

**NUMERICAL SIMULATION OF EARTHQUAKE GROUND  
MOTIONS IN THE UPPER MISSISSIPPI EMBAYMENT**

A Dissertation  
Presented to  
The Academic Faculty

by

José Alfredo Fernández León

In Partial Fulfillment  
of the Requirements for the Degree  
Doctor of Philosophy in the  
School of Civil and Environmental Engineering

Georgia Institute of Technology  
December 2007

# **NUMERICAL SIMULATION OF EARTHQUAKE GROUND MOTIONS IN THE UPPER MISSISSIPPI EMBAYMENT**

Approved by:

Dr. Glenn J. Rix, Advisor  
School of Civil and Environmental  
Engineering  
*Georgia Institute of Technology*

Dr. Dominic Assimaki  
School of Civil and Environmental  
Engineering  
*Georgia Institute of Technology*

Dr. Bruce R. Ellingwood  
School of Civil and Environmental  
Engineering  
*Georgia Institute of Technology*

Dr. Laurence J. Jacobs  
School of Civil and Environmental  
Engineering  
*Georgia Institute of Technology*

Dr. L. Timothy Long  
School of Earth and Atmospheric  
Sciences  
*Georgia Institute of Technology*

Date Approved: November 12, 2007

To my wife and my family

## ACKNOWLEDGEMENTS

I would especially like to express my gratitude to my advisor, Dr. Glenn J. Rix, for his guidance, support, and advice during my masters and doctoral studies. His knowledge and experience have greatly contributed to my academic pursuits.

I also want to acknowledge my other thesis committee members including Dr. Dominic Assimaki, Dr. Bruce R. Ellingwood, Dr. Laurence J. Jacobs, and Dr. L. Timothy Long for their insightful comments that improved the quality of this study. I would like to extend my gratitude to the other faculty members of the Geosystems Group at Georgia Tech including Dr. Carlos Santamarina, Dr. David Frost, and Dr. Paul Mayne for their contribution to my education.

I wish to acknowledge all the students of the Geosystems Group, particularly to Andrew Fuggle, Pierre Ramondenc, and Mehmet Iscimen for their friendship and support through these five years at Georgia Tech. I also want to thank Varun for his help on running some Matlab simulations.

The financial and technical support for this investigation provided by the Mid-America Earthquake (MAE) Center is greatly appreciated.

I have no words to express my sincere gratitude to my wife Mercedes, my parents Alfredo and María Teresa, my sisters Lissette and Mariela, family and friends in Guatemala for their continuous love, encouragement and support through the years. None of this would have been possible without them.

# TABLE OF CONTENTS

	Page
ACKNOWLEDGEMENTS.....	iv
LIST OF TABLES.....	viii
LIST OF FIGURES .....	ix
LIST OF SYMBOLS AND ABBREVIATIONS .....	xxii
SUMMARY .....	xxix
CHAPTER1. INTRODUCTION.....	1
1.1. Objective of this Study .....	3
1.2. Organization of this Study .....	4
CHAPTER 2. UPPER MISSISSIPPI EMBAYMENT.....	6
CHAPTER 3. SOIL ATTENUATION RELATIONSHIPS IN THE UPPER MISSISSIPPI EMBAYMENT .....	15
3.1. Ground Motion Uncertainties .....	17
3.2. Stochastic Method.....	18
3.2.1. The Source Effect .....	20
3.2.2. The Path Effect .....	25
3.2.3. The Site Effect .....	25
3.2.4. Type of Ground Motion.....	26
3.2.5. Random Vibration Theory .....	28
3.3. Validation of the Use of an Equivalent Linear Approach for Site Response Analyses in the Upper Mississippi Embayment .....	32
3.4. Models and Variability .....	38
3.4.1. Source Model .....	40
3.4.2. Stress Drop.....	47
3.4.3. Source Depth.....	50
3.4.4. Crustal and Near-Surface Attenuation .....	50
3.4.5. Crustal Shear-Wave Velocity.....	51
3.4.6. Soil Shear-Wave Velocity.....	51

3.4.7. Dynamic Soil Properties .....	54
3.4.8. Embayment Depth .....	60
3.5. Randomization of Parameters .....	60
3.6. Attenuation Relationships .....	62
3.7. Discussion of Results .....	100
3.8. Conclusions .....	116
<b>CHAPTER 4. SEISMIC HAZARD ANALYSES AND PROBABILISTIC GROUND MOTION TIME HISTORIES IN THE UPPER MISSISSIPPI EMBAYMENT .....</b>	<b>119</b>
4.1. Seismic Hazard Analysis .....	123
4.2. Seismic Hazard Analyses in the Upper Mississippi Embayment .....	136
4.2.1. Seismic Sources Characterization .....	137
4.2.1.1 Spatial Characterization .....	137
4.2.1.2 Size Characterization .....	139
4.2.2. Ground Motion Attenuation Relationships .....	146
4.2.3. Seismic Hazard Analyses for Selected Cities .....	146
4.2.3.1 Seismic Hazard Deaggregation .....	152
4.2.3.2 Uniform Hazard Spectra .....	189
4.2.3.3 Comparison with other studies .....	213
4.2.4. Regional Seismic Hazard Maps .....	219
4.3. Spectrum-Compatible Time Histories .....	233
4.4. Conclusions .....	247
<b>CHAPTER 5. BASIN EFFECTS IN THE UPPER MISSISSIPPI EMBAYMENT .....</b>	<b>253</b>
5.1. Site Effects .....	256
5.1.1. Surface Topography .....	257
5.1.2. Soil Layers .....	257
5.1.3. Subsurface Topography and Lateral Discontinuities .....	258
5.2. Methods to Evaluate Site Effects .....	259
5.2.1. Empirical Methods .....	259
5.2.2. Experimental Methods .....	260
5.2.3. Theoretical Methods .....	261
5.3. Seismic Response of Sedimentary Basins to SH Waves .....	262
5.4. Description of the Method .....	267

5.4.1. Wave field outside basin .....	268
5.4.2. Wave field inside basin .....	271
5.4.3. Non-linear soil behavior .....	274
5.5. Assessment of the Method .....	279
5.5.1. Semi-circular basin .....	279
5.5.2. Parabolic basin .....	280
5.6. Basin Effects in the Upper Mississippi Embayment .....	292
5.6.1. Application of method to the Upper Mississippi Embayment.....	294
5.6.2. Results and Discussion .....	295
5.7. Conclusions.....	312
CHAPTER 6. SUMMARY, CONCLUSIONS, AND RECOMENDATIONS .....	314
6.1. Summary and Conclusions .....	314
6.2. Recommendations.....	316
APPENDIX A. MODEL REGRESSION COEFFICIENTS FOR THE SOIL ATTENUATION EQUATION .....	318
APPENDIX B. SEISMIC HAZARD DEAGGREGATION .....	319
REFERENCES .....	337
VITA.....	365

## LIST OF TABLES

	Page
Table 2.1. Stratigraphic column of the sediments of Mississippi Embayment near Memphis, TN (Brahana et al., 1987; Romero, 2001; Van Arsdale and TenBrink, 2000).....	12
Table 3.1. Uncertainties in ground motion estimation (modified from Silva et al. (1997) and Toro et al. (1997)) .....	19
Table 3.2. Alternative models .....	38
Table 3.3. Randomized model parameters and distributions .....	39
Table 3.4. Source models parameters .....	41
Table 4.1. Parameters for exponential part of the recurrence model of New Madrid and Charleston, SC sources .....	144
Table 4.2. Logic tree for characteristic magnitude of New Madrid seismic sources.....	145
Table 4.3. Logic tree for characteristic magnitude of Charleston, SC seismic sources.	145
Table 4.4. Logic tree for attenuation relationship .....	147
Table 4.5. Selected cities included in the seismic hazard analysis .....	147

## LIST OF FIGURES

	Page
Figure 1.1. Source, path, and site effects in the earthquake process generation and seismic wave propagation.....	2
Figure 2.1. Extent of the Upper Mississippi Embayment and near surface geologic deposits.....	7
Figure 2.2. Regional seismicity from 1974 to 2007 (CERI, 2007) and fictitious faults used to the characterize the New Madrid Seismic Zone (Frankel et al., 2002) .....	8
Figure 2.3. Extent of the Upper Mississippi Embayment along with the geographical location of the New Madrid Seismic Zone.....	9
Figure 2.4. Alternative seismic sources used by Toro and Silva (2001) to characterize the NMSZ .....	10
Figure 2.5. Sediment thickness contours of the Upper Mississippi Embayment.....	11
Figure 2.6. East-West cross-sectional view of the Embayment near Memphis, TN (Brahana et al., 1987) .....	14
Figure 2.7. East-West cross-sectional view of the Embayment near Memphis, TN (vertical-to-horizontal scale ratio = 10:1).....	14
Figure 3.1. Source spectrum scaling for one-corner $\omega$ -square model.....	23
Figure 3.2. Comparison of one- and two-corner source models.....	24
Figure 3.3. Band-limited spectra predicted by the stochastic method .....	27
Figure 3.4. Modeling bias and variability estimates of the Stochastic Method using a one-corner, point-source model and the equivalent linear analysis for site response (from Silva et al. (1997)) .....	33
Figure 3.5. Upper-bound envelope approach used by Park and Hashash (2005) to develop site factors for Embayment depths of 500 and 1000 m .....	35
Figure 3.6. Comparison of $F_a$ site factors for the Upper Mississippi Embayment computed by equivalent linear and true non-linear analyses.....	36
Figure 3.7. Geometrical attenuation functions.....	42

Figure 3.8. Seismic attenuation functions.....	43
Figure 3.9. Path duration.....	44
Figure 3.10. High-frequency filters .....	45
Figure 3.11. Comparison of Fourier acceleration spectra.....	48
Figure 3.12. Attenuation of Fourier acceleration amplitudes .....	49
Figure 3.13. Crustal shear-wave velocity profile (Catchings, 1999) .....	52
Figure 3.14. Near-surface shear-wave velocity profiles .....	53
Figure 3.15. EPRI (1993) modulus reduction curves and their depth range of applicability .....	55
Figure 3.16. EPRI (1993) damping ratio curves and their depth range of applicability..	56
Figure 3.17. Upper and lower bounds of EPRI (1993) modulus reduction curves.....	57
Figure 3.18. Upper and lower bounds of EPRI (1993) damping ratio curves .....	58
Figure 3.19. Density and small-strain damping ratio profiles .....	59
Figure 3.20. Examples of randomized soil parameters.....	63
Figure 3.21. Example of simulations and attenuation relationship for PGA using the Atkinson and Boore (1995) model .....	66
Figure 3.22. Example of simulations and attenuation relationship for PGA using the Frankel et al. (1996) model .....	67
Figure 3.23. Example of simulations and attenuation relationship for PGA using the Silva et al. (2003) model.....	68
Figure 3.24. Example of simulations and attenuation relationship for 1-second spectral acceleration using the Atkinson and Boore (1995) model .....	69
Figure 3.25. Example of simulations and attenuation relationship for 1-second spectral acceleration using the Frankel et al. (1996) model.....	70
Figure 3.26. Example of simulations and attenuation relationship for 1-second spectral acceleration using the Silva et al. (2003) model.....	71

Figure 3.27. Normalized residuals of 1-second spectral accelerations vs. epicentral distance for the Atkinson and Boore (1995) model.....	72
Figure 3.28. Normalized residuals of 1-second spectral accelerations vs. epicentral distance for the Frankel et al. (1996) model.....	73
Figure 3.29. Normalized residuals of 1-second spectral accelerations vs. epicentral distance for the Silva et al. (2003) model.....	74
Figure 3.30. Normalized residuals of 1-second spectral accelerations vs. magnitude for the Atkinson and Boore (1995) model .....	75
Figure 3.31. Normalized residuals of 1-second spectral accelerations vs. magnitude for the Frankel et al. (1996) model.....	76
Figure 3.32. Normalized residuals of 1-second spectral accelerations vs. magnitude for the Frankel et al. (1996) model.....	77
Figure 3.33. Normalized residuals of PGA vs. epicentral distance for the Atkinson and Boore (1995) model.....	78
Figure 3.34. Normalized residuals of PGA vs. epicentral distance for the Frankel et al. (1996) model .....	79
Figure 3.35. Normalized residuals of PGA vs. epicentral distance for the Silva et al. (2003) model .....	80
Figure 3.36. Normalized residuals of PGA vs. magnitude for the Atkinson and Boore (1995) model .....	81
Figure 3.37. Normalized residuals of PGA vs. magnitude for the Frankel et al. (1996) model .....	82
Figure 3.38. Normalized residuals of PGA vs. magnitude for the Silva et al. (2003) model .....	83
Figure 3.39. Example of total aleatory variability for the Atkinson and Boore (1995) model .....	85
Figure 3.40. Example of total aleatory variability for the Frankel et al. (1996) model ....	86
Figure 3.41. Example of total aleatory variability for the Silva et al. (2003) model .....	87
Figure 3.42. Example of parametric variability for M 4 and M 7 using the Atkinson and Boore (1995) model.....	88

Figure 3.43. Example of parametric variability for M 4 and M 7 using the Frankel et al. (1996) model .....	89
Figure 3.44. Example of parametric variability for M 4 and M 7 using the Silva et al. (2003) model .....	90
Figure 3.45. Example of parametric variability vs. embayment depth for the Atkinson and Boore (1995) model.....	92
Figure 3.46. Example of parametric variability vs. embayment depth for the Frankel et al. (1996) model .....	93
Figure 3.47. Example of parametric variability vs. embayment depth for the Silva et al. (2003) model .....	94
Figure 3.48. Total aleatory variability of PGA vs. magnitude.....	95
Figure 3.49. Total aleatory variability of 0.2-seconds spectral acceleration vs. magnitude .....	96
Figure 3.50. Total aleatory variability of 1-second spectral acceleration vs. magnitude .	97
Figure 3.51. Parametric variability of PGA vs. magnitude.....	98
Figure 3.52. Parametric variability of 1-second spectral acceleration vs. magnitude .....	99
Figure 3.53. Comparison of attenuation relationships for M 4.....	101
Figure 3.54. Comparison of attenuation relationships for M 7.....	102
Figure 3.55. Comparison of response spectra for M 6.....	104
Figure 3.56. Comparison of response spectra for magnitude-dependent and constant stress drop source models.....	106
Figure 3.57. Comparison of response spectra for one- and two-corner source models..	107
Figure 3.58. Effect of stress drop epistemic uncertainty on response spectra .....	109
Figure 3.59. Effect of earthquake magnitude on spectral shape .....	110
Figure 3.60. Effect of embayment depth on response spectra .....	112
Figure 3.61. Effect of embayment depth on attenuation of ground amplitude .....	113
Figure 3.62. Effect of soil shear-wave velocity profile on response spectra .....	115

Figure 4.1. Peak ground acceleration (PGA) hazard curve for Atlanta, GA on rock site conditions given by the 2002 USGS National Hazard Maps .....	128
Figure 4.2. Geographical location of seismic sources considered in the analysis along with the extent of the Upper Mississippi Embayment.....	138
Figure 4.3. Extent of the background seismicity areas, Wabash Valley (east zone) and cratonic zones (west zone), and maximum magnitude assigned to each zone (Frankel et al., 2002) .....	140
Figure 4.4. Gutenberg-Richter recurrence relation (from Kramer, 1996) .....	142
Figure 4.5. Characteristic magnitude recurrence model proposed by Schwartz and Coppersmith (1984) (from McGuire, 2004).....	143
Figure 4.6. Upper Mississippi Embayment and selected cities included in the seismic hazard analysis.....	148
Figure 4.7. Peak ground acceleration hazard curves for Memphis, TN .....	150
Figure 4.8. One-second spectral period hazard curves for Memphis, TN .....	151
Figure 4.9. Peak ground acceleration mean and +/- 1 standard deviation hazard curves for Memphis, TN (Lowlands).....	153
Figure 4.10. One-second spectral period mean and +/- 1 standard deviation hazard curves for Memphis, TN (Lowlands).....	154
Figure 4.11. Peak ground acceleration mean and +/- 1 standard deviation hazard curves for Memphis, TN (Uplands).....	155
Figure 4.12. One-second spectral period mean and +/- 1 standard deviation hazard curves for Memphis, TN (Uplands).....	156
Figure 4.13. Peak ground acceleration mean and +/- 1 standard deviation hazard curves for Jonesboro, AR.....	157
Figure 4.14. One-second spectral period mean and +/- 1 standard deviation hazard curves for Jonesboro, AR.....	158
Figure 4.15. Peak ground acceleration mean and +/- 1 standard deviation hazard curves for Jackson, TN .....	159
Figure 4.16. One-second spectral period mean and +/- 1 standard deviation hazard curves for Jackson, TN .....	160

Figure 4.17. Peak ground acceleration mean and +/- 1 standard deviation hazard curves for Blytheville, AR .....	161
Figure 4.18. One-second spectral period mean and +/- 1 standard deviation hazard curves for Blytheville, AR .....	162
Figure 4.19. Peak ground acceleration mean and +/- 1 standard deviation hazard curves for Paducah, KY .....	163
Figure 4.20. One-second spectral period mean and +/- 1 standard deviation hazard curves for Paducah, KY .....	164
Figure 4.21. Peak ground acceleration mean and +/- 1 standard deviation hazard curves for Cape Girardeau, MO .....	165
Figure 4.22. One-second spectral period mean and +/- 1 standard deviation hazard curves for Cape Girardeau, MO .....	166
Figure 4.23. Peak ground acceleration mean and +/- 1 standard deviation hazard curves for Little Rock, AR .....	167
Figure 4.24. One-second spectral period mean and +/- 1 standard deviation hazard curves for Little Rock, AR .....	168
Figure 4.25. Hazard curves for Memphis, TN using the Atkinson and Boore (1995) model with and without aleatory uncertainty .....	170
Figure 4.26. Hazard deaggregation for peak ground acceleration and return period of 2475 years in Memphis, TN using the Atkinson and Boore (1995) model	173
Figure 4.27. Hazard deaggregation for peak ground acceleration and return period of 2475 years in Memphis, TN using the Frankel et al. (1996) – median $\Delta\sigma$ model .....	174
Figure 4.28. Hazard deaggregation for peak ground acceleration and return period of 2475 years in Memphis, TN using the Frankel et al. (1996) – high $\Delta\sigma$ model .....	175
Figure 4.29. Hazard deaggregation for peak ground acceleration and return period of 2475 years in Memphis, TN using the Frankel et al. (1996) – low $\Delta\sigma$ model .....	176
Figure 4.30. Hazard deaggregation for peak ground acceleration and return period of 2475 years in Memphis, TN using the Silva et al. (2003) – median $\Delta\sigma$ model .....	177

Figure 4.31. Hazard deaggregation for peak ground acceleration and return period of 2475 years in Memphis, TN using the Silva et al. (2003) – high $\Delta\sigma$ model .....	178
Figure 4.32. Hazard deaggregation for peak ground acceleration and return period of 2475 years in Memphis, TN using the Silva et al. (2003) – low $\Delta\sigma$ model .....	179
Figure 4.33. Mean hazard deaggregation for peak ground acceleration and return period of 2475 years in Memphis, TN .....	181
Figure 4.34. Hazard deaggregation for peak ground acceleration and return period of 975 years in Memphis, TN .....	182
Figure 4.35. Hazard deaggregation for peak ground acceleration and return period of 475 years in Memphis, TN .....	183
Figure 4.36. Hazard deaggregation for peak ground acceleration and return period of 475 years in Memphis, TN .....	184
Figure 4.37. Hazard deaggregation for 1-second spectral period and return period of 2475 years in Memphis, TN .....	185
Figure 4.38. Joint magnitude and distance hazard deaggregation for peak ground acceleration and return period of 2475 years in Memphis, TN .....	186
Figure 4.39. Joint magnitude and distance hazard deaggregation for 1-second spectral period and return period of 2475 years in Memphis, TN .....	187
Figure 4.40. Procedure to calculate the uniform hazard spectrum .....	190
Figure 4.41. Contribution of small nearby and large distant earthquakes to the uniform hazard spectrum (from Reiter, 1990).....	191
Figure 4.42. Rock and soil hazard curves for peak ground acceleration in Memphis, TN .....	193
Figure 4.43. Hazard deaggregation for rock site conditions in Memphis, TN .....	195
Figure 4.44. Hazard deaggregation for soil site conditions in Memphis, TN using soil attenuation relationships .....	196
Figure 4.45. Soil mean uniform hazard spectrum and its associated variability for return period of 2475 years in Memphis, TN (Lowlands) .....	197
Figure 4.46. Soil mean uniform hazard spectrum and its associated variability for return period of 2475 years in Memphis, TN (Uplands).....	198

Figure 4.47. Soil mean uniform hazard spectrum and its associated variability for return period of 2475 years in Jonesboro, AR .....	199
Figure 4.48. Soil mean uniform hazard spectrum and its associated variability for return period of 2475 years in Jackson, TN .....	200
Figure 4.49. Soil mean uniform hazard spectrum and its associated variability for return period of 2475 years in Blytheville, AR.....	201
Figure 4.50. Soil mean uniform hazard spectrum and its associated variability for return period of 2475 years in Paducah, KY .....	202
Figure 4.51. Soil mean uniform hazard spectrum and its associated variability for return period of 2475 years in Cape Girardeau, MO .....	203
Figure 4.52. Soil mean uniform hazard spectrum and its associated variability for return period of 2475 years in Little Rock, AR .....	204
Figure 4.53. Soil mean uniform hazard spectra for return periods of 475, 975, and 2475 years in Memphis, TN (Lowlands).....	205
Figure 4.54. Soil mean uniform hazard spectra for return periods of 475, 975, and 2475 years in Memphis, TN (Uplands) .....	206
Figure 4.55. Soil mean uniform hazard spectra for return periods of 475, 975, and 2475 years in Jonesboro, AR.....	207
Figure 4.56. Soil mean uniform hazard spectra for return periods of 475, 975, and 2475 years in Jackson, TN.....	208
Figure 4.57. Soil mean uniform hazard spectra for return periods of 475, 975, and 2475 years in Blytheville, AR .....	209
Figure 4.58. Soil mean uniform hazard spectra for return periods of 475, 975, and 2475 years in Paducah, KY .....	210
Figure 4.59. Soil mean uniform hazard spectra for return periods of 475, 975, and 2475 years in Cape Girardeau, MO .....	211
Figure 4.60. Soil mean uniform hazard spectra for return periods of 475, 975, and 2475 years in Little Rock, AR.....	212
Figure 4.61. Five-second spectral period hazard curves for Blytheville, AR.....	214
Figure 4.62. Comparison of uniform hazard spectra for return period of 2475 years in Memphis, TN.....	216

Figure 4.63. Division of the Upper Mississippi Embayment according to soil type – Lowlands (Lwld) and Uplands (Upld) – and depth bin – 6 m (bin 1) to 1220 m (bin 7) – .	220
Figure 4.64. Seismic hazard map for peak ground acceleration and return period of 475 years; mean values.	221
Figure 4.65. Seismic hazard map for peak ground acceleration and return period of 975 years; mean values.	222
Figure 4.66. Seismic hazard map for peak ground acceleration and return period of 2475 years; mean values.	223
Figure 4.67. Seismic hazard map for 1-second spectral acceleration and return period of 475 years; mean values.	224
Figure 4.68. Seismic hazard map for 1-second spectral acceleration and return period of 975 years; mean values.	225
Figure 4.69. Seismic hazard map for 1-second spectral acceleration and return period of 2475 years; mean values.	226
Figure 4.70. Seismic hazard map for 4-second spectral acceleration and return period of 475 years; mean values.	227
Figure 4.71. Seismic hazard map for 4-second spectral acceleration and return period of 975 years; mean values.	228
Figure 4.72. Seismic hazard map for 4-second spectral acceleration and return period of 2475 years; mean values.	229
Figure 4.73. Seismic hazard maps developed by Cramer (2006b) using SHAKE91 (blue line represents the boundary of the Upper Mississippi Embayment).	231
Figure 4.74. Seismic hazard maps developed by Cramer (2006b) using TREMORKA (blue line represents the boundary of the Upper Mississippi Embayment)	232
Figure 4.75. Uniform hazard spectrum simulations for return period of 2475 years along with the mean (target) uniform hazard spectrum in Memphis, TN	238
Figure 4.76. Selected uniform hazard spectrum simulations for return period of 2475 years along with the mean (target) uniform hazard spectrum in Memphis, TN	239
Figure 4.77. Example of the spectral matching process	241

Figure 4.78. Example of the initial and final time histories corresponding to the spectral matching process shown in Figure 4.77 .....	243
Figure 4.79. Cosine taper function applied to acceleration time histories.....	245
Figure 4.80. Acceleration, velocity, and displacement time histories before and after the drift correction. ....	246
Figure 4.81. Acceleration time histories consistent with hazard levels of 2% PE in 50 years for Memphis, TN.....	248
Figure 4.82. Velocity time histories consistent with hazard levels of 2% PE in 50 years for Memphis, TN .....	249
Figure 4.83. Displacement time histories consistent with hazard levels of 2% PE in 50 years for Memphis, TN.....	250
Figure 5.1. Extent of the Upper Mississippi Embayment along with the geographical location of the 2-D and 3-D models used by Saikia et al. (2006) (dotted line and rectangle) and 2-D model implemented in this study (solid line) .....	266
Figure 5.2. Stratified basin embedded in a half-space (from Zeng and Benites (1998)) .....	268
Figure 5.3. Hysteresis shear stress-strain loop (from Kramer (1996)). ....	275
Figure 5.4. Iterative procedure used by the equivalent linear analysis (from Kramer (1996)). Numbers in parentheses indicate number of iteration .....	276
Figure 5.5. Model of semi-circular basin.....	280
Figure 5.6. Surface displacement amplification of a semi-circular basin due to a unitary incident motion.....	281
Figure 5.7. Model of parabolic basin .....	281
Figure 5.8. Surface displacement amplification of a parabolic basin due to a unitary incident motion.....	282
Figure 5.9. Comparison of surface displacement amplification of the parabolic basin model shown in Figure 5.7 to a unitary incident motion with incident angle of $0^\circ$ computed with 1-D and 2-D models.....	283
Figure 5.10. Comparison of surface displacement amplification of the parabolic basin shown in Figure 5.7 to a unitary incident motion with incident angle of $60^\circ$ computed with 1-D and 2-D models .....	284

Figure 5.11. Surface displacement time histories of the parabolic basin shown in Figure 5.7 due to a Ricker pulse with incident angle of $0^\circ$ computed with a 2-D model (9 stations only) .....	286
Figure 5.12. Surface displacement time histories of the parabolic basin shown in Figure 5.7 due to a Ricker pulse with incident angle of $0^\circ$ computed with a 2-D model .....	287
Figure 5.13. Surface displacement time histories of the parabolic basin shown in Figure 5.7 due to a Ricker pulse with incident angle of $60^\circ$ computed with a 2-D model (9 stations only) .....	288
Figure 5.14. Surface displacement time histories of the parabolic basin shown in Figure 5.7 due to a Ricker pulse with incident angle of $60^\circ$ computed with a 2-D model .....	289
Figure 5.15. Significant duration of the surface displacement time histories shown in Figure 5.12.....	290
Figure 5.16. Significant duration of the surface displacement time histories shown in Figure 5.14.....	291
Figure 5.17. Model of the Upper Mississippi Embayment implemented in the analyses .....	292
Figure 5.18. Response spectra of incident motions used in the analyses .....	296
Figure 5.19. Fourier displacement amplification at the surface of the Upper Mississippi Embayment.....	298
Figure 5.20. Comparison of 1-D and 2-D Fourier displacement amplifications vs. distance for the incident motion with PGA of 0.40g and incident angle of $0^\circ$ .....	299
Figure 5.21. Comparison of 1-D and 2-D Fourier displacement amplifications vs. distance for the incident motion with PGA of 0.40g and incident angles of $30^\circ$ and $-30^\circ$ .....	300
Figure 5.22. Comparison of 1-D and 2-D Fourier displacement amplifications vs. distance for the incident motion with PGA of 0.40g and incident angles of $60^\circ$ and $-60^\circ$ .....	301
Figure 5.23. Comparison of 1-D and 2-D Fourier displacement amplifications vs. distance and spectral period for the incident motion with PGA of 0.40g .....	303

Figure 5.24. Comparison of 1-D and 2-D Fourier displacement amplifications vs. frequency for the incident motion with PGA of 0.40g and incident angle of 0° .....	304
Figure 5.25. Comparison of 1-D and 2-D Fourier displacement amplifications vs. frequency for the incident motion with PGA of 0.40g and incident angles of 30° and -30° .....	305
Figure 5.26. Comparison of 1-D and 2-D Fourier displacement amplifications vs. frequency for the incident motion with PGA of 0.40g and incident angles of 60° and -60° .....	306
Figure 5.27. Comparison of 1D and 2D soil amplification for an incident motion with PGA of 0.40g.....	307
Figure 5.28. Comparison of 1D and 2D soil amplification for an incident motion with PGA of 0.50g.....	308
Figure 5.29. Comparison of 1D and 2D soil amplification for an incident motion with PGA of 0.75g.....	309
Figure B.1 Hazard deaggregation for peak ground acceleration and return period of 2475 years in Jonesboro, AR.....	319
Figure B.2. Hazard deaggregation for 1-second spectral period and return period of 2475 years in Jonesboro, AR.....	320
Figure B.3. Joint magnitude and distance hazard deaggregation for peak ground acceleration and return period of 2475 years in Jonesboro, AR.....	321
Figure B.4. Hazard deaggregation for peak ground acceleration and return period of 2475 years in Jackson, TN.....	322
Figure B.5. Hazard deaggregation for 1-second spectral period and return period of 2475 years in Jackson, TN.....	323
Figure B.6. Joint magnitude and distance hazard deaggregation for peak ground acceleration and return period of 2475 years in Jackson, TN .....	324
Figure B.7. Hazard deaggregation for peak ground acceleration and return period of 2475 years in Blytheville, AR .....	325
Figure B.8. Hazard deaggregation for 1-second spectral period and return period of 2475 years in Blytheville, AR .....	326

Figure B.9. Joint magnitude and distance hazard deaggregation for peak ground acceleration and return period of 2475 years in Blytheville, AR .....	327
Figure B.10. Hazard deaggregation for peak ground acceleration and return period of 2475 years in Paducah, KY .....	328
Figure B.11. Hazard deaggregation for 1-second spectral period and return period of 2475 years in Paducah, KY .....	329
Figure B.12. Joint magnitude and distance hazard deaggregation for peak ground acceleration and return period of 2475 years in Paducah, KY .....	330
Figure B.13. Hazard deaggregation for peak ground acceleration and return period of 2475 years in Cape Girardeau, MO .....	331
Figure B.14. Hazard deaggregation for 1-second spectral period and return period of 2475 years in Cape Girardeau, MO .....	332
Figure B.15. Joint magnitude and distance hazard deaggregation for peak ground acceleration and return period of 2475 years in Cape Girardeau, MO .....	333
Figure B.16. Hazard deaggregation for peak ground acceleration and return period of 2475 years in Little Rock, AR .....	334
Figure B.17. Hazard deaggregation for 1-second spectral period and return period of 2475 years in Little Rock, AR .....	335
Figure B.18. Joint magnitude and distance hazard deaggregation for peak ground acceleration and return period of 2475 years in Little Rock, AR .....	336

## LIST OF SYMBOLS AND ABBREVIATIONS

$a$	Half-width of a basin model, intercept of the Gutenberg-Richter relation
ab95	Atkinson and Boore (1995) source model
$A$	Amplitude of incident wave
$A(f)$	Amplification function
$A_{loop}$	Area of hysteresis loop
$b$	Slope of the Gutenberg-Richter relation
$B_m$	Complex coefficients of the propagator matrices formulation
$c_i$	Regression coefficients of attenuation equation ( $i = 1$ to $10$ )
$c_Q$	Seismic velocity
$C$	Auxiliary curve where sources are located
CERI	Center for Earthquake Research and Information
CEUS	Central and Eastern United States
$d_s$	Distance from sources to basin interface
$d_w$	Distance between adjacent collocation points
$D(f)$	Attenuation function
DEEPSOIL	True non-linear site response computer program
DSHA	Deterministic seismic hazard analysis
$E(M_0, f)$	Source spectrum
EPRI	Electric Power Research Institute
EZFRISK <sup>TM</sup>	Computer program for earthquake ground motion estimation
$f$	Frequency
$f(M, R)$	Functional form of attenuation equation
$f_X(x)$	Probability density function of $x$
$f_a$	Corner frequency related to the length of the earthquake rupture

$fa96$	Frankel et al. (1996) source model
$f_b$	Corner frequency related to the width of the earthquake rupture
$f_e$	Rate of occurrence of extrema
$f_{max}$	Cut-off frequency
$f_0$	Corner frequency of source spectrum
$f_z$	Rate of occurrence of zero crossings
$F_a$	Site coefficient at short-periods
FEMA	Federal Emergency Management Agency
$g$	Acceleration due to gravity
$G$	Shear modulus
$G^*$	Complex shear modulus
$G(f)$	Site spectrum
$G_f(P,Q)$	Green's function
$G_{max}$	Maximum shear modulus
$G_{sec}$	Secant shear modulus
$H$	Source depth; soil layer thickness
$H[\cdot]$	Heaviside step function
$H_0^{(1)}(\cdot)$	Hankel function of the first kind and order zero
$H_1^{(1)}(\cdot)$	Hankel function of the first kind and order one
$H/V$	Ratio between spectra of the horizontal and vertical components of a ground motion
$H_{Low}$	Lower limit of source depth
$H_{Up}$	Upper limit of source depth
$I(f)$	Function that controls the type of motion
IBEM	Indirect boundary element method
$K$	Covariance matrix
$l_1$	First element of the motion-stress vector

$l_2$	Second element of the motion-stress vector
$L$	Lower triangular matrix
$L_{wld}$	Lowlands soil profile
$m$	Earthquake magnitude
$m_b$	Body wave magnitude
$m_k$	Moments of the power spectral density
$m_{max}$	Maximum earthquake magnitude expected to occur on the source
$m_{min}$	Minimum earthquake magnitude of engineering significance
$M$	Number of wavenumbers
$\mathbf{M}$	Moment magnitude
$M_L$	Richter local magnitude
$M_S$	Surface wave magnitude
$M_0$	Seismic moment
MAE	Mid-America Earthquake Center
$\mathbf{n}$	Unit vector
$N$	Number of sources
$N(m)$	Number of earthquakes of magnitude $m$ or greater per unit of time
$N_z$	Number of zero crossings
$N_e$	Number of extrema
NCSA	National Center for Supercomputing Applications
NEHRP	National Earthquake Hazards Reduction Program
NGA	Next Generation Attenuation Model
NMSZ	New Madrid Seismic Zone
$\mathbf{P}$	Propagator matrix
$P[\cdot]$	Probability operator
$P(R,f)$	Path spectrum
PGA	Peak ground acceleration

PSHA	Probabilistic seismic hazard analysis
$Q(f)$	Seismic attenuation function
$Q_0$	Crustal attenuation coefficient
$Q_s$	Quality factor
$r$	Source-to-site distance
$R$	Epicentral distance, source-to-site distance
$R_\gamma$	Ratio of the effective shear strain to the peak shear strain
$R_M$	Equivalent epicentral distance
$\langle R_{\Theta\Phi} \rangle$	Radiation factor of the total shear-wave radiation
RANPAR	Computer program for randomization of site response input
RASCALS	Equivalent-linear site response computer program
rms	Root-mean-square
RP	Return period
RVT	Random vibration theory
$S(M_0, f)$	Displacement source spectrum
$S_a$	Spectral acceleration
si03	Silva et al. (2003) source model
$S_s$	Mapped maximum considered earthquake spectral response acceleration at short periods
SSR	Standard spectral ratio
SHAKE91	Equivalent-linear site response computer program
$t$	Time; traction
$t_0$	Time corresponding to the beginning of the window function; free-field traction
$t_b$	Duration of the beginning of the taper of the window function
$t_B$	Traction inside basin
$t_d$	Duration of the ground motion after the beginning taper of the window function; scattered-field traction

$t_e$	Duration of the ending the taper of the window function
$t_H$	Traction in the half-space
$T$	Period, ground motion duration
$T_d$	Faulting duration
TREMORKA	Equivalent-linear site response computer program
$u$	Displacement
$u_0$	Free-field displacement
$u_B$	Displacement inside the basin
$u_d$	Scattered-field displacement
$u_H$	Displacement in the half-space
$u_{inc}$	Incident displacement
$U$	Upper triangular matrix
Upld	Uplands soil profile
UHS	Uniform hazard spectrum
UHRs	Uniform hazard response spectrum
USGS	United States Geological Survey
$V$	Factor accounting for partitioning of energy onto 2 horizontal components
$w$	Weighting factor; uncorrelated standard normal random numbers
$W$	Number of collocation points along basin interface
WUS	Western United States
$x$	Horizontal coordinates
$y$	Ground motion amplitude; non-conditional, autocorrelated simulation of a random function
$y_{max}$	Peak amplitude
$y_{rms}$	Root-mean-square amplitude
$Y(M_0, R, f)$	Surface Fourier spectrum
$z$	Vertical coordinate, depth

$Z(R)$	Geometrical spreading function
$\beta$	Shear-wave velocity; parameter of the truncated exponential distribution
$\beta_s$	Shear-wave velocity in the vicinity of the earthquake source
$\gamma_{\text{eff}}$	Effective shear strain
$\gamma_{\text{peak}}$	Peak shear strain
$\gamma_s$	Shear strain
$\gamma_{s \text{ max}}$	Maximum shear strain
$\gamma_{s \text{ rms}}$	Root-mean-square shear strain
$\delta(\cdot)$	Dirac delta function
$\Delta\kappa$	Wavenumber interval
$\Delta\sigma$	Stress drop
$\varepsilon$	Standard Gaussian variable
$\theta_0$	Incident angle with respect to vertical
$\kappa$	Near-surface attenuation coefficient; wavenumber
$\lambda$	Annual frequency that a ground motion parameter exceeds a particular level; wavelength
$\lambda_{\text{inc}}$	Incident wavelength
$\nu$	Annual rate of occurrence of earthquakes
$\xi$	Damping ratio
$\xi(x)$	Interface between basin and half-space
$\rho$	Density; correlation coefficient
$\rho_s$	Density in the vicinity of the earthquake source
$\sigma$	Standard deviation
$\sigma(\mathbf{Q})$	Source density function
$\sigma_{\ln y}$	Standard deviation of the natural log of the ground motion amplitude $y$
$\tau_s$	Shear stress

$\phi(\mathbf{Q})$	Source strength at point $\mathbf{Q}$
$\omega$	Circular frequency

## SUMMARY

Earthquake ground motions are needed to evaluate the seismic performance of new and existing structures and facilities. In seismically active regions the strong ground motion recordings database is usually sufficiently large to physically constrain the earthquake estimation for seismic risk assessment. However, in areas of low seismicity rate, particularly in the Central and Eastern United States, the estimation of strong ground motions for a specified magnitude, distance, and site conditions represents a significant issue. The only available approach for ground motion estimation in this region is numerical simulation.

In this study, earthquake ground motions have been generated for the Upper Mississippi Embayment using a numerical wave propagation formulation. The effects of epistemic and aleatory uncertainties in the earthquake source, path, and site processes, the effect of non-linear soil behavior, and the effects of the geometry of the Embayment have been incorporated. The ground motions are intended to better characterize the seismic hazard in the Upper Mississippi Embayment by representing the amplitude and variability that might be observed in real earthquakes and to provide resources to evaluate the seismic risk in the region.

# CHAPTER 1

## INTRODUCTION

Earthquakes are a natural hazard that causes death, injuries, and property damage. Earthquakes caused an average of 17,000 fatalities per year in the 20th century and represent the natural hazard that has caused the largest economic losses, including \$100 billion due to the 1995 Hyogo-ken Nambu, Japan earthquake ( $M = 6.9$ ) (Scawthorn, 2003). The adverse social and economic impact of earthquakes has led to the creation of earthquake hazard reduction programs to mitigate earthquake risk. A main objective of earthquake hazard reduction programs is to identify and characterize earthquakes that have occurred in the past in a given region and based on this information, to provide tools to estimate the impact that future earthquakes may have in order to reduce earthquake risk. The characterization of earthquakes in seismically active regions is relatively straight forward because observed records exist to physically constrain and validate the estimation of future earthquakes. In low-seismicity regions, the database of real earthquakes records is scarce, particularly for earthquakes of engineering interest, and ground motion predictions must be based on numerical simulations of earthquake processes.

The earthquake process involves contributions of source, path, and site effects. Figure 1.1 illustrates the propagation of seismic waves from the earthquake source to the recording site at the surface of the earth. Seismologists often perform empirical studies and numerical simulations of the source and path effects incorporating their variability and provide ground motions at the bedrock level beneath the site to be used in engineering applications. Engineers evaluate site effects for specific applications and incorporate these effects with the source and path effects to estimate surface ground

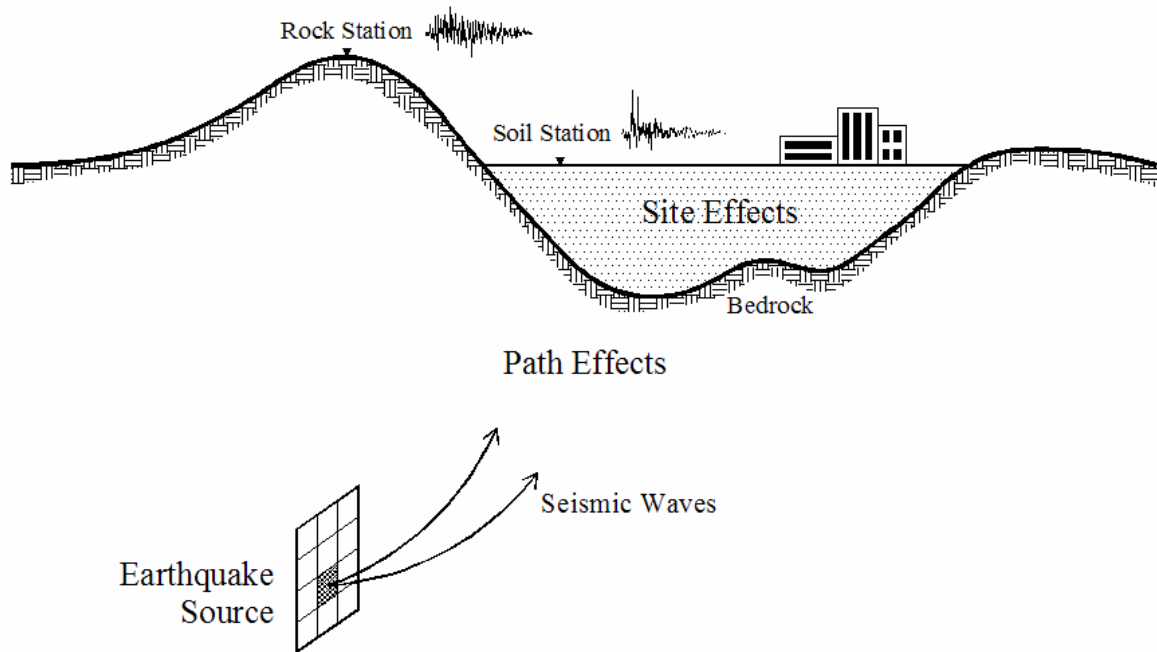


**Figure 1.1.** Source, path, and site effects in the earthquake process generation and seismic wave propagation

motions. Site effects are usually evaluated using the best estimates of the soil parameters and therefore the characterization of the variability in the earthquake process is lost. As indicated by several researchers (e.g., Bazzurro and Cornell, 2004b; Goulet et al., 2007), the coupling of source and path effects with site effects to estimate surface ground motions is not a trivial task, and an incorrect procedure may lead to an overestimation of the surface ground motion amplitude. A better approach would be to consider the three earthquake processes simultaneously when estimating surface ground motions.

The Central and Eastern United States (CEUS) is a stable continental region where no large earthquake records exist but the potential for occurrence of such an event is high. The 1811-1812 sequence of earthquakes in New Madrid, MO ( $M = 7.0$  to  $8.1$ ) and the 1886 earthquake in Charleston, SC ( $M = 7.3$ ) are examples of large, damaging earthquakes that have occurred in the CEUS and illustrate the seismic potential in the region. However the annual rate of occurrence of moderate and large earthquakes in the

CEUS is relatively low. The lack of real recordings leads to large uncertainties in the causes and characteristics of earthquakes in the CEUS (EPRI, 1993; Toro and McGuire, 1987), and makes the estimation of strong ground motions for a specified magnitude, distance, and site conditions in the region a challenging problem (Silva and Costantino, 2002).

The Mississippi Embayment is a wedge-shaped syncline structure that extends from southern Illinois to the Gulf of Mexico and is centered along the Mississippi River. The Upper Mississippi Embayment consists of soft sediments with thickness varying from a few meters to a maximum of about 1200 meters south of Memphis, TN. Many urban centers are located within the Embayment, and it is the most seismically active region of the CEUS (Schweig and Van-Arsdale, 1996). The New Madrid Seismic Zone (NMSZ), epicenter of the 1811-1812 sequence of earthquakes in New Madrid, MO, is located beneath the Upper Mississippi Embayment.

### **1.1. Objective of this Study**

The objective of this study is to develop earthquake ground motions for soil sites in the Upper Mississippi Embayment. The ground motions are intended to better characterize the seismic hazard in the region by representing the amplitude and variability that might be observed in real earthquakes and to provide resources to evaluate the seismic risk in the Embayment. The earthquake ground motions have been generated using a numerical wave propagation formulation. Source, path, and site effects have been considered simultaneously to properly account for the coupling between them, and the variability in the entire earthquake process has been incorporated. The effects of epistemic and aleatory uncertainties in the earthquake processes, the effects of non-linear soil behavior, and the effects of the geometry of the Embayment have been included. Previous studies have developed soil ground motions for applications in the Embayment (e.g., Atkinson and Beresnev, 2002; Toro and Silva, 2001; Wen and Wu, 2001).

However, none of them has included the variability in the entire earthquake process in a manner as extensive and rigorous as in this study. Accurately modeling the variability is important in probabilistic seismic hazard analysis as well in deterministic seismic hazard analysis involving the median-ground motion plus a multiple of the standard deviation.

The results of this study have been incorporated into MAEviz ([http://mae.ce.uiuc.edu/software\\_and\\_tools/maeviz.html](http://mae.ce.uiuc.edu/software_and_tools/maeviz.html)) to estimate surface ground motions in the Upper Mississippi Embayment. MAEviz is a seismic risk assessment software developed by the Mid-America Earthquake (MAE) Center and the National Center for Supercomputing Applications (NCSA).

## **1.2. Organization of this Study**

This study is divided into four main chapters that describe the generation and evaluation of earthquake ground motions in the Upper Mississippi Embayment.

Chapter 2 provides a summary of the geographical location, geology, seismicity, and geometry of the Upper Mississippi Embayment.

Chapter 3 describes the development of attenuation relationships for soil sites in the Upper Mississippi Embayment. Typical geological units of the region, Embayment depth, and non-linear soil behavior have been considered. The effects of epistemic and aleatory variability in the entire earthquake process have been incorporated. These soil attenuation relationships provide a direct approach for developing hazard-consistent soil ground motions in the region.

Chapter 4 documents the regional and site-specific seismic hazard analyses performed in the Upper Mississippi Embayment using the soil attenuation relationships developed in Chapter 3. It also describes the development of hazard-consistent time histories for selected cities within the Embayment. The seismic hazard analyses incorporate the geological conditions and uncertainties in the earthquake process characterized in the attenuation relationships.

Chapter 5 evaluates the two-dimensional effects of the geometry of the Upper Mississippi Embayment on earthquake ground motions in the region. The seismic response of the Embayment was computed using 1-D and 2-D models. The effects of non-linear soil behavior were incorporated in the analyses.

Chapter 6 presents a summary and main conclusions of the study and recommendations for future work.

## CHAPTER 2

### UPPER MISSISSIPPI EMBAYMENT

The Mississippi Embayment is a wedge-shaped syncline structure that extends from southern Illinois to the Gulf of Mexico and is centered along the Mississippi River as shown in Figure 2.1. The New Madrid Seismic Zone (NMSZ), epicenter of the 1811-1812 sequence of earthquakes ( $M = 7.0$  to  $8.1$ ) in New Madrid, MO, is located beneath the Upper Mississippi Embayment. Figure 2.2 shows the regional seismicity from 1974 to 2007 (CERI, 2007) along with the fictitious faults used by the U.S. Geological Survey to characterize the NMSZ in the development of the 2002 Seismic Hazard Maps (Frankel et al., 2002). Figure 2.3 shows the extent of the Upper Mississippi Embayment used in this study along with the geographical location of the NMSZ. Figure 2.4 illustrates alternative seismic sources used by Toro and Silva (2001) to characterize the NMSZ including the SE Flank of the Reelfoot rift, the Blytheville Arch, the Reelfoot fault, the East Prairie fault, and the Commerce-Benton Hills fault. This characterization is consistent with the spatial distribution of the seismicity shown in Figure 2.2. The seismic activity rate in the Upper Mississippi Embayment is low compared to regions located at the margins of tectonic plates. However, it is the most seismically active region of the Central and Eastern United States (CEUS) (Schweig and Van-Arsdale, 1996).

The Upper Mississippi Embayment consists of soft sediments with thickness varying from a few meters to a maximum of about 1200 meters south of Memphis, TN as illustrated in Figure 2.5. The sediments of the Mississippi Embayment consist of layers of clay, silt, sand, and gravel with variable amounts of pyrite, lignite, and mica. The age of the sediments ranges from the most recent Holocene period (approximately 11,000 years ago) to the Cretaceous period (approximately 100 million years ago). Table 2.1

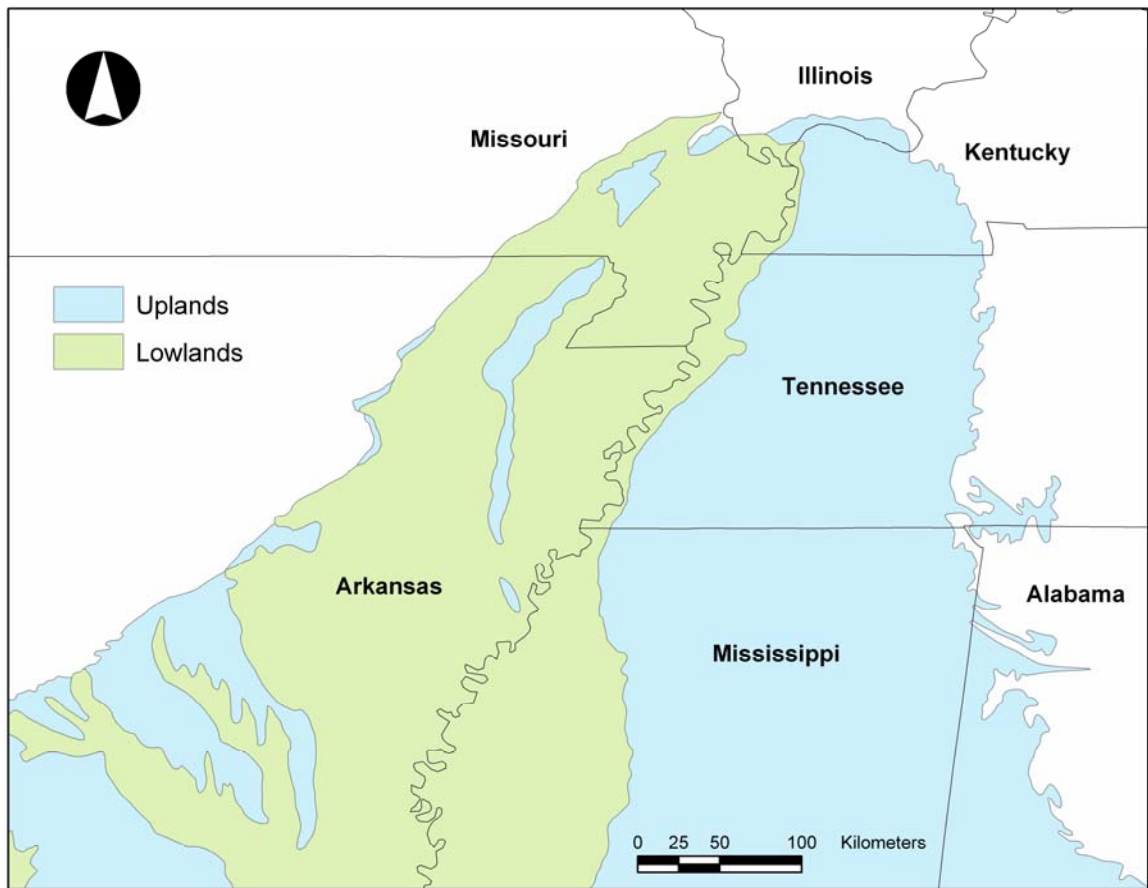


**Figure 2.1.** Extent of the Upper Mississippi Embayment and near surface geologic deposits

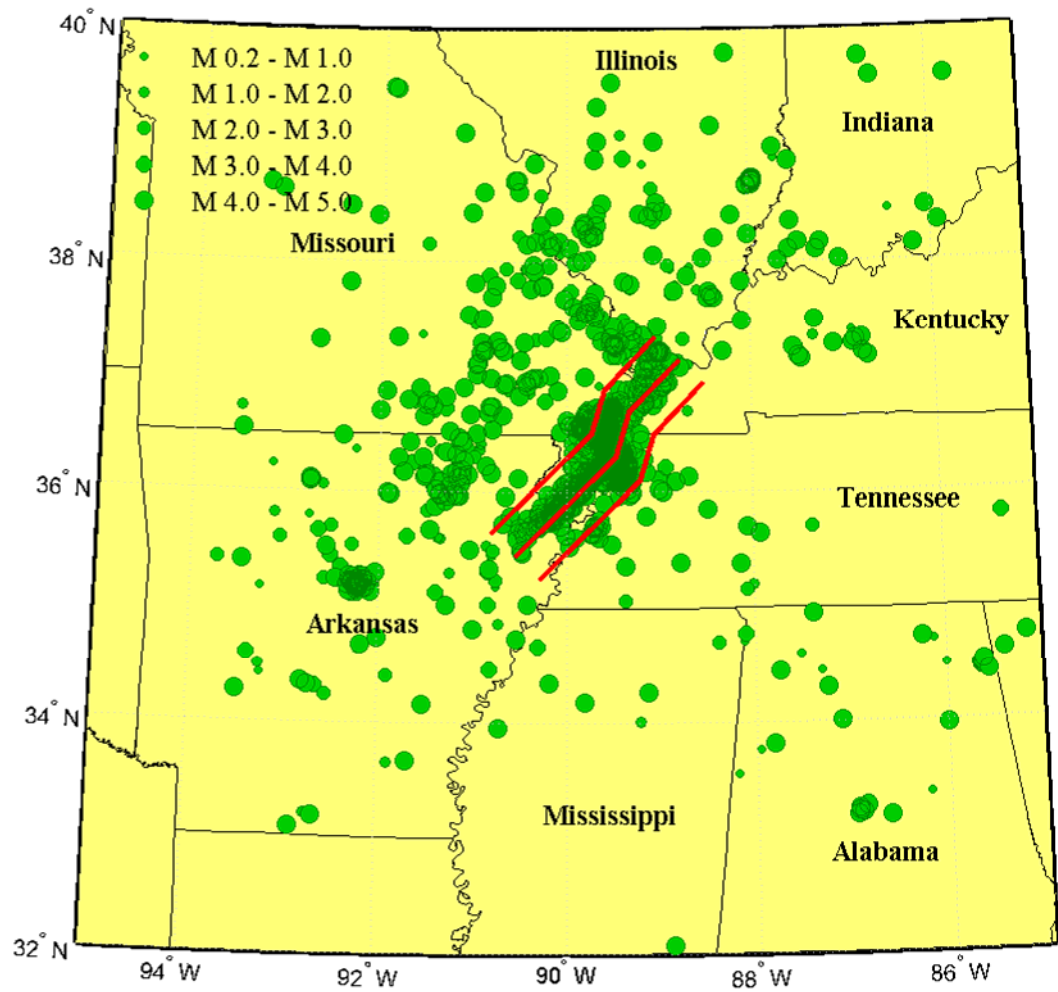


**Figure 2.2.** Regional seismicity from 1974 to 2007 (CERI, 2007) and fictitious faults used to the characterize the New Madrid Seismic Zone (Frankel et al., 2002)

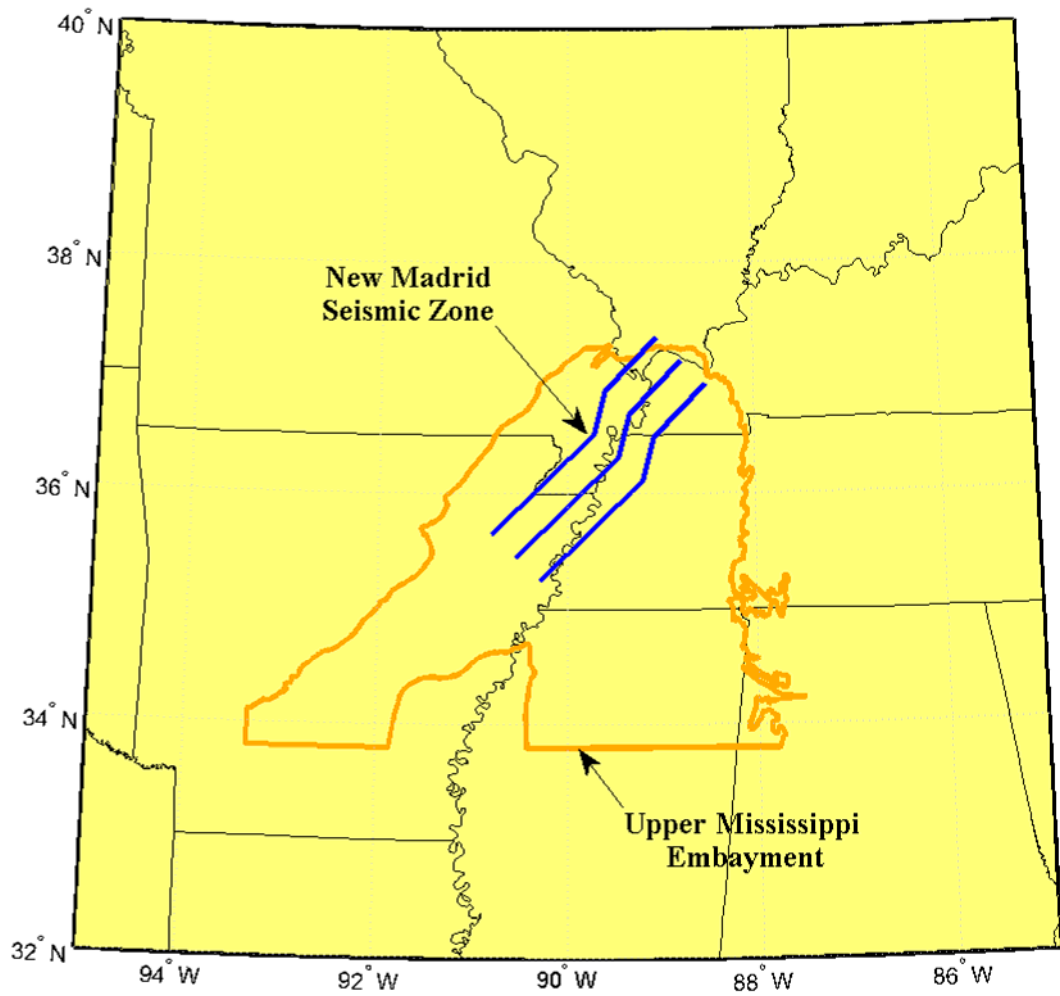


**Figure 2.3.** Extent of the Upper Mississippi Embayment along with the geographical location of the New Madrid Seismic Zone

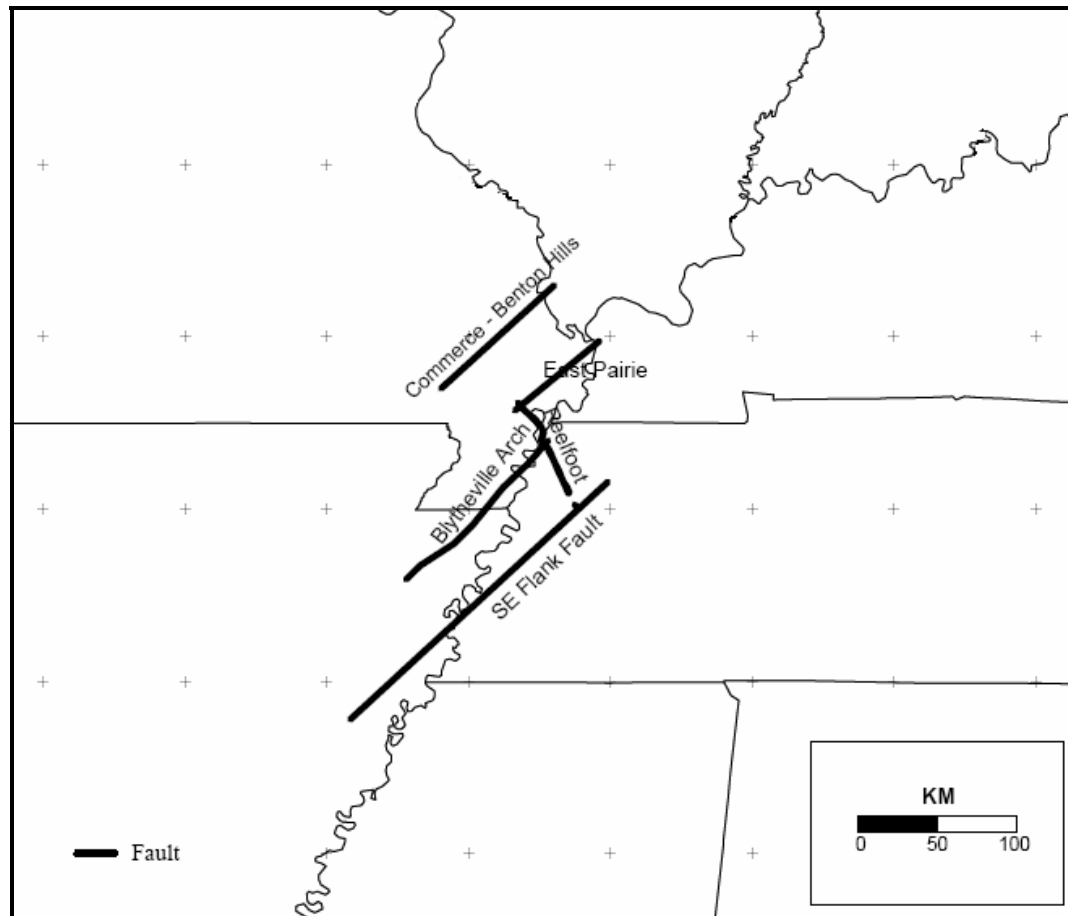


**Figure 2.4.** Alternative seismic sources used by Toro and Silva (2001) to characterize the NMSZ

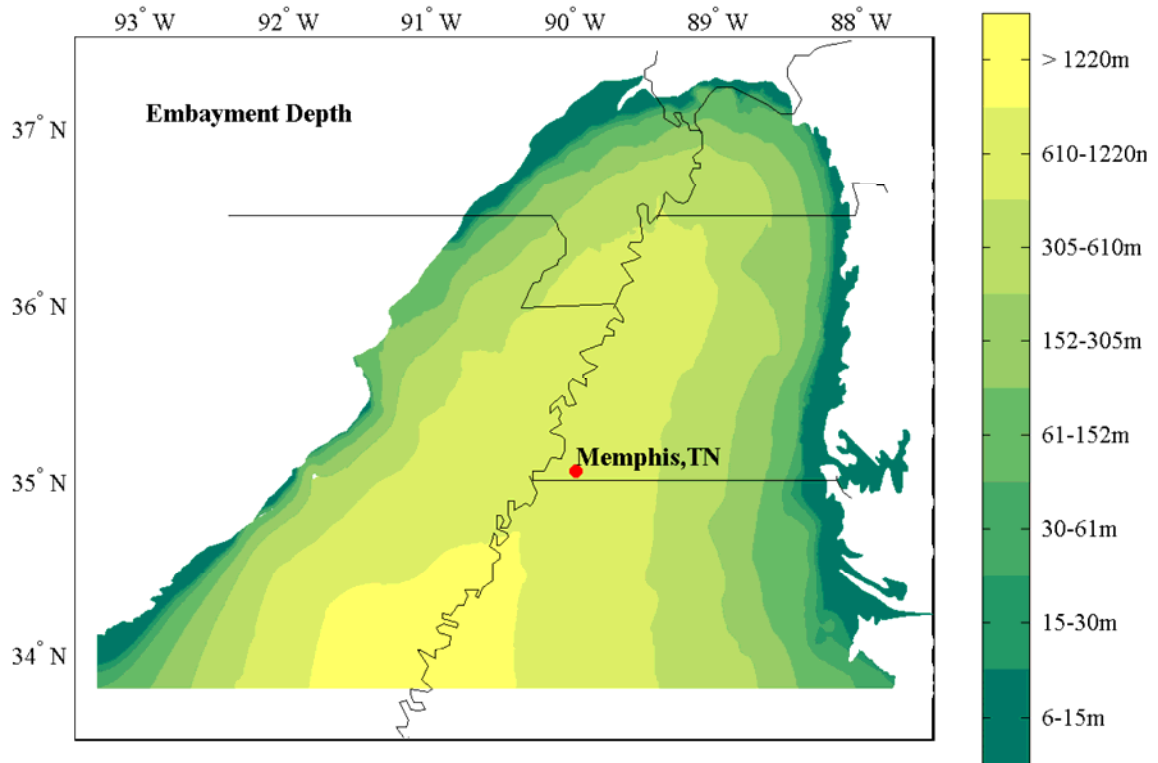


**Figure 2.5.** Sediment thickness contours of the Upper Mississippi Embayment

shows the stratigraphic column of the sediments in the Mississippi Embayment near Memphis, TN, and Figure 2.6 shows an East-West cross-sectional view of the Embayment passing through Memphis, TN. It is important to note that the vertical scale in Figure 2.6 has been greatly exaggerated. The surface deposits of the Upper Mississippi Embayment can be classified in two different categories: the Lowlands profile representing Holocene deposits typically found on the alluvial plains in the Mississippi River flood plain, and the Uplands profile consisting of Pleistocene deposits located on terraces overlooking the Mississippi River. Figure 2.1 shows the extent of these deposits within the Upper Mississippi Embayment.

**Table 2.1.** Stratigraphic column of the sediments of Mississippi Embayment near Memphis, TN (Brahana et al., 1987; Romero, 2001; Van Arsdale and TenBrink, 2000)

Period	Era	Series	Group	Stratigraphic Unit	Thickness [m]	Description	
Cenozoic	Quaternary	Holocene		Alluvium	0 - 57	Sand, gravel, silt, and clay within Mississippi alluvial plain and alluvial plains of streams	
		Pleistocene		Loess	0 - 21	Silt, silty clay, and minor sand; found in upland areas, thickest on bluffs and thins eastward	
		Pliocene/ Pleistocene		Lafayette Formation (Upland Gravel, fluvial deposits)	0 - 33	Sand, gravel, minor clay and ferruginous sandstone, underlies loess in upland areas	
	Tertiary	Oligocene		Jackson Formation	0 - 121	Clay, silt, sand, and lignite	
		Eocene	Claiborne Group	Cockfield Formation		Light-gray to light-brown silt and clay interbedded with medium- to fine-grained sand, lignite common	
				Cook Mountain Formation		Light-gray to light-buff clay and silt; contains variable amounts of sand and lignite	
				Memphis Sand ("500 ft-sand")	164 - 292	Fine- to very coarse-grained, light gray-white, quartzose sand, contains pyrite, lignite, and rock fragments; principal aquifer within Memphis	
		Paleocene	Wilcox Group	Flour Island Formation	62 - 102	Medium- to light-gray silty clay and clayey silt containing thin beds of fine- to very fine grained sand; commonly contains lignite, pyrite, and mica	
				Fort Pillow Sand ("1400-ft sand")	38 - 93	Fine- to very coarse-grained, quartzose sand; commonly contains pyrite, lignite, and mica; aquifer for regions west of Mississippi River	
				Old Breastworks Formation	55 - 107	Clay, silt, sand, and lignite	
			Midway Group	Porters Creek Clay	76 - 98	Steel-gray to dark-gray, hard, micaceous clay; disseminated organic material common; locally mottled yellow-buff, locally fossiliferous; becomes calcareous and very glauconitic near the base; confining unit for Fort Pillow Sand & McNairy Sand	
				Clayton Formation	12 - 37	Light-green-gray, glauconitic, fossiliferous, clay interbedded with green-white fossiliferous marl	
	Mesozoic	Upper Cretaceous		Owl Creek Formation		12 - 27	Samples from the Owl Creek Formation missing, but geophysical logs indicate it is present
				McNairy Sand		110 - 174	Fine- to coarse-grained sand, commonly containing pyrite, mica, and wood fragments, and traces of glauconite interbedded with steel-gray, soft, micaceous silty clay
Demopolis Formation				82 - 119	Massively-bedded, fossiliferous, argillaceous, gray marls		
Coffee Formation				0 - 37	Well-sorted, loose white sands interbedded with laminated to thin-bedded, brownish-gray carbonaceous clays with clean quartz silt partings		
Paleozoic / Upper Cambrian			Knox Dolomite of Ordovician age	--	White to dark-gray, fine- to coarse-crystalline dolomite; locally recrystallized; trace vuggy porosity; pyrite common; trace quartz crystals		

The interface between the Paleozoic rock and the sediments of the Embayment dip gently toward the axis at a rate of 1.9 to 6.6 m/km (Brahana et al., 1987). Figure 2.7 shows an East-West cross-section of the Embayment similar to the view shown in Figure 2.6, but using a vertical-to-horizontal scale ratio of 10:1. As observed in Figure 2.7, in the context of seismic wave propagation, the Upper Mississippi Embayment can be considered as a 1-D structure, and consequently the earthquake ground motions developed in Chapters 3 and 4 will be generated using a 1-D wave propagation formulation. The validity of this assumption will be evaluated in Chapter 5, and site conditions where this assumption is not valid will be identified.

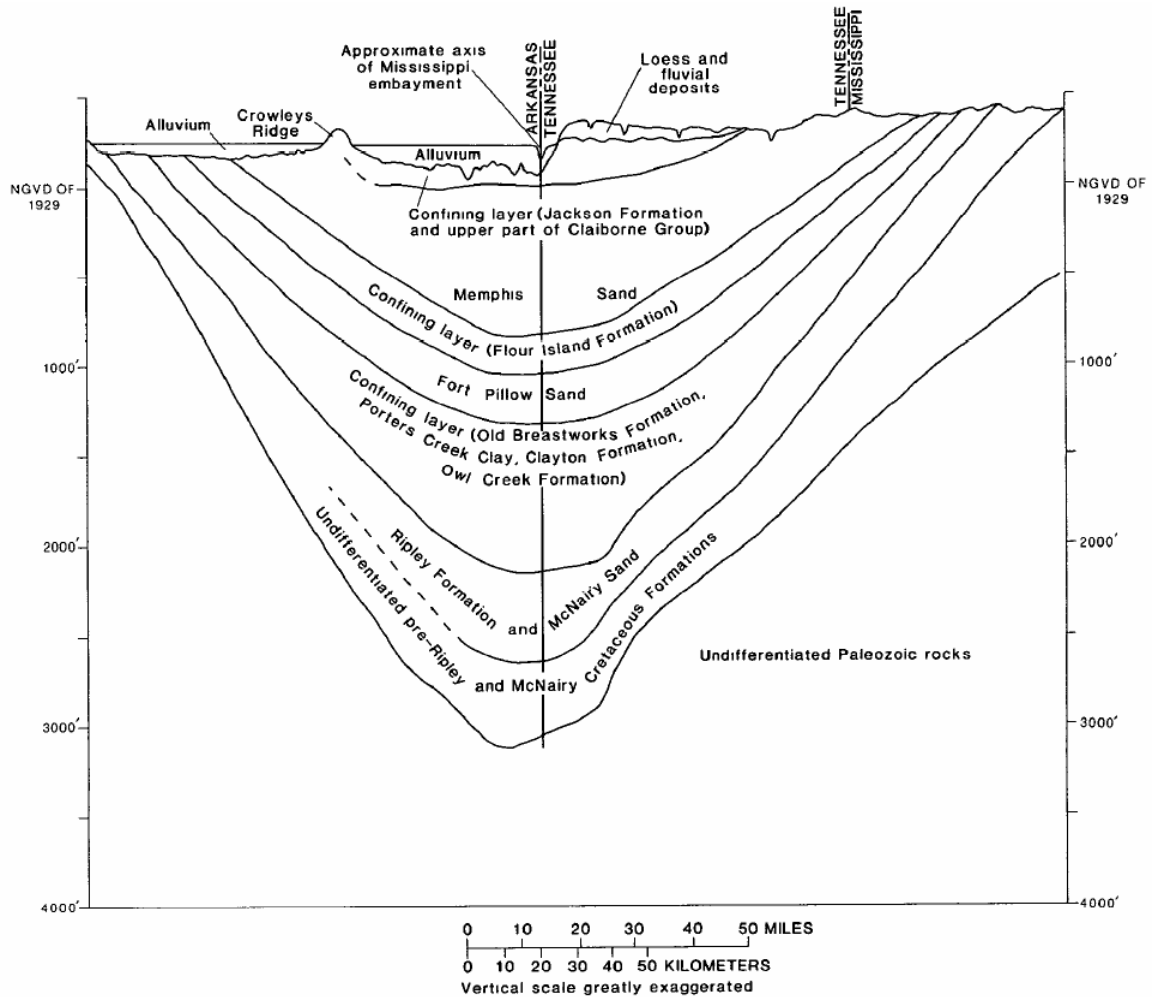


**Figure 2.6.** East-West cross-sectional view of the Embayment near Memphis, TN (Brahana et al., 1987)

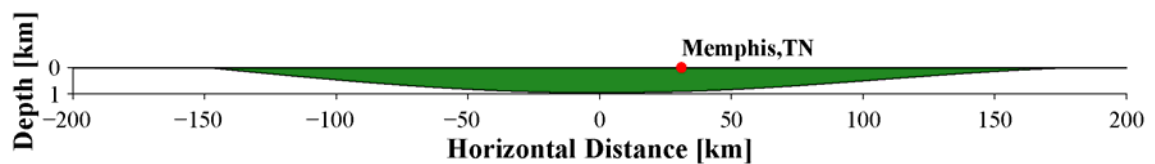


**Figure 2.7.** East-West cross-sectional view of the Embayment near Memphis, TN (vertical-to-horizontal scale ratio = 10:1)

# **CHAPTER 3**

## **SOIL ATTENUATION RELATIONSHIPS IN THE UPPER MISSISSIPPI EMBAYMENT**

Large damaging earthquakes have occurred in the Central and Eastern United States (CEUS). The 1811-1812 sequence of earthquakes in New Madrid, MO and the 1886 earthquake in Charleston, SC (Scawthorn, 2003) illustrate the seismic potential in the region. However, the annual rate of occurrence of moderate and large earthquakes in the CEUS is relatively low, and empirical earthquake data in the region is scarce. The lack of real recordings leads to large uncertainties in the causes and characteristics of earthquakes in the CEUS (EPRI, 1993; Toro and McGuire, 1987), and makes the estimation of strong ground motions for a specified magnitude, distance, and site conditions in the region a significant issue (Silva and Costantino, 2002).

Typically, ground motions are developed for rock conditions using attenuation relationships, which provide an equation to estimate median response and its associated uncertainty for a given combination of magnitude and source-to-site distance. To obtain site-specific estimates of ground motion, the rock motions are modified by the local soil profile using either an equivalent linear or a non-linear site response analysis, or by using soil amplification functions. The characterization of variability in dynamic soil properties and in the wave propagation model formulation is often lost in this type of approach. To calculate the variability in soil ground motions, the variability of the site response should be divided according to the rock motion level: variability for low and moderate levels of shaking, and variability of non-linear response for high levels of shaking (EPRI, 1993; Toro et al., 1997). This division is necessary since the effect of the non-linear soil response is to reduce the variability in soil ground motions (Bazzurro and

Cornell, 2004a; Campbell and Bozorgnia, 2006; EPRI, 1993; Toro et al., 1997). This negative correlation between rock motion level and site response must be taken into account when coupling the variability of both processes; otherwise the variability of soil ground motions would be overestimated (Bazzurro and Cornell, 2004b; Silva and Costantino, 2002; Silva et al., 2000).

The coupling process is not easy to perform in practice. Recent studies have proposed probabilistic procedures to incorporate the variability in site response into existing rock attenuation equations to develop site-specific ground motions (Bazzurro and Cornell, 2004b; Cramer, 2003; Goulet et al., 2007; Stewart et al., 2006). Although these more refined procedures take into account the variability in the entire earthquake process, the most accurate approach to develop site-specific ground motions is by using site-specific soil attenuation relationships, assuming that appropriate epistemic and aleatory uncertainties are incorporated in the development of the attenuation relationship (Bazzurro and Cornell, 2004b; Field et al., 2000; Goulet and Stewart, 2007; Goulet et al., 2007; Silva and Costantino, 2002). Soil attenuation relationships already account for correlations in the processes of the earthquake generation, and therefore avoid the process of coupling the variability in rock motions and in site response. This approach facilitates the development of site-specific ground motions either by probabilistic or deterministic analysis since the process requires only the selection of the dependent variables in the attenuation equation.

Many researchers have developed rock attenuation relationships for the CEUS conditions (Atkinson and Boore, 1995, 2006; Campbell, 2003b; EPRI, 1993; Frankel et al., 1996; Hwang and Huo, 1997; Silva et al., 2002, 2003; Somerville and Saikia, 2001; Toro et al., 1997; Toro and Silva, 2001) to characterize strong ground motions in this area. Some of them (EPRI, 1993; Hwang and Huo, 1997; Toro and Silva, 2001) have also provided soil amplification functions to modify the rock motions and obtain ground motions at the soil surface. However, soil attenuation relationships that take into account

the source, path, and site effects simultaneously have not been developed for the region. Hence, to better accommodate the variability of the earthquake process in site-specific ground motions, soil attenuation relationships have been developed for the Upper Mississippi Embayment that include the effects of epistemic and aleatory uncertainties in earthquake source, path, and site processes, and the effects of non-linear soil behavior. Epistemic uncertainties were included by using alternative models for each aspect of the earthquake process and aleatory uncertainties were included by considering random variations in parameter values. Using a stochastic point-source model, combinations of model parameters were considered using a Monte Carlo approach that yielded median attenuation relationships and their respective variability.

### **3.1. Ground Motion Uncertainties**

In the context of ground motion models, the total uncertainty associated with a ground motion prediction is usually subdivided into modeling and parametric uncertainties. The modeling uncertainty represents the difference between the ground motions generated by the actual earthquake process and the ground motions predicted by a given model. It is a measure on how well the model works when its parameters are known. Modeling uncertainty is calculated by comparing ground motion predictions with observed earthquake data, and therefore it captures all the factors that affect actual ground motions but are not included in the model. Parametric uncertainty represents the uncertainty in the values of model parameters for future earthquakes. It is estimated by comparing ground motion predictions generated by probabilistic varying model parameters with the mean predicted ground motion. Parametric uncertainty is a measure of the sensitivity of the model to a range of values for model parameters (Abrahamson et al., 1990; Silva et al., 1997; Toro et al., 1997; Toro and McGuire, 1987).

In seismic hazard analyses, the total ground motion uncertainty is subdivided into epistemic and aleatory uncertainties. Epistemic uncertainty is related to the incomplete

knowledge and data about the physics of the earthquake process. In principle it can be reduced as additional information becomes available. Aleatory uncertainty is the inherent component of variability for a given model or parameter. It cannot be reduced by collection of additional information. Both epistemic and aleatory uncertainties have components of modeling and parametric uncertainties. Uncertainty resulting from model assumptions and simplifications due to limited data is epistemic modeling uncertainty. It can be reduced by adjusting the model as more observed earthquake data is available. Observed scatter due to physical processes not included in the model is aleatory modeling uncertainty, since it cannot be reduced for a given model form. Uncertainty resulting from incomplete data to characterize median parameter values and their probability distributions is epistemic parametric uncertainty. It can be reduced by collecting additional data to better constrain model parameters. The event-to-event variation in model parameters is aleatory parametric uncertainty and cannot be reduced by collecting additional information (Silva et al., 1997; Toro et al., 1997; Toro and McGuire, 1987). Table 3.1 summarizes the components of the total uncertainty in the context of ground motion estimation.

### **3.2. Stochastic Method**

The preferred approach to develop attenuation relationships is the direct use of empirical strong ground motion recordings. However, the ground motion database in the CEUS is sparse, and the only available approach to develop appropriate attenuation relationships for this region is numerical simulations (EPRI, 1993). Ground motions can be modeled using different wave propagation methods (e.g. stochastic modeling techniques, ray theory, finite element method, finite difference method, discrete-wave number method, indirect-boundary element method, hybrid methods). The stochastic method has been widely used to predict ground motions for regions where records of damaging earthquakes are not available (Boore, 2003a). Many researchers have

**Table 3.1.** Uncertainties in ground motion estimation (modified from Silva et al. (1997) and Toro et al. (1997))

		Seismic Hazard Analysis	
		Epistemic	Aleatory
<b>Ground-Motion Predictions</b>	<b>Modeling</b>	Uncertainty related to model assumptions and simplifications	Uncertainty related to differences between model and actual earthquake process
	<b>Parametric</b>	Uncertainty related to the lack of data to properly characterize model parameters	Uncertainty related to intrinsic variability of model parameter values

implemented this method for ground motion prediction in the CEUS (e.g. Atkinson and Beresnev, 2002; Atkinson and Boore, 1995, 2006; Campbell, 2003b; EPRI, 1993; Frankel et al., 1996; Harik et al., 1997; Hwang and Huo, 1997; Silva et al., 2002, 2003; Toro et al., 1997; Toro and Silva, 2001; Wen and Wu, 2001) as an evidence of the acceptance of this ground motion model in the seismological community. Silva et al. (1997) performed an extensive quantitative evaluation of the prediction ability of the stochastic method by estimating model bias and variability in the prediction of 16 earthquakes recorded at 503 sites over distances ranged from 1 to 177 km (460 km for the 1988 **M** 5.8 Saguenay, Canada earthquake). Silva et al. (1997) found that when using correct assumptions about the earthquake process the stochastic method can accurately predict observed variations in ground motions and provide reliable estimates of design strong ground motions.

The stochastic method is based on the work done by Hanks and McGuire (1981), who stated that far-field, high-frequency, strong ground motions on an elastic half-space are finite duration, band-limited, Gaussian white noise. They assumed that acceleration amplitudes within the time interval  $0 \leq t - R/\beta \leq T_d$ , where  $R$  is distance,  $\beta$  is shear wave

velocity, and  $T_d$  is the faulting duration, are stationary (their statistics do not change with time) and can be modeled by a Gaussian distribution in the frequency band  $f_0 \leq f \leq f_{\max}$ , where  $f_0$  is the spectral corner frequency, a definition of which is given below; and  $f_{\max}$  is the highest frequency passed by the attenuation of the Earth or the instrumental recording system. Based on these assumptions, Hanks and McGuire (1981) derived a simple expression to estimate peak and root-mean-square (rms) accelerations that were in good agreement with data from 16 earthquakes. Boore (1983) extended the method of Hanks and McGuire (1981) to the simulation of time series and to the estimation of peak velocity, Wood-Anderson instrument response, and response spectra.

The stochastic method states that the physics of the earthquake process and wave propagation phenomenon can be put in the form of simple equations that, when combined, result in the spectrum of the ground motion at a site. Following the notation and expressions by Boore (2003a), the total Fourier spectrum ( $Y$ ) at a given site is calculated as the contribution of earthquake source ( $E$ ), path ( $P$ ) and site ( $G$ ) processes, and instrument or type of motion ( $I$ ), such that:

$$Y(M_0, R, f) = E(M_0, f) \cdot P(R, f) \cdot G(f) \cdot I(f) \quad 3.1$$

where  $M_0$  is the seismic moment,  $R$  is a measure of distance from source to site, and  $f$  is the frequency.

### 3.2.1. The Source Effect

The source effects are related to the characteristics of earthquake energy release. The shape and amplitude of the source spectrum  $E(M_0, f)$  are specified by defining a displacement spectrum as a function of earthquake size. The source spectrum is given by the following equation:

$$E(M_0, f) = C \cdot M_0 \cdot S(M_0, f) \quad 3.2$$

where  $C$  is a constant and  $S$  is the displacement source spectrum. The constant  $C$  is given by:

$$C = \frac{\langle R_{\Theta\Phi} \rangle \cdot V \cdot F}{4\pi \cdot \rho_s \cdot \beta_s^3 \cdot R_0} \quad 3.3$$

where  $\langle R_{\Theta\Phi} \rangle$  is the radiation factor of the total shear-wave radiation,  $V$  represents the partition of total shear-wave energy into horizontal components,  $F$  is the effect of the free surface,  $\rho_s$  and  $\beta_s$  are the density and shear wave velocity in the vicinity of the source, and  $R_0$  is a reference distance. Usual values used for  $V$ ,  $F$ , and  $R_0$  are  $1/\sqrt{2}$ , 2, and 1 km respectively (Boore, 2003a; 2003b). Recommended values of  $\langle R_{\Theta\Phi} \rangle$  are provided by Boore and Boatwright (1984).

The seismic moment  $M_0$  relates to the moment magnitude  $\mathbf{M}$  by the following relation (Hanks and Kanamori, 1979):

$$\mathbf{M} = \frac{2}{3} \cdot \log(M_0) - 10.7 \quad 3.4$$

The most widely used and qualitatively validated displacement source spectrum is the  $\omega$ -square model (Aki, 1967), which is given by:

$$S(M_0, f) = \frac{1}{1 + \left( \frac{f}{f_0} \right)^2} \quad 3.5$$

where  $f_0$  is the corner frequency and is given by the following equation (Brune, 1970, 1971):

$$f_0 = 4.9 \times 10^6 \cdot \beta_s \cdot \left( \frac{\Delta\sigma}{M_0} \right)^{1/3} \quad 3.6$$

where  $f_0$  is in Hz,  $\beta_s$  is in km/sec,  $\Delta\sigma$  is the stress drop in bars, and  $M_0$  is in dyne-cm. The corner frequency is inversely proportional to the source duration, and is the transition point from a rapid increase in spectral amplitude to a nearly flat spectrum in the higher frequency band (Anderson, 2003). The corner frequency increases with shear-wave velocity and stress drop, parameters that are region dependent. The stress drop scales the source spectrum for frequencies above the corner frequency; therefore high-frequency

ground motion predictions are sensitive to this parameter (Silva et al., 1997). Since the corner frequency is also inversely proportional to the fault dimension, an inspection of Equation 3.6 shows that the stress drop replaces the fault dimension in the source description of the one-corner  $\omega$ -square model (Atkinson and Beresnev, 1997). The stress drop has a physical interpretation only if earthquakes truly follow the one-corner  $\omega$ -square model (Equation 3.6). In this case the stress drop values correspond to the stresses that induce the relative slip across the rupture surface; otherwise the stress drop is only a scaling or fitting parameter (Silva et al., 1997). Figure 3.1 compares the Fourier acceleration source spectrum,  $E$ , for different moment magnitudes and stress drops,  $\Delta\sigma$ . Figure 3.1 illustrates the high-frequency scaling by  $\Delta\sigma$ , and the relation between corner frequency, moment magnitude, and stress drop.

Although the one-corner  $\omega$ -square model is the most common source description, other models have also been implemented in applications of the stochastic method. The one-corner model is based on the principle of similarity (Aki, 1967), which states that the length and width of the rupture increase with magnitude. Joyner (1984) proposed a two-corner source model for large earthquakes where the width of the fault reaches its limit and only the length increases. In these cases, the principle of similarity no longer applies. The two-corner model is intended for earthquakes with magnitudes greater than a critical magnitude corresponding to the rupture of the entire width of the fault. For magnitudes smaller than the critical magnitude, the one-corner and two-corner source models are consistent. In the two-corner source model, the spectral corners,  $f_A$  and  $f_B$ , are proportional to the length and width of the rupture, respectively (Joyner, 1984). Figure 3.2 compares the Fourier acceleration source spectrum,  $E$ , predicted by the one-corner (Frankel et al., 1996) and the two-corner (Atkinson and Boore, 1995) source models. The low-frequency amplitudes for  $M$  4.5 are similar for both source models because the critical magnitude for the Atkinson and Boore (1995) model is  $M$  4.0. Examples of

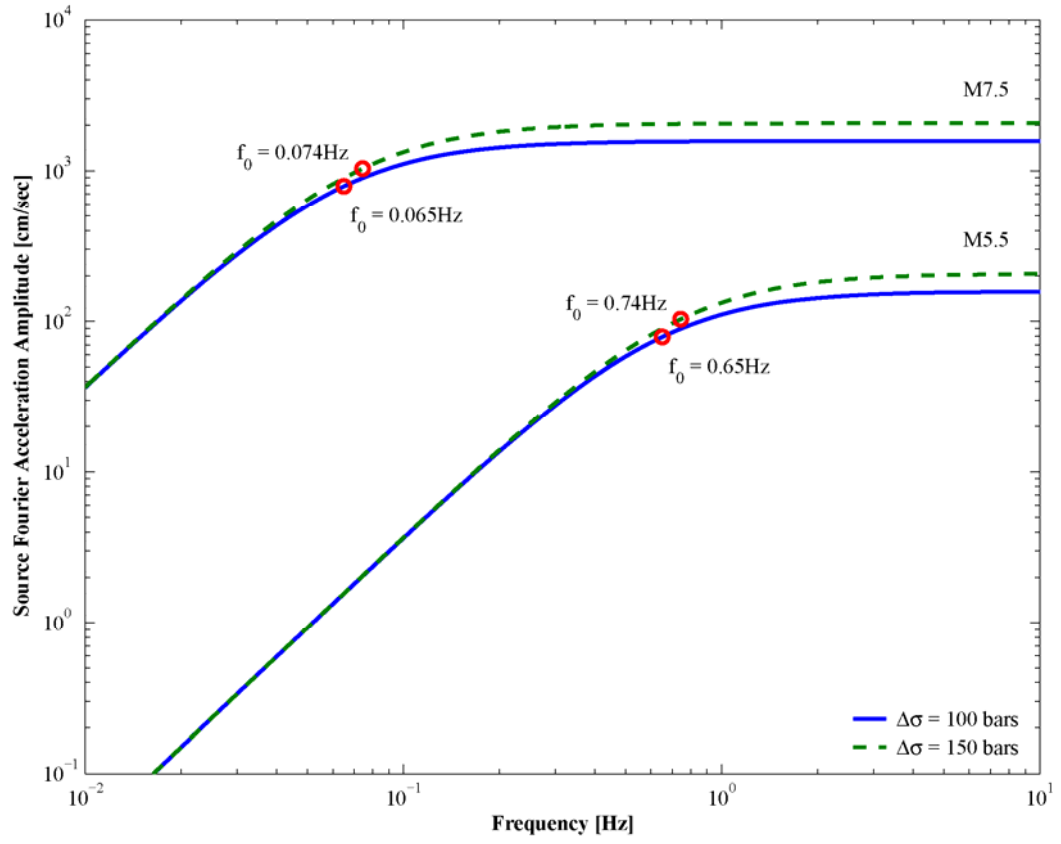


**Figure 3.1.** Source spectrum scaling for one-corner  $\omega$ -square model

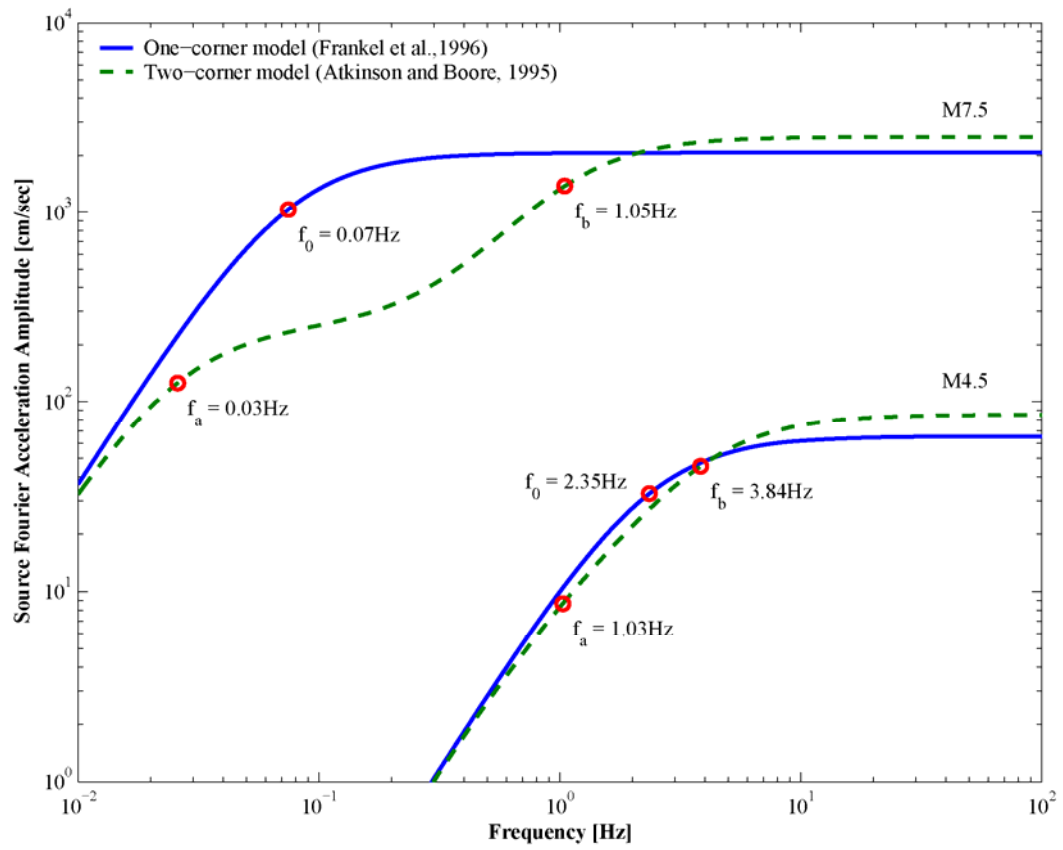


**Figure 3.2.** Comparison of one- and two-corner source models

applications of the two-corner source model can be found in Atkinson and Boore (1995), Atkinson and Silva (2000), and Haddon (1996).

### 3.2.2. The Path Effect

The path effect spectrum,  $P(R,f)$ , is used to model the effects on seismic waves due to the distance traveled from the earthquake source to the bedrock beneath the site. The path effect is given by the multiplication of a geometrical spreading function,  $Z$ , and a seismic attenuation function  $Q$ :

$$P(R,f) = Z(R) \cdot \exp\left(-\frac{\pi \cdot f \cdot R}{Q(f) \cdot c_Q}\right) \quad 3.7$$

where  $R$  is usually the closest distance to the rupture surface, and  $c_Q$  is the seismic velocity used in the determination of  $Q(f)$ . The geometrical spreading function,  $Z$ , models the geometric attenuation, which accounts for the decrease in seismic wave amplitude with traveled distance due to an increase in the wave front size (Santamarina et al., 2001). The seismic attenuation function (i.e. anelastic attenuation),  $Q$ , represents the effects of intrinsic material loss and scattering attenuation, a process that redistributes wave energy by reflection, refraction, and conversion at irregularities in the propagation medium (Lay and Wallace, 1995). The  $Q$  function corresponding to high frequency attenuation is usually expressed in the form (Nuttli, 1981):

$$Q(f) = Q_0 \cdot f^\eta \quad 3.8$$

where  $Q_0$  and  $\eta$  are parameters obtained from analysis of ground motion data.

### 3.2.3. The Site Effect

The site effect spectrum,  $G(f)$ , accounts for the modification of the seismic waves by the local site conditions. The function  $G$  is calculated by the multiplication of amplification,  $A(f)$ , and attenuation,  $D(f)$ , functions. The amplification function depends on the shear-wave velocity profile and on the dynamic properties of the soil column. It

can include geometrical and topographical effects. The attenuation function accounts for the path-independent loss of high-frequency in the ground motions and is implemented by a multiplicative filter. Two filters that are in common use are the  $f_{\max}$  filter and the  $\kappa$  filter:

$$D(f) = \left[ 1 + \left( \frac{f}{f_{\max}} \right)^8 \right]^{-1/2} \quad (\text{Boore, 1983}) \quad 3.9$$

$$D(f) = \exp(-\pi \cdot \kappa \cdot f) \quad (\text{Anderson and Hough, 1984}) \quad 3.10$$

The attenuation function  $D$  models the observed sharp decrease in ground motion amplitudes of frequencies higher than a region-dependent maximum frequency, which is characterized by the  $f_{\max}$  and  $\kappa$  factors in the Equations 3.9 and 3.10. The function  $D$  is responsible for the band-limited characteristic of the stochastic method. The frequency limits of the ground motion spectrum are given by the source corner frequency and the high frequency spectral attenuation (Silva et al., 1997). Figure 3.3 shows the Fourier acceleration source spectrum,  $E$ , for the Frankel et al. (1996) model multiplied by a  $f_{\max}$  filter (Equation 3.9) with  $f_{\max} = 50$  Hz. Figure 3.3 illustrates the band-limited characteristic of the ground motion predictions by the stochastic method.

### 3.2.4. Type of Ground Motion

The function  $I(f)$  controls the type of ground motion calculated by Equation 3.1 and is given by:

$$I(f) = (2\pi \cdot f \cdot i)^n \quad 3.11$$

where  $i = \sqrt{-1}$ , and  $n = 0, 1$ , or  $2$  for ground displacement, velocity, or acceleration, respectively.

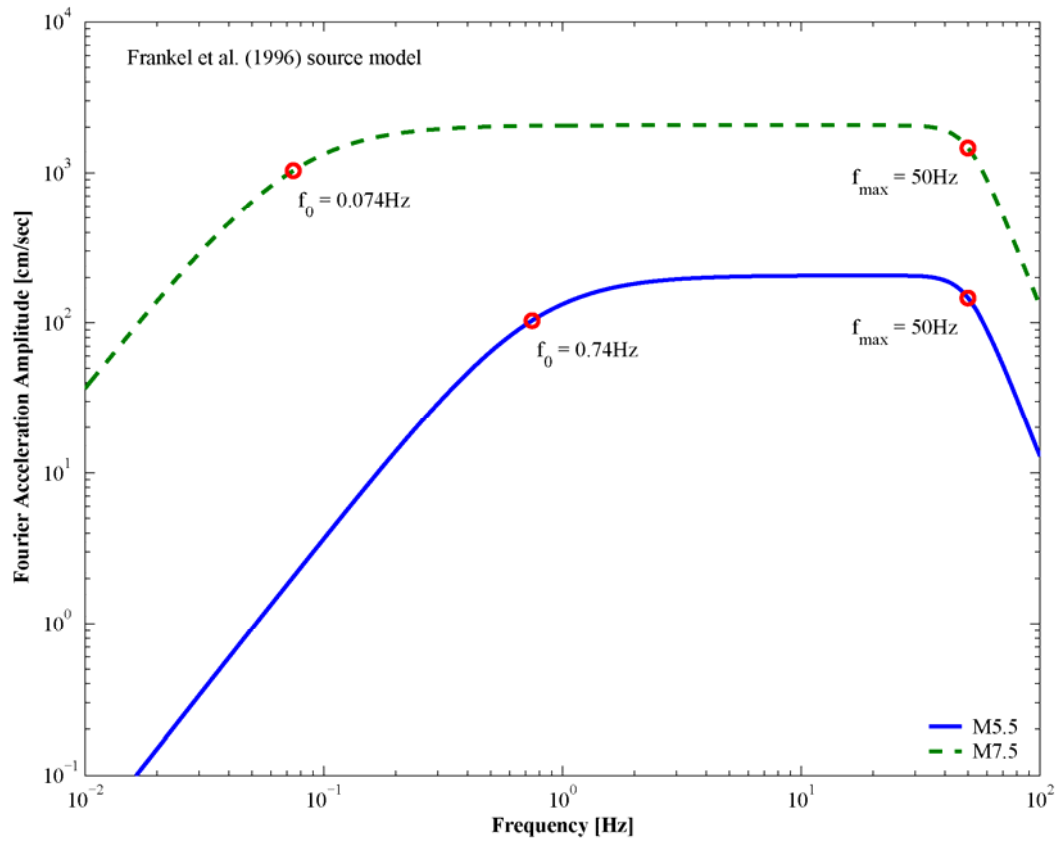


**Figure 3.3.** Band-limited spectra predicted by the stochastic method

### 3.2.5. Random Vibration Theory

Random vibration theory (RVT) provides an estimate of peak values (i.e. peak acceleration, peak velocity, peak displacement, response spectrum) by calculating the ratio of peak motion to root-mean-square (rms) motion. The rms motion is obtained by applying the Parseval's theorem to the ground motion spectrum,  $Y$  (see Equation 3.1).

Cartwright and Longuet-Higgins (1956) developed a method to estimate extremes, (i.e. points where the first derivative of the motion is zero) of ocean waves by using spectral characteristics of a continuous record of sea heights. Boore (1983) adapted this method to estimate extremes of transient earthquake records. The ratio of peak to rms motion is given by (Cartwright and Longuet-Higgins, 1956):

$$\frac{y_{\max}}{y_{\text{rms}}} = 2 \cdot \int_0^{\infty} \left\{ 1 - \left[ 1 - \xi \cdot \exp(-z^2) \right]^{N_e} \right\} \cdot dz \quad 3.12$$

where  $\xi$  is defined as the ratio of the number of zero crossings,  $N_z$ , to the number of extremes,  $N_e$ :

$$\xi = \frac{N_z}{N_e} \quad 3.13$$

For large  $N_z$ , a good approximation of Equation 3.12 is given by the following asymptotic expression (Cartwright and Longuet-Higgins, 1956):

$$\frac{y_{\max}}{y_{\text{rms}}} = \left[ 2 \cdot \ln(N_z) \right]^{1/2} + \frac{\gamma}{\left[ 2 \cdot \ln(N_z) \right]^{1/2}} \quad 3.14$$

where  $\gamma$  is the Euler's constant ( $\gamma = 0.5772$ ). Equation 3.14 is based on the assumption that the crossings of a relatively high threshold occur as a Poisson arrival process (Vanmarcke and Lai, 1980).

The number of zero crossings and extremes,  $N_z$  and  $N_e$ , are related to the frequencies or rate of occurrence of zero crossings,  $f_z$ , and extrema,  $f_e$ , and to duration,  $T$ , by the equation:

$$N_{z,e} = 2 \cdot f_{z,e} \cdot T \quad 3.15$$

For a stationary Gaussian process the occurrence rate of zero crossings and extremes are given by (Lutes and Sarkani, 1997):

$$f_z = \frac{1}{2\pi} \cdot \left( \frac{m_2}{m_0} \right)^{1/2} \quad 3.16$$

$$f_e = \frac{1}{2\pi} \cdot \left( \frac{m_4}{m_2} \right)^{1/2} \quad 3.17$$

and the moments of the power spectral density,  $m_k$ ,  $k = 0, 2, 4$ , are defined by:

$$m_k = 2 \cdot \int_0^\infty (2\pi \cdot f)^k \cdot |Y(f)|^2 df \quad 3.18$$

where  $Y$  is the ground motion spectrum calculated by Equation 3.1. The rms motion,  $y_{rms}$ , is calculated by:

$$y_{rms} = \left( \frac{m_0}{T} \right)^{1/2} \quad 3.19$$

The RVT equations presented above to calculate  $y_{max}$  and  $y_{rms}$  assume the signal is stationary Gaussian noise with uncorrelated adjacent peaks. This assumption is not strictly valid for real earthquake records, however it permits the theory to work very well in predicting ground motions as have been shown in various comparisons with recorded earthquakes (Atkinson and Silva, 2000; Boore, 1983; Boore and Atkinson, 1987; EPRI, 1993; Hanks and McGuire, 1981; Silva et al., 1997).

In spite of its simplicity (see Equation 3.1), the stochastic method is suitable for the characterization of ground motions for engineering applications because by using only a few parameters, it captures the general features of strong ground motions in terms of peak values and spectral content (Silva et al., 1997).

The stochastic method can be evaluated by using a point or a finite representation of the earthquake source. The point-source model has been validated using many earthquakes with a wide range of magnitudes, rupture distances, and site conditions (Silva et al., 1997). The objective of these comprehensive validation exercises is to estimate the model uncertainty and model bias of the point-source model, which are shown in the next section. The model uncertainty captures factors that affect ground motions but are not considered in the model (e.g. surface topography, finite and propagating seismic sources, heterogeneities in the propagation medium); and the model bias accounts for the inherent tendency of the model to over or underestimate mean ground motions. A stochastic point-source model was selected in this study to perform the ground motion simulations, which has been proven to accurately reflect average source-site geometries and average properties of ground motions (Boore, 1983; Hanks and McGuire, 1981; Silva et al., 1997), and along with its extensive validation, it represents a robust model for engineering characterization of ground motions (Silva et al., 1997).

According to Silva et al. (1997), there are three general applications of the stochastic method. It can be used to simulate ground motions for a particular source, path, and site scenario as implemented in Lawrence et al. (2006) to validate ground motion predictions in the Upper Mississippi Embayment. Due to the simplicity of the model, the stochastic method can also be used to assess parameter sensitivity as used in Silva (1992) and Roblee et al. (1996) to evaluate the sensitivity of ground motions to variations in source, path, and site parameters. A third application of the method is to simulate ground motions over a magnitudes, distances, and sites ranges, to develop regional and site specific attenuation relationships. In this study a combination of the second and third applications was implemented. The source, path, and site parameters were randomly varied using probability distributions and uncertainties observed in previous studies (EPRI, 1993; Silva et al., 1997; Silva et al., 2003). Then using a Monte

Carlo approach, ground motions were simulated for sets of source models and soil profiles, and ranges of magnitudes, epicentral distances, and embayment depths, to develop regional soil attenuation relationships for the Upper Mississippi Embayment that incorporate epistemic and aleatory uncertainties associated with the earthquake process.

A similar methodology has been used in the literature to incorporate epistemic and aleatory uncertainties in ground motions predictions in the CEUS (Atkinson and Boore, 2006; EPRI, 1993; Hwang and Huo, 1997; Silva et al., 2002, 2003; Toro et al., 1997; Toro and Silva, 2001). However, none of the previous studies have considered the incorporation of uncertainty in the entire earthquake process, including source, path, and site effects. Some of them (EPRI, 1993; Hwang and Huo, 1997; Toro and Silva, 2001) have provided soil amplification functions to modify the rock motion predictions and obtain ground motions estimates at the soil surface. EPRI (1993) and Toro and Silva (2001) have accounted for the deep soil profile in the Upper Mississippi Embayment. The soil amplification function of Hwang and Huo (1997) considers only generic soil profiles. However to obtain the variability in soil ground motion estimates using these predictions, the variability in rock estimates must be coupled with the variability in site amplification. As discussed previously this process must account for the correlation between both variables, otherwise the ground motion variability at the soil surface could be overestimated (Bazzurro and Cornell, 2004b; Silva and Costantino, 2002; Silva et al., 2000). The approach followed in this study predicts more accurate soil ground motions (Bazzurro and Cornell, 2004b; Silva and Costantino, 2002) and avoid the coupling process of the earthquake source and path variability with the variability in site effects.

The stochastic method was implemented using the computer program RASCALS, which stands for Response Spectra and Acceleration Scaling (Silva and Lee, 1987). To incorporate non-linear soil behavior in the simulations, RASCALS implements an equivalent linear approach based on random vibration theory. In this way the site amplification function  $A(f)$  is calculated using an algorithm of 1-D wave propagation

through a layered system developed by Silva (1976). Only SH-waves are considered in the formulation.

### **3.3. Validation of the Use of an Equivalent Linear Approach for Site Response**

#### **Analyses in the Upper Mississippi Embayment**

The equivalent linear approach is an approximation to the actual non-linear response of the soil to seismic loading. However it is easy to implement and provides reasonable results for many engineering problems (Kramer, 1996). The equivalent linear analysis does not need the definition of all the parameters required by complex non-linear models, such as the specification of the hysteresis loops. Furthermore the principle of superposition applies to the solution of an equivalent linear analysis allowing spectral analysis of wave fields and frequency domain solutions. Equivalent linear analyses for site response calculations with accurate profiles of soil properties provides a reliable approach to predict soil effects on strong ground motions. However it does not provide reasonable results when the analysis involves large soil deformations and liquefaction (EPRI, 1993), or when estimating the surface response of a deep, soft soil deposit (Hashash and Park, 2001; Kausel and Assimaki, 2002). In the last case the equivalent linear analysis causes an overdamping of the high-frequency content of the surface ground motions.

The stochastic method and the particular form of the equivalent linear analysis implemented in RASCALS have been extensively validated by Silva et al. (1997). Figure 3.4 shows the model bias and variability estimates resulting from this validation exercise with 16 earthquakes ( $M$  5.3 to 7.4) at 503 sites with rupture distances ranging from 1 to 460 km using a one-corner, point-source model. This broad range in magnitude and distance and number of earthquakes and sites result in the most comprehensively validated model currently available to simulate strong ground motions (Silva et al., 2003). While there are shortcomings associated with the model, they are represented by

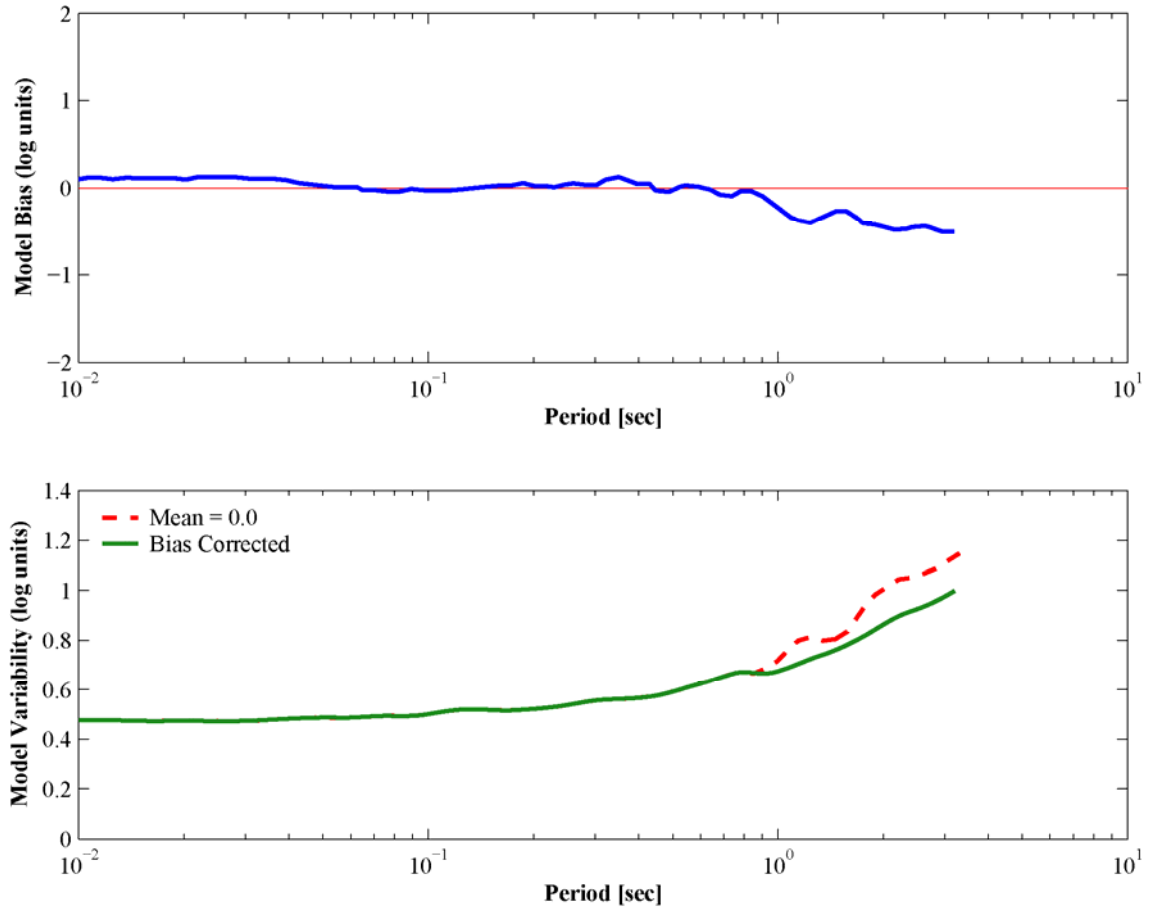


**Figure 3.4.** Modeling bias and variability estimates of the Stochastic Method using a one-corner, point-source model and the equivalent linear analysis for site response (from Silva et al. (1997))

the model variability shown in Figure 3.4, and this variability has been incorporated in this study as described later.

Cramer (2006b) evaluated different site response computer programs for applications in the Upper Mississippi Embayment. The evaluation included SHAKE91 (traditional equivalent linear analysis), TREMORKA (equivalent linear analysis with frequency-dependent dynamic soil properties), and DEEPSOIL (true non-linear analysis). As indicated by Kausel and Assimaki (2002) and Hashash and Park (2001), the use of the equivalent linear analysis for deep soil sites may yield unrealistic surface ground motions, particularly in the high-frequency range, if the entire soil column is allowed to undergo non-linear behavior. Therefore, Cramer (2006b) implemented three variations of the traditional equivalent linear analysis by limiting the non-linear soil behavior to the upper 80, 300, and 400 m of the profile. For low amplitudes of the input motion (i.e.  $PGA = 0.11g$ ), SHAKE91, TREMORKA, and DEEPSOIL resulted in similar surface ground motions amplitudes, independent of the maximum depth of non-linear behavior permitted in the traditional equivalent linear analysis. For high amplitudes of the input motion (i.e.  $PGA = 0.55g$ ), Cramer (2006b) concluded that by limiting the non-linear soil behavior to the upper 300 m, the traditional equivalent linear analysis yielded similar results to the other two formulations, except between 0.2 and 0.5 sec. where SHAKE91 underestimated the surface response compared to TREMORKA and DEEPSOIL. This conclusion is consistent with previous studies (Romero, 2001; Silva et al., 1997; Toro and Silva, 2001), that recommended to limit the non-linear behavior to the upper 150 m of the soil column when using the equivalent linear analysis in the Upper Mississippi Embayment.

To perform an additional evaluation of the differences between surface ground motions estimated by equivalent linear and true non-linear analyses, site amplification factors developed for the Upper Mississippi Embayment using these two approaches were compared. Knapp (2003) developed site amplification factors using the equivalent

linear analysis implemented in RASCALS with non-linear soil behavior constrained to the upper 150 m. Knapp (2003) divided the Embayment in seven depth bins and randomized soil parameters within each depth bin to characterize their variability, and thus, provided site factors corresponding to the median value, 84<sup>th</sup>, and 95<sup>th</sup> percentiles. Park and Hashash (2005) obtained similar site amplification factors but they used a true non-linear wave propagation formulation. Park and Hashash (2005) used two sets of dynamic soil properties to define upper and lower bounds to the site factors and considered a single shear wave velocity profile for each of six Embayment depths. The soil parameters were not randomized and only the median values were used in the analyses. The site factors were selected such that the response spectrum calculated by the procedure provided in FEMA (2001a) resulted in an upper-bound envelope to the simulations, as illustrated in Figure 3.5.

Figure 3.6 compare  $F_a$  site factors as a function of Embayment depth calculated by both studies for spectral accelerations at  $T = 0.2$  sec. of 0.25 g and 1.0 g. Only the short-period site factor  $F_a$  is compared because the largest difference between equivalent linear and true non-linear analyses is expected to occur in this period range. Figure 3.6

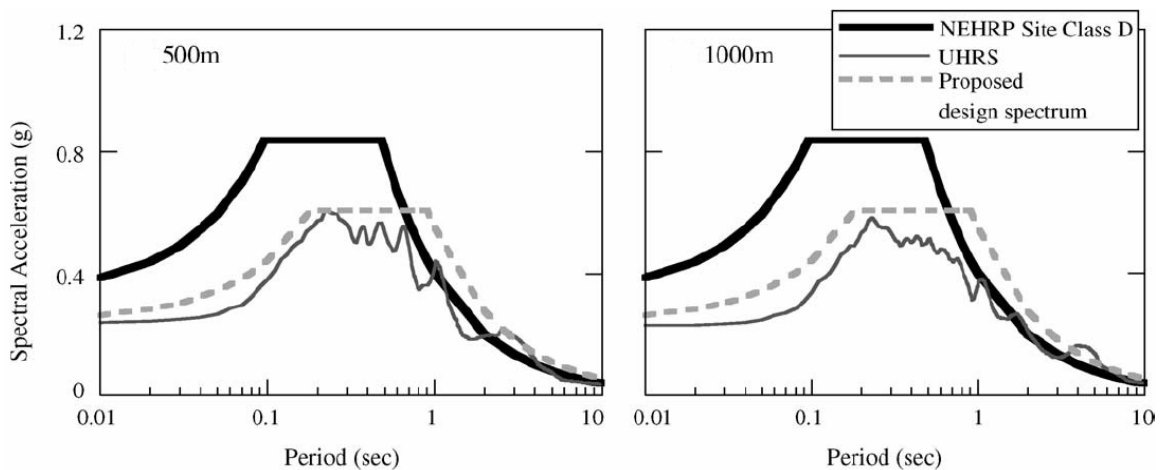


**Figure 3.5.** Upper-bound envelope approach used by Park and Hashash (2005) to develop site factors for Embayment depths of 500 and 1000 m

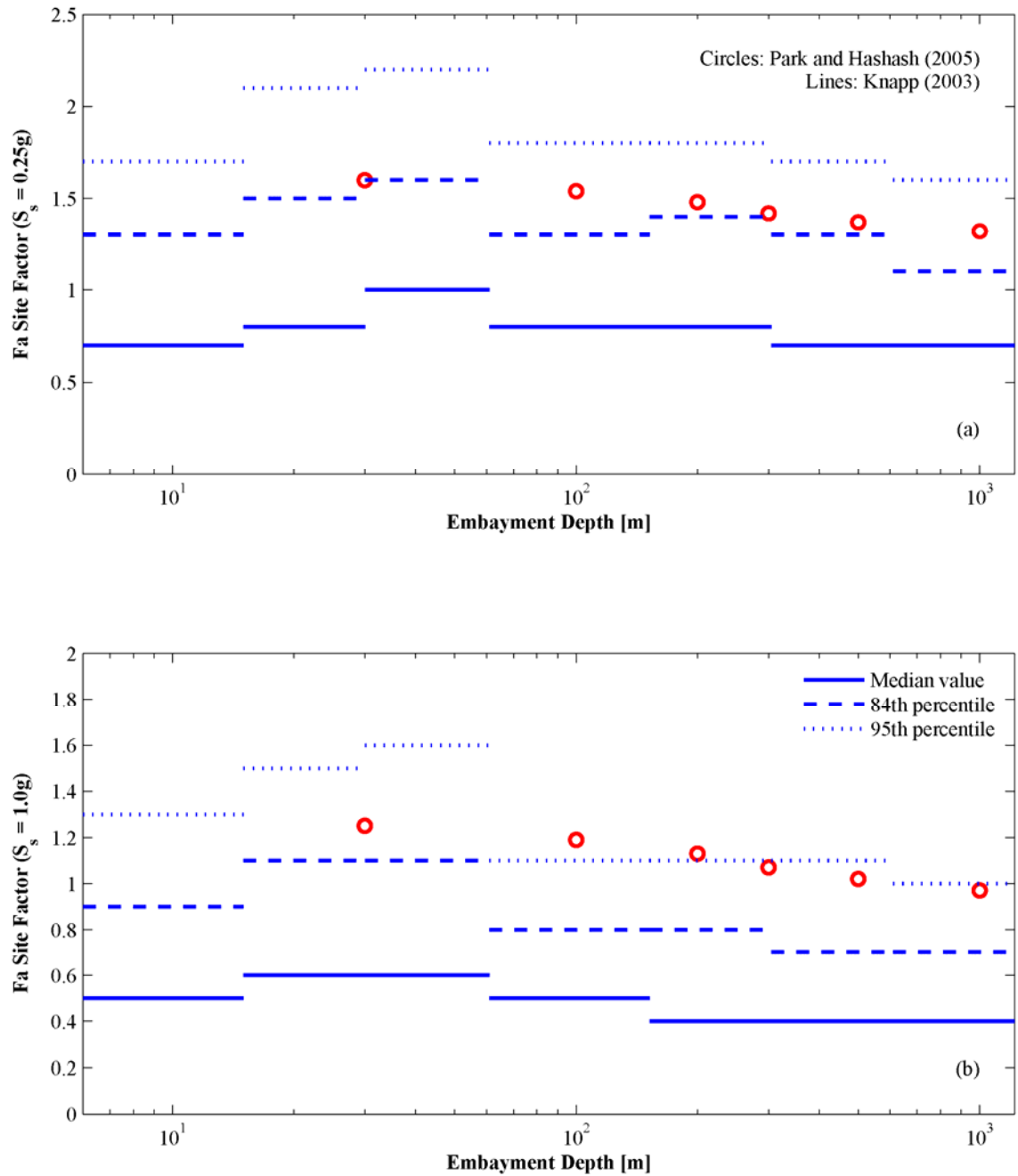


**Figure 3.6.** Comparison of  $F_a$  site factors for the Upper Mississippi Embayment computed by equivalent linear and true non-linear analyses

corresponds to site factors developed for the Uplands soil profile using the EPRI (1993) dynamic soil properties. Similar results are obtained for the Lowlands soil profile. Figure 3.6 indicates that the high percentiles of the site factors developed by Knapp (2003) compare well with the site factors proposed by Park and Hashash (2005). This observation is consistent with the envelope approach used by the latter to obtain the site factors. Furthermore, the use of the median values of the soil parameters in a non-linear process does not necessarily yield the median site response, and therefore it is difficult to evaluate whether the Park and Hashash (2005) site factors correspond to the envelope of the median values or other percentile.

The equivalent linear analysis is an approximation to the non-linear process of seismic site response with recognized limitations. However, the discussion presented above has shown that by imposing some restrictions in the implementation of the equivalent linear analysis in the Upper Mississippi Embayment, it can generate surface ground motions comparable to the ground motions estimated by true non-linear analyses. Furthermore, the validation performed by Silva et al. (1997) provides information on the bias and variability of the modified equivalent linear approach that is incorporated into ground motion estimates developed in this study.

The equivalent linear analysis implemented in RASCALS is based on random vibration theory. RVT is used to estimate peak time domain values of shear strains based on the shear strain power spectrum. The procedure is similar to the estimation of peak shear strains values in the time domain used by the program SHAKE (Schnabel et al., 1972). However the frequency domain approach eliminates the need of a suite of time domain control motions to obtain a statistically stable estimate of site response (Silva et al., 1991). A time domain approach would require many more simulations to obtain stable estimates of the median and variability of the site response and would raise additional uncertainties regarding the selection of control motions.

A recommendation for future work is to include other site response formulations to better characterize epistemic variability.

### 3.4. Models and Variability

Table 3.2 lists the alternative models used in the simulations to accommodate epistemic variability and Table 3.3 shows the median values of the randomized earthquake parameters along with the standard deviations and distributions used to characterize aleatory variability. The randomized model parameters included stress drop  $\Delta\sigma$ , source depth  $H$ , crustal attenuation coefficient  $Q_0$ , near-surface attenuation coefficient  $\kappa$ , crustal velocity, near-surface shear wave velocity, and modulus reduction and damping ratio curves.

**Table 3.2.** Alternative models

<b>Variable</b>	<b>Alternatives</b>
<b>Source Models</b>	Atkinson and Boore (1995) Frankel et al. (1996) Silva et al. (2003)
<b>Stress Drops</b>	Medium case 100% Higher 100% Lower
<b>Soil Profiles</b>	Lowlands Uplands
<b>Non-linear Soil Properties</b>	EPRI (1993)
<b>Embayment Depth</b>	6 – 15 m 15 – 30 m 30 – 61 m 61 – 152 m 152 – 305 m 305 – 610 m 610 – 1220 m

**Table 3.3.** Randomized model parameters and distributions

Parameter		Median				Std. Dev.	Distribution
Source	Stress Drop, $\Delta\sigma$	<ul style="list-style-type: none"><li>• ab95: <math>\Delta\sigma = 100</math> bars</li><li>• fa96: <math>\Delta\sigma = 150</math> bars</li><li>• si03: <math>\Delta\sigma = f(M)</math></li></ul>				0.5	Log-Normal
		<b>M</b>	<b><math>\Delta\sigma</math> (bars)</b>				
		4.0	160				
		4.5	160				
		5.0	160				
		5.5	160				
		6.0	140				
		6.5	120				
		7.0	105				
	7.5	90					
Source Depth, H (km)	<b>M</b>	<b>H<sub>Low</sub></b>	<b><math>\bar{H}</math></b>	<b>H<sub>up</sub></b>	0.6	Log-Normal truncated between lower and upper limits	
	4.0	2	5	12.5			
	4.5	2	6	15			
	5.0	2	6	15			
	5.5	2	6	15			
	6.0	3	7	17.5			
	6.5	4	8	20			
	7.0	4.5	9	20			
	7.5	5	10	20			
Path	Crustal Attenuation Coefficient, $Q_0$	<ul style="list-style-type: none"><li>• ab95: <math>Q_0 = 680.0</math></li><li>• fa96: <math>Q_0 = 680.0</math></li><li>• si03: <math>Q_0 = 351.0</math></li></ul>				0.4	Log-Normal
	Near-Surface Attenuation, $\kappa$	<ul style="list-style-type: none"><li>• ab95: <math>\kappa = 0.0</math></li><li>• fa96: <math>\kappa = 0.006</math></li><li>• si03: <math>\kappa = 0.006</math></li></ul>				0.3	Log-Normal
	Crustal Velocity	1 profile				0.3	Log-Normal
Site	Near-Surface Velocity, $V_s$	2 profiles				0.4	Log-Normal
	Modulus Reduction, $G/G_{\max}$	1 curve set				0.3	Log-Normal
	Damping Ratio	1 curve set				0.3	Log-Normal

**Note:** ab95: Atkinson and Boore (1995), fa96: Frankel et al. (1996), si03: Silva et al. (2003)

### 3.4.1. Source Model

For the stochastic model considered herein, three source models were implemented including a two-corner frequency model: Atkinson and Boore (1995) and two, one-corner frequency models: Frankel et al. (1996) and Silva et al. (2003). These source models were developed particularly for the CEUS conditions. Table 3.4 summarizes the source models' parameters. Figure 3.7 through Figure 3.10 compare the mean values of the geometrical attenuation function, seismic attenuation function  $Q$ , path duration, and high-frequency filter implemented in each source model.

The occurrence of the 1988 **M** 5.8 Saguenay, Canada earthquake, which was one of the largest earthquakes recorded in Eastern North America, has generated considerable confusion in the ground motion prediction in the CEUS due to its unusual high amplitudes in the high-frequency range (Atkinson and Boore, 1998, 2006). The two-corner frequency model matches the spectral shape of this earthquake better than the one-corner model but underpredicts the absolute motion levels (Silva et al., 1997). Furthermore, stress drops higher than 500 bars are required in order to predict its high-frequency spectra levels, but this results in overestimation of the ground motion amplitudes at low and intermediate frequencies (Silva and Costantino, 2002). Some source models match the Saguenay earthquake data (e.g. Haddon, 1996); however these models in general do not fit the rest of the CEUS ground motion recordings, suggesting the unusual nature of this event (Atkinson and Boore, 1998). The Atkinson and Boore (1995) and Frankel et al. (1996) models are not consistent with the data of this event (Atkinson and Boore, 1998), whereas the seismic attenuation function  $Q$  of the Silva et al. (2003) model is based on inversions of this particular earthquake (Cramer, 2006a). It is clear that one source model is not capable of predicting the broad range of possible earthquakes in the CEUS. While it appears that the two-corner frequency model is more appropriate to model CEUS ground motions, there is value in considering more epistemic

**Table 3.4.** Source models parameters

	Atkinson and Boore (1995)	Frankel et al. (1996)	Silva et al. (2003)
Density	2.8 g/cm <sup>3</sup>	2.8 g/cm <sup>3</sup>	2.78 g/cm <sup>3</sup>
Shear-wave Velocity	3.8 km/sec	3.6 km/sec	3.75 km/sec
Geometrical Spreading	$\frac{1}{R}$ ; $R < 70\text{km}$ $\frac{1}{70}$ ; $70\text{km} \leq R < 130\text{km}$ $\frac{1}{70} \cdot \left(\frac{130}{R}\right)^{0.5}$ ; $R \geq 130\text{km}$		$R^{-[a+b(M-6.5)]}$ ; $R \leq 80\text{km}$ $R^{\frac{[a+b(M-6.5)]}{2}}$ ; $R > 80\text{km}$ $a = 1.0296$ $b = -0.0422$
Seismic Attenuation			
	$Q(f) = 680 \cdot f^{0.36}$		$Q(f) = 351 \cdot f^{0.84}$
Path Duration	$0$ ; $R < 10\text{km}$ $0.16(R-10)$ ; $10 \leq R < 70\text{km}$ $9.6-0.03(R-70)$ ; $70 \leq R < 130\text{km}$ $7.8+0.04(R-130)$ ; $R \geq 130\text{km}$	$0.05 \cdot R$	
$f_{\max}$ filter	50.0 Hz	100.0 Hz	0.0 Hz
$\kappa$ filter	0.0 sec	0.006 sec	0.006 sec

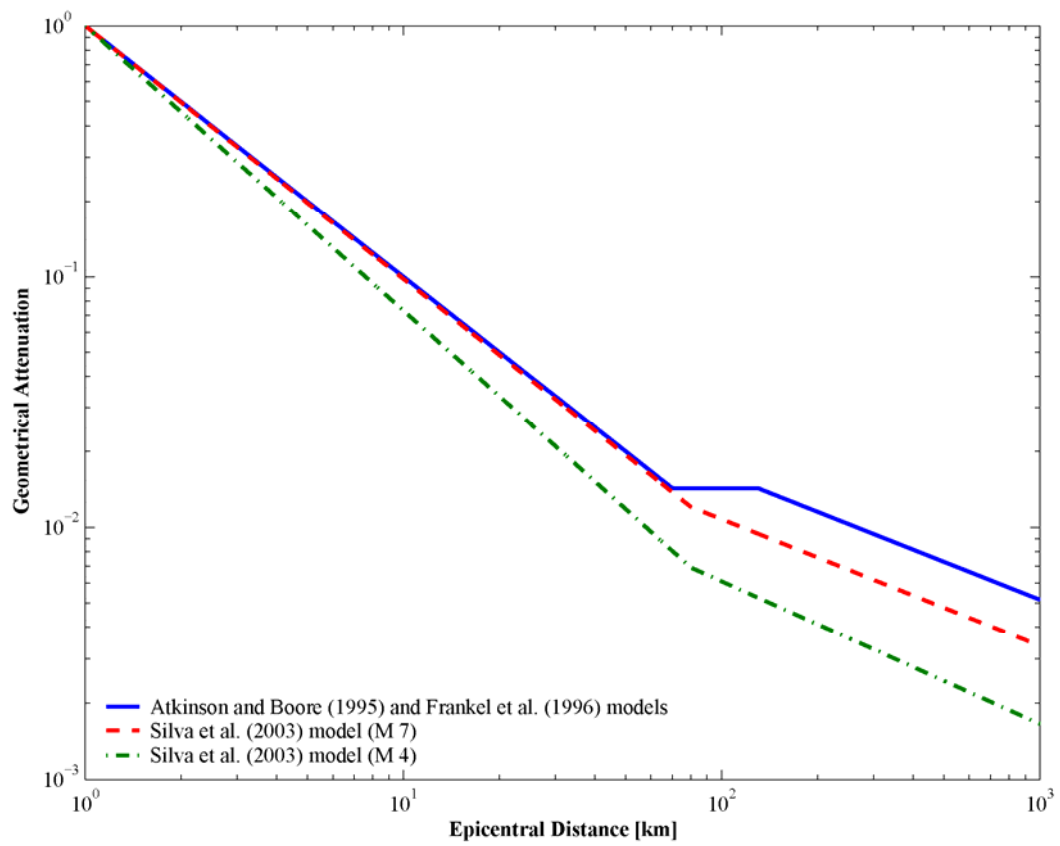


**Figure 3.7.** Geometrical attenuation functions

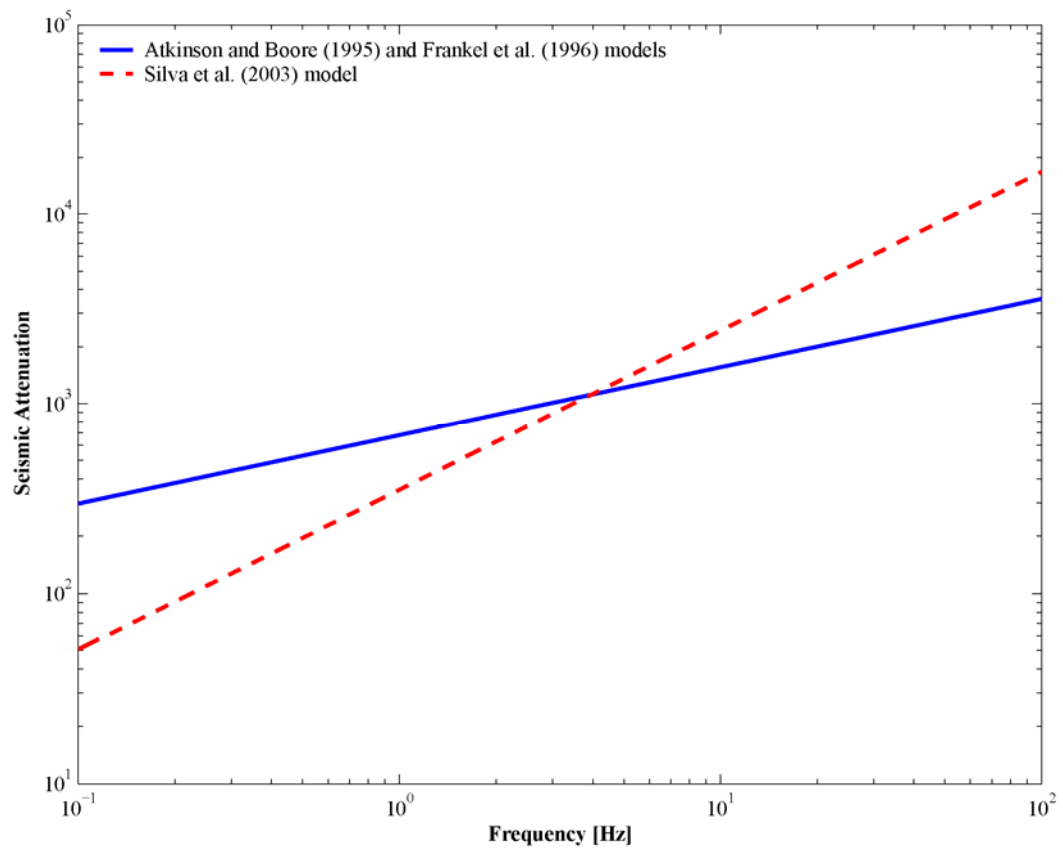


**Figure 3.8.** Seismic attenuation functions

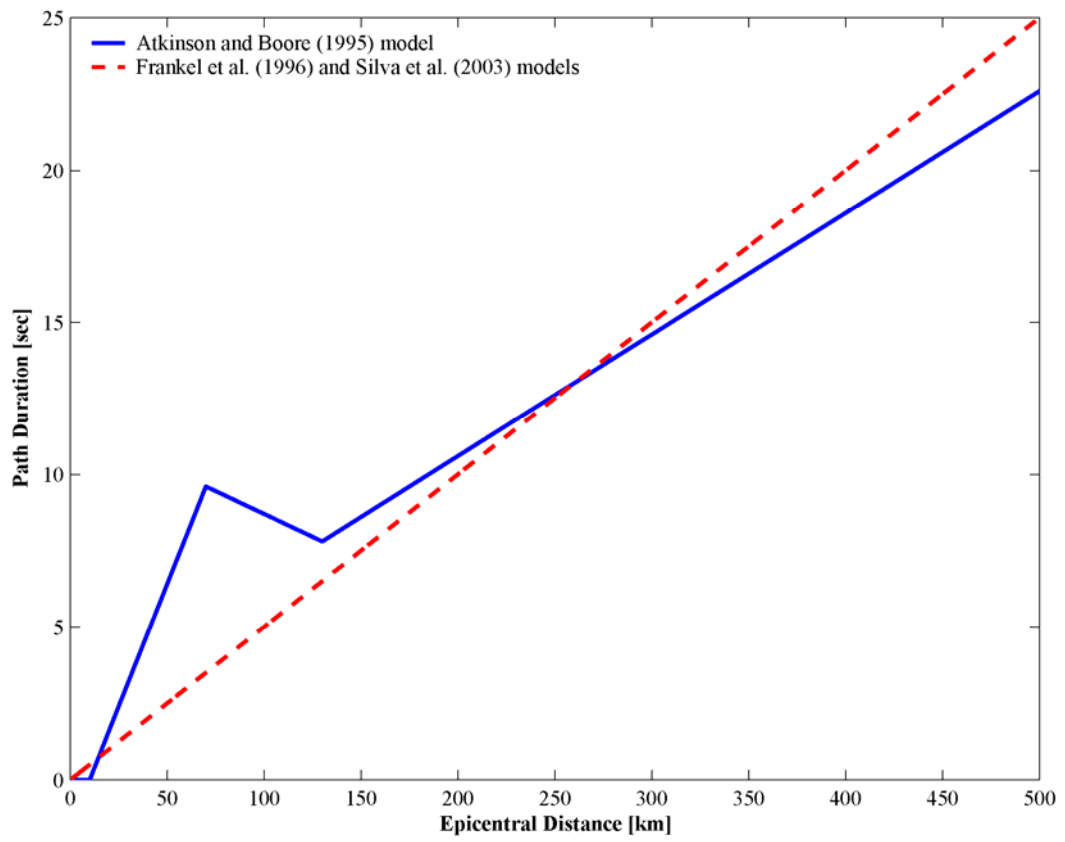


**Figure 3.9.** Path duration

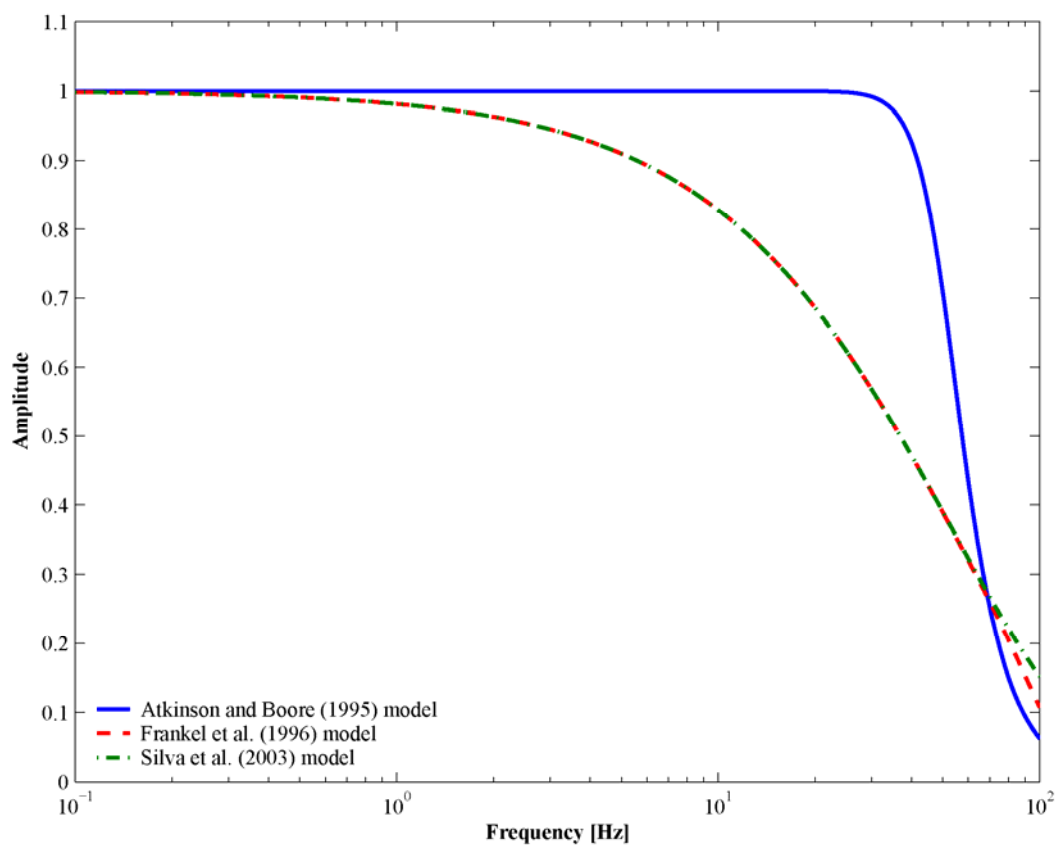


**Figure 3.10.** High-frequency filters

variability in predicting strong ground motions for engineering design (Silva and Costantino, 2002).

The point source model does not capture near-field effects (e.g. directivity effects, rupture propagation). However, in most engineering applications only high frequencies are important, and far-field effects dominate the response (Boore, 2003a). Nevertheless, average finite-fault effects can be incorporated in a point-source model in several ways.

Atkinson and Silva (2000) demonstrated that the use of a two-corner point-source model is equivalent to the use of a finite-fault model. Atkinson and Silva (2000) found that two-corner point-source and finite-fault models predict the same median levels of ground motions when averaged over all azimuths, and noted the advantage of simplicity and stability of using a point source model in ground motion predictions, because a finite fault model requires more parameters and involves averaging simulations over many azimuths and slips distributions. This observation is supported by Atkinson and Boore (2006), who found similarities between the two-corner point-source model ground motion predictions of Atkinson and Boore (1995) and their new prediction equations based on a finite-fault model. Silva et al. (2002; 2003) proposed another way to incorporate finite-fault effects in a point-source model. Silva et al. (2002; 2003) provides evidence that when multiple earthquakes are considered, finite source effects coupled with variability in source depth and crustal structure are adequately modeled by using a point-source model with a magnitude-dependent geometrical attenuation function. Furthermore, Silva et al. (2003) stated that a magnitude-dependent stress drop provides an empirical mechanism to incorporate magnitude saturation due to finite-fault effects. In addition, Boore (2003a) mentions that the use of the closest distance to the fault rupture in ground motion prediction equations captures the finite-fault effects averaged over many sites distributed around the fault.

Although a point source model was selected to perform the simulations in this study, average-finite fault effects are captured in the ground motions predictions by using

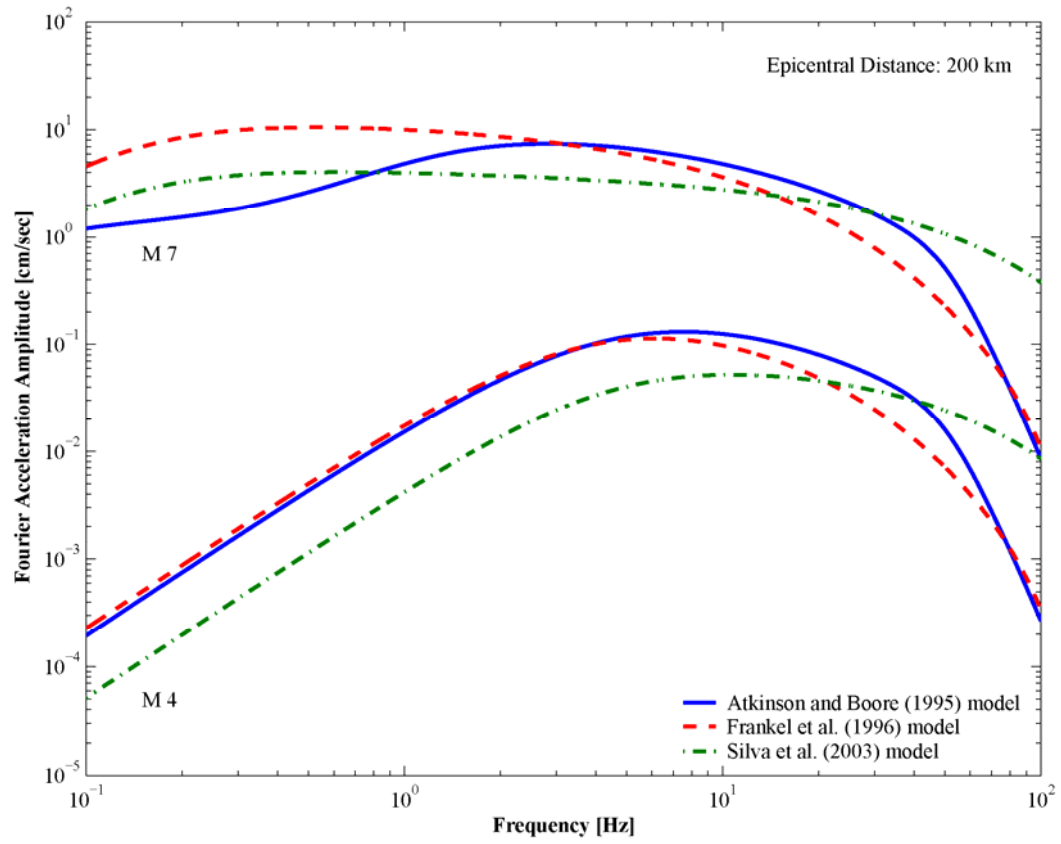
a two-corner source spectrum (Atkinson and Boore, 1995), a magnitude-dependent geometrical attenuation function and a magnitude-dependent stress drop as implemented in the Silva et al. (2003) model, and the epicentral distance as the source-to-site distance in the attenuation relationships, as discussed below (Boore, 2003a).

Figure 3.11 and Figure 3.12 compare the Fourier acceleration amplitudes estimated by the three source models. Figure 3.11 shows the Fourier acceleration spectra for an epicentral distance of 200 km, and Figure 3.12 shows the decay of Fourier acceleration amplitudes with distance for low and high frequencies. The ground motion amplitudes include source and path effects, and the high-frequency filters shown in Figure 3.10. It is important to note the difference in amplitudes and decay rate among source models, because these differences help to explain the ground motion amplitudes obtained at the soil surface as discussed later.

### **3.4.2. Stress Drop**

The stress drop is not explicitly defined for the Atkinson and Boore (1995) model, but a value of 100 bars was selected to run the simulations (Boore and Atkinson, 1987). Silva et al. (2003) considered constant and magnitude-dependent stress drop models. The latter was implemented in this study to better characterize epistemic variability in the source model because both Atkinson and Boore (1995) and Frankel et al. (1996) consider a magnitude-independent stress drop. Moreover, a magnitude-dependent stress drop model provides a method to incorporate average finite-source effects in point-source simulations as discussed previously.

Table 3.3 lists the median stress drop values for the three source models. For a point source model, the stress drop is the parameter that most contributes to the variability of ground motions (Atkinson and Boore, 2006; Silva, 1992; Toro et al., 1997) and therefore an explicit characterization of epistemic and aleatory variability in stress drop is required. Epistemic uncertainty in the stress drop was included by varying the



**Figure 3.11.** Comparison of Fourier acceleration spectra

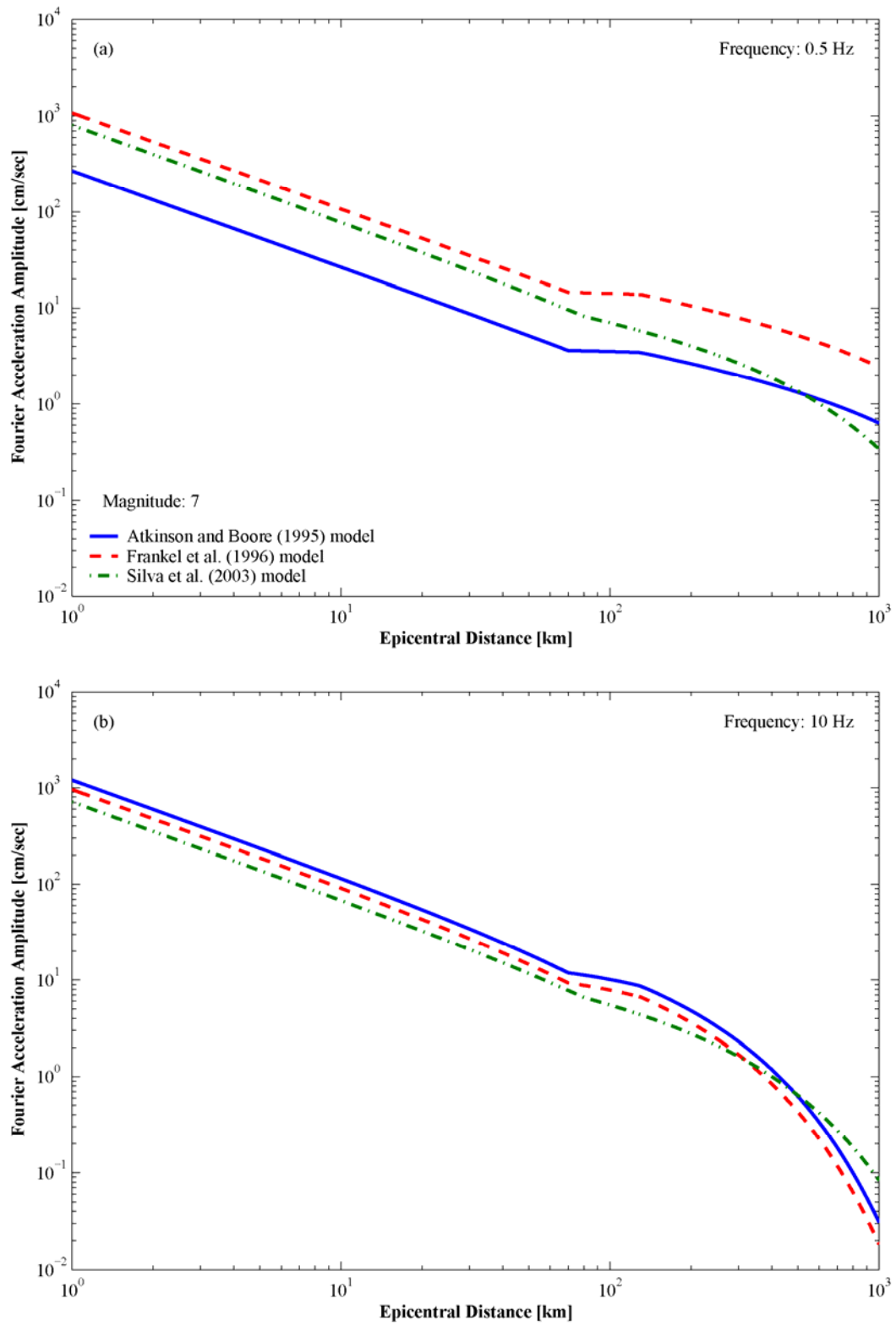


**Figure 3.12.** Attenuation of Fourier acceleration amplitudes

median value by a factor of two. A logarithmic standard deviation of 0.5 was used for the aleatory uncertainty of the stress drop (Silva et al., 1997). If only the median case of the stress drop is considered in the analysis, it is recommended to use a logarithmic standard deviation of 0.7 to characterize both epistemic and aleatory variability (Silva, personal communication).

### **3.4.3. Source Depth**

The source depth was assumed to be magnitude-dependent with a logarithmic standard deviation of 0.6 (EPRI, 1993; Silva et al., 2003).

Table 3.3 shows the magnitude-dependent depth distribution implemented herein, which is based on seismicity in stable continental regions (EPRI, 1993). Bounds were used for the source depth distribution to prevent non-physical realizations (Silva et al., 2003).

### **3.4.4. Crustal and Near-Surface Attenuation**

Table 3.3 lists the median values used for the crustal attenuation coefficient  $Q_0$  and near-surface attenuation  $\kappa$ . The logarithmic standard deviation used for  $Q_0$  and  $\kappa$  were 0.4 (Silva et al., 1997) and 0.3 (EPRI, 1993), respectively. Toro and Silva (2001) recognize that this value of uncertainty in  $\kappa$  is low to characterize epistemic and aleatory variability and attribute this to the fact that the point source modeling variability already includes the effects of the  $\kappa$  uncertainty. Double counting of uncertainties might overestimate the total variability of the attenuation relationships; however there are no ground motion validations for deep soil sites in the CEUS and it seems necessary to follow this approach in order to not underestimate ground motion uncertainty (Toro and Silva, 2001). The variability in the seismic attenuation function  $Q$  is taken only on  $Q_0$  (see Equation 3.8), whose  $\pm 1\sigma$  variation is sufficient to cover the range of CEUS inversions from 1 to 20 Hz (Silva et al., 2003). According to Roblee et al. (1996), only

parametric variability for  $\Delta\sigma$ , H and Q are required to be reflected in the source model simulations. However,  $\kappa$  was also randomized because its value is based on data from regions other than the CEUS, and few CEUS sites were available for validation exercises (Silva et al., 1997; 2002).

#### **3.4.5. Crustal Shear-Wave Velocity**

Catchings (1999) used seismic refraction and gravity modeling to develop velocity models of the crustal structure of the New Madrid rift along a profile from Memphis, TN to St. Louis, MO. The crustal velocity model implemented in this study was the model developed by Catchings (1999) for the city of Memphis, TN, which was considered to be appropriate for the entire region. This model was used for geologic deposits below 1 km. Romero (2001) summarizes other crustal velocity models that have been proposed for the CEUS; however these models are applicable to the northern part of the Mississippi Embayment where the depth to the bedrock is approximately 650 meters (Chiu et al., 1992). Figure 3.13 shows the crustal velocity profile used in the simulations. The logarithmic standard deviation used for the crustal velocity was 0.3 (EPRI, 1993).

#### **3.4.6. Soil Shear-Wave Velocity**

The surface deposits of the Upper Mississippi Embayment can be classified in two different categories: the Lowlands and Uplands profiles as discussed in Chapter 2 and shown in Figure 2.1. Figure 3.14 shows the shear-wave velocity profiles implemented in the simulations for both geologic deposits. These profiles are the smoothed, weighted average of the generic profiles developed by Romero (2001), the profiles derived by Street et al. (2004), and two borehole geophysical logs located near Memphis, TN, and Keiser, AR. A logarithmic standard deviation of 0.4 was used for the near-surface velocity (EPRI, 1993).

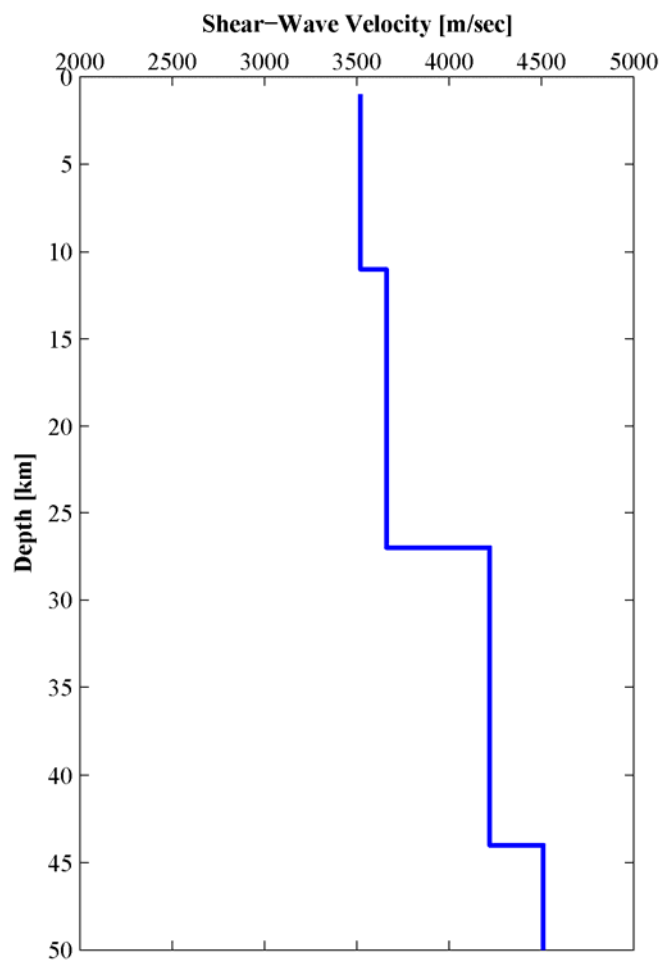


**Figure 3.13.** Crustal shear-wave velocity profile (Catchings, 1999)

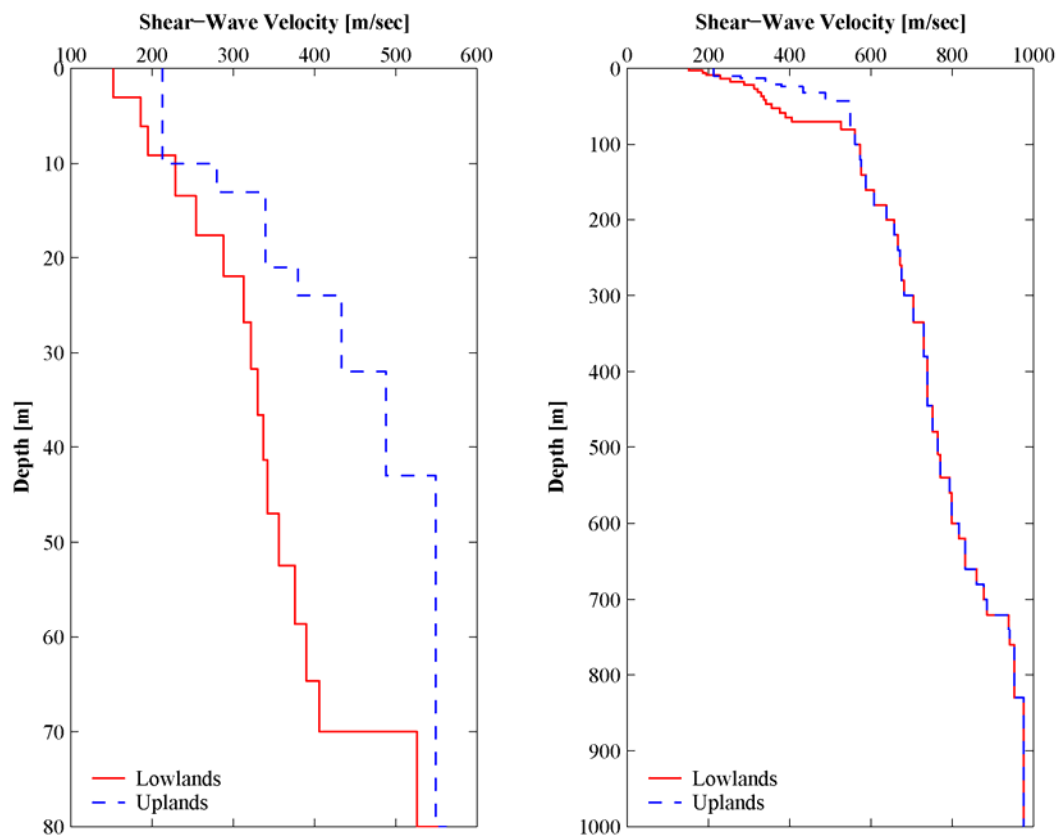


**Figure 3.14.** Near-surface shear-wave velocity profiles

### 3.4.7. Dynamic Soil Properties

The shear modulus and damping are critical dynamic properties of the soil to evaluate the non-linear behavior of the site (Kramer, 1996). During dynamic shear loading, shear modulus and damping values vary with shear strain amplitude. Usually the shear modulus is normalized to the maximum shear modulus,  $G_{\max}$ , and the variation of this modulus ratio with shear strain is described by a modulus reduction curve. The damping ratio is defined as the ratio of the strain energy dissipated in one loading cycle to the maximum strain energy, and its variation with shear strain is described by a damping ratio curve. Generic modulus reduction and damping ratio curves developed by EPRI (1993) were used in the simulations. These sets of curves are based on an extensive database of field and laboratory investigations and quantify the variability due to different factors affecting the shear modulus and material damping ratio (EPRI, 1993). The EPRI (1993) curves have been validated at 48 San Francisco Bay area soil sites through modeling strong ground motions from observed earthquakes (Silva et al., 1997). Furthermore, these sets of curves were used to develop soil amplification factors for power plants in the CEUS (EPRI, 1993). Figure 3.15 and Figure 3.16 show the mean modulus reduction and damping ratio curves developed by EPRI (1993) along with their depth range of applicability. A logarithmic standard deviation of 0.3 was used for both modulus reduction and damping ratio curves (Silva, personal communication). Upper and lower bounds were imposed to avoid unrealistic values of material properties (EPRI, 1993). Figure 3.17 and Figure 3.18 show the bounds for the modulus reduction and damping ratio curves. Only the upper 150 m of the soil column was allowed to undergo non-linear behavior as discussed previously.

Figure 3.19 shows the variation of mass density and small-strain damping ratio with depth implemented in the simulations. The mass density profile was taken from Romero (2001). The initial value of small-strain damping ratio profile is based on the damping curves developed by EPRI (1993).

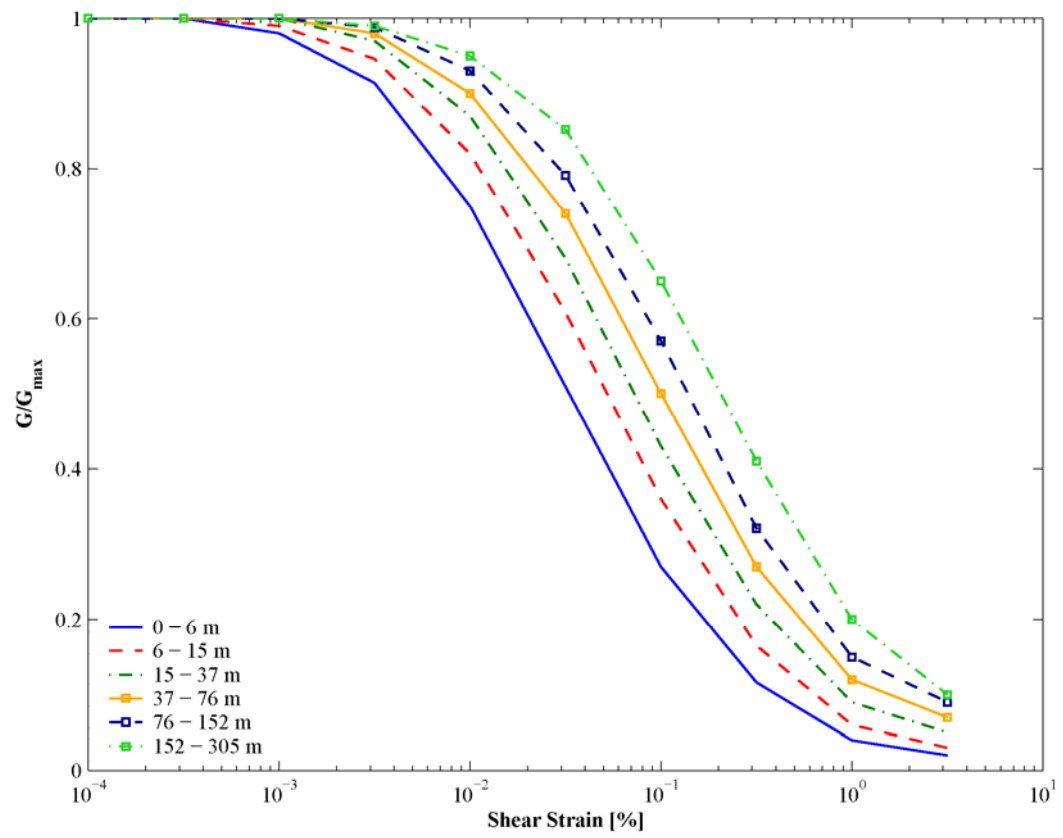


**Figure 3.15.** EPRI (1993) modulus reduction curves and their depth range of applicability

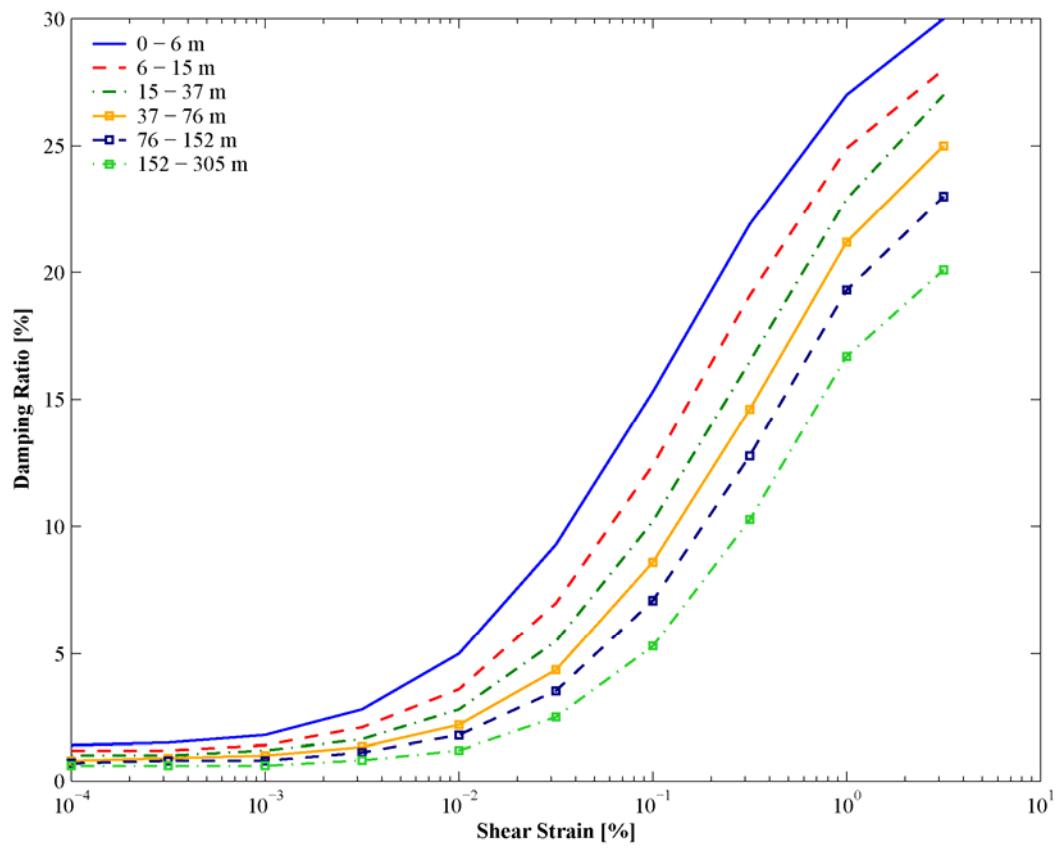


**Figure 3.16.** EPRI (1993) damping ratio curves and their depth range of applicability

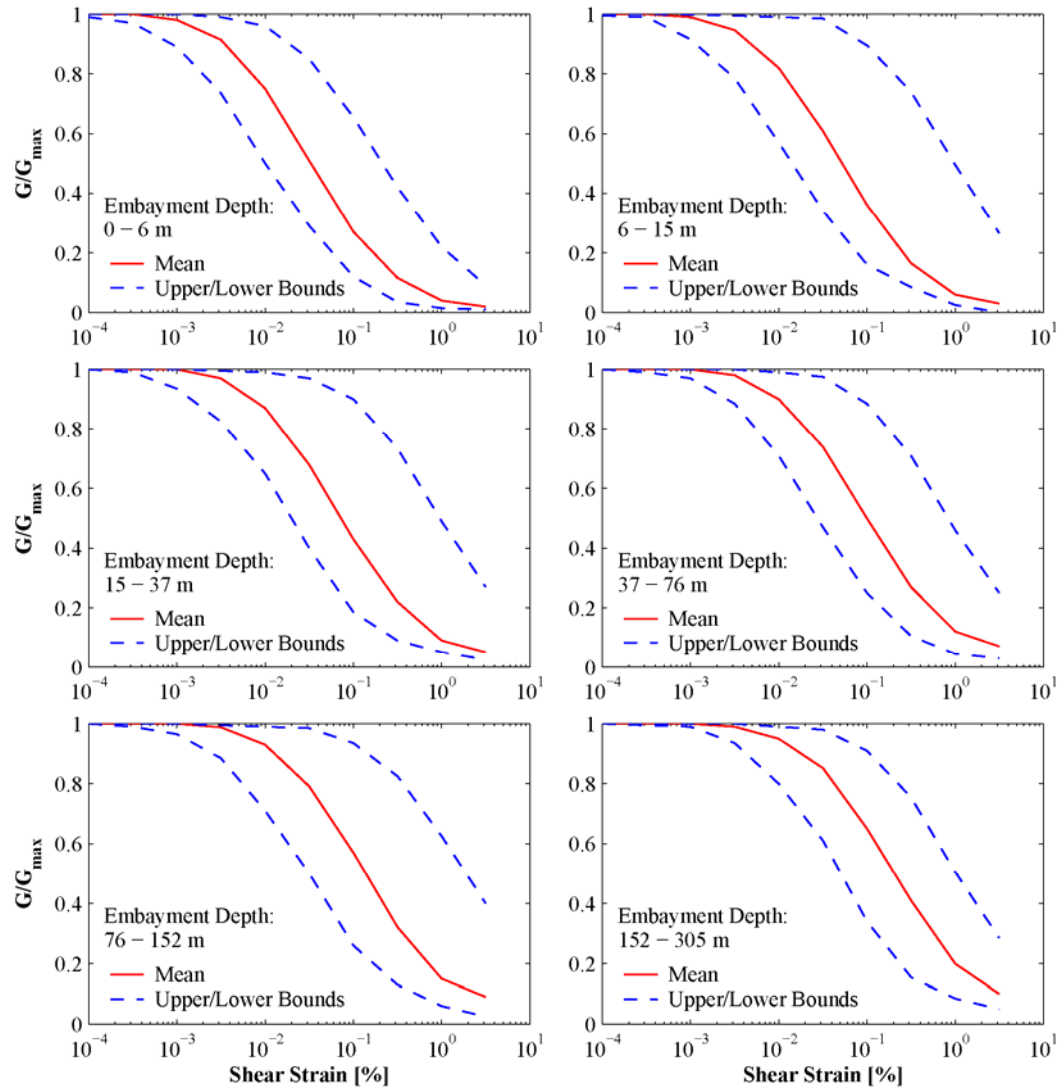


**Figure 3.17.** Upper and lower bounds of EPRI (1993) modulus reduction curves

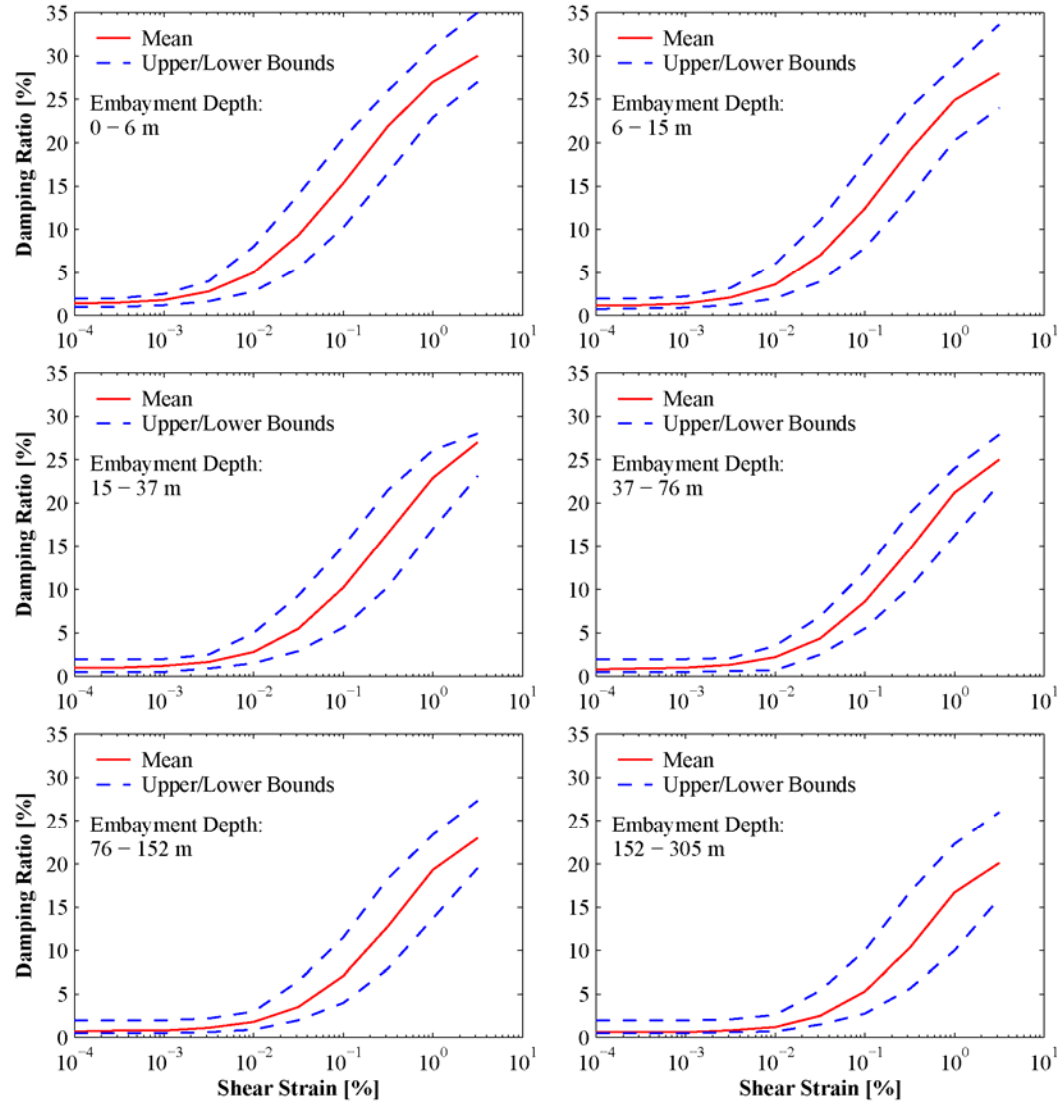


**Figure 3.18.** Upper and lower bounds of EPRI (1993) damping ratio curves

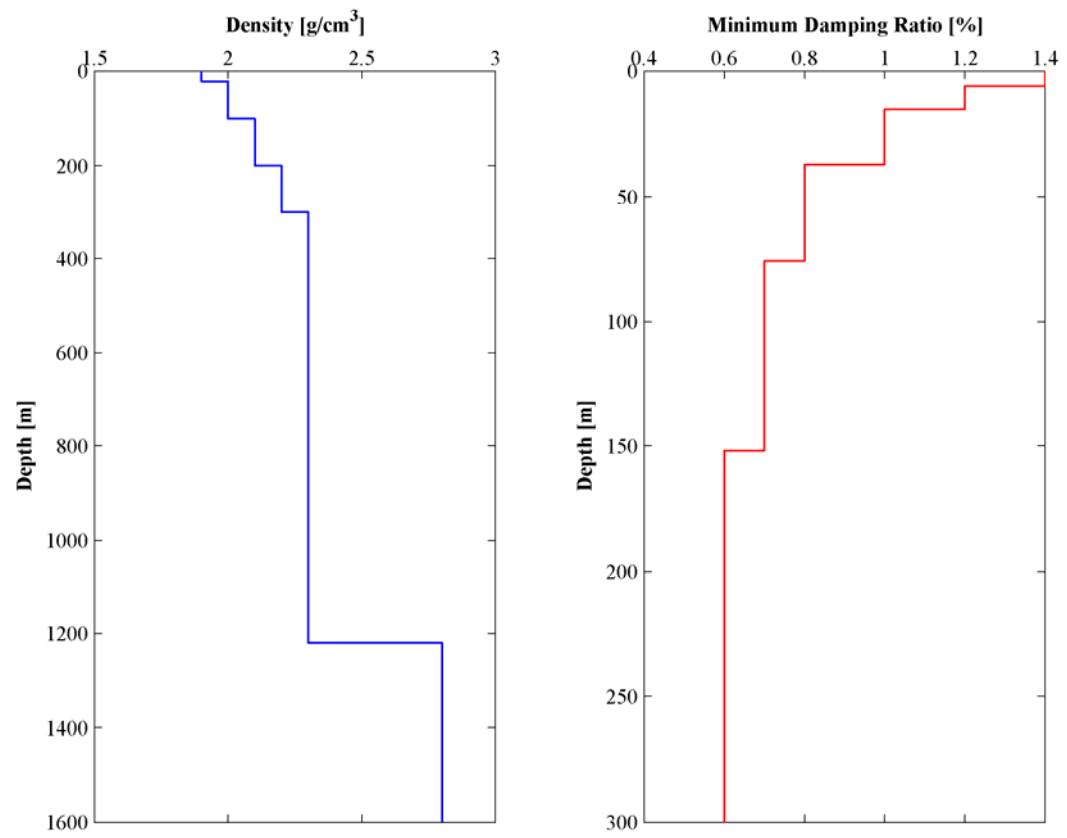


**Figure 3.19.** Density and small-strain damping ratio profiles

#### **3.4.8. Embayment Depth**

The Embayment profile was subdivided into seven depth bins to accommodate likely soil profile depth ranges (Toro and Silva, 2001). The depth of the soil profile was randomized within the depth bins' limits using a uniform distribution. Table 3.2 shows the depth bins used in this study, which range from 6 m to 1220 m. The depth bins follow a geometric distribution, where the mean depth of each bin is associated with a resonant frequency of the Embayment.

### **3.5. Randomization of Parameters**

For each combination of variables including source model, stress drop, soil profile, dynamic soil properties and depth bin, 550 realizations of the earthquake parameters were simulated for epicentral distances uniformly distributed (in logarithmic units) between 1 to 750 km and eight moment magnitudes:  $M$  4, 4.5, 5, 5.5, 6, 6.5, 7, and 7.5.

Several definitions of source-to-site distance exist to characterize the seismic waves travel path in ground motion relations. For point-source models, the definitions reduce to hypocentral and epicentral distances. Hypocentral distance measures the distance from the site to the hypocenter of the earthquake (i.e. distance to the rupture starting point). Epicentral distance is the distance from the observing point to the surface projection of the hypocenter. Most damaging earthquakes occur in the top 30 km of the crust, and therefore the difference between hypocentral and epicentral distances is small for intermediate and large distances (Douglas, 2003). It is difficult to obtain an accurate estimation of the hypocenter depth, and therefore for shallow crustal earthquakes the use of hypocentral distance is unlikely to reduce the standard deviation of the ground motion relation equation (Douglas, 2003). For these reasons, epicentral distance was selected to measure the source-to-site distance.

Previous studies (Bollinger et al., 1993; Nuttli, 1981) have shown the large damaged areas associated with CEUS earthquakes are due to the low attenuation rates in the region, i.e. high values of  $Q$ . An isoseismal map of the 1811-1812 New Madrid, MO earthquakes sequence shows Modified Mercalli Intensities of II-III in Boston, Massachusetts (Johnston and Schweig, 1996; Stover and Coffman, 1993), approximately 1,800 km from the epicenter. The 1886 Charleston, SC earthquake was felt over 2.5 million square miles, from Cuba to New York and Bermuda to St. Louis (Scawthorn, 2003). Attenuation models developed for CEUS conditions have considered source-to-site distances ranging from 500 km (Atkinson and Boore, 1995; EPRI, 1993; Somerville and Saikia, 2001; Toro et al., 1997) to 1000 km (Campbell, 2003b; Frankel et al., 1996) due to the low anelastic attenuation observed in the region. Following these previous models, the ground motions in this study were simulated up to epicentral distances of 750 km.

The selection of moment magnitude over other earthquake magnitudes scales (e.g. Richter local magnitude  $M_L$ , body wave magnitude  $m_b$ , or surface wave magnitude  $M_S$ ) has some advantages. Moment magnitude is the only definition that has a physical meaning, because it is based on the seismic moment (see Equation 3.4), which is directly related to the size of the earthquake fault and the slip along the fault (Douglas, 2003; Kramer, 1996). Furthermore  $M_L$ ,  $m_b$ , and  $M_S$  are calculated by making frequency-dependent amplitude measurements of the earthquake spectrum at about 1.2, 1.0, and 0.05 Hz respectively (Lay and Wallace, 1995). For earthquakes larger than a specific size, these frequencies will be higher than the corner frequency (see Figure 3.1), and therefore all earthquakes above this size will have the same magnitude. This phenomenon is called magnitude saturation (Lay and Wallace, 1995). Moment magnitude does not saturate due to its direct relation to the factors that produce fault rupture, and hence can be used to characterize the entire magnitude range (Kramer, 1996; Lay and Wallace, 1995).

Atkinson and Boore (1995), Frankel et al. (1996), and Silva et al. (2003) used maximum magnitudes of **M** 7.25, **M** 8.2, and **M** 8.5 respectively, when implementing their source models. The maximum magnitude considered in the simulations, **M** 7.5, follows the minimum magnitude of the three source models. However, probabilistic seismic hazard analyses using the attenuation relationships developed herein show that the extrapolation of the model to magnitudes up to **M** 8.5 yields adequate results.

The randomization routines are implemented in the computer program RANPAR (Silva, personal communication). RANPAR randomizes the model parameters and creates a RASCALS input file for each set of randomized set of parameters. The number of realizations of the earthquake parameters was determined in order to obtain a stable estimate of the median and standard deviation of the distributions. To evaluate a single realization of the dynamic soil properties curves, the algorithm generates a random value at the strain where the largest difference between the upper and lower bounds occurs, and calculates a scaling relationship to find values for the entire strain range. This procedure ensures that the realizations preserve the shape of the median curves. This algorithm does not consider coupling between the modulus reduction and damping ratio curves, and therefore it might misestimate parametric variability associated with the non-linear soil response (Roblee et al., 1996). The shear wave velocity profiles are randomized using an algorithm implemented in RANPAR by Toro (1995). This algorithm simulates velocity profiles by using a correlation model that depends on the depth and distance between layers midpoints. Figure 3.20 shows an example of the randomized soil parameters.

### **3.6. Attenuation Relationships**

The regression equation was developed by combining features of functional forms used in previous studies. Among all the variations used in the regression analyses, the functional form that provided the smallest residuals was selected to fit to the simulations and is given by:

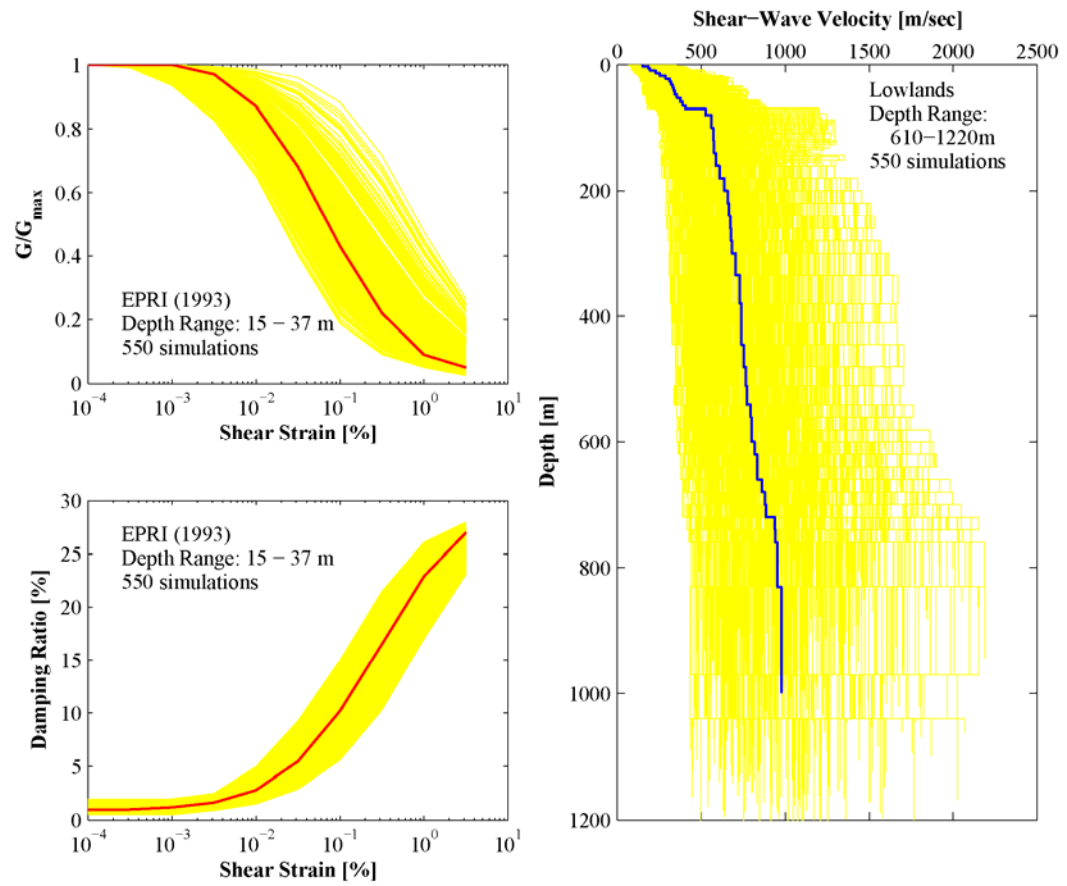


**Figure 3.20.** Examples of randomized soil parameters

$$\ln y = c_1 + c_2 \cdot \mathbf{M} + c_3 \cdot (\mathbf{M} - 6)^2 + c_4 \cdot \ln R_M + c_5 \cdot \max \left[ \ln \left( \frac{R}{70} \right), 0 \right] + c_6 \cdot R_M \quad 3.20$$

$$R_M = R + c_7 \cdot \exp(c_8 \cdot \mathbf{M}) \quad 3.21$$

$$\sigma_{\ln y} = c_9 \cdot \mathbf{M} + c_{10} \quad 3.22$$

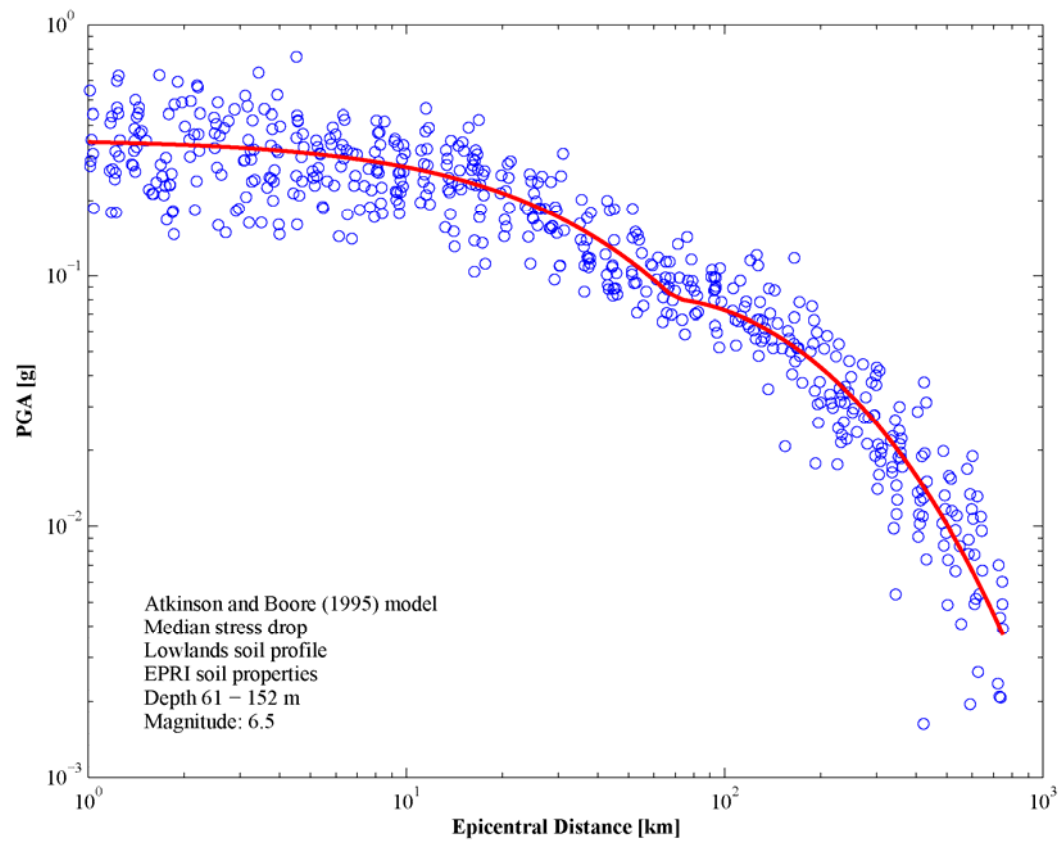
where  $y$  is peak ground displacement in cm, peak ground velocity in cm/sec, or 5% damped spectral acceleration in units of  $g$ ,  $R$  is the epicentral distance in km,  $\mathbf{M}$  is the moment magnitude,  $\sigma_{\ln y}$  is the logarithmic standard deviation of  $y$ , and  $c_1$  through  $c_{10}$  are the regression coefficients. The model regression coefficients are available at [http://geosystems.ce.gatech.edu/soil\\_dynamics](http://geosystems.ce.gatech.edu/soil_dynamics) and are given in an electronic supplement in Appendix A.

The equivalent distance term  $R_M$  accounts for the increase in traveling distance by the seismic waves due to the increase in fault rupture size with magnitude (Kramer, 1996). Moreover it incorporates the belief that high-frequency ground motion should become less dependent on magnitude close to the earthquake fault (Campbell, 2003a). The  $c_2$  term in Equation 3.20 is consistent with the original definition of earthquake magnitude, which states that earthquake magnitude is proportional to the logarithm of some peak motion parameter (Campbell, 2003a; Kramer, 1996). The  $c_3$  term provides a better fit to the simulations for low-frequency ground motions (EPRI, 1993; Toro et al., 1997). The  $c_4$  and  $c_5$  terms represent the geometrical attenuation of the seismic wave front with the  $c_4$  term for  $R < 70$  km and both terms for  $R > 70$  km (EPRI, 1993; Toro et al., 1997). The  $c_5$  expression accommodates crustal effects incorporated in the source models. The epicentral distance  $R$  is used in the  $c_5$  term rather than the equivalent distance  $R_M$  because  $R$  provided better fit to the simulations. The  $c_6$  expression models anelastic attenuation. The exponential term in Equation 3.21 accounts for the exponential magnitude dependence of the energy released by an earthquake (Douglas, 2003).

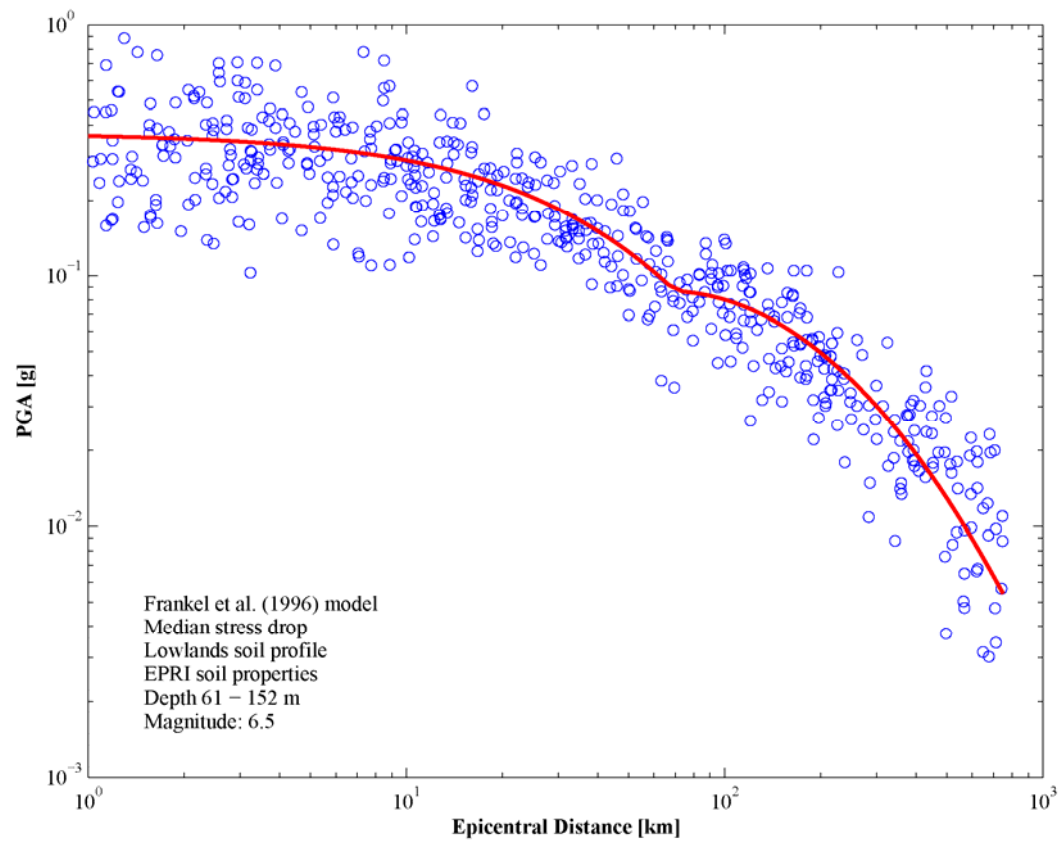
Figure 3.21 through Figure 3.26 show samples of peak ground acceleration and 1-second spectral acceleration simulations along with the proposed attenuation relationship equation for the three source models considered in this study. In general, the model fits the central trends of the simulations and captures the crustal reflections at about  $R = 70$  km for the Atkinson and Boore (1995) and Frankel et al. (1996) models due to their geometrical attenuation function shown in Figure 3.7. The Silva et al. (2003) model uses a bilinear model for the geometrical attenuation function, as shown in Figure 3.7, that smoothes the crustal reflections (Cramer, 2006a) and yet the same functional form captures the behavior of the simulations.

Figure 3.27 through Figure 3.29 show examples of normalized residuals (i.e. the simulated value minus the predicted value divided by the standard deviation (Campbell, 1997)) for 1-second spectral acceleration as a function of epicentral distance, and Figure 3.30 through Figure 3.32 show samples of normalized residuals for the same spectral period as a function of moment magnitude. Solid circles show mean residuals and one standard deviation in distance and magnitude bins. The entire epicentral distance range was subdivided into ten equally spaced (in logarithmic units) distance bins. The mean residual was calculated for each bin and plotted at the epicentral distance corresponding to the midpoint in each bin. Figure 3.33 through Figure 3.38 show the normalized PGA residuals for all stress drop cases, soil profiles, and depth bins as a function of epicentral distance and magnitude. These figures show that the attenuation equation does not systematically over- or under-predict ground motion amplitudes, and therefore the proposed model is in general unbiased for the entire range of epicentral distances and magnitudes considered in the analyses.

Figure 3.39 through Figure 3.41 show samples of the estimation of the total aleatory variability. The modeling variability is taken from Silva et al. (1997) and the parametric variability is calculated from the regression analysis. Independence is assumed between the modeling and parametric variability, and therefore the total



**Figure 3.21.** Example of simulations and attenuation relationship for PGA using the Atkinson and Boore (1995) model



**Figure 3.22.** Example of simulations and attenuation relationship for PGA using the Frankel et al. (1996) model

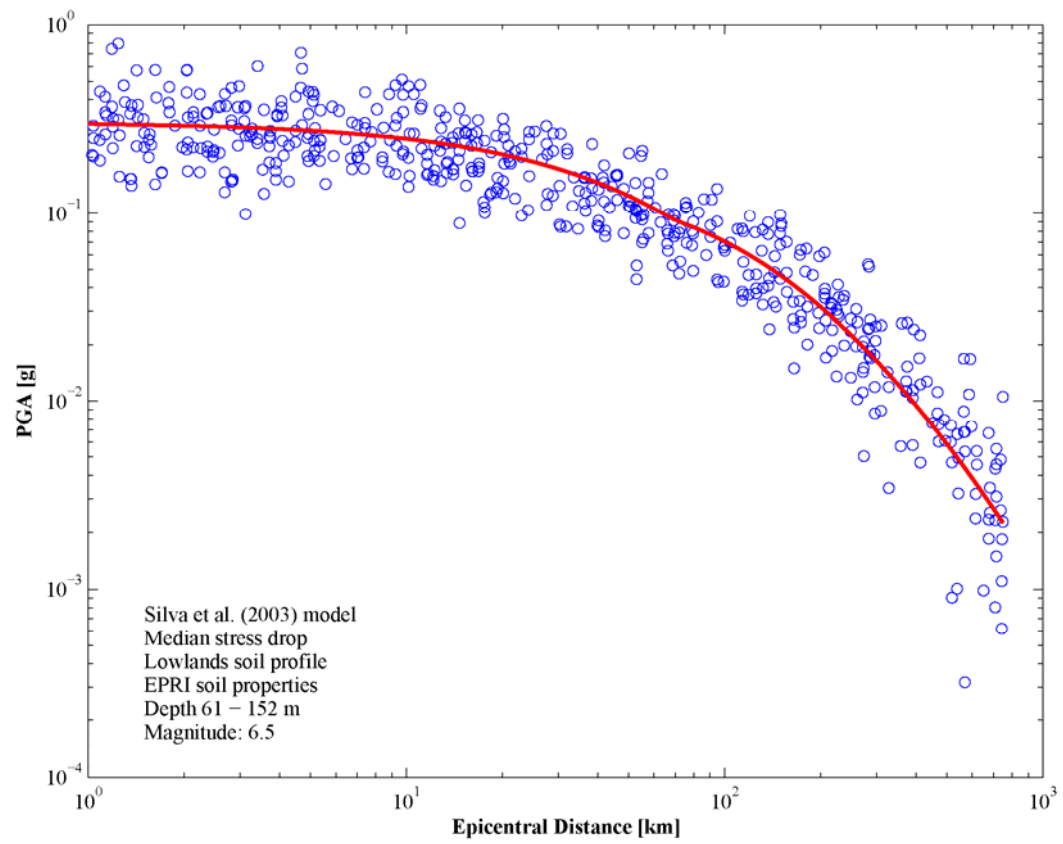


**Figure 3.23.** Example of simulations and attenuation relationship for PGA using the Silva et al. (2003) model

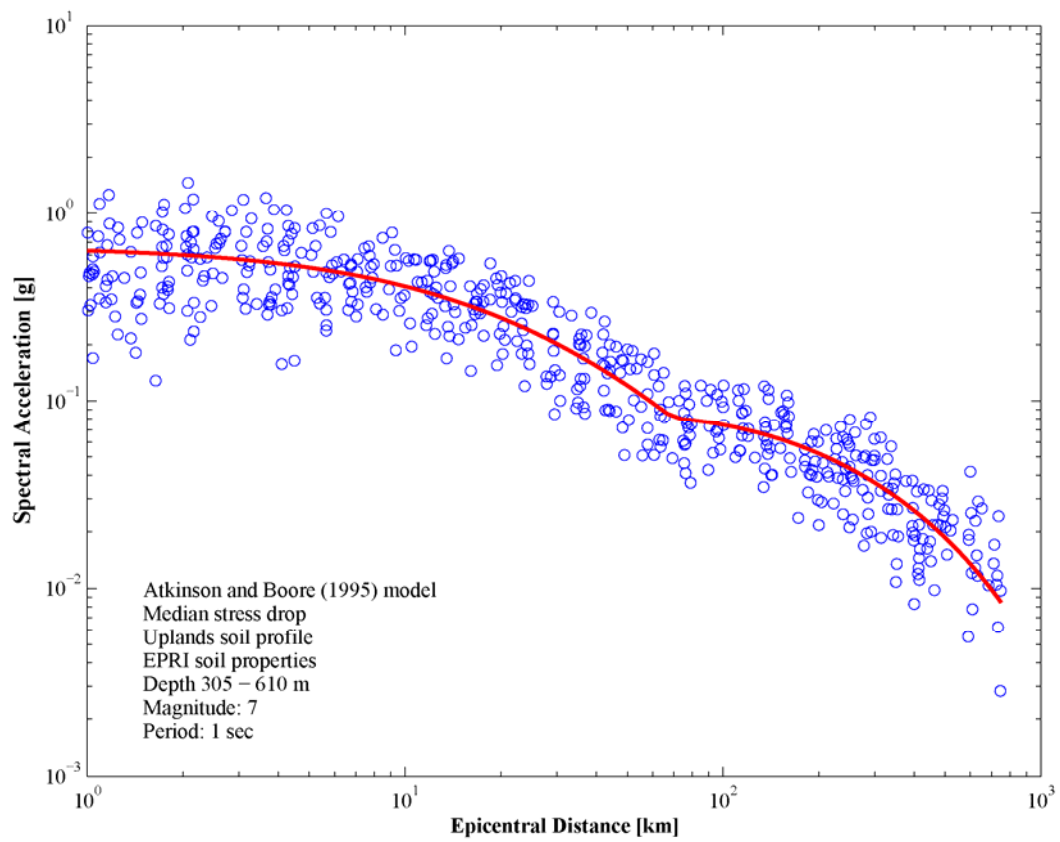


**Figure 3.24.** Example of simulations and attenuation relationship for 1-second spectral acceleration using the Atkinson and Boore (1995) model

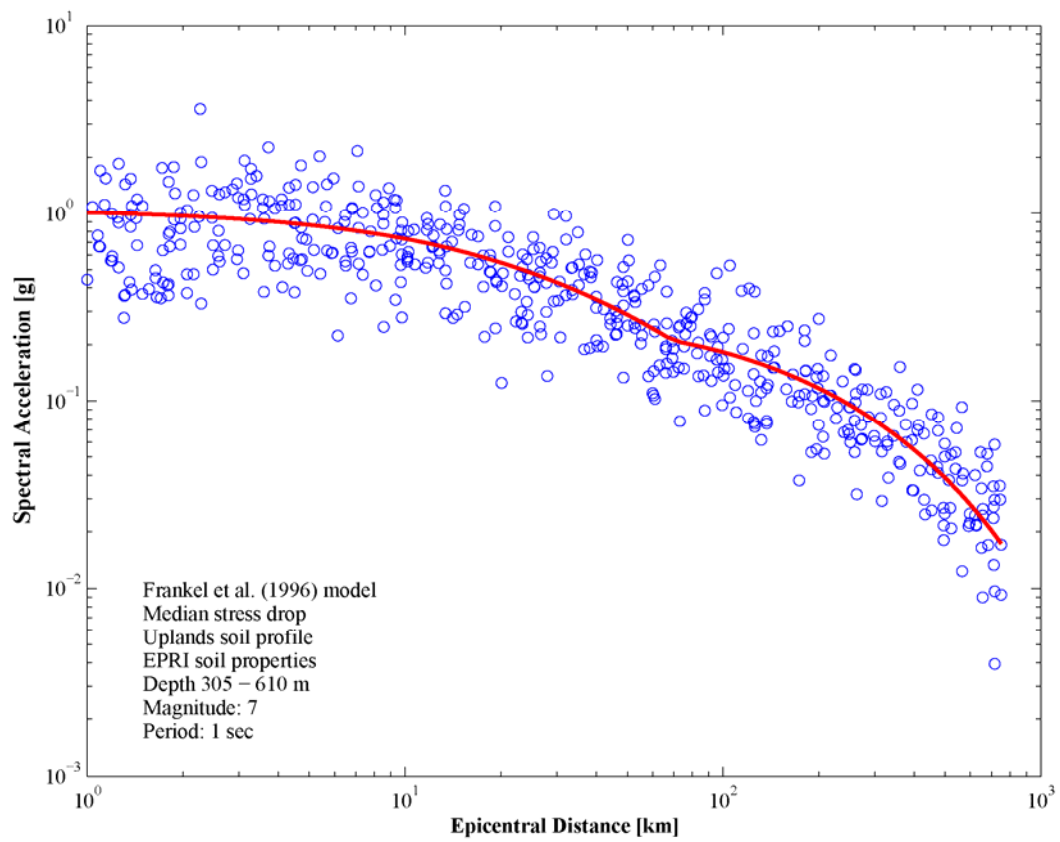


**Figure 3.25.** Example of simulations and attenuation relationship for 1-second spectral acceleration using the Frankel et al. (1996) model

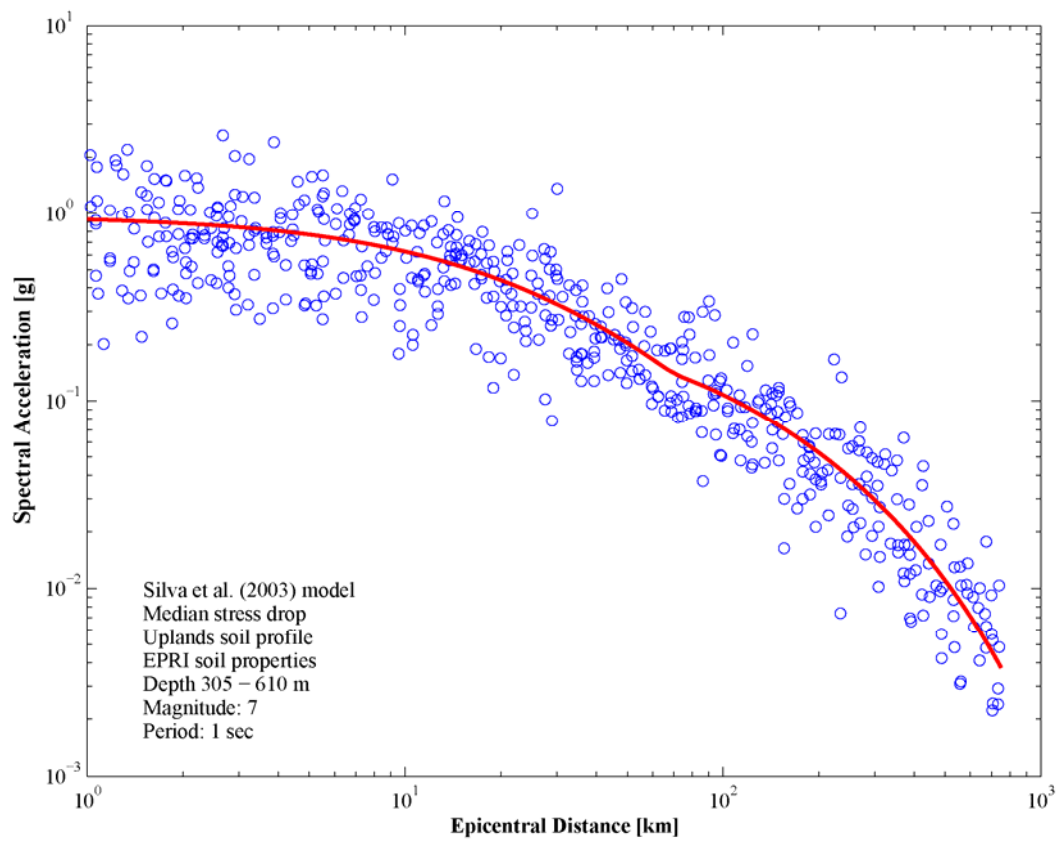


**Figure 3.26.** Example of simulations and attenuation relationship for 1-second spectral acceleration using the Silva et al. (2003) model

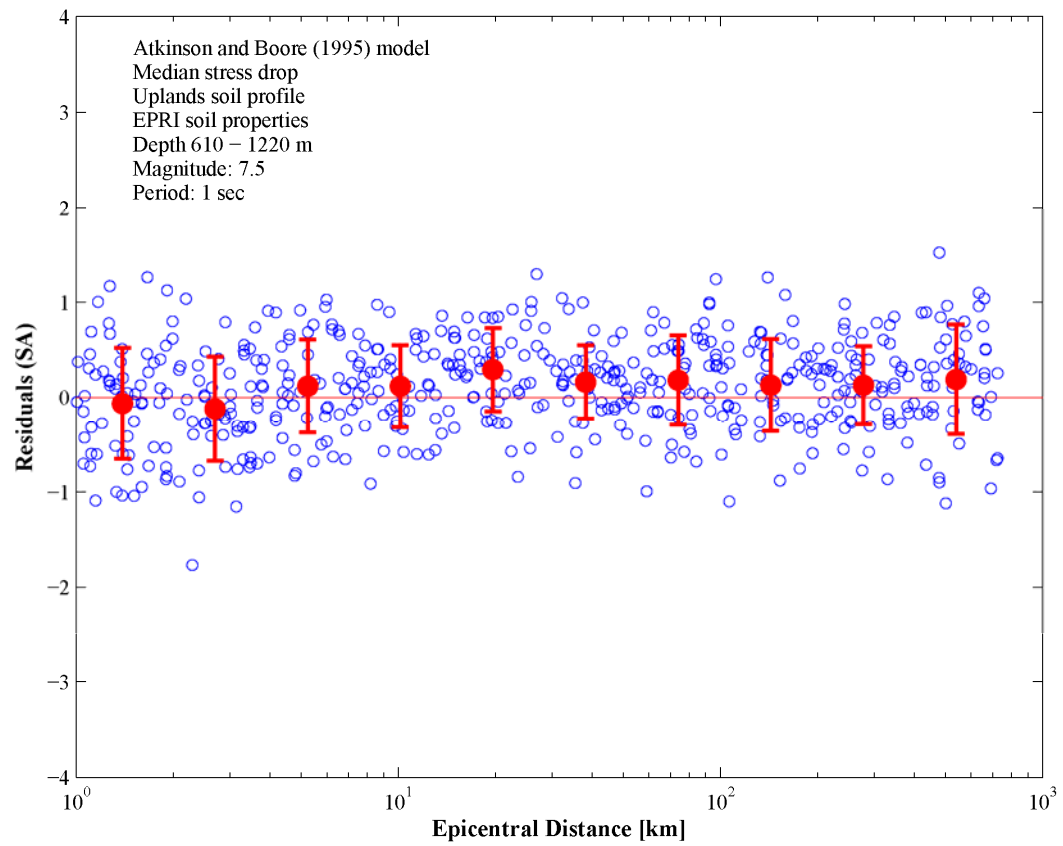


**Figure 3.27.** Normalized residuals of 1-second spectral accelerations vs. epicentral distance for the Atkinson and Boore (1995) model

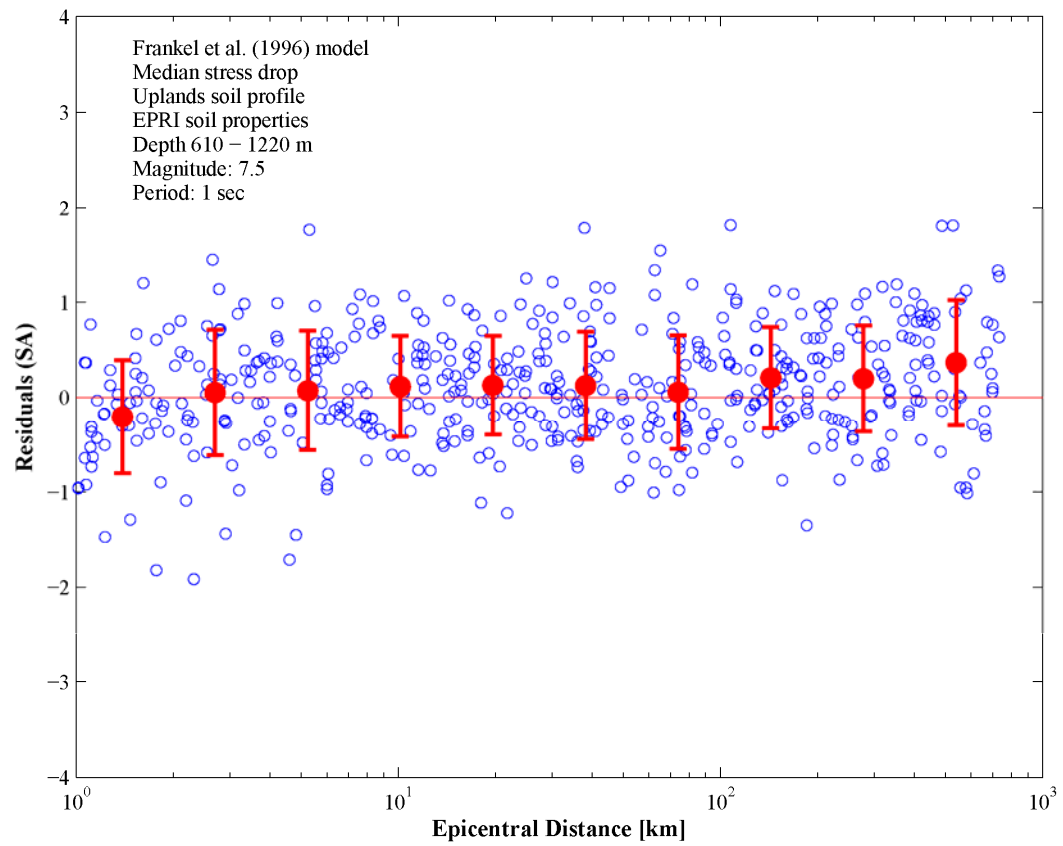


**Figure 3.28.** Normalized residuals of 1-second spectral accelerations vs. epicentral distance for the Frankel et al. (1996) model

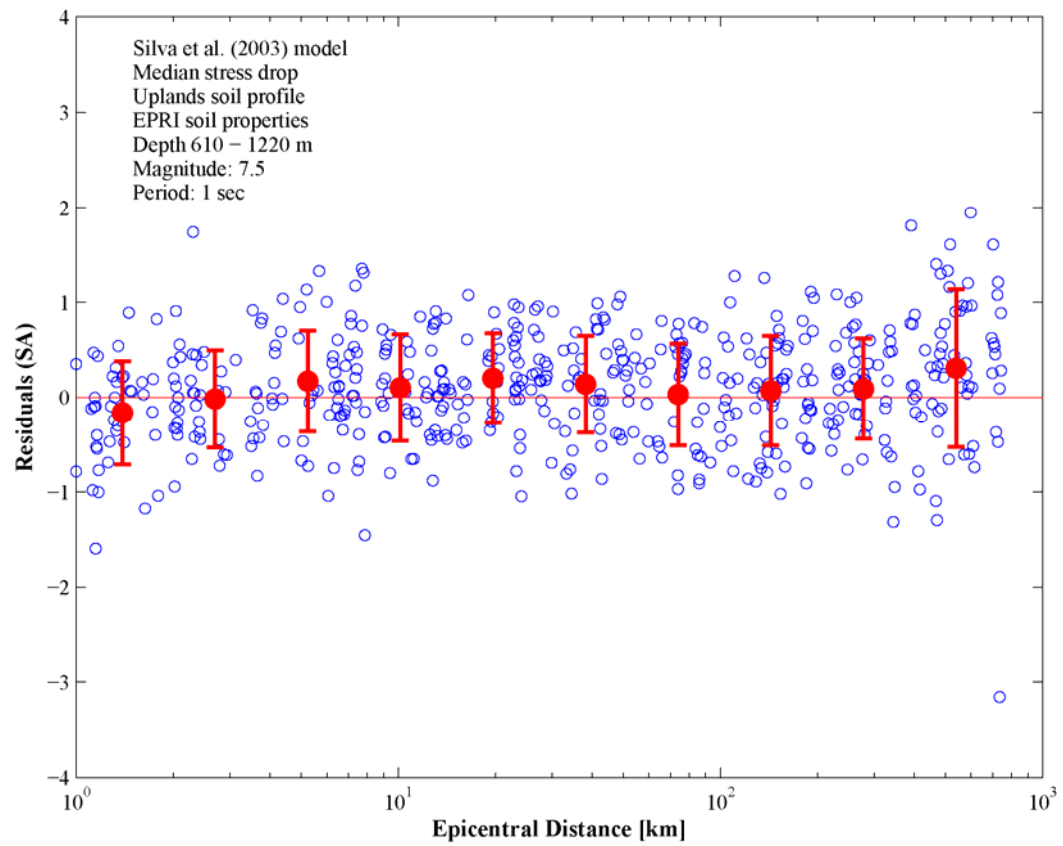


**Figure 3.29.** Normalized residuals of 1-second spectral accelerations vs. epicentral distance for the Silva et al. (2003) model

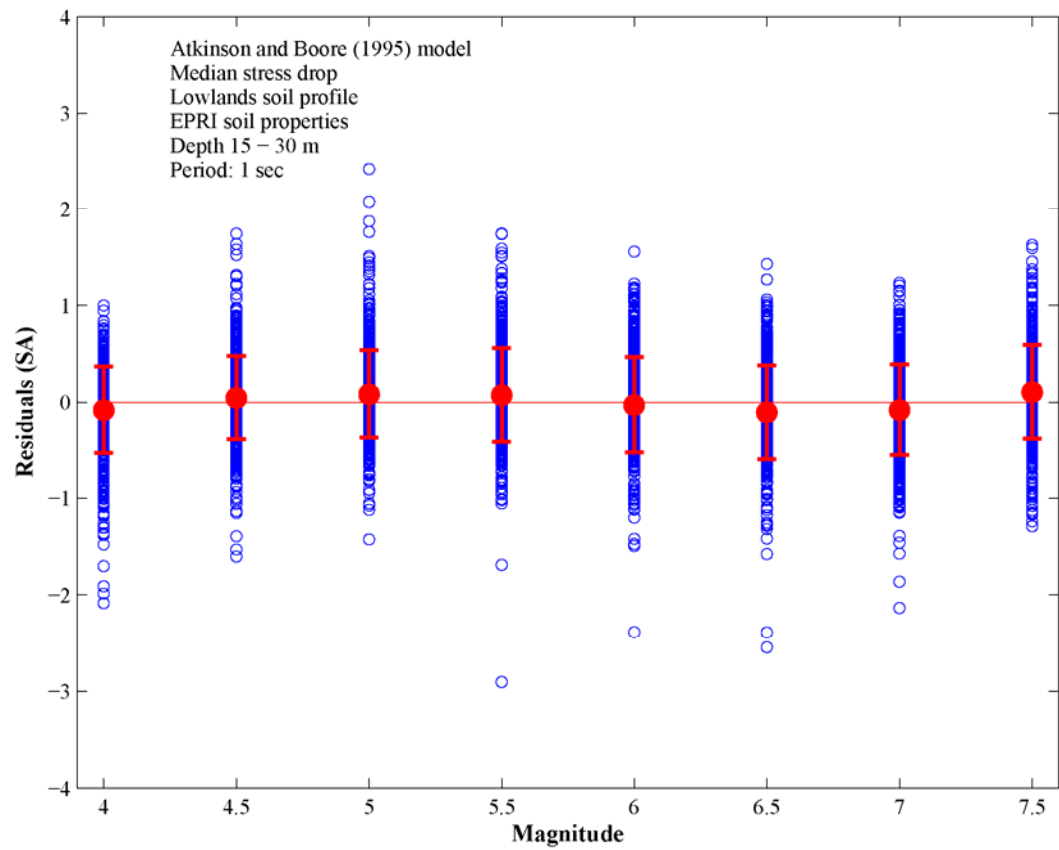


**Figure 3.30.** Normalized residuals of 1-second spectral accelerations vs. magnitude for the Atkinson and Boore (1995) model

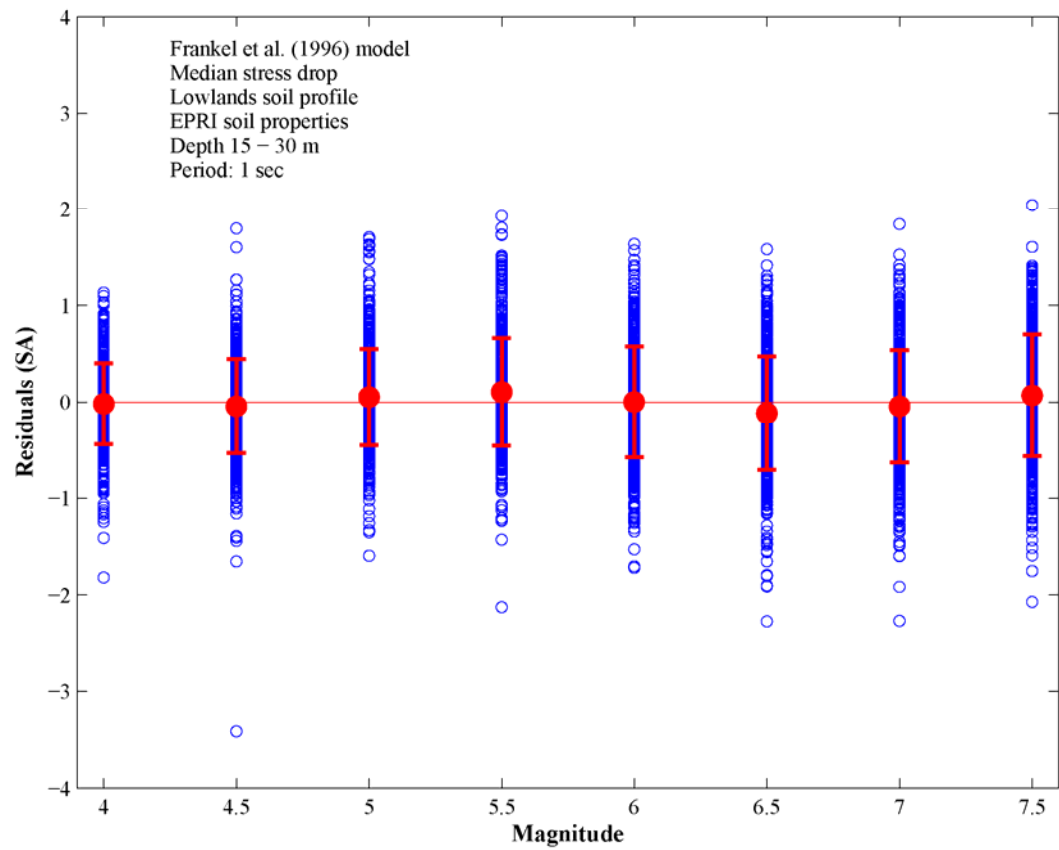


**Figure 3.31.** Normalized residuals of 1-second spectral accelerations vs. magnitude for the Frankel et al. (1996) model

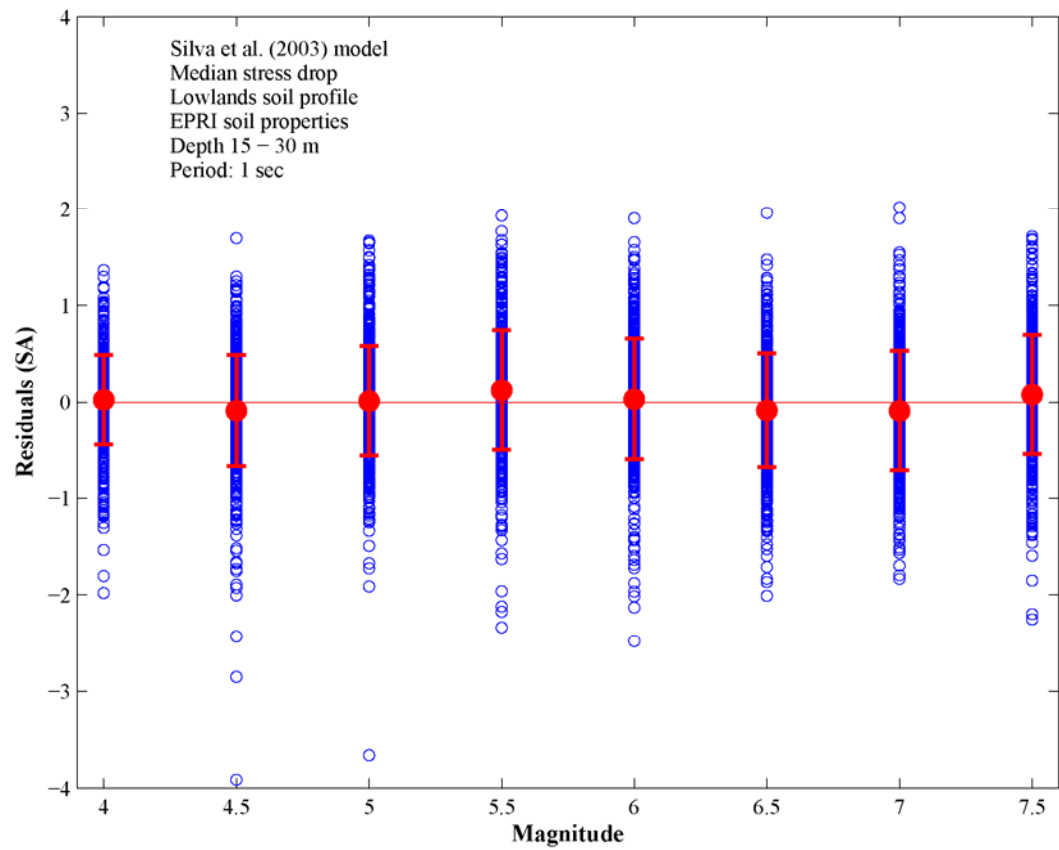


**Figure 3.32.** Normalized residuals of 1-second spectral accelerations vs. magnitude for the Frankel et al. (1996) model

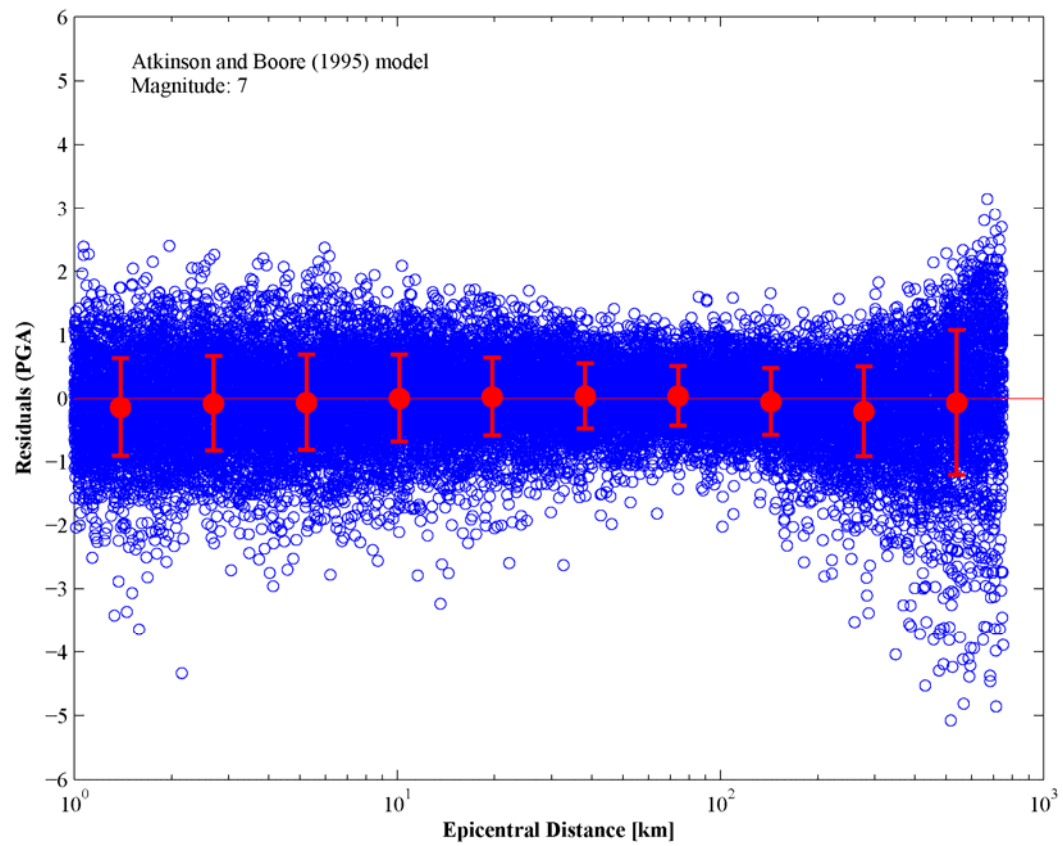


**Figure 3.33.** Normalized residuals of PGA vs. epicentral distance for the Atkinson and Boore (1995) model

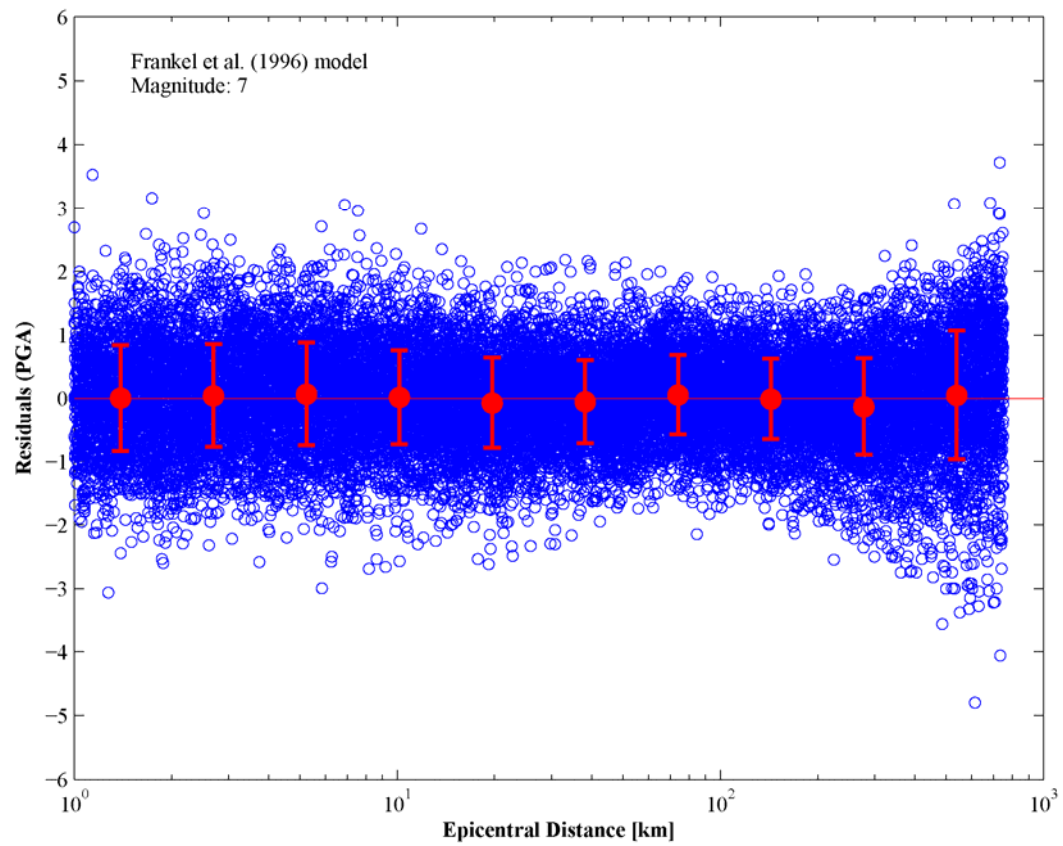


**Figure 3.34.** Normalized residuals of PGA vs. epicentral distance for the Frankel et al. (1996) model

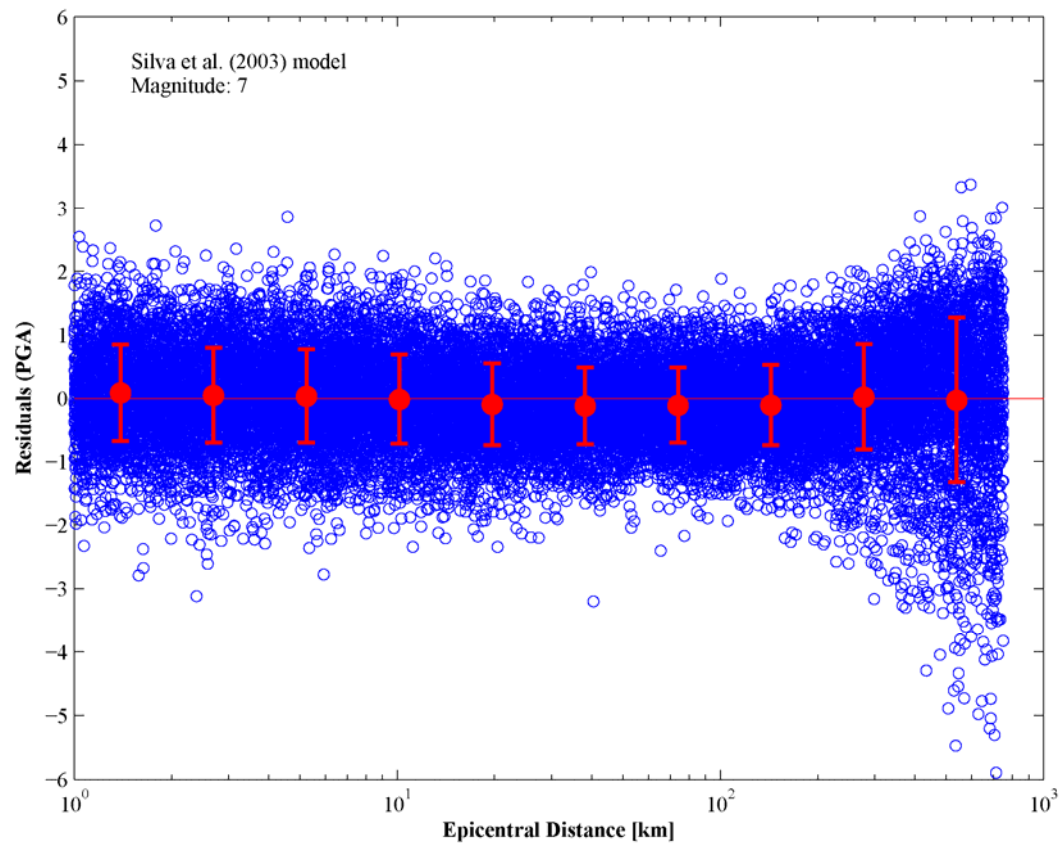


**Figure 3.35.** Normalized residuals of PGA vs. epicentral distance for the Silva et al. (2003) model

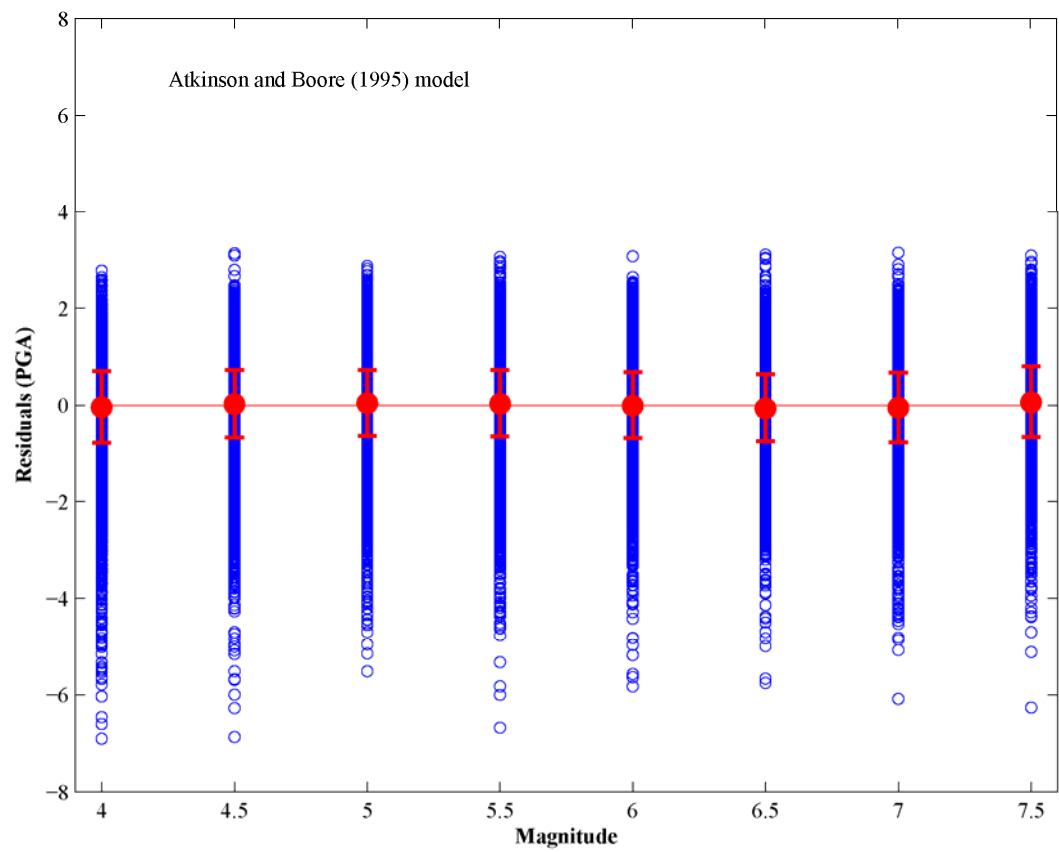


**Figure 3.36.** Normalized residuals of PGA vs. magnitude for the Atkinson and Boore (1995) model

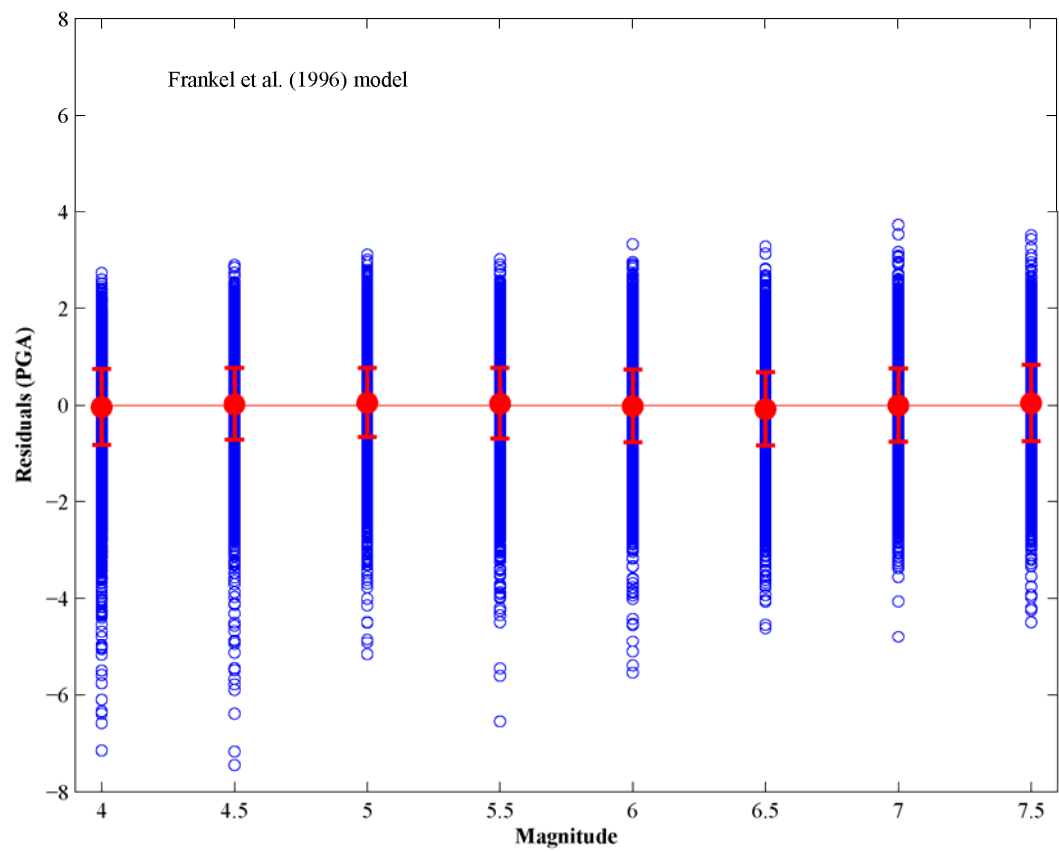


**Figure 3.37.** Normalized residuals of PGA vs. magnitude for the Frankel et al. (1996) model

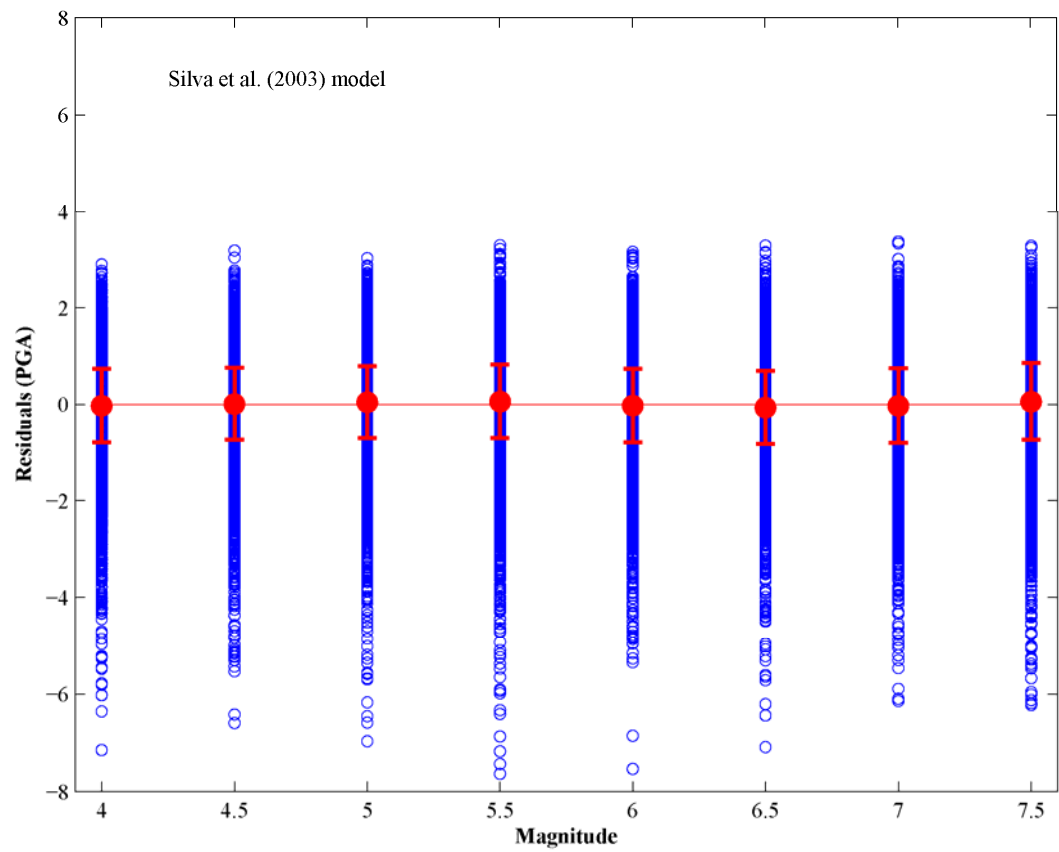


**Figure 3.38.** Normalized residuals of PGA vs. magnitude for the Silva et al. (2003) model

variability is calculated simply as the sum of the variances. The modeling variability corresponds to the one-corner source model, since the two-corner model was not available when the stochastic method validation was performed (Silva et al., 1997). Using this modeling variability for the two-corner-frequency model is considered conservative since this model provides a better fit to CEUS ground motions than the one-corner-frequency model (Silva and Costantino, 2002; Silva et al., 2003). The one-corner point-source model tends to overpredict low-frequency motions at large magnitudes, which is reflected in the higher modeling variability at long periods (EPRI, 1993; Silva et al., 2003).

The stress drop directly scales the ground motion amplitudes at short periods or high frequencies above the corner frequency and, as discussed previously, it is the parameter that most contributes to ground motion uncertainty. This high contribution of the stress drop to ground motion variability particularly at short and intermediate periods causes the decrease of parametric variability at long periods observed in Figure 3.39 through Figure 3.41. This conclusion is supported by Figure 3.42 through Figure 3.44, which show parametric variability as a function of period for **M** 4 and **M** 7. Circles indicate the corner frequency for each curve. Parametric variability starts to decrease more rapidly at periods close to the corner frequency.

Figure 3.42 through Figure 3.44 also illustrate the reduction in parametric variability at short periods as the level of ground motion increases. This observation is consistent with the negative correlation between rock ground motions and soil response variability observed in real records due to the non-linear response of the soil column (Bazzurro and Cornell, 2004a; Campbell and Bozorgnia, 2006; EPRI, 1993; Toro et al., 1997). This result suggests that the effect of the non-linear response is to reduce the variability of soil ground motions and compensate for the additional variability due to variations of soil properties (EPRI, 1993; Toro et al., 1997).

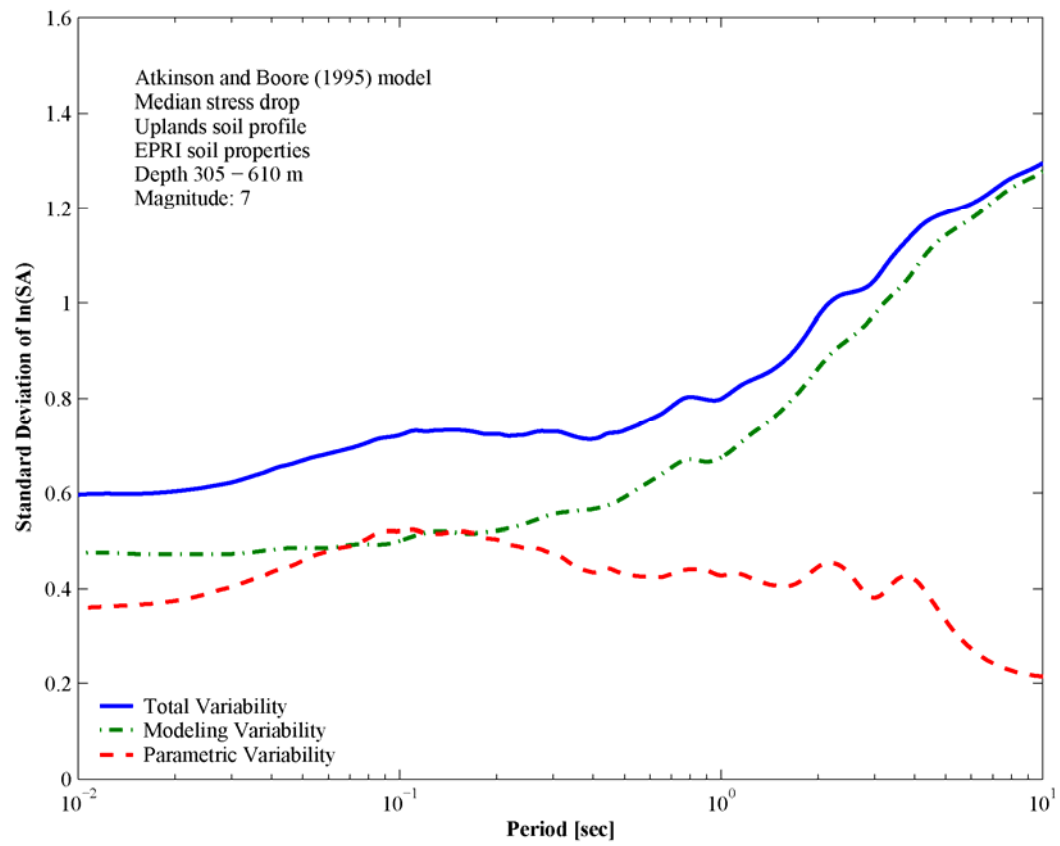


**Figure 3.39.** Example of total aleatory variability for the Atkinson and Boore (1995) model

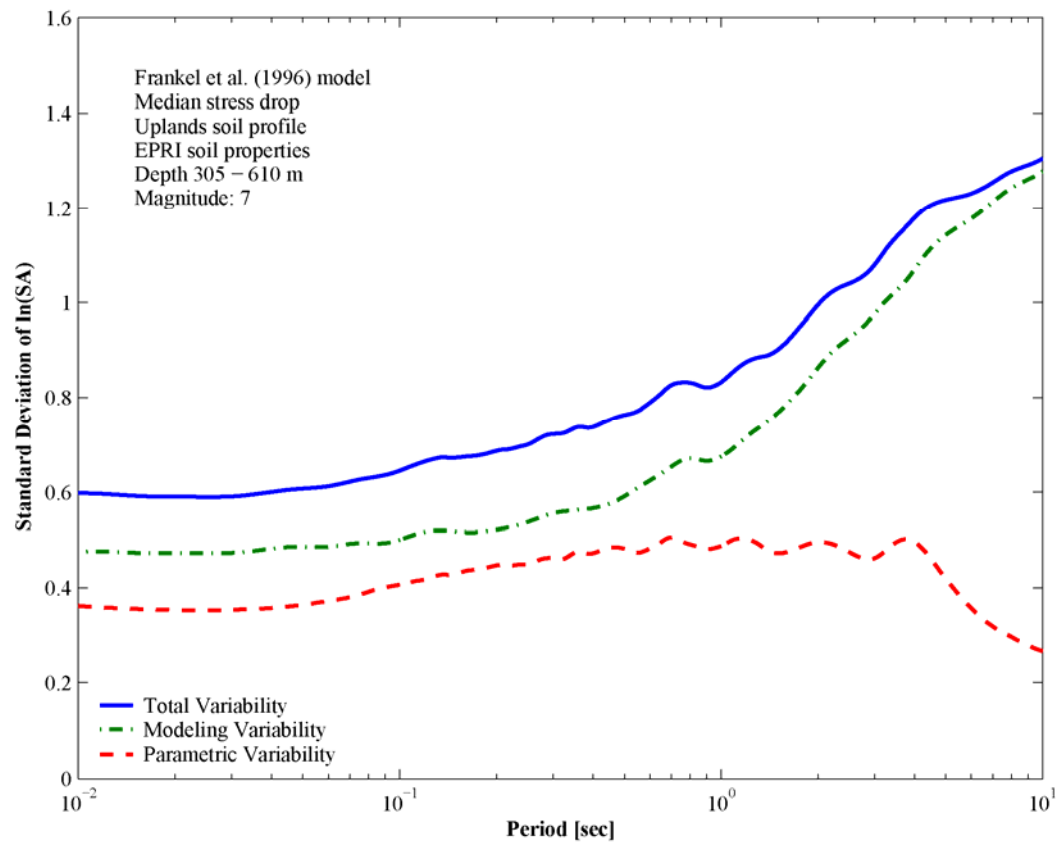


**Figure 3.40.** Example of total aleatory variability for the Frankel et al. (1996) model

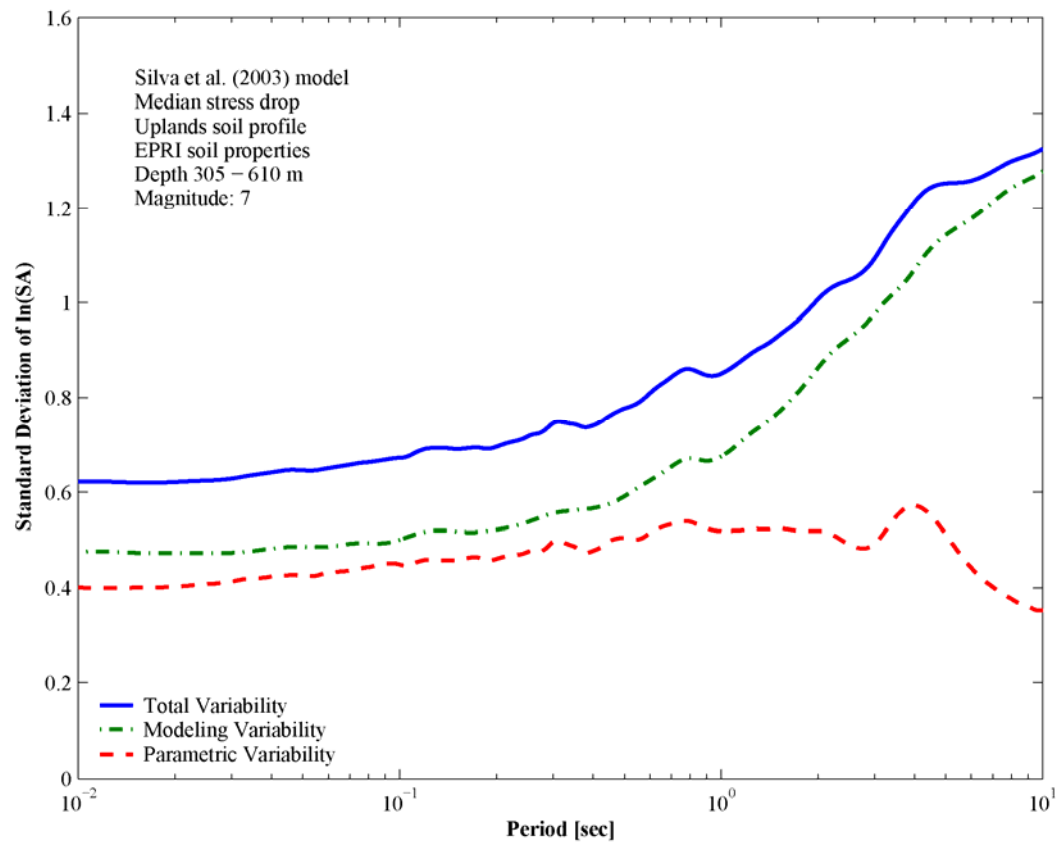


**Figure 3.41.** Example of total aleatory variability for the Silva et al. (2003) model

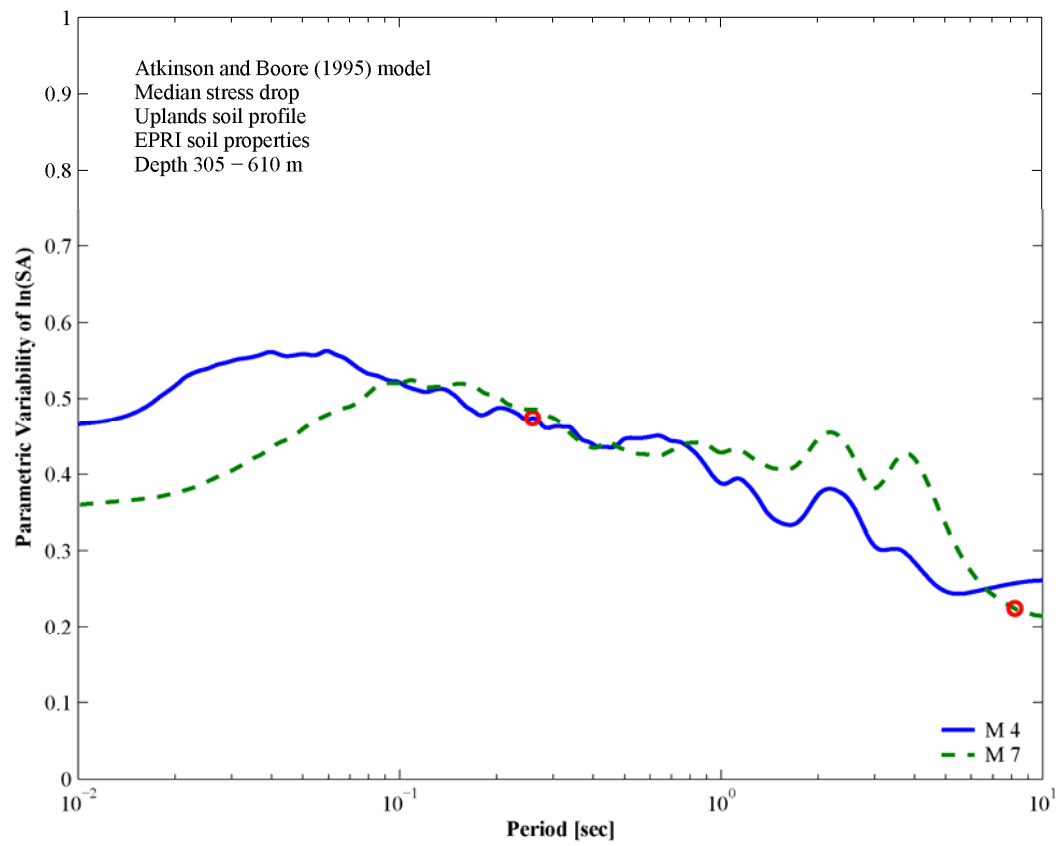


**Figure 3.42.** Example of parametric variability for M 4 and M 7 using the Atkinson and Boore (1995) model

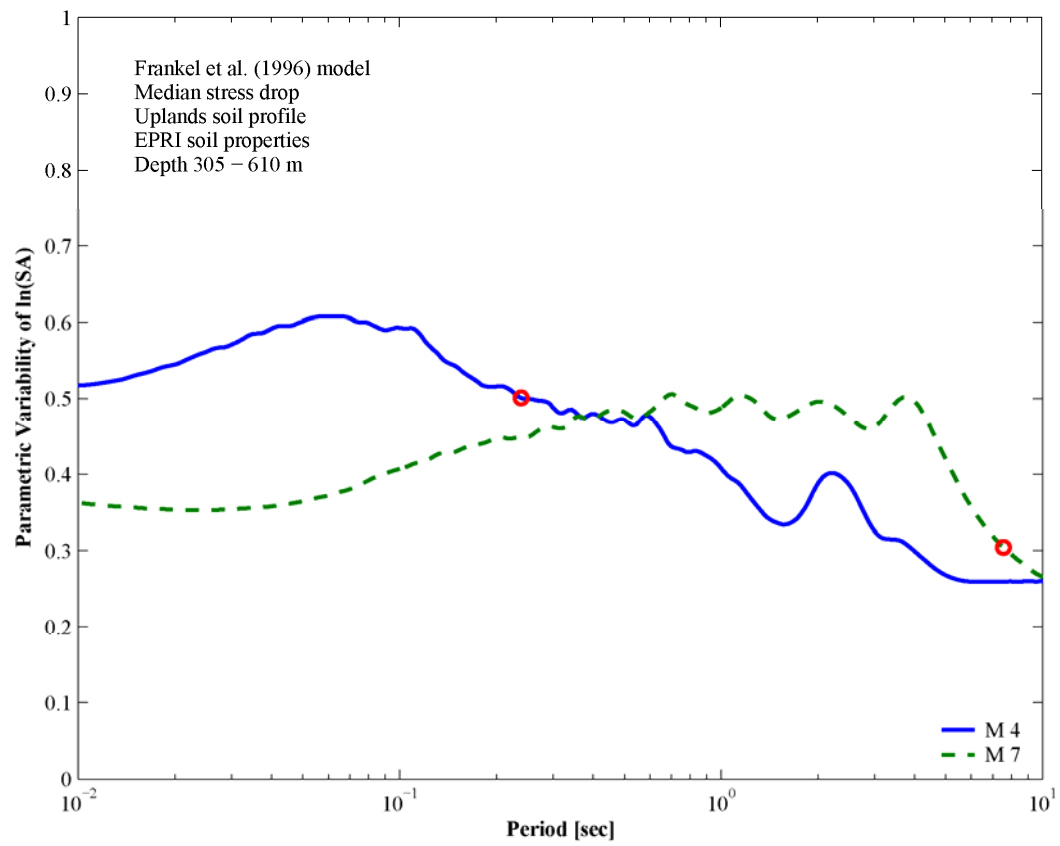


**Figure 3.43.** Example of parametric variability for M 4 and M 7 using the Frankel et al. (1996) model

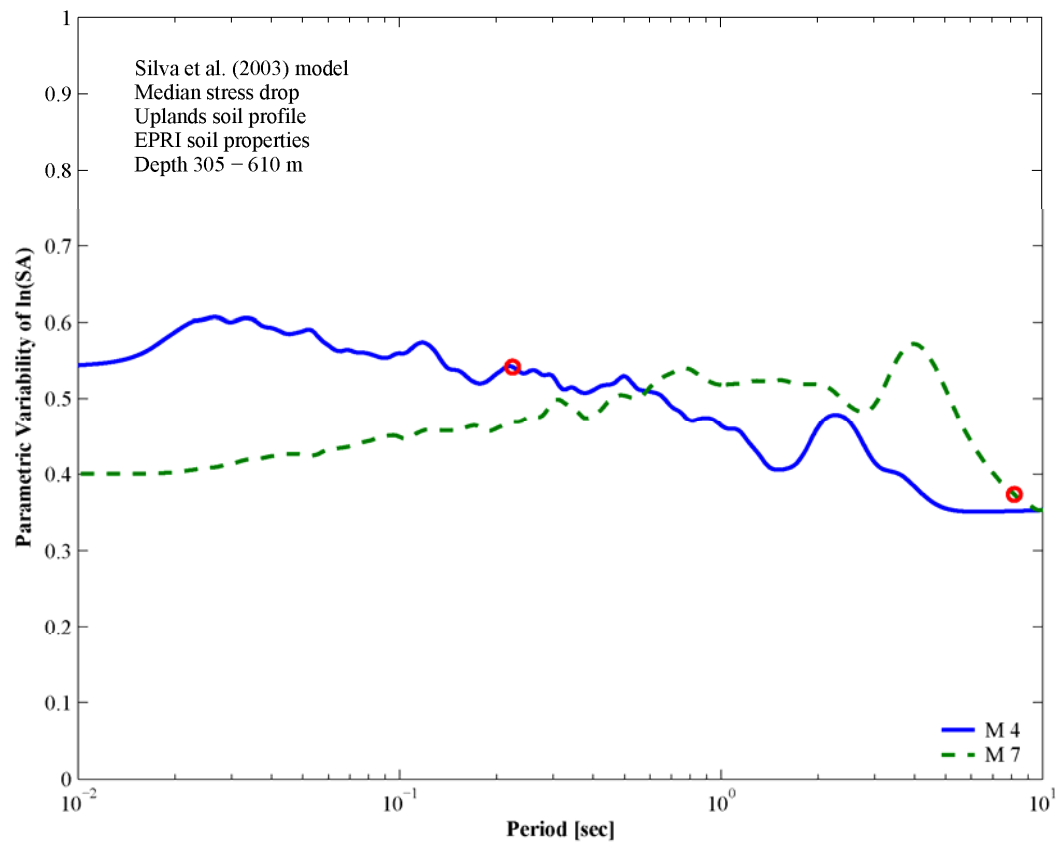


**Figure 3.44.** Example of parametric variability for M 4 and M 7 using the Silva et al. (2003) model

Figure 3.45 through Figure 3.47 compare the parametric variability with embayment depth. Shallow profiles exhibit higher variability at short periods whereas the variability is higher for deep profiles at long periods. The importance of this observation is discussed later when ground motion amplitudes are compared with embayment depth.

In this study the total aleatory variability is considered to be magnitude-dependent as expressed by Equation 3.22. Previous studies have also considered the aleatory variability dependent on the magnitude of the earthquake (e.g. Abrahamson and Silva, 1997; Campbell, 2003b). Figure 3.48 through Figure 3.50 show the total aleatory variability as function of magnitude for different spectral periods. The aleatory variability slightly changes with magnitude, particularly for magnitudes above 5, and this tendency is independent of source model. This observation is consistent with recent findings of the Next Generation Attenuation model (NGA) project where aleatory variability is considered to be independent of magnitude (Boore and Atkinson, 2006; Campbell and Bozorgnia, 2006; Chiou and Youngs, 2006). The simple linear relationship considered herein between aleatory variability and magnitude can capture reasonably well a constant or a linear trend.

Figure 3.51 and Figure 3.52 show the parametric variability as a function of magnitude for PGA and 1-second spectral acceleration. In general the Atkinson and Boore (1995) model has the lowest parametric variability throughout the entire magnitude range considered. This difference might be a consequence of the fact that the stress drop is not a parameter in this model. Previous studies have used the parametric variability of the one-corner model with variable stress drop for the two-corner model in order to not underestimate its total aleatory variability (Silva et al., 2003). As shown in Figure 3.48 through Figure 3.50, when the modeling variability is added to the parametric variability, the difference between the one- and two-corner models is not significant, and therefore the variability computed for each model was used in this study.

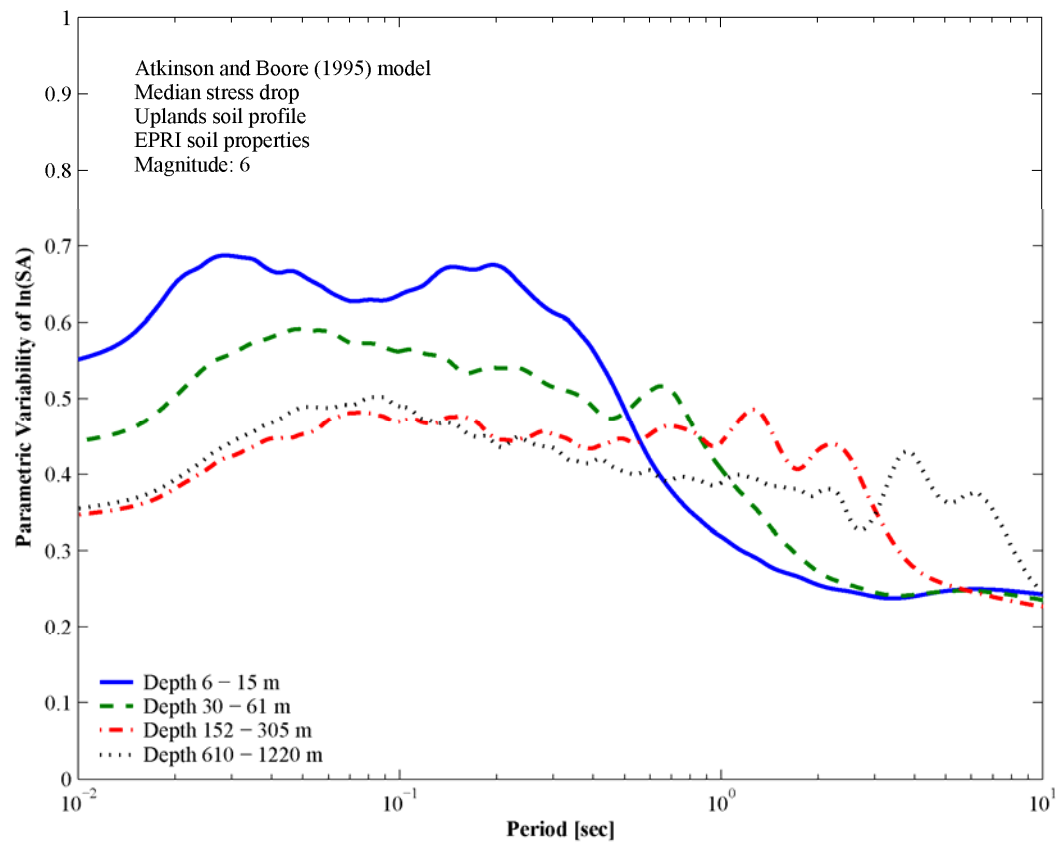


**Figure 3.45.** Example of parametric variability vs. embayment depth for the Atkinson and Boore (1995) model

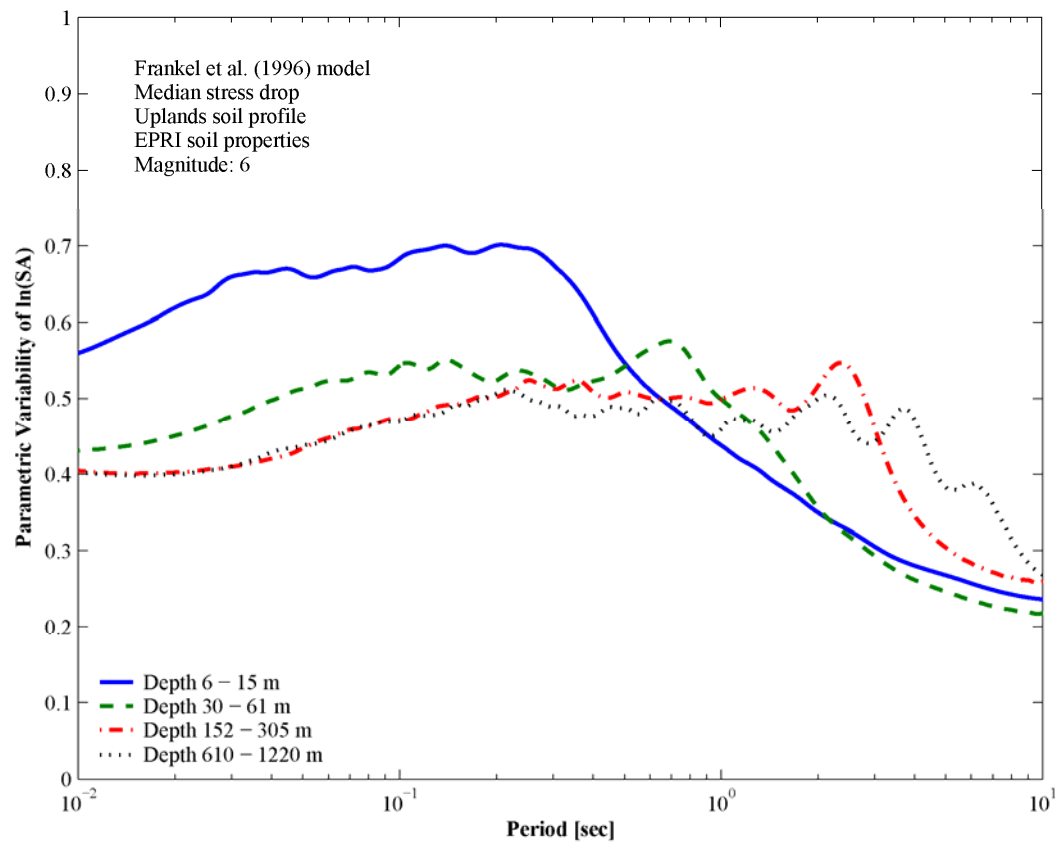


**Figure 3.46.** Example of parametric variability vs. embayment depth for the Frankel et al. (1996) model

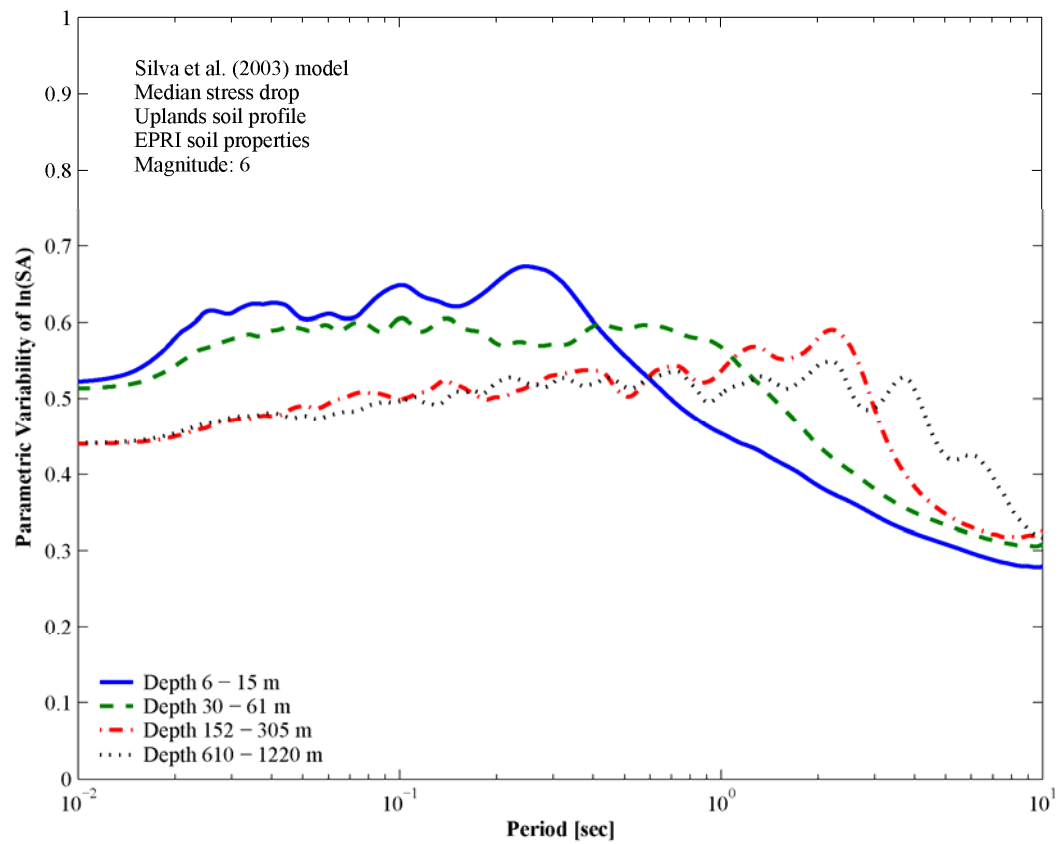


**Figure 3.47.** Example of parametric variability vs. embayment depth for the Silva et al. (2003) model

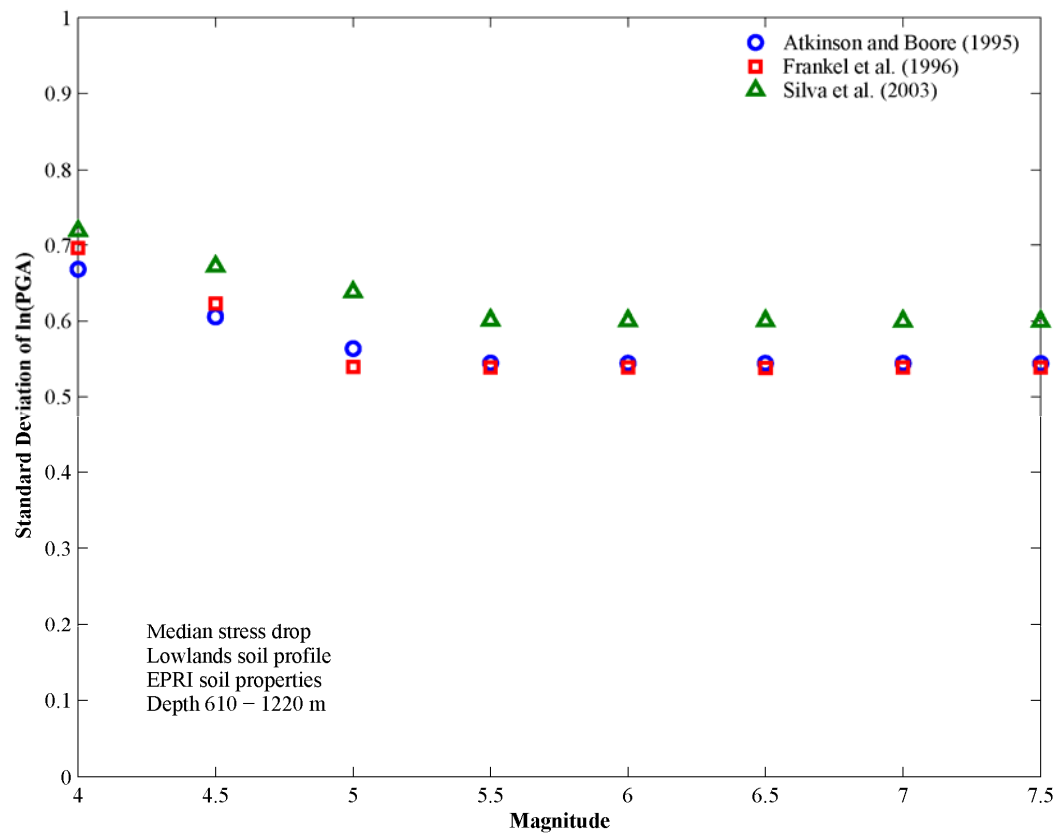


**Figure 3.48.** Total aleatory variability of PGA vs. magnitude

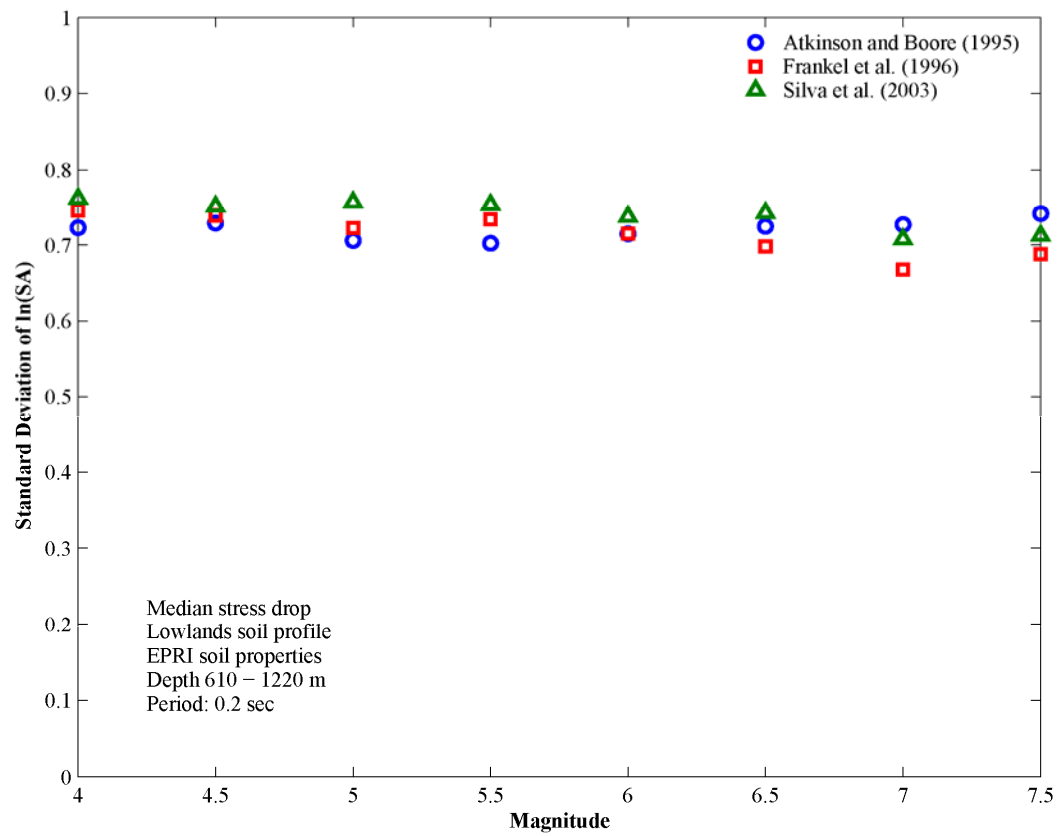


**Figure 3.49.** Total aleatory variability of 0.2-seconds spectral acceleration vs. magnitude

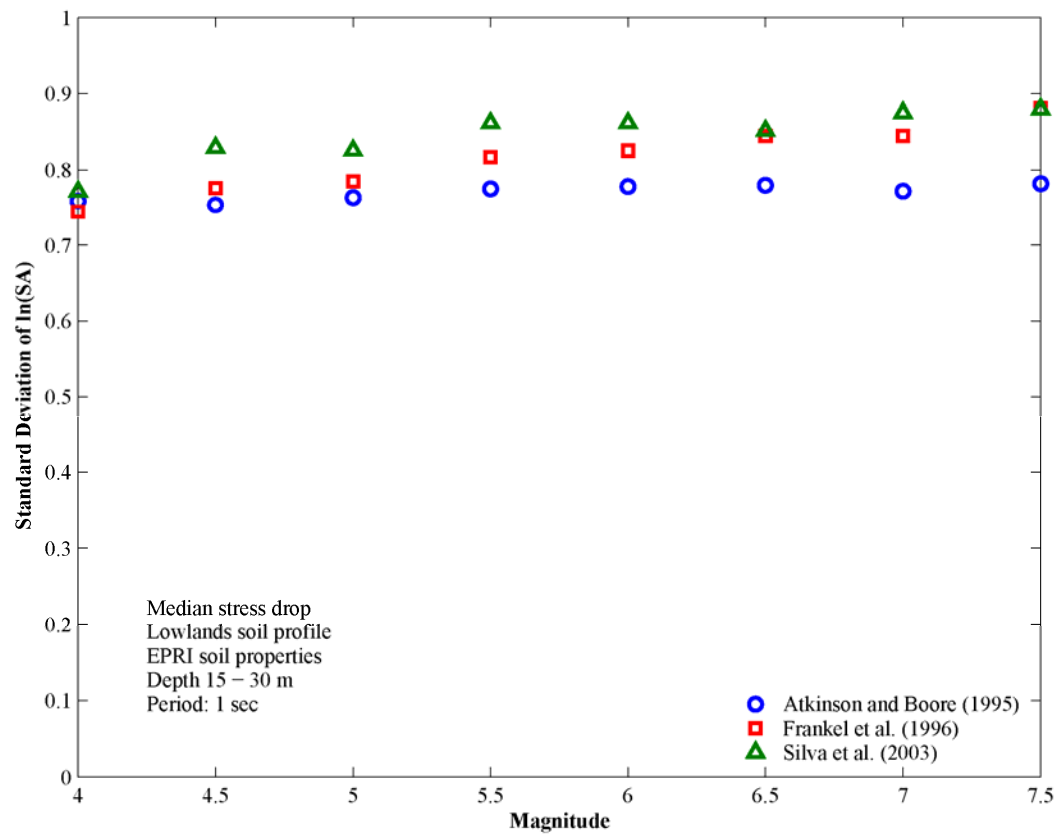


**Figure 3.50.** Total aleatory variability of 1-second spectral acceleration vs. magnitude

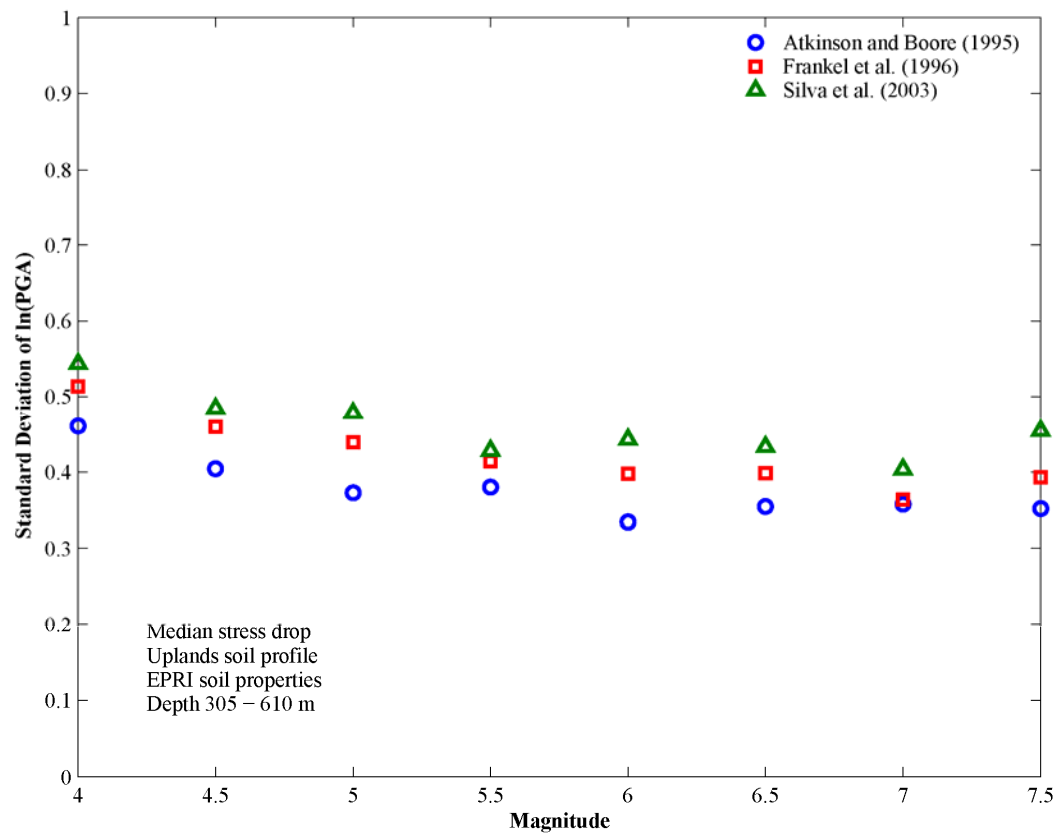


**Figure 3.51.** Parametric variability of PGA vs. magnitude

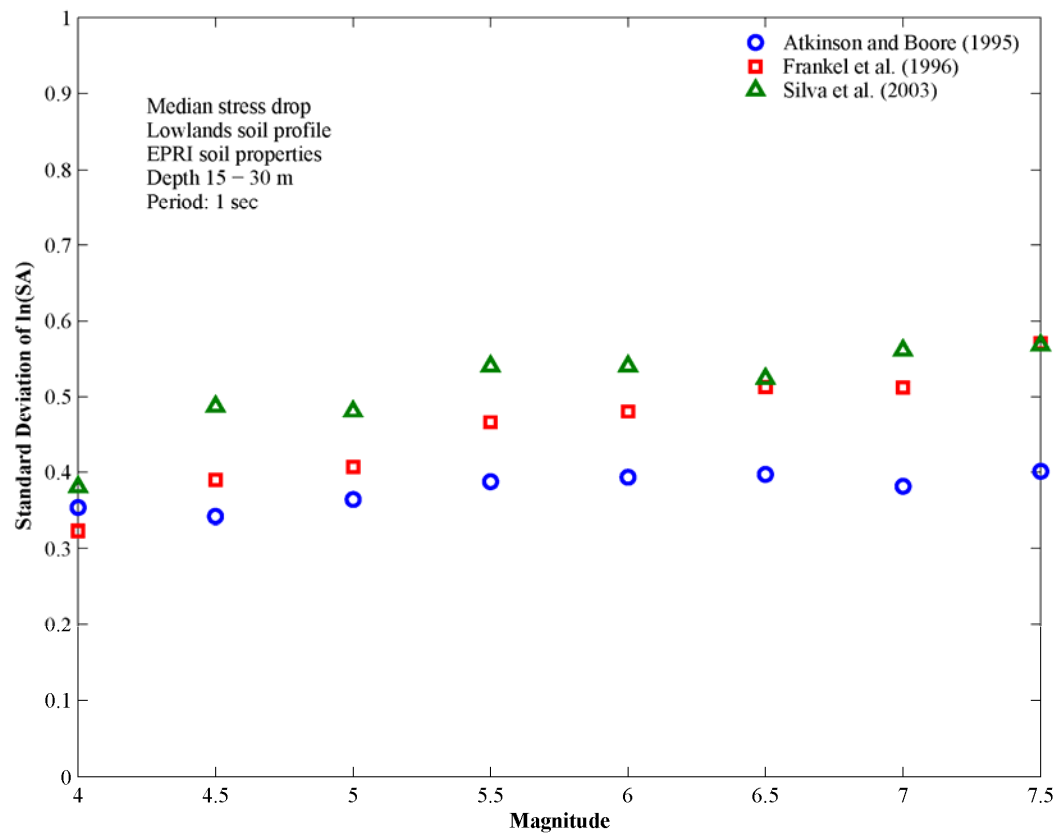


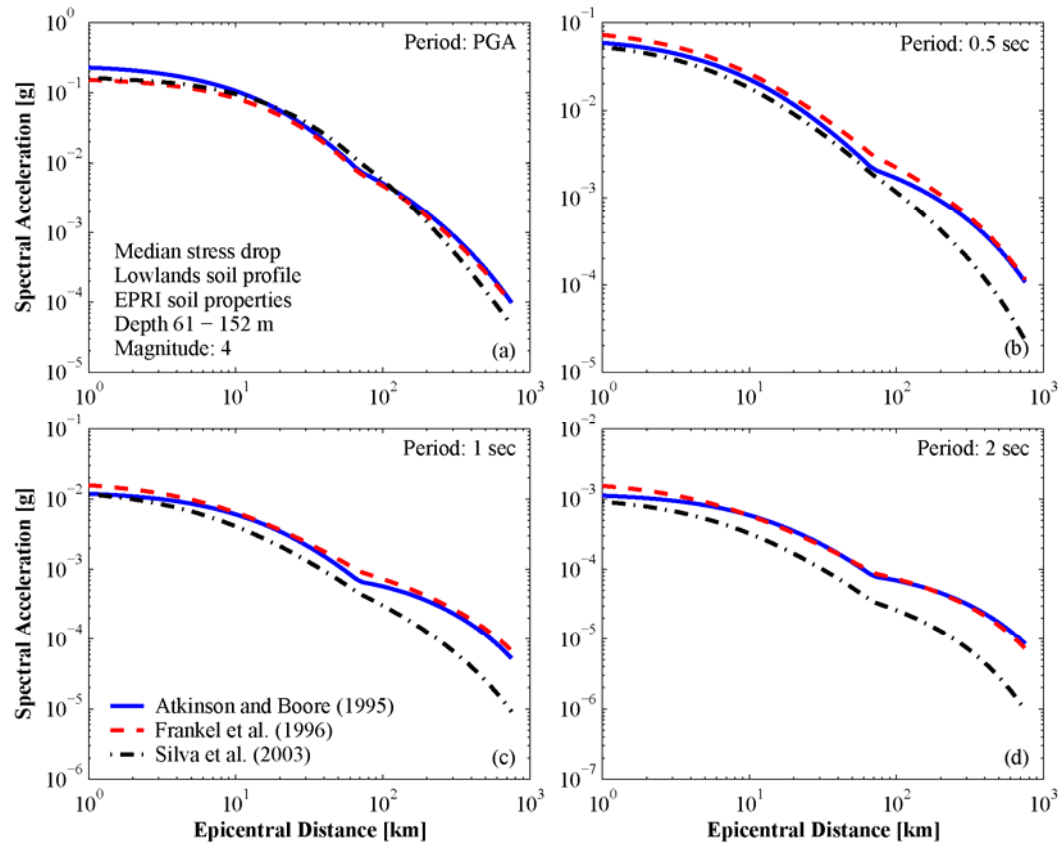
**Figure 3.52.** Parametric variability of 1-second spectral acceleration vs. magnitude

### 3.7. Discussion of Results

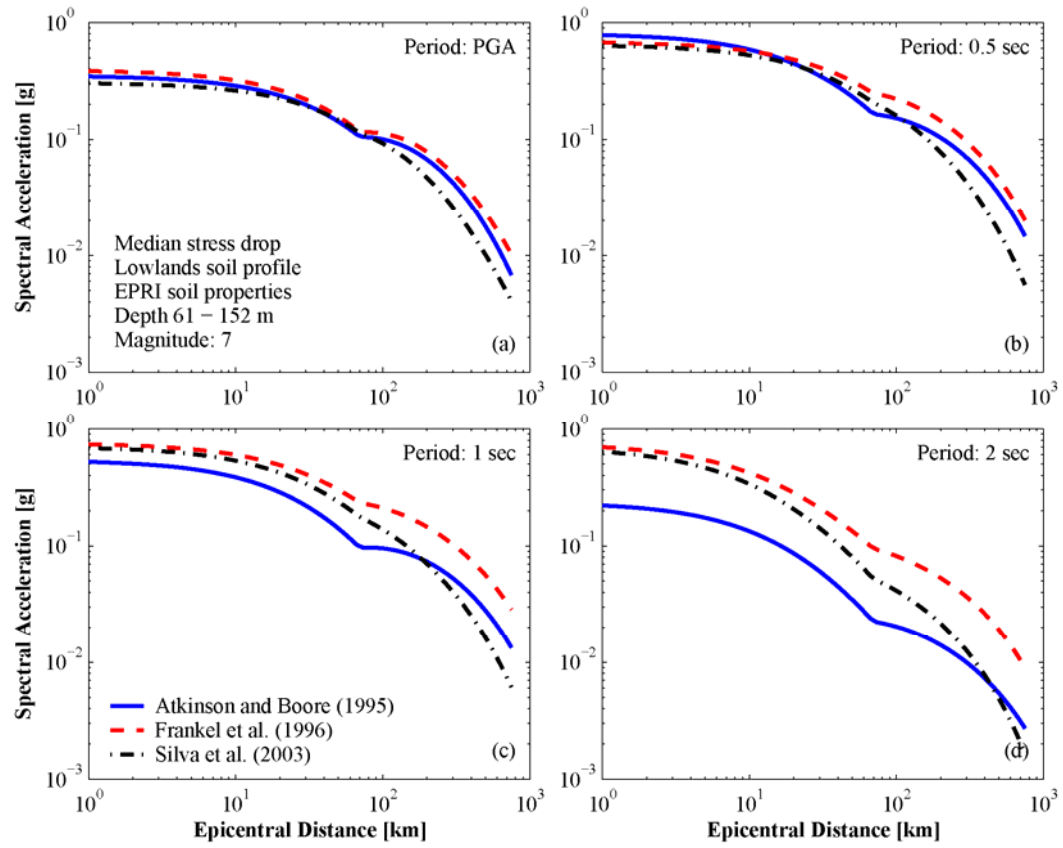
Most of the Fourier and response spectra shown in this section are plotted as a function of frequency. This facilitates the discussion of the results by comparing them directly with the parameters of the source models that are usually frequency dependent.

Figure 3.53 and Figure 3.54 compare the attenuation of spectral acceleration with epicentral distance for **M** 4 and **M** 7, and for different spectral periods and source models. The Atkinson and Boore (1995) and Frankel et al. (1996) models predict similar attenuation of ground motion amplitude with distance since both models use the same geometrical and anelastic attenuation functions. The Silva et al. (2003) model uses a magnitude-dependent geometrical spreading model with geometrical attenuation increasing with decreasing magnitude. Figure 3.7 and Figure 3.8 show the geometrical spreading and seismic attenuation functions implemented in the three source models. For epicentral distances shorter than 70 km, all models use a similar geometrical attenuation, with slightly lower values for small magnitudes in the Silva et al. (2003) model. For longer distances, the bilinear model implemented in Silva et al. (2003) uses a higher attenuation compared to the trilinear model used in the Atkinson and Boore (1995) and Frankel et al. (1996) models for distances greater than 130 km. Furthermore, as shown in Figure 3.8, the anelastic attenuation function implemented in the Silva et al. (2003) model gives lower attenuation values at high frequencies and higher attenuation values at low frequencies compared to the attenuation function used by the Atkinson and Boore (1995) and Frankel et al. (1996) models.

Figure 3.53a and Figure 3.53b show that for small magnitudes and high frequencies, the lower  $Q$  values compensate for the higher geometrical spreading attenuation at short distances implemented in Silva et al. (2003), and the resulting ground motion amplitude decay is similar to the predicted by the Atkinson and Boore (1995) and Frankel et al. (1996) models. At long distances, the geometrical attenuation dominates



**Figure 3.53.** Comparison of attenuation relationships for M 4



**Figure 3.54.** Comparison of attenuation relationships for M 7

because the Silva et al. (2003) model predicts a faster decay in ground motion amplitudes.

For small magnitudes and low frequencies, Figure 3.53c and Figure 3.53d show that the combined effect of higher Q and geometrical attenuation values causes the higher attenuation of ground motion amplitudes as predicted by the Silva et al. (2003) model. As observed in the high-frequency motions, the geometrical attenuation function at long distances implemented in the Silva et al. (2003) model causes a faster amplitude decay compared to the other two source models.

Similar results are observed in Figure 3.54 for large magnitudes. However in this case the difference in the amplitude decay rate at short distances is due mainly to the different Q models since the geometrical attenuation function is the same for all source models.

Figure 3.53 and Figure 3.54 show that the largest difference in ground motion attenuation is observed at large distances, independent of magnitude and frequency. Therefore the bilinear and trilinear geometrical spreading models are one of the major contributors to the difference observed in ground motion attenuation. Other embayment depths and magnitudes show similar results.

Figure 3.55 compares response spectra with epicentral distance for all source models. Figure 3.55 illustrates the effect of different geometrical spreading and anelastic attenuation models. As discussed above, the geometrical spreading effects dominate at high frequencies, particularly at long distances. At low frequencies, the addition of a higher anelastic attenuation as used in the Silva et al. (2003) model causes the increase of ground motion attenuation compared to the other source models. The spectral sag observed at intermediate frequencies and long distances in the Silva et al. (2003) model resembles the spectral shape of the two-corner model of Atkinson and Boore (1995). For this reason Cramer (2006a) states that for long distances the Silva et al. (2003) model behaves as a two-corner model.

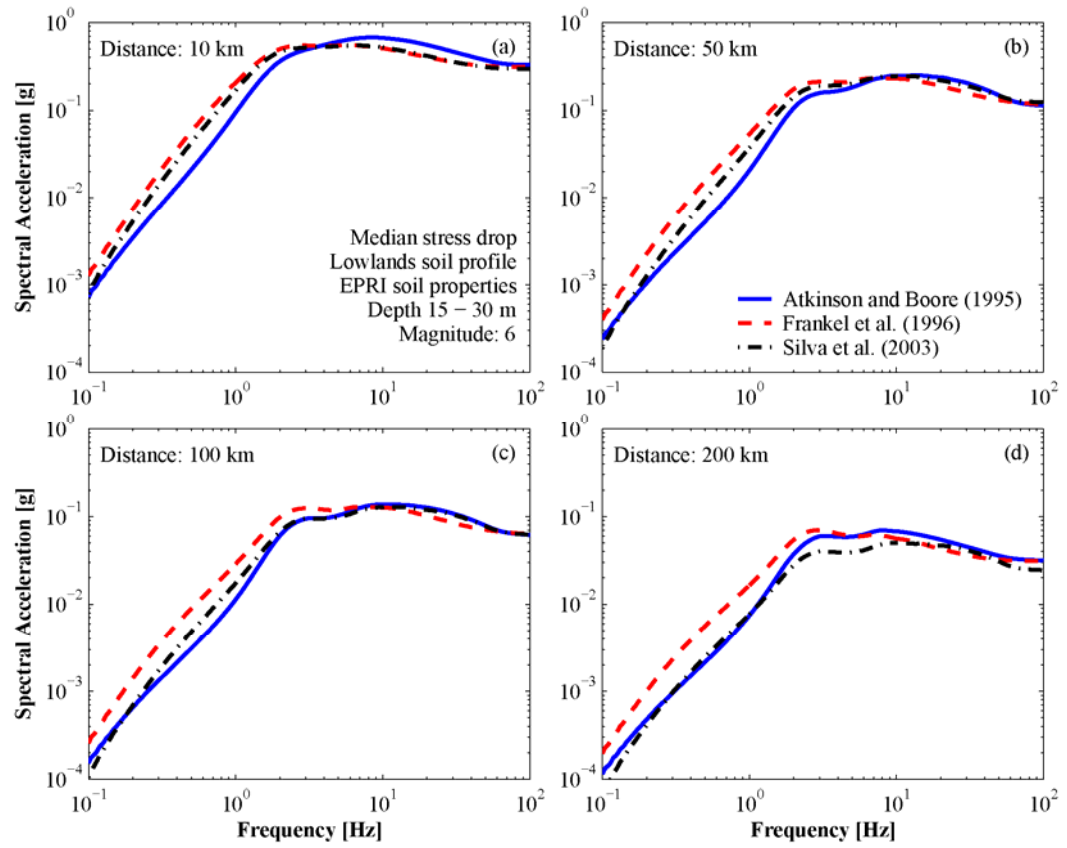
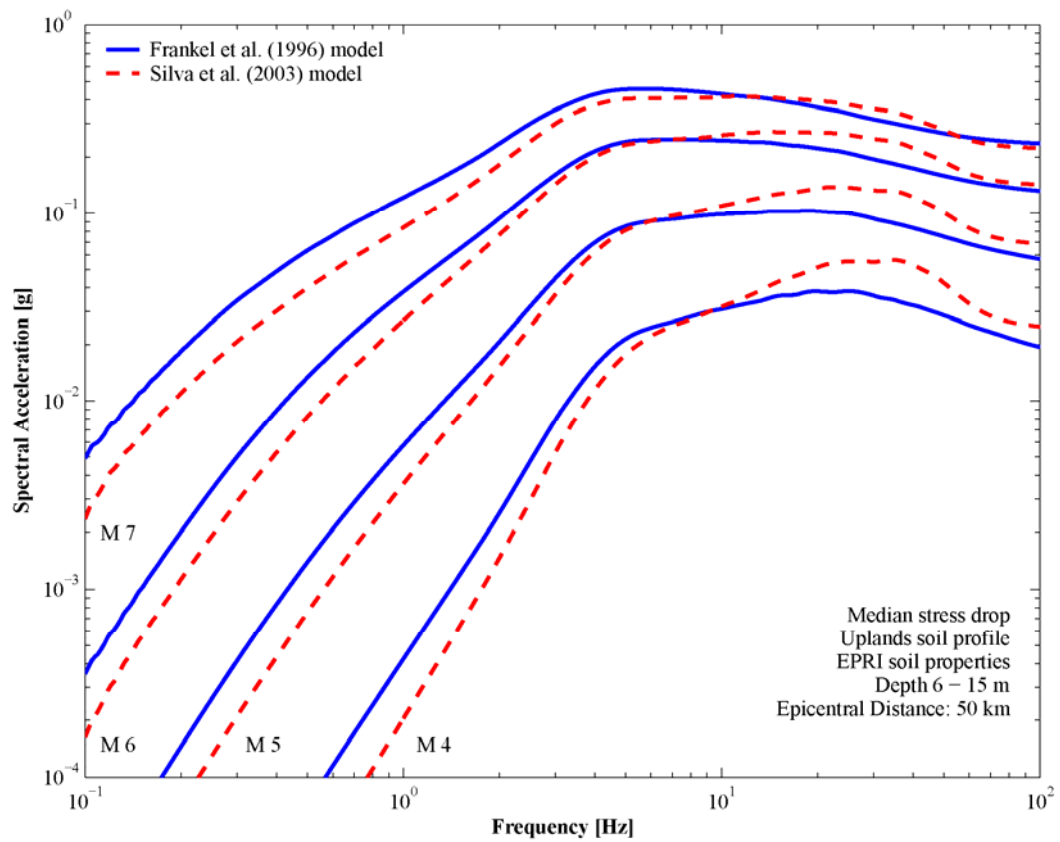


**Figure 3.55.** Comparison of response spectra for M 6

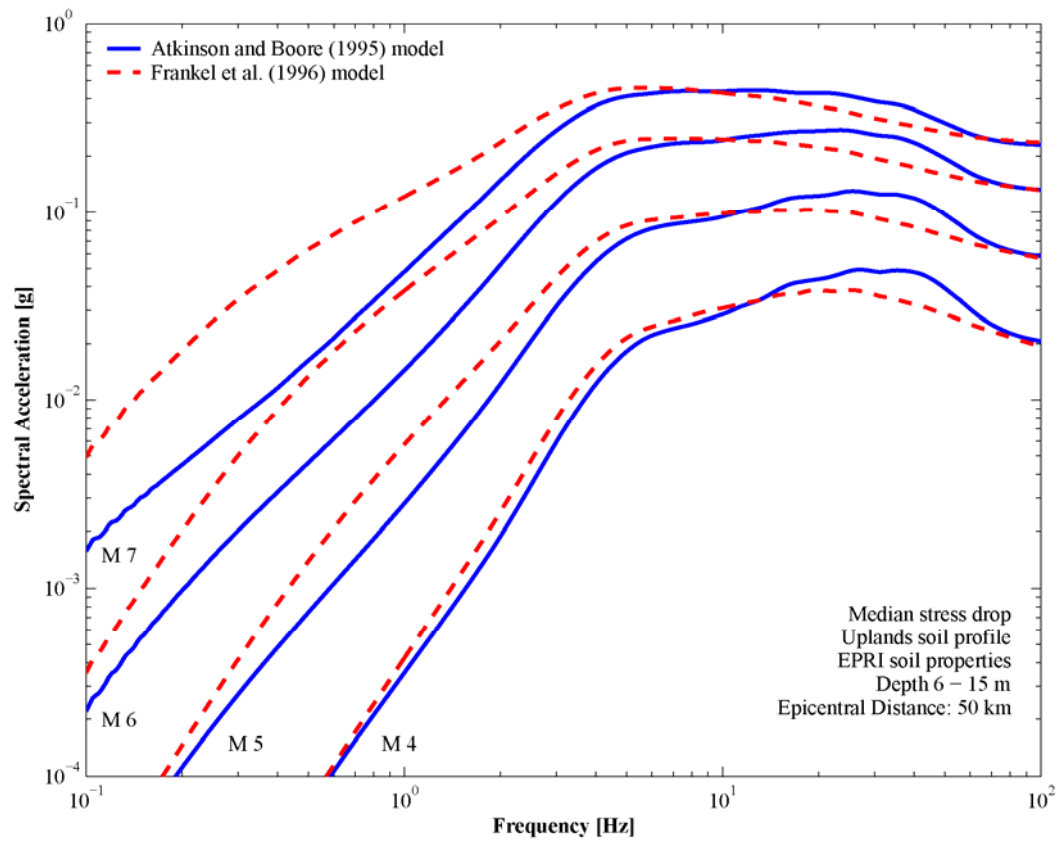
The difference in absolute ground motion amplitude among source models observed in Figure 3.53 through Figure 3.55 is due to the spectral shape assumed in the one- and two-corner source models as discussed below.

Figure 3.56 compares response spectra of constant (Frankel et al., 1996) and magnitude-dependent (Silva et al., 2003) stress drop models. For small magnitudes (**M** 4 and **M** 5) the corner frequencies corresponding to the Silva et al. (2003) model are slightly higher compared to the Frankel et al. (1996) model due to its higher median stress drop values used in this magnitude range (see Table 3.3). The opposite occurs for larger magnitudes (**M** 6 and **M** 7) due to the decrease in stress drop implemented in the Silva et al. (2003) model as the magnitude increases. Figure 3.56 also shows the different high-frequency scaling of ground motions associated with the two source models. It would be expected that the magnitude-dependent stress drop model of Silva et al. (2003) would predict higher ground motion amplitudes for small magnitudes and lower amplitudes for large magnitudes compared to the constant stress drop model of Frankel et al. (1996). Figure 3.56 shows that this is true for small magnitudes, however for large magnitudes the Silva et al. (2003) model still predicts slightly higher amplitudes. These higher amplitudes might be due to the higher  $Q$  model at high frequencies implemented in Silva et al. (2003). The geometrical attenuation effect is small at large magnitudes because both models use a similar geometrical spreading function at an epicentral distance of 50 km. The lack of a  $f_{\max}$  filter in the Silva et al. (2003) model also contributes to the slightly higher PGA values predicted by this model. Both models use the same  $\kappa$  filter, but additionally Frankel et al. (1996) implements a  $f_{\max}$  filter as illustrated in Figure 3.10. The difference in low-frequency ground motion amplitude observed in Figure 3.56 is mainly due to the lower  $Q$  model at low frequencies implemented in the Silva et al. (2003) model.

Figure 3.57 compares response spectra of the one-corner (Frankel et al., 1996) and two-corner (Atkinson and Boore, 1995) source models. At low frequencies, the



**Figure 3.56.** Comparison of response spectra for magnitude-dependent and constant stress drop source models



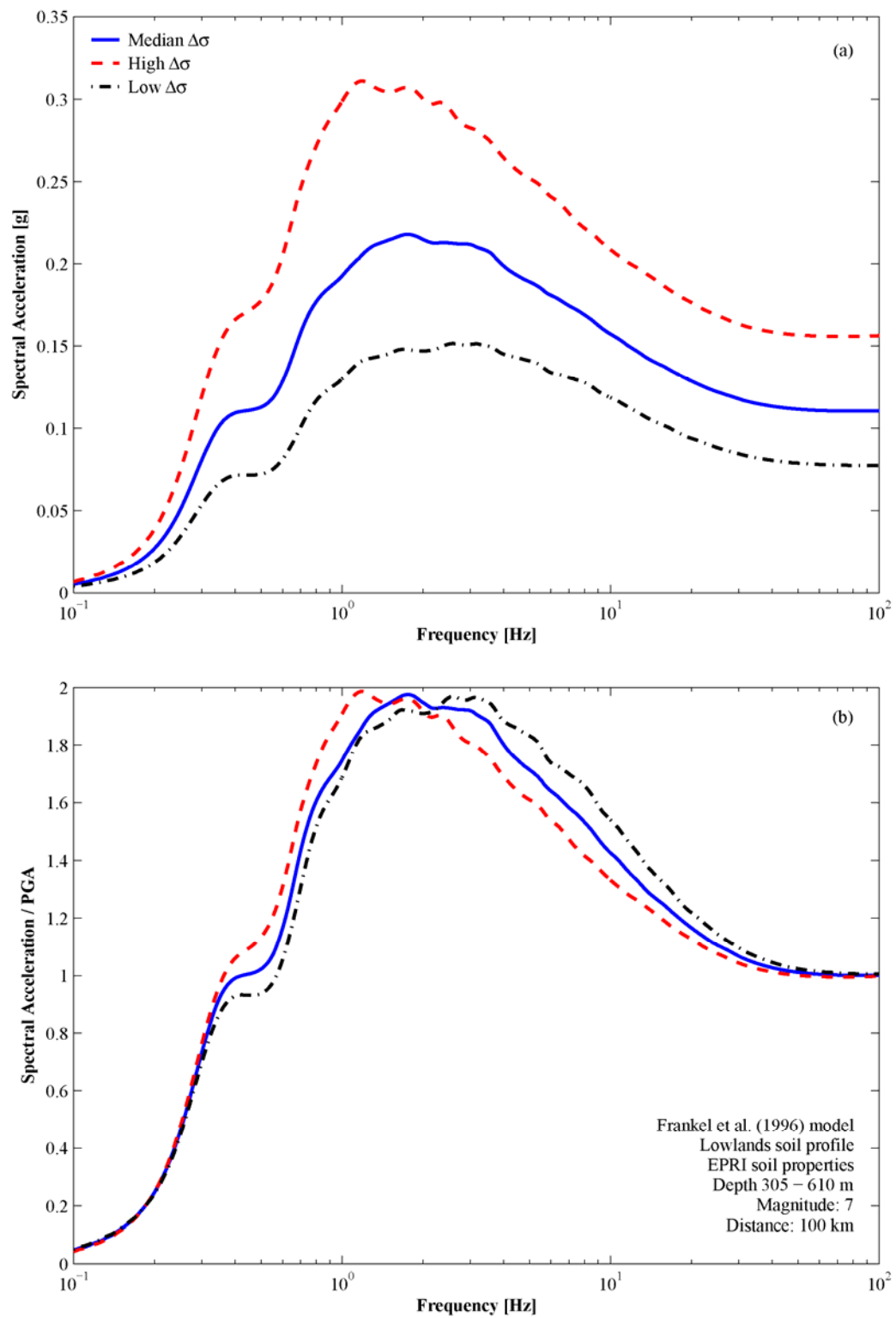
**Figure 3.57.** Comparison of response spectra for one- and two-corner source models

difference in amplitude is due to the different source spectrum shapes assumed in the one- and two-corner models, as discussed previously (see Figure 3.2). For  $M$  4 or less the difference between source models is small because  $M$  4 corresponds to the critical magnitude where the Atkinson and Boore (1995) two-corner model starts behaving as a one-corner source model. The difference in amplitude at high frequencies is controlled mainly by the  $\kappa$  and  $f_{\max}$  filters. In addition to a  $f_{\max}$  filter the Frankel et al. (1996) model implements a  $\kappa$  filter which reduces high-frequency motion amplitudes more than the  $f_{\max}$  filter implemented in the Atkinson and Boore (1995) model, as illustrated in Figure 3.10.

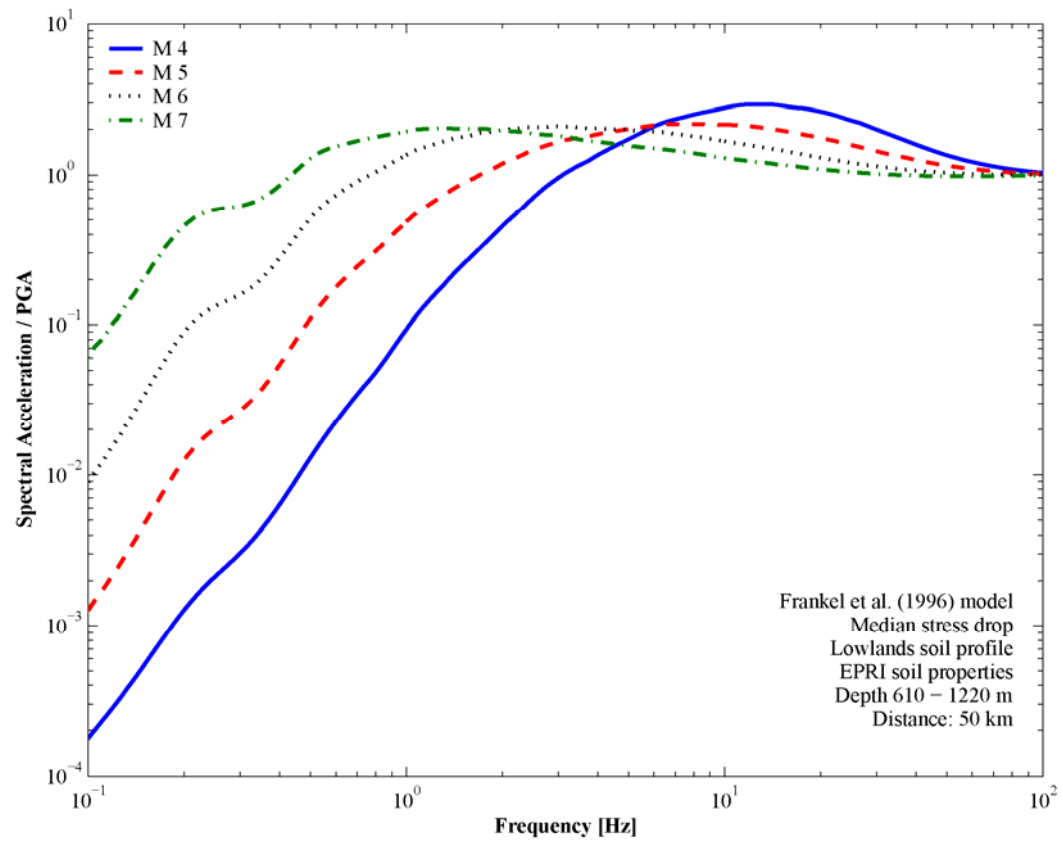
Figure 3.53 through Figure 3.57 illustrate the high variability in ground motion amplitude predicted by the three source models. Epistemic variability in source model is an important factor to consider when estimating ground motion amplitudes of future earthquakes, particularly for areas with a low seismicity rate but capable of generating large earthquakes like in the CEUS.

Figure 3.58 shows the effect of epistemic variability in stress drop on ground motion amplitude and spectral shape. As expected the largest difference among response spectra with different stress drops values occurs in the high frequency ( $f > 1$  Hz) range. This difference becomes smaller as the response spectra approach the corner frequency. A higher stress drop results in an increase in ground motion amplitude, which causes the resonant peak of the soil response shift towards lower frequencies due to softening of the soil column caused by the reduction in the shear modulus. The spectral shapes are similar for different levels of stress drop suggesting a weak dependency of the spectral shape on this parameter (Silva et al., 1997). The large difference in mean ground motion amplitude due to the consideration of epistemic variability in stress drop, illustrates the importance of this parameter when estimating high-frequency ground motions.

Figure 3.59 shows the dependency of spectral shape on magnitude. Larger earthquakes excite a larger range of frequencies, whereas smaller earthquakes show a narrower bandwidth. This result is a direct consequence of the relation between corner



**Figure 3.58.** Effect of stress drop epistemic uncertainty on response spectra



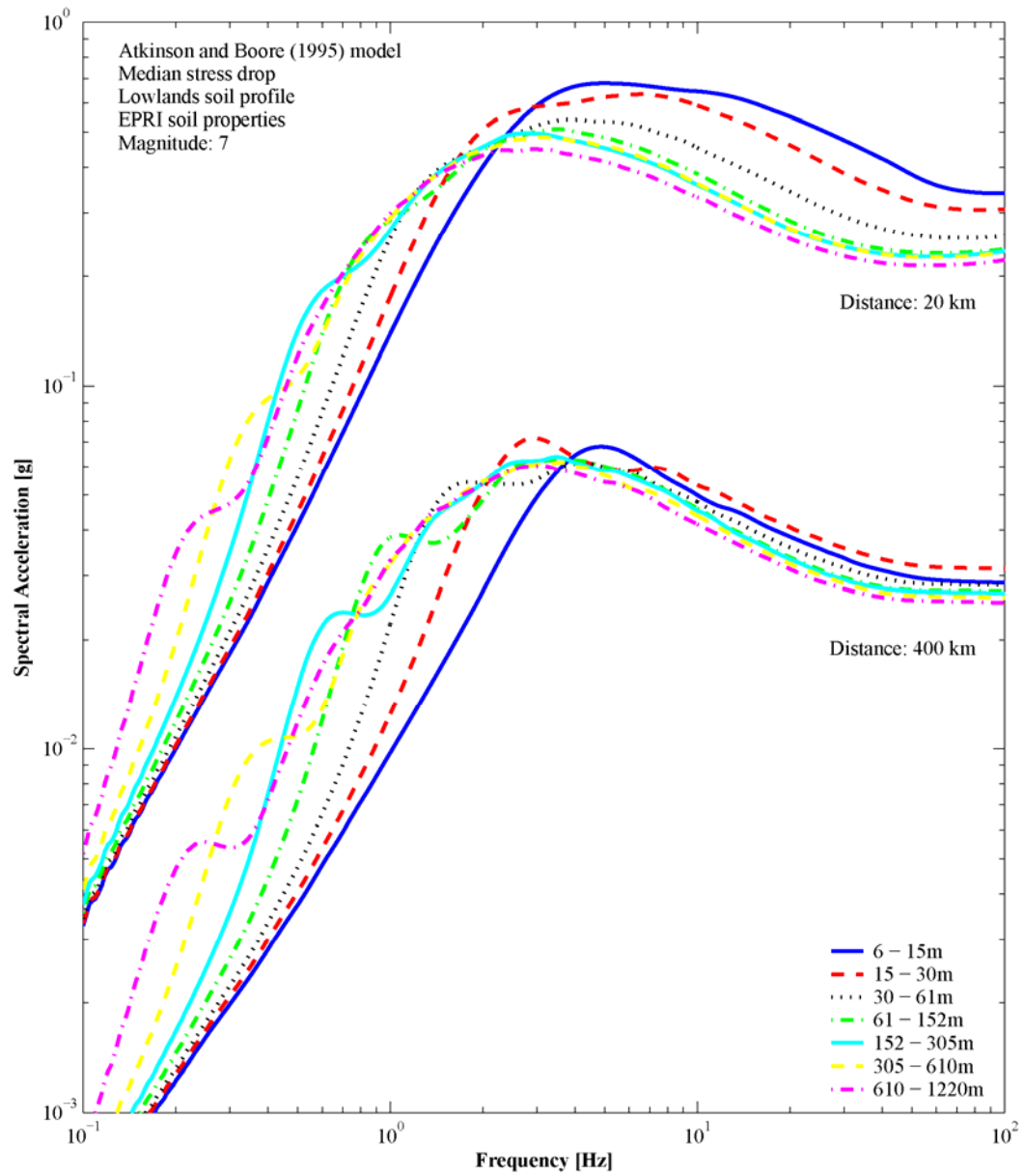
**Figure 3.59.** Effect of earthquake magnitude on spectral shape

frequency and magnitude, as stated in Equation 3.6. Larger earthquakes have lower corner frequencies and therefore wider bandwidth, as illustrated in Figure 3.3 and Figure 3.11.

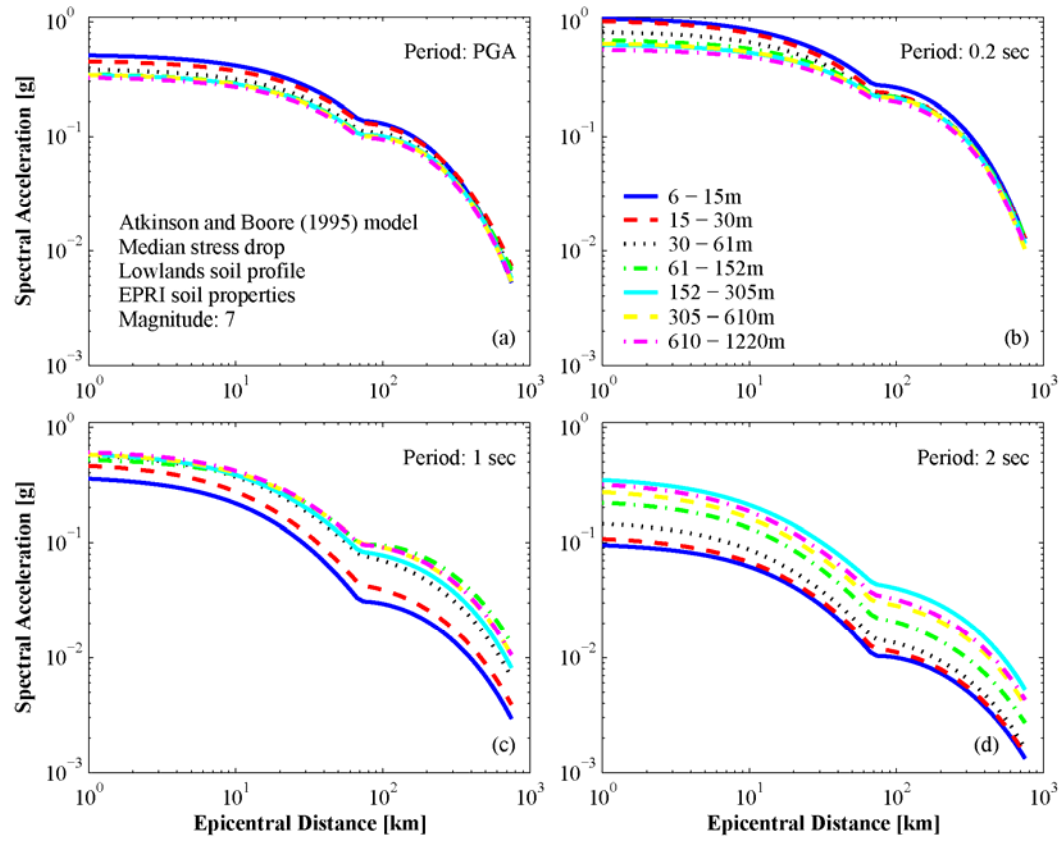
Figure 3.60 and Figure 3.61 show the effect of embayment depth on ground motions amplitude. Figure 3.60 shows that peak amplitudes of response spectra shift to lower frequencies as the embayment depth increases. Fundamental frequencies are inversely proportional to the thickness of the soil column, and thus deep profiles show lower resonant frequencies than shallow profiles. The reduction in peak amplitudes observed as the depth of the soil column increases is due to the additional viscous damping at depth found in deep profiles (Park and Hashash, 2005; Romero, 2001).

Figure 3.60 illustrates that response spectra at long distances show a decrease in high-frequency amplitudes compared to response spectra at short distances. This is consistent with the higher attenuation with distance suffered by high-frequency motions observed in Figure 3.12. The effect of attenuation of high frequencies with distance is more evident on shallow profiles, as their resonant frequencies occur in this frequency range. The spectral shape of deep profiles remains approximately unchanged; however shallow profiles show a narrower bandwidth with distance. This effect is also observed in Figure 3.61a and Figure 3.61b. A direct conclusion of these observations is that embayment depth is not an important factor to characterize high-frequency motions at distances greater than about 200 km.

Figure 3.60 also shows that resonant peaks are sharper at long distances. The high levels of rock motions at short distances cause the soil to behave nonlinearly. The non-linear behavior reduces the peak amplitudes and smoothes the response spectra near the peaks. However, as the distance increases, the rock motion amplitude decreases due to geometrical and anelastic attenuation. This reduction in amplitude causes the soil to behave in the linear range causing a sharpening of the resonant peaks.



**Figure 3.60.** Effect of embayment depth on response spectra



**Figure 3.61.** Effect of embayment depth on attenuation of ground amplitude

Figure 3.60 shows that the ground motion amplitude follows the same trend as the parametric variability as illustrated in Figure 3.45 through Figure 3.47. Thus, the parametric variability increases as the ground motion amplitude increases. This relationship between ground motion amplitude and variability has also been observed in real ground motions (Bazzurro and Cornell, 2004a; Campbell and Bozorgnia, 2006; EPRI, 1993; Toro et al., 1997) and supports the results shown in Figure 3.42 through Figure 3.44.k

Figure 3.60 and Figure 3.61 show the importance of soil column thickness to characterize surface ground motions in the Upper Mississippi Embayment. The difference in ground motion amplitude can be up to four times between shallow and deep profiles.

Figure 3.62 compares response spectra of the Lowlands and Uplands soil profiles for different epicentral distances. The difference between the seismic responses of the soil profiles is more important at high frequencies. Although Figure 3.62 shows only response spectra for a particular embayment depth, similar results were found for other depth bins. For high levels of rock ground motion, the non-linear behavior induced in the soil causes a reduction on surface amplitudes in soft soil profiles compared to stiffer profiles, i.e. profiles with higher shear wave velocities. The Uplands profile results in higher ground motion amplitudes due to its higher shear wave velocities in the upper 70 m, which is the depth range that most contributes to the non-linear response of the soil column (Romero, 2001). Non-linear effects are more important for the softer Lowlands profile causing more deamplification of the rock ground motions. As the epicentral distance increases, the rock ground motion amplitudes decreases and the difference between the Lowlands and Uplands response spectra becomes less significant. For low levels of rock ground motion, the soil column behaves linearly and the difference in shear wave velocity profiles becomes less important. The resonant peaks of the Lowlands profile occur at slightly lower frequencies compared to the Uplands profile due to its

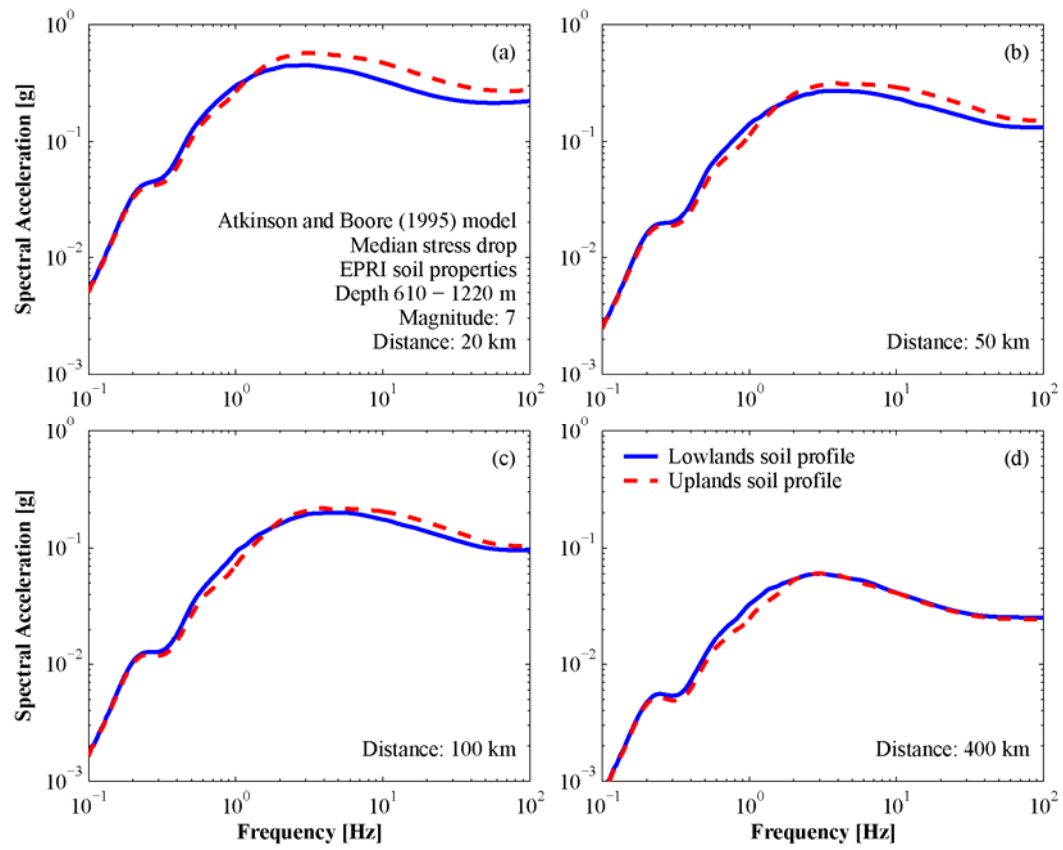


**Figure 3.62.** Effect of soil shear-wave velocity profile on response spectra

lower shear wave velocities. Figure 3.62 illustrates the importance of near-surface characterization in the estimation of strong ground motions, particularly in the high frequency range.

### **3.8. Conclusions**

Attenuation relationships have been developed to estimate median soil ground motions and their respective variability in the Upper Mississippi Embayment. Typical geological units of the region, Embayment depth, and non-linear soil behavior have been considered. Epistemic variability is accommodated with the use of three source models and three stress drop values. Aleatory variability is accommodated by the randomization of site, path, and site parameters.

The proposed attenuation model fits the central trends of the simulations and captures the crustal reflections for the Atkinson and Boore (1995) and Frankel et al. (1996) models. The model provides unbiased ground motion estimates for the entire range of epicentral distances and magnitudes considered in the analyses.

The parametric variability follows the same trend as the ground motion amplitude when non-linear soil behavior is considered. Shallow profiles and small magnitudes exhibit higher variability at short periods, whereas the variability is higher for deep profiles and large magnitudes at long periods. This relationship between ground motion amplitude and variability has also been observed in real ground motions and is one of the most important factors to consider when coupling the source and path effects with the site effects to estimate surface ground motions. The total aleatory variability is considered to be magnitude-dependent. The simple linear relationship considered herein between aleatory variability and magnitude can capture reasonably well the trend observed in the ground motion simulations.

The largest difference in ground motion attenuation among source models is observed at large distances, independent of magnitude, frequency, and embayment depth.

Therefore the bilinear and trilinear geometrical spreading models are one of the major contributors to the difference observed in the attenuation of ground motion amplitudes. The difference in absolute ground motion amplitude among source models observed in the low-frequency range is mainly due to the spectral shape assumed in the one- and two-corner source models. In the high-frequency range, the difference in ground motion amplitude is caused by the  $\kappa$  and  $f_{\max}$  filters implemented in the source models. In general, the ground motions predicted by the three source models show a high variability. This observation leads to the conclusion that epistemic variability in source model is an important factor to consider when estimating ground motion amplitudes of future earthquakes, particularly for areas with a low seismicity rate but capable of generating large earthquakes like in the CEUS.

The effect of the stress drop on spectral shape is not significant; however the consideration of epistemic variability in stress drop causes large difference in the mean ground motion amplitudes in the high frequency range ( $f > 1$  Hz), illustrating the importance of this parameter when estimating high-frequency ground motions.

The difference in ground motion amplitude between shallow and deep profiles can be up to four times. Furthermore, fundamental frequencies are inversely proportional to the thickness of the soil column and thus deep profiles show lower resonant frequencies than shallow profiles. This shows the importance of soil column thickness to characterize surface ground motions in the Upper Mississippi Embayment. However the effect of Embayment depth in the high-frequency range and for epicentral distances greater than 200 km is not significant.

The characterization of the near-surface deposits, i.e., Lowlands and Uplands profiles, is particularly important in the high-frequency range and for high levels of rock motions where the non-linear soil behavior becomes an important factor.

A major advantage of using soil attenuation equations in seismic hazard analyses is that no coupling between probabilistic hazard analyses for rock conditions and site

response is necessary when developing soil ground motions. These soil attenuation relationships already account for correlation among the processes of the earthquake generation and seismic wave propagation and therefore provide a direct approach for developing hazard-consistent soil motions.

Recent site investigations in the southern part of the Upper Mississippi Embayment have determined shear modulus reduction and damping ratio curves that show a more linear behavior than the predicted by the EPRI (1993) curves (Silva, personal communication). The development of additional soil attenuations relationships using this new set of dynamic soil properties will help to better characterize their epistemic variability. As discussed above, the source model is an important factor to consider when estimating ground motions in the Embayment, and therefore the consideration of other source models (e.g., Boatwright and Choy, 1992; Haddon, 1996; Joyner, 1997) in the analyses will also improve the characterization of epistemic variability. As indicated by Cramer (2006b), the selection of the site response formulation may contribute to the uncertainty in soil ground motions estimation, and therefore the incorporation of other site response models such as a true non-linear analysis (e.g., Hashash and Park, 2001) and an equivalent linear analysis with frequency-dependent dynamic soil properties (e.g., Assimaki and Kausel, 2002; Kausel and Assimaki, 2002) can also improve the characterization of epistemic variability.

The attenuation relationships developed in this study have been incorporated into MAEviz ([http://mae.ce.uiuc.edu/software\\_and\\_tools/maeviz.html](http://mae.ce.uiuc.edu/software_and_tools/maeviz.html)) to estimate deterministic scenario ground motions in the Upper Mississippi Embayment. MAEviz is a seismic risk assessment software developed by the Mid-America Earthquake (MAE) Center and the National Center for Supercomputing Applications (NCSA).

# **CHAPTER 4**

## **SEISMIC HAZARD ANALYSES AND PROBABILISTIC GROUND MOTION TIME HISTORIES IN THE UPPER MISSISSIPPI EMBAYMENT**

The evaluation of the seismic hazard for a particular site involves the estimation of ground motions associated with potentially damaging earthquakes. The seismic hazard may be evaluated by deterministic or probabilistic procedures. In a deterministic analysis, a particular earthquake scenario is assumed by specifying an earthquake size and location. A probabilistic analysis explicitly considers the uncertainties in earthquake size, location, and time of occurrence, and along with the use of attenuation relationships it provides estimates of the likelihood of earthquake ground motions of varying levels at a given site. Typically the seismic hazard is first computed at the bedrock level either by performing a site-specific seismic hazard analysis or by using regional seismic hazard maps (e.g. Frankel et al., 2002; Leyendecker et al., 2000). To obtain the seismic hazard at the soil surface, the mean rock hazard is usually multiplied either by a mean amplification function, as in the hybrid method in Cramer (2003), or by a set of average site amplification factors, as in the site coefficients proposed in FEMA (2001a) or in Park and Hashash (2005). In the first approach, the amplification function is determined by driving through the soil column a small suite of acceleration time histories compatible with the rock hazard level using an equivalent linear or fully non-linear site response analysis. An average of the response spectral ratios of ground surface to rock motions is used to obtain the soil response spectrum (FEMA, 2001b). Typically, the local site conditions are characterized by using the best estimates of the dynamic soil properties

and shear wave velocity profile. In the second approach, average site coefficients for different ranges of natural period are used to adjust the rock hazard to account for site effects. As discussed later, these methodologies produce soil ground motion levels with unknown exceedance rates when combined with probabilistic seismic hazard analysis (PSHA) at the rock level (Bazzurro and Cornell, 2004b; Goulet et al., 2007). Moreover the characterization of variability in dynamic soil properties is often lost in this type of approach.

Some recent studies have proposed methods to account for the site response in probabilistic seismic hazard analyses using a probabilistic procedure (Baturay and Stewart, 2003; Bazzurro and Cornell, 2004b, 2006; Cramer, 2003; Goulet et al., 2007; Stewart et al., 2006; Stewart and Goulet, 2006). Bazzurro and Cornell (2004b; 2006) proposed two analytical procedures to implement site response analyses into PSHA. One approach involves the convolution of the probability distribution of the amplification function with the rock hazard curve. The second approach modifies a rock attenuation relationship to account for the site response effects, and then uses the resulting soil attenuation relationship directly into PSHA calculations. Stewart et al. (Baturay and Stewart, 2003; Goulet et al., 2007; Stewart et al., 2006; Stewart and Goulet, 2006) proposed an empirical approach to integrate site effects into PSHA. The approach is similar to the proposed method by Bazzurro and Cornell (2004b; 2006) that modifies the median and standard deviation of a rock attenuation relationship to obtain a soil attenuation equation, but in this case the standard deviation is an empirical value obtained by comparing a ground motion model with observed data for different site categories. The negative correlation observed between the rock hazard level and the site effects (Bazzurro and Cornell, 2004a; Campbell and Bozorgnia, 2006; EPRI, 1993; Toro et al., 1997) due to the non-linear soil behavior is taken into account in these procedures. The method proposed by Cramer (2003) is similar to the approaches described above and uses site amplification distributions to modify existing rock attenuation relationships prior to

PSHA calculations. However in this approach no negative correlation is considered when the site response variability is coupled with the rock hazard. The negative correlation between rock motion level and site response observed in real records must be taken into account when coupling the variability of both processes, otherwise the variability of soil ground motions will be overestimated (Bazzurro and Cornell, 2004b; Silva and Costantino, 2002; Silva et al., 2000).

Although these more refined procedures take into account the variability in the entire earthquake process, the most accurate approach to develop site-specific ground motions is by using site-specific soil attenuation relationships in the probabilistic seismic hazard calculations, assuming that appropriate epistemic and aleatory uncertainties are incorporated in the development of the attenuation relationship (Bazzurro and Cornell, 2004b; Field et al., 2000; Goulet and Stewart, 2007; Goulet et al., 2007; Silva and Costantino, 2002). Soil attenuation relationships consider source, path, and site effects simultaneously, and therefore account for correlations in the earthquake processes. Thus, soil attenuation relationships avoid the need to coupling the variability in rock motions and in site response. The attenuation relationships developed in this study for soil sites in the Upper Mississippi Embayment have been used for deterministic and probabilistic seismic hazard analyses for the region. The seismic hazard estimation incorporates epistemic variability in the attenuation relationships via the use of three source models and three stress drop values. The two typical geological units of the region – Lowlands and Uplands –, Embayment depth, and non-linear soil behavior have been considered by the use of site-specific soil attenuation relationships. The regional analyses have been used to generate seismic hazard maps for the Upper Mississippi Embayment. Suites of probabilistic ground motion time histories consistent with three hazard levels have been generated for selected cities within the Embayment.

Previous studies (Cramer, 2006b; Cramer et al., 2004; Park and Hashash, 2005; Toro and Silva, 2001; Wen and Wu, 2001) have performed probabilistic analysis for soil

sites in the region. All the studies consider the non-linear soil behavior and the deep sediments in the Mississippi Embayment, except for Wen and Wu (2001) who used a linear algorithm to compute the site response. Cramer et al. (2004) generated seismic hazard maps of return periods of 475, 975, and 2475 years for Memphis, TN, using the method proposed by Cramer (2003). The methodology used by Cramer et al. (2004) was implemented by Cramer (2006b) to develop seismic hazard maps for the Upper Mississippi Embayment. Park and Hashash (2005) developed site amplification coefficients similar to the coefficients proposed by FEMA (2001a) that account for the Upper Mississippi Embayment conditions. Uniform hazard spectra (UHS) corresponding to a return period of 2475 years were generated for six soil sites in the Embayment, and then amplification coefficients were chosen such that an envelope of the UHS was obtained. Toro and Silva (2001) performed regional probabilistic seismic hazard analysis for rock conditions in the Mississippi Embayment and then soil ground motions were obtained by modifying the rock hazard with median soil amplification functions. The soil ground motions were generated for St. Louis, MO and Memphis, TN, and for return periods of 475 and 2475 years. Wen and Wu (2001) developed probabilistic soil ground motions for return periods of 475 and 2475 years for the cities of Memphis, TN, St. Louis MO, and Carbondale, IL, by using soil amplification functions to modify the rock motions. The main difference between the different approaches is the characterization of variability in the earthquake process. The methods described above required coupling the rock hazard with site effects, and except for Cramer et al. (2004) and Cramer (2006b), none of the methods performed the coupling process using a probabilistic approach. The methodology followed in this study predicts more accurate soil ground motions (Bazzurro and Cornell, 2004b; Goulet and Stewart, 2007; Goulet et al., 2007; Silva and Costantino, 2002) and avoids the need to couple the earthquake source and path variability with the variability in site effects.

#### **4.1. Seismic Hazard Analysis**

Seismic hazard refers to the potential occurrence of damaging natural phenomena related to earthquakes at a given location, such as ground shaking, soil liquefaction, tsunamis, and landslides. More specifically, seismic hazard analysis refers to the estimation of ground motion intensity (e.g., peak ground acceleration, peak ground velocity, spectral acceleration) at a particular location. Sometimes seismic hazard is mistakenly used to refer to seismic risk, which is related to the consequences caused by the occurrence of these damaging earthquakes such as the loss of life, direct physical damage, or business interruption losses.

The seismic hazard for a particular site may be evaluated by deterministic and probabilistic procedures. In a deterministic seismic hazard analysis (DSHA), a single or a few earthquake scenarios are assumed by specifying an earthquake size and location for each event. The location is defined by identifying earthquakes sources in the vicinity of the site at which the seismic hazard is to be estimated. The earthquake sources' geometry can be defined by points, lines, areas, or volumes. The earthquake potential must be defined for each earthquake source in terms of a maximum earthquake. The maximum earthquake is defined by its size, which is usually described by an earthquake magnitude. Each pair of source-magnitude is associated with a source-to-site distance, usually the shortest distance to the site, and therefore a deterministic analysis assumes that the representative earthquake for each source occurs at the shortest distance between the earthquake source and the site. To determine the seismic hazard at the site, an earthquake ground motion attenuation equation is selected, which provides estimates of ground motions amplitudes given the earthquake magnitude and distance. Thus, ground motion amplitudes are estimated at the site for each pair of earthquake magnitude and source-to-site distance. The controlling earthquake, which is the earthquake expected to produce the strongest level of shaking at the site, is selected by comparing the ground motion amplitudes produced by all considered earthquake sources. The controlling earthquake is

defined by its size (i.e. magnitude) and distance from the site, and is the most important event in defining the seismic hazard. The seismic hazard at the site is described by a ground motion parameter such as peak ground acceleration or response spectrum generated by the controlling earthquake. When the seismic hazard is described by more than one ground motion parameter (e.g. peak ground acceleration and peak ground velocity), it is possible that different earthquakes control different ground motion measures, and therefore there will be more than one controlling earthquake (Reiter, 1990). Kramer (1996) and Reiter (1990) provide a more detailed description of deterministic seismic hazard analysis methodology.

A deterministic analysis does not consider the effects of uncertainties in the location, size, and frequency of occurrence of the controlling earthquake, or in the variation of the ground motion amplitude with earthquake magnitude and source-to-site distance (Kramer, 1996; Reiter, 1990; Thenhaus and Campbell, 2003). A probabilistic analysis provides a methodology that explicitly considers these uncertainties in the seismic hazard calculations (Kramer, 1996). Furthermore, in a probabilistic analysis the description of the seismic hazard is not restricted to discrete, scenario events, but incorporates the effects of all possible earthquakes capable of affecting the site (Reiter, 1990).

The methodology to conduct a probabilistic seismic hazard analysis (PSHA) is well established in the literature (Cornell, 1968; Kramer, 1996; McGuire, 2004; Reiter, 1990; Thenhaus and Campbell, 2003). A PSHA determines the frequency with which a ground motion parameter (e.g. peak ground acceleration, peak ground velocity, a level of Modified Mercalli Intensity) exceeds a certain value (e.g. 0.3 g) during some fixed time in the future (McGuire, 2004).

The PSHA computation is based on the total probability theorem that states that the probability that a ground motion parameter  $Y$  will exceed a particular value  $y$  can be calculated by (Kramer, 1996):

$$P[Y > y] = \int P[Y > y | \mathbf{X}] \cdot f_{\mathbf{x}}(\mathbf{X}) \cdot d\mathbf{x} \quad 4.1$$

where  $\mathbf{X}$  is a vector of random variables that affect the parameter  $Y$ .  $P[Y > y | \mathbf{X}]$  is the probability that a given set of variables  $\mathbf{X}$  will cause that a ground motion parameter  $Y$  will exceed a particular value  $y$ , and  $f_{\mathbf{x}}(\mathbf{X})$  is the probability density distribution of  $\mathbf{X}$ . Usually the vector  $\mathbf{X}$  only includes the earthquake magnitude,  $M$ , and the distance from source to site,  $R$ . However, other parameters can also be considered like seismic moment, stress drop, and rupture direction and velocity (McGuire, 2004). The consideration of additional parameters increases the accuracy of the results, but additional calculations are required to integrate over these parameters, and in many cases no advantage is obtained (McGuire, 2004). If  $M$  and  $R$  are assumed to be independent, the probability of exceedance can be written as:

$$P[Y > y] = \iint P[Y > y | m, r] \cdot f_M(m) \cdot f_R(r) \cdot dr \cdot dm \quad 4.2$$

where  $P[Y > y | m, r]$  is the probability that a given earthquake of magnitude  $m$  and distance  $r$  from the site will cause ground motions that exceeds a particular value  $y$ , and  $f_M(m)$  and  $f_R(r)$  are the probability density distributions of magnitude and source-to-site distance, respectively. If the effect of  $N$  earthquake sources is considered in the analysis, the annual frequency that a ground a motion at the site exceeds a particular level  $y$  is given by:

$$\lambda[Y \geq y] = \sum_{i=1}^N v_i \int_{m_0}^{m_{\max}} \int_R P[Y \geq y | m, r] \cdot f_{M_i}(m) \cdot f_{R_i}(r) \cdot dr \cdot dm \quad 4.3$$

where  $v_i$  is the annual rate of occurrence of earthquakes between magnitudes  $m_0$  and  $m_{\max}$  on seismic source  $i$ ,  $m_0$  is the minimum magnitude of engineering significance,  $m_{\max}$  is maximum magnitude expected to occur on the source,  $P[Y \geq y | m, r]$ ,  $f_{M_i}(m)$ , and  $f_{R_i}(r)$  were defined in Equation 4.2, and subindex  $i$  refers to earthquake source  $i$ .

The aleatory variability of the ground motion attenuation equation can be included explicitly in Equation 4.3 (McGuire, 1995):

$$\lambda[Y \geq y] = \sum_{i=1}^N v_i \int_{m_0}^{m_{\max}} \int_R \int_{\varepsilon} P[Y \geq y | m, r, \varepsilon] \cdot f_{M_i}(m) \cdot f_{R_i}(r) \cdot f_{\varepsilon}(\varepsilon) \cdot d\varepsilon \cdot dr \cdot dm \quad 4.4$$

where epsilon,  $\varepsilon$ , represents the number of standard deviations (logarithmic units) by which the ground motion (logarithmic units) deviates from the median value predicted by the attenuation equation. Epsilon is a standard Gaussian variable and it can be represented in a generic ground motion attenuation equation by:

$$\ln Y = f(M, R) + \varepsilon \cdot \sigma_{\ln Y} \quad 4.5$$

where  $Y$  is a ground motion parameter,  $f(M, R)$  is the functional form of the attenuation equation, and  $\sigma_{\ln Y}$  is the standard deviation of  $\ln Y$ , which is defined by the scatter around the attenuation equation (e.g., Figure 3.21).

Equation 4.4 is often called the Cornell-McGuire method because it is based on the original formulation of Cornell (1968) and modified by McGuire (1976) to include the aleatory variability of the attenuation equation in the formulation. The PSHA integral is solved numerically and the range of possible values of magnitude, distance, and epsilon for each source is divided in bins, which do not need to be constant throughout the domain of the variables, and thus the integrals of Equation 4.4 are replaced by summations.

As expressed in Equation 4.4, the probabilistic approach requires the specification of three components of the uncertainty in the generation and propagation of seismic waves from the earthquake source to the site in study. A PSHA requires the identification and characterization of earthquakes sources by defining the source geometry and distribution of rupture locations in order to obtain the probability distribution of distance from source to site,  $f_{R_i}(r)$ . This step is similar to DSHA, except that the probability distribution of earthquake locations must also be specified.

Characterization of the seismicity is another component of the PSHA methodology, and it is evaluated by specifying the earthquake recurrence frequency and size distribution (i.e. magnitude distribution) of the defined seismic sources,  $f_{M_i}(m)$ . The magnitude distribution includes the maximum earthquake, but it is not limited to this earthquake as in the case of DSHA. Finally attenuation relationships and their inherent uncertainty must be specified to estimate ground motions at the site as a function of earthquake magnitude and distance to the seismic source,  $P[Y > y | m, r, \epsilon]$  and  $f_\epsilon(\epsilon)$ . Attenuation relationships are also used in DSHA, but usually only the median or the median + 1 standard deviation value is used in the analysis and therefore ground motion amplitudes are not considered as random variables. The probability term in Equation 4.4 is evaluated by the Heaviside step function:

$$P[Y > y | m, r, \epsilon] = H[\ln Y(m, r, \epsilon) - \ln y] \quad 4.6$$

which is 0 if  $\ln Y(m, r, \epsilon)$  predicted by the attenuation equation is less than the target ground motion value  $\ln y$ , and 1 otherwise.

The probabilistic methodology combines the uncertainty in earthquake location, earthquake size, and ground motion amplitude to obtain the frequency that a ground motion exceeds a chosen level at the site in a given period of time, which is usually set to one year. The main result of a PSHA is a hazard curve, which plots annual probabilities of exceedance versus the amplitude of a ground motion parameter (e.g. peak ground acceleration). Figure 4.1 shows an example of a hazard curve for Atlanta, Georgia. This hazard curve corresponds to the peak ground acceleration on rock site conditions given by the 2002 USGS National Hazard Maps.

Aleatory variability is accommodated in the probabilistic methodology by means of mathematical integration of the probability distribution of all sources of uncertainty in the earthquake process and it is represented by a complementary cumulative distribution function (e.g., Figure 4.1). Epistemic variability is included in the analysis by

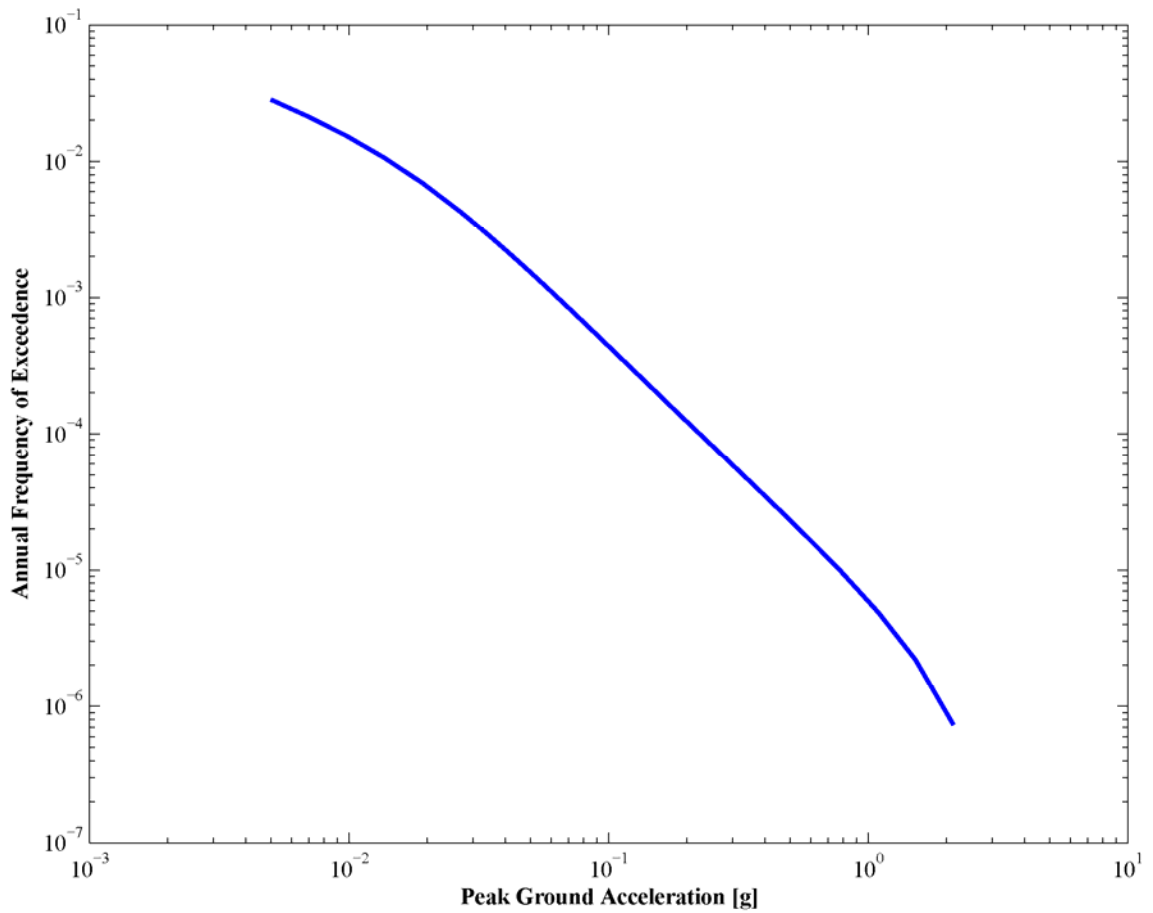


**Figure 4.1.** Peak ground acceleration (PGA) hazard curve for Atlanta, GA on rock site conditions given by the 2002 USGS National Hazard Maps

considering alternative models for the characterization of earthquakes sources, seismicity, and ground motion attenuation relationships. Each model is used to calculate a single hazard curve. Weights are assigned to each alternative input, and the results are usually described by a set of hazard curves that represent the central value and the scatter of the alternative models (McGuire, 2004; Reiter, 1990; Thenhaus and Campbell, 2003). The mean hazard curve is often used as the single measure of the seismic hazard at a site (McGuire, 2004). Abrahamson and Bommer (2005) have proposed the use of other fractiles for the selection of design ground motions. Abrahamson and Bommer (2005) argue that the mean values at very low annual probabilities of exceedance (i.e.  $10^{-7}$  or  $10^{-8}$ ) are greatly affected by the most severe of the alternative models considered in the analysis, even if small weights are assigned to them. This results in high mean hazard values comparable to the higher fractiles curves. McGuire et al. (2005) and Musson (2005) support the use of the mean hazard curve when a single representation of the seismic hazard is required, and state that the validity of those extreme cases that may affect the mean curve should be studied before they are included in the analysis. Furthermore, the mean hazard curve is not affected by the decision of treating the variability as aleatory or epistemic in seismic hazard analysis (McGuire et al., 2005). If a portion of the aleatory variability is considered as epistemic variability during a seismic hazard analysis, the median curve and other fractiles will be affected, but the mean hazard curve will not change (McGuire et al., 2005). Musson (2005) adds that each fractile curve represents one state of epistemic variability, and it can only be true if all the model parameters associated with this curve are true. The mean curve is the only one that takes into account all possible cases.

The probability that a ground motion parameter  $Y$  will be greater than or equal to a particular value  $y$  in the next  $t$  years can be computed assuming a Poisson distribution for earthquake occurrence:

$$P[Y \geq y] = 1 - \exp(-t \cdot \lambda[Y \geq y]) \quad 4.7$$

The return period in years of an event exceeding a particular ground motion level  $y$  can be computed by:

$$RP = \frac{1}{\lambda[Y \geq y]} = \frac{-t}{\ln(1 - P[Y \geq y])} \quad 4.8$$

A common probability value used in PSHA are ground motions that have a 10% probability of being exceeded in a period of 50 years. The return period corresponding to this probability of exceedence can be calculated by Equation 4.8:

$$RP = \frac{-50}{\ln(1 - 0.1)} = 475 \text{ years} \quad 4.9$$

An alternative to Equation 4.4 in calculating the seismic hazard at a site in a probabilistic manner is the Monte Carlo simulation method or stochastic modeling (Musson, 1998, 1999, 2000). The method uses the same input needed to evaluate Equation 4.4: source geometry and distribution of rupture locations, earthquake recurrence frequency and magnitude distribution of the defined seismic sources, and attenuation relationships and their uncertainty. Typically a Poisson model is used to randomly determine the number of earthquakes occurring on each seismic source in the next  $t$  years. Epicenter location, source depth, and magnitude are simulated for each earthquake using the probability distribution of each parameter for each earthquake source zone. The output of this process represents a synthetic catalogue of the region in the next  $t$  years. For each synthetic earthquake, the ground motion amplitudes are estimated at the site using attenuation relationships and their distribution. After a very large number of simulations, probabilities of exceedence can be calculated by counting the number of earthquakes exceeding a particular ground motion value. Previous studies (Musson, 1998, 2000; Park and Hashash, 2005; Wen and Wu, 2001) have demonstrated

that when using the same input parameters, conventional PSHA (Equation 4.4) and Monte Carlo simulation yield the same results.

Other methodologies have been proposed to perform probabilistic seismic hazard analysis that avoid the uncertainty associated with the definition of seismic sources and use seismic catalogues to predict future earthquakes. These methods are based on the assumption that future seismicity of a particular region can be represented by its history (McGuire, 1993). Tsang and Chandler (2006) proposed a method that replaces the sources characterization used in the Cornell-McGuire method (Equation 4.4) by considering an infinite number of sources. This method was developed particularly for regions where seismic sources are difficult to identify, i.e. stable continental intraplate areas; however the method can be extended to active seismic zones (Tsang and Chandler, 2006). Ebel and Kafka (1999) have proposed a similar methodology to the Monte Carlo approach described previously. This method generates the synthetic earthquake catalog by resampling an observed catalog. Earthquake sources, seismicity rates, and ground motion attenuation relationships are implicit in the real seismic catalog and in the ground motions observations, and therefore these inputs are not required in the analysis. A Gutenberg-Richter recurrence relationship is needed if the largest earthquake required in the analysis is larger than the largest earthquake in the observed catalog. Another method that eliminates the need to define seismic sources is the approach developed by Frankel (1995). For regions without identified active faults, the method calculates the seismic hazard by smoothing historical seismicity. The uncertainty associated with the historical catalog is reduced by smoothing spatially the historical seismicity. This approach along with the separate treatment of known active faults has been used in developing the U.S. National Seismic Hazard Maps (Frankel et al., 1996; 2002).

Usually PSHA assumes that the occurrence of earthquakes follows a Poisson process, i.e. earthquakes occur independently of each other in space and time; however this is not a requirement in the calculations and others models can be implemented. The

Poisson model assumption is not consistent with the elastic rebound theory (Lay and Wallace, 1995). The theory of elastic rebound states that earthquakes occur on a particular portion of a fault where the stress has reached a certain level imposed by the material properties of the rock and fault surface. The earthquake relieves this stress and subsequent earthquakes will not occur along this portion of the fault until stresses build up again. These cycles of stress accumulation and release continue during the active life of the fault. Thus, the probability of occurrence of an earthquake on this segment of the fault should be related to the time when the last earthquake occurred and to the amount of energy that was released (Kramer, 1996). Various models that account for past seismicity have been proposed including Non-homogenous Poisson models, Renewal models, Time-predictable models, Slip-predictable models, Markov models, Semi-Markov models, and Trigger models (Kramer, 1996; Thenhaus and Campbell, 2003).

Cornell and Winterstein (1988) have shown that the Poisson model is a reasonable assumption for most engineering applications. Furthermore each of the more refined models requires additional parameters whose evaluation needs empirical earthquake data that it is often not available (Kramer, 1996).

Bommer (2002) provides a comprehensive comparison of the deterministic and probabilistic approaches for seismic hazard evaluation. The identification of potential earthquake sources and the use of attenuation relations to estimate ground motion amplitudes at a site are features common to both methodologies. However, there are important differences between both methods. The identification of the representative earthquake for each seismic source in DSHA involves subjective decisions that result in ambiguity in its selection (Kramer, 1996; Reiter, 1990; Thenhaus and Campbell, 2003). A PSHA eliminates the difficulties on the selection of the representative magnitude since it quantifies the effects of all possible earthquakes for each source. Another important difference is the treatment of the earthquake sources in the seismic hazard calculations. DSHA considers each seismic source independently, and the seismic hazard results

clearly show the effects of each source. PSHA combines the effects of all potential sources into one hazard curve. However, the integration of all possible magnitudes and relevant sources implemented in PSHA may create some problems in further analysis involving the seismic hazard results as discussed below.

The DSHA is very simple and transparent, and therefore easy to review by the analyst and the user. A PSHA integrates large sets of input earthquake parameters to obtain the seismic hazard at a site, and therefore one of the disadvantages of the probabilistic approach is the loss of transparency in the analysis. The output of a PSHA is the probability that a ground motion parameter exceeds a given value, but it does not indicate if this ground motion value is produced by a small local earthquake or by a large distant earthquake. This information is important, for example, to define the duration of time histories for dynamic structural analyses or for liquefaction potential evaluations. It is difficult for the user and even sometimes for the analyst to relate the output of a PSHA to the factors that influence the hazard. The problem of identifying the dominant earthquakes in PSHA is created by the total probability theorem (Equation 4.4), which requires that all possible earthquakes must be considered simultaneously when calculating the probabilities of exceedence of a given ground motion level (Bommer, 2002). Due to this difficulty in identifying the magnitude-distance pair or pairs that dominate the hazard at a site, some researchers (Bommer et al., 2000; Krinitzsky, 1995, 1998) have recommended the use of DSHA for critical structures or high hazard levels, since the DSHA explicitly identifies these dominant earthquakes. The Monte Carlo simulation method does not have this weakness because the design earthquakes can be determined by selecting from the synthetic earthquake catalogues the events that match the hazard level and examining the distribution obtained (Musson, 1999).

DSHA does not consider the inherent uncertainty in seismic hazard estimation, i.e. uncertainty of the location and magnitude of future earthquakes. Many large earthquakes have occurred in areas where only small earthquakes were expected (e.g.

1988 Saguenay, Quebec earthquake). A deterministic approach does not take into account the frequency of earthquake occurrence. Two earthquake sources having the same maximum magnitude, but different recurrence intervals (e.g., 100 and 1000 years) will yield similar seismic hazard results if performed using a deterministic approach. However the two scenarios have different likelihood of occurrence and a DSHA will result in inconsistent levels of hazard (Reiter, 1990). Conversely, a PSHA explicitly incorporates the frequency of earthquake occurrence. The units of time included in PSHA represent one of the fundamental differences between the two approaches (Bommer, 2002).

Deterministic and probabilistic seismic hazard analyses have advantages and disadvantages, and integrated approaches have been proposed to implement the strengths on each methodology. Seismic hazard deaggregation methods (Bazzurro and Cornell, 1999; Chapman, 1995; McGuire, 1995; Scott et al., 1998) identify the earthquakes (i.e. magnitude and distance) that contribute to the seismic hazard estimated by probabilistic methods. Thus, the representative magnitude-distance pairs can be used to select ground motion time histories for further analyses (Cornell, 2005; Somerville and Collins, 2003; Stewart et al., 2002) or to deterministically estimate ground motions consistent with a given return period or probability of exceedence. This characterization of the hazard also facilitates the understanding of the nature of the seismic hazard in a given site. These methods will be discussed in detail later.

Krinitzsky (2002b; 2003) proposes procedures to combine probabilistic and deterministic analysis and to estimate ground motions for engineering design. Krinitzsky (2002b) recommends the use of the median plus one standard deviation (84th percentile) when calculating ground motions for each scenario event, as opposed to the median (50th percentile) ground motion used in the DSHA described in Reiter (1990) and Kramer (1996). The selection of the 84th percentile implicitly reflect a choice based on probability (Bommer, 2003). Krinitzsky (2003) recommends the use of DHSA for design

of critical structures or for high hazard levels, and recommends PSHA for preliminary analysis, for design of non-critical structures, and for design based on the operating basis earthquake (OBE), i.e. the earthquake for which the structure is designed to remain operational. Bommer et al. (2000) supports the recommendations of Krinitzsky (2002b; 2003), and proposed the use of DSHA when realistic acceleration time histories are needed for engineering design.

McGuire (2001) states that deterministic and probabilistic analysis are not mutually exclusive approaches, but they are complimentary. A probabilistic analysis should include all credible deterministic events and it can be used to check whether a deterministic scenario is realistic and reasonably probable or not. Deterministic analysis can be used to check if realistic hypotheses were included in a probabilistic analysis. McGuire (2001) provides a scheme to select deterministic or probabilistic approaches for seismic hazard evaluations based on the type of risk mitigation decision, level of seismicity of the region, and scope of the assessment. A probabilistic analysis is more appropriate for applications that requires quantitative decisions (i.e. seismic design and retrofit, insurance decisions), for low and moderate seismic regions, or for site-specific or multiple-site assessments. When the application requires more qualitative decisions (i.e. plans for emergency response, plans for post-earthquake recovery), for high seismicity regions, or for regional assessments, a deterministic analysis is preferred (McGuire, 2001). McGuire (2001) remarks that the most insightful seismic hazard evaluation should include both methodologies using an iterative approach. A probabilistic analysis will identify the deterministic scenarios that dominate the hazard at a given site. Then the dominant deterministic events will be modeled in more detail, and this information will be used for a refined probabilistic analysis (McGuire, 2001).

The maximum considered earthquake maps for the 1997 NEHRP Recommended Provisions for Seismic Regulations for New Buildings (Leyendecker et al., 2000) were developed using a combination of deterministic and probabilistic analysis. Probabilistic

maps were generated for ground motions corresponding to a return period of 2475 years, and deterministic maps were developed using active faults and the median ground motions predicted by the attenuation relationships multiplied by 1.5. The deterministic values are used as an upper bound for the probabilistic maps. This methodology was used to obtain a uniform margin against collapse throughout the United States, by considering the rare but possible ground motions in the Central and Eastern United States and the earthquake performance of structures in the Western United States (Leyendecker et al., 2000).

The method selected for seismic hazard evaluations should reflect the state of knowledge of the earthquake generation and propagation processes in a given region or site, and should describe the hazard results in a way that can be used properly by peer reviewers and end users (Bommer, 2003; Reiter, 1990). Despite all the critics of the probabilistic approach (Bommer et al., 2000; Krinitzsky, 1995, 1998, 2002a, 2002b, 2003; Paul, 2002), PSHA is the most widely used approach for seismic hazard assessments.

#### **4.2. Seismic Hazard Analyses in the Upper Mississippi Embayment**

The soil attenuations relationships developed in this study were used to perform seismic hazard analyses in the Upper Mississippi Embayment. Deterministic and probabilistic analyses were performed for seven selected cities. Probabilistic analyses were performed for the entire region to develop probabilistic seismic hazard maps. The probabilistic hazard analyses were performed using EZ-FRISK<sup>TM</sup>, a widely used computer program for earthquake ground motion estimation developed by Risk Engineering, Inc. EZ-FRISK<sup>TM</sup> implements the Cornell-McGuire method to compute the hazard analyses. Other computer programs are available to perform PSHA (e.g., EQRISK, SEISRISK III, OpenSHA, CRISIS2003), however the main advantage of using

EZ-FRISK<sup>TM</sup> is that it includes the seismic sources characterization used by the U.S. Geological Survey to describe the seismicity in the United States.

#### **4.2.1. Seismic Sources Characterization**

The characterization of seismic sources implemented in the PSHA is the same characterization that the U.S. Geological Survey used to develop the Seismic Hazard Maps 2002 for the CEUS region (Frankel et al., 2002) including the New Madrid and Charleston, SC seismic sources and background seismicity of the CEUS. The characterization of these seismic sources is implemented within EZ-FRISK<sup>TM</sup> and a brief description is given below. A more detailed description can be found in Frankel et al. (1996; 2002).

##### **4.2.1.1 Spatial Characterization**

Figure 4.2 shows the geographical location of the seismic sources considered in the analysis along with the extent of the Upper Mississippi Embayment. The three S-shaped sources in the New Madrid region do not represent actual active faults, but they are fictitious faults used to express the uncertainty in the location of large earthquakes such as the sequence of 1811-1812 New Madrid earthquakes (Frankel et al., 1996). The three sources are identified as NW New Madrid, C New Madrid, and SE New Madrid faults. The earthquake sources are considered vertical with the shallowest part of the fault at a depth of 10 km and the deepest part at 50 km (Frankel et al., 1996).

The broad areal seismic zone in Charleston, SC, is the same source used in the development of the 1996 U.S. National Seismic Hazard Maps (Frankel et al., 1996). The extent of the zone was constrained by paleoliquefaction sites (Frankel et al., 1996). The narrow zone was added in 2002 to encompass a more concentrated zone of seismicity following the Woodstock fault and a “zone of river anomalies” (Frankel et al., 2002; Wheeler and Perkins, 2000). These areal zones are implemented in the PSHA by dividing the zones into grid cells and converting each of them into equivalent faults using the expressions of

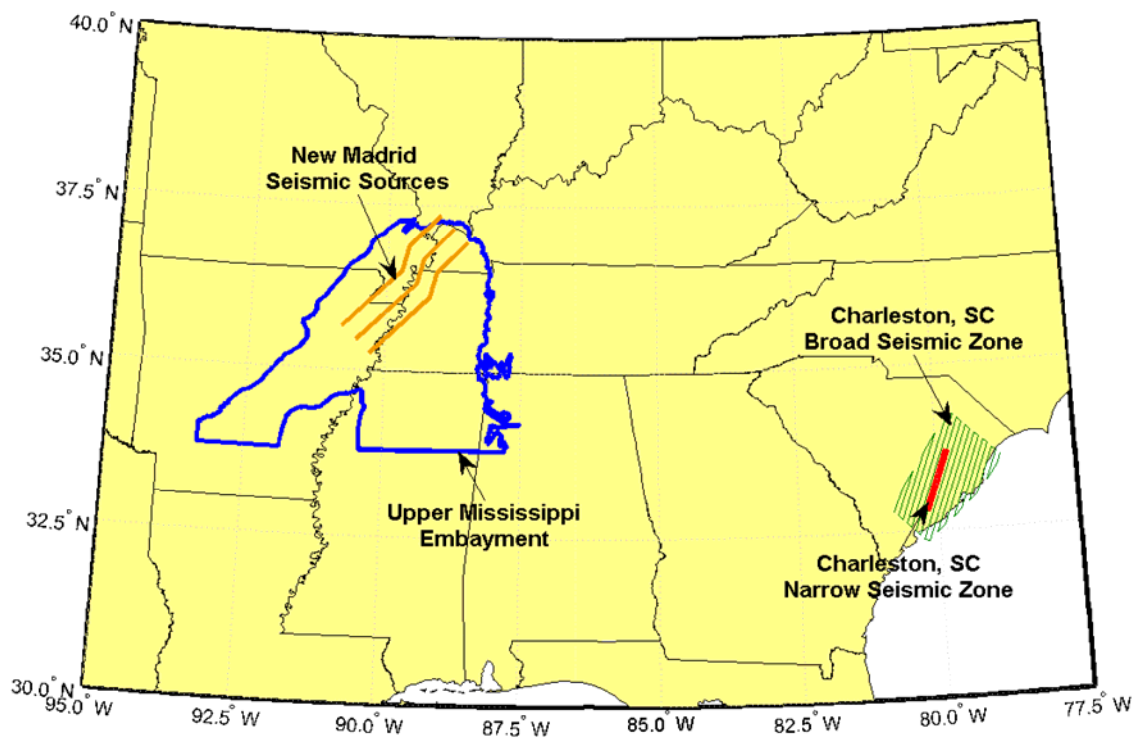


**Figure 4.2.** Geographical location of seismic sources considered in the analysis along with the extent of the Upper Mississippi Embayment

(Wells and Coppersmith, 1994). The midpoint of the fault is located at the center of the cell. The strike of the fault is considered parallel to the long axis of the narrow zone. Each of the equivalent faults are considered vertical with the same vertical location and dimension as the New Madrid faults (Frankel et al., 1996; 2002).

The background seismic zones are used to represent the seismicity of a region where large events have not occurred in the past, but that have the potential to generate large earthquakes in the future. Figure 4.3 shows the extent of the background seismicity areas, Wabash Valley and cratonic zones, implemented in the analysis along with the maximum magnitudes assigned to each zone (Frankel et al., 2002). A craton refers to an area of a continental plate that has been relatively undisturbed in the past. The background sources are included in the analysis in similar fashion as the Charleston, SC aeral zones, with the difference that the strike of the fictitious faults used to represent the background sources is considered random (Frankel et al., 2002).

The location of earthquakes within a particular source zone is assumed to follow a uniform distribution, i.e. earthquakes are considered equally likely to occur at any location within the source (Kramer, 1996).

#### 4.2.1.2 Size Characterization

The evaluation of the earthquake sizes that a particular seismic source is capable of generating is performed by a recurrence model, which describes the distribution of earthquakes sizes in a given period of time (Kramer, 1996). The exponential distribution is the most basic relationship and is expressed by the Gutenberg-Richter relation:

$$\log N(m) = a - b \cdot m \quad 4.10$$

where  $N(m)$  is the number of earthquakes of magnitude  $m$  or greater per unit of time,  $10^a$  is the number of earthquakes with  $m \geq 0$  per unit of time, and  $b$  (the  $b$ -value) is the slope of the regression line and describes the relative likelihood of small and large earthquakes. A low  $b$ -value implies a relative higher proportion of large earthquakes compared to a

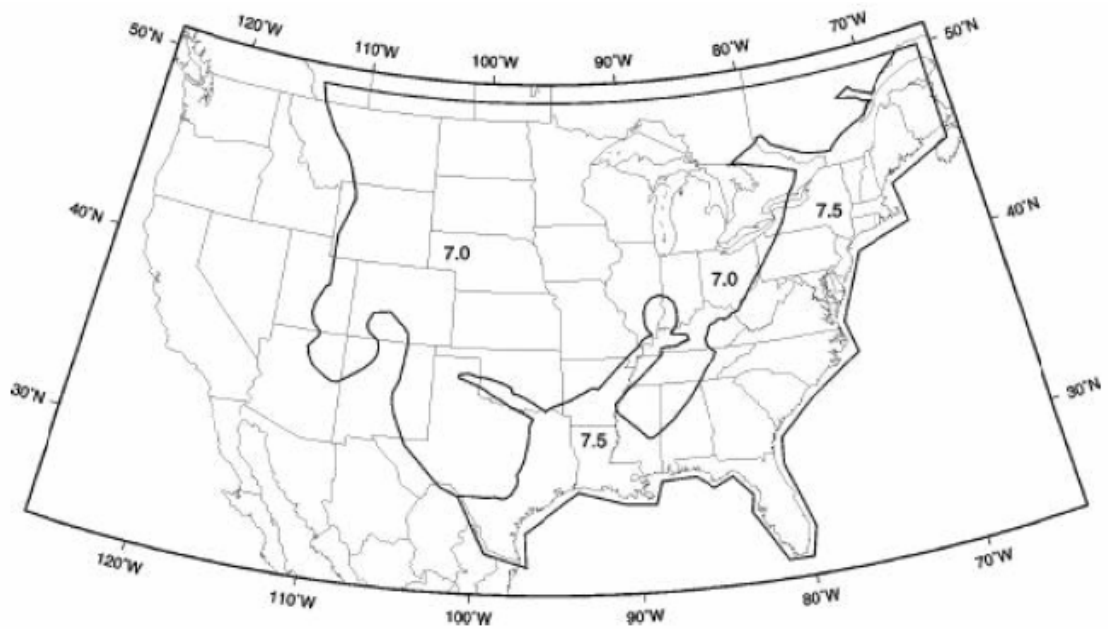


**Figure 4.3.** Extent of the background seismicity areas, Wabash Valley (east zone) and cratonic zones (west zone), and maximum magnitude assigned to each zone (Frankel et al., 2002)

high b-value (Kramer, 1996; McGuire, 2004; Reiter, 1990). Figure 4.4 illustrates the Gutenberg-Richter relation.

Equation 4.10 considers an infinite range of magnitudes. However in PSHA for engineering purposes is common to disregard the effects of small magnitudes less than  $m_{\min}$  because they are not capable of causing significant damage, and discard earthquakes above a particular magnitude,  $m_{\max}$ , because they are not physically possible for a given seismic source. A truncated exponential distribution accounts for these lower and upper bounds and is expressed by the following relation (Kramer, 1996):

$$N(m) = v \cdot \frac{\exp[-\beta \cdot (m - m_{\min})] - \exp[-\beta \cdot (m_{\max} - m)]}{1 - \exp[-\beta \cdot (m_{\max} - m)]} \quad m_{\min} \leq m \leq m_{\max} \quad 4.11$$

where  $v = \exp(\alpha - \beta \cdot m_{\min})$  is the number of earthquakes with  $m \geq m_{\min}$  in a given period of time,  $\alpha = a \cdot \ln(10)$ , and  $\beta = b \cdot \ln(10)$ .

Equations 4.10 and 4.11 describe the frequency of earthquake occurrence in a region that involves many seismic sources, but they do not provide a good representation of the frequency of occurrence on individual faults (Schwartz and Coppersmith, 1984). Geologic investigations indicate that individual faults tend to generate earthquakes within a narrow range of magnitudes (a half magnitude unit) at or near their maximum magnitude. These earthquakes are known as characteristic earthquakes. The characteristic recurrence model (Youngs and Coppersmith, 1985) combines the exponential magnitude distribution (i.e. Equation 4.11) for small and moderate magnitudes earthquakes with a uniform distribution for large magnitude earthquakes near the characteristic earthquake. The exponential part of the distribution is estimated from historical seismicity, and the characteristic part is controlled by geologic data. Figure 4.5 illustrates the characteristic recurrence model proposed by Schwartz and Coppersmith (1984) to characterize the frequency of occurrence on individual faults.

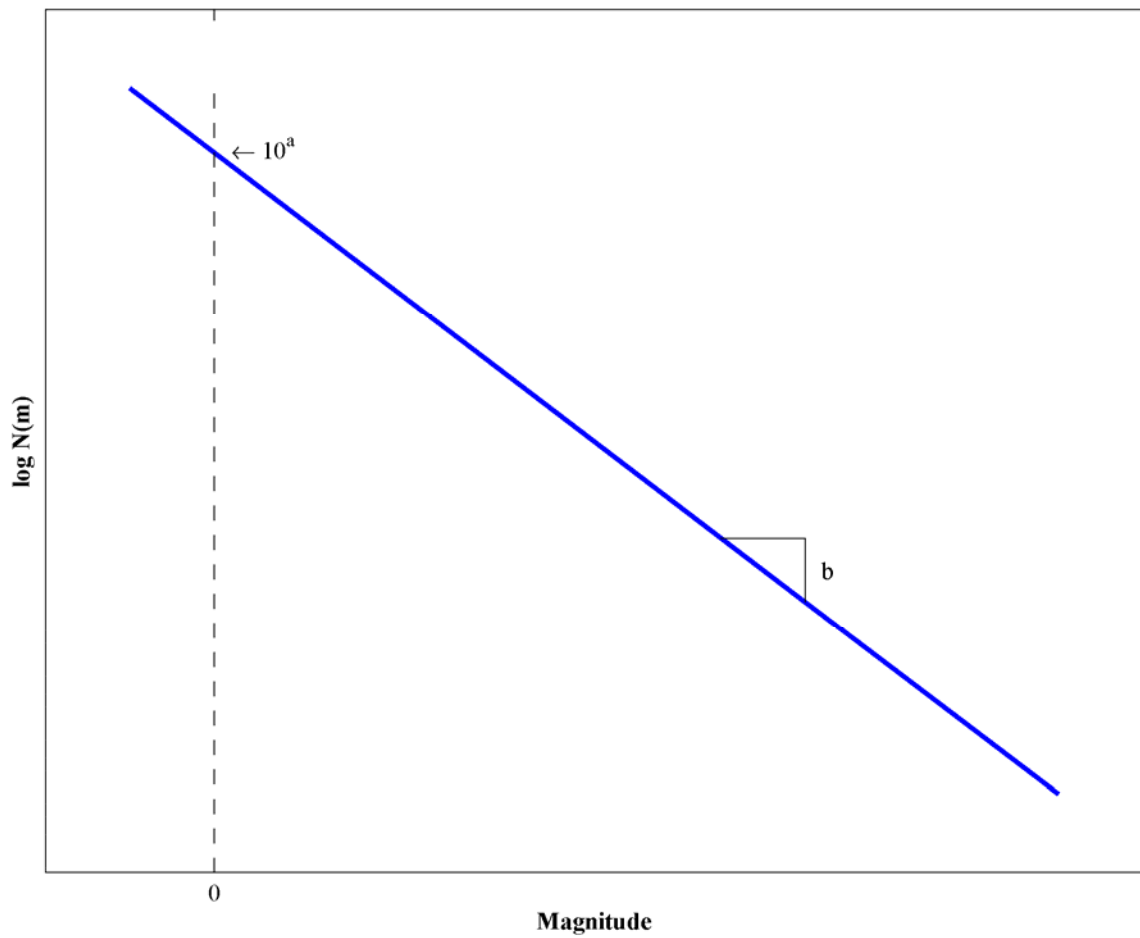


**Figure 4.4.** Gutenberg-Richter recurrence relation (from Kramer, 1996)

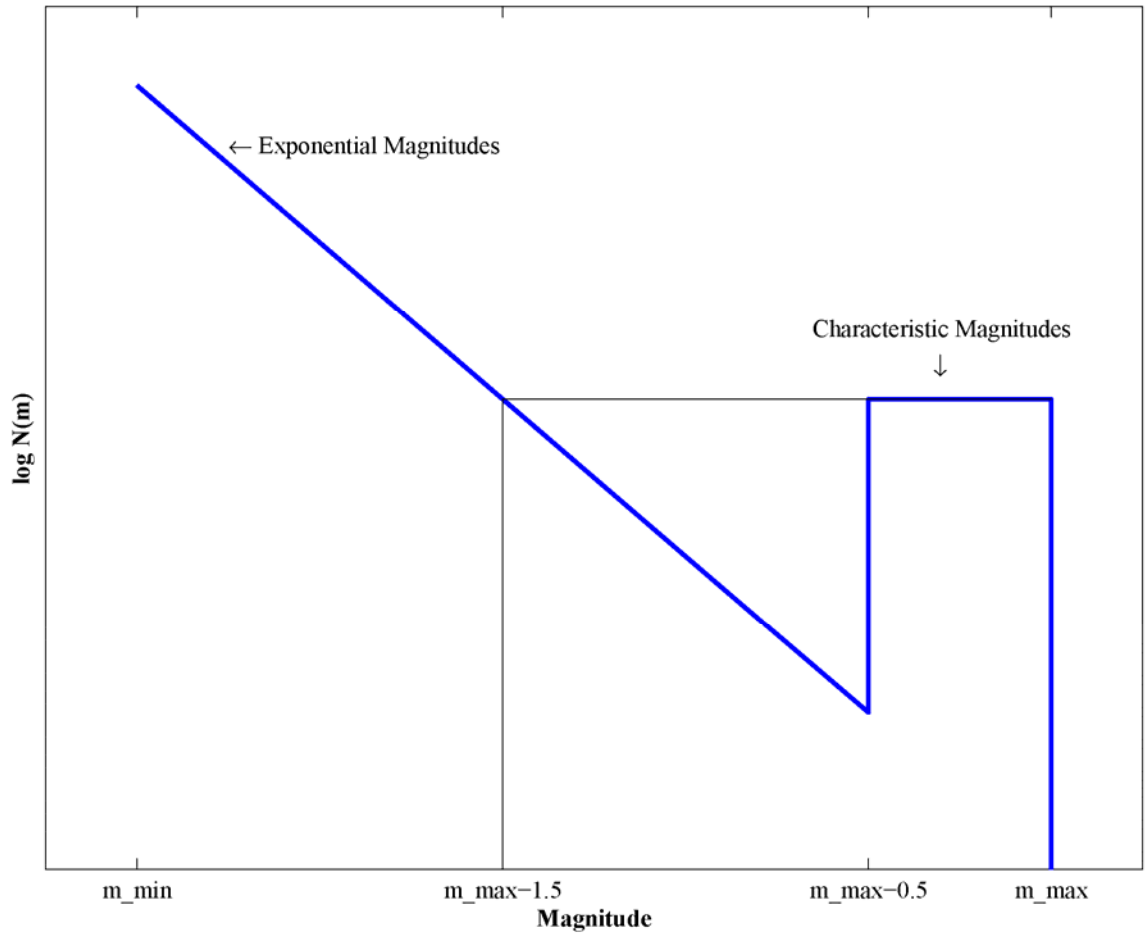


**Figure 4.5.** Characteristic magnitude recurrence model proposed by Schwartz and Coppersmith (1984) (from McGuire, 2004)

The seismicity of the New Madrid and Charleston, SC sources is characterized by a characteristic recurrence model and the background seismicity sources are described by a truncated exponential recurrence model.

The parameters of the exponential part of the recurrence model and weights assigned to the New Madrid and Charleston, SC sources are given in Table 4.1. The annual rate of occurrence is based on events of magnitude higher than **M** 4.5. The analysis uses a logic tree to incorporate epistemic variability in the characteristic magnitude of the New Madrid sources, i.e. the maximum magnitude of the sequence of earthquakes in 1811-1812. The weights assigned to each hypothesis are shown in Table 4.2. This logic tree results in the same hazard as if only the **M** 7.7 hypothesis were considered in the analysis with a weight of 1.0 (Frankel et al., 2002). A mean recurrence time of 500 years is used for the characteristic earthquakes, which equals the inverse of the total rate resulting by adding the equivalent rates computed by multiplying the rates and weights shown in Table 4.1 (Frankel et al., 2002).

**Table 4.1.** Parameters for exponential part of the recurrence model of New Madrid and Charleston, SC sources

<b>Seismic Source</b>	<b>Rate (events/year)<sup>1</sup></b>	<b>b-value</b>	<b>Weight</b>
C New Madrid	0.002	0.95	0.50
NW New Madrid	0.002	0.95	0.25
SE New Madrid	0.002	0.95	0.25
Broad zone, Charleston, SC	0.00182	0.95	0.50
Narrow zone, Charleston, SC	0.00182	0.95	0.50

<sup>1</sup> Events with  $m_b > 5$  (i.e.  $\sim$ **M** 4.5)

**Table 4.2.** Logic tree for characteristic magnitude of New Madrid seismic sources

<b>Magnitude</b>	<b>Weight</b>
<b>M 7.3</b>	0.15
<b>M 7.5</b>	0.20
<b>M 7.7</b>	0.50
<b>M 8.0</b>	0.15

Table 4.1 lists the seismic parameters for the exponential portion of the recurrence model for the Charleston, SC sources, and Table 4.3 shows the logic tree implemented in the analysis for the characteristic magnitude for the Charleston, SC sources. A mean recurrence time of 550 years is used for the characteristic earthquakes (Frankel et al., 2002).

Figure 4.3 shows the maximum magnitude assigned to the background seismicity. A minimum magnitude of  $m_b$  3 (i.e.  $\sim M$  2.5) and a b-value of 0.95 are used for the exponential recurrence model of the background seismicity used in the analysis.

**Table 4.3.** Logic tree for characteristic magnitude of Charleston, SC seismic sources

<b>Magnitude</b>	<b>Weight</b>
<b>M 6.8</b>	0.20
<b>M 7.1</b>	0.20
<b>M 7.3</b>	0.45
<b>M 7.5</b>	0.15

#### **4.2.2. Ground Motion Attenuation Relationships**

Attenuation relationships and their inherent uncertainty must be specified to estimate ground motions at the site as a function of earthquake magnitude and distance to the seismic source. The soil attenuation relationships developed in Chapter 3 for the Upper Mississippi Embayment were selected to perform the seismic hazard analysis. The attenuation relationships incorporate the entire earthquake process including source, path, and site effects, and the non-linear behavior of the deep soil profile in the Embayment. As discussed previously, the use of soil attenuation relationships in PSHA represents the most accurate approach to develop probabilistic soil ground motions (Bazzurro and Cornell, 2004b; Silva and Costantino, 2002). The correlation among the earthquake generation and propagation processes is directly taken into account.

The epistemic variability on attenuation relationship is incorporated by using three source models – Atkinson and Boore (1995), Frankel et al. (1996), and Silva et al. (2003) –, and three values of the stress drop parameter,  $\Delta\sigma$  – median case, 100% higher (high case), and 100% lower (low case) –. The Atkinson and Boore (1995) model is insensitive to the stress drop and therefore only one case is implemented for this source model. The weights assigned to each hypothesis in the analysis are 2/3, 1/6, and 1/6 for the median, high and low stress drop values (Silva et al., 2003) and 1/3, 1/3, and 1/3 for the three source models. Table 4.4 lists the weights assigned to each combination of source model and stress drop value.

#### **4.2.3. Seismic Hazard Analyses for Selected Cities**

Deterministic and probabilistic seismic hazard analyses were performed for seven selected cities within the Upper Mississippi Embayment including Memphis, TN; Jonesboro, AR; Jackson, TN; Blytheville, AR; Paducah, KY; Cape Girardeau, MO; and Little Rock, AR. Figure 4.6 shows a map of the Embayment along with the location of the selected cities and Table 4.5 lists the latitude, longitude, soil profile, and soil column

**Table 4.4.** Logic tree for attenuation relationship

<b>Attenuation Relationship</b>	<b>Weight</b>
Atkinson and Boore (1995)	1/3
Frankel et al. (1996) – median case of $\Delta\sigma$	2/9
Frankel et al. (1996) – high case of $\Delta\sigma$	1/18
Frankel et al. (1996) – low case of $\Delta\sigma$	1/18
Silva et al. (2003) – median case of $\Delta\sigma$	2/9
Silva et al. (2003) – high case of $\Delta\sigma$	1/18
Silva et al. (2003) – low case of $\Delta\sigma$	1/18

**Table 4.5.** Selected cities included in the seismic hazard analysis

<b>City</b>	<b>Latitude</b>	<b>Longitude</b>	<b>Soil Profile</b>	<b>Soil Column Depth (approx.) (m)</b>
Memphis, TN	35.050	-90.000	Lowlands	900
Memphis, TN	35.050	-90.000	Uplands	900
Jonesboro, AR	35.833	-90.700	Uplands	600
Jackson, TN	35.600	-88.917	Uplands	350
Blytheville, AR	35.950	-89.950	Lowlands	850
Paducah, KY	37.067	-88.767	Uplands	120
Cape Girardeau, MO	37.233	-89.583	Lowlands	10
Little Rock, AR	34.733	-92.233	Uplands	10

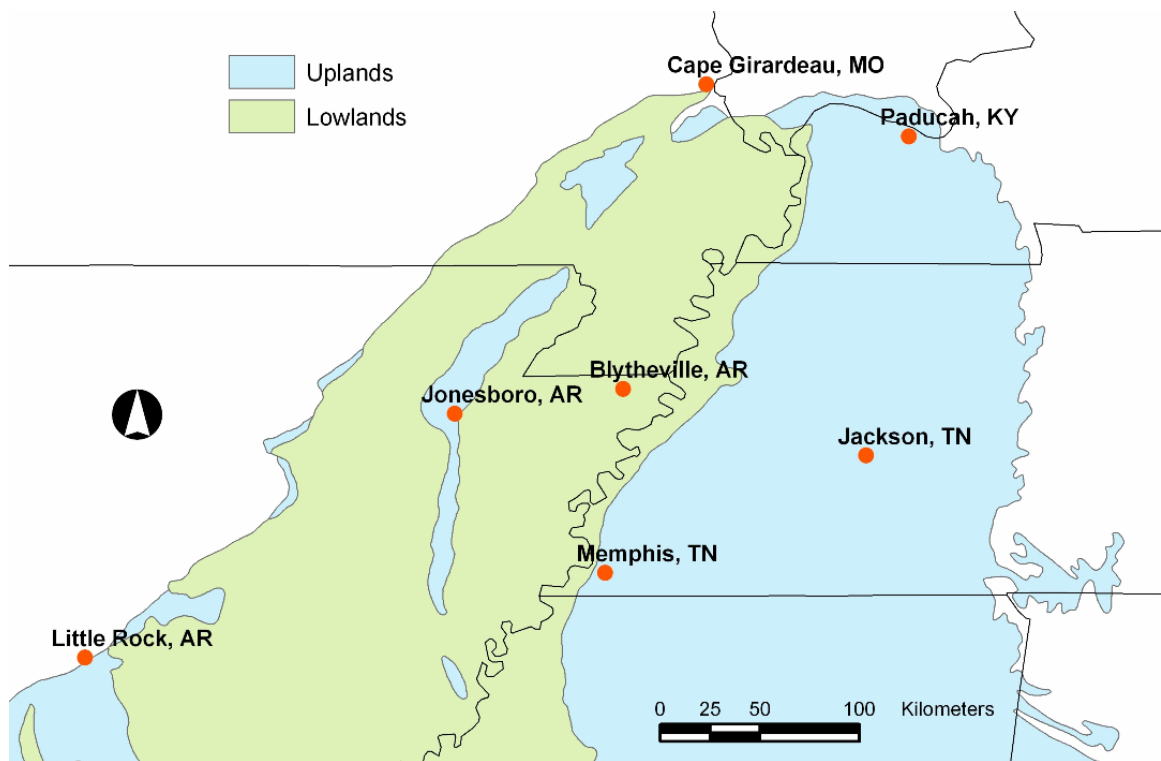


**Figure 4.6.** Upper Mississippi Embayment and selected cities included in the seismic hazard analysis

depth used in the analyses for each city. Both Lowlands and Uplands soil profiles were considered for the city of Memphis, TN, because portions of the city are in each soil type.

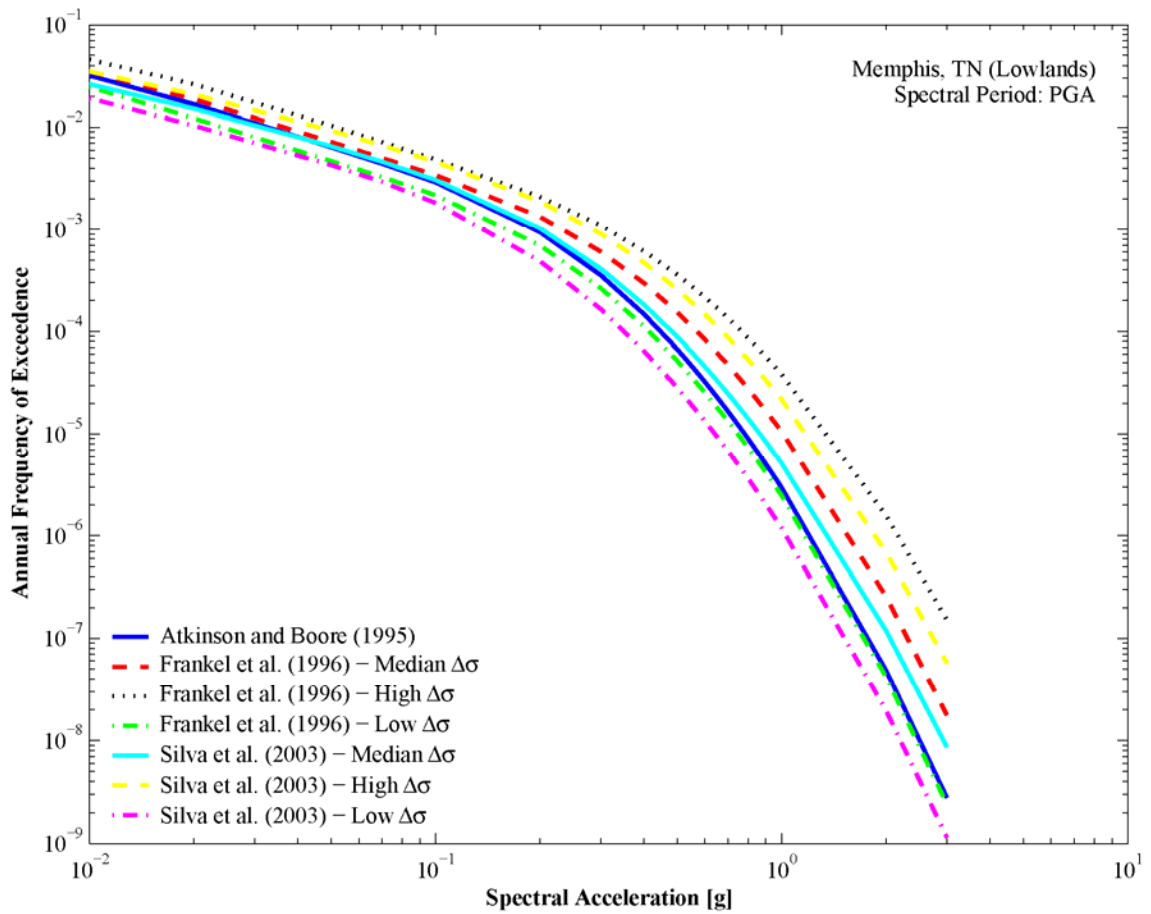
The attenuation relationships used in the PSHA for each city were selected based upon the type of soil profile and depth to the bedrock as defined in Table 4.5. The epistemic variability in characteristic magnitude of the New Madrid and Charleston, SC seismic sources shown in Table 4.2 and Table 4.3 is included in the analysis by EZ-FRISK<sup>TM</sup>, so the seismic hazard results shows only one hazard curve per attenuation relationship. The combination of source models and stress drop values, as listed in Table 4.4, results in seven independent hazard curves for each city.

Figure 4.7 and Figure 4.8 compare the seven different soil hazard curves for Memphis, TN, corresponding to PGA and 1-second spectral period. The figures show the scatter due to the epistemic variability in source model and stress drop value.

The seven hazard curves for a particular city are combined into a single mean hazard curve (McGuire, 2004; McGuire et al., 2005; Musson, 2005). The mean hazard curve is computed as the weighted average of the seven individual hazard curves using the weights listed in Table 4.4. This calculation is performed using the following equation:

$$\ln \bar{\lambda} = \frac{\sum_{i=1}^N w_i \cdot \ln \lambda_i}{\sum_{i=1}^N w_i} \quad 4.12$$

where  $\lambda$  is the annual frequency that a ground motion exceeds a particular level,  $N$  is the number of hazard curves,  $w$  is the weighting factor, and subindex  $i$  refers to a particular hazard curve. The weighted variance associated with the weighted mean is calculated by:



**Figure 4.7.** Peak ground acceleration hazard curves for Memphis, TN

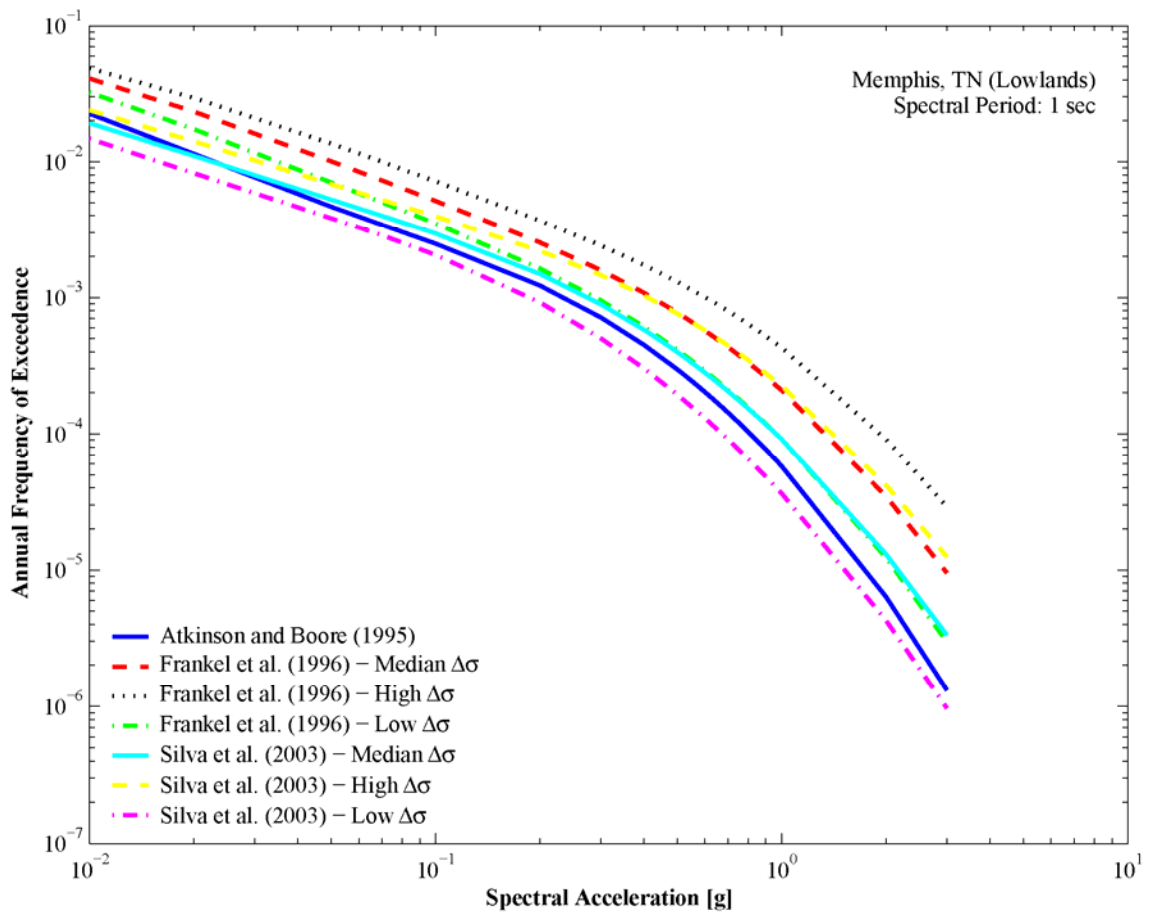


**Figure 4.8.** One-second spectral period hazard curves for Memphis, TN

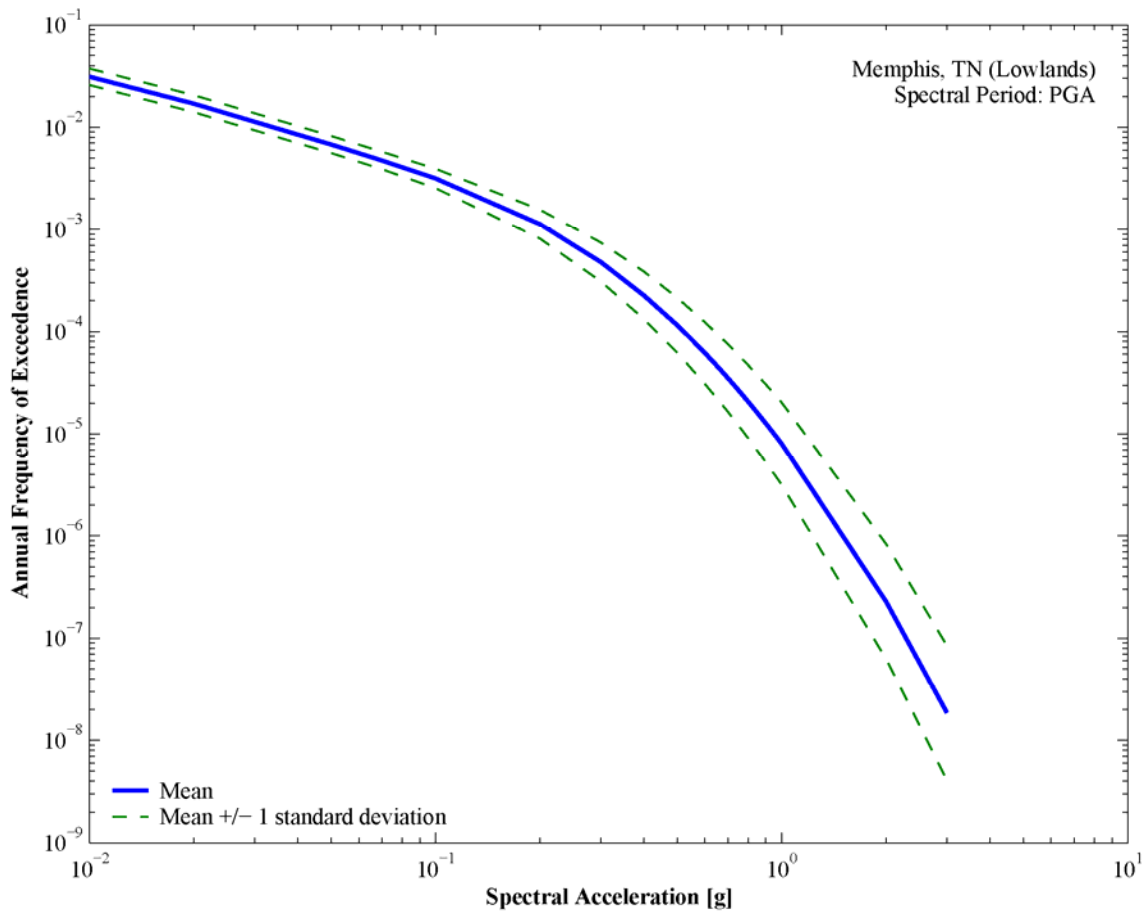
$$\sigma_{\ln \bar{\lambda}}^2 = \frac{\sum_{i=1}^N w_i \cdot (\ln \lambda_i - \ln \bar{\lambda})^2}{\sum_{i=1}^N w_i} \quad 4.13$$

Figure 4.9 through Figure 4.24 show the mean hazard curve and its associated variability for the seven cities listed in Table 4.5, corresponding to PGA and 1-second spectral period. Similar curves were obtained for 50 spectral periods distributed between 0.01 and 5 seconds. The hazard values depend on the location of the city with respect to the seismic sources and to the Embayment depth in each city, as discussed later.

#### 4.2.3.1 Seismic Hazard Deaggregation

Probabilistic seismic hazard analysis in the form of Equation 4.4 combines the effects of all possible magnitudes and relevant sources into one hazard curve. The output of a PSHA is the probability that a ground motion parameter exceeds a given value, but it does not indicate if this ground motion value is produced by a small local earthquake or by a large distant earthquake. Seismic hazard deaggregation methods (Bazzurro and Cornell, 1999; Chapman, 1995; McGuire, 1995; Scott et al., 1998) identify the earthquakes (i.e. magnitude, distance, and epsilon) that contribute to the seismic hazard estimated by probabilistic methods.

Several methods have been proposed to determine the dominant magnitude-distance pairs in a PSHA. Chapman (1995) proposed an approach where the modal events (i.e. the most frequent events), defined in terms of magnitude and distance, are selected as the earthquakes that dominate the seismic hazard. Chapman (1995) defines the modal event for a given ground motion amplitude  $y$  and earthquake source  $i$ , as the earthquake of magnitude  $m$  and distance  $r$  that maximizes the integrand of Equation 4.3  $v_i \cdot P[Y \geq y | m, r] \cdot f_{M_i}(m) \cdot f_{R_i}(r)$ . This approach does not consider the aleatory variability in the ground motion attenuation equation, which causes the difference observed between the design ground motion calculated by the seismic hazard analysis



**Figure 4.9.** Peak ground acceleration mean and +/- 1 standard deviation hazard curves for Memphis, TN (Lowlands)

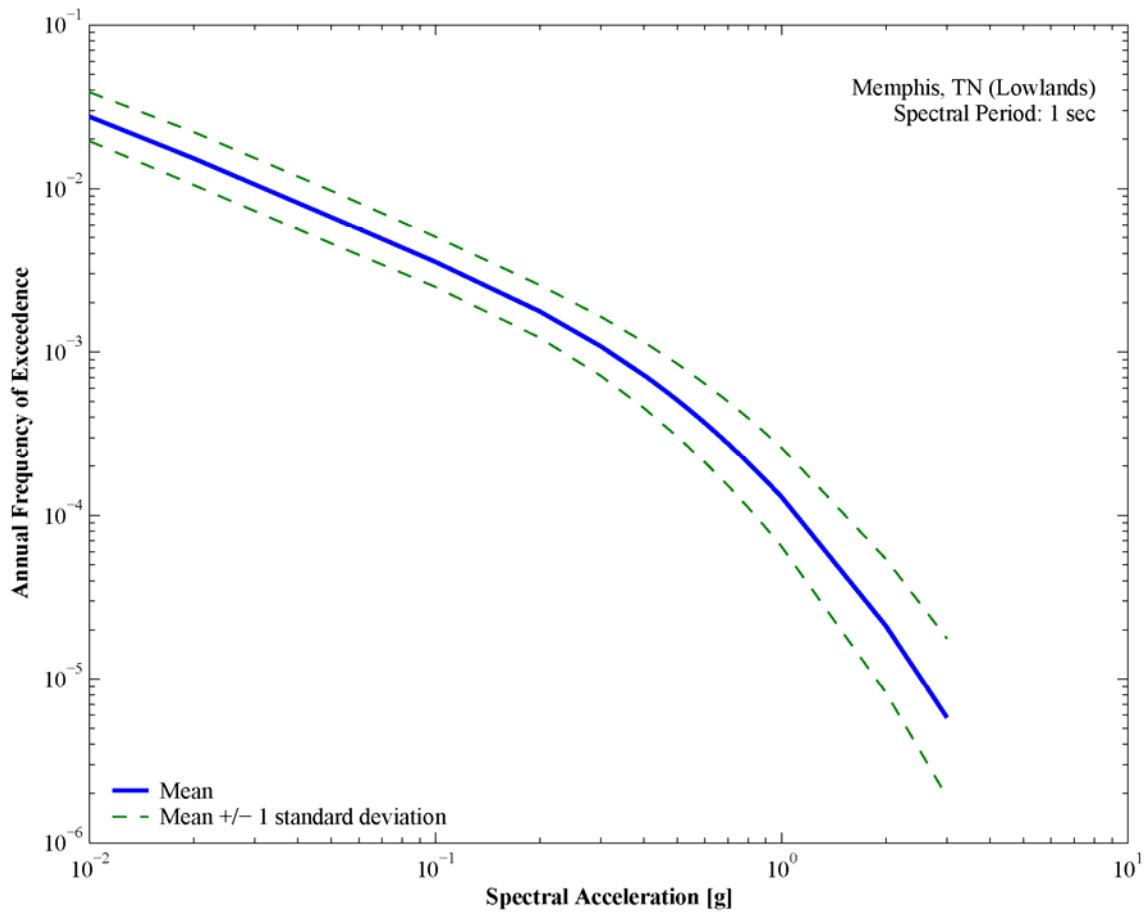


**Figure 4.10.** One-second spectral period mean and  $\pm$  1 standard deviation hazard curves for Memphis, TN (Lowlands)

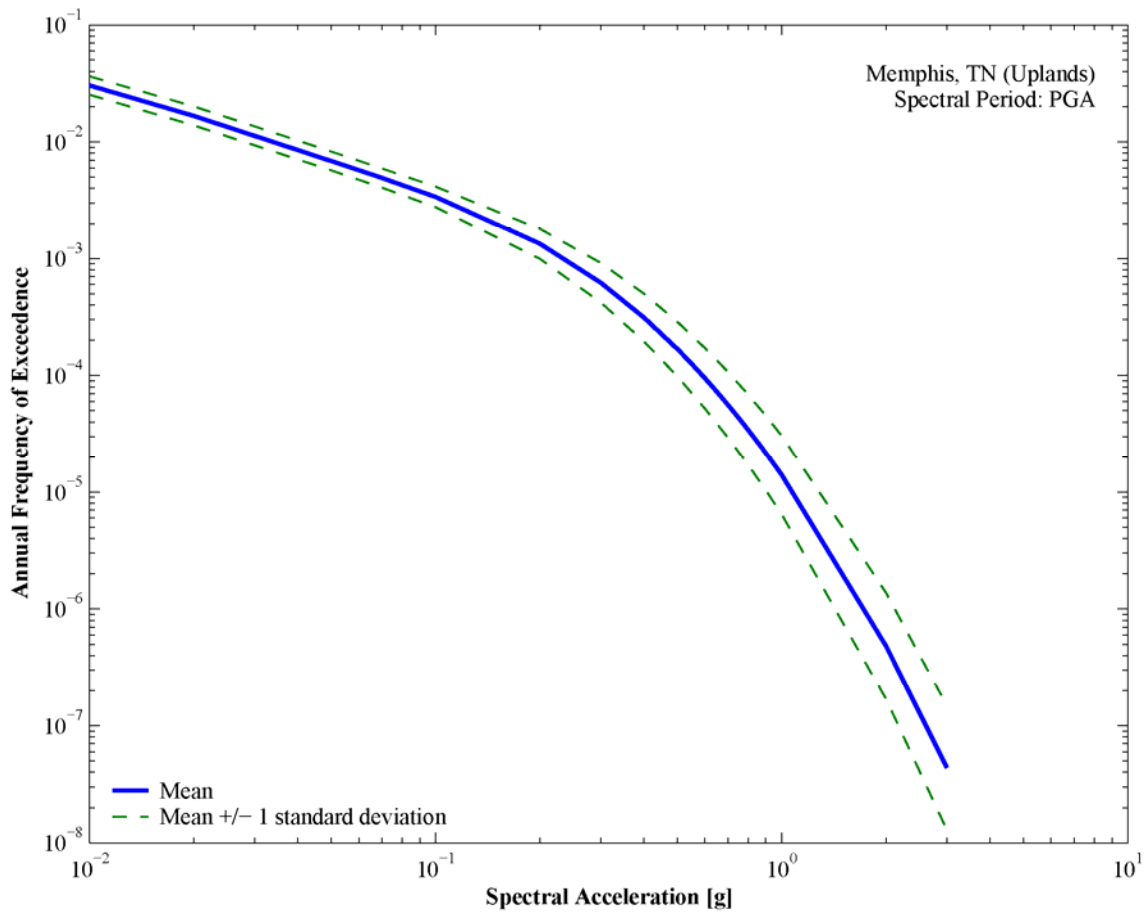


**Figure 4.11.** Peak ground acceleration mean and +/- 1 standard deviation hazard curves for Memphis, TN (Uplands)

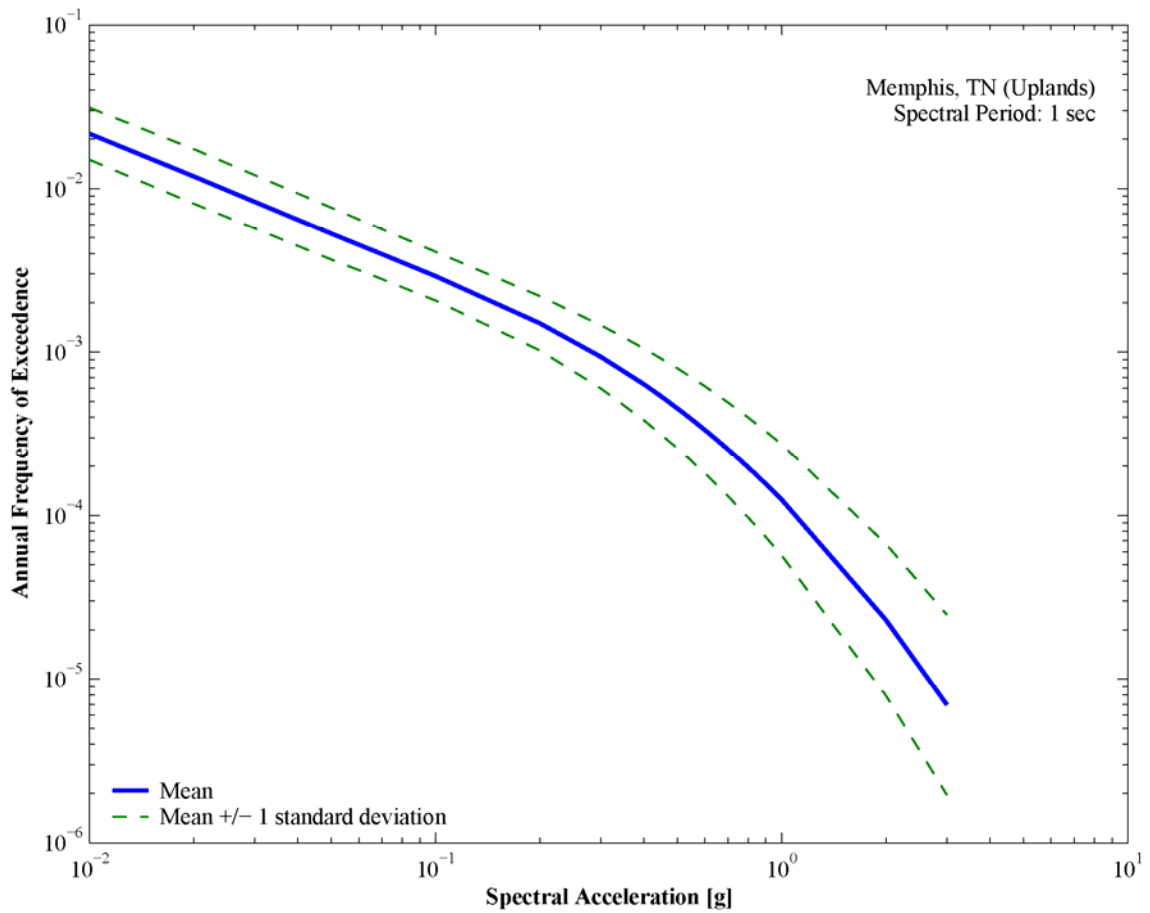


**Figure 4.12.** One-second spectral period mean and  $\pm$  1 standard deviation hazard curves for Memphis, TN (Uplands)

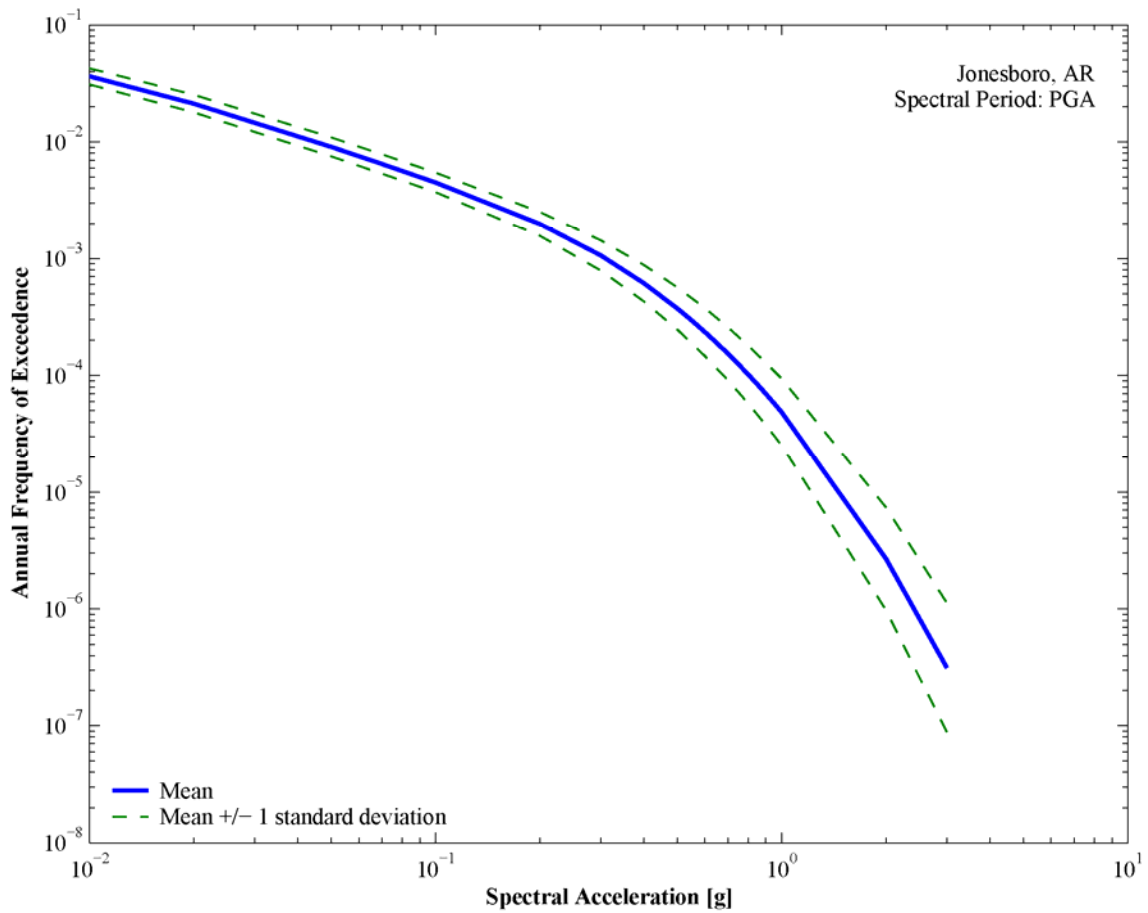


**Figure 4.13.** Peak ground acceleration mean and  $\pm$  1 standard deviation hazard curves for Jonesboro, AR

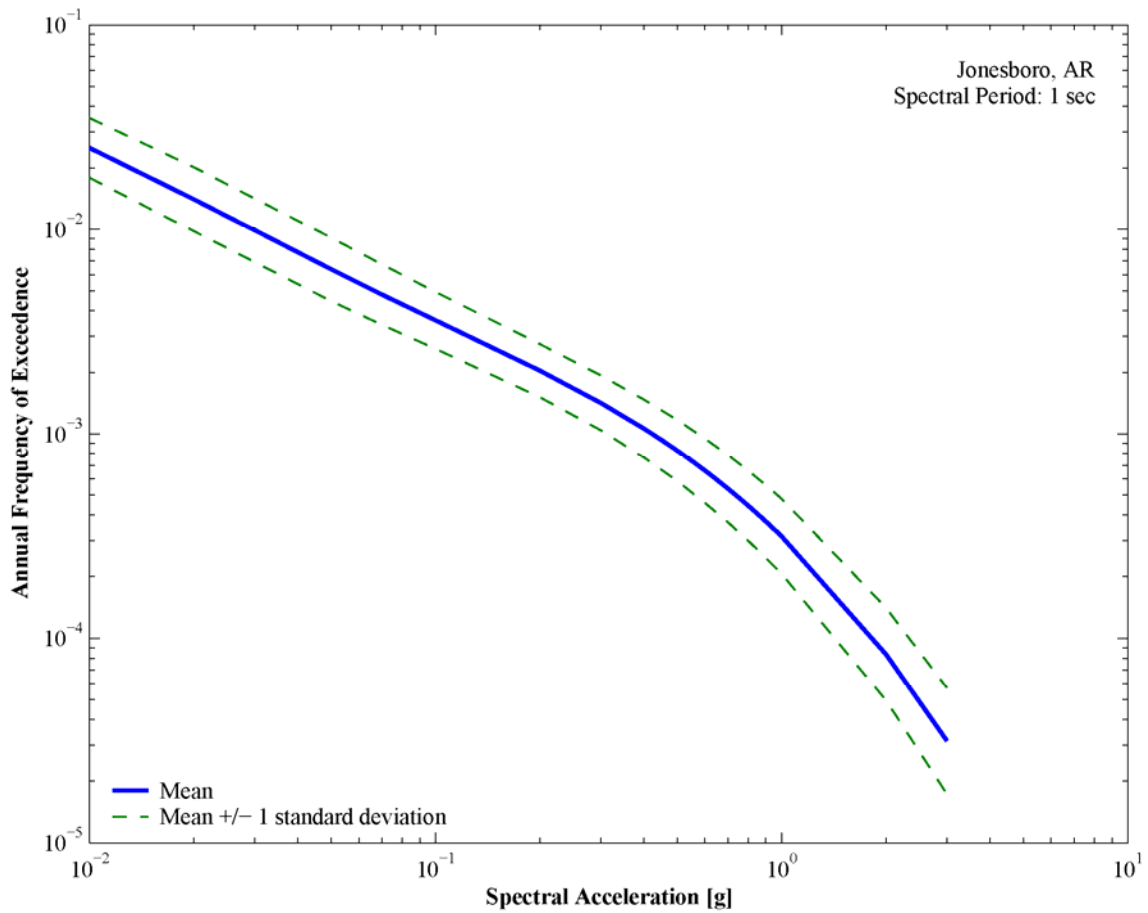


**Figure 4.14.** One-second spectral period mean and  $\pm 1$  standard deviation hazard curves for Jonesboro, AR

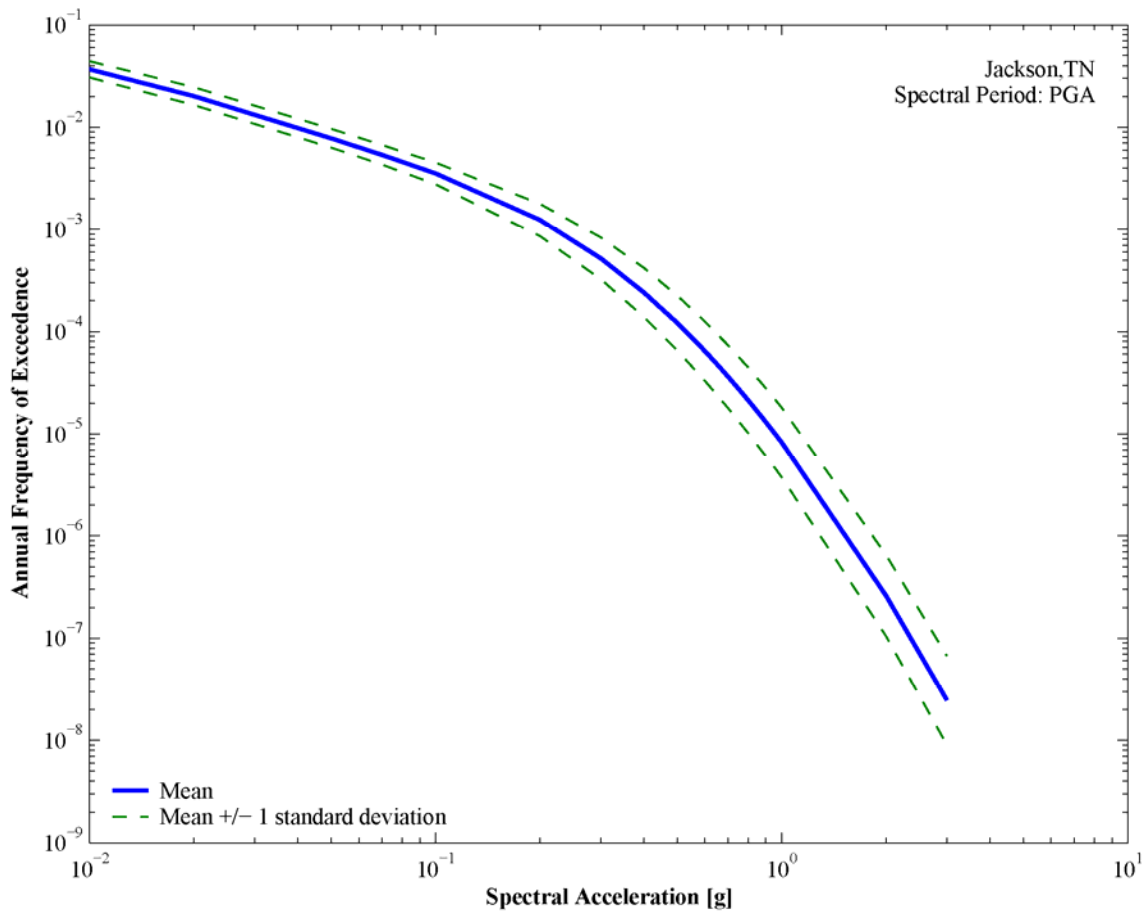


**Figure 4.15.** Peak ground acceleration mean and  $\pm$  1 standard deviation hazard curves for Jackson, TN

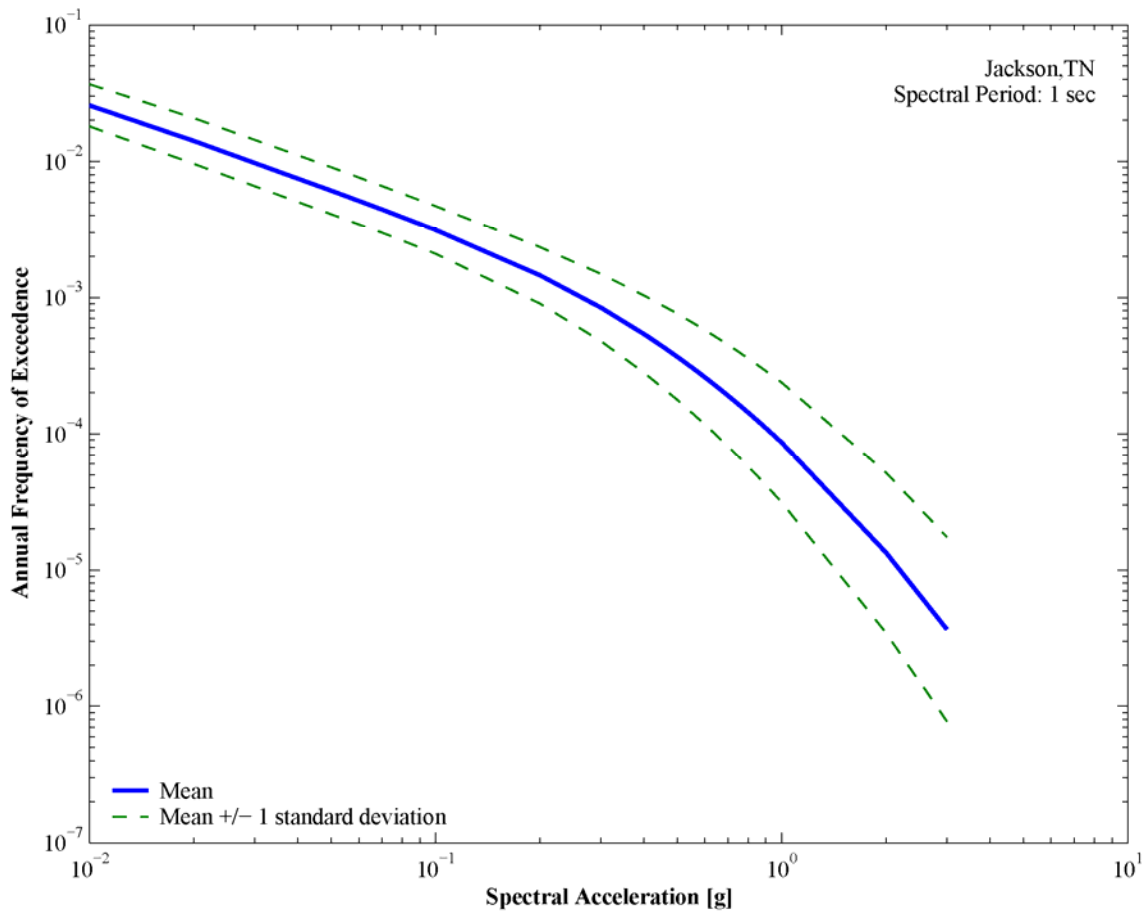


**Figure 4.16.** One-second spectral period mean and  $\pm$  1 standard deviation hazard curves for Jackson, TN

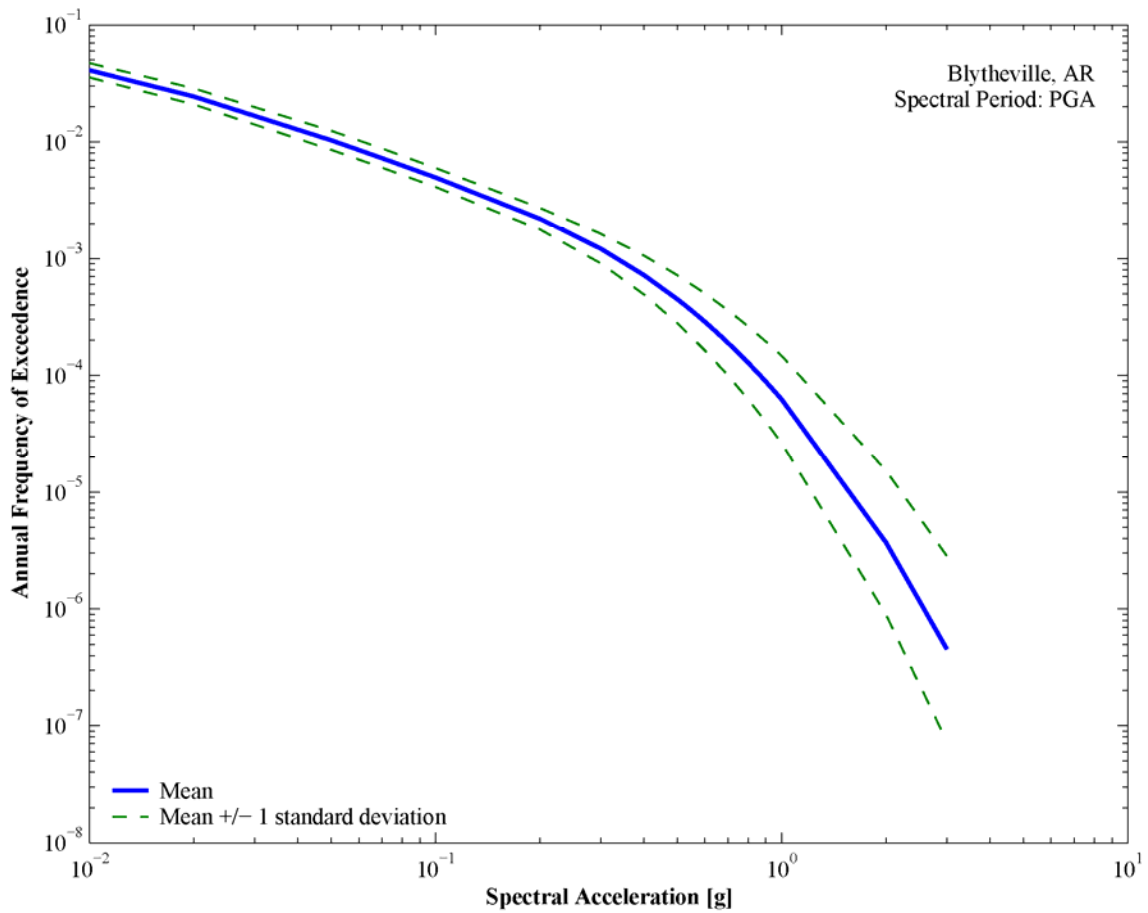


**Figure 4.17.** Peak ground acceleration mean and +/- 1 standard deviation hazard curves for Blytheville, AR

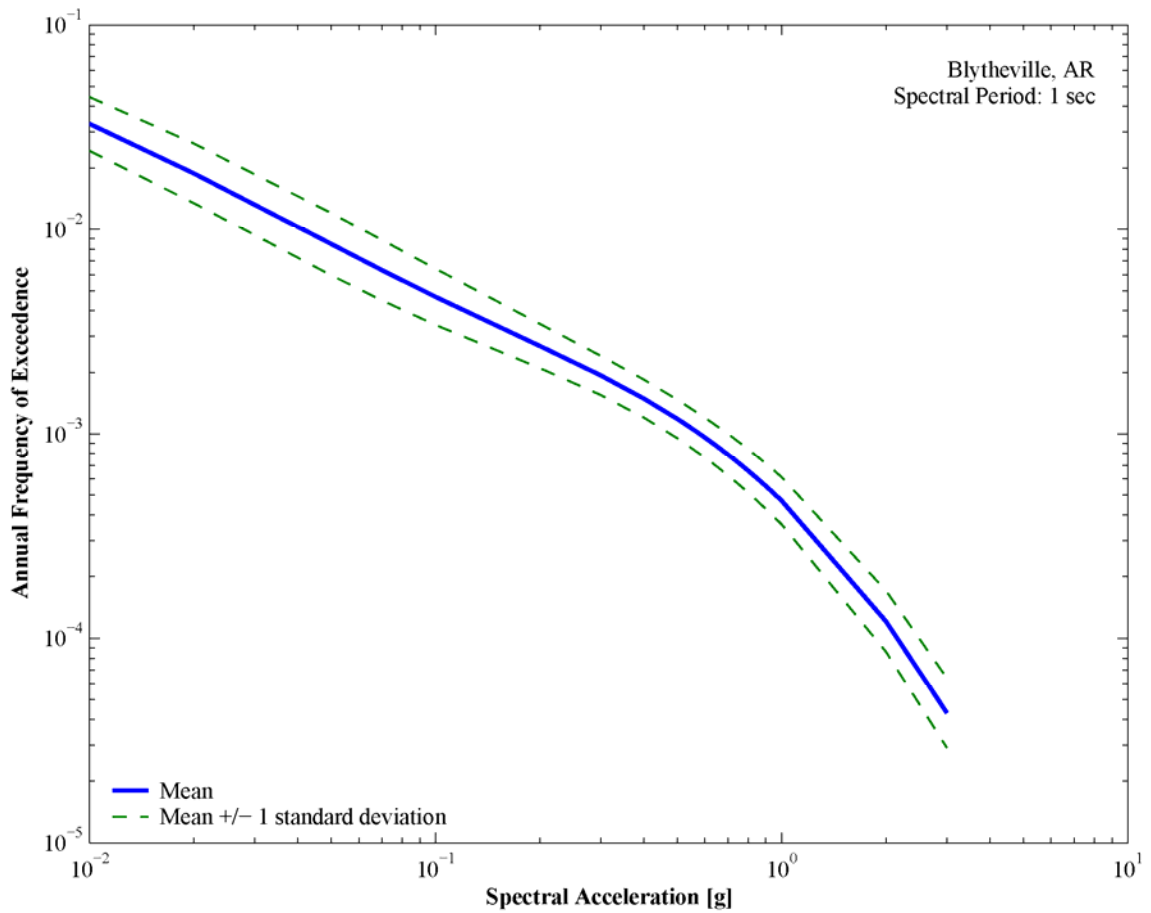


**Figure 4.18.** One-second spectral period mean and  $\pm$  1 standard deviation hazard curves for Blytheville, AR

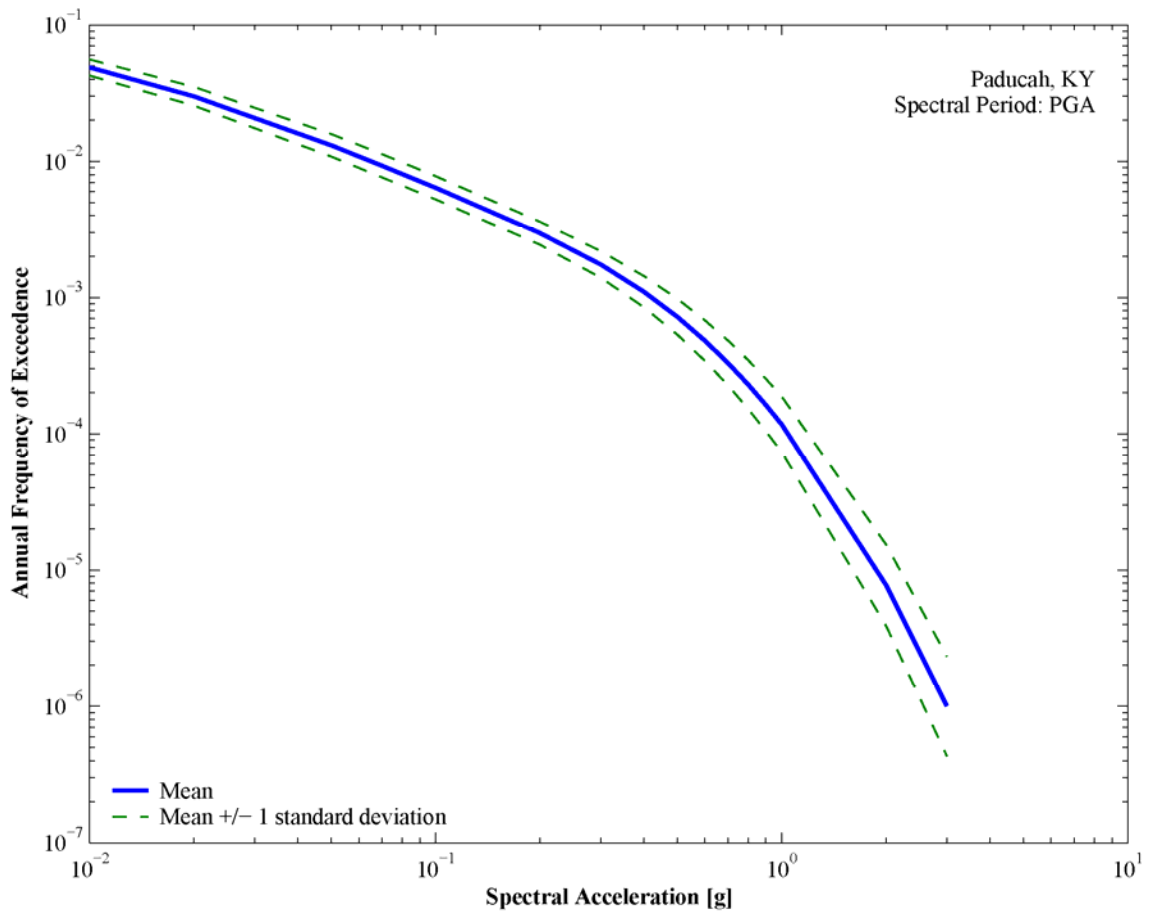


**Figure 4.19.** Peak ground acceleration mean and +/- 1 standard deviation hazard curves for Paducah, KY

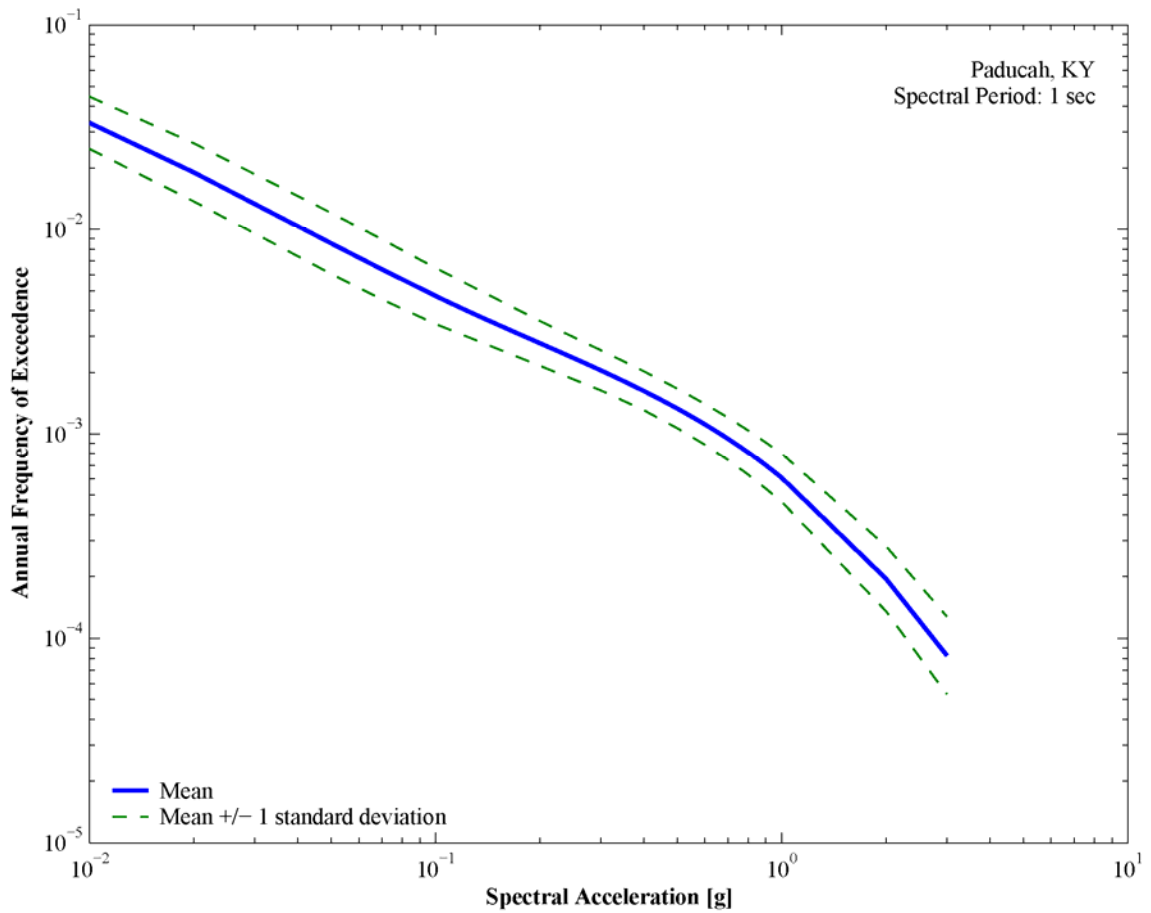


**Figure 4.20.** One-second spectral period mean and +/- 1 standard deviation hazard curves for Paducah, KY

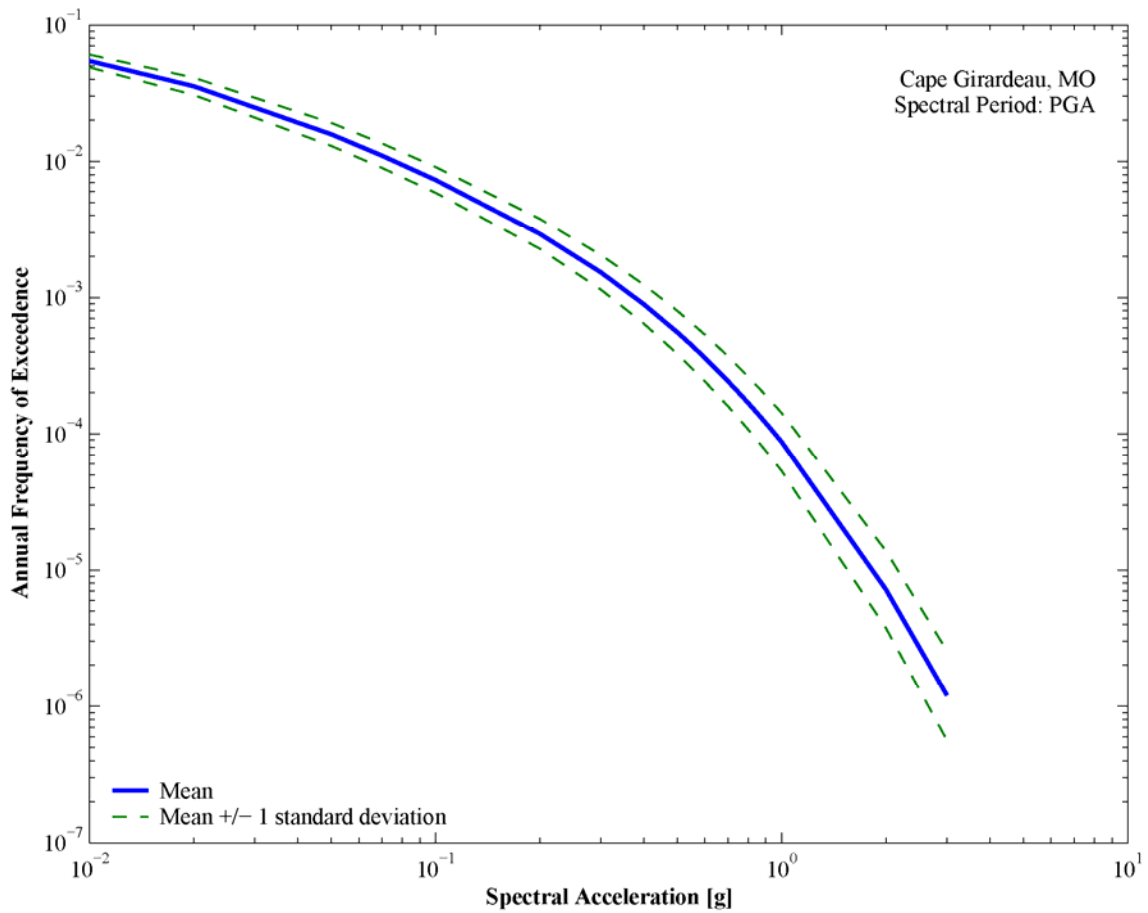


**Figure 4.21.** Peak ground acceleration mean and +/- 1 standard deviation hazard curves for Cape Girardeau, MO

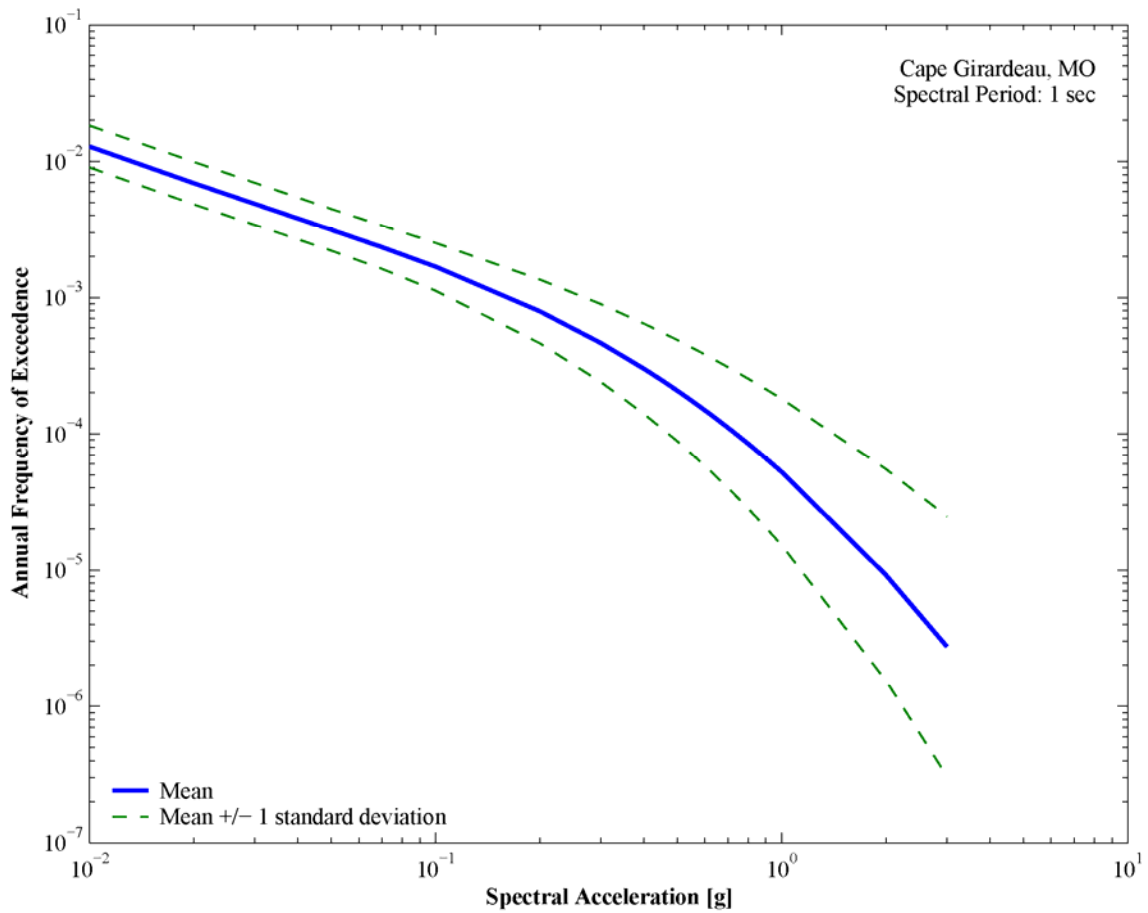


**Figure 4.22.** One-second spectral period mean and  $\pm$  1 standard deviation hazard curves for Cape Girardeau, MO

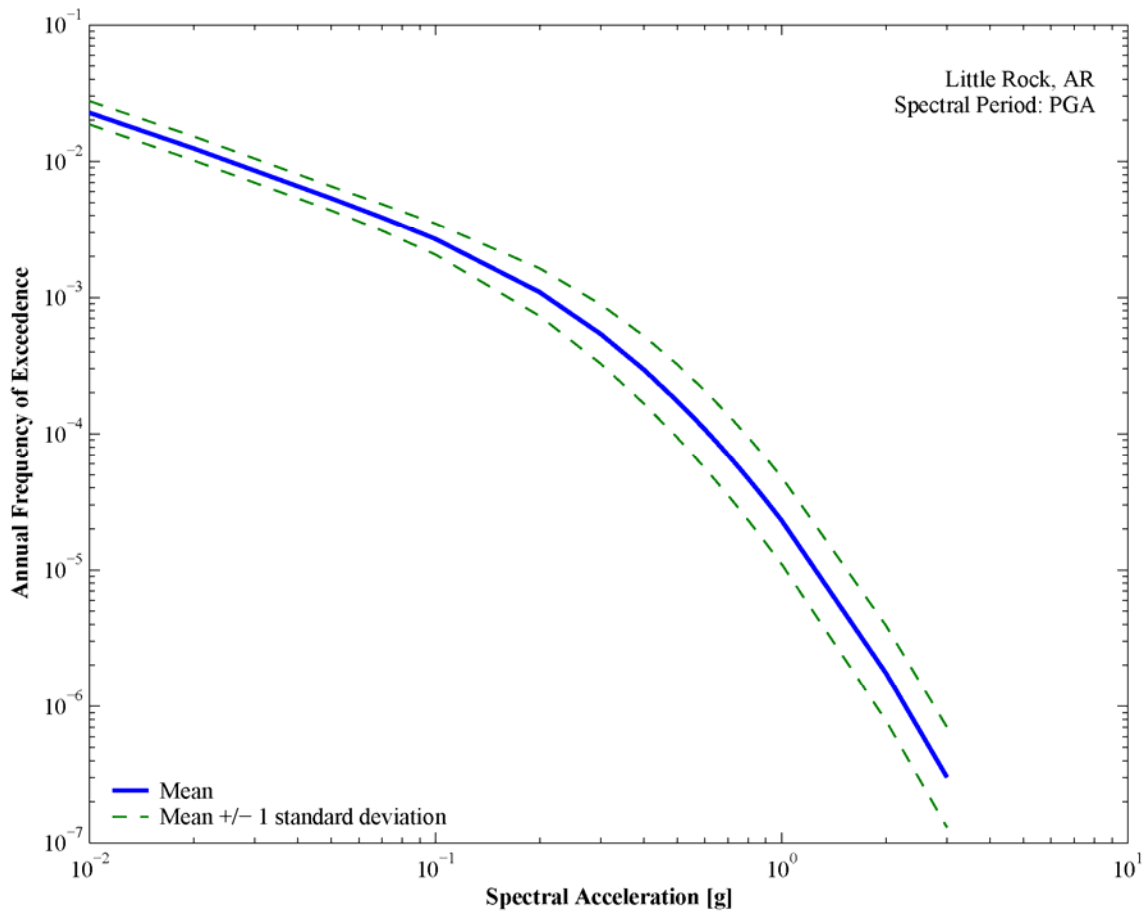


**Figure 4.23.** Peak ground acceleration mean and  $\pm$  1 standard deviation hazard curves for Little Rock, AR

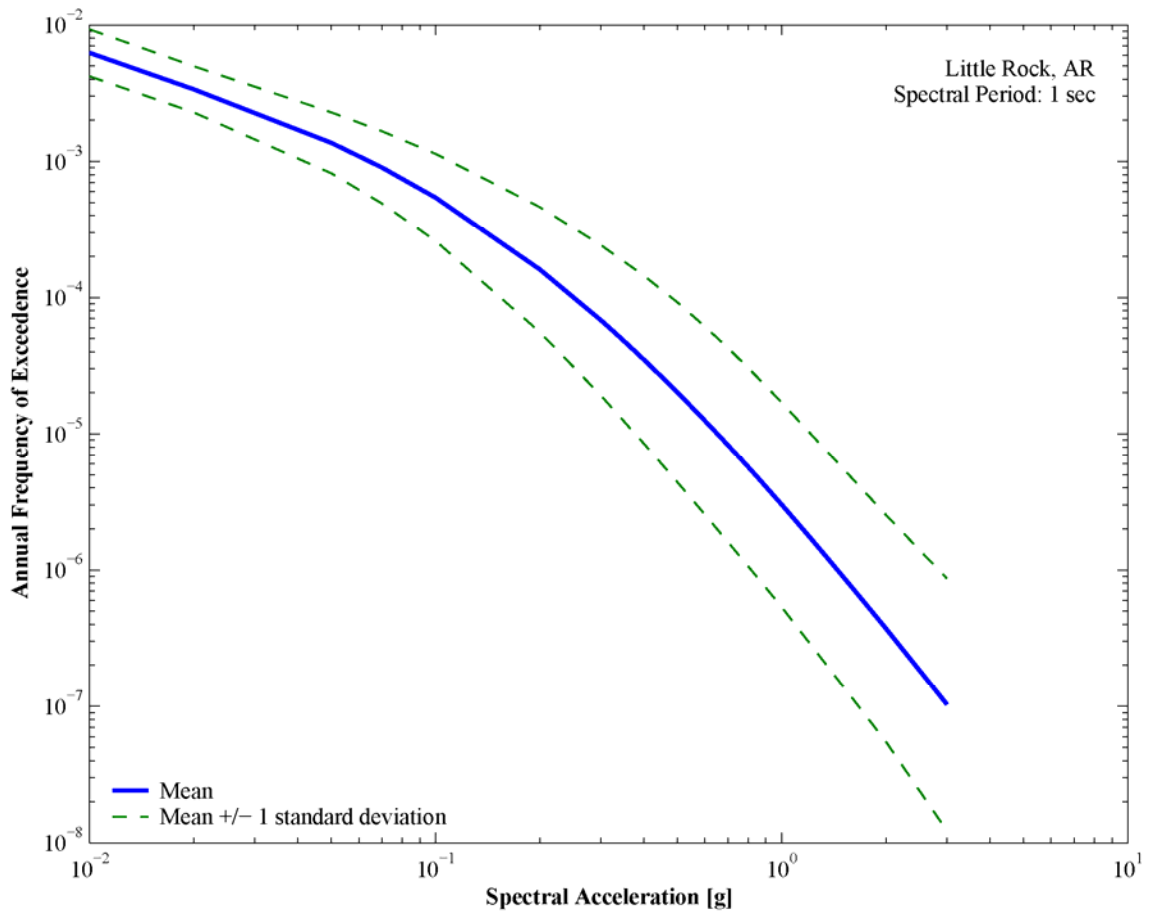


**Figure 4.24.** One-second spectral period mean and  $\pm$  1 standard deviation hazard curves for Little Rock, AR

and the modal event computed by substituting the dominant magnitude and distance in the attenuation equation (Chapman, 1995). Chapman (1995) proposed to scale the amplitude of the modal event such that it matches the design ground motion amplitude. This procedure obtains indirectly the epsilon value of the modal event, although not in a fully probabilistic manner.

Scott et al. (1998) suggest a methodology that uses the inversion of the attenuation equation to select the dominant magnitude and distance. A hazard analysis is performed for each seismic source without taking into account the uncertainty in the attenuation equation. A ground motion amplitude is calculated given a probability of exceedence, and inserted into the attenuation relation. The resulting equation is solved to find the magnitude and distance that satisfies the relationship. The solution of the equation does not define a unique event, and a curve of magnitude versus distance is constructed with all possible solutions. Different curves are calculated using different ground motion parameters (e.g. peak ground acceleration, peak ground velocity, ground motion duration, spectral acceleration), and the intersection of the curves defines the magnitude-distance pair that contribute the most to the seismic hazard. Time histories are selected based on the dominant earthquake, expecting that the variability in time histories compensates for the fact that the variability in the ground motion equation was not considered in the seismic hazard calculations. However the selection of a few time histories can not represent the entire range of the ground motion amplitude scatter (Musson, 1999).

A weakness of the approaches proposed by Chapman (1995) and Scott et al. (1998) is that they do not consider the inherent uncertainty in ground motion estimation, which may cause a large difference in the seismic hazard calculation (Reiter, 1990). Figure 4.25 compares hazard curves for Memphis, TN computed using the Atkinson and Boore (1995) model attenuation equation with and without the aleatory variability. Figure 4.25 shows the difference in ground motion amplitude for a given probability of

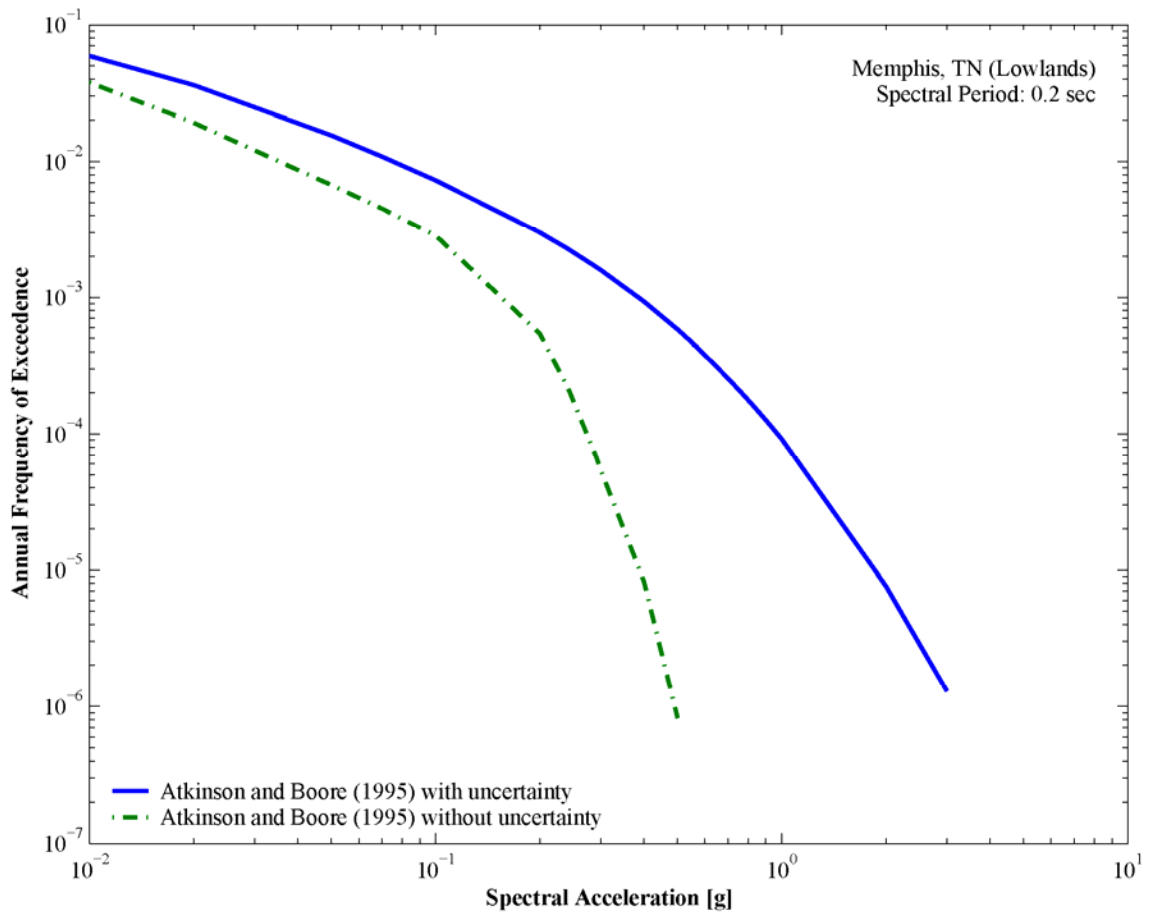


**Figure 4.25.** Hazard curves for Memphis, TN using the Atkinson and Boore (1995) model with and without aleatory uncertainty

exceedence when the variability in the attenuation equation is not included in the analysis.

The most widely used deaggregation method is the methodology proposed by McGuire (1995). The deaggregation is calculated by accumulating in each magnitude, distance, and epsilon bins the annual frequencies of exceedence of a particular ground motion level and spectral period during the numerical integration of Equation 4.4. At the end of the calculations the frequencies of exceedence accumulated in each bin are divided by the total annual frequency of exceedence to obtain the probability that a combination of magnitude, distance, and epsilon caused the exceedence of a given ground motion amplitude. The contribution of each combination of magnitude, distance, and epsilon is computed by substituting the probability term in Equation 4.4 by (McGuire, 1995):

$$P[Y > y | m, r, \epsilon] = \delta[\ln Y(m, r, \epsilon) - \ln y] \quad 4.14$$

where  $\delta$  is the Dirac delta function. Thus, the method only accumulates frequencies of exceedence when  $\ln Y(m, r, \epsilon) = \ln y$ . The main goal of this formulation is to identify the combination of magnitude, distance, and epsilon values that when inserted in the attenuation equation, the predicted ground motion equals the target amplitude. This procedure finds the earthquake that matches the target ground motion, but it does not guarantee that this earthquake is the most likely to exceed the target amplitude at the site (Bazzurro and Cornell, 1999).

The deaggregation results are presented as histograms showing the contribution of each magnitude, distance, and epsilon bin to the total hazard. The histograms are usually represented in terms of probability density functions, and the contribution of each bin can be found by computing the area under the curve. The dominant events can be different for different spectral periods and probabilities of exceedence, since the scaling of ground motion amplitudes depends on magnitude and distance. Thus, small local earthquakes

may dominate the hazard at short periods and large distant earthquakes may dominate at long periods.

Bazzurro and Cornell (1999) extended the method proposed by McGuire (1995) to deaggregate the seismic hazard by latitude, longitude, magnitude, and epsilon. The methodology explicitly finds the geographical location of the contributing earthquakes, and thus identifies the earthquakes sources that dominate the hazard at a given site. The procedure is useful for areas that are affected by multiple faults located at similar distances but with different azimuths from the site (e.g. Western United States). In the CEUS, particularly in the Upper Mississippi Embayment, only a few potential earthquakes sources exist and the dominant faults can be identified by using the method of McGuire (1995).

The deaggregation method proposed by McGuire (1995) is used in this study, which is implemented in EZ-FRISK<sup>TM</sup>. The hazard deaggregation should be performed for each individual attenuation equation and then each probability density function should be combined using the same weights assigned to each attenuation equation to calculate the hazard deaggregation of the mean hazard curve (Bazzurro and Cornell, 1999).

In this study the width of the magnitude, distance, and epsilon bins was 0.1, 2.5, and 0.2 respectively. Figure 4.26 through Figure 4.32 show the hazard deaggregation for PGA and return period of 2475 years in Memphis, TN, for each individual attenuation equation used in the analysis. These figures represent the earthquake magnitudes, epicentral distances, and epsilon values (see Equation 4.5) that contribute to the seismic hazard at the site. For example, Figure 4.26 indicates that for the Atkinson and Boore (1995) attenuation model, PGA, and return period of 2475 years, earthquakes of **M** 7.7 located at 35 km from the site with ground motion amplitudes equal to the median +  $0.75 \cdot \sigma$  dominate the seismic hazard in Memphis, TN.

Figure 4.26 through Figure 4.32 show that the hazard deaggregation by magnitude and distance are similar for the three  $\Delta\sigma$  cases. However some variations are observed

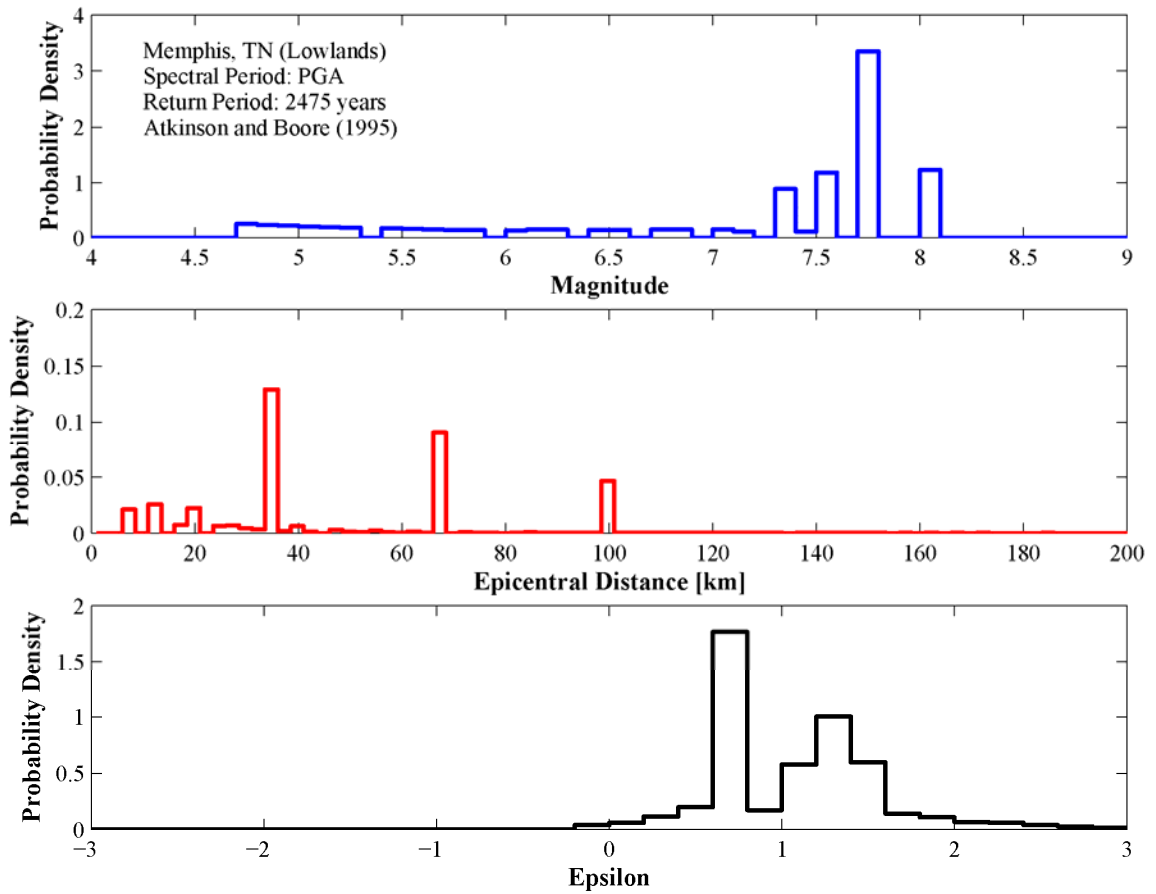


**Figure 4.26.** Hazard deaggregation for peak ground acceleration and return period of 2475 years in Memphis, TN using the Atkinson and Boore (1995) model

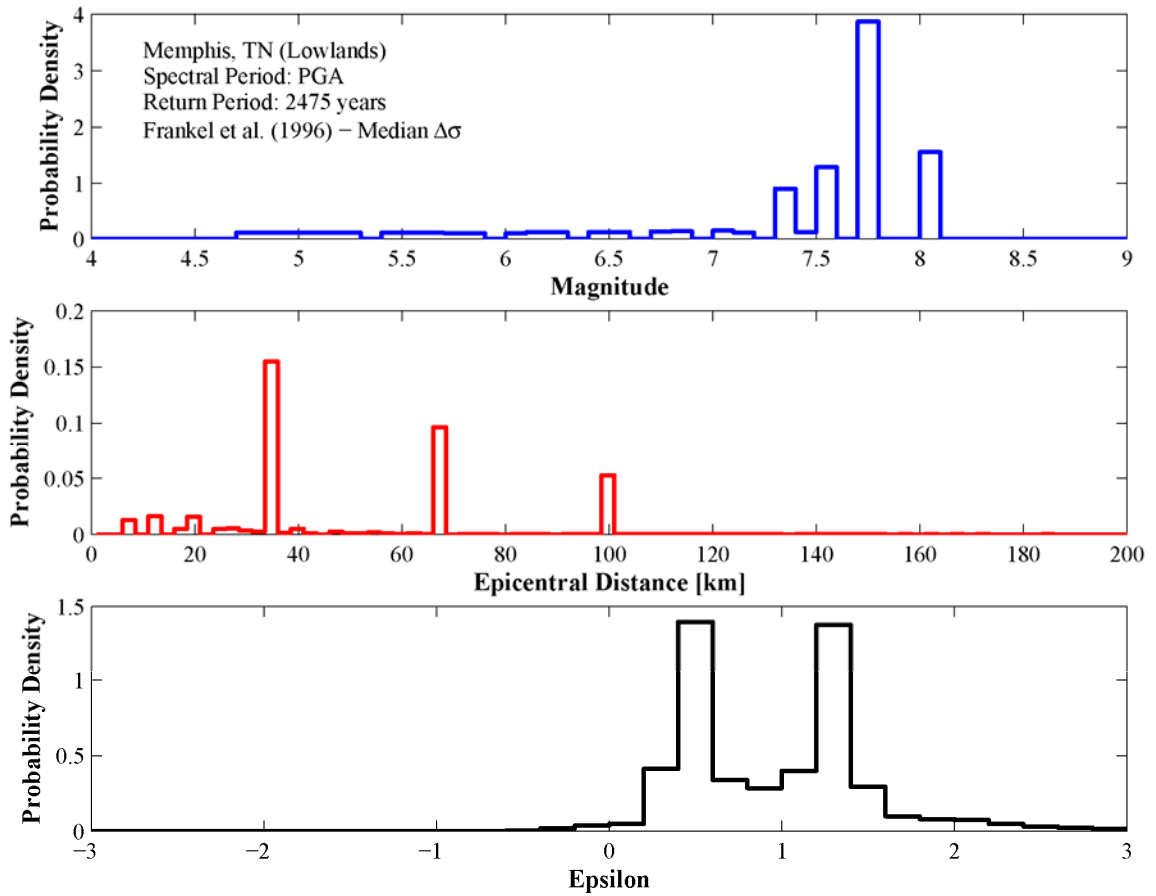


**Figure 4.27.** Hazard deaggregation for peak ground acceleration and return period of 2475 years in Memphis, TN using the Frankel et al. (1996) – median  $\Delta\sigma$  model

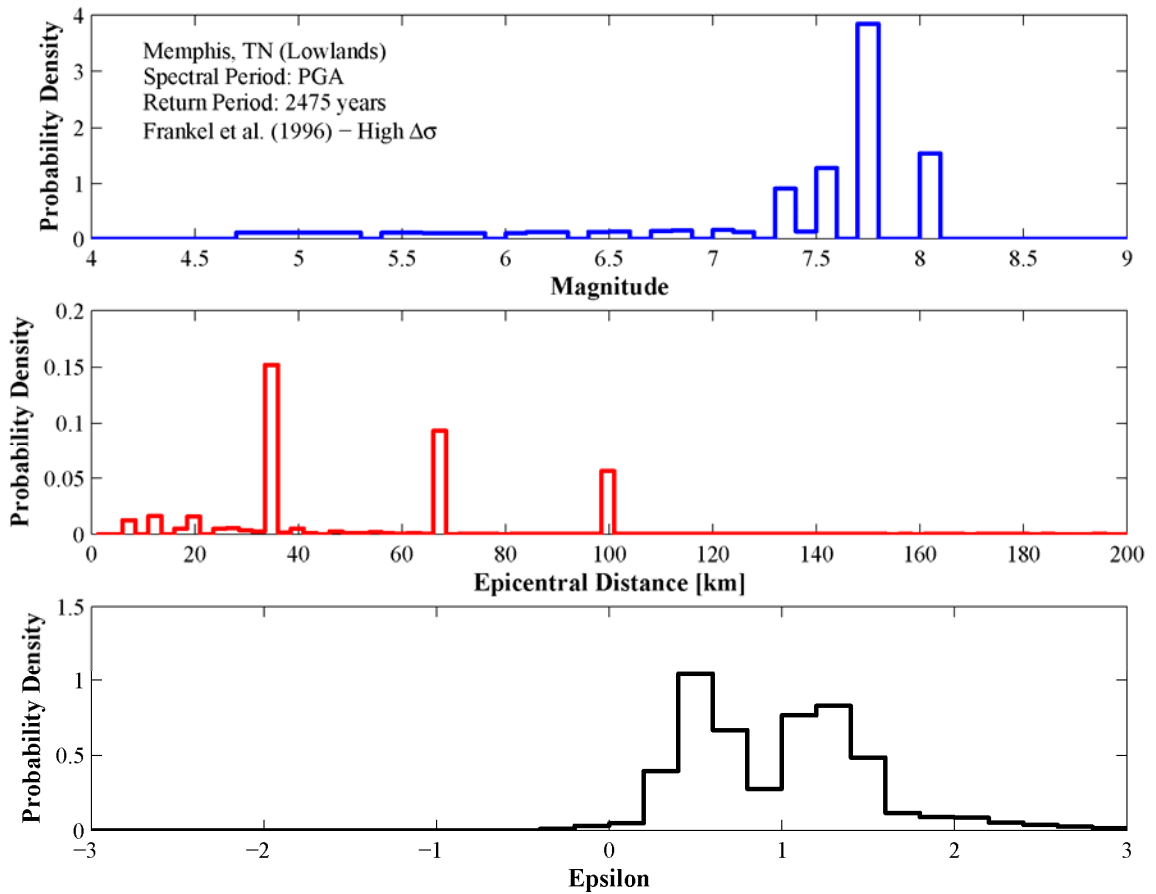


**Figure 4.28.** Hazard deaggregation for peak ground acceleration and return period of 2475 years in Memphis, TN using the Frankel et al. (1996) – high  $\Delta\sigma$  model

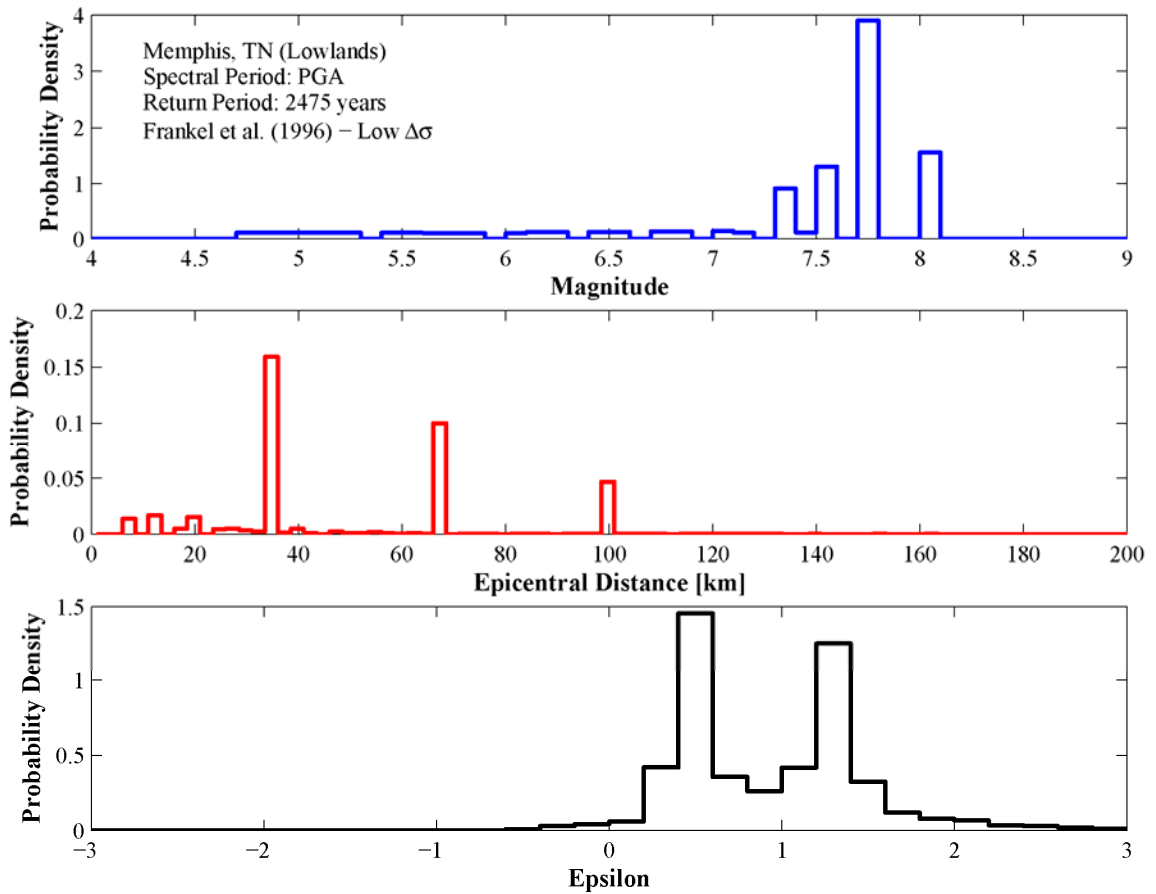


**Figure 4.29.** Hazard deaggregation for peak ground acceleration and return period of 2475 years in Memphis, TN using the Frankel et al. (1996) – low  $\Delta\sigma$  model

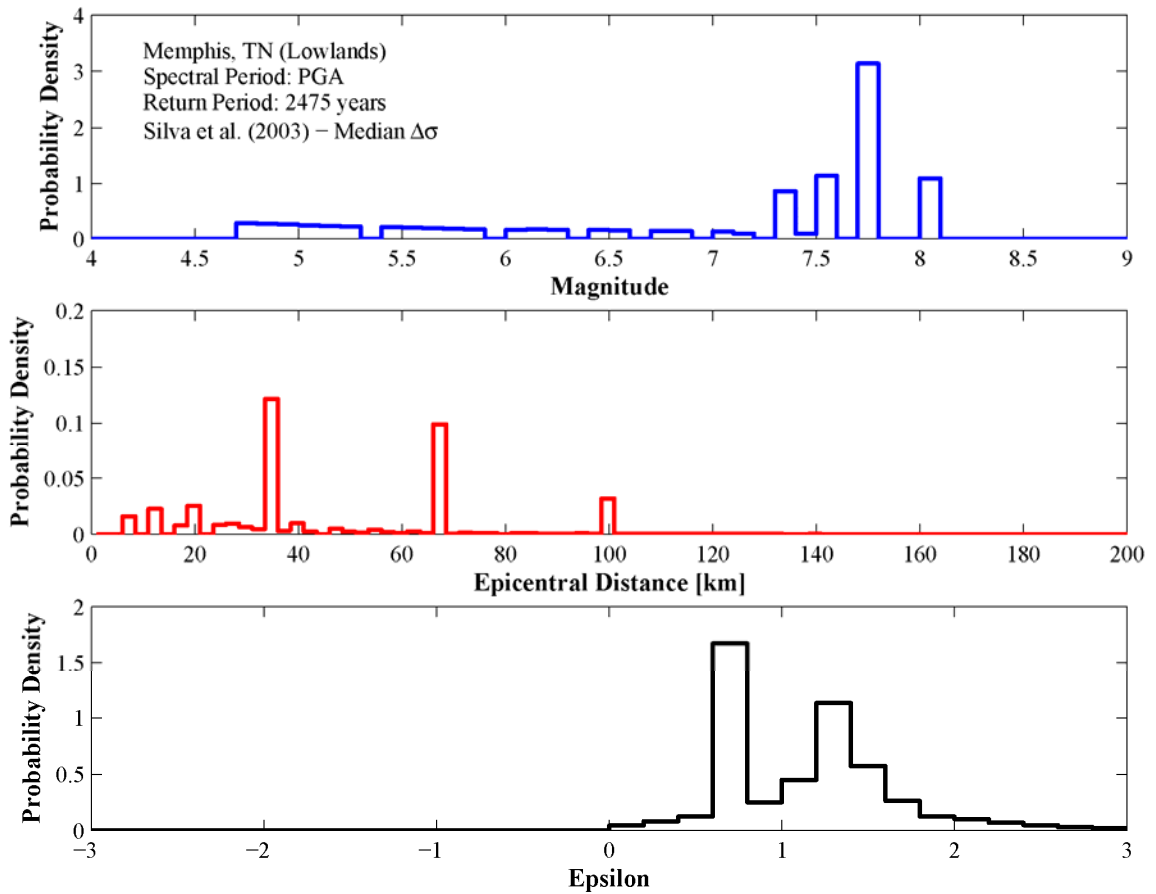


**Figure 4.30.** Hazard deaggregation for peak ground acceleration and return period of 2475 years in Memphis, TN using the Silva et al. (2003) – median  $\Delta\sigma$  model

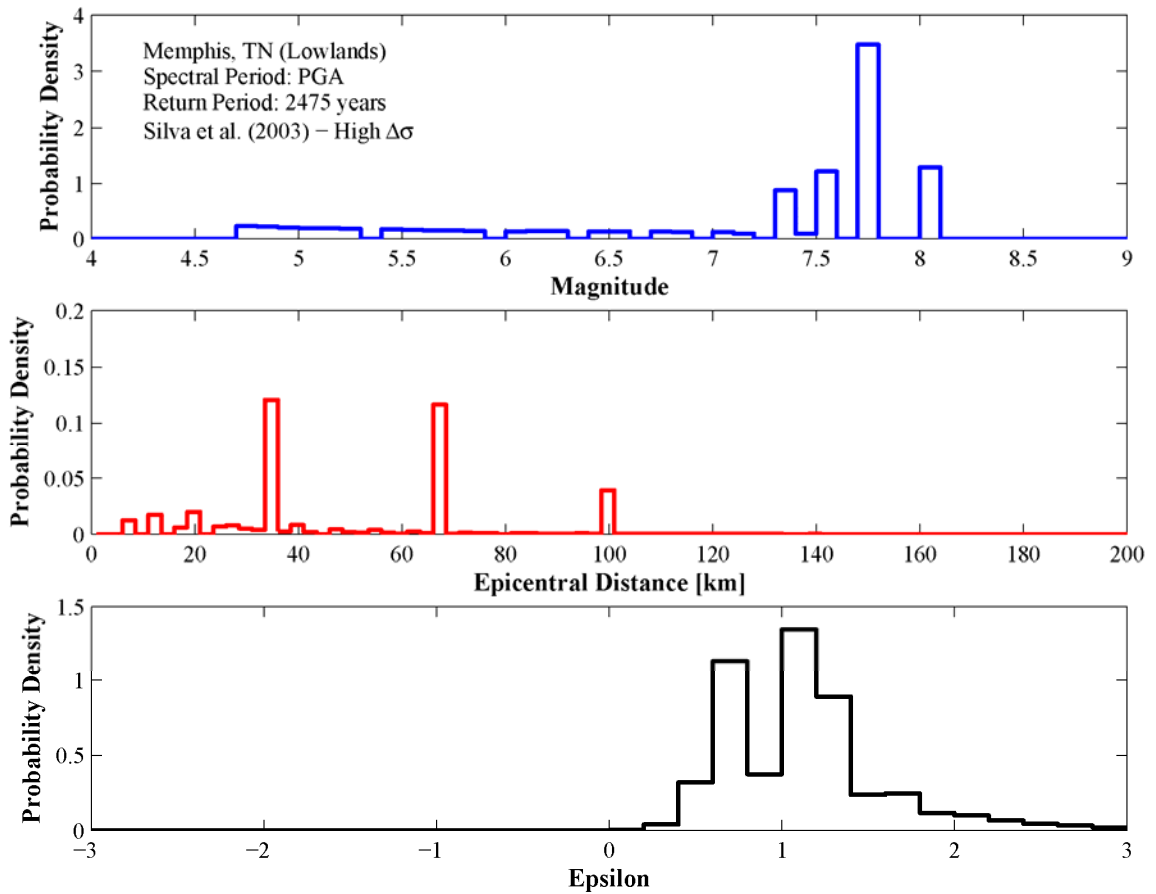


**Figure 4.31.** Hazard deaggregation for peak ground acceleration and return period of 2475 years in Memphis, TN using the Silva et al. (2003) – high  $\Delta\sigma$  model

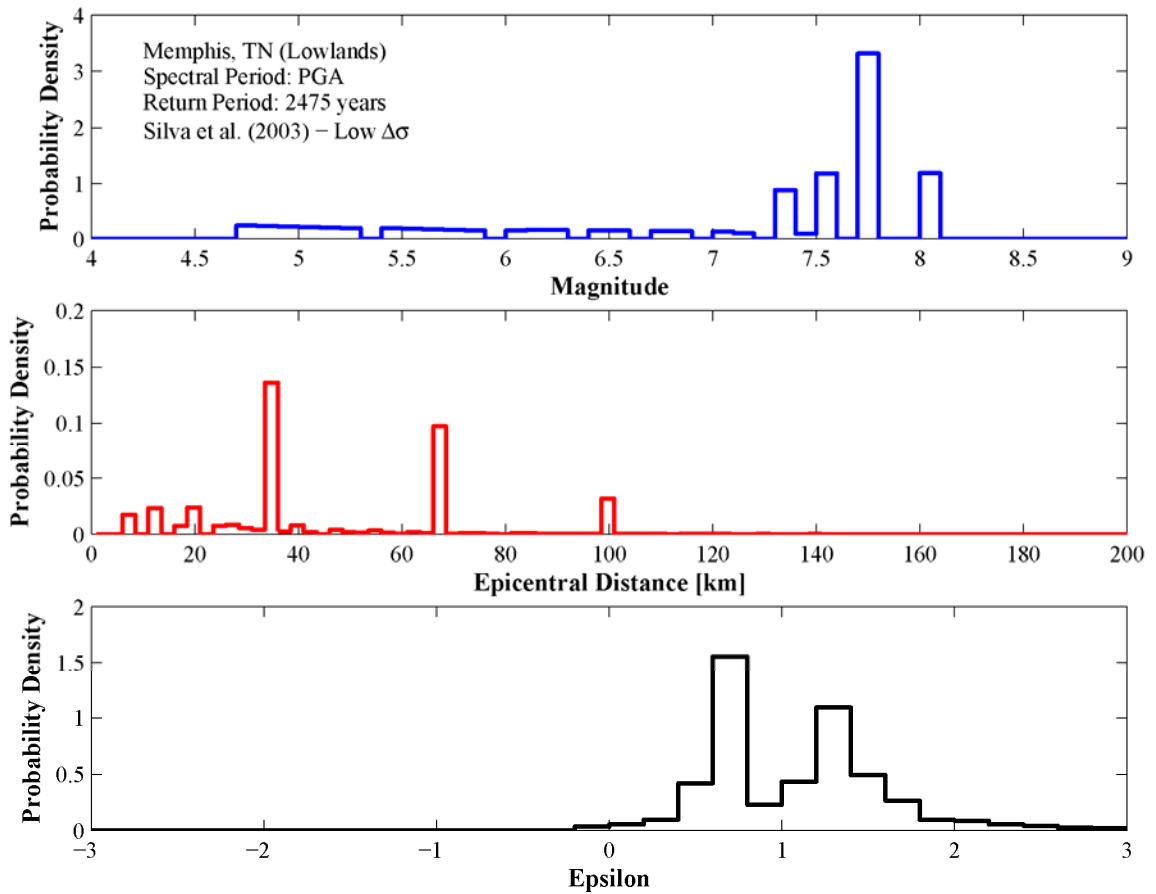


**Figure 4.32.** Hazard deaggregation for peak ground acceleration and return period of 2475 years in Memphis, TN using the Silva et al. (2003) – low  $\Delta\sigma$  model

among source models due to the different attenuation rates implemented in each model. The deaggregation by epsilon shows lower contribution from the high  $\Delta\sigma$  models because their median ground motion values are higher compared to the other two  $\Delta\sigma$  cases for the same source model. Figure 4.33 shows the combined seismic deaggregation using the weights listed in Table 4.4. In this case the mean hazard deaggregation is very similar to deaggregation curves of each individual attenuation model. Hereafter all the hazard deaggregation curves presented in this study will refer to the mean hazard deaggregation.

Figure 4.34 and Figure 4.36 show the hazard deaggregation for PGA in Memphis, TN corresponding to return periods of 975 and 475 years, respectively. The comparison of the hazard deaggregation curves for the three return periods (i.e. Figure 4.33 through Figure 4.36) show that the distributions of magnitude and distance are independent of the hazard level for this case. The deaggregation by magnitude for the return period of 475 years shows a higher contribution from small magnitudes; however the dominant magnitudes are clearly the same for the three hazard levels. This observation indicates that the characteristic earthquakes defined in Table 4.2 for the New Madrid seismic sources dominate the seismic hazard. The epsilon distribution moves toward higher values as the hazard level or return period increases, indicating that higher percentiles of the ground motion distribution are needed to match higher target amplitudes. Similar results were obtained for the rest of the cities, and therefore only hazard deaggregation curves for return periods of 2475 years will be presented. Figure 4.37 shows the hazard deaggregation for 1-second spectral period and return period of 2475 years in Memphis, TN. The magnitude distribution for PGA shows higher contribution from small magnitudes, and the distance distribution for 1-second spectral period indicates a small increase in the contribution from the C New Madrid fault. However the dominant magnitudes and distances are the same for both periods. The epsilon distribution for PGA shows larger contribution from higher percentiles. Figure 4.38 and Figure 4.39 show the 2D hazard deaggregation of magnitude and distance for PGA and 1-second

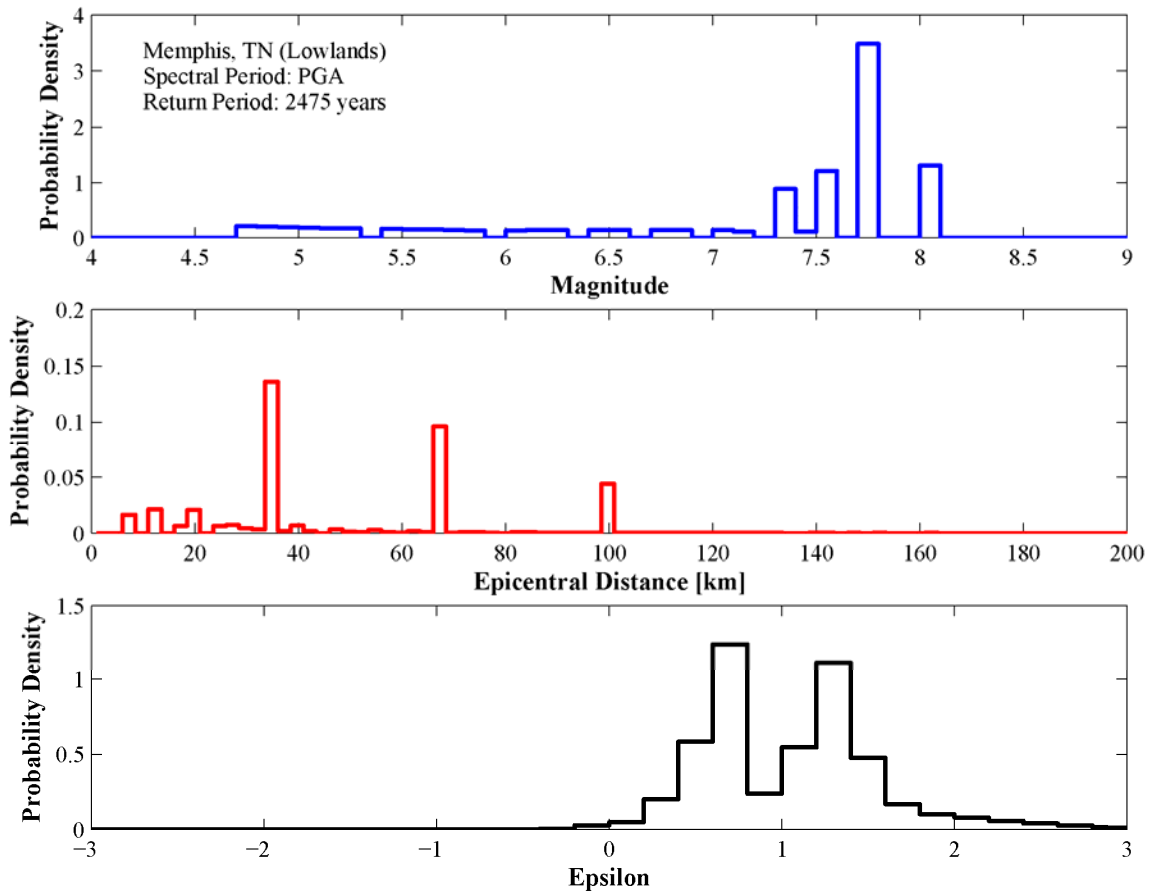


**Figure 4.33.** Mean hazard deaggregation for peak ground acceleration and return period of 2475 years in Memphis, TN

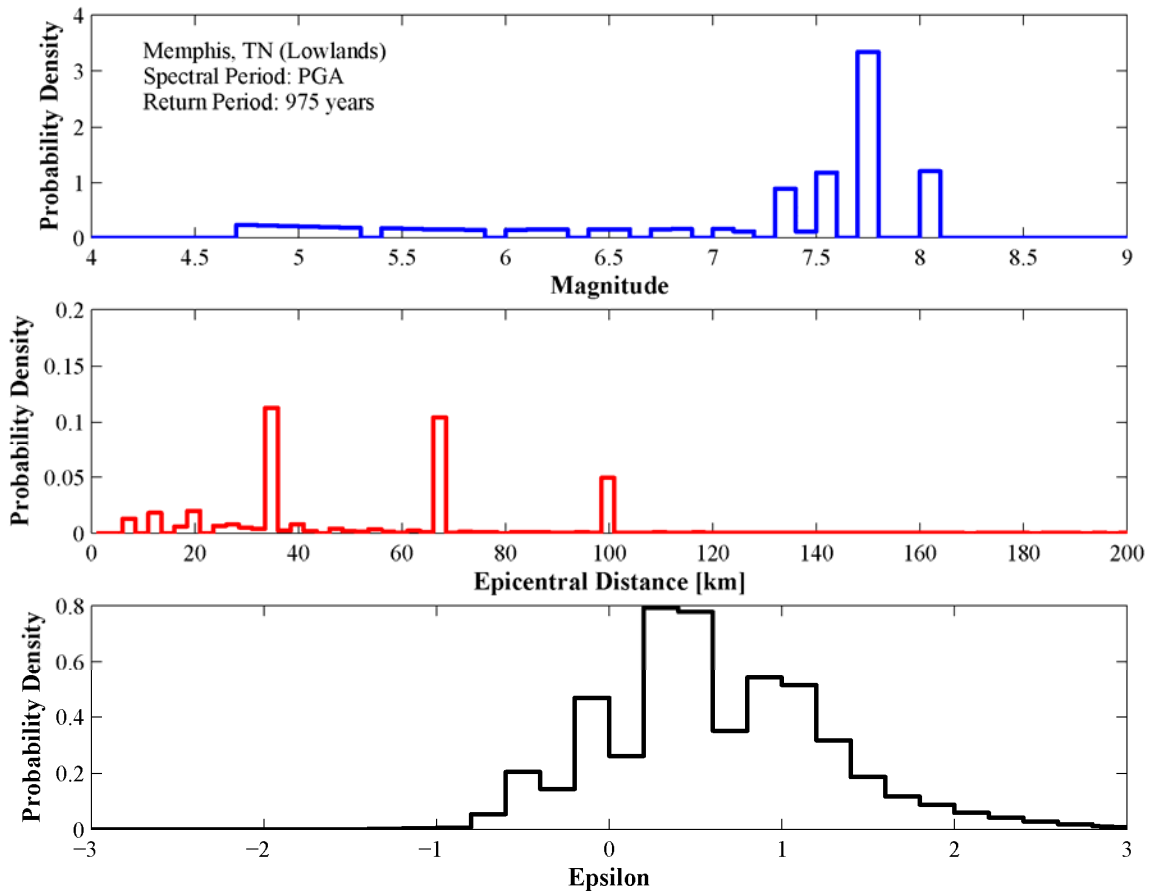


**Figure 4.34.** Hazard deaggregation for peak ground acceleration and return period of 975 years in Memphis, TN

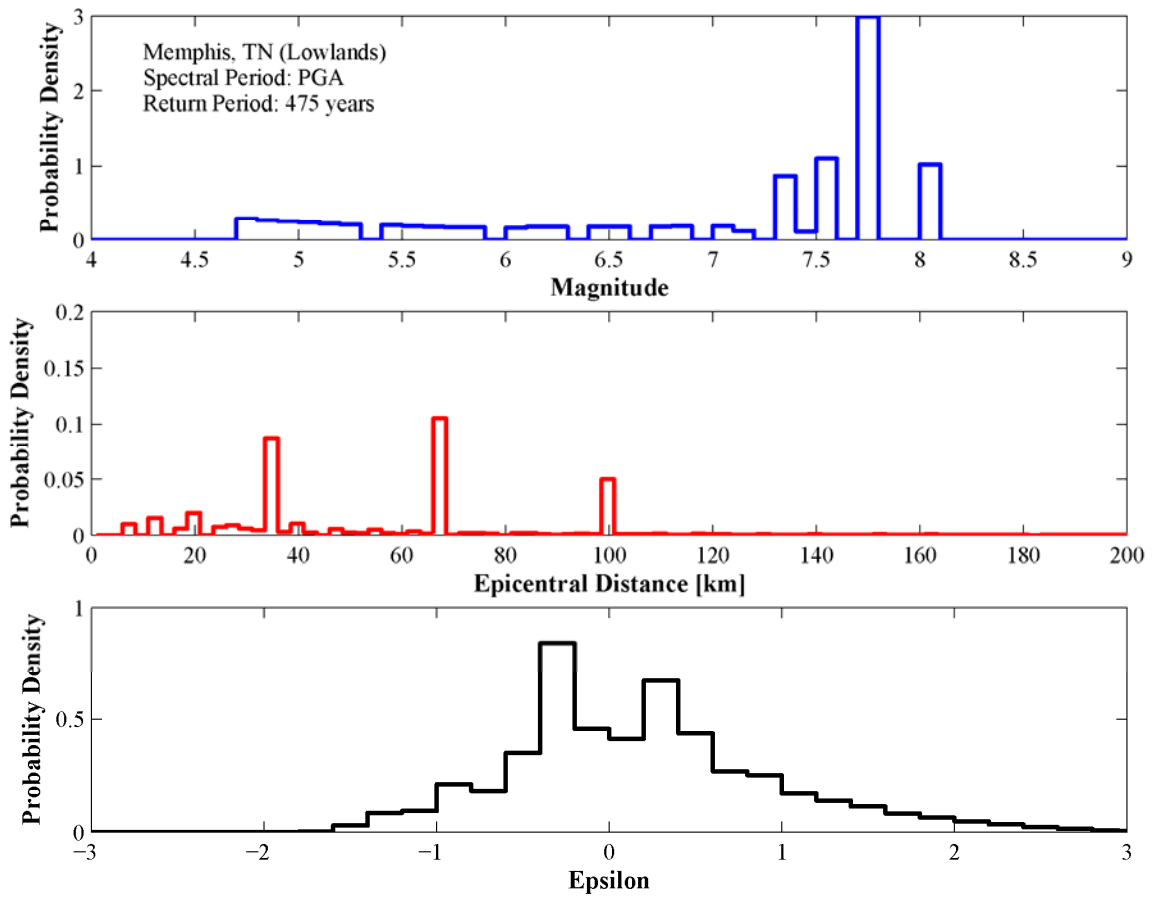


**Figure 4.35.** Hazard deaggregation for peak ground acceleration and return period of 475 years in Memphis, TN

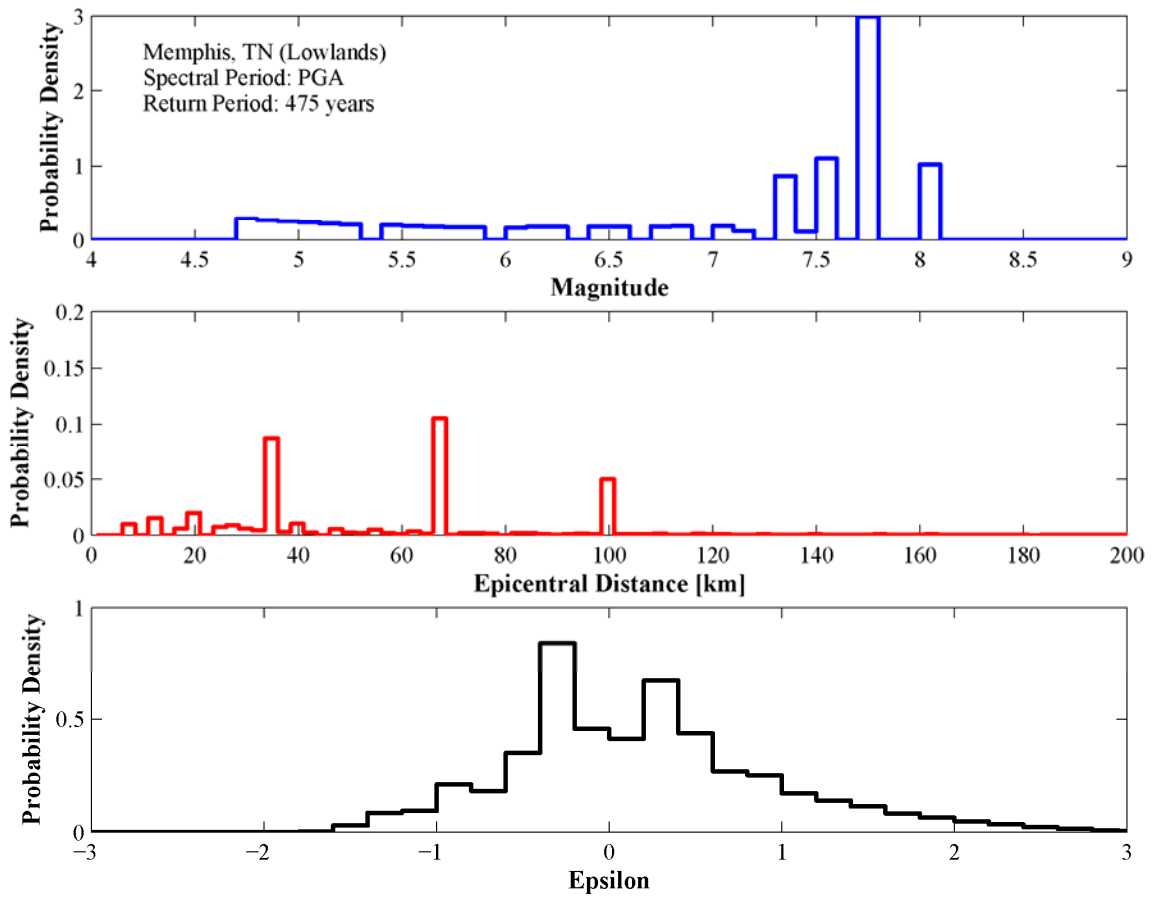


**Figure 4.36.** Hazard deaggregation for peak ground acceleration and return period of 475 years in Memphis, TN

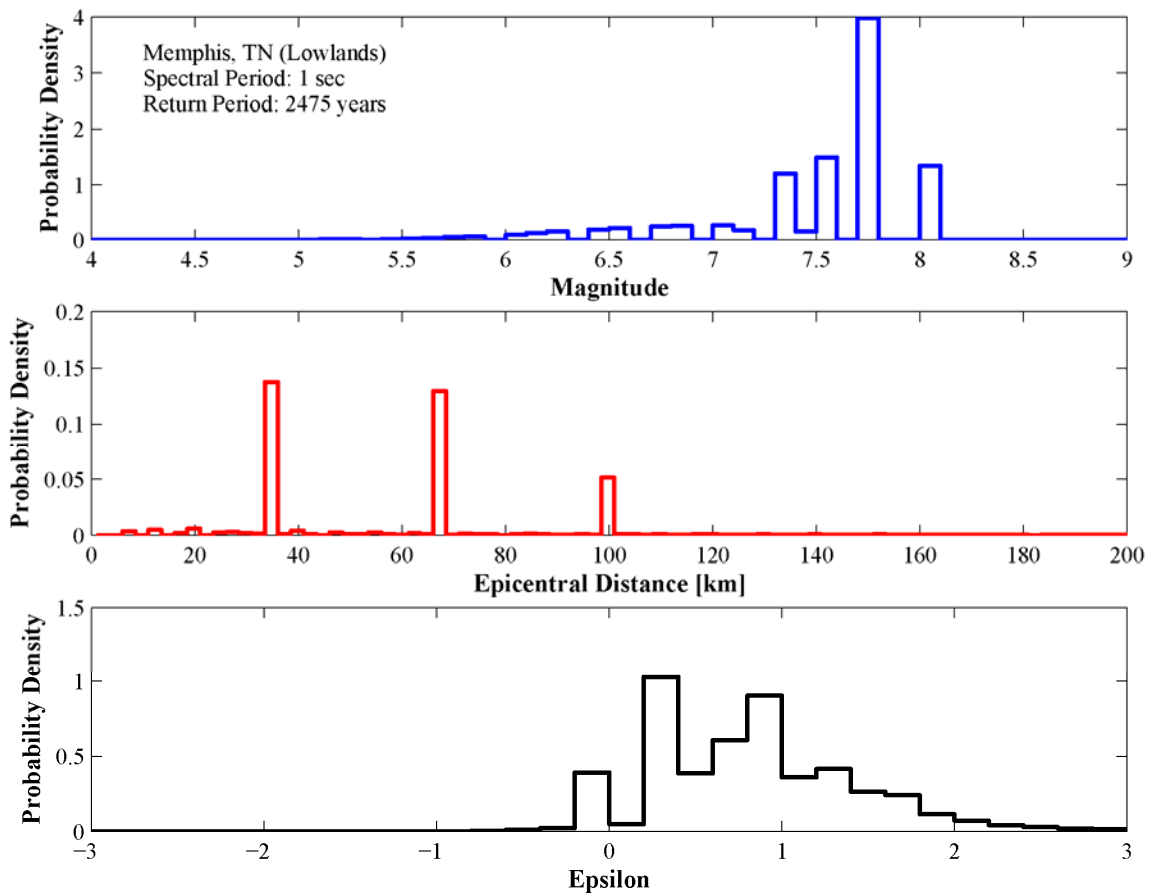


**Figure 4.37.** Hazard deaggregation for 1-second spectral period and return period of 2475 years in Memphis, TN

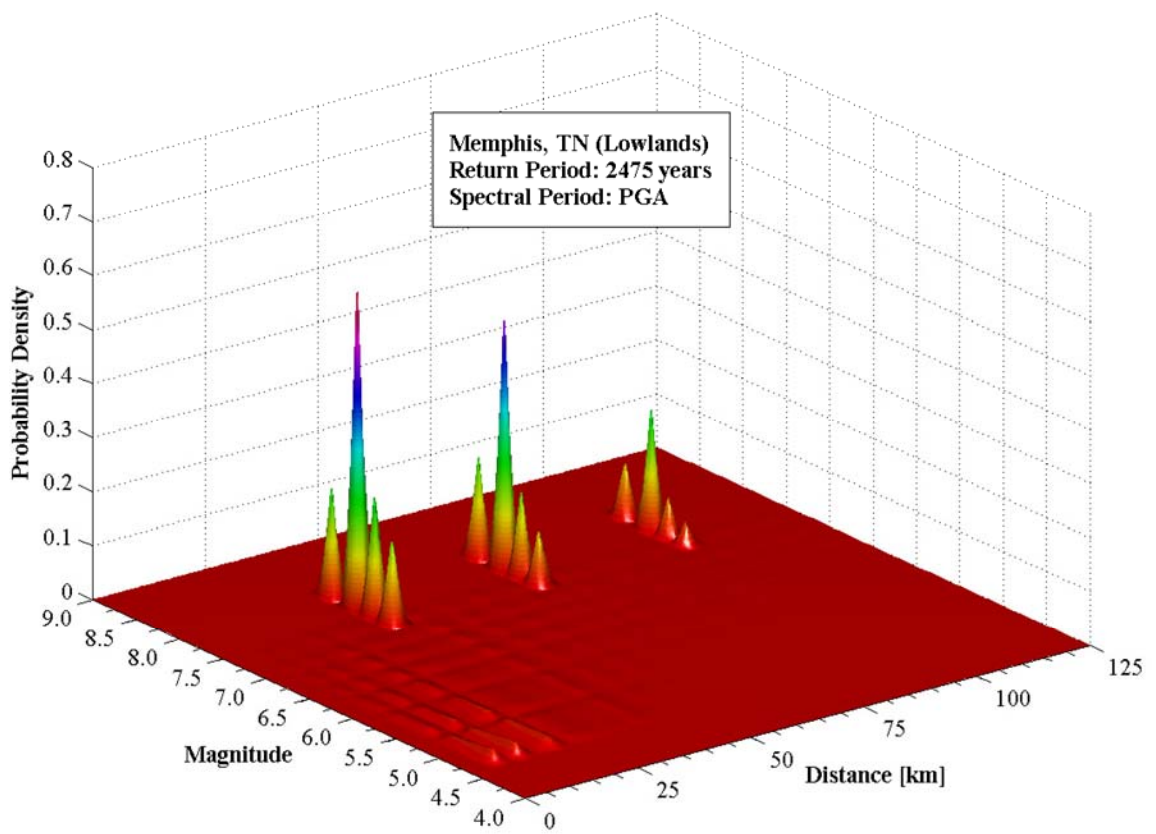


**Figure 4.38.** Joint magnitude and distance hazard deaggregation for peak ground acceleration and return period of 2475 years in Memphis, TN

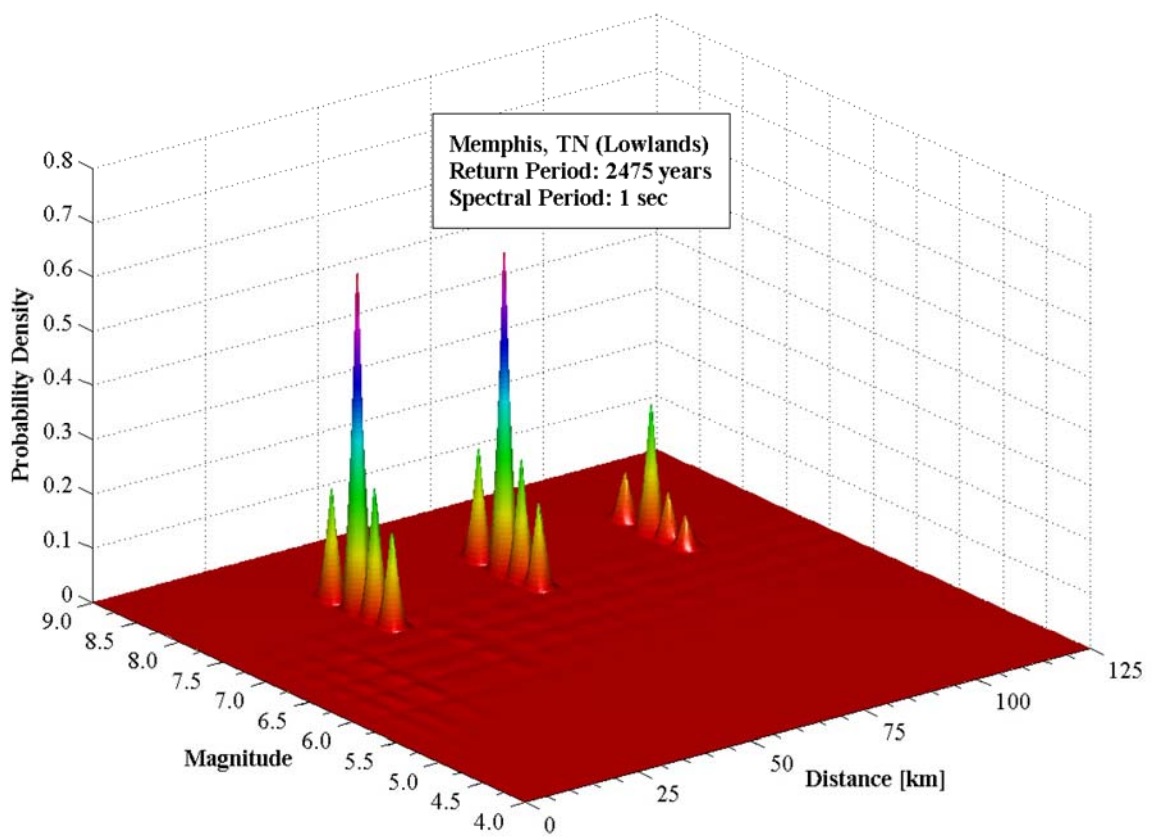


**Figure 4.39.** Joint magnitude and distance hazard deaggregation for 1-second spectral period and return period of 2475 years in Memphis, TN

spectral period in Memphis, TN. This type of joint deaggregation indicates the contribution of the different magnitude-distance pairs to the seismic hazard. The 2D hazard deaggregation is useful for selecting time histories compatible with the hazard level because it directly shows the combination of magnitude and distance that dominate the hazard at a given site. The 1D hazard deaggregation (e.g. Figure 4.37) identifies the dominant magnitudes and distances, but it does not indicate the relationships between these two variables. It is a projection of the 2D curve. In this particular case, the advantages of the 2D hazard deaggregation are not obvious because the site is affected by very few faults. However for sites affected by many faults (e.g. sites located in the Western United States), the 2D hazard deaggregation facilitates the identification of the dominant magnitude-distance pairs. Appendix B shows the hazard deaggregation for the rest of the selected cities.

The hazard deaggregation by distance for PGA indicate that the three fictitious faults used to characterize the uncertainty in source location in the New Madrid seismic zone (Frankel et al., 1996) dominate the hazard. The distance distribution also shows that there is a small contribution from nearby earthquakes due to the background sources. Similar results are obtained for 1-second spectral period, but in this case the background sources do not contribute to the hazard. The distance deaggregation curves indicate that the Charleston, SC seismic zone does not affect the seismic hazard in the Upper Mississippi Embayment. The hazard deaggregation by distance for Memphis, TN is consistent with Toro and Silva (2001), who found that the SE Flank of the Reelfoot rift, the Blytheville Arch, and the Reelfoot fault (see Figure 2.4) at distances approximately of 20 km, 65 km, and 100 km, respectively, from Memphis, TN, dominate the seismic hazard in this city. The hazard deaggregation by magnitude for PGA shows that **M** 7.3 to **M** 8.0 are the most important contributors to the hazard, with **M** 7.7 having the highest contribution. However, there is a small contribution from small earthquakes corresponding to background sources. These small earthquakes do not contribute to the

hazard for 1-second spectral period. These results are consistent with the logic tree for the characteristic magnitude of the New Madrid seismic zone implemented in the analyses and listed in Table 4.2. The magnitude distribution shows that the contribution to the hazard from **M** 7.3, **M** 7.5, **M** 7.7, and **M** 8.0 is proportional to the weights assigned in the logic tree to each magnitude. The distribution of epsilon indicates that the seismic hazard for a return period of 2475 years is associated with the mean + 1 standard deviation ground motions, which is also consistent with findings by Toro and Silva (2001) for Memphis, TN.

In conclusion, the seismic hazard deaggregation indicates that small magnitudes and short distances (i.e. background sources) contribute to the hazard mainly at short periods and low hazard levels. However, the New Madrid seismic zone is the dominant hazard contributor in the Upper Mississippi Embayment. The Charleston, SC seismic sources do not contribute to the seismic hazard in the region.

#### 4.2.3.2 Uniform Hazard Spectra

Hazard curves are used to calculate response spectra of constant probability or uniform hazard spectra (UHS). A uniform hazard spectrum represents the ground motion amplitudes that share the same probability of exceedence or return period. Figure 4.40 illustrates the procedure to construct the UHS from the hazard curves. In summary, each ordinate of the UHS is read from the abscissa on the hazard curve corresponding to a given probability of exceedence or return period. This process is repeated for all spectral periods.

The UHS is usually smoother with a wider band-width than the response spectrum of a real earthquake record. The UHS is not associated with a particular earthquake scenario but results from the contribution of all possible magnitudes and distances that may affect the site. As mentioned previously, small local earthquakes may dominate the

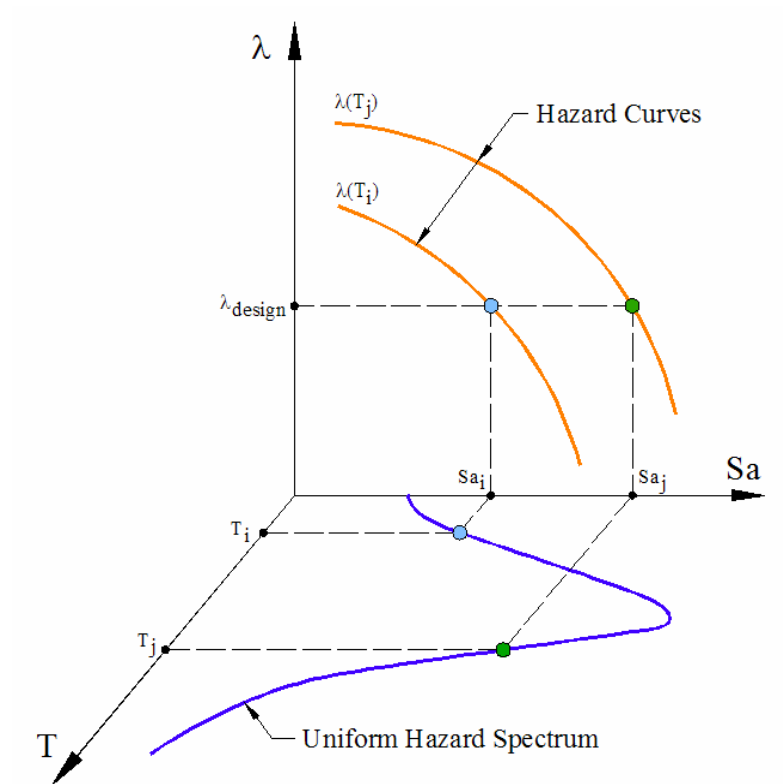


**Figure 4.40.** Procedure to calculate the uniform hazard spectrum

hazard at short periods and large distant earthquakes may dominate at long periods as illustrated in Figure 4.41.

If multiple hypotheses are considered in the seismic hazard analysis, a PSHA results in multiple hazard curves and uniform hazard spectra. The mean ground motion is usually computed as a single representative measure of the different hypotheses. However if one computes the UHS corresponding to the mean hazard curve, it does not necessarily match the mean UHS calculated from the individual UHS. If the multiple hazard curves were all parallel to each other then both methods would yield the same mean UHS. In reality the hazard curves computed from different models are not parallel. If for example a PSHA is performed using multiple attenuation equation models, each model will assume different propagation and attenuation characteristics of the seismic waves and therefore the different hazard curves obtained will not be necessarily parallel

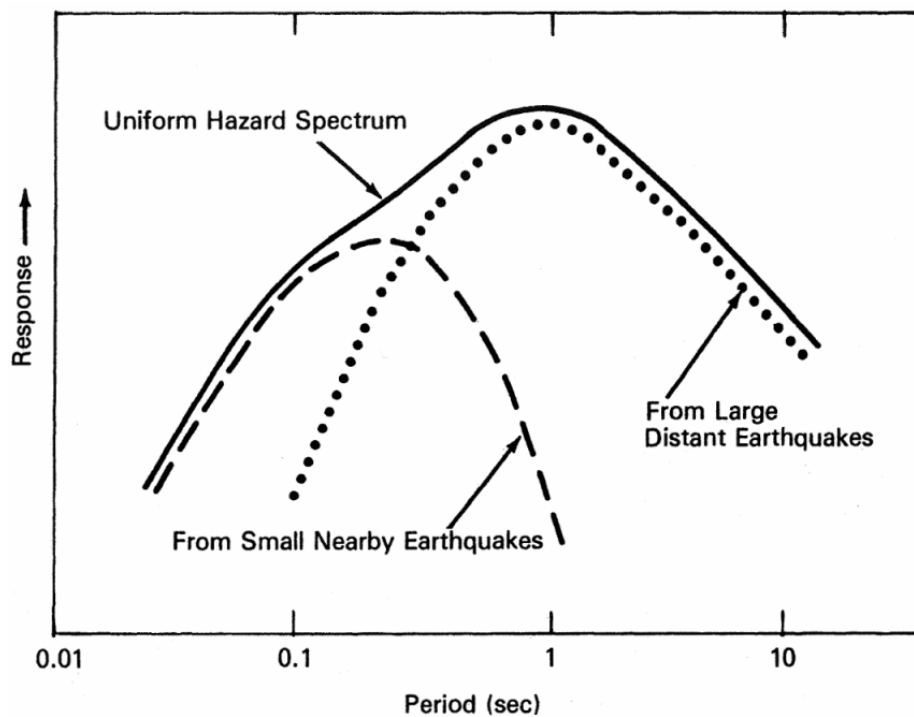


**Figure 4.41.** Contribution of small nearby and large distant earthquakes to the uniform hazard spectrum (from Reiter, 1990)

to each other. The mean UHS should be calculated using the mean hazard curve and not by averaging the individual UHS curves of the different models (Toro, personal communication).

Usually deterministic amplification factors are applied to a rock UHS to obtain a UHS for soil conditions. The probability of exceedence of the soil UHS estimated by this probabilistic-deterministic approach is not necessarily the same as the probability of exceedence of the rock UHS. The probability of exceedence of the soil ground motions given by this procedure is unknown (Bazzurro and Cornell, 2004b; Goulet et al., 2007). Figure 4.42 compares PGA hazard curves for rock and soil conditions in Memphis, TN. The rock hazard curve was calculated by using the Atkinson and Boore (1995) rock attenuation relationships that were developed for the CEUS. The soil hazard curves were estimated using two different approaches. The first procedure calculates the soil hazard curve by using the soil attenuation relationships developed in this study corresponding to the Atkinson and Boore (1995) source model. The second procedure uses the site coefficients proposed by FEMA (2001a) and Park and Hashash (2005) for site class D to modify the rock hazard curve and obtain hazard curves for soil conditions. Both sets of site coefficients account for soil nonlinearity, and the Park and Hashash (2005) coefficients also incorporate the effect of the deep soil column in the Embayment. An important difference between the soil hazard curves is that the site coefficients cannot capture the non-linear behavior of the soil column when subjected to high levels of ground motion (i.e. low annual frequency of exceedence) as shown in Figure 4.42. Even if site-specific amplification functions or site factors that account for soil nonlinearity and Embayment depth are used to modify the rock hazard curve, different soil hazard amplitudes will be obtained compared to those calculated by using soil attenuation relationships.

The difference between both methodologies results from the assumption made by the probabilistic-deterministic approach that rock and soil hazard are controlled by the

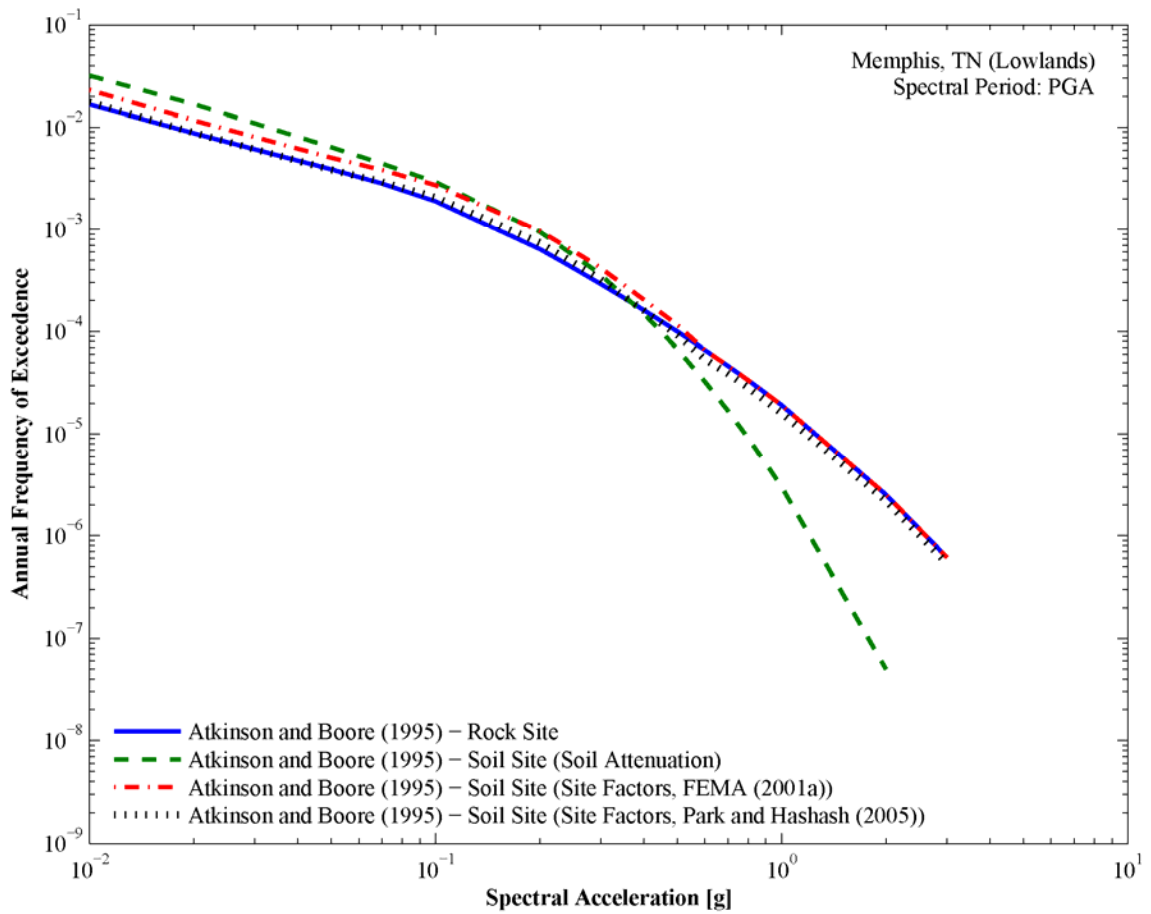


**Figure 4.42.** Rock and soil hazard curves for peak ground acceleration in Memphis, TN

same earthquakes (i.e. same magnitude, distance, and epsilon) (Goulet and Stewart, 2007; Goulet et al., 2007). Figure 4.43 and Figure 4.44 show the hazard deaggregation for rock and soil conditions respectively. The soil hazard deaggregation was computed using the soil attenuation relationship. The distributions of magnitude, distance, and epsilon indicate that the rock and soil hazard are controlled by different earthquakes. In this case, small nearby earthquakes with negative epsilon contribute significantly to the rock hazard. Conversely, large distant earthquakes with positive epsilon dominate the soil hazard, which leads to the high nonlinearity observed in the hazard curve. If this difference between the controlling earthquakes is not considered in the analysis, the multiplication of the rock hazard by a deterministic amplification factors may bias the estimation of soil ground motions (Goulet and Stewart, 2007; Goulet et al., 2007).

The mean hazard curves were used to calculate soil uniform hazard spectra for three return periods — 475, 975 and 2475 years — corresponding to a 10%, 5%, and 2% of probability of exceedance in 50 years, respectively. Figure 4.45 through Figure 4.52 show the mean UHS and its associated variability for a return period of 2475 years for the selected cities. The resonant peaks of the UHS reflect the Embayment depth at each city as listed in Table 4.5. The standard deviation represents the scatter observed in the hazard curves due to the different attenuation models and not in the individual UHS. Figure 4.53 through Figure 4.60 compare the mean UHS for three return periods. The resonant peaks of the UHS shift to longer periods as the level of hazard increases due to the non-linear behavior of the soil column.

The UHS for the city of Blytheville, AR illustrated in Figure 4.49 and Figure 4.57 show an unusual shape with high ground motion amplitudes at long periods and amplitudes starting to decay after a period 4.5 seconds, particularly for a return period of 2475 years. Due to this long-period amplitude decay, the seismic hazard analyses for this city were performed for periods up to 10 seconds. This unusual UHS shape is caused by the proximity of the city of Blytheville, AR to the New Madrid seismic sources along

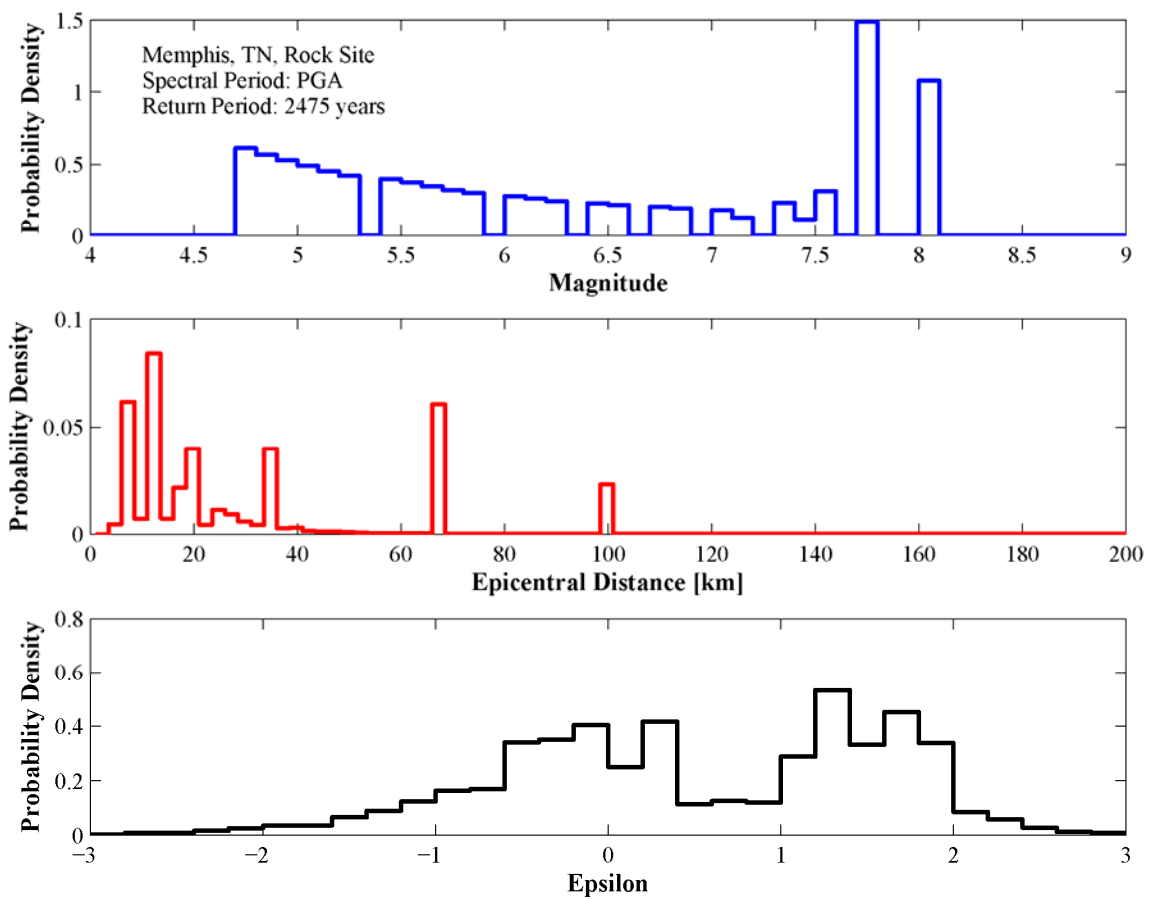


**Figure 4.43.** Hazard deaggregation for rock site conditions in Memphis, TN

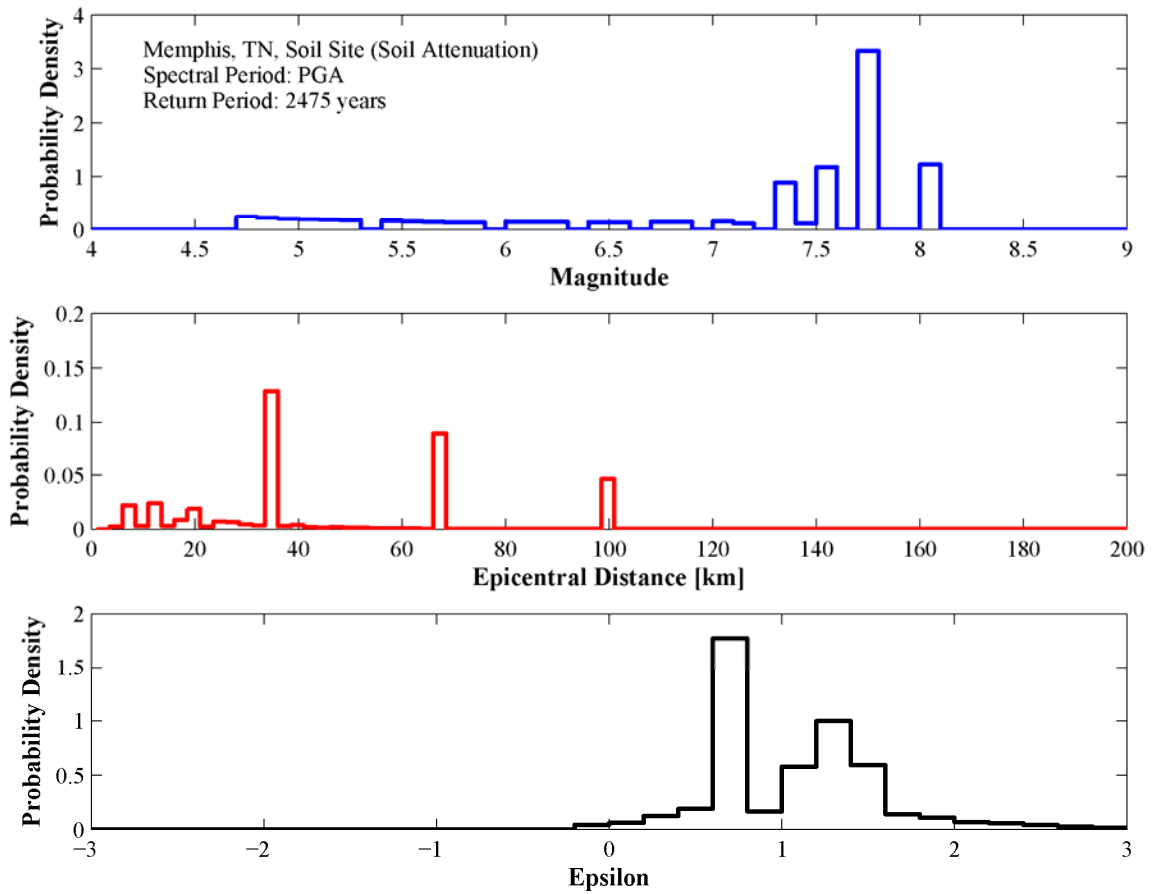


**Figure 4.44.** Hazard deaggregation for soil site conditions in Memphis, TN using soil attenuation relationships

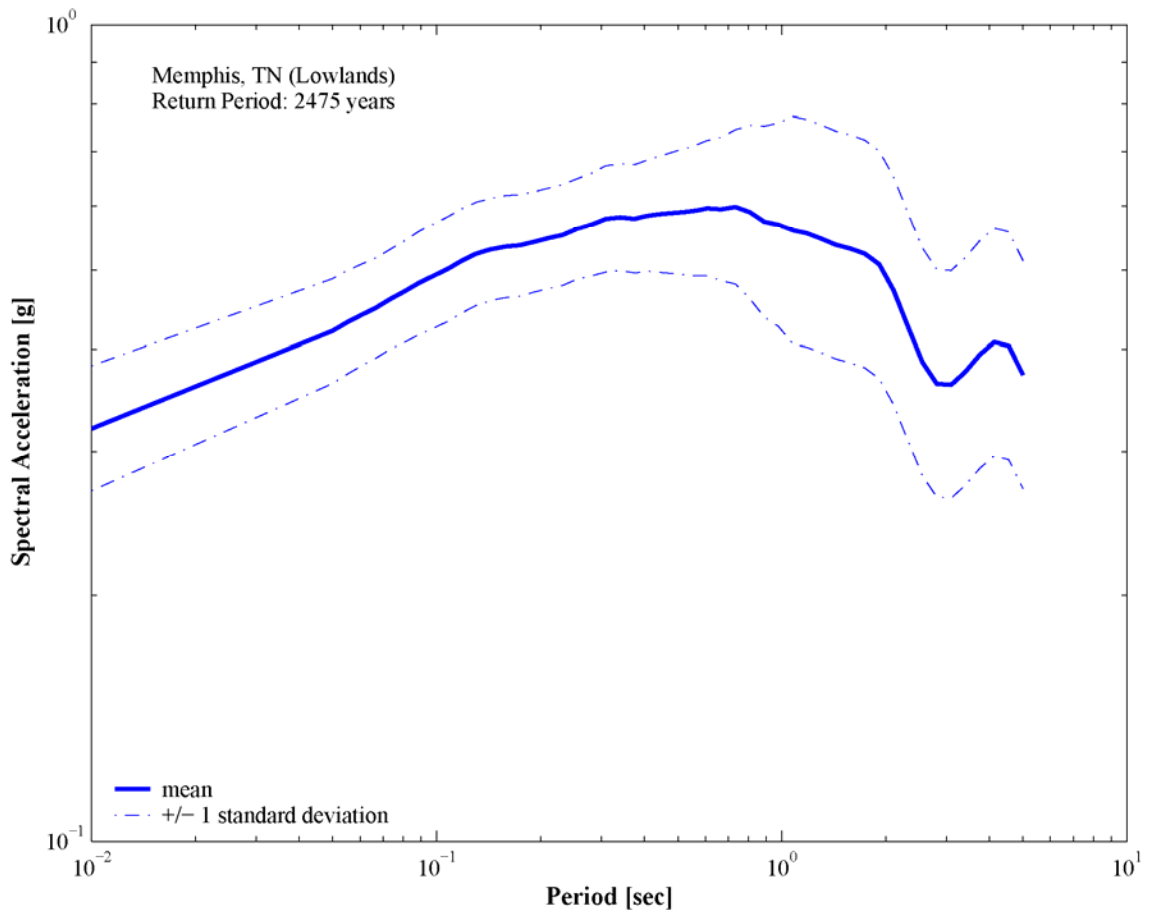


**Figure 4.45.** Soil mean uniform hazard spectrum and its associated variability for return period of 2475 years in Memphis, TN (Lowlands)

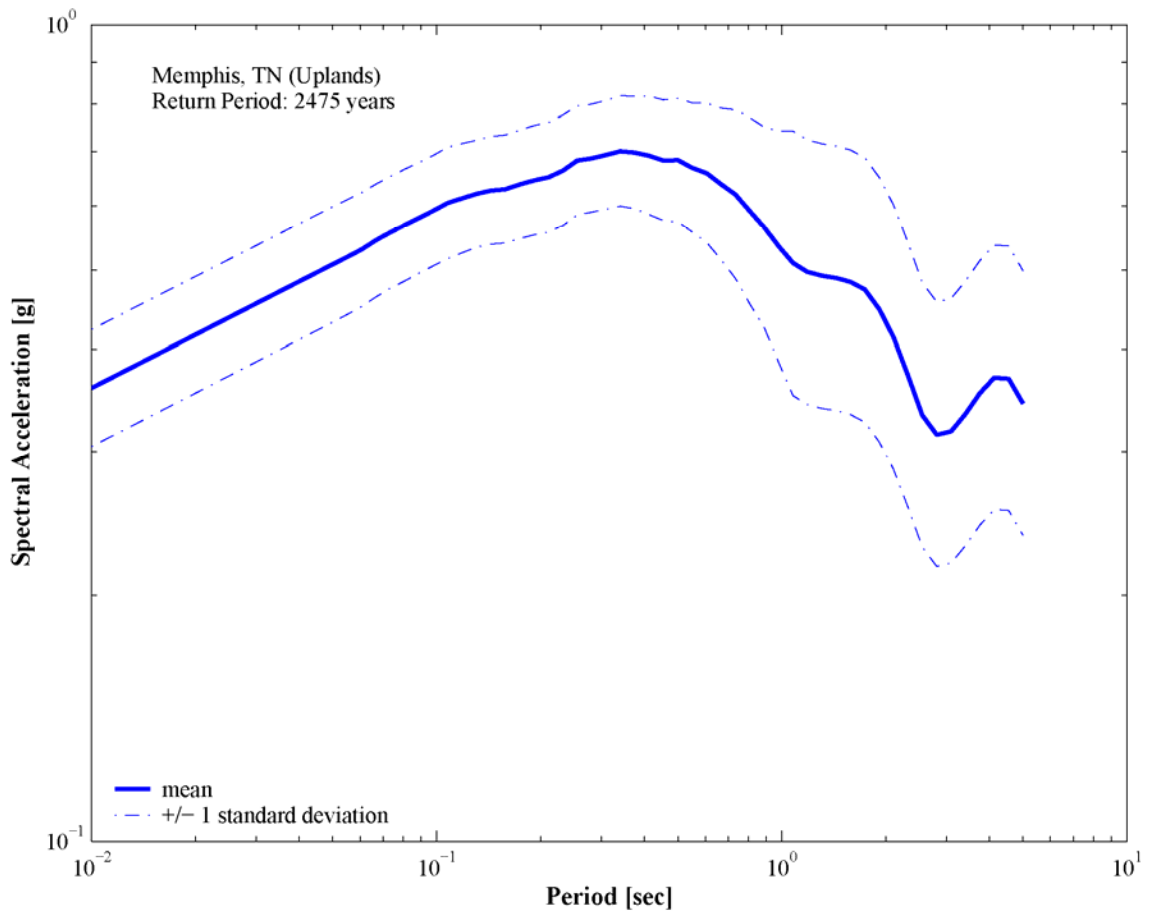


**Figure 4.46.** Soil mean uniform hazard spectrum and its associated variability for return period of 2475 years in Memphis, TN (Uplands)

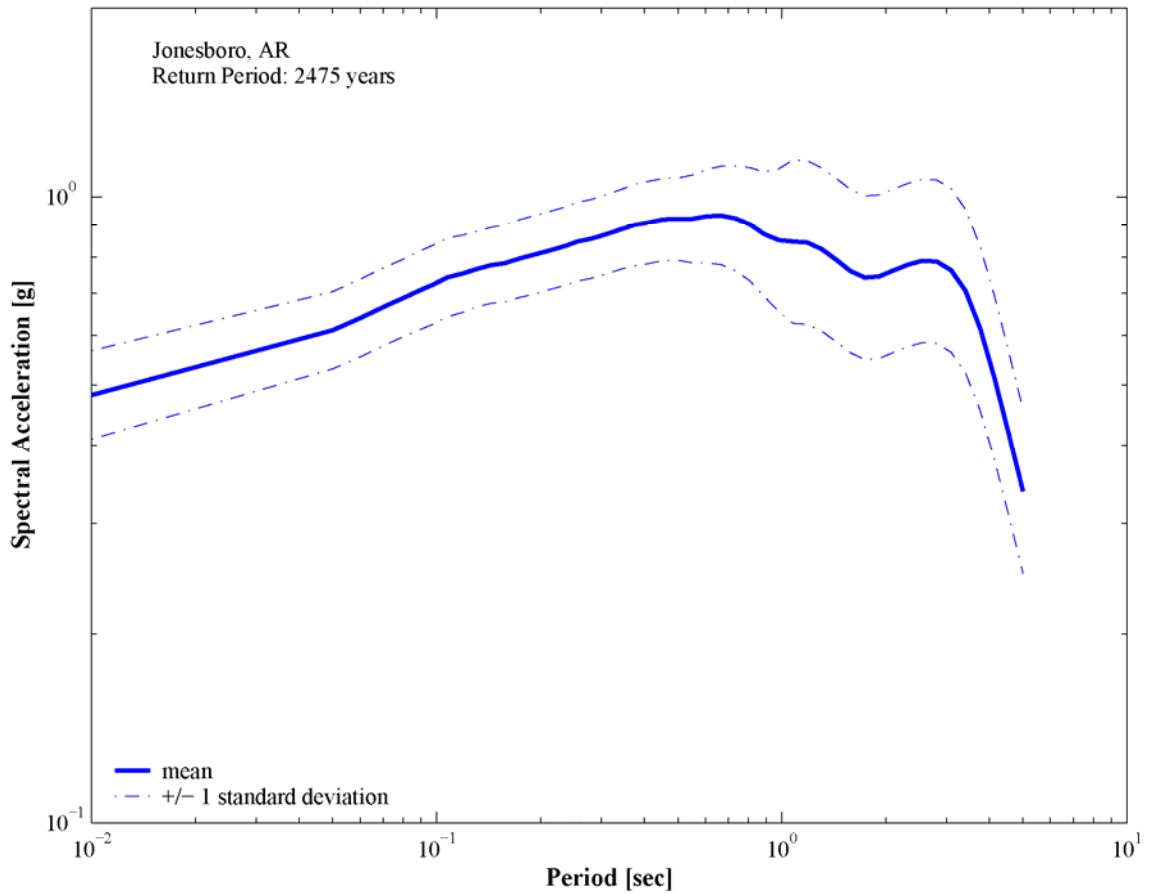


**Figure 4.47.** Soil mean uniform hazard spectrum and its associated variability for return period of 2475 years in Jonesboro, AR

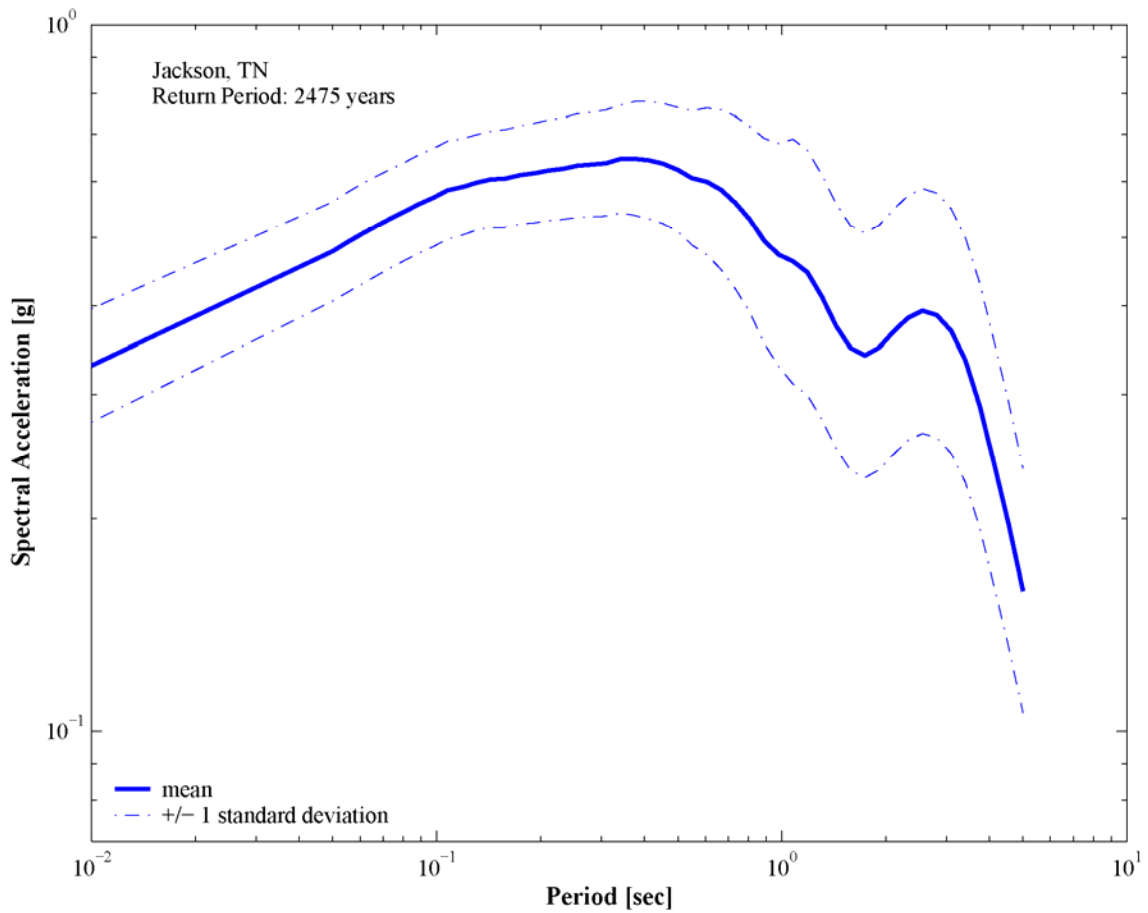


**Figure 4.48.** Soil mean uniform hazard spectrum and its associated variability for return period of 2475 years in Jackson, TN

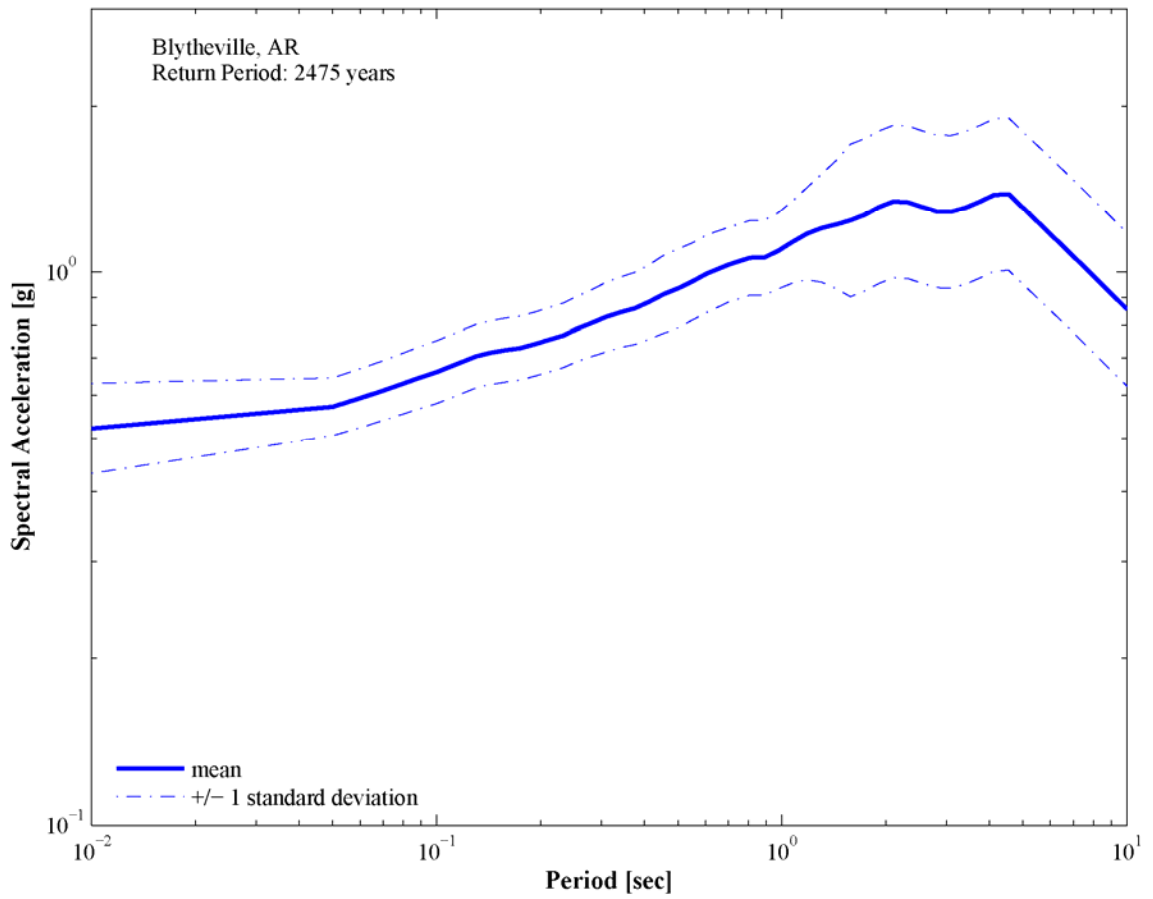


**Figure 4.49.** Soil mean uniform hazard spectrum and its associated variability for return period of 2475 years in Blytheville, AR

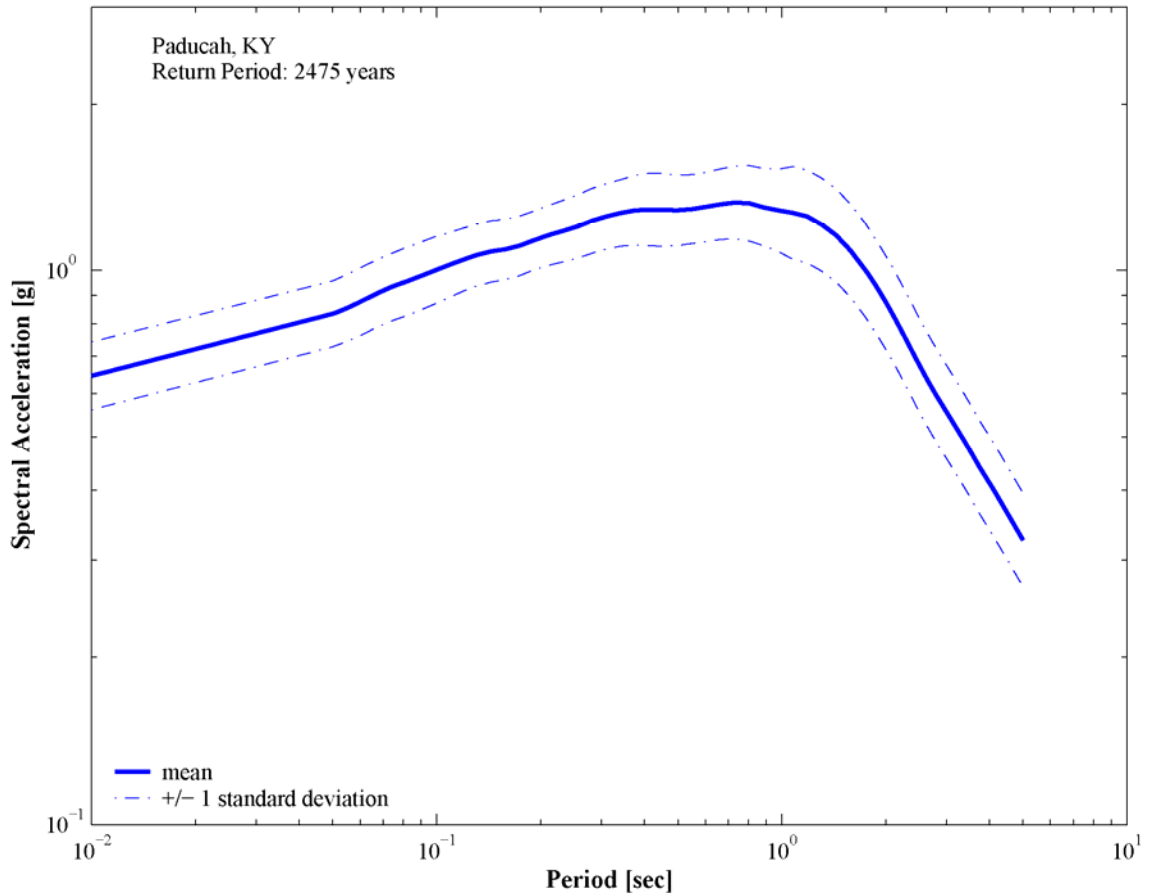


**Figure 4.50.** Soil mean uniform hazard spectrum and its associated variability for return period of 2475 years in Paducah, KY

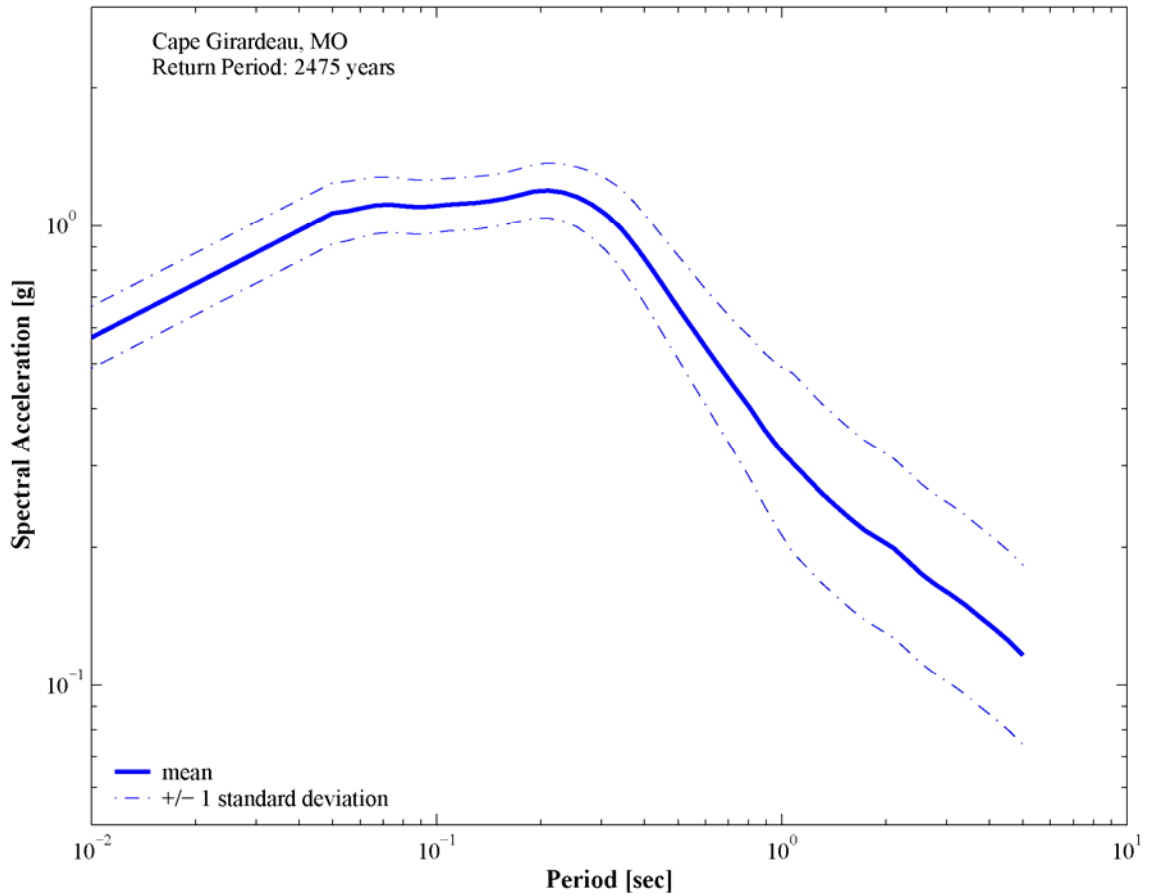


**Figure 4.51.** Soil mean uniform hazard spectrum and its associated variability for return period of 2475 years in Cape Girardeau, MO

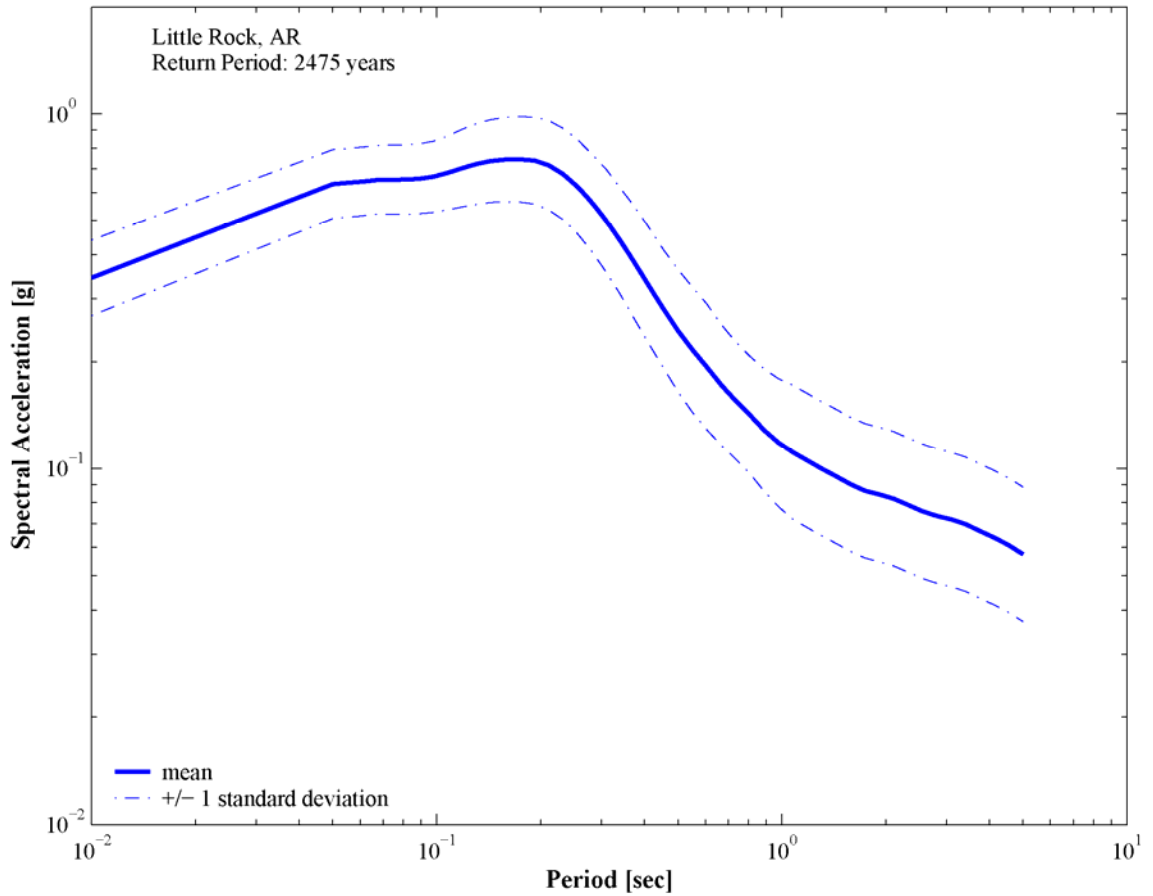


**Figure 4.52.** Soil mean uniform hazard spectrum and its associated variability for return period of 2475 years in Little Rock, AR

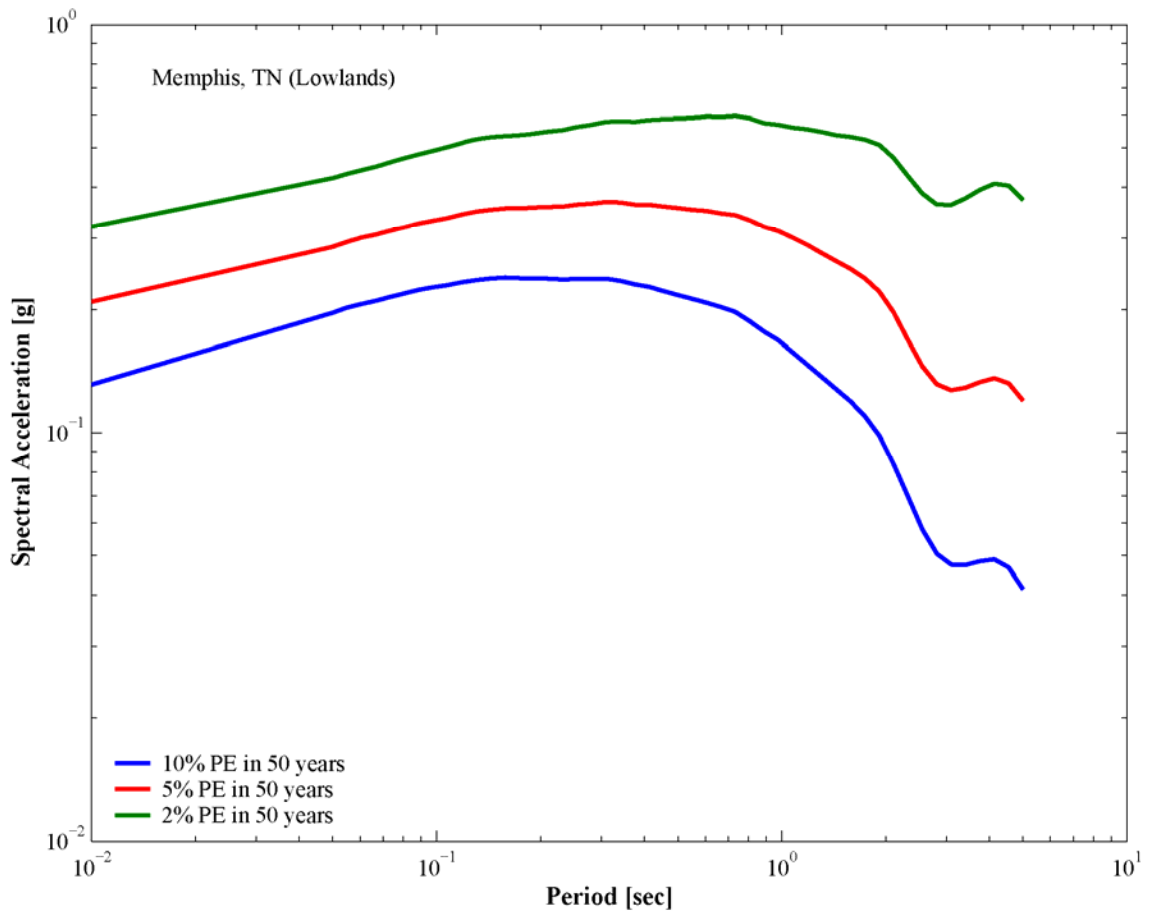


**Figure 4.53.** Soil mean uniform hazard spectra for return periods of 475, 975, and 2475 years in Memphis, TN (Lowlands)

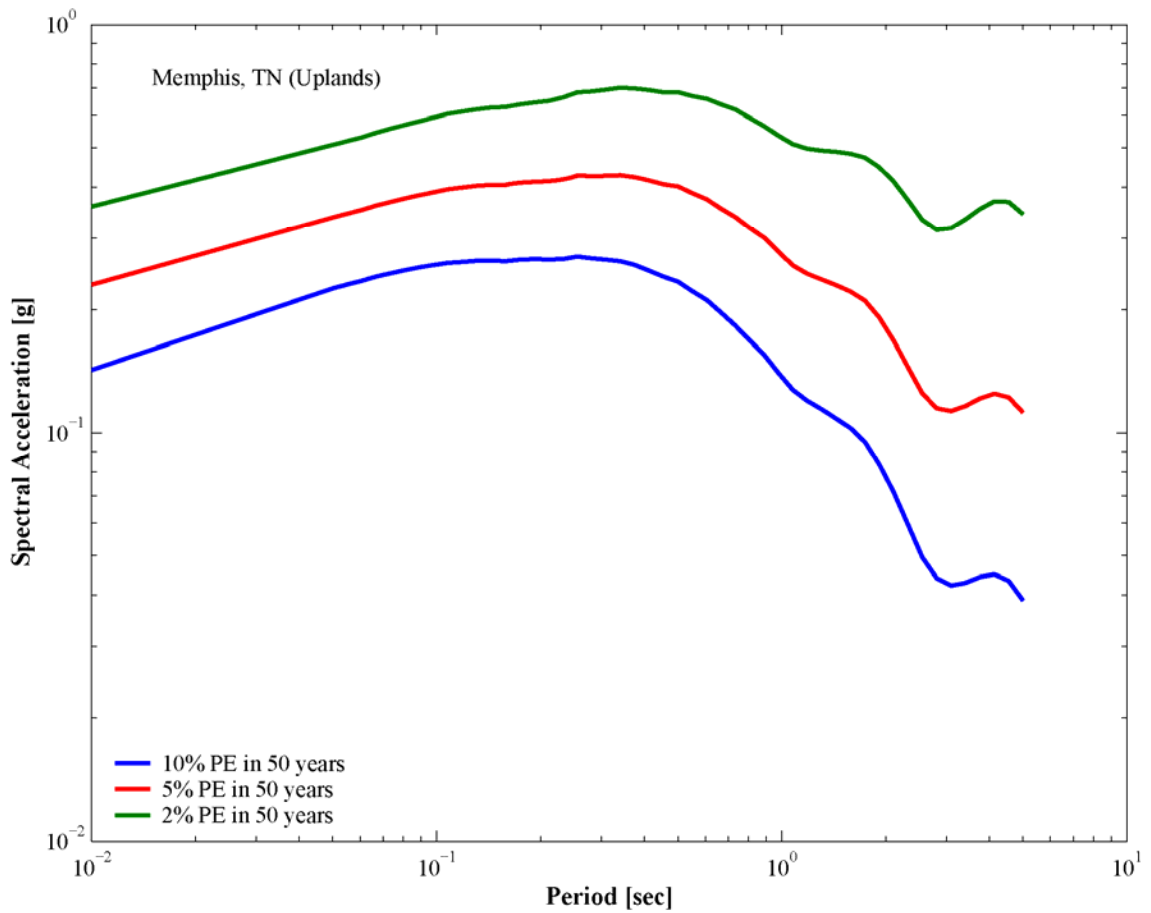


**Figure 4.54.** Soil mean uniform hazard spectra for return periods of 475, 975, and 2475 years in Memphis, TN (Uplands)

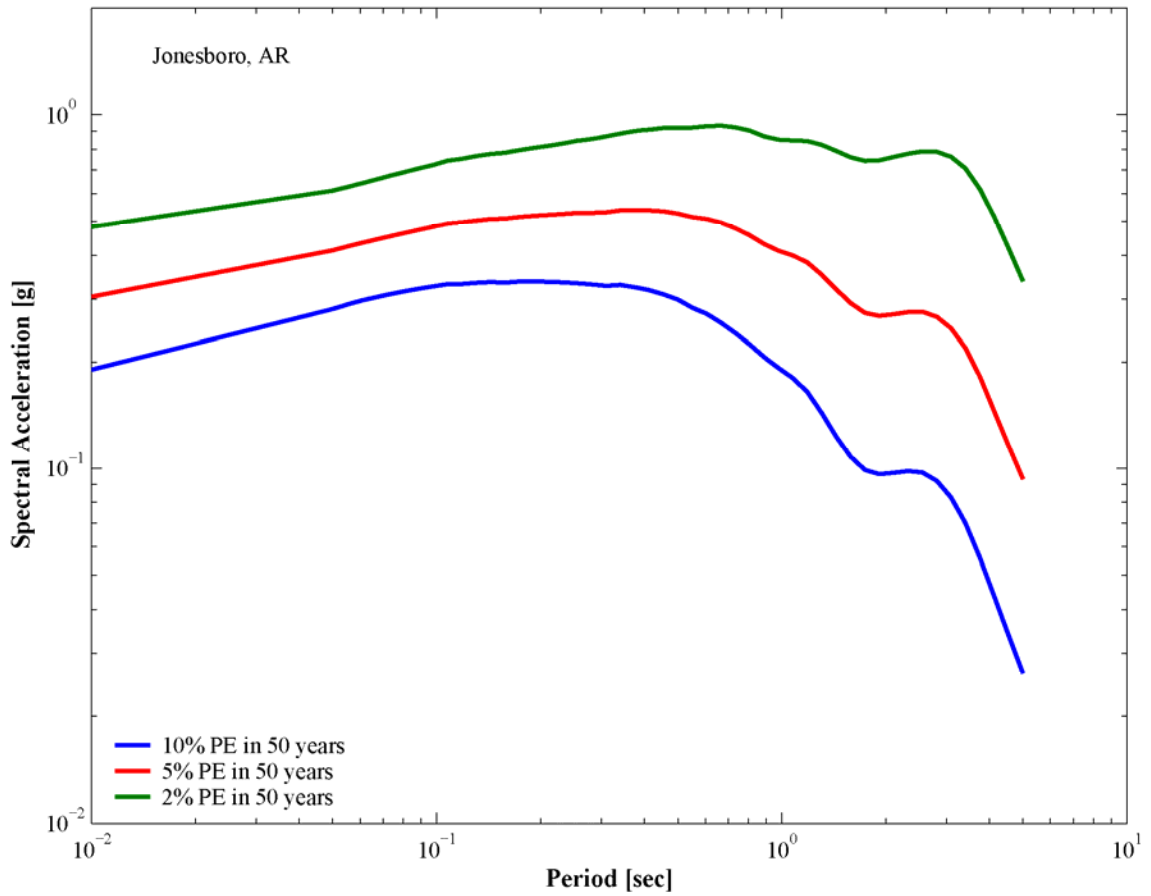


**Figure 4.55.** Soil mean uniform hazard spectra for return periods of 475, 975, and 2475 years in Jonesboro, AR

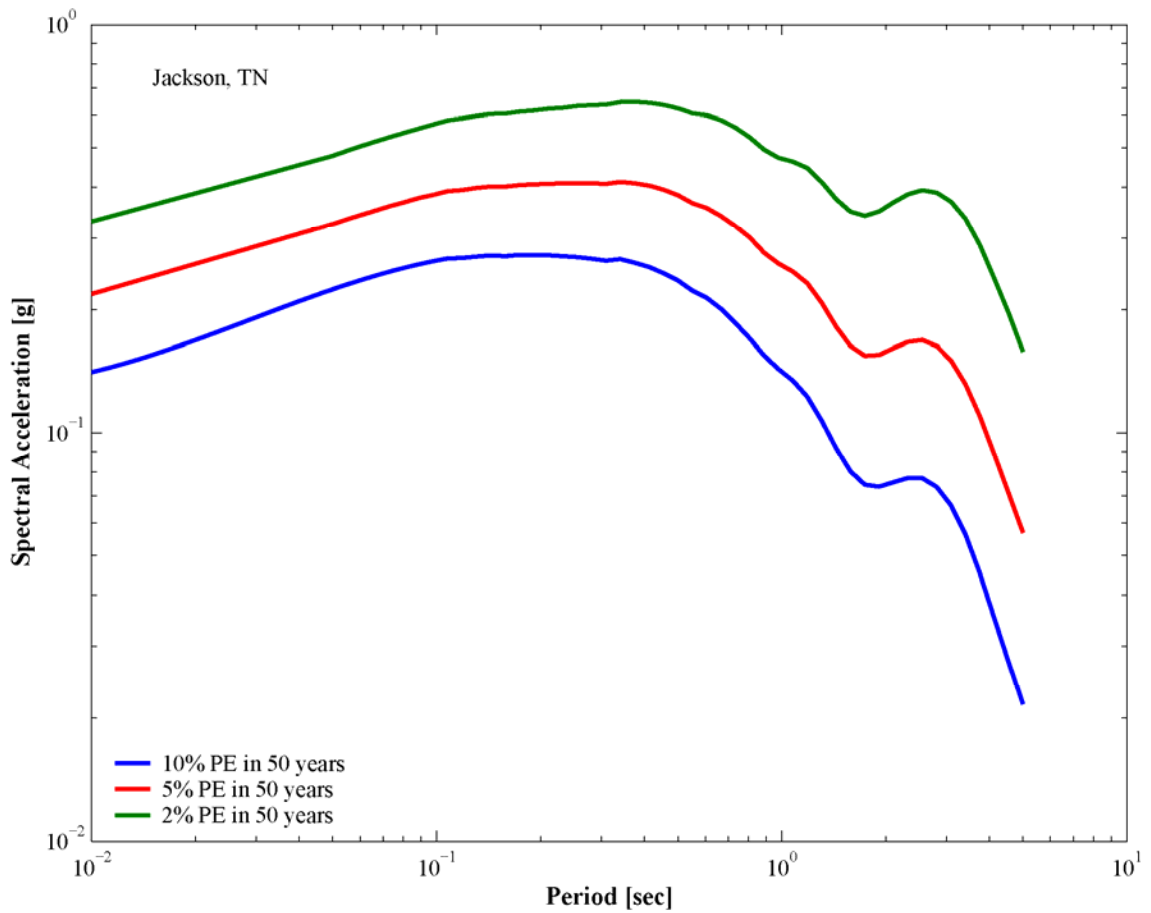


**Figure 4.56.** Soil mean uniform hazard spectra for return periods of 475, 975, and 2475 years in Jackson, TN

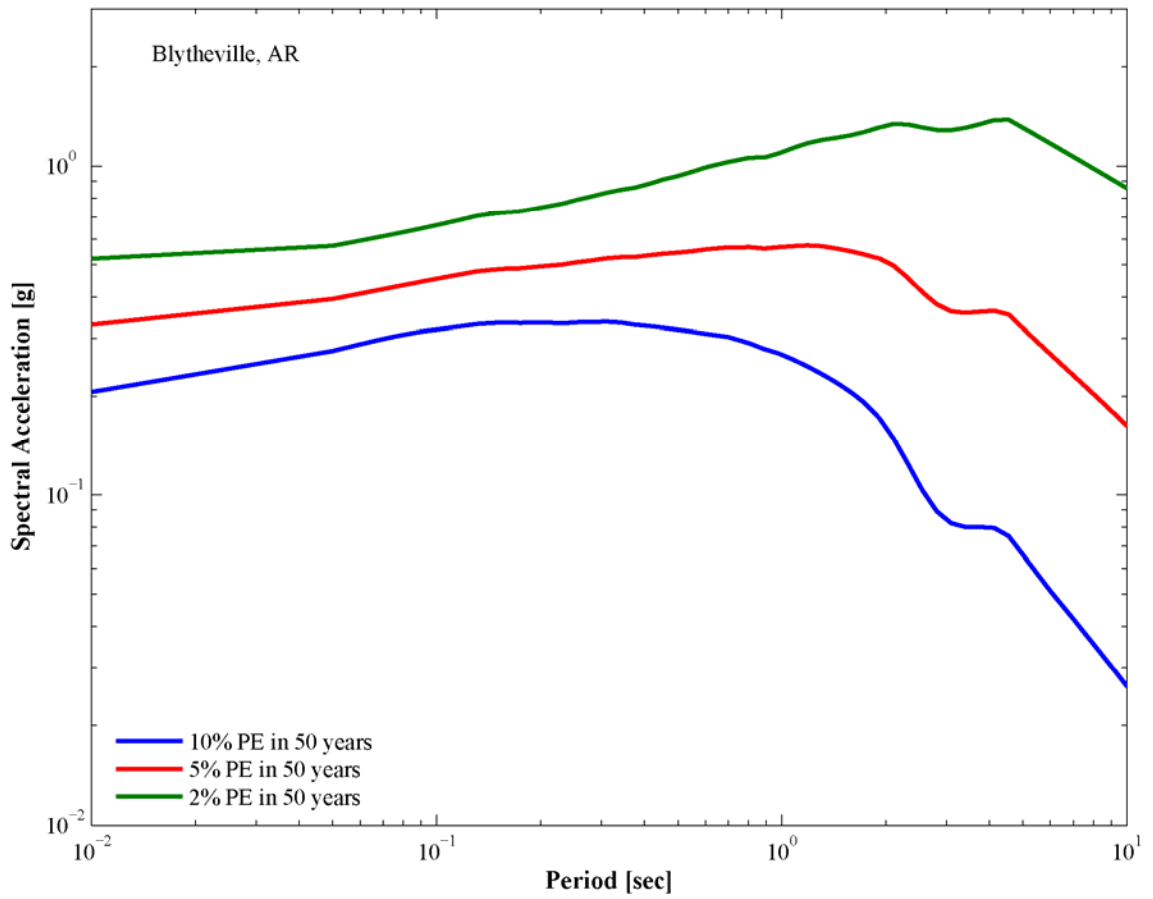


**Figure 4.57.** Soil mean uniform hazard spectra for return periods of 475, 975, and 2475 years in Blytheville, AR

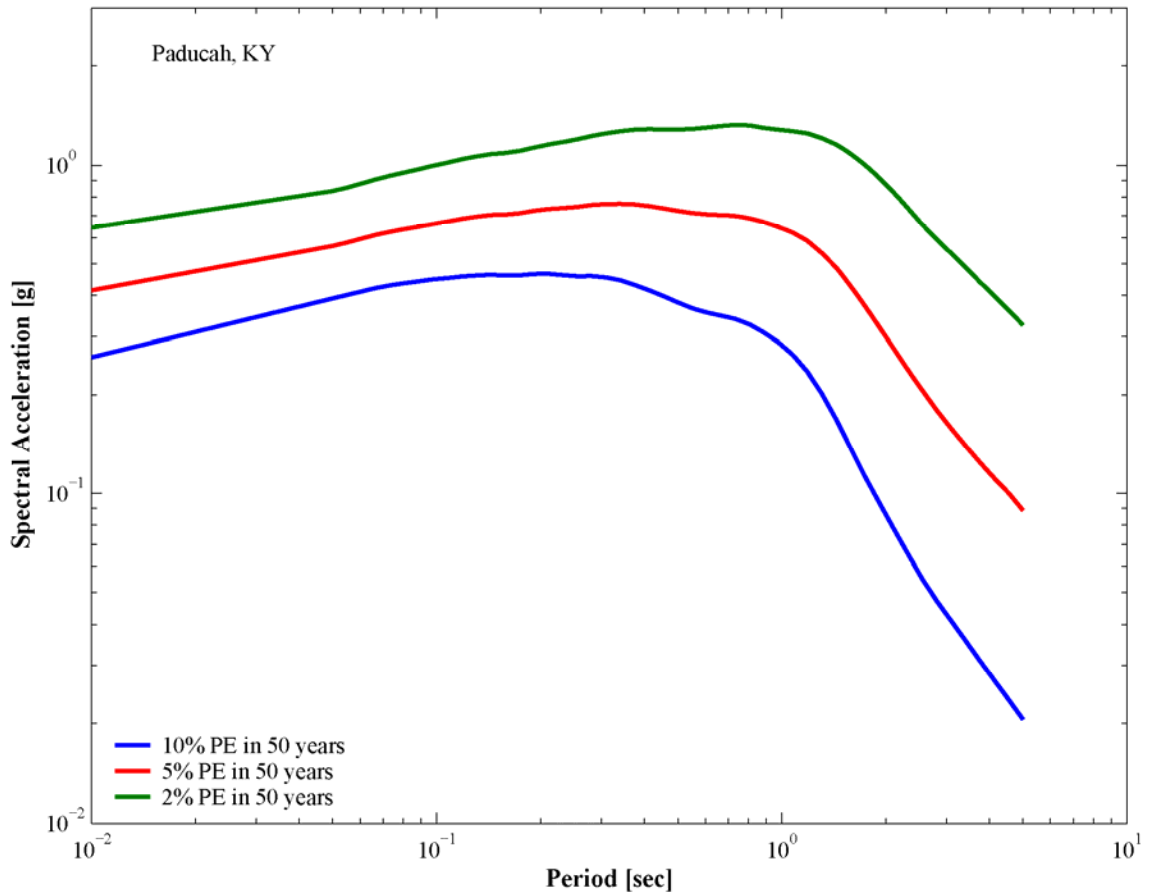


**Figure 4.58.** Soil mean uniform hazard spectra for return periods of 475, 975, and 2475 years in Paducah, KY

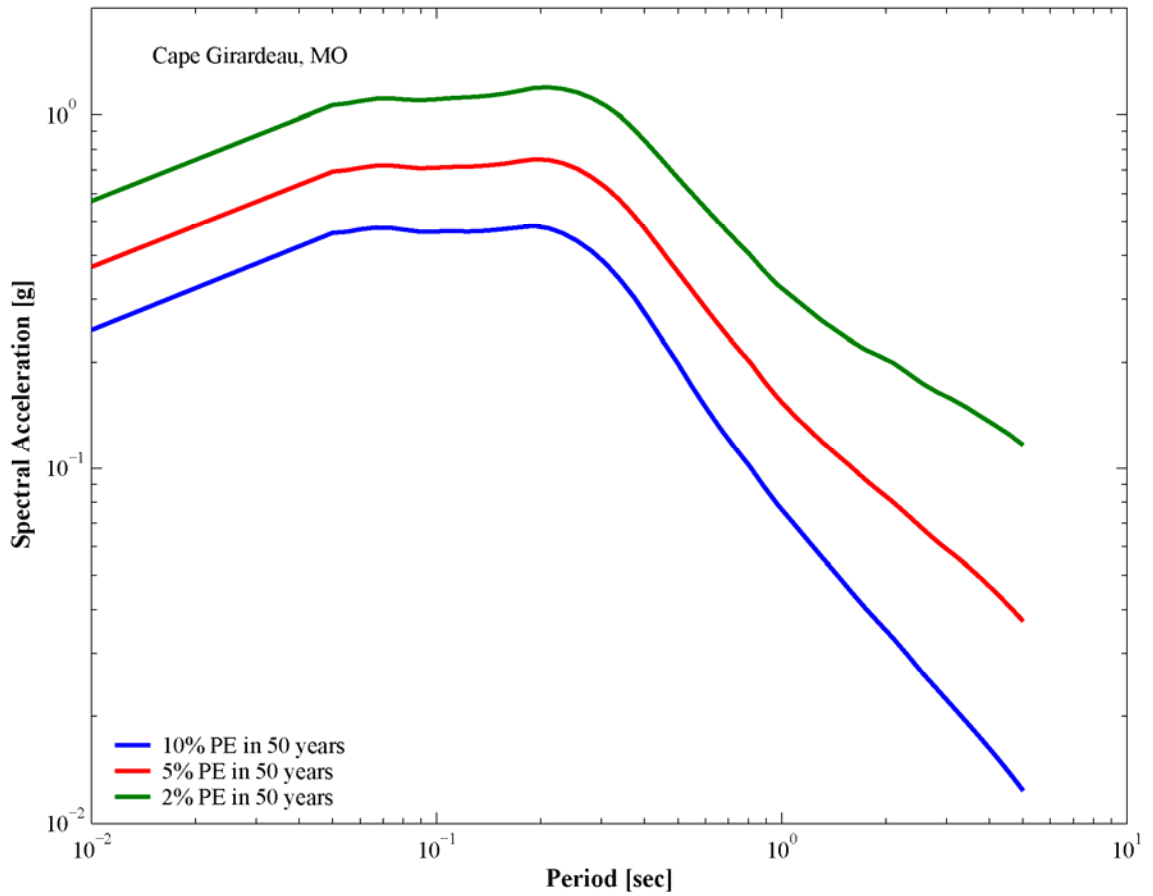


**Figure 4.59.** Soil mean uniform hazard spectra for return periods of 475, 975, and 2475 years in Cape Girardeau, MO

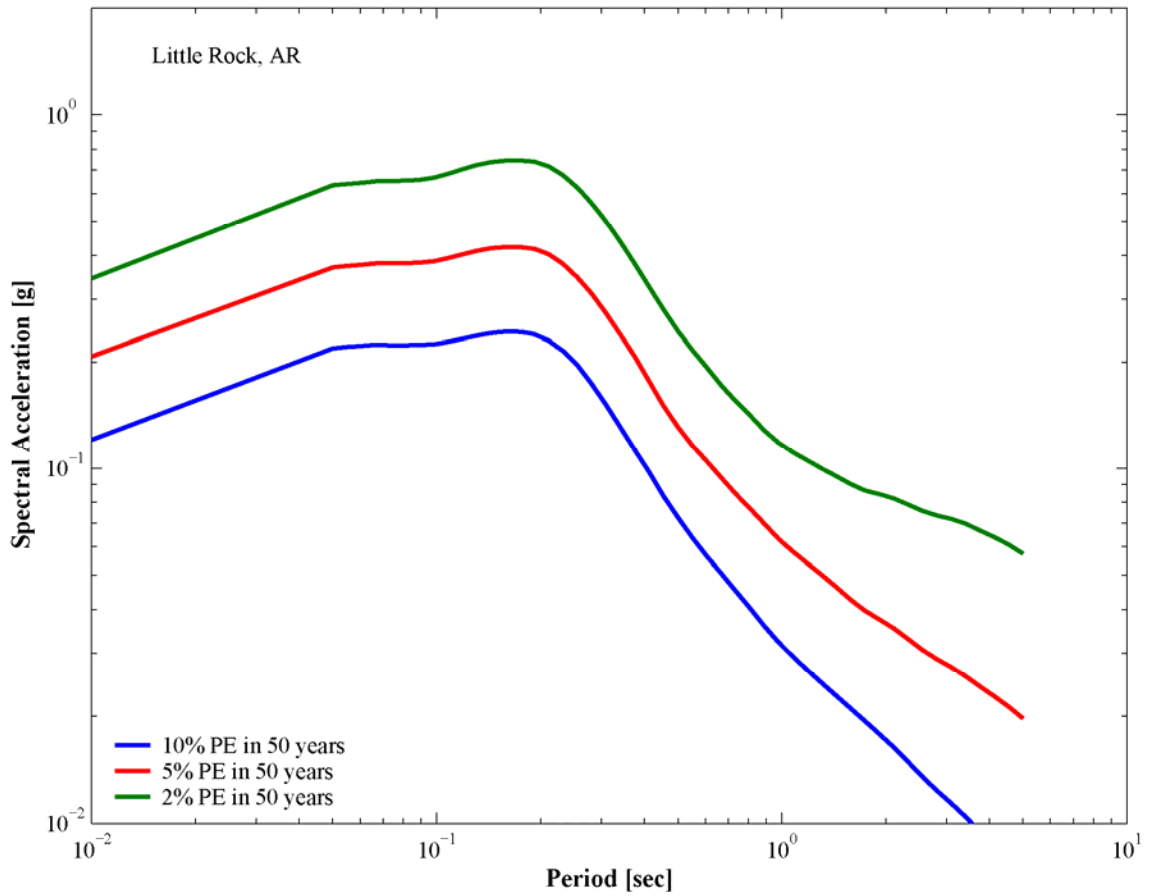


**Figure 4.60.** Soil mean uniform hazard spectra for return periods of 475, 975, and 2475 years in Little Rock, AR

with the effect of the Embayment depth at the site (850 m). The hazard deaggregation shown in Figure B.8 for this city indicates that earthquakes located at 10 km from the site dominate the seismic hazard. Figure 4.61 compare the seven soil hazard curves for 5-second spectral period in Blytheville, AR. The difference between ground motion amplitudes predicted by the Atkinson and Boore (1995) model (one-corner source model) and the Frankel et al. (1996) and Silva et al. (2003) models (two-corner source models) observed in Figure 4.61 is caused by the shape of the source spectrum at low frequencies and the attenuation functions at short distances implemented in each source model as illustrated in Figure 3.2 and Figure 3.12. This difference between the source models is reflected in the hazard curves shown in Figure 4.61. The effect of the Embayment depth on the shape of the UHS can be evaluated by comparing the UHS for Blytheville, AR and Paducah, KY shown in Figure 4.57 and Figure 4.58 respectively. The hazard deaggregation for Paducah, KY shown in Figure B.11 indicates that the dominant epicentral distance is 12 km, which is similar to the dominant distance in Blytheville, AR. However the Embayment depth at Paducah, KY is 120 m and the resonance of the soil column at this site occurs at a shorter period compared to Blytheville, AR. Hence, the decay of ground motion amplitudes in Paducah, KY starts at shorter periods, and the UHS for this city do not show the unusual shape shown by the UHS in Blytheville, AR. Therefore, the high amplitudes predicted by the Frankel et al. (1996) and Silva et al. (2003) models at short distances and low frequencies along with the long-period resonance of the soil column at Blytheville, AR cause the unusual UHS shape for this city shown in Figure 4.49 and Figure 4.57.

#### 4.2.3.3 Comparison with other studies

Figure 4.62 compares the mean UHS calculated in this study for Memphis, TN, to uniform response spectra calculated in previous studies including the analysis for Shelby County, TN performed by Cramer et al. (2004), the probabilistic ground motions for

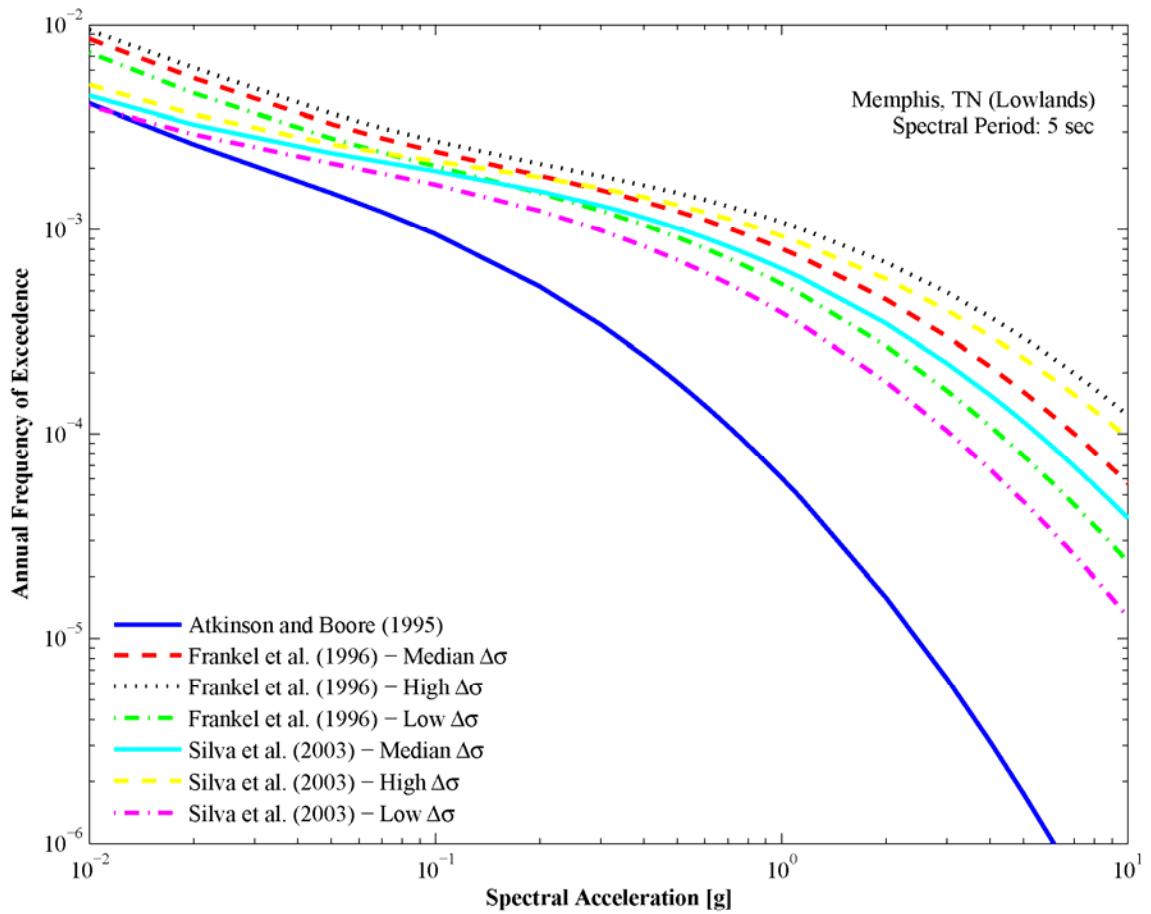


**Figure 4.61.** Five-second spectral period hazard curves for Blytheville, AR

Memphis, TN developed by Toro and Silva (2001) and Wen and Wu (2001), and the rock seismic hazard values for Memphis, TN given by the 2002 USGS National Hazard Maps (Frankel et al., 2002) and modified for soil conditions using the site coefficients provided by FEMA (2001a) and Park and Hashash (2005).

To construct the response spectra using the site coefficients provided by FEMA (2001a) and Park and Hashash (2005), the rock seismic hazard at Memphis, TN was first determined using the 2002 USGS National Hazard Maps (Frankel et al., 2002). The procedure specified in FEMA (2001a) was used to obtain the entire spectrum at the soil surface using the site coefficients corresponding to site class D. The factor of 2/3 specified in this procedure to obtain a design spectrum was not included when computing the response spectra shown in Figure 4.62. The UHS computed using the site coefficients provided by FEMA (2001a) gives the largest difference compared to the mean UHS computed in this study since this set of coefficients does not account for the deep soil profile in Memphis, TN, and therefore it does not capture resonance at long periods and a decrease in amplitude due to viscous damping at depth (Park and Hashash, 2005). Furthermore, as discussed previously and shown in Figure 4.42, these site coefficients do not capture the deamplification of the rock ground motion due to the non-linear soil behavior.

Park and Hashash (2005) provide site coefficients for two sets of soil properties: EPRI and ME (Mississippi Embayment) properties, which they developed specifically for the Mississippi Embayment. The site coefficients corresponding to the EPRI soil properties were used to develop the response spectrum shown in Figure 4.62 because the same set of soil properties was used to develop the soil attenuation relationships used in the PSHA calculations in this study. The response spectrum calculated using this set of site coefficients captures the effect of the embayment depth at Memphis, TN and the non-linear soil behavior, by showing a decrease in amplitude and longer resonance periods compared to the response spectrum calculated using the site coefficients provided by

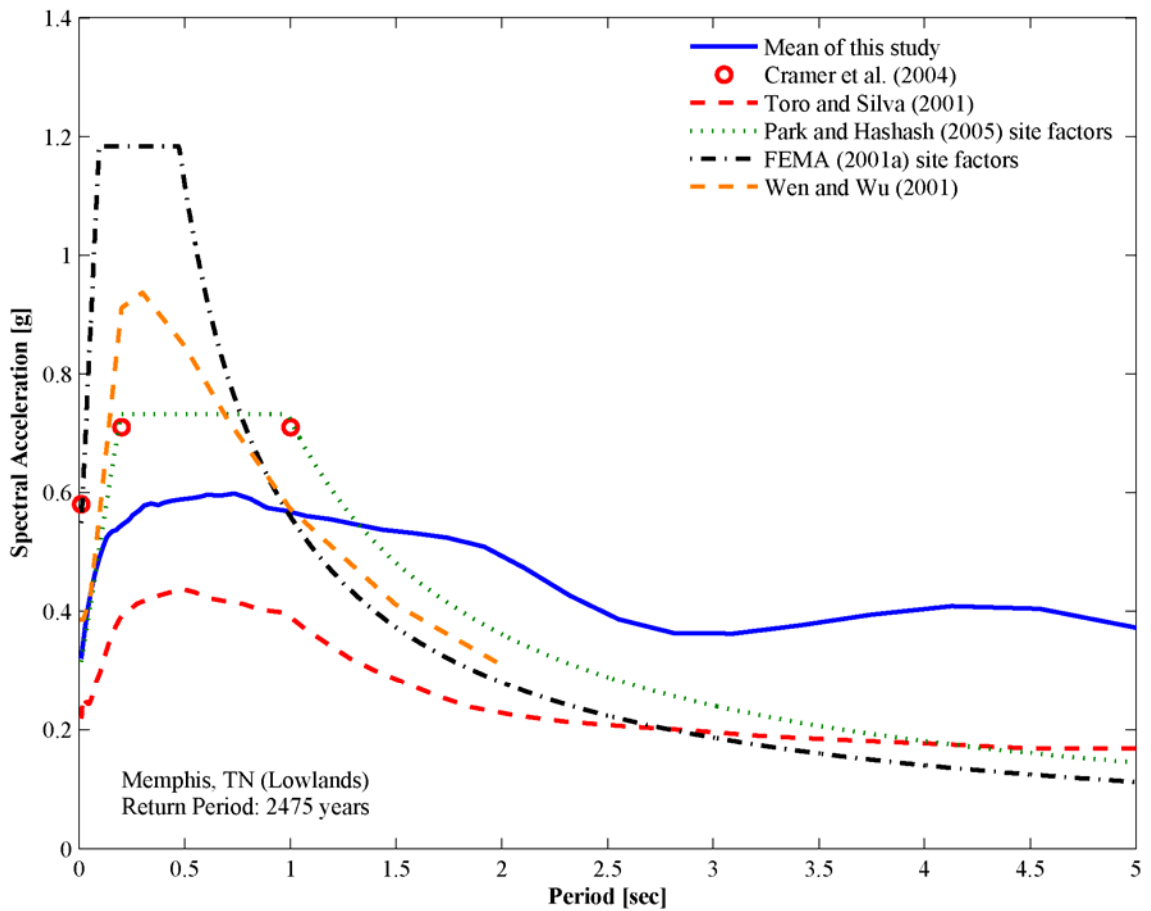


**Figure 4.62.** Comparison of uniform hazard spectra for return period of 2475 years in Memphis, TN

FEMA (2001a); however the Park and Hashash (2005) response spectrum still shows higher amplitudes compared to the mean UHS of this study. As discussed previously, the multiplication of a rock UHS by deterministic amplification factors may bias the estimation of soil ground motions. Moreover, the probabilistic-deterministic procedure results in soil UHS with unknown exceedance rate (Bazzurro and Cornell, 2004b; Goulet et al., 2007). Therefore, as in the case of the FEMA (2001a) response spectrum, a direct comparison can not be made between the mean UHS of this study and the response spectrum calculated with the Park and Hashash (2005) site coefficients. The assumed shape of the FEMA (2001a) and Park and Hashash (2005) UHS, particularly in the long-period range where the amplitude is inversely proportional to the period, is another factor for the difference with the UHS calculated in this study.

Figure 4.62 also shows the average ground motion values calculated by Cramer et al. (2004) for Shelby County, TN, corresponding to 2% probability of exceedence in 50 years. These ground motion values are higher than the mean UHS computed in this study. Cramer et al. (2004) used the method proposed by Cramer (2003) to couple the uncertainty in site response with PSHA computations at the rock level to estimate the seismic hazard at the soil surface. According to Bazzurro and Cornell (2004b) and Silva et al. (2000), this methodology generates artificially high amplitudes of the seismic hazard at the soil surface since the coupling procedure does not consider the negative correlation between the site response and the rock hazard when the amplitudes of the rock motions are high enough to induce non-linear behavior of the soil column (Bazzurro and Cornell, 2004a; Campbell and Bozorgnia, 2006; EPRI, 1993; Toro et al., 1997). The lack of the negative correlation may be responsible for the difference in amplitude observed in Figure 4.62.

Toro and Silva (2001) developed probabilistic ground motions for Memphis, TN that include the effect of the soil thickness, local geology, and non-linear soil behavior. Toro and Silva (2001) developed soil amplification functions for the deep soil profile of

the Upper Mississippi Embayment and applied the median of these amplification functions to the rock UHS to obtain ground motions at the soil surface. Figure 4.62 shows that the UHS calculated by Toro and Silva (2001) gives lower amplitude values compared to the mean UHS computed herein. A possible cause of this difference might be the different source characterization performed in both studies. Toro and Silva (2001) used a longer recurrence interval compared to the mean recurrence time of 500 years used in the source characterization implemented in this study. Toro and Silva (2001) considered recurrence times of 1000 and 500 years, but a larger weight (70%) was assigned to the longer recurrence interval. According to Cramer (2001) the uncertainty in rupture model is one of the most important contributors to the variability in seismic hazard estimates in the New Madrid region. Furthermore, Toro and Silva (2001) acknowledge that the simple multiplication of the rock UHS by a median amplification function neglects the uncertainty in the soil response. This factor might be another source of the differences observed in Figure 4.62.

Wen and Wu (2001) developed probabilistic soil ground motions for Memphis, TN by using soil amplification functions to modify rock UHS. The soil amplification was computed using the quarter-wavelength method (Joyner et al., 1981). Figure 4.62 shows that this site response method does not model the non-linear soil behavior and the resonance peaks at long periods due to the deep soil profile in Memphis, TN. In fact, none of the previous studies capture the resonance of the deep sediments in the Embayment observed at about 4 to 5 sec in the UHS of this study as shown in Figure 4.62. Moreover, the method used by Wen and Wu (2001) suffers the disadvantages of the probabilistic-deterministic approach discussed above.

In general the results of this study are comparable with probabilistic ground motions calculated in previous studies. However the UHS computed herein are believed to be more accurate since the variability in the entire earthquake process and site-specific conditions are included directly in the PSHA calculations by using soil attenuation

relationships in the hazard integral (Equation 4.4) (Bazzurro and Cornell, 2004b; Goulet and Stewart, 2007; Goulet et al., 2007; Silva and Costantino, 2002).

#### **4.2.4. Regional Seismic Hazard Maps**

The soil attenuation relationships developed herein were also used to perform probabilistic seismic hazard analyses for the entire region. The seismic sources characterization described previously for the PSHA of selected cities within the Embayment was also implemented in the regional seismic hazard analyses.

The soil attenuation relationships were developed for the two typical soil profiles in the Embayment – Lowlands and Uplands – and seven Embayment depth bins, ranging from 6 m to 1220 m. Thus, to perform the regional seismic hazard analyses the entire Upper Mississippi Embayment was subdivided in 14 areas, corresponding to the two soil profiles and seven depth bins. Appropriate soil attenuation relationships were selected for the PSHA calculations on each area. Figure 4.63 illustrates the 14 regions delimited according to the Embayment depth and soil type. In this study the southernmost limit of the Upper Mississippi Embayment is latitude 33.8° N. Figure 4.63 shows an area on the south part of the Embayment where no analyses were performed, since the Embayment depth in this region exceeds the depth limit of 1220 m of the attenuation relationships.

The regional probabilistic seismic hazard analyses were computed on a 0.1-degree square grid. Epistemic variability was incorporated in the analyses by using the seven attenuation relationships corresponding to the source models and stress drop values listed in Table 4.4. These hazard analyses incorporate the non-linear soil behavior implemented in the soil attenuation relationships.

These regional analyses were used to generate seismic hazard maps for the Upper Mississippi Embayment. The seven hazard values obtained at each grid point were combined using the weights listed in Table 4.4 to generate seismic hazard maps for three ground motion amplitudes, mean and +/- 1 standard deviation. Following the same

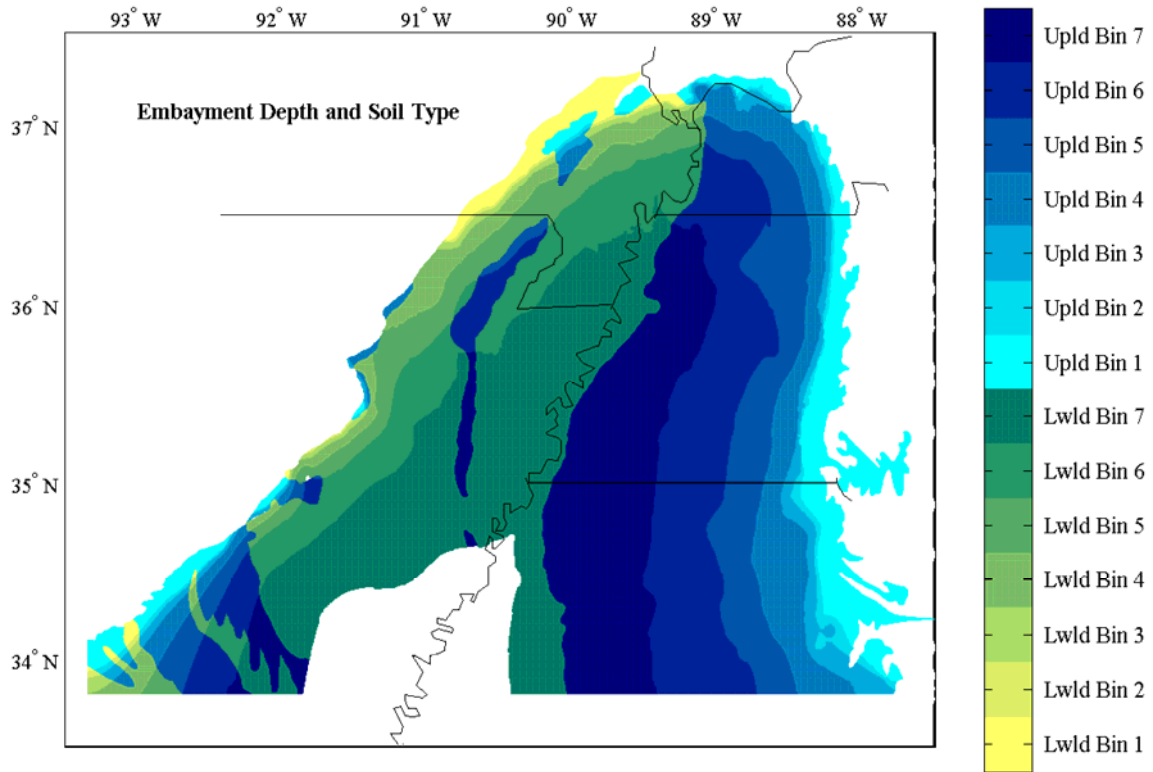


**Figure 4.63.** Division of the Upper Mississippi Embayment according to soil type – Lowlands (Lwld) and Uplands (Upld) – and depth bin – 6 m (bin 1) to 1220 m (bin 7) –.

procedure used in analysis of the selected cities, the combination of the different models was computed in the frequency of exceedence space and then transformed into uniform hazard spectra. The seismic hazard maps were generated for three return periods, 475, 975 and 2475 years, and for 50 spectral periods distributed between 0.01 and 5 seconds. The maps were constructed by interpolating hazard values at points located on a 0.025-degree square grid using a triangle-based linear interpolation. For points located outside the 0.1-degree square grid, the extrapolation was performed using the Ordinary Kriging method using the four closest hazard values. Figure 4.64 through Figure 4.72 show samples of the hazard maps generated. The maps illustrate that for short spectral periods the seismic hazard in the Embayment is controlled by the depth to the bedrock, whereas

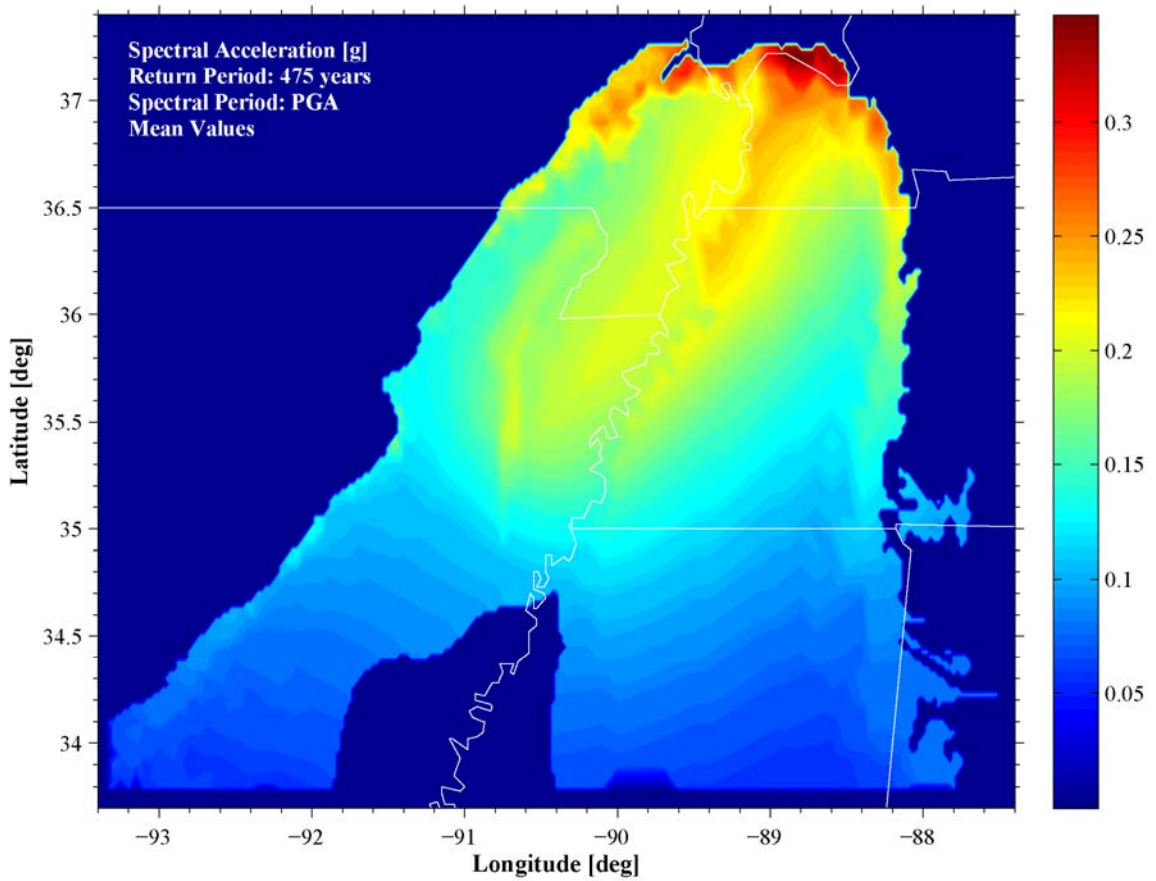


**Figure 4.64.** Seismic hazard map for peak ground acceleration and return period of 475 years; mean values

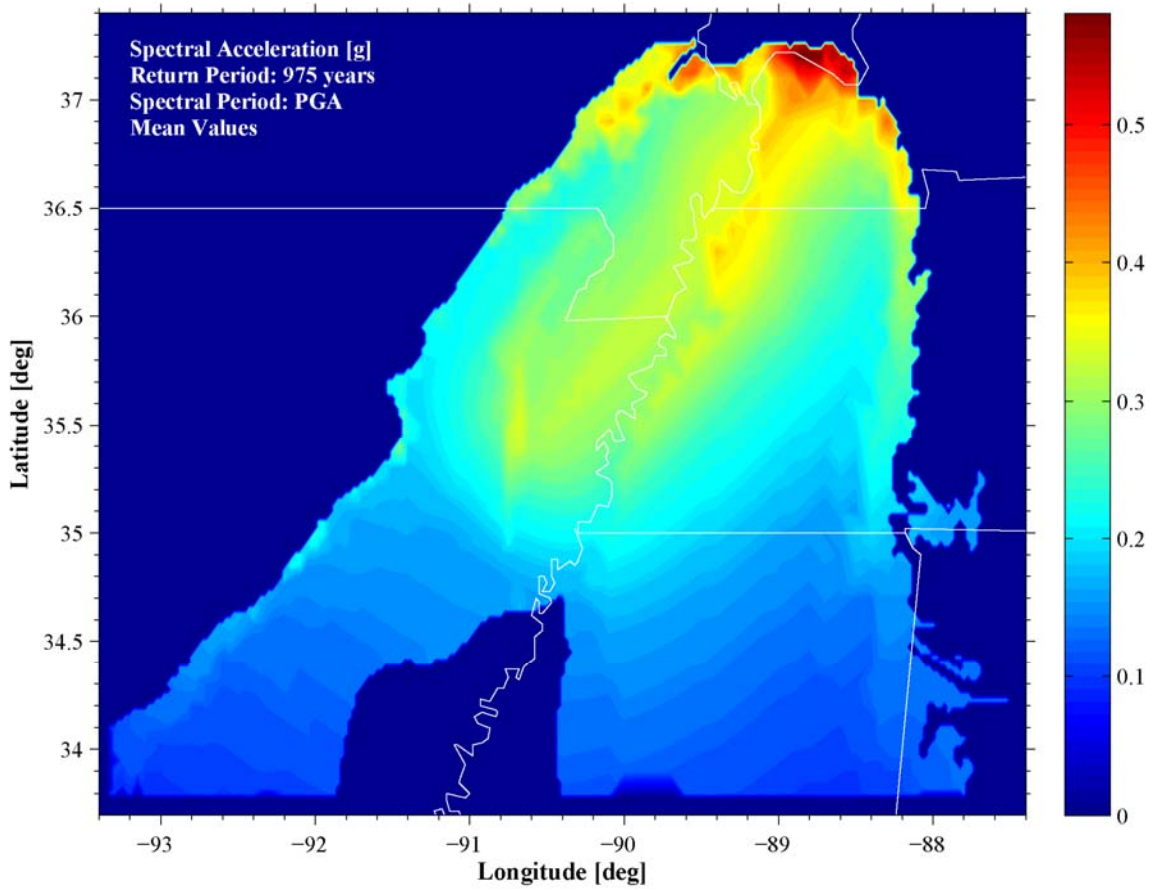


**Figure 4.65.** Seismic hazard map for peak ground acceleration and return period of 975 years; mean values

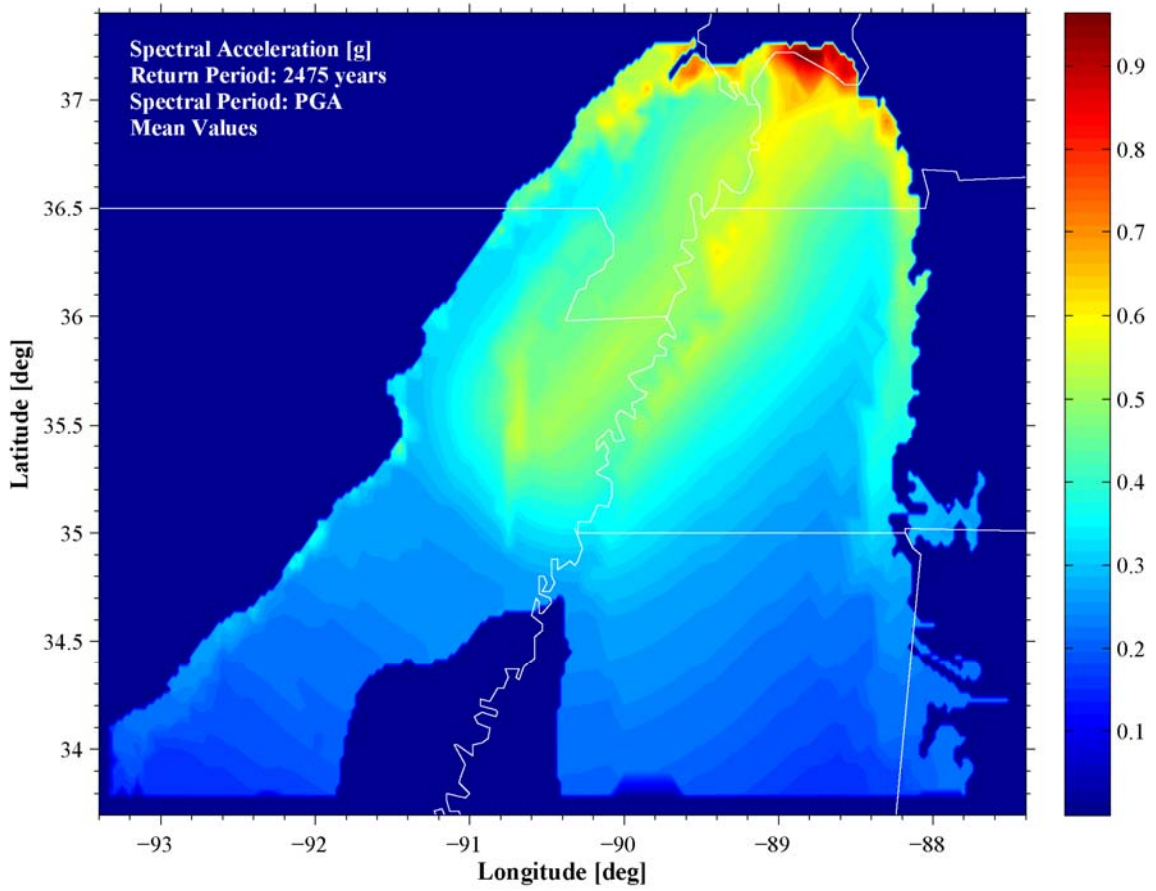


**Figure 4.66.** Seismic hazard map for peak ground acceleration and return period of 2475 years; mean values

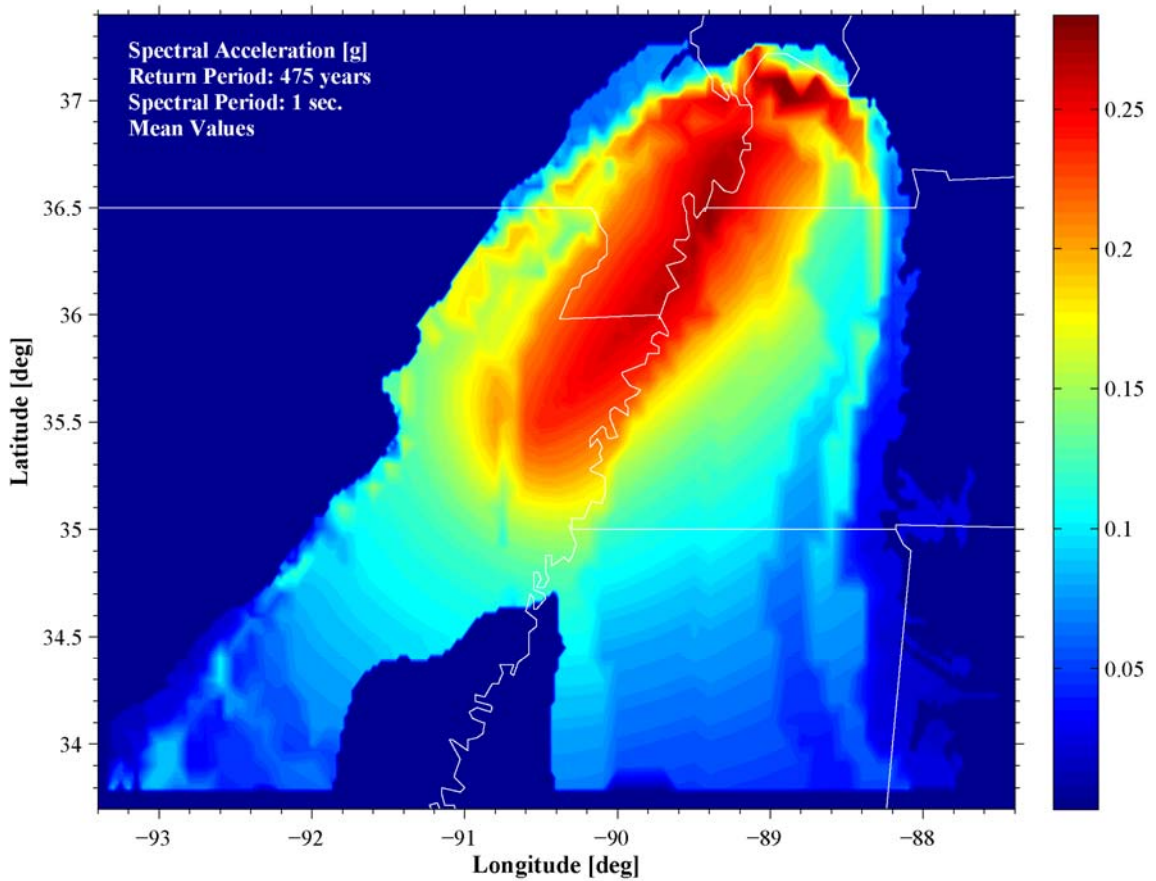


**Figure 4.67.** Seismic hazard map for 1-second spectral acceleration and return period of 475 years; mean values

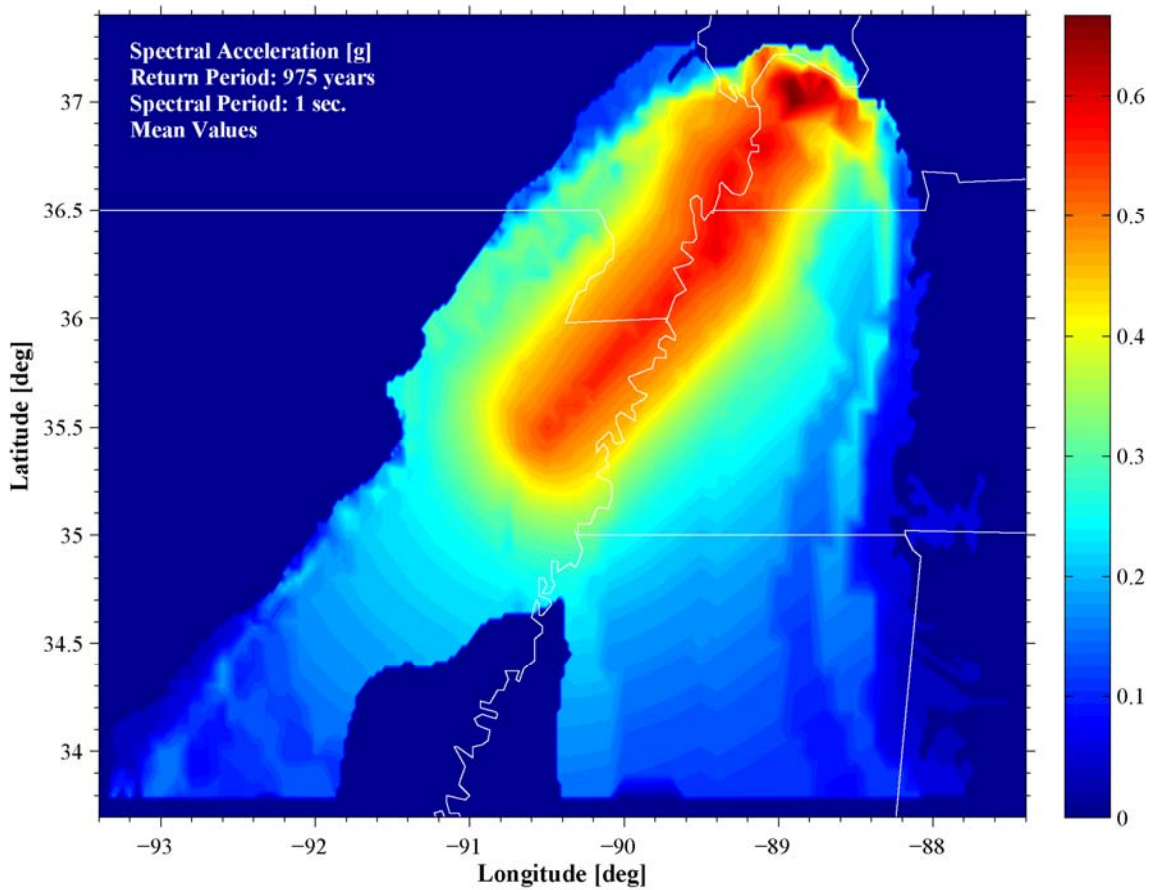


**Figure 4.68.** Seismic hazard map for 1-second spectral acceleration and return period of 975 years; mean values

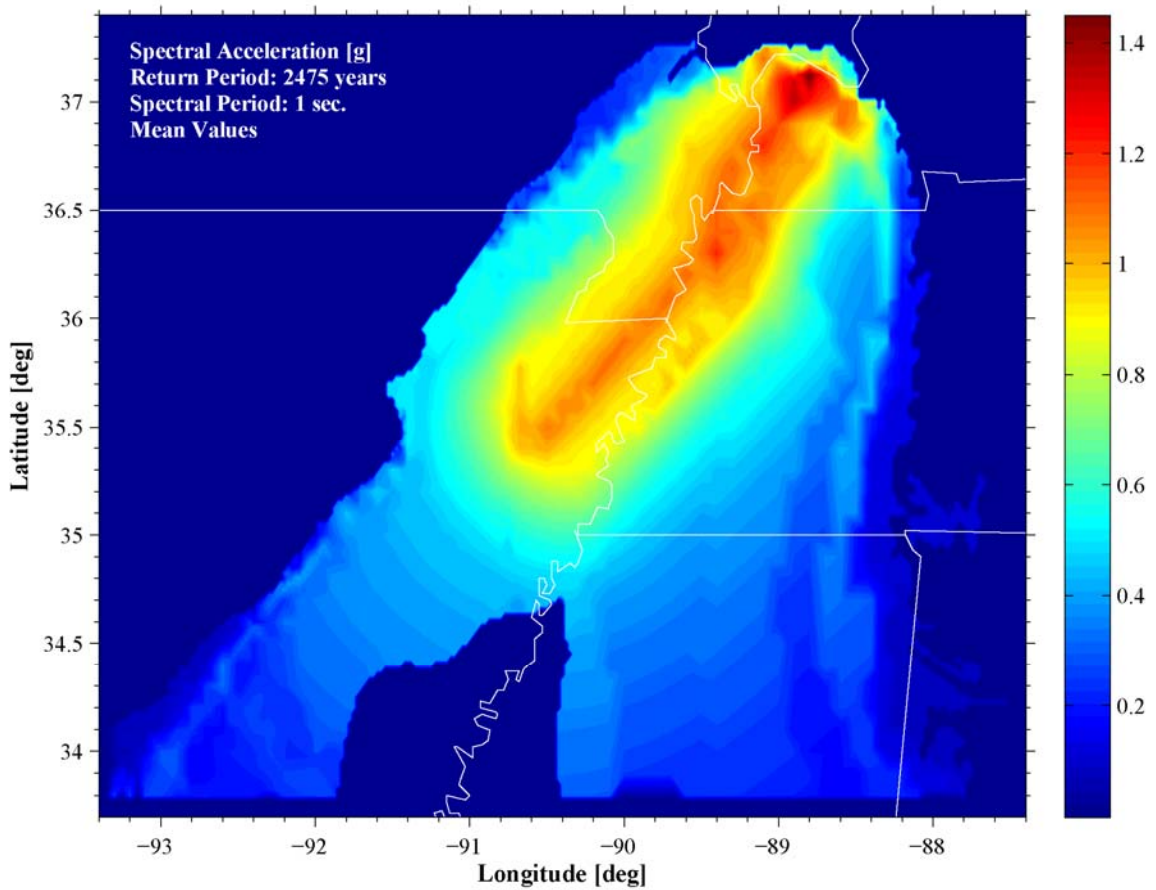


**Figure 4.69.** Seismic hazard map for 1-second spectral acceleration and return period of 2475 years; mean values

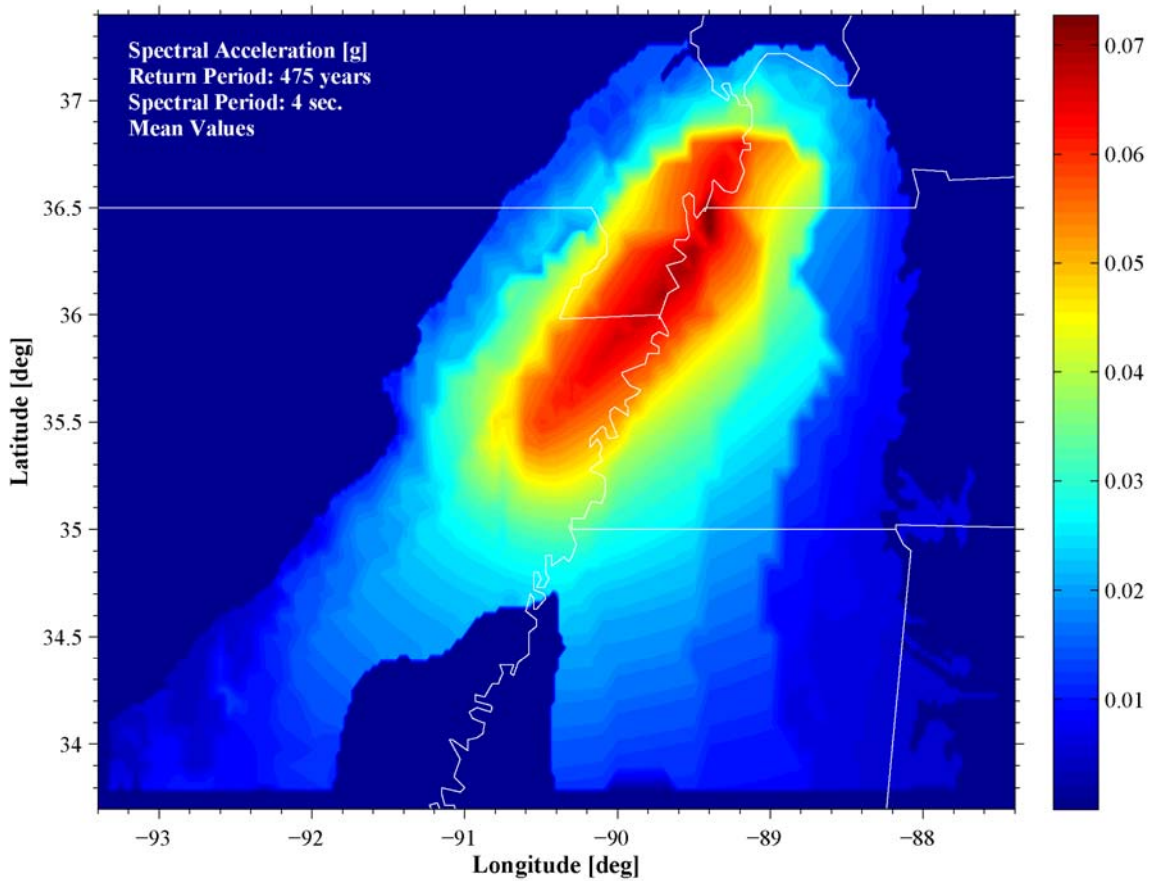


**Figure 4.70.** Seismic hazard map for 4-second spectral acceleration and return period of 475 years; mean values

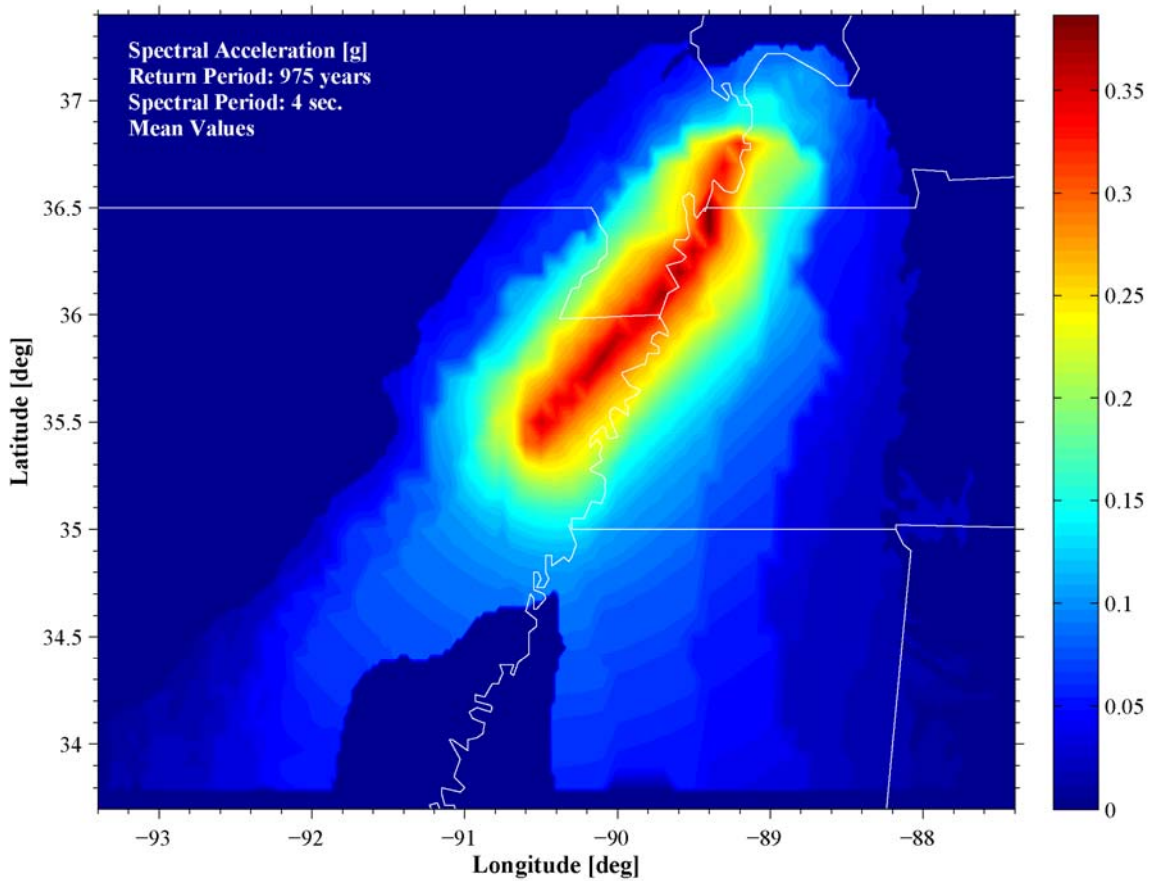


**Figure 4.71.** Seismic hazard map for 4-second spectral acceleration and return period of 975 years; mean values

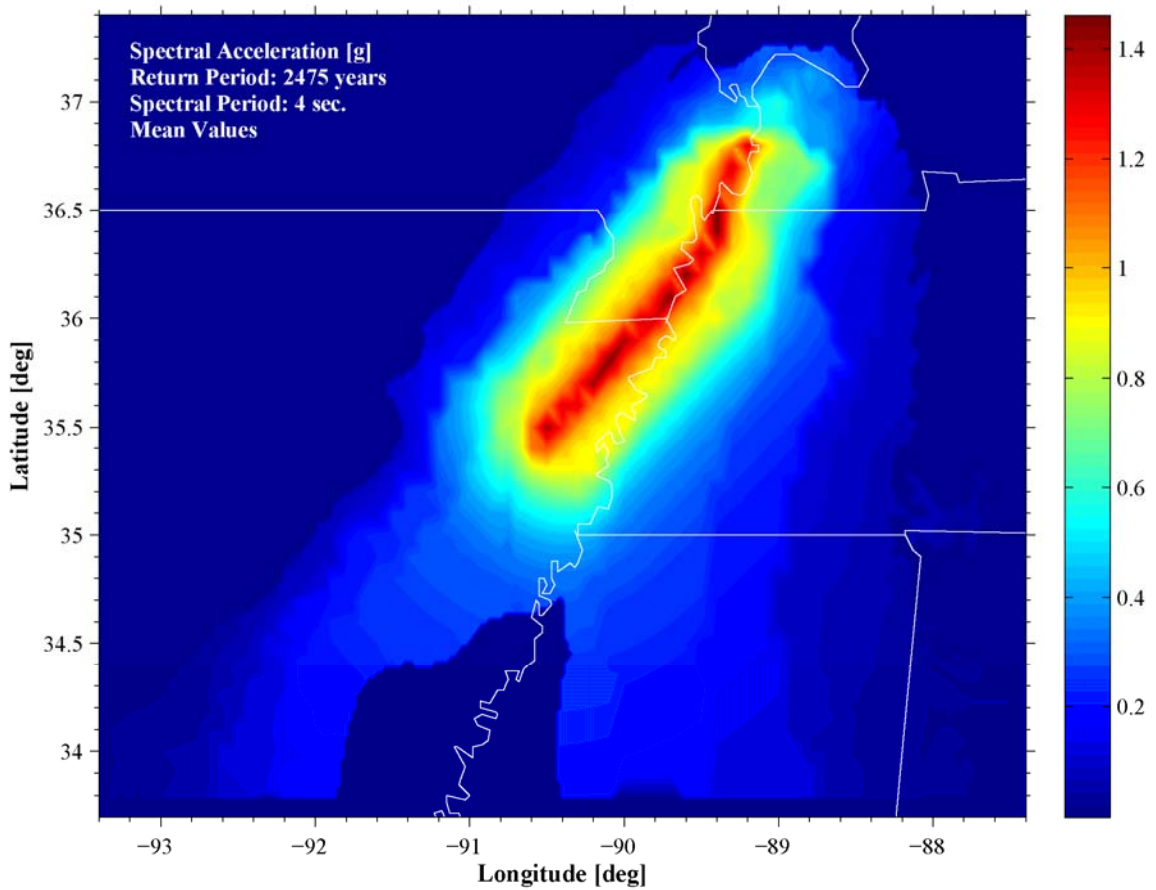


**Figure 4.72.** Seismic hazard map for 4-second spectral acceleration and return period of 2475 years; mean values

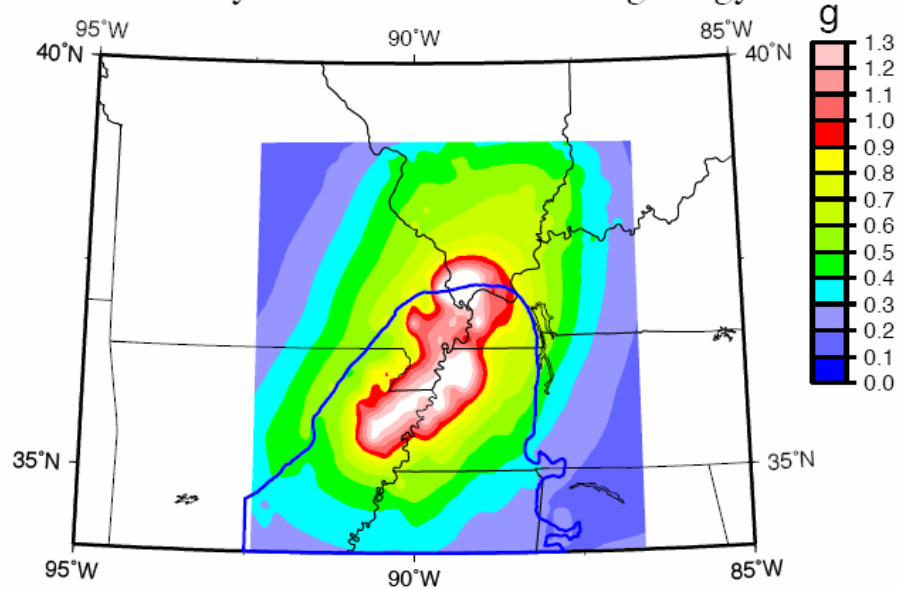
the New Madrid seismic faults control the seismic hazard at long spectral periods independent of the hazard level.

The methodology used by Cramer et al. (2004) to develop probabilistic ground motions for Shelby County, TN was implemented by Cramer (2006b) to develop seismic hazard maps for the Upper Mississippi Embayment. Cramer (2006b) used two site response formulations to generate the seismic hazard maps: a traditional equivalent linear analysis implemented in the program SHAKE91 (Idriss and Sun, 1992) limiting the non-linear soil behavior to the upper 300 m of the soil profile, and an equivalent linear analysis using frequency-dependent soil dynamic properties to account for the deep soil column in the Embayment (Assimaki and Kausel, 2002; Kausel and Assimaki, 2002) implemented in the program TREMORKA (Hartzell et al., 2004).

Figure 4.73 and Figure 4.74 show the seismic hazard maps developed by Cramer (2006b) using SHAKE91 and TREMORKA, respectively. The maps correspond to a 2% probability of exceedence in 50 years (i.e. return period of 2475 years) and are for PGA and 1-second spectral acceleration. The blue line represents the boundary of the Upper Mississippi Embayment. The relative ground motion amplitude distribution shown in Figure 4.66 and Figure 4.69 for PGA and 1-second spectral acceleration, respectively, and return period of 2475 years, shows higher amplitudes in the northern part of the Embayment. This relative amplitude distribution compares better to the relative amplitudes of the seismic hazard map generated using TREMORKA shown in Figure 4.74. However the absolute ground motion amplitudes obtained in this study are lower than those predicted by Cramer (2006b), particularly the ground motions generated using SHAKE91. The methodology used by Cramer (2006b) for coupling the site response variability with the rock ground motions may be responsible for the difference observed in ground motion amplitudes, as discussed above.

## 2005 Embayment PGA Hazard Map

2% in 50 years with effects of site geology



## 2005 Embayment 1s Sa Hazard Map

2% in 50 years with effects of site geology

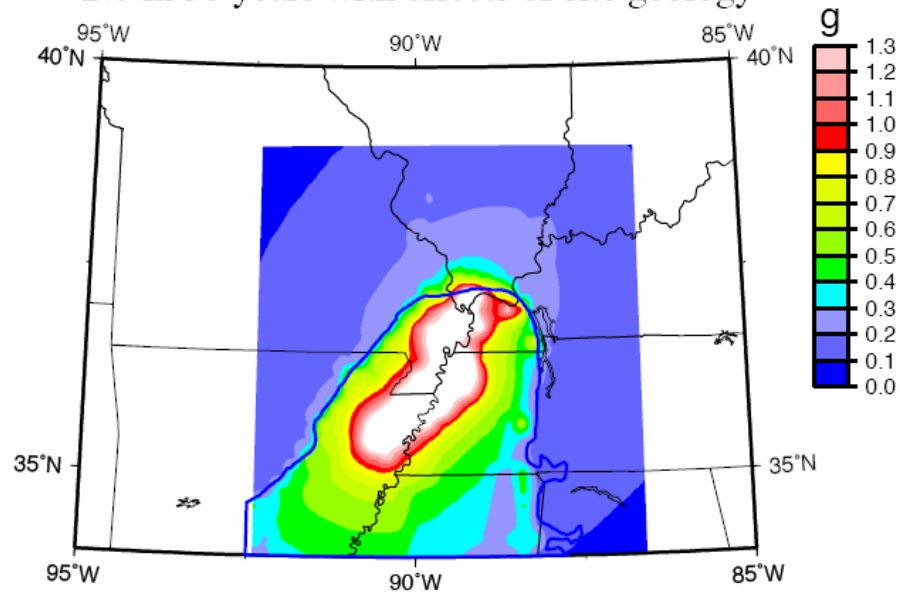
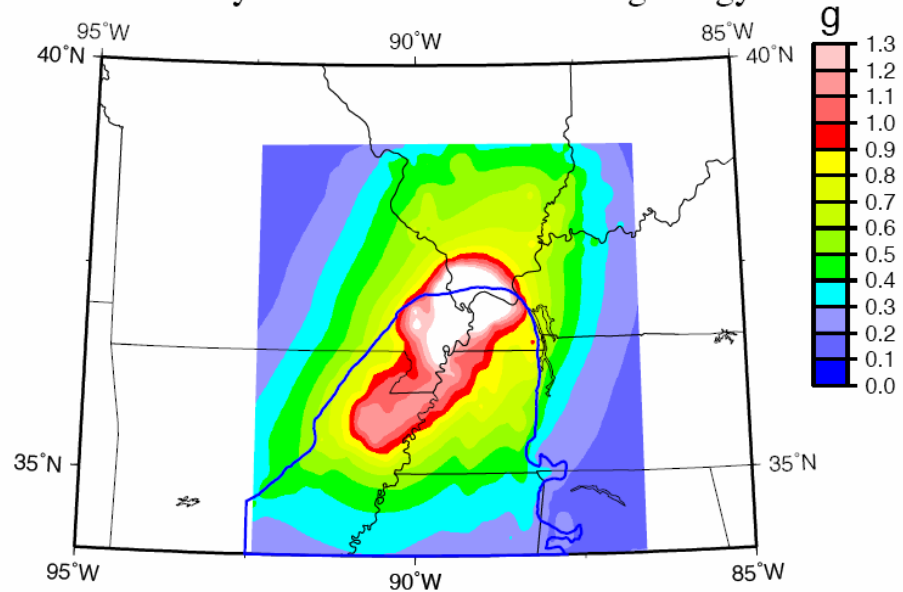


**Figure 4.73.** Seismic hazard maps developed by Cramer (2006b) using SHAKE91 (blue line represents the boundary of the Upper Mississippi Embayment)

## Alternate Embayment PGA Hazard Map

2% in 50 years with effects of site geology



## Alternate Embayment 1s Sa Hazard Map

2% in 50 years with effects of site geology

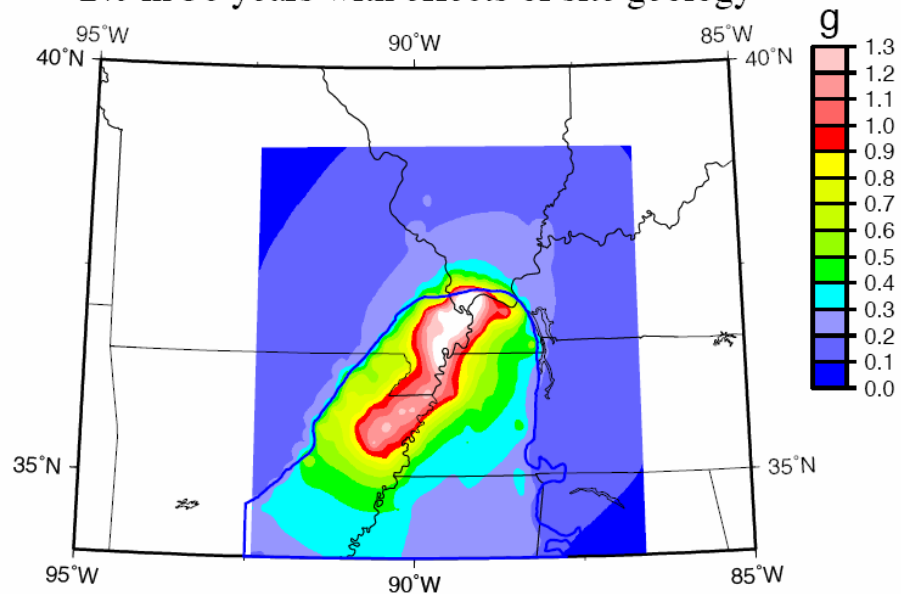


**Figure 4.74.** Seismic hazard maps developed by Cramer (2006b) using TREMORKA (blue line represents the boundary of the Upper Mississippi Embayment)

### 4.3. Spectrum-Compatible Time Histories

Non-linear structural analyses require site-specific, time domain representation of the seismic hazard. The recorded ground motions database in the Central and Eastern United States (CEUS) is sparse particularly for magnitudes and distances relevant to engineering design. Previous studies of seismic hazard in the CEUS (Atkinson and Beresnev, 2002; McGuire et al., 2001; Somerville and Collins, 2003; Wen and Wu, 2001) have generated time series of earthquake ground motions for the CEUS using a variety of approaches involving artificial, simulated, or real earthquake motions.

Wen and Wu (2001) developed artificial time histories for soil and rock conditions by combining windowed Gaussian white noise with a Fourier amplification spectrum computed with a seismological model (Boore, 2003c). Linear site amplification was incorporated using the quarter-wavelength method. The time histories are consistent with hazard levels corresponding to return periods of 2475 and 475 years and were developed for three cities – Memphis, TN, St. Louis, MO, and Carbondale, IL.

Atkinson and Beresnev (2002) also generated artificial rock and soil ground motions for **M** 7.5 and **M** 8.0 scenarios using a finite-fault stochastic method for the cities of Memphis, TN, and St. Louis, MO. The non-linear site response was modeled by an empirical approach using a combination of the amplification factors of Abrahamson and Silva (1997), NEHRP (FEMA, 2001a), and Atkinson and Boore (2001). Atkinson and Beresnev (2002) considered basin effects in Memphis by using the empirical correction factors of Joyner (2000).

Somerville and Collins (2003) used a broadband strong ground motion simulation method to develop synthetic time histories for rock conditions that were consistent with the USGS 2002 National Seismic Hazard Maps. The time histories were obtained by scaling simulated ground motions to match a target response spectrum. Sets of time histories were developed for three return periods – 2475, 475, and 108 years – and 25 major cities in the CEUS.

Another approach to develop time histories is the method recommended by McGuire et al. (2001), where the acceleration time history of a real earthquake is modified to be compatible with a target response spectrum. McGuire et al. (2001) scaled soil and rock time histories recorded for Western United States conditions to more closely represent CEUS conditions. The scaling process involved computing response spectral transfer functions between WUS and CEUS conditions using the single-corner-frequency, point-source model. The transfer functions were then applied to the WUS empirical rock and soil spectra resulting in scaled CEUS empirical rock and soil motions. This process provides CEUS ground motions with realistic phase and amplitude relationships between components and frequency-to-frequency variability (McGuire et al., 2001). The scaling process produces CEUS rock ground motions that have significantly higher spectral content at high frequencies compared to WUS rock motions for comparable magnitudes and distances due to differences in shallow (1-2 km) crustal damping, which is much greater in the soft crustal rock of the WUS (Silva and Costantino, 2002). However, the dynamic properties of the deep soils located in CEUS are considered similar to the deep soils located in the WUS, and therefore the filtering properties of the soil profile should significantly reduce the differences observed between the CEUS and WUS rock motions (McGuire et al., 2001). This set of time histories is intended to use in scaling or spectral matching applications in the CEUS to obtain a desired hazard level.

None of the previous studies have developed UHS-compatible time histories for engineering design applications in the Upper Mississippi Embayment region that specifically account for the combined effects of the deep sediment profile found in the Embayment and non-linear soil behavior. Thus, the soil UHS calculated in this study were used to generate suites of spectrum-compatible time histories for each city listed in Table 4.5 for three hazard levels corresponding to return periods of 2475, 975, and 475 years. The database of scaled motions for CEUS conditions developed by McGuire et al.

(2001) was used in this process because they are based on real earthquake motions rather than artificial or simulated time histories.

The UHS is usually a smooth curve that results from the combination of many magnitudes and distances, and lacks the period-to-period variability observed in the response spectrum of real earthquakes recordings. A smooth response spectrum and a real earthquake spectrum will yield different results when used as inputs in non-linear structural analyses (Carballo and Cornell, 2000; Somerville and Collins, 2003; Watson-Lamprey and Abrahamson, 2006b). In order to provide time histories with similar characteristics of observed records, the smooth UHS was modified by adding spectral ordinates variations in such a way that the general spectral shape was preserved but it more closely resembled a real earthquake response spectrum.

Spectral variations were introduced by adding the frequency-to-frequency variability observed in real earthquakes to the mean UHS. This variability was taken from the correlation function developed by Baker and Cornell (2006a). Baker and Cornell (2006a) defined the standard normal variable  $\varepsilon$  that accounts for the aleatory variability of the observations and given by:

$$\varepsilon = \frac{\ln Sa_{\text{data}} - \ln \bar{Sa}}{\sigma_{\ln \bar{Sa}}} \quad 4.15$$

where  $Sa_{\text{data}}$  is the spectral acceleration of the observation, and  $\bar{Sa}$  and  $\sigma_{\ln \bar{Sa}}$  are the mean and standard deviation of the spectral acceleration predicted by a ground motion attenuation model. The correlation between  $\varepsilon$  values of a single horizontal ground motion component at two different periods is given by (Baker and Cornell, 2006a):

$$\rho = 1 - \cos \left[ \frac{\pi}{2} - \left( 0.359 + 0.163 \cdot I_{T_{\min} < 0.189} \cdot \ln \frac{T_{\min}}{0.189} \right) \cdot \ln \frac{T_{\max}}{T_{\min}} \right] \quad 4.16$$

where

$$I_{T_{\min} < 0.189} = \begin{cases} 1 & \text{if } T_{\min} < 0.189 \\ 0 & \text{otherwise} \end{cases} \quad 4.17$$

and  $T_{\min}$  and  $T_{\max}$  are the smaller and larger of the two periods in consideration, respectively.

The UHS simulations were performed using the unconditional LU method (Davis, 1987). The simulation method is based on the Cholesky LU triangular decomposition of the covariance matrix  $K$  associated with data locations:

$$K = L \cdot U \quad 4.18$$

where  $L$  and  $U$  are lower and upper triangular matrices. An important condition of the method is that the  $L$  matrix should be the transpose of the  $U$  matrix:

$$L = U^T \quad 4.19$$

The Cholesky decomposition can be used to factorize the matrix  $K$  to satisfy this condition. If a vector  $w$  of uncorrelated standard normal random numbers is multiplied by the  $L$  matrix, such that:

$$y = L \cdot w \quad 4.20$$

then the resulting vector  $y$  is a non-conditional, autocorrelated simulation of the random function at data locations with covariance matrix  $K$  (Davis, 1987). The correlation matrix  $K$  is calculated by:

$$K_{ij} = \sigma_i \cdot \sigma_j \cdot \rho_{ij} \quad 4.21$$

where  $\sigma$  is the standard deviation of the spectral acceleration,  $\rho$  is the correlation coefficient computed by Equation 4.16, and subindexes  $i$  and  $j$  refer to the two periods in consideration. The correlated errors  $y$  computed by Equation 4.20 were added to the mean UHS using the following expression:

$$\ln Sa_i = \ln \overline{Sa_i} + y_i \cdot \sigma_{\ln Sa_i} \quad 4.22$$

where  $S_a$  is the simulated spectral acceleration,  $\overline{S_a}$  is the mean spectral acceleration,  $\sigma_{\ln \overline{S_a}}$  is the standard deviation of the logarithm of the spectral acceleration, and subindex  $i$  refers to the period in consideration.

The methodology described above was used to simulate 1000 response spectra for each hazard level. Figure 4.75 shows the 1000 simulations along with the mean response spectrum for Memphis, TN for a return period of 2475 years. The UHS was simulated for 49 periods uniformly distributed (in logarithmic units) between 0.05 and 5 seconds. The mean of the simulations matches the target UHS. The simulations were truncated at two standard deviations to be compatible with the seismic hazard deaggregation by epsilon. The truncation also avoids unrealistic realizations of the response spectrum. The correlation function (Equation 4.16) is valid for periods between 0.05 and 5 seconds. To obtain the PGA value of the simulations, the PGA of the target UHS was modified by adding or subtracting the difference between spectral accelerations of the simulations and the target UHS at 0.05 seconds. Ten simulations (Cornell, 2005) were selected at random to use for spectral matching to obtain time histories compatible with the UHS. Figure 4.76 shows the ten selected response spectra from the 1000 simulations shown in Figure 4.75. The PGA of the selected response spectra was calculated as described above.

The spectral matching process involves the modification of an initial response spectrum to match a target spectrum preserving the non-stationary characteristics of the initial time history. The spectral matching procedure can be performed using frequency or time domain approaches. The frequency domain approach (Silva and Lee, 1987) iteratively adjusts the Fourier amplitudes of the initial spectrum until it matches the Fourier amplitude spectrum of the target ground motion while keeping the phase spectrum unchanged. The time domain approach (Abrahamson, 1992; Mukherjee and Gupta, 2002) adds or subtracts finite-duration wavelets to or from the initial time history with the assumption that the time of the peak response will not be modified by

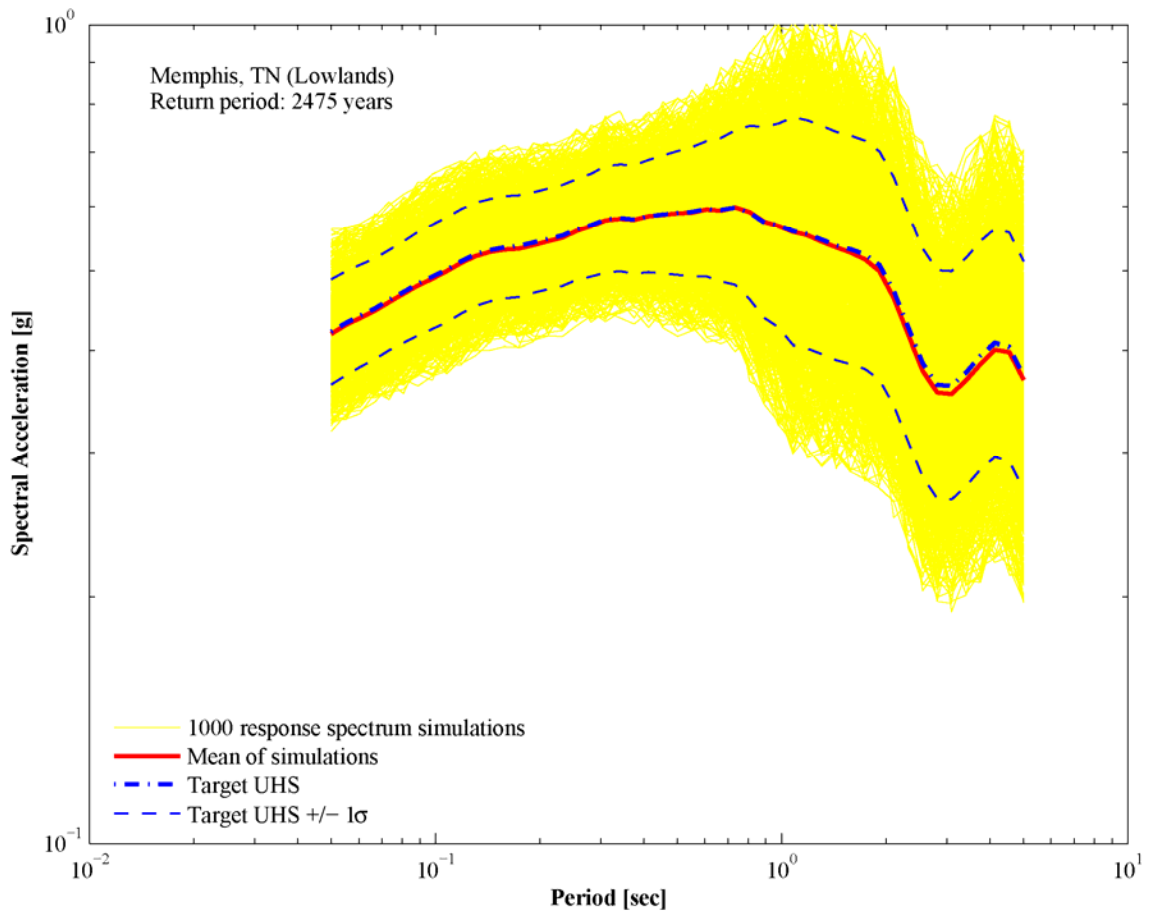


**Figure 4.75.** Uniform hazard spectrum simulations for return period of 2475 years along with the mean (target) uniform hazard spectrum in Memphis, TN

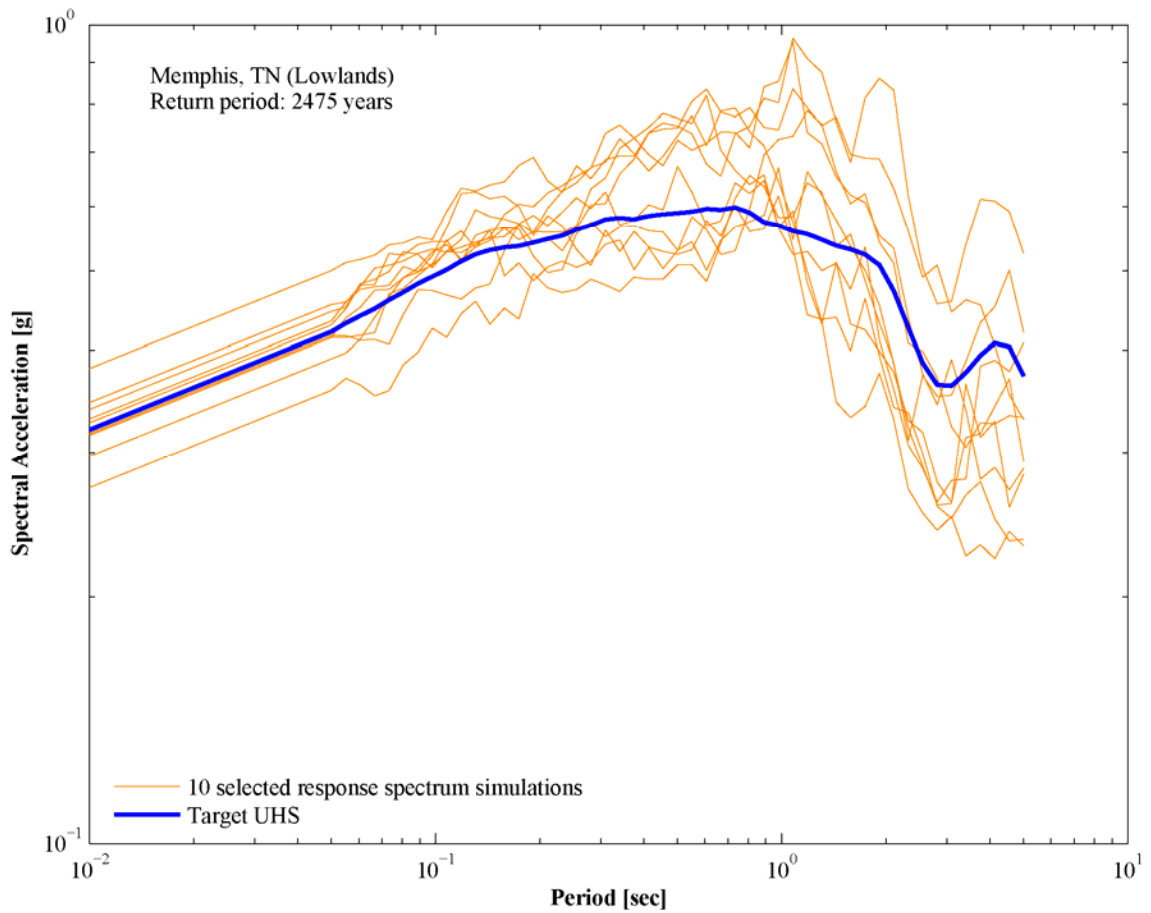


**Figure 4.76.** Selected uniform hazard spectrum simulations for return period of 2475 years along with the mean (target) uniform hazard spectrum in Memphis, TN

adding small adjustments to the initial time history. Each wavelet is intended to match the response spectrum at one period. Usually the time domain approach provides a better match, and the frequency domain approach generates greater visual differences between the initial and final time histories (Acevedo, 2003; Walsh, 2003).

The spectral matching process in this study was performed in EZFRISK<sup>TM</sup> using a time domain approach based on the RSMP99 code of the computer program SpectralMatch developed by Norman Abrahamson (Risk Engineering, 2005). The initial ground motions were selected from the time history database developed by McGuire et al. (2001) as described previously. The selection of the initial time histories was performed from records having similar magnitudes, epicentral distances, and site conditions to the earthquakes that dominate the hazard in each city as given by the hazard deaggregation (Cornell, 2005; Somerville and Collins, 2003; Stewart et al., 2002). This practice is supported by the effect that magnitude has on the spectral shape, which is an important factor to consider when selecting time histories to match a target spectrum. Among the time histories that met the magnitude, distance, and site conditions criteria, the records with the longest duration were selected to perform the spectral matching process as recommended by McGuire et al. (2001) when using the ground motions library in CEUS applications. Few observed earthquakes of magnitudes and distances of engineering significance exist in the CEUS, particularly for the soil conditions of the Upper Mississippi Embayment, and an assessment of observed ground motion durations cannot be performed in the region at this moment.

Figure 4.77 illustrates one example of the spectral matching process. The original response spectrum corresponds to the initial time history selected from the ground motion database. The PGA of the original spectrum is scaled to match the PGA of the target response spectrum, and this scaled response spectrum is used as input for the spectral matching process. The final spectrum was calculated after ten iterations of the matching process. A perfect match between the target and final spectra can be obtained by using

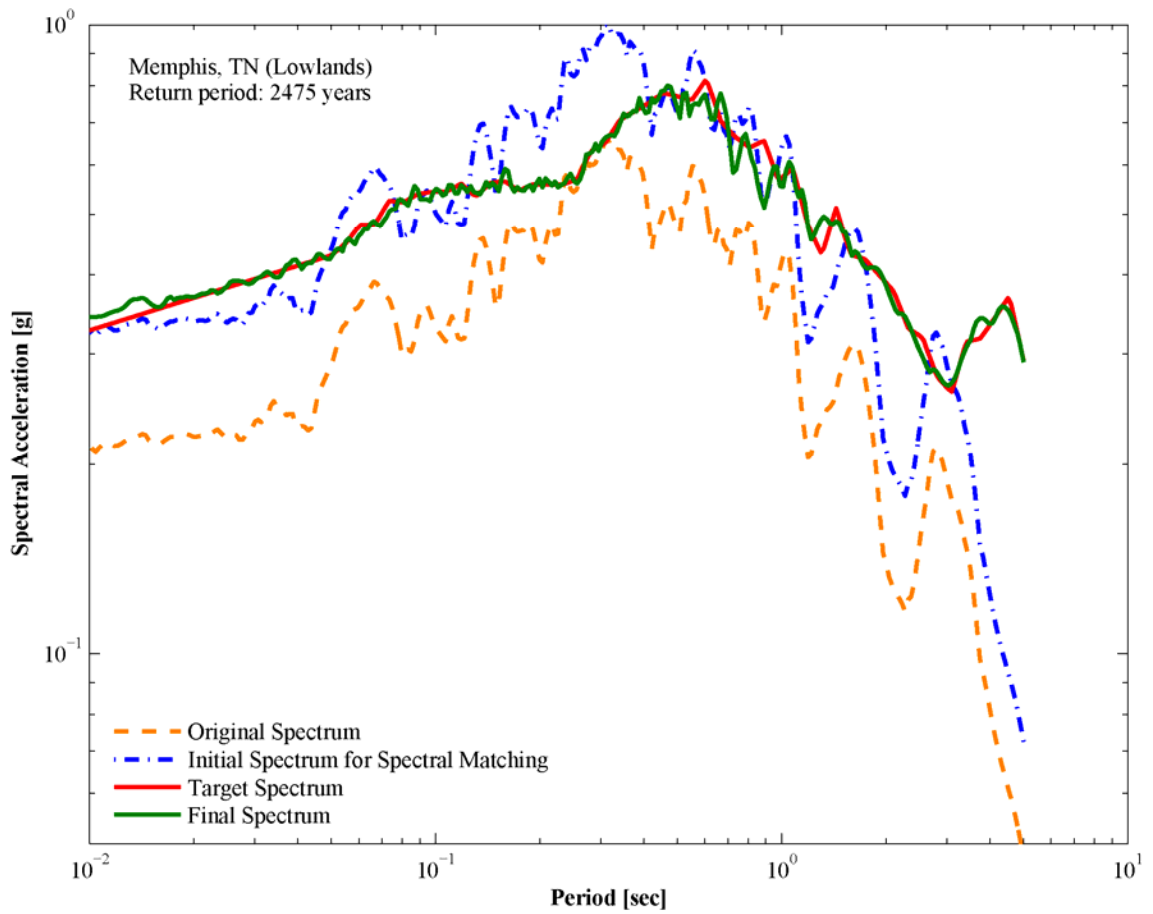


**Figure 4.77.** Example of the spectral matching process

several iterations, however the match shown in Figure 4.77 was considered acceptable. Figure 4.78 shows the acceleration, velocity, and displacement time histories of the initial and final response spectra shown in Figure 4.77. Small drifts are observed in the final ground motion, particularly in the displacement time history; however the drifts are removed later in the process as discussed subsequently. In general, the time domain characteristics of the initial time history are preserved such as the duration and the time of occurrence of the peaks. Thus, the duration of the time histories generated herein represents the duration of observed earthquakes in the ground motion database provided by McGuire et al. (2001).

Another approach to obtain ground motions compatible with a desired hazard level is the multiplication of ground motions by a scale factor in order to match a target ground motion parameter. There are several scaling ground motion measures including peak ground acceleration, peak ground velocity, Arias intensity, root-mean-square acceleration, spectral acceleration level averaged over a frequency band, spectral acceleration at a particular spectral period, among others (Acevedo, 2003). Typical scaling factors range from 0.5 to 4 (Vanmarcke, 1979), however these limits are based on the comfort level of the engineer and not on quantitative evaluations of the scaling process (Watson-Lamprey and Abrahamson, 2006a). Previous studies (Acevedo, 2003; Baker and Cornell, 2006b; Cornell, 2005; Iervolino and Cornell, 2005; Somerville et al., 1997; Watson-Lamprey and Abrahamson, 2006a) have demonstrated that as long as the target and initial ground motions have similar spectral shape, the scaling factor may be larger than these limits without introducing bias in the structural response estimation.

Some researchers (Cornell, 2005; Shome et al., 1998) have suggested that the most efficient scaling approach to estimate the median non-linear response of a structure is the scaling of ground motions to the target spectral acceleration corresponding to the fundamental period of the structure. An advantage of the scaling approach over the spectral matching method is that the original spectral shape is not modified. However the

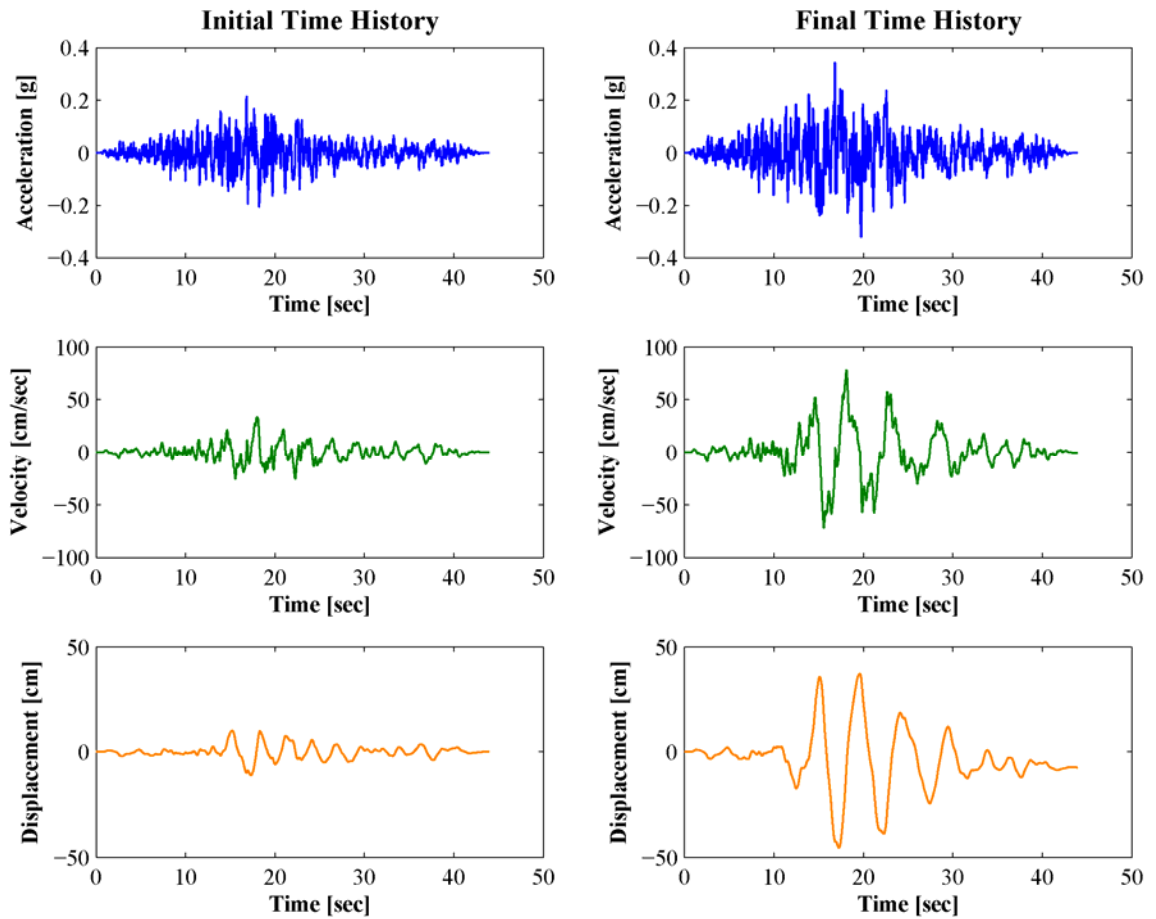


**Figure 4.78.** Example of the initial and final time histories corresponding to the spectral matching process shown in Figure 4.77

fundamental period of the structure involved in the analysis must be known in advance. In this study the ground motions are developed for structural analysis in general and not for the analysis of a particular structure. Thus, the ground motions were matched to the target spectrum in the entire frequency range. However the analyst or user can perform an additional scaling of the time histories according to the needs of their particular application.

Baseline correction was applied to the acceleration time histories resulting from the spectral matching process. This correction was performed using the computer program BLPadFlt.for written by Dr. David Boore. The baseline correction process adds zeros before and after the time history to assure an appropriate filtering. To avoid incompatibility between the acceleration, velocity, and displacement time histories, Boore (2005) recommends not to remove the padded portions of the record. This process may also cause low-frequency drifts in the velocity and displacement time histories (Boore, 2005). However to reduce the computational effort in further analysis involving the ground motions generated, the acceleration time histories were windowed using a cosine taper function of the form (Keaton et al., 2000):

$$f(t) = \begin{cases} \frac{1 - \cos\left(\frac{\pi \cdot (t - t_0)}{t_b}\right)}{2} & \text{if } t_0 < t < t_0 + t_b \\ 1 & \text{if } t_0 + t_b < t < t_0 + t_b + t_d \\ \frac{1 + \cos\left(\frac{\pi \cdot (t - t_0 - t_b - t_d)}{t_e}\right)}{2} & \text{if } t_0 + t_b + t_d < t < t_0 + t_b + t_d + t_e \\ 0 & \text{otherwise} \end{cases} \quad 4.23$$

where  $t_0$  is the time corresponding to the beginning of the window,  $t_b$  is the duration of the beginning taper,  $t_d$  is the duration of the ground motion after the beginning taper, and  $t_e$  is the duration of the ending taper. The durations  $t_b$  and  $t_e$  were set to two seconds, and the duration  $t_d$  was calculated as the time between the 0.5% and 99.5% of the total Arias intensity (Arias, 1970), which is related to the damage potential and calculated by:

$$AI = \frac{\pi}{2g} \cdot \int_0^{\infty} [a(t)]^2 \cdot dt \quad 4.24$$

where  $a(t)$  is the acceleration time history. Figure 4.79 illustrates the window function defined by Equation 4.23.

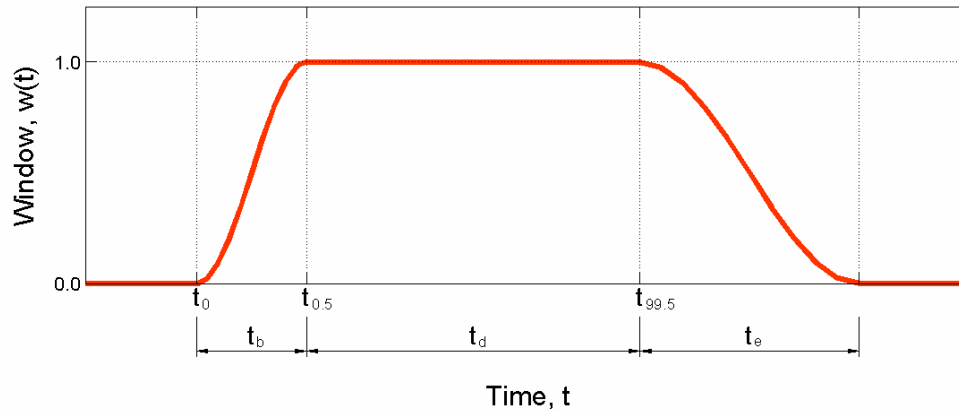


**Figure 4.79.** Cosine taper function applied to acceleration time histories

Velocity and displacement time histories were computed by numerical integration using the trapezoidal rule of the corrected and windowed acceleration time history. The small drifts observed in the resulting velocity and displacement records were corrected by fitting a straight line to the data and then subtracting this line from the records (Boore and Bommer, 2005). Figure 4.80 shows an example of velocity and displacement time histories before and after the drift correction. The acceleration time history shown in Figure 4.80 is not drift corrected and is the direct result of the application of the cosine taper function of Equation 4.23 to the padded time history calculated by the program BLPadFlt.for. The correction to the velocity time history is minimal for most of the time histories in this study.

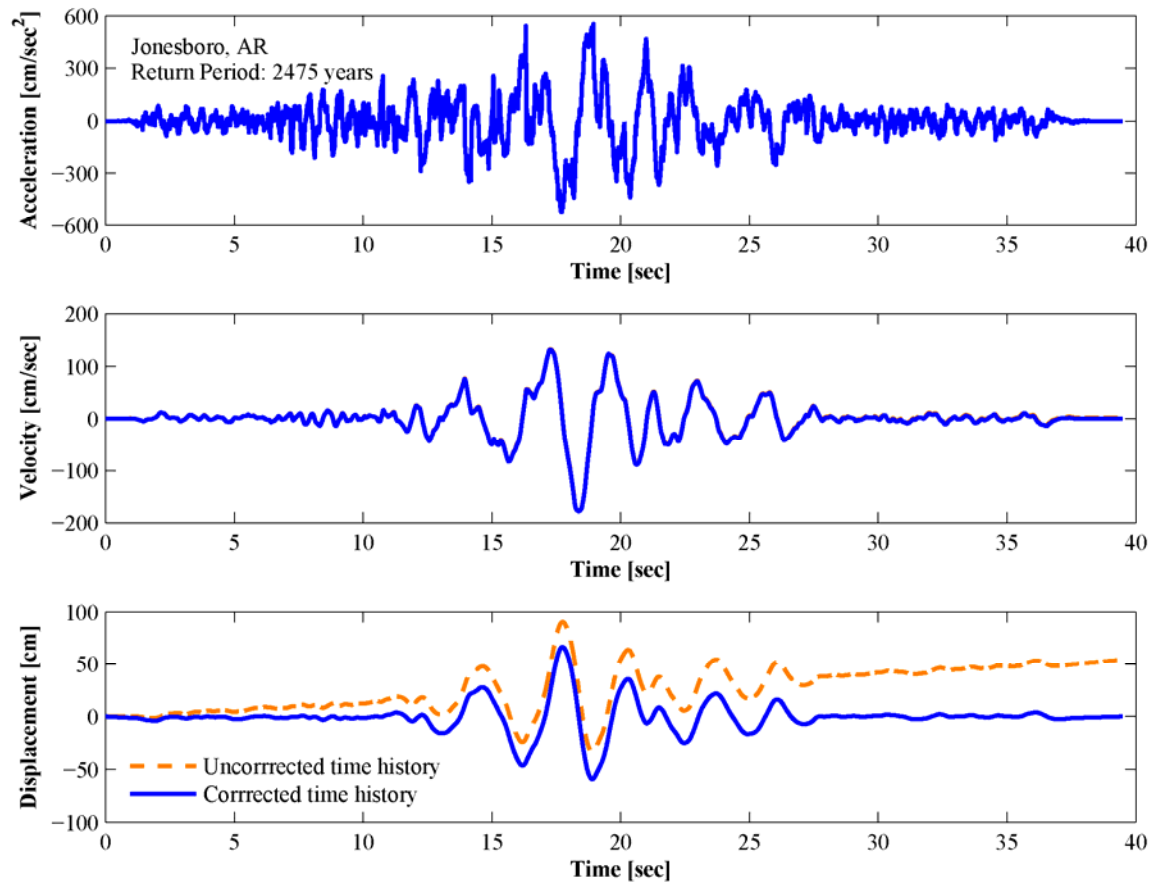


**Figure 4.80.** Acceleration, velocity, and displacement time histories before and after the drift correction.

The resulting time histories are consistent with hazard levels of 10%, 5%, and 2% of probability of exceedence in 50 years. Ten acceleration, velocity, and displacement time histories were generated for each hazard level, for a total of 30 ground motions for each city. The suites of ground motions are intended to represent the epistemic and aleatory variability characterized in the soil attenuation relationships developed for the region. The ground motions are available at [http://geosystems.ce.gatech.edu/soil\\_dynamics](http://geosystems.ce.gatech.edu/soil_dynamics). Figure 4.81 through Figure 4.83 show an example of the acceleration, velocity, and displacement time histories generated for Memphis, TN, for 2% of probability of exceedence in 50 years.

#### **4.4. Conclusions**

Seismic hazard analyses have been performed in the Upper Mississippi Embayment using the soil attenuation relationships developed in this study. A major advantage of using soil attenuation equations in the analyses is that no coupling between probabilistic hazard analyses for rock conditions and site response is necessary. These soil attenuation relationships already account for correlation among the processes of the earthquake generation and seismic wave propagation and therefore provide a direct approach for developing hazard-consistent soil motions.

Seismic hazard analyses were performed for seven selected cities in the Upper Mississippi Embayment. Regional analyses were also performed to develop probabilistic seismic hazard maps for the entire region. The hazard curves and uniform hazard spectra generated herein incorporate the epistemic variability represented in the attenuation relationships by the use of three source models and three stress drop values. Typical geological units of the region, Embayment depth, and non-linear soil behavior have been considered by the use of site-specific soil attenuation relationships.

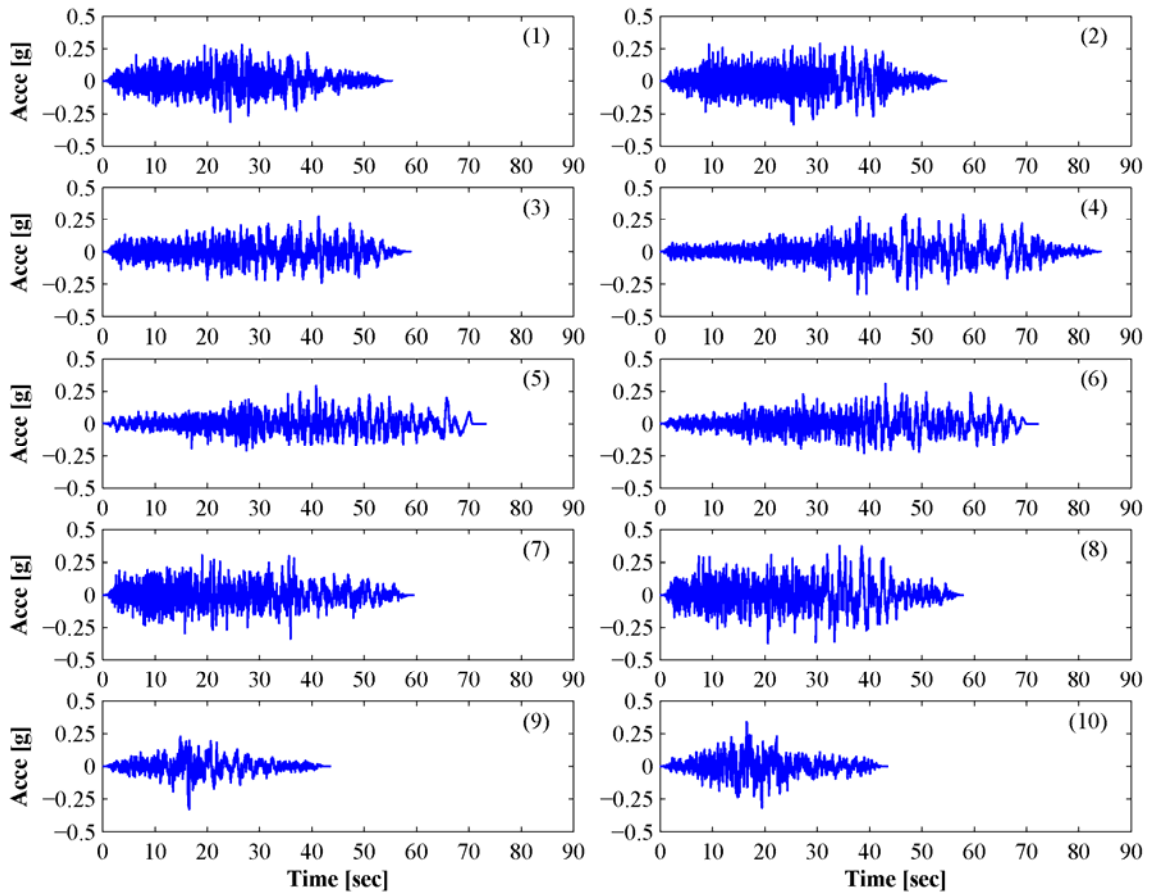


**Figure 4.81.** Acceleration time histories consistent with hazard levels of 2% PE in 50 years for Memphis, TN

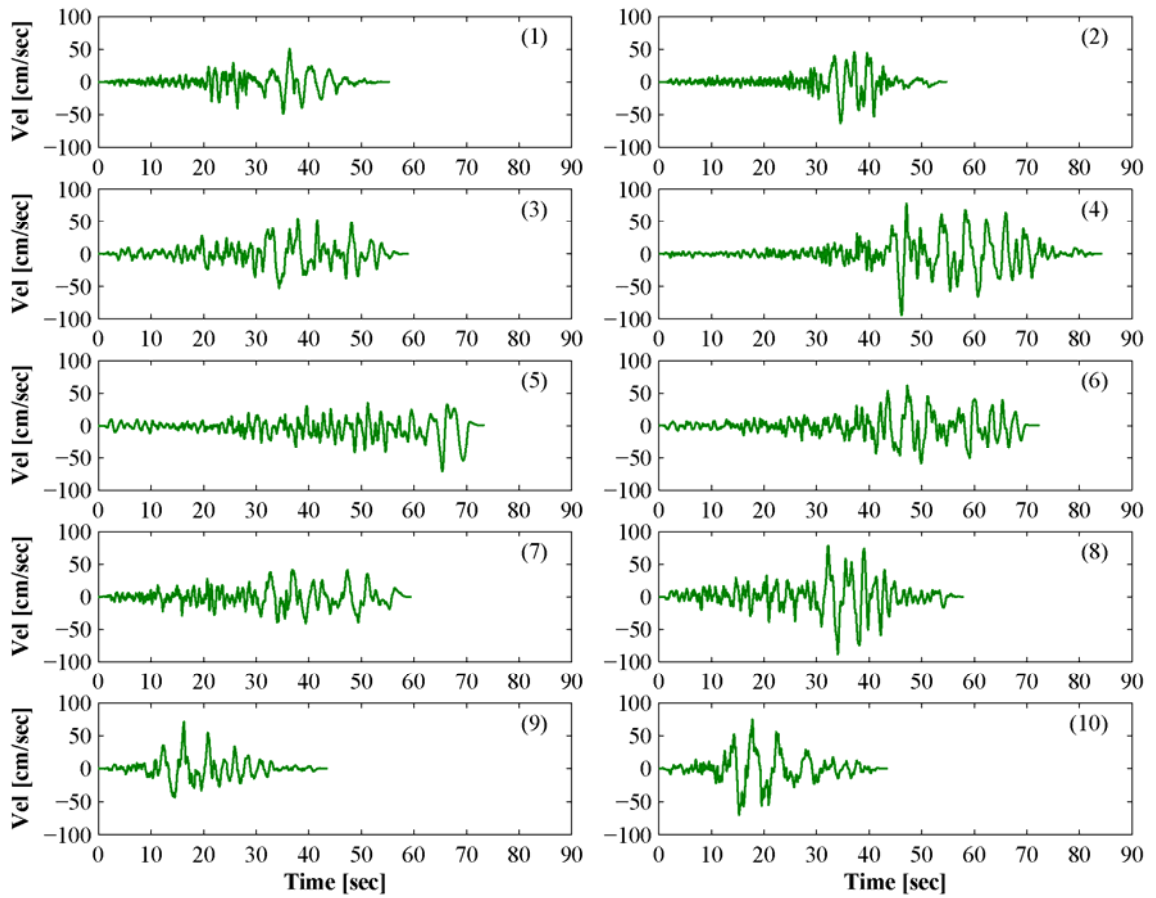


**Figure 4.82.** Velocity time histories consistent with hazard levels of 2% PE in 50 years for Memphis, TN

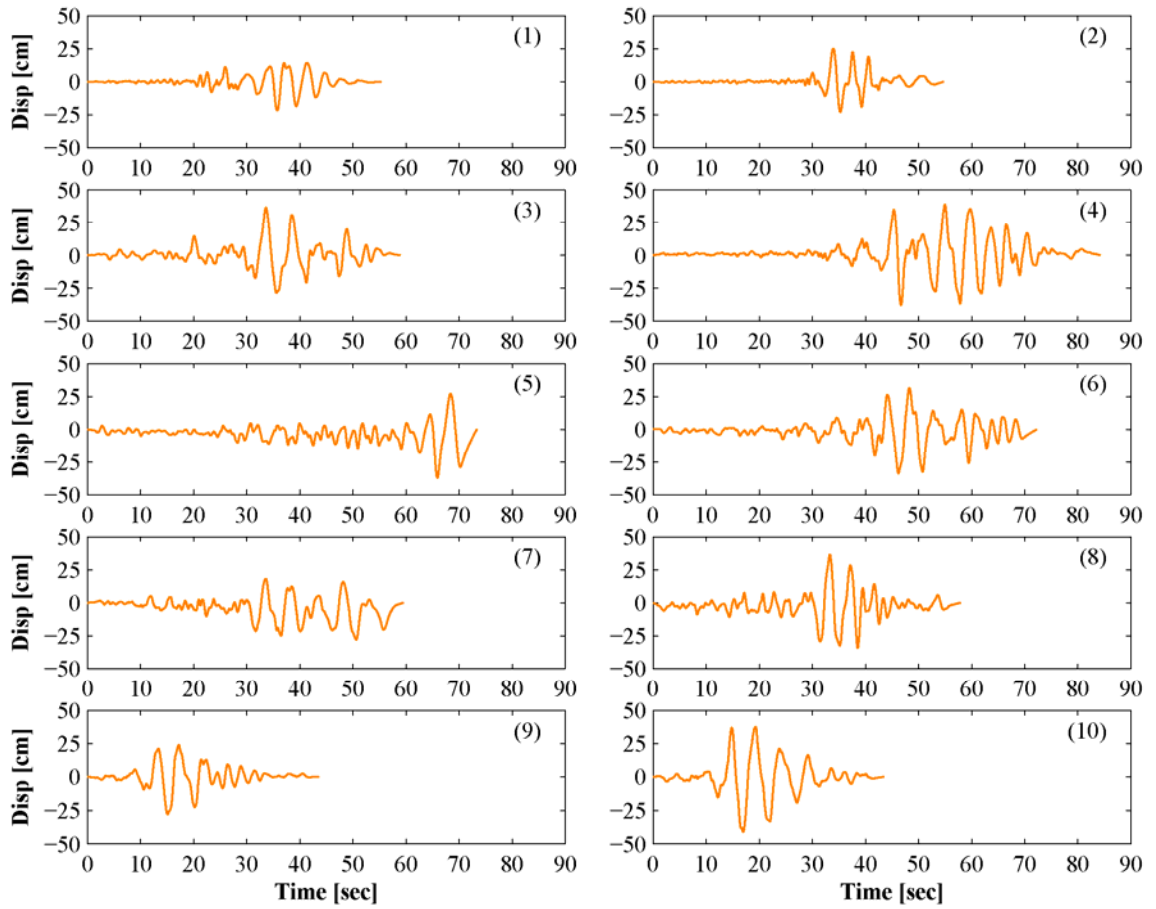


**Figure 4.83.** Displacement time histories consistent with hazard levels of 2% PE in 50 years for Memphis, TN

The seismic hazard deaggregation indicates that small magnitudes and short distances (i.e. background sources) contribute to the hazard at short periods and low hazard levels. However, the New Madrid seismic zone is the dominant contributor to hazard in the Upper Mississippi Embayment. The Charleston, SC seismic sources do not contribute to the seismic hazard in the region. In general, the seismic hazard corresponding to a return period of 2475 years is associated to the mean + 1 standard deviation ground motions.

The multiplication of the probabilistic seismic hazard at the bedrock level by deterministic amplification factors to account for site effects, i.e. a probabilistic-deterministic approach, may bias the estimation of soil ground motions. It is recommended to include site effects in the probabilistic seismic hazard calculations by using soil attenuation relationships.

The probabilistic seismic hazard maps show that for short spectral periods the seismic hazard in the Embayment is controlled by the depth to the bedrock, whereas the New Madrid seismic zone controls the seismic hazard at long spectral periods independent of the hazard level.

Acceleration, velocity, and displacement time histories consistent with three hazard levels corresponding to return periods of 475, 975, and 2475 years have been developed for seven selected cities in the Upper Mississippi Embayment. The suites of ground motions are intended to represent the epistemic and aleatory variability characterized in the soil attenuation relationships developed for the region. The ground motion time histories were developed for structural analysis in general and not for the analysis of a particular structure. Thus, the time histories were matched to the target spectrum in the entire frequency range. However the analyst or user can perform an additional scaling of the time histories according to the needs of their particular application. Few observed earthquakes of magnitudes and distances of engineering significance exist in the CEUS, particularly for the soil conditions of the Upper

Mississippi Embayment, and an assessment of observed ground motion durations cannot be performed in the region at this moment. Therefore, the duration of the time histories might not represent the actual duration of large earthquakes observed in the Embayment. However, time domain scaling of ground motions is not recommended because the frequency content is modified and the process may generate unrealistic motions (Acevedo, 2003). Additional research is needed to evaluate the duration of ground motions in the Embayment and determine a methodology to incorporate it in the numerical simulations.

In general the results of this study are broadly comparable with probabilistic ground motions calculated in previous studies. However the UHS computed herein are believed to be more accurate since the variability in the entire earthquake process and site-specific conditions are included directly in the PSHA calculations by using soil attenuation relationships in the hazard integral.

The probabilistic seismic hazard analyses performed in this study have been incorporated into MAEviz ([http://mae.ce.uiuc.edu/software\\_and\\_tools/maeviz.html](http://mae.ce.uiuc.edu/software_and_tools/maeviz.html)) to estimate probabilistic ground motions in the Upper Mississippi Embayment. MAEviz is a seismic risk assessment software developed by the Mid-America Earthquake (MAE) Center and the National Center for Supercomputing Applications (NCSA).

## CHAPTER 5

### BASIN EFFECTS IN THE UPPER MISSISSIPPI EMBAYMENT

Many earthquakes have provided evidence of the important influence of local site conditions on earthquake ground motions. During the 1985 Michoacán, Mexico earthquakes ( $M = 8.1$  and  $M = 7.5$ ) peak ground accelerations (PGA) of the order of 0.10 g to 0.17 g were observed at stations located on thick saturated soft soil deposits (i.e. the “lake-bed” zone) in the Mexico valley, almost 350 km from the epicenter. At this epicentral distance, small PGA values were expected as confirmed by earthquake records at rock sites (i.e. the “hill” zone) located on the west side of the Mexico valley, where PGA’s of 0.03 g and 0.04 g were recorded. Furthermore the duration of ground motions in the “lake bed” zone were significantly longer compared to the “hill” zone. Considering the epicentral distance and the large difference in ground motion amplitude and duration between soil and rock sites, local site conditions played an important role in the ground motion amplification of this earthquake (Bard et al., 1988; Chavez-Garcia and Bard, 1994; Sanchez-Sesma et al., 1988). A similar strong influence of local site conditions was observed during the 1989 Loma Prieta earthquake ( $M = 6.9$ ). The ground motions recorded on Yerba Buena Island and on Treasure Island provide a good example. Both islands are located in San Francisco Bay and approximately at the same distance from the epicenter. Yerba Buena Island is a rock outcrop and Treasure Island is a man-made island underlain by the natural bay sediments, called Bay Mud. The PGA’s recorded for the N-S and E-W components of motion were 0.03 g and 0.07 g on the Yerba Buena Island, and 0.10 g and 0.16 g on Treasure Island. Moreover the ground motions recorded on Treasure Island showed higher amplitudes in the long-period range (Seed et al., 1990).

The characterization of site effects in the estimation of earthquake ground motions is one of the main goals of earthquake hazard reduction programs. Several methods have been developed to quantify site effects and determine the characteristics of earthquake ground surface motions including site amplification factors based on soil type, ratio of horizontal-to-vertical components of surface ground motions, and physical modeling of seismic wave propagation through local site conditions. The last approach is the most rigorous method to characterize site effects (Kawase, 2003), particularly for low-seismicity regions where the lack of real earthquakes recordings prevents the use of empirical approaches. Usually the influence of soil conditions on strong ground motions is evaluated using a 1-D wave propagation formulation where the soil profile is modeled by horizontal layers over a half-space (Ching and Glaser, 2001; Haskell, 1953; Idriss and Seed, 1968; Kausel and Roesset, 1984; Schnabel et al., 1972; Thomson, 1950). In general this simple model is capable of representing the basic characteristics of the site amplification provided that the dynamic soil properties are assigned properly (Darragh et al., 2006; EPRI, 1993; Satoh et al., 1995).

However, there are ground response problems where more complex analyses are required. Examples of these cases are locations where the soil layers are confined by the surrounding rock to form a sedimentary basin. The assumptions of the 1-D model are not valid for this type of geometry, and a 2-D or 3-D model is needed to evaluate the seismic response of these structures. At the edges of the basin, strong diffraction takes place due to the large velocity contrast between soil and rock. Such diffraction creates basin-induced surface waves that propagate in the horizontal direction inside the basin, and depending on the geometry of the structure and properties of the sediments, the surface waves may become trapped inside the basin. Thus basin edges can be considered as secondary seismic sources. Basin effects result in longer ground motions with an increase in low-frequency energy compared to those predicted by 1-D models (Kawase, 2003).

Extensive evidence of these long-period waves in real earthquakes can be found in the literature. Hanks (1975) found that surface waves contributed significantly to the long-period motions in the 1971 San Fernando, California, earthquake ( $M = 6.6$ ). Kawase (1996; 2003) showed that the damage that occurred in the city of Kobe after the 1995 Hyogo-ken Nambu earthquake ( $M = 6.9$ ) was caused by the constructive interference of direct body waves and basin-induced surface waves generated at the northwestern edge of the Osaka basin. The large ground motion amplification observed during the 1994 Northridge earthquake ( $M = 6.8$ ) in the Santa Monica area was attributed to surface waves generated at the northwest part of the Los Angeles basin (Graves et al., 1998). Pei and Papageorgiou (1996) provided evidence of basin-induced surface waves on ground motion recorded by the Gilroy array on the Santa Clara valley during the 1989 Loma Prieta ( $M = 7.1$ ) and 1984 Morgan Hill ( $M = 6.2$ ) earthquakes. Boore (1999) showed that a sea-floor recording of the 1990 Upland, California earthquake ( $M = 5.6$ ) was dominated by long-period, late-arriving surface waves generated at the edge of the Los Angeles basin. Graves and Wald (2004) demonstrated that the longer duration and amplification of motion observed during the 1999 Hector Mine earthquake ( $M = 7.0$ ) were caused by the generation of surface waves in the San Bernardino basin. Earthquake observations at Euroseistest located in the Mygdonian basin in northern Greece have shown large amplification levels and ground motion durations that cannot be predicted by a 1-D site response model and have been attributed to the contribution of locally generated surface waves (Makra et al., 2002; Raptakis et al., 2000). Comparison of theoretical 1-D transfer functions and earthquake observations at Euroseistest have shown large differences in amplification levels due to the contribution of locally generated surface waves.

There are also sedimentary basins where 1-D and 2-D/3-D site response models predicted similar results as in the case of the Taipei basin (Sokolov et al., 2000), Turkey Flat test area near Parkfield, California (Real et al., 2006; Stepp and Cramer, 1992), and

Ashigara Valley test site in Japan (Kudo and Sawada, 1992; Shinozaki and Irikura, 1992). Basin effects must be evaluated on a case-by-case basis and cannot be extrapolated from site to site because the basin geometry and physical properties of the sediments play an important role.

The geometry of the Upper Mississippi Embayment described in Chapter 2 may potentially generate basin surface waves that affect the earthquake ground motions in the region. Previous studies have investigated basin effects and resonances in the Embayment (Atkinson and Beresnev, 2002; Bodin and Horton, 1999; Bodin et al., 2001; Saikia et al., 2006). In general, they have concluded that a 1-D wave propagation model is adequate to estimate earthquake ground motions in the region. However, a detailed characterization of the sediments and the non-linear soil behavior were not incorporated in the studies.

Numerical analyses using a 3-D model of the entire Upper Mississippi Embayment and a detailed profile of the sediments incorporating non-linear soil behavior are needed to evaluate basin effects in the region and thus confirm the conclusions of previous studies. However, this would require significant computational resources due to the vast size of the Embayment. Due to this limitation, a 2-D model has been selected to evaluate the non-linear seismic response of the Upper Mississippi Embayment. In this study a combination of the methods proposed by Bravo et al. (1988) and Zheng and Dravinski (1998) to evaluate the linear response of sedimentary basins under incident SH waves is implemented to evaluate the 2-D seismic response of the Embayment, and the non-linear soil behavior is incorporated by using an equivalent linear approach.

### **5.1. Site Effects**

The earthquake generation and wave propagation process can be divided into source, path, and site effects. Despite the variability of the earthquake source characteristics and the several kilometers that seismic waves might travel from the source

to the bedrock underneath the site, the last tens or hundreds of meters before the seismic waves reach the earth surface play the most important role in defining the characteristics of surface earthquake ground motions. Surface and subsurface topography, lateral discontinuities, and soil layering are local site conditions that greatly affect the amplitude, frequency content, and time-domain characteristics of ground motions. The degree of the influence of local site conditions depends on many factors including the amplitude of the incident motion, incidence angle of the seismic waves, site geometry (i.e. length, width, and thickness of the site structure), and irregularity of the interface between the site and the underlying bedrock. Comprehensive reviews of site effects on earthquake ground motions can be found in the literature (Aki, 1988; Bard and Riepl-Thomas, 2000; Kawase, 2003; Pitilakis, 2004; Rathje et al., 2000; Seed and Idriss, 1969), and only a brief description is given herein.

#### **5.1.1. Surface Topography**

Earthquake observations (Celebi, 1987, 1991; Kawase and Aki, 1990; Restrepo and Cowan, 2000) and instrumental evidence and numerical models (Bard, 1982; Bard and Tucker, 1985; Boore et al., 1981; Geli et al., 1988; Pedersen et al., 1994) have shown that convex topographic structures like ridge crests and cliffs cause ground motion amplification which increases with the topographic slope, whereas deamplification occurs in concave structures such as valleys, canyons, and the base of hills. These effects are related to three physical phenomena: the sensitivity of surface motions to the incidence angle, focusing and defocusing of seismic waves along the topographic feature, and interference between the direct and diffracted waves (Bard and Riepl-Thomas, 2000).

#### **5.1.2. Soil Layers**

Extensive evidence has shown that soil sites experience larger earthquake ground motion amplitudes than rock sites (Bard et al., 1988; Chavez-Garcia and Bard, 1994;

Seed et al., 1991; Su et al., 1998). The soil amplification is mainly caused by the trapping of seismic waves within the soil layers. For 1-D structures where the soil layers extend horizontally, the trapping affects body waves only. For 2-D and 3-D structures with lateral discontinuities the trapping also affects surface waves. The constructive interference of the trapped waves causes resonance effects that depend on the geometrical and mechanical characteristics of the site. The thickness and shear-wave velocity of the soil layers will determine the dominant frequencies of the ground motion, and the spectral amplitude of the resonant peaks will depend on the material contrast between the soil layers and the underlying bedrock (Kramer, 1996).

Large earthquakes may induce large shear strains in the soil. If the shear strains reach a certain threshold, the soil will behave non-linearly (Kramer, 1996). The non-linear behavior of the soil is characterized by a decrease in shear modulus (i.e. a reduction in the shear-wave velocity) and an increase in damping. The non-linear soil behavior induces a decrease in the fundamental frequency of the soil column due to the softening of the material, and causes a deamplification or reduces the amplification of the incident ground motion due to the increase in damping (Kramer, 1996).

Previous studies have also shown that surface ground motions on soil sites exhibit longer duration relative to rock sites (Dobry et al., 1978; Kempton and Stewart, 2006; Shoji et al., 2005). This phenomenon is closely related to the effect of trapping seismic waves by the sediments.

### **5.1.3. Subsurface Topography and Lateral Discontinuities**

Subsurface topography, as in the case of sedimentary basins where the soil layers are confined by the surrounding rock, may generate surface waves due to the conversion of body waves at the edges of the structure. These basin-induced surface waves become trapped inside the basin, increasing the amplitude and duration of ground motions compared to the case of 1-D structures (Aki, 1988; Bard and Riepl-Thomas, 2000;

Kawase, 2003). This phenomenon also causes a very complex spatial distribution of the ground motion amplitudes. Several earthquake observations have provided evidence of existence of such surface waves as described in the introduction of this chapter.

For basins with a large width-to-depth ratio, the basin-induced surface waves will arrive later than the direct body waves at a given surface point located in the central part of the basin because the surface waves must travel a longer distance (Kawase, 2003). However, for sites located near the edges of the basin, large ground motion amplification has been observed due to the constructive interference between basin-induced surface waves and direct body waves propagating vertically from the bottom of the basin (Bakir et al., 2002; Chavez-Garcia and Bard, 1994; Graves et al., 1998; Kawase, 1996, 2003). Kawase (1996) called this phenomenon “the basin edge effect” after the 1995 Hyogo-ken Nambu earthquake, where a damage area of ~20 km long and ~1 km wide occurred in the city of Kobe along the northwestern edge of the Osaka basin (Kawase, 2003).

## **5.2. Methods to Evaluate Site Effects**

Methods to estimate site effects can be classified in empirical, experimental, and theoretical approaches. The method selected for the analysis will depend on the availability of data and the importance of the project for which it is applied (Bard and Riepl-Thomas, 2000).

### **5.2.1. Empirical Methods**

Empirical methods are based on correlations derived from earthquake observations for given site conditions, which then are applied to other locations where only the site conditions are known. In this type of approach, the site conditions are usually characterized by the age of the sediments, soil type, or by geotechnical parameters such as the shear-wave velocity, standard penetration test resistance, or undrained shear strength. The ground motion parameters that have been used in the

correlations include earthquake intensity (Astroza and Monge, 1991; Giammarinaro et al., 2005), site amplification (Borcherdt et al., 1991; Lachet et al., 1996), and spectral accelerations (Abrahamson and Silva, 1997; Dobry et al., 2000). Usually these methods are incorporated in seismic code provisions (Pitilakis, 2004).

### **5.2.2. Experimental Methods**

Experimental approaches are based on observed data including microtremors, weak-motion, and strong-motion records.

Microtremors are related to small amplitude vibrations of the ground due to ambient disturbances like wind, sea waves, traffic, etc. Kanai et al. (1962; 1961; 1965) were the first to propose that microtremors exhibit some correlation with site conditions. The ratio between the Fourier spectra of the horizontal and vertical components of microtremors at the same station (i.e. the H/V ratio) has been used to identify the fundamental frequencies and amplification at the site (Nakamura, 1989). Several experimental studies (Field and Jacob, 1995; Lachet et al., 1996; Seekins et al., 1996; Wollery and Street, 2002) and theoretical analysis (Field and Jacob, 1993; Lachet and Bard, 1994; Lermo and Chavez-Garcia, 1994) have shown a good correlation between the peak frequency of the H/V ratio and the fundamental frequency of the site, particularly in the long-period range ( $T > 1$  sec.). However, some studies have reported that the peak amplitude of the H/V ratio does not correlate well with shear-wave amplification. According to these results, this method provides a simple and inexpensive approach to estimate the fundamental resonant frequency of the site, but it can not predict the absolute site amplification.

Weak ground motions refer to small-to-moderate seismic events such as small-magnitude earthquakes, aftershocks of large earthquakes, nuclear tests, etc. (Bard and Riepl-Thomas, 2000). The most common approach to estimate site effects is the Standard Spectral Ratio, SSR, which compares the spectral characteristics of a ground

motion recorded at a reference site and at the site of analysis (Borcherdt, 1970). In order to estimate the site response by this method, both site locations should share the same source and path effects, and the reference site should be free of any type of site effects (Bard and Riepl-Thomas, 2000; Pitilakis, 2004). This method has been extended to consider large data sets recorded on local or regional networks simultaneously and to estimate site effects by solving a large inversion problem (Andrews, 1986). In practice is difficult to find a reference site that satisfies these conditions. For this reason several methods have been developed that do not need a reference site to estimate the site effects (e.g., Boatwright et al., 1991). As in the case of microtremors, this method offers reliable estimates of the fundamental frequencies of the site (Bard and Riepl-Thomas, 2000; Pitilakis, 2004).

An important limitation of using microtremors and weak ground motion data to estimate site effects is that their low amplitude level is not capable of predicting how the soil profile will behave under strong earthquake ground motions (i.e. non-linear soil behavior). Methods developed for weak ground motions have been applied to strong ground motions with the advantage that non-linear effects are included in the analysis.

### **5.2.3. Theoretical Methods**

The physical modeling of the seismic wave propagation from the source or a reference position to the receiver is the most rigorous approach to evaluate site effects (Kawase, 2003). This approach requires information about the geotechnical parameters and geometrical characteristics of the site. The 1-D model is the most simple and widely used model to estimate site effects. It considers only a vertical variation of the soil parameters assuming that the soil deposit is comprised of horizontal layers of infinite horizontal extent (Ching and Glaser, 2001; Haskell, 1953; Idriss and Seed, 1968; Kausel and Roesset, 1984; Schnabel et al., 1972; Thomson, 1950).

In general, the 1-D wave propagation model is capable of representing the basic characteristics of the site amplification provided that the dynamic soil properties are assigned properly (Darragh et al., 2006; EPRI, 1993; Satoh et al., 1995). For complex surface or subsurface topographies the assumptions of the 1-D model are not valid, and a 2-D or 3-D model is required to evaluate the seismic response of these structures. These more complex analyses can be performed by analytical methods, ray methods, boundary element methods, and domain-based methods (i.e. finite-difference or finite-element methods) (Bard and Riepl-Thomas, 2000). Analytical methods can be used for very simple geometries (e.g. homogenous circular or elliptical basins (Trifunac, 1971; Wong and Trifunac, 1974)). Ray methods are applicable only to high-frequencies and difficult to use for wavelengths comparable to the size of the heterogeneities (Bard and Riepl-Thomas, 2000). Boundary element methods (Herrera, 1984; Manolis and Beskos, 1988) are efficient for large-size structures because only the discretization of the boundaries of the domains is needed and the radiation conditions are satisfied; however the resulting system is dense, and it is difficult to apply the method to highly heterogeneous media. Domain-based methods can consider very complex geometries, but require large computational resources and truncation of the semi-infinite medium by the introduction of an artificial boundary to avoid wave reflections (Bielak et al., 1999). In general numerical methods are very flexible and versatile, but require detailed geotechnical or geophysical investigations to determine the input parameters.

### **5.3. Seismic Response of Sedimentary Basins to SH Waves**

The evaluation of the seismic response of sedimentary basins has been performed by empirical, analytical, and numerical methods. The examples of analytical and numerical methods presented in this section refer to studies involving SH waves because this study focuses on the seismic response of the Upper Mississippi Embayment to this type of wave for reasons discussed later.

Empirical methods have been developed based on earthquake observations for locations with extensive data sets. Hruby and Beresnev (2003) and Joyner (2000) have provided amplification factors based on earthquakes recorded in the Los Angeles basin that account for basin effects to correct ground motions estimated with 1-D models. Field (2000) and Lee and Anderson (2000) provided attenuation relationships for Southern California that accounted for basin effects based on basin depth. An advantage of these empirical amplification factors is that they are based on real records; however a large data set is needed and the results are region-specific. Usually few real data exist for a given site to empirically study basin effects, and the site effects evaluation must be based on analytical and numerical methods.

Since the early work by Aki and Larner (1970), several analytical and numerical methods have been developed to estimate the seismic response of irregular underground structures to incident SH waves. A review of available methods can be found in Aki (1988), Sanchez-Sesma (1987), and Takenaka et al. (1998).

Analytical methods have been developed to estimate the seismic response of homogenous semi-circular (Trifunac, 1971) and semi-elliptical (Wong and Trifunac, 1974) sedimentary basins. These methods are applicable only to simple geometries; however these analytical solutions have been used to validate the results obtained with numerical methods.

Aki and Larner (1970) introduced a numerical method that stated that the wave field in an elastic medium can be calculated as the superposition of homogenous and inhomogeneous plane waves of complex amplitudes propagating in many directions. Examples of the application of the Aki-Larner method to estimate the seismic response of sedimentary basins can be found in the literature (Aki and Larner, 1970; Bard and Bouchon, 1985; Bard et al., 1988; Boore et al., 1971). The Aki-Larner method has been extended to time domain calculations (Bard and Bouchon, 1980) and to incorporate vertical velocity gradients (Bard and Gariel, 1986).

Sanchez-Sesma (1982) introduced the boundary element method to investigate the scattering and diffraction of SH waves by surface irregularities. Several studies have applied boundary element methods to estimate the response of sedimentary basins (Alvarez-Rubio et al., 2004; Dravinski, 2003; Luzon et al., 2004; Moeen-Vaziri and Trifunac, 1988; Papageorgiou and Pei, 1998; Pedersen et al., 1995; Semblat et al., 2002).

The discrete wavenumber representation of seismic source wave fields is an extension of the Aki-Larner method based on the spatial periodicity of sources to discretize the radiated wave field (Bouchon, 2003; Bouchon and Aki, 1977). It has been applied to study the response of two-dimensional structures to incident SH waves (Fu and Bouchon, 2004).

The finite-difference method has been extensively used in the estimation of the seismic response of sedimentary basins (Boore et al., 1971; Chavez-Garcia et al., 2000; Frankel, 1993; Graves and Wald, 2004; Moczo et al., 1996). The finite-element method is another powerful domain method to study wave propagation in complex media; however it has not been as popular as the finite-difference method to predict the seismic response of sedimentary basins (Bao et al., 1998; Bielak et al., 1998; Bielak et al., 1999; Toshinawa and Ohmachi, 1992).

All these methods provide different approaches to evaluate basin effects in the Upper Mississippi Embayment. The best approach would be the empirical method; however due to the lack of strong ground motion records, this method can not be applied to the region. Previous studies have accounted for these effects in numerical simulations of ground motions in the Embayment. Atkinson and Beresnev (2002) simulated ground motions for the city of Memphis, TN using the finite-fault stochastic method and incorporated the possible basin effects by modifying the simulated response spectra with empirical amplification factors developed by Joyner (2000) from earthquakes recorded in the Los Angeles basin. More recently Saikia et al. (2006) evaluated the effects of the Mississippi Embayment on the amplification of seismic waves by using 2-D and 3-D

finite-difference simulations. Figure 5.1 shows the extent of the Upper Mississippi Embayment along with the geographical location of the 2-D and 3-D models used by Saikia et al. (2006). The dotted line from Memphis, TN to St. Louis, MO corresponds to the cross-section used in the 2-D model, and the rectangular area shows the location of the 3-D model. They concluded that a 1-D model will estimate ground motions adequately for engineering purposes at sites located in the central part of the Embayment for earthquakes generated in the New Madrid seismic zone. However due to the large size of the Embayment, the 3-D model implemented considered only a portion of the Embayment, the minimum grid spacing was 500 m, and a single layer with a shear wave velocity of 600 m/sec represented the sediments. A more detailed model is needed to confirm the results for sites located near the edges of the basin. Furthermore the non-linear behavior of the sediments was not incorporated in the simulations.

Numerical analyses using a 3-D model of the entire Upper Mississippi Embayment along with a detailed profile of the sediments incorporating non-linear soil behavior are needed to evaluate basin effects in the region and thus confirm the conclusions of Saikia et al. (2006). However this would require significant computational resources due to the vast size of the Embayment. Due to this limitation, a 2-D model has been selected to evaluate the non-linear seismic response of the Upper Mississippi Embayment. The continuous line shown in Figure 5.1 represents the location of the 2-D model implemented herein. Numerical analyses via domain approaches (i.e. finite-differences or finite-elements) would still require large computational resources because a detailed profile of the soil layers is needed to incorporate their non-linear behavior. The boundary element method is considered more suitable for the analysis of the Embayment because it requires only the discretization of the boundaries of the domains. In this study a combination of the methods proposed by Bravo et al. (1988) and Zheng and Dravinski (1998) to evaluate the linear response of sedimentary basins under

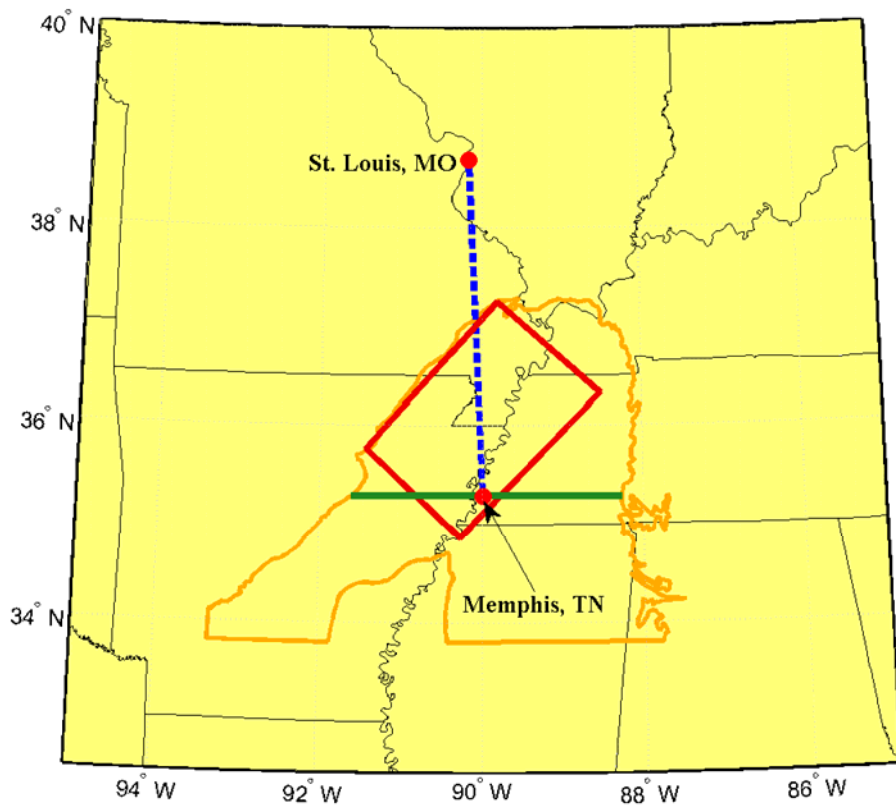


**Figure 5.1.** Extent of the Upper Mississippi Embayment along with the geographical location of the 2-D and 3-D models used by Saikia et al. (2006) (dotted line and rectangle) and 2-D model implemented in this study (solid line)

incident SH plane waves is implemented to evaluate the 2-D seismic response of the Embayment.

#### **5.4. Description of the Method**

Bravo et al. (1988) proposed a method to evaluate the linear response of stratified sedimentary basins to incident SH plane waves. The procedure combines the indirect boundary element method (IBEM) to analyze the seismic wave field in the half-space with the discrete wavenumber representation (Bouchon, 2003; Bouchon and Aki, 1977) of propagator matrices to study the seismic wave field in the sediments inside the basin. It is called an indirect method because the unknowns of the problem are source strengths located at the boundaries, which are then used to compute the wave field in the domains, as opposed to the direct methods where displacements and tractions are directly solved in the formulation (Sanchez-Sesma et al., 1993). In the approach proposed by Bravo et al. (1988), the IBEM sources are not located at the boundaries to avoid singularities of the Green's function, resulting when the source and the point of application are placed at the same location. Gil-Zepeda et al. (2003) extended the approach by placing the IBEM sources on the boundary between the half-space and the sediments, and Zeng and Benites (1998) incorporated the effect of the vertical variation of the shear-wave velocity of the sediments. Zheng and Dravinski (1998) proposed a similar method where the IBEM is used to investigate the scattering of SH waves by a sedimentary basin of arbitrary shape. This approach treats the half-space and the basin with the IBEM. In this study the formulation of Zheng and Dravinski (1998) is used to solve the wave field in the half-space because it is more computationally efficient, and the discrete wavenumber representation of propagator matrices proposed by Bravo et al. (1988) is used to solve the wave field in the basin. In this way only the discretization of the interface between the basin and the half-space is needed, and the propagator matrices provide high resolution of the sediment profile to incorporate the non-linear soil behavior. Furthermore, the

propagator matrices provide a detailed characterization of the geometry and properties of the soil layers required to obtain reliable estimates of ground motions in sedimentary basins (Narayan and Singh, 2006; Semblat et al., 2005). The analyses are performed for SH waves only because it is believed that site response is caused mainly by this type of wave (Kramer, 1996). In general this assumption has resulted in reasonable agreement with recorded data. Furthermore the incorporation of the non-linear soil behavior is based on the properties of soil during shear loading.

#### 5.4.1. Wave field outside basin

Figure 5.2 shows a horizontally stratified basin embedded in a half-space. The displacement at point  $P(x,z)$  in the half-space is given by:

$$u_H(x,z) = u_0(x,z) + u_d(x,z) \quad 5.1$$

where  $u_0$  is the free-field displacement (i.e. the displacement in the absence of the basin) and  $u_d$  is the scattered-field displacement due to the presence of the basin. For an incident SH wave of the form (Zheng and Dravinski, 1998):

$$u_{inc}(x,z) = A \cdot \exp[i(\kappa x \sin \theta_0 - \kappa z \cos \theta_0 - \omega t)] \quad 5.2$$

the free-field displacement resulting from the sum of incident and refracted waves is given by:

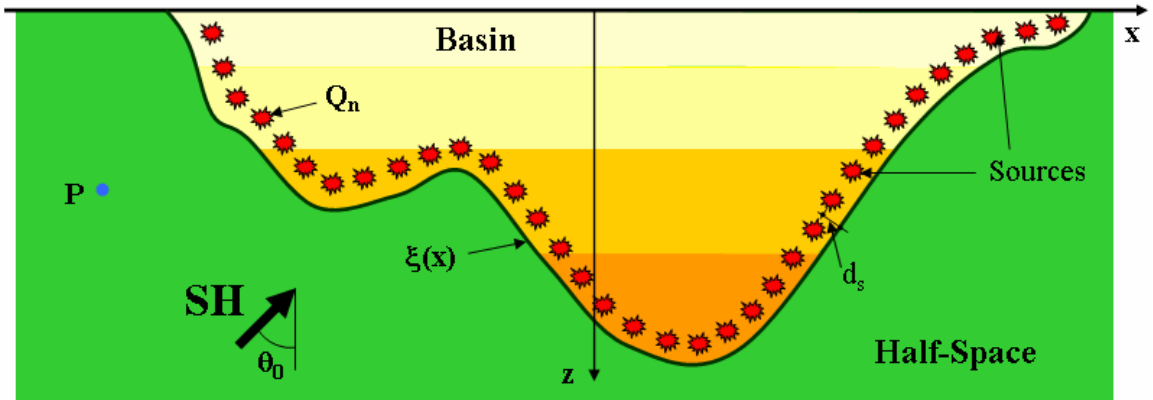


**Figure 5.2.** Stratified basin embedded in a half-space (from Zeng and Benites (1998))

$$u_0(x, z) = 2 \cdot A \cdot \exp(i\kappa x \sin \theta_0) \cdot \cos(\kappa z \cos \theta_0) \cdot \exp(-i\omega t) \quad 5.3$$

where  $A$  is the amplitude of the incident wave,  $\kappa = \omega/\beta$  is the wave number,  $\omega$  is the circular frequency,  $\beta$  is the shear wave velocity of the half-space, and  $\theta_0$  is the incident angle with respect to vertical.

The scattered-field displacement can be written in terms of single layer potentials over the auxiliary curve  $C$  parallel to interface  $\xi(x)$  (Sanchez-Sesma and Esquivel, 1979; Zheng and Dravinski, 1998):

$$u_d(\mathbf{P}) = \int_C \sigma(\mathbf{Q}) \cdot G_f(\mathbf{P}, \mathbf{Q}) \cdot dS_Q \quad 5.4$$

where  $\sigma(\mathbf{Q})$  is the source density function, and  $G_f(\mathbf{P}, \mathbf{Q})$  is the Green's function associated with a line source in a half-space. Assuming that  $\sigma(\mathbf{Q})$  represents a system of  $N$  discrete point sources along the auxiliary curve  $C$ , it follows that:

$$\sigma(\mathbf{Q}) = \sum_{n=1}^N \phi(\mathbf{Q}_n) \cdot \delta(|\mathbf{Q} - \mathbf{Q}_n|) \quad 5.5$$

where  $\phi(\mathbf{Q}_n)$  is the unknown source strength at point  $\mathbf{Q}_n$ . Replacing Equation 5.5 in Equation 5.4, the scattered-field displacement is given as:

$$u_d(\mathbf{P}) = \sum_{n=1}^N \phi(\mathbf{Q}_n) \cdot G_f(\mathbf{P}, \mathbf{Q}_n) \quad 5.6$$

where the Green's function  $G_f(\mathbf{P}, \mathbf{Q}_n)$  represents the response at point  $\mathbf{P}$  to a unit forcing at point source  $\mathbf{Q}_n$ . Thus the scattered-field is computed as the superposition of point sources and can be seen as a numerical representation of Huygens' principle (Sanchez-Sesma et al., 1993). The half-space is considered to undergo elastic linear behavior due to the low strains induced in the bedrock, and non-linear behavior was considered only for the sediments as described later.

The Green's function in this problem is given by (Zheng and Dravinski, 1998):

$$G_f(\mathbf{P}, \mathbf{Q}_n) = \frac{i}{4} \cdot [H_0^{(1)}(\kappa r) + H_0^{(1)}(\kappa r')] \quad 5.7$$

where  $H_0^{(1)}(\cdot)$  is the Hankel function of the first kind and order zero,  $\kappa$  is the wavenumber, and  $r$  and  $r'$  are the distances from point  $\mathbf{P}$  to sources located at  $(x_{Q_n}, z_{Q_n})$  and  $(x_{Q_n}, -z_{Q_n})$  respectively.

As in the case of displacements, the traction at point  $\mathbf{P}$  in the half-space is given by:

$$t_H(x, z) = t_0(x, z) + t_d(x, z) \quad 5.8$$

where  $t_0$  is the free-field traction and  $t_d$  is the scattered-field traction due to the presence of the basin. The traction can be calculated as:

$$t = G \cdot \frac{\partial u}{\partial \mathbf{n}} = G \cdot \left( \frac{\partial u}{\partial x} \cdot \mathbf{n}_x + \frac{\partial u}{\partial z} \cdot \mathbf{n}_z \right) \quad 5.9$$

where  $G$  is the shear modulus,  $u$  is the displacement, and  $\mathbf{n}$  is a unit vector pointing outward and normal to interface  $\xi(x)$ . Applying Equation 5.9 to the free-field displacement given by Equation 5.3, the free-field traction can be calculated as:

$$t_0(x, z) = G \cdot \left( \frac{\partial u_0}{\partial x} \cdot \mathbf{n}_x + \frac{\partial u_0}{\partial z} \cdot \mathbf{n}_z \right) \quad 5.10$$

$$\frac{\partial u_0}{\partial x} = 2i \cdot A \cdot \kappa \cdot \sin(\theta_0) \cdot \exp[i\kappa x \sin(\theta_0)] \cdot \cos[\kappa z \cos(\theta_0)]$$

$$\frac{\partial u_0}{\partial z} = -2 \cdot A \cdot \kappa \cdot \cos(\theta_0) \cdot \exp[i\kappa x \sin(\theta_0)] \cdot \sin[\kappa z \cos(\theta_0)]$$

The scattered-field traction is computed by applying Equation 5.9 to Equation 5.6:

$$t_d(\mathbf{P}) = \sum_{n=1}^N \phi(\mathbf{Q}_n) \cdot \left[ G \cdot \left( \frac{\partial G_f(\mathbf{P}, \mathbf{Q}_n)}{\partial x} \cdot \mathbf{n}_x + \frac{\partial G_f(\mathbf{P}, \mathbf{Q}_n)}{\partial z} \cdot \mathbf{n}_z \right) \right] \quad 5.11$$

$$\frac{\partial G_f(\mathbf{P}, \mathbf{Q}_n)}{\partial x} = -\frac{i}{4} \cdot \kappa \cdot (x - x_{Q_n}) \cdot \left[ H_1^{(1)}(\kappa r) \cdot \frac{1}{r} + H_1^{(1)}(\kappa r') \cdot \frac{1}{r'} \right]$$

$$\frac{\partial G_f(\mathbf{P}, \mathbf{Q}_n)}{\partial z} = -\frac{i}{4} \cdot \kappa \cdot \left[ H_1^{(1)}(\kappa r) \cdot \frac{(z - z_{Q_n})}{r} + H_1^{(1)}(\kappa r') \cdot \frac{(z + z_{Q_n})}{r'} \right]$$

where  $H_1^{(1)}(\cdot)$  is the Hankel function of the first kind and order one.

#### 5.4.2. Wave field inside basin

The displacements inside the basin are calculated by using a discrete wavenumber representation of the propagator matrices (Bravo et al., 1988; Gil-Zepeda et al., 2003):

$$u_B(x, z) = \sum_{m=-M}^M B_m \cdot l_1(\kappa_m, z, \omega) \cdot \exp(-i\kappa_m x) \quad 5.12$$

where  $M$  is the number of wavenumbers needed for the convergence of the summation,  $B_m$  are unknown complex coefficients, and  $l_1(\kappa_m, z, \omega)$  is the first element of the motion-stress vector at depth  $z$  and horizontal discrete wavenumber  $\kappa_m$ . The principle of the discrete wavenumber method is that the source can be represented as a discrete superposition of homogeneous and inhomogeneous plane waves propagating from periodic sources (Bouchon, 2003; Bouchon and Aki, 1977).

The motion-stress vector at depth  $z$  can be calculated as:

$$\begin{bmatrix} l_1 \\ l_2 \end{bmatrix}_z = \mathbf{l}(z) = \mathbf{P}(z, z_0) \cdot \mathbf{l}(z_0) = \mathbf{P}(z, z_0) \cdot \begin{bmatrix} l_1 \\ l_2 \end{bmatrix}_{z_0} \quad 5.13$$

where  $\mathbf{l}(z_0)$  is the motion-stress vector at depth  $z_0$  and the propagator matrix  $\mathbf{P}(z, z_0)$  for  $z_j \geq z \geq z_{j-1}$  is calculated as:

$$\mathbf{P}(z, z_0) = \mathbf{P}(z, z_{j-1}) \cdot \mathbf{P}(z_{j-1}, z_{j-2}) \cdots \mathbf{P}(z_1, z_0) \quad 5.14$$

The propagator matrix  $\mathbf{P}(z_j, z_{j-1})$  for Love waves is given by (Aki and Richards, 1980):

$$\mathbf{P}(z_j, z_{j-1}) = \begin{bmatrix} \cos \eta(z_j - z_{j-1}) & \frac{1}{\eta G} \sin \eta(z_j - z_{j-1}) \\ -\eta G \sin \eta(z_j - z_{j-1}) & \cos \eta(z_j - z_{j-1}) \end{bmatrix} \quad 5.15$$

where  $\eta = (\omega^2/\beta^2 - \kappa_m^2)^{0.5}$  and  $G$  and  $\beta$  are the shear modulus and shear-wave velocity of the layer, respectively, which are related to the density  $\rho$  by the following relation:

$$G = \rho \cdot \beta^2 \quad 5.16$$

The tractions inside the basin are calculated by applying Equation 5.9 to Equation 5.12:

$$t_B(x, z) = \sum_{m=-M}^M B_m \cdot [-i \cdot \mu \cdot \kappa_m \cdot l_1(\kappa_m, z, \omega) \cdot n_x + l_2(\kappa_m, z, \omega) \cdot n_z] \cdot \exp(-i\kappa_m x) \quad 5.17$$

where  $l_2(\kappa_m, z, \omega)$  is the second element of the motion-stress vector at depth  $z$  and horizontal discrete wavenumber  $\kappa_m$ .

The continuity of displacements  $u$  and tractions  $t$  at  $W$  number of points located on interface  $\xi(x)$  results in a system of equations of the form:

$$u_d(x, z) - u_B(x, z) = -u_0(x, z) \quad 5.18$$

$$t_d(x, z) - t_B(x, z) = -t_0(x, z) \quad 5.19$$

Equations 5.18 and 5.19 can be written as:

$$\mathbf{A} \cdot \mathbf{b} = \mathbf{f} \quad 5.20$$

where matrix  $\mathbf{A}$  of size  $2W \times (N + 2M + 1)$  and vector  $\mathbf{f}$  of size  $2W \times 1$  are known, and vector  $\mathbf{b}$  contains the  $N$  unknown source strengths,  $\phi(\mathbf{Q}_n)$ , and the  $2M+1$  unknown complex coefficients,  $B_m$ . Once the system of equations defined by Equation 5.20 is solved, the displacements and tractions inside the basin can be calculated using Equations 5.12 and 5.17, and in the half-space using Equations 5.6 and 5.11.

The convergence of the method depends on the number of collocation points  $W$  on interface  $\xi(x)$ , number of sources  $N$  in Equations 5.6 and 5.11, number of wavenumbers  $M$  in Equations 5.12 and 5.17, and the distance  $d_s$  from the auxiliary curve  $C$  to interface  $\xi(x)$ .

The distance between adjacent collocation points,  $d_w$ , is related to the incident wave length,  $\lambda_{inc}$ , by (Ding and Dravinski, 1996; Zheng and Dravinski, 1998):

$$d_w < \frac{1}{10} \cdot \lambda_{inc} \quad 5.21$$

The distance  $d_w$  defines the minimum number of collocation points  $W$  needed in the analysis. Due to the singularity of the Green's function when evaluated at interface  $\xi(x)$ , the sources must be located at a distance  $d_s$  from this boundary. The distance  $d_s$  from the auxiliary curve  $C$  to interface  $\xi(x)$  is related to the distance  $d_w$  by (Ding and Dravinski, 1996; Zheng and Dravinski, 1998):

$$d_s \cong 3 \cdot d_w \quad 5.22$$

Zheng and Dravinski (1998) uses two auxiliary curves (i.e. two sets of point sources), one inside and one outside the basin to calculate the wave field on the half-space and in the basin respectively. Zheng and Dravinski (1998) provide a relationship between the total number of sources on the two auxiliary curves and the number of collocation points. The approach presented herein uses only one set of point sources, and therefore the relationship between the number of sources  $N$  and the number of collocation points  $W$  was modified from the one given by Zheng and Dravinski (1998) and expressed as:

$$N \cong 0.4 \cdot W \quad 5.23$$

The range of horizontal discrete wavenumbers in Equations 5.12 and 5.17 should be from  $-\infty$  to  $\infty$ ; however in practice the discretization of wavenumbers is truncated between  $-\kappa_{max}$  and  $\kappa_{max}$ . The discrete wavenumbers are equally spaced in a range that gives only homogeneous planes waves for the displacement field in the softest layer (Bravo et al., 1988), that is:

$$\kappa_{max} = \frac{\omega}{\beta_{min}} \quad 5.24$$

Equation 5.24 implies that inhomogeneous waves can exist in the other layers. To obtain stable results the wavenumber interval should be defined as (Zeng and Benites, 1998):

$$\Delta\kappa \leq 0.85 \cdot \frac{2\pi}{4a} \quad 5.25$$

where  $a$  is the half-width of the basin. The number of discrete wavenumbers  $M$  is calculated using Equations 5.24 and 5.25:

$$M = \frac{\kappa_{\max}}{\Delta\kappa} \quad 5.26$$

### 5.4.3. Non-linear soil behavior

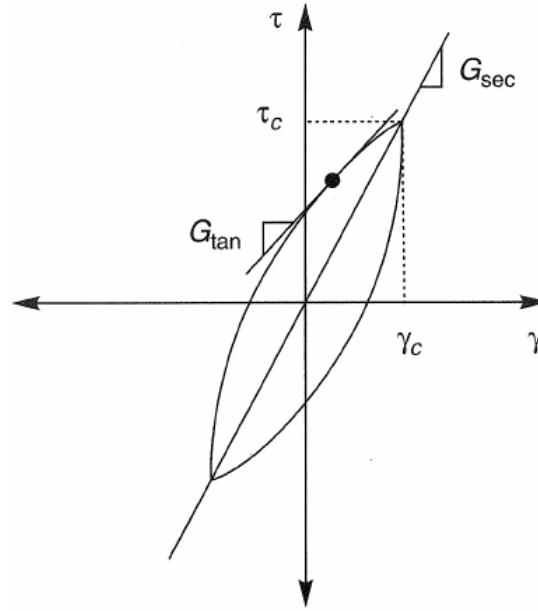
The linear approach described above must be modified to account for non-linear behavior of the sediments inside the basin. The non-linear hysteretic stress-strain behavior for cyclically loaded soils can be approximated by using an iterative procedure using equivalent linear soil properties (Idriss and Seed, 1968; Kramer, 1996).

Figure 5.3 illustrates a hysteresis shear stress-strain loop experienced by a mass of soil subjected to cyclic loads. The hysteresis loop can be described by the actual path of the loop or by parameters that describe its general shape. Inclination and width are the most important characteristics of the shape of the loop. The inclination depends on the stiffness of the soil, and its average value can be approximated by the secant shear modulus, which is defined as the slope of the line that joins the extreme points of the hysteresis loop (Kramer, 1996):

$$G_{\text{sec}} = \frac{\tau_s}{\gamma_s} \quad 5.27$$

where  $\tau_s$  and  $\gamma_s$  are the shear stress and shear strain amplitudes, respectively. The width of the loop is related to its area, which is a measure of energy dissipation and can be described by the damping ratio (Kramer, 1996):

$$\xi = \frac{1}{2\pi} \frac{A_{\text{loop}}}{G_{\text{sec}} \cdot \gamma_s^2} \quad 5.28$$



**Figure 5.3.** Hysteresis shear stress-strain loop (from Kramer (1996)).

where  $A_{\text{loop}}$  is the area of the loop. The parameters  $G_{\text{sec}}$  and  $\xi$  are referred to as equivalent linear soil properties. Equations 5.27 and 5.28 indicate that shear modulus and damping values vary with shear strain amplitude during dynamic shear loading.

The linear approach requires that the shear modulus,  $G$ , and damping ratio,  $\xi$ , be constant for each soil layer. Hence an equivalent linear analysis consists of determining the equivalent linear material properties compatible with the shear strain level induced in each layer. The shear strain time history for an earthquake record is very irregular and defining the strain level of a harmonic load by the peak amplitude of a transient record represents a more severe loading condition because only a few spikes may approach the peak amplitude of a transient record. Consequently the strain level of an earthquake record is usually characterized by an effective shear strain that has been found to range between 50% and 70% of the peak shear strain (Kramer, 1996). Idriss and Sun (1992) suggested a relationship between the ratio of the effective shear strain to the peak shear strain,  $R_\gamma$ , and earthquake magnitude:

$$R_\gamma = \frac{M-1}{10} \quad 5.29$$

The response of the system is not highly sensitive to this percentage, and the  $R_\gamma$  factor is typically taken as 65% (Kramer, 1996).

The calculated effective shear strain depends on the values of the equivalent linear soil properties, and therefore an iterative approach is required to obtain material properties compatible with the calculated strain levels. Figure 5.4 illustrates the iterative procedure used by the equivalent linear analysis, and which be described in the following steps (Kramer, 1996):

1. The initial estimates of  $G$  and  $\xi$  are determined from the low-strain values (i.e.  $G_{\max}$  and  $\xi_{\min}$ ).
2. The estimates of  $G$  and  $\xi$  are used to perform the site response analysis using a linear approach.
3. The effective shear strain in each soil layer is computed from the peak shear strain:

$$\gamma_{\text{eff}} = R_\gamma \cdot \gamma_{\text{peak}} \quad 5.30$$

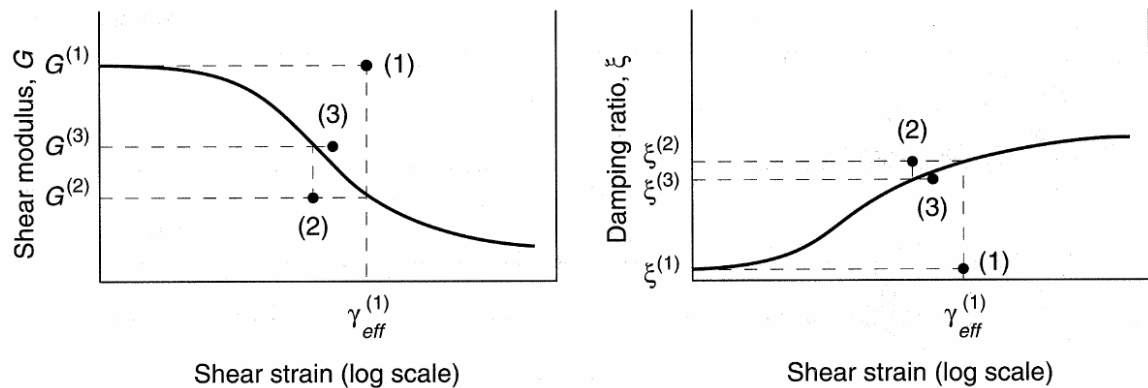


**Figure 5.4.** Iterative procedure used by the equivalent linear analysis (from Kramer (1996)). Numbers in parentheses indicate number of iteration

4. The calculated effective shear strain is used to select new equivalent linear values of  $G$  and  $\xi$  for the next iteration.

5. Steps 2 to 4 are repeated until a predetermined tolerance between the differences of the computed values of  $G$  and  $\xi$  in two successive iterations is achieved. Tolerances of 5% to 10% are usually achieved in three to five iterations.

To incorporate the material damping in the analysis, soils are usually characterized by the Kelvin-Voight model, where the shear modulus is estimated as the sum of an elastic term and a viscous term and can be represented by a spring and dashpot in parallel (Kramer, 1996). Thus the shear modulus can be written as (Kramer, 1996; Sanchez-Sesma et al., 2000):

$$G^* = G \cdot (1 + 2i \cdot \xi) \quad 5.31$$

where  $G^*$  is the complex shear modulus. Thus viscoelastic soil behavior can be incorporated in the formulation by using complex material properties.

The peak shear strain used in Step 3 can be computed by time and frequency domain approaches. In the time domain approach as used by the program SHAKE (Schnabel et al., 1972), the peak shear strains are directly measured from the shear strain time histories. In the frequency-domain approach, random vibration theory is used to estimate peak time domain values of shear strains based on the shear strain power spectrum. In this study an equivalent linear approach based on random vibration theory is used to account for the non-linear soil behavior. The validity of the use of the equivalent linear approach for site response analyses in the Upper Mississippi Embayment, and the advantages of the random vibration theory methodology over the traditional time domain approach have been discussed in Chapter 3.

Once the system of equations defined by Equation 5.20 is solved, the shear strain spectrum  $\gamma_s(f)$  is calculated at the midpoints of each layer. The shear strains are computed using the following relation (Silva, 1976):

$$\gamma_s(f) = \left| \frac{\tau_s(f)}{G} \cdot \frac{2}{1 + \sqrt{1 + Q_s^{-2}}} \cdot \left( 1 - \frac{i}{Q_s} \right) \right| \quad 5.32$$

where  $\tau_s(f)$  is the shear stress computed at the midpoints of each layer,  $G$  is the shear modulus, and  $Q_s$  is the quality factor, which is defined as:

$$Q_s = \frac{1}{2 \cdot \xi} \quad 5.33$$

For large values of zero crossings,  $N_z$ , the maximum shear strain  $\gamma_{s \max}$  can be estimated as (Cartwright and Longuet-Higgins, 1956):

$$\frac{\gamma_{s \max}}{\gamma_{s \text{rms}}} = [2 \cdot \ln(N_z)]^{1/2} + \frac{\gamma}{[2 \cdot \ln(N_z)]^{1/2}} \quad 5.34$$

where  $\gamma$  is the Euler's constant ( $\gamma = 0.5772$ ),  $\gamma_{s \text{rms}}$  is the root-mean-square (rms) value of the shear strains.  $N_z$  is related to the frequencies or rate of occurrence of zero crossings,  $f_z$ , and to duration,  $T$ , by the equation:

$$N_z = 2 \cdot f_z \cdot T \quad 5.35$$

For a stationary Gaussian process, the occurrence rate of zero crossings is given by (Lutes and Sarkani, 1997):

$$f_z = \frac{1}{2\pi} \cdot \left( \frac{m_2}{m_0} \right)^{1/2} \quad 5.36$$

The moments of the power spectral density of shear strains,  $m_k$ ,  $k = 0, 2$  are defined by:

$$m_k = 2 \cdot \int_0^\infty (2\pi \cdot f)^k \cdot |\gamma_s(f)|^2 df \quad 5.37$$

The rms shear strain value in Equation 5.34,  $\gamma_{s \text{rms}}$ , is calculated by:

$$\gamma_{s \text{rms}} = \left( \frac{m_0}{T} \right)^{1/2} \quad 5.38$$

The definition of duration  $T$  proposed by Herrmann (1985) is used in this study. The duration of the motion  $T$  in seconds is related to the corner frequency of the source spectrum  $f_0$  and to the traveled distance of the seismic waves  $R$  in km by:

$$T = \frac{1}{f_0} + 0.05 \cdot R \quad 5.39$$

The corner frequency of the source spectrum can be estimated by Equation 3.6.

The effective shear strain in each layer is determined as the 65% of the peak shear strain calculated by Equation 5.34. Due to the 2-D nature of the problem, the value of the shear strain in a given layer varies horizontally across the layer. To calculate the effective shear strain in each layer, the representative peak shear strain is estimated as the maximum of the peak shear strains computed by Equation 5.34 at different points horizontally distributed along the layer. This homogenization of shear strains across each soil layer is an approximation of the real 2-D response, and it was incorporated in the analysis to be consistent with the propagator matrices approach. Future analyses are required to evaluate the significance of this assumption on the results calculated by proposed method.

The methodology described above was implemented in this study in a Matlab program.

## 5.5. Assessment of the Method

The performance of the method has been evaluated by comparing the linear response of a homogeneous, semi-circular basin and a layered, parabolic basin calculated by the proposed method with solutions provided in the literature.

### 5.5.1. Semi-circular basin

The linear response of a homogeneous, semi-circular basin to an incident plane SH wave calculated by the presented method has been compared with the closed-form solution provided by Trifunac (1971). Figure 5.5 shows the model of the basin used in

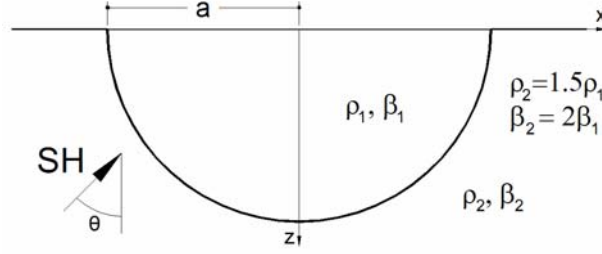


**Figure 5.5.** Model of semi-circular basin

the example. The model consists of a cylindrical basin with a semi-circular cross-section of radius (i.e. half-width)  $a$ . The values of the density and shear-wave velocity of the half-space and sediments are given in Figure 5.5. In order to evaluate the performance of the propagator matrices, the sediments inside the basin were subdivided in three layers with identical material properties. Figure 5.6 compares the surface displacement amplification with respect to a unitary incident motion for different angles of incidence due to an incident SH wave of unitary amplitude and wavelength equal to the diameter of the basin. The agreement of the surface basin response calculated by both methods is excellent. Similar results were obtained for other incident wavelengths. It is important to note the dependence of the basin response on the incident angle. Only positive angles were considered in the analysis, since the basin is symmetric with respect to the  $z$ -axis.

### 5.5.2. Parabolic basin

The implementation of the method has also been evaluated by comparing the linear response of a layered, parabolic basin computed by the presented method with the results provided by Bravo et al. (1988) and Gil-Zepeda et al. (2003). Figure 5.7 shows the model of the basin used in the comparison. The model consists of a cylindrical basin with a parabolic cross-section with half-width  $a$  and maximum depth of  $a/2$ . The basin is comprised of two layers with thicknesses of  $H_1 = a/6$  and  $H_2 = a/3$ . The shear-wave velocity and mass density of the soil layers are given in terms of the material properties

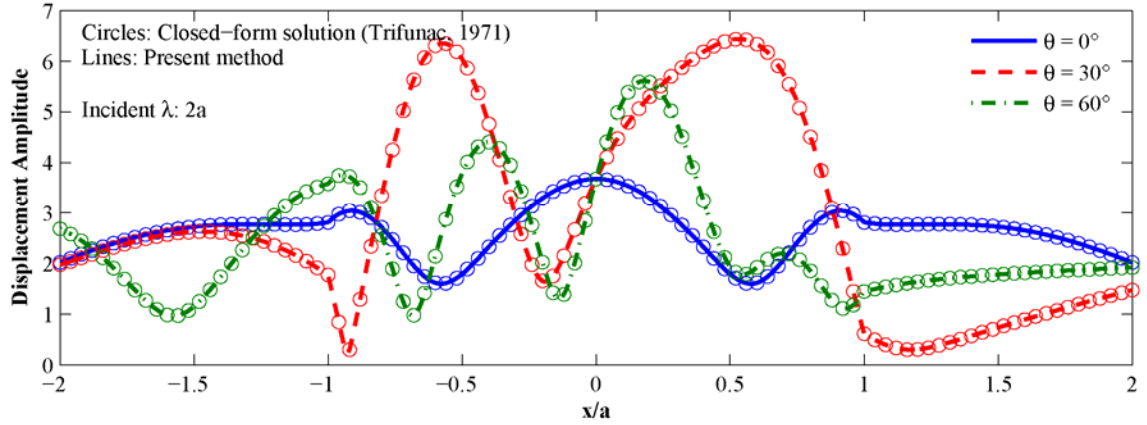


**Figure 5.6.** Surface displacement amplification of a semi-circular basin due to a unitary incident motion

of the half-space (subindex H):  $\beta_1/\beta_H = 1/3$ ,  $\beta_2/\beta_H = 2/3$ ,  $\rho_1/\rho_H = 3/4$ , and  $\rho_2/\rho_H = 0.85$ . The damping ratios for each soil layer are  $\xi_1 = 0.05$  and  $\xi_2 = 0.02$ .

Figure 5.8 compares the surface displacement amplification with respect to a unitary incident motion computed herein with the results obtained by Bravo et al. (1988), which are the same as the results provided by Gil-Zepeda et al. (2003). The incident motion is a plane SH wave of unitary amplitude and wavelength equal to the total width of the basin,  $2a$ . The agreement between both solutions is excellent. Similar results were obtained for other incident wavelengths.

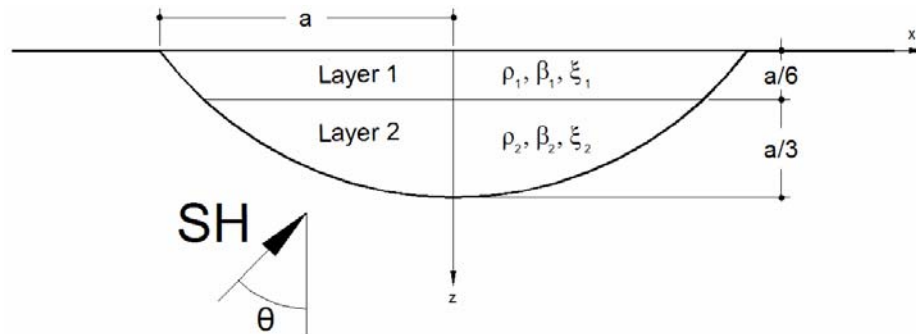


**Figure 5.7.** Model of parabolic basin

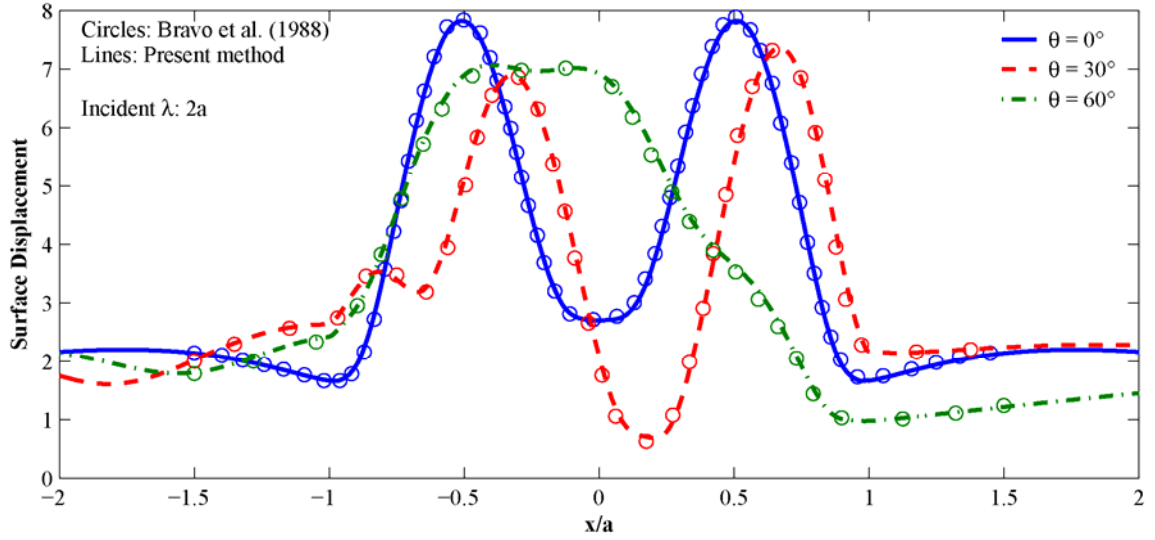


**Figure 5.8.** Surface displacement amplification of a parabolic basin due to a unitary incident motion

The 2-D response of the basin was compared to the response of a 1-D model (i.e. flat layer response (Aki and Larner, 1970)), which is the response in the absence of the basin interface, assuming uniform layer thicknesses equal to local profile for each point at the surface. The 1-D response was calculated using the propagator matrices formulation provided by Ben-Menahem and Singh (1981). Figure 5.9 and Figure 5.10 compare the 1-D and 2-D surface amplification with respect to a unitary incident motion for different incident angles and stations at the surface. The 2-D response shows more defined resonant frequencies and higher amplitudes compared to the 1-D model.

Displacement time histories were calculated at the surface of the basin due to an incident Ricker wavelet of the form (Zheng and Dravinski, 1998):

$$f(t) = \frac{\sqrt{\pi}}{2} \cdot (\tau - 0.5) \cdot \exp(-\tau) \quad (5.40)$$

$$\tau = \left( \pi \cdot \frac{t - t_s}{t_p} \right)^2$$

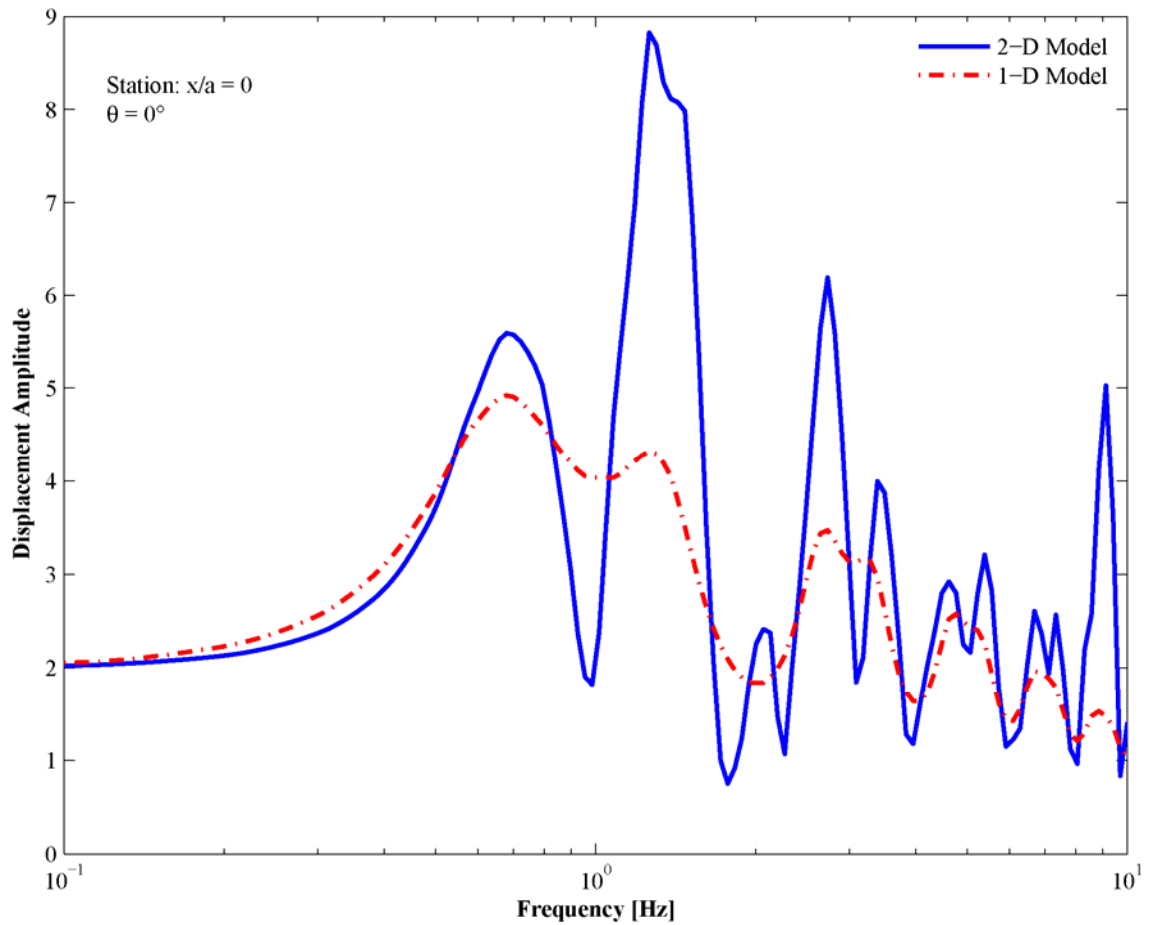


**Figure 5.9.** Comparison of surface displacement amplification of the parabolic basin model shown in Figure 5.7 to a unitary incident motion with incident angle of  $0^\circ$  computed with 1-D and 2-D models

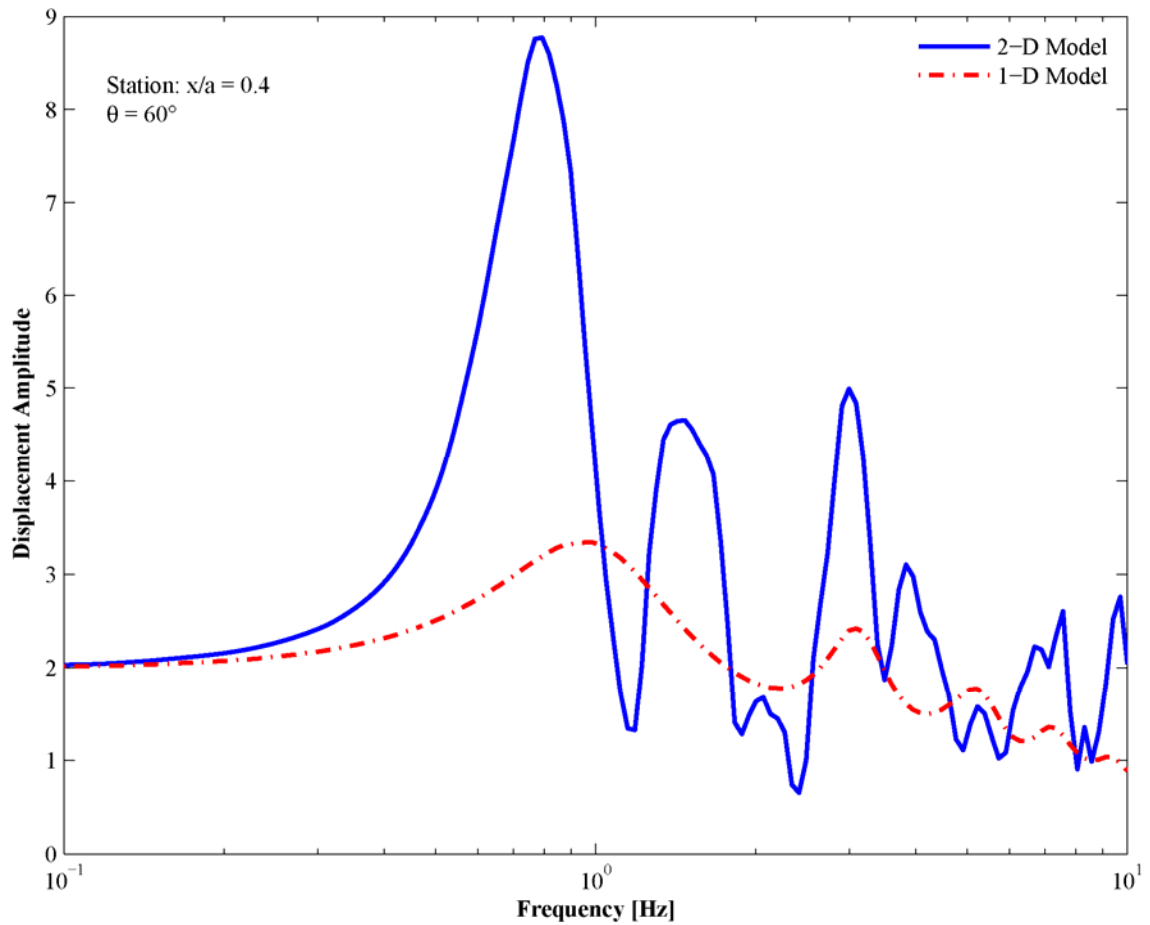


**Figure 5.10.** Comparison of surface displacement amplification of the parabolic basin shown in Figure 5.7 to a unitary incident motion with incident angle of  $60^\circ$  computed with 1-D and 2-D models

where  $t_s$  is the time of maximum amplitude and  $t_p$  is related to the frequency of maximum amplitude by  $\omega_p = 2\pi/t_p$ . The values of these parameters used in the example are  $t_s = 2$  sec and  $t_p = 1$  sec, which result in a characteristic wavelength of the incident pulse of  $2a$ . The time histories are obtained by convolving the Fourier transform of the input motion,  $f(\omega)$  with the displacement spectrum calculated at the surface of the basin,  $u(\omega)$ , and then converting to the time domain using the inverse Fourier transform:

$$u(t) = \frac{1}{2\pi} \cdot \int_{-\infty}^{\infty} f(\omega) \cdot u(\omega) \cdot \exp(i\omega t) \cdot d\omega \quad 5.41$$

Figure 5.11 through Figure 5.14 show surface displacement time histories for two angles of incidence. Figure 5.11 and Figure 5.13 show time histories only for nine stations horizontally distributed along the width of the basin in order to better identify the shape and amplitude of the waveforms. For an incidence angle of  $0^\circ$ , the surface waves generated at both edges of the basin travel towards the center where they converge creating a constructive interference pattern. For an incidence angle of  $60^\circ$ , the surface waves generated at the incident edge travel towards the opposite side where the waves are refracted back into the basin. The complexity of the response increases near the opposite edge of the basin. Figure 5.15 and Figure 5.16 show the significant duration of the time histories shown in Figure 5.12 and Figure 5.14. The significant duration (Trifunac and Brady, 1975) is defined as the interval between the 5% and 95% of the Arias intensity, which is related to the damage potential and is calculated by Equation 4.24. Both cases show an increase in ground motion duration due to the generation of surface waves. For an incidence angle of  $0^\circ$ , longer durations are observed near the edges of the basin due to waves reflected back from the edge as shown in Figure 5.12. For an incidence angle of  $60^\circ$ , the duration increases as the waves approach the opposite edge of the basin. For this particular case, the 2-D effects cause an increase in duration of about 3 to 3.5 times with respect to the free-field duration.

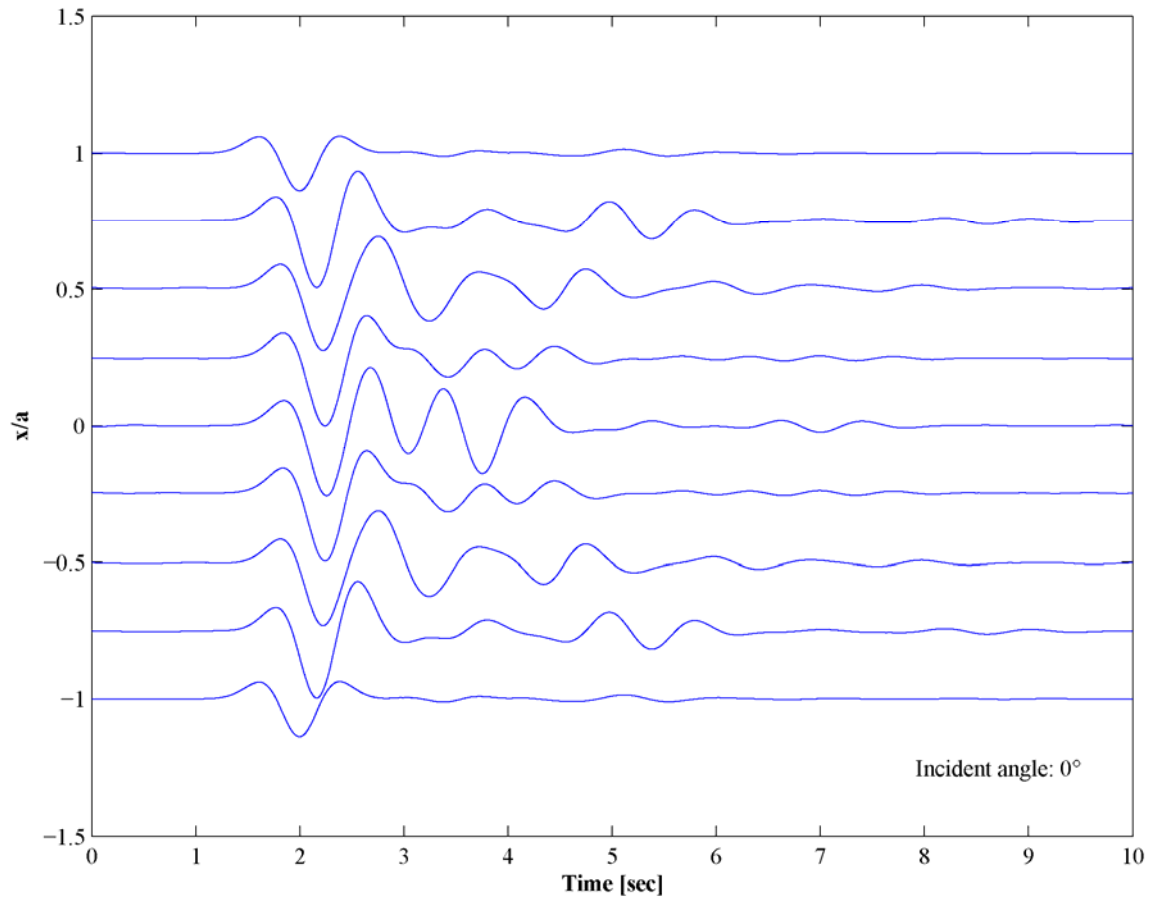


**Figure 5.11.** Surface displacement time histories of the parabolic basin shown in Figure 5.7 due to a Ricker pulse with incident angle of  $0^\circ$  computed with a 2-D model (9 stations only)

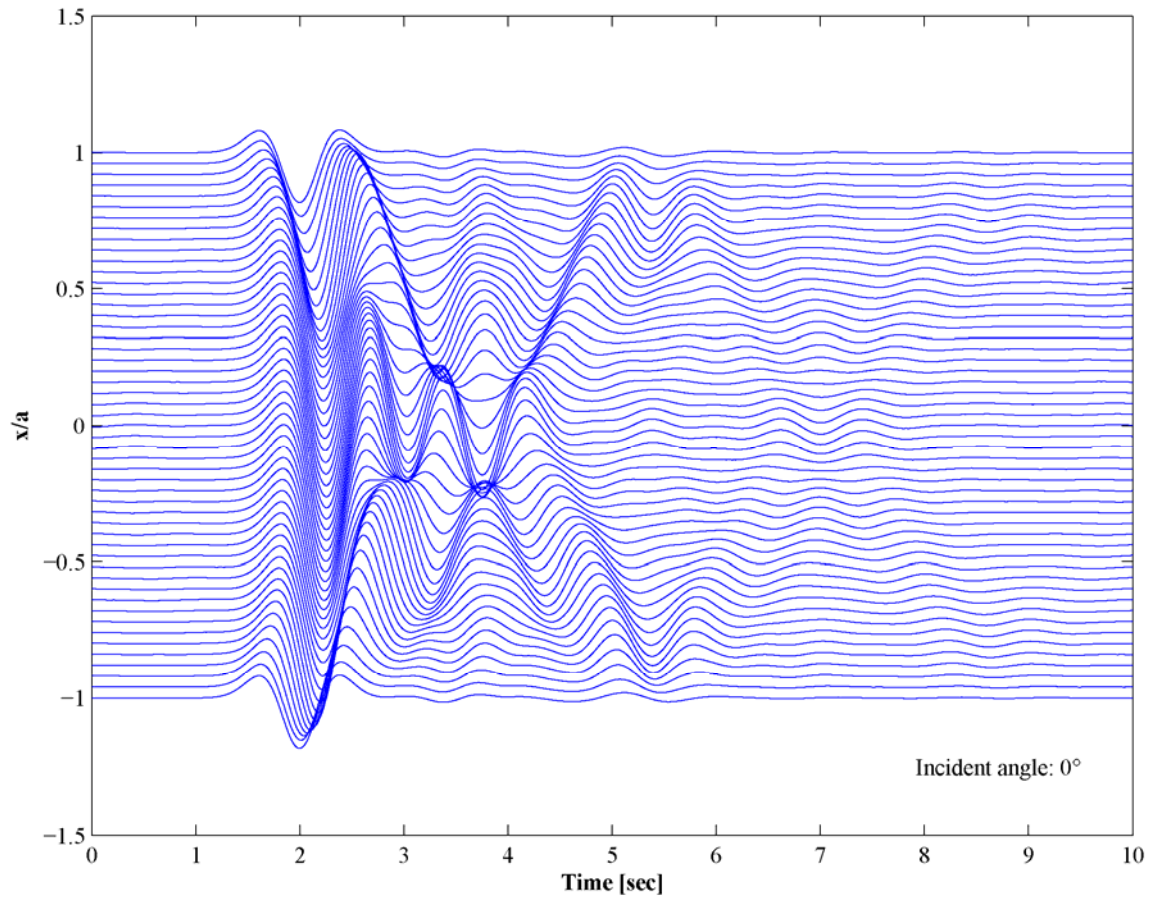


**Figure 5.12.** Surface displacement time histories of the parabolic basin shown in Figure 5.7 due to a Ricker pulse with incident angle of  $0^\circ$  computed with a 2-D model

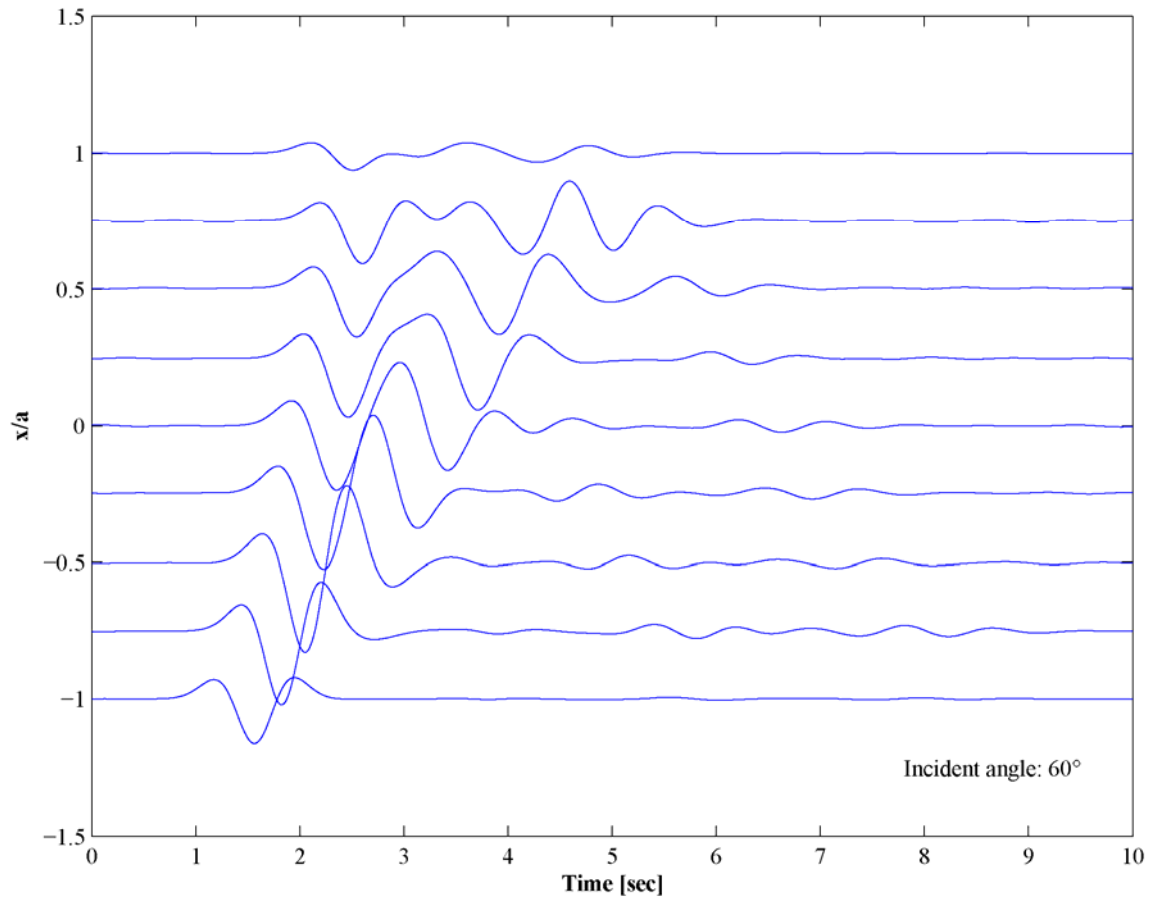


**Figure 5.13.** Surface displacement time histories of the parabolic basin shown in Figure 5.7 due to a Ricker pulse with incident angle of  $60^\circ$  computed with a 2-D model (9 stations only)

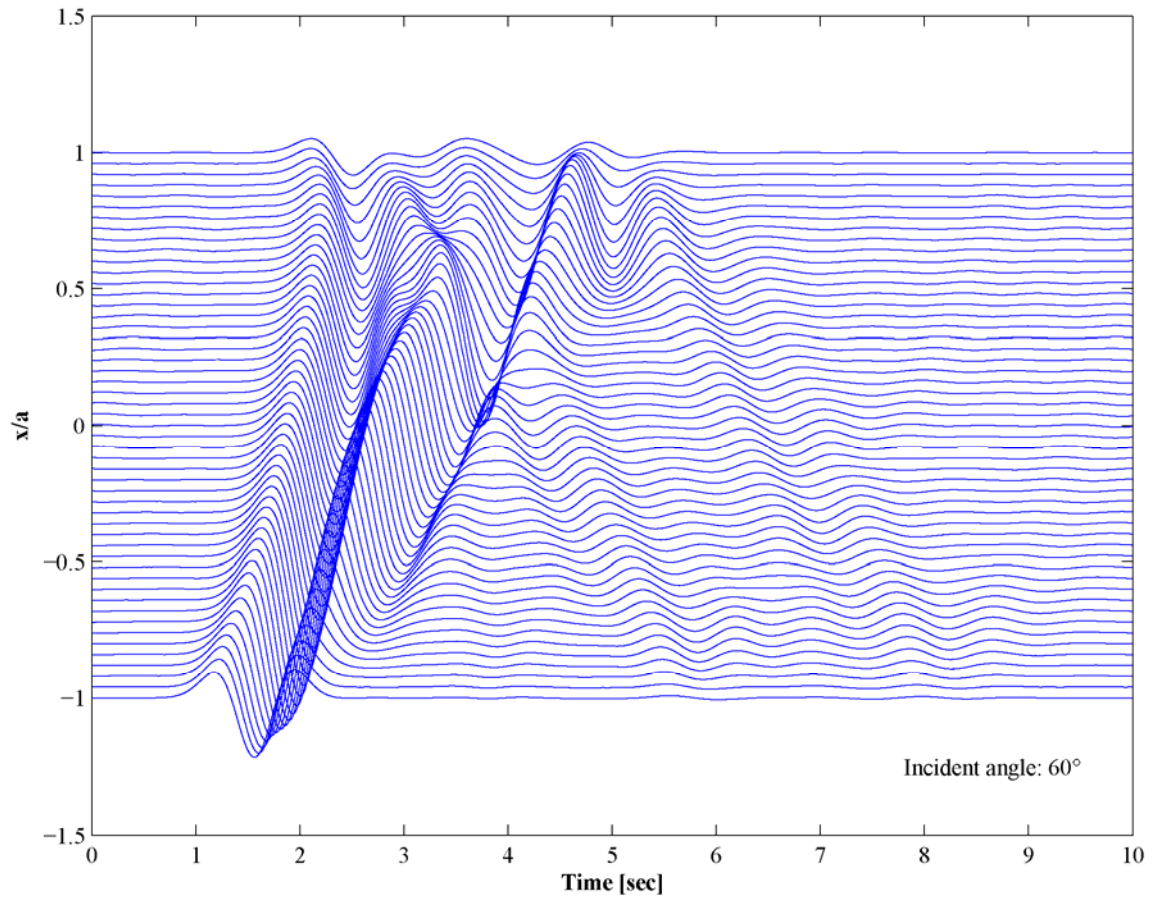


**Figure 5.14.** Surface displacement time histories of the parabolic basin shown in Figure 5.7 due to a Ricker pulse with incident angle of  $60^\circ$  computed with a 2-D model

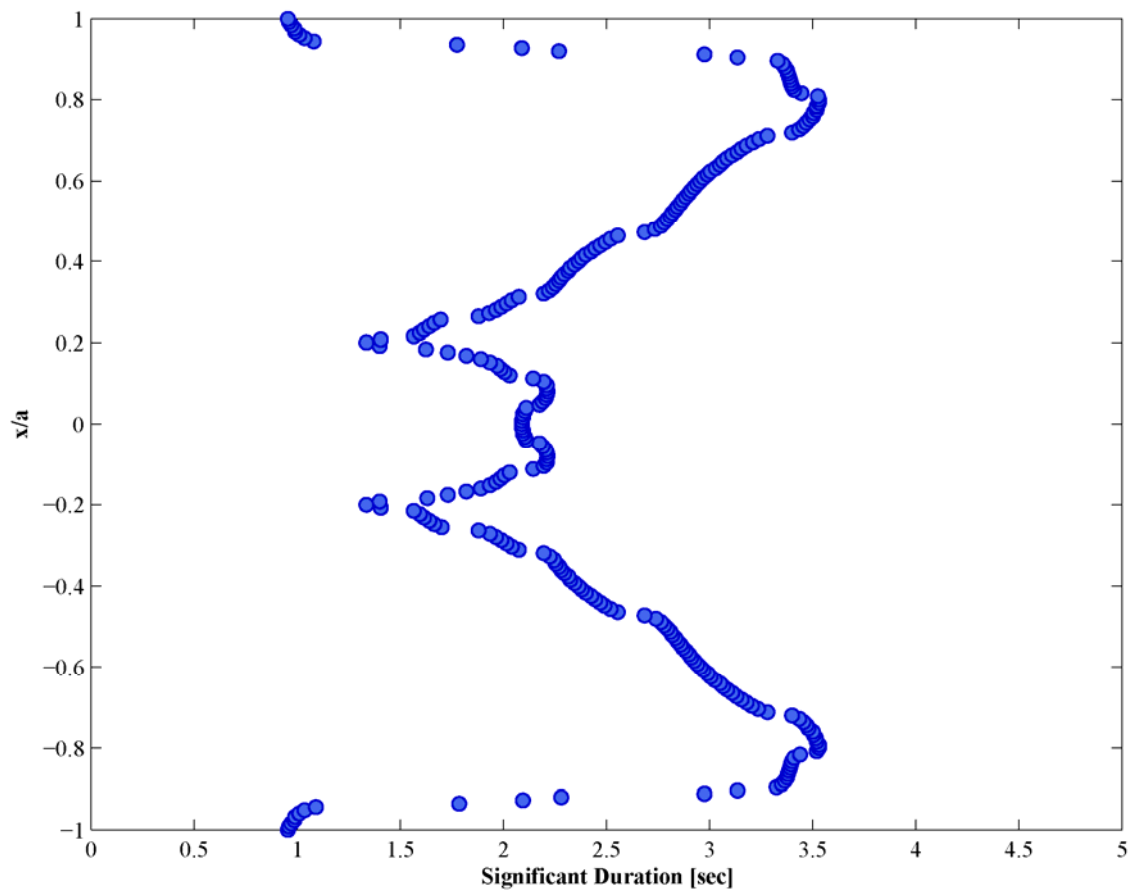


**Figure 5.15.** Significant duration of the surface displacement time histories shown in Figure 5.12

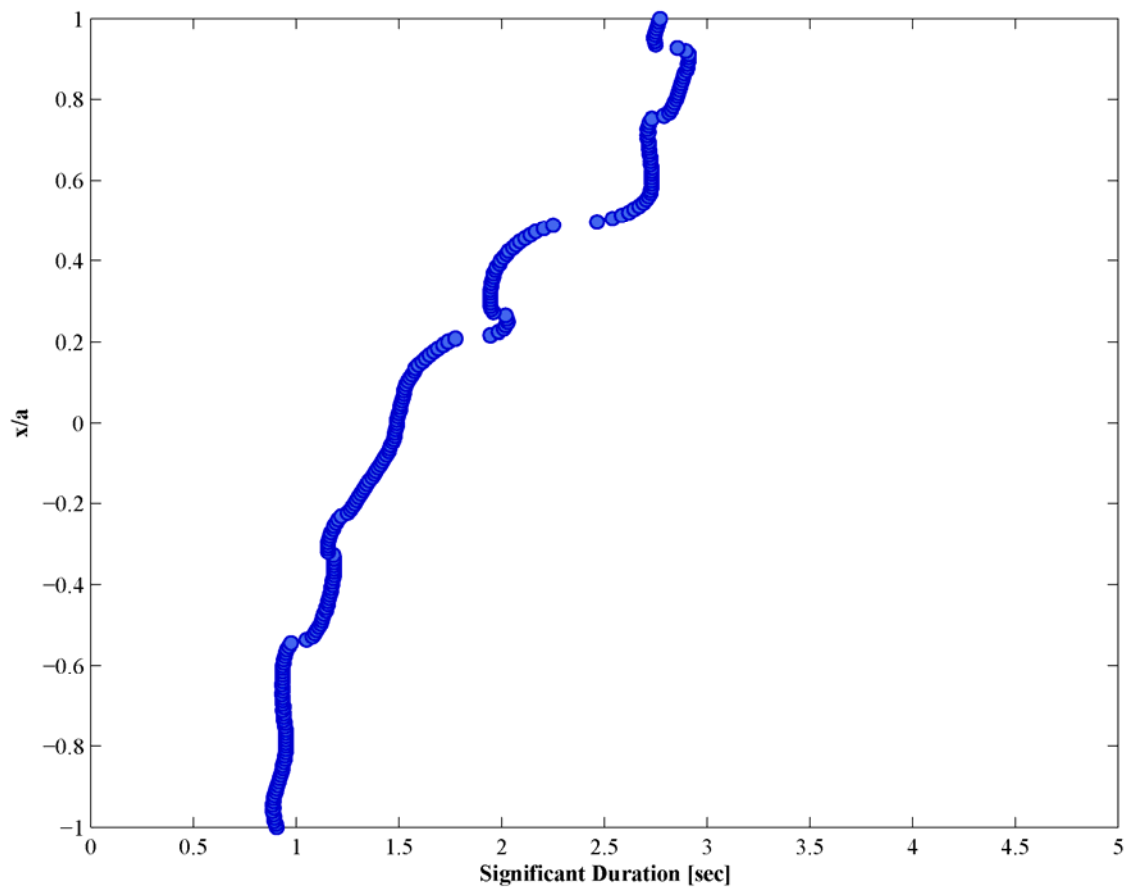


**Figure 5.16.** Significant duration of the surface displacement time histories shown in Figure 5.14

This simple parabolic basin model has illustrated the general features of basin effects in ground motions. The 2-D basin response shows high amplitudes at low frequencies that can not be captured by a 1-D model. The surface waves generated at the basin edges may generate complex surface amplitude patterns and longer surface ground motions that also can not be predicted by using a 1-D analysis. The influence of the incident angle on ground motion amplitude and spatial variability is significant.

### 5.6. Basin Effects in the Upper Mississippi Embayment

The method presented herein has been used to evaluate the 2-D non-linear seismic response of the Upper Mississippi Embayment. The ground response analyses were performed at an East-West cross-section passing through Memphis, TN as shown in Figure 5.1 and Figure 5.17.

The sediments of the Upper Mississippi Embayment can be classified in two different categories: the Lowlands and Uplands profiles, which are described in Chapter 2. Figure 2.1 shows the extent of each soil category and Figure 3.14 shows the shear-wave velocity profiles for both geologic deposits. The method cannot incorporate lateral heterogeneities inside the basin and therefore both profiles cannot be considered at the

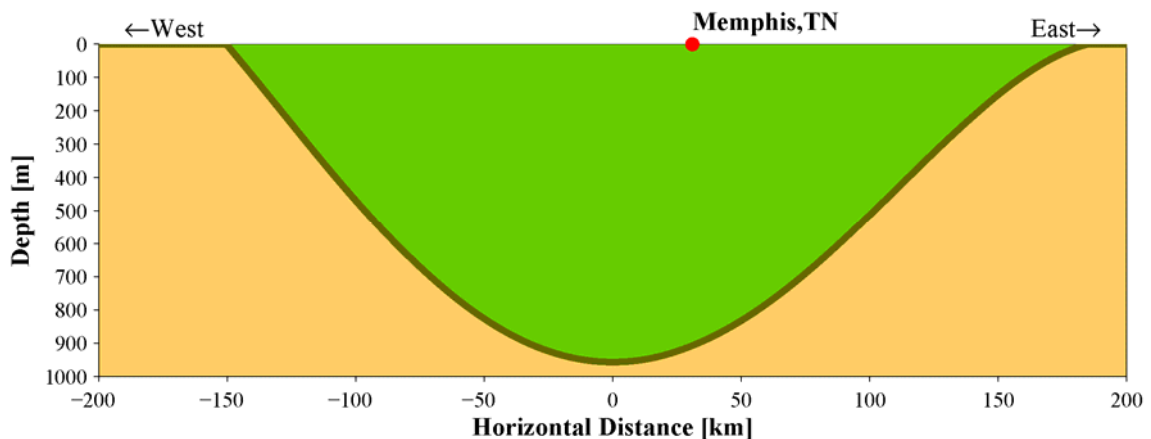


**Figure 5.17.** Model of the Upper Mississippi Embayment implemented in the analyses

same time. Figure 3.62 shows that both soil profiles induce similar one-dimensional ground motion amplification in the low-frequency range, which is where basin effects are expected to occur. For these reason, only the Lowlands shear-wave velocity profile was implemented in the simulations. The shear-wave velocity of the half-space corresponds to the value at a depth of 1 km of the crustal velocity model developed by Catchings (1999) for the city of Memphis, TN. This shear-wave velocity value is 3520 m/sec.

As discussed previously the shear modulus and damping are critical dynamic properties of the soil to evaluate the non-linear behavior of site response (Kramer, 1996). During dynamic shear loading shear modulus decreases and damping values increase with shear strain amplitude. Usually the shear modulus is normalized to the maximum shear modulus,  $G_{\max}$ , and the variation of this modulus ratio with shear strain is described by a modulus reduction curve. The damping ratio is defined as the ratio of the strain energy dissipated in one loading cycle to the maximum strain energy, and its variation with shear strain is described by a damping ratio curve. Generic modulus reduction and damping ratio curves developed by EPRI (1993) were used in the simulations. These sets of curves were also used in Chapter 3 to develop soil attenuation relationships in the Upper Mississippi Embayment. Figure 3.15 and Figure 3.16 show the mean modulus reduction and damping ratio curves along with their depth range of applicability. Only the upper 150 m of the soil column was allowed to undergo non-linear behavior as discussed in Chapter 3.

Figure 3.19 shows the variation of mass density and small-strain damping ratio with depth implemented in the simulations. The mass density profile was taken from Romero (2001). The initial value of small-strain damping ratio profile is based on the damping curves developed by EPRI (1993).

### 5.6.1. Application of method to the Upper Mississippi Embayment

The value of the distance  $d_s$  provided by Equation 5.22 does not ensure convergence of the method when applied to the Upper Mississippi Embayment. The convergence distance  $d_s$  was found to be 10% of the maximum depth of the basin model, which is similar to the convergence criteria suggested by Zeng and Benites (1998). Due to the large extent of the Embayment, Equation 5.21 and Equation 5.23 give large numbers of collocation points,  $W$ , and point sources,  $N$ , and large numbers of discrete wavenumbers,  $M$ , must be used to ensure convergence. This results in a large, full, ill-conditioned matrix  $\mathbf{A}$  in Equation 5.20. To solve the system of equations defined in Equation 5.20, a regularization method was used to ensure a stable solution. The regularization approach used is the Tikhonov method which is implemented in a Matlab script by Hansen (2001).

The main idea of the Tikhonov regularization method is to find a regularized solution  $\mathbf{b}_\lambda$  such that (Hansen, 2001; Santamarina and Fratta, 1998):

$$\mathbf{b}_\lambda = \arg \min \left\{ \|\mathbf{A} \cdot \mathbf{b} - \mathbf{f}\|_2^2 + \lambda^2 \|\mathbf{L} \cdot (\mathbf{b} - \mathbf{b}_0)\|_2^2 \right\} \quad 5.42$$

where  $\lambda$  is the regularization parameter,  $\mathbf{L}$  is usually the identity matrix  $\mathbf{I}$  or a discrete derivative operator, and  $\mathbf{b}_0$  is an initial estimate of the solution. In this study  $\mathbf{L} = \mathbf{I}$  and  $\mathbf{b}_0 = 0$ , which reduces Equation 5.42 to:

$$\mathbf{b}_\lambda = \arg \min \left\{ \|\mathbf{A} \cdot \mathbf{b} - \mathbf{f}\|_2^2 + \lambda^2 \|\mathbf{b}\|_2^2 \right\} \quad 5.43$$

The solution of Equation 5.43 implemented by Hansen (2001) is:

$$\mathbf{b}_\lambda = \sum_{i=1}^n x_i \cdot \frac{\mathbf{u}_i^T \mathbf{f}}{\sigma_i} \cdot \mathbf{v}_i \quad 5.44$$

where  $x_i$  are filter factors,  $n$  is the number of columns of matrix  $\mathbf{A}$ ,  $\mathbf{u}_i$  and  $\mathbf{v}_i$  are the left and right singular vectors of  $\mathbf{A}$ , and  $\sigma_i$  are the singular values of  $\mathbf{A}$ , which are given by the singular value decomposition of matrix  $\mathbf{A}$ :

$$\mathbf{A} = \mathbf{U} \cdot \mathbf{\Sigma} \cdot \mathbf{V}^T = \sum_{i=1}^n \mathbf{u}_i \cdot \sigma_i \cdot \mathbf{v}_i^T \quad 5.45$$

The filter factors  $x_i$  are computed as (Hansen, 2001):

$$x_i = \frac{\sigma_i^2}{\sigma_i^2 + \lambda^2} \quad 5.46$$

The regularization parameter  $\lambda$  is calculated using the plot of  $\|\mathbf{L} \cdot \mathbf{b}_\lambda\|_2$  versus  $\|\mathbf{A} \cdot \mathbf{b}_\lambda - \mathbf{f}\|_2$ , which is called the L-curve because when plotted in log-log space the curve resembles an L shape (Hansen, 2001). The vertical leg of the L-curve represent solutions where  $\|\mathbf{L} \cdot \mathbf{b}_\lambda\|_2$  is very sensitive to  $\lambda$ , and conversely the horizontal leg represent solutions where  $\|\mathbf{A} \cdot \mathbf{b}_\lambda - \mathbf{f}\|_2$  is very sensitive to  $\lambda$ . Therefore the optimal value of  $\lambda$  corresponds to the corner of the L-curve.

### 5.6.2. Results and Discussion

The soil amplification factors developed for the region by Toro and Silva (2001) using a 1-D model were used to compare the results of the 2-D response computed herein. To evaluate the effects of the non-linear soil behavior in site response, Toro and Silva (2001) used seven rock input motions corresponding to PGA's ranging from 0.05g to 0.75g. The rock ground motions corresponding to a PGA of 0.40g, 0.50g, and 0.75g were used as input motions in this study. Figure 5.18 shows the 5% damped response spectra of the input motions used in the simulations. Toro and Silva (2001) provide the earthquake parameters used to generate the input motions, which are required to estimate the ground motion duration as defined by Equation 5.39. The stress drop value and moment magnitude are 110 bars and **M** 6.5 for the three input motions, and the epicentral distances are 13 km, 9.3 km, and 3 km which correspond to PGA's of 0.40g, 0.50g, and 0.75g respectively.

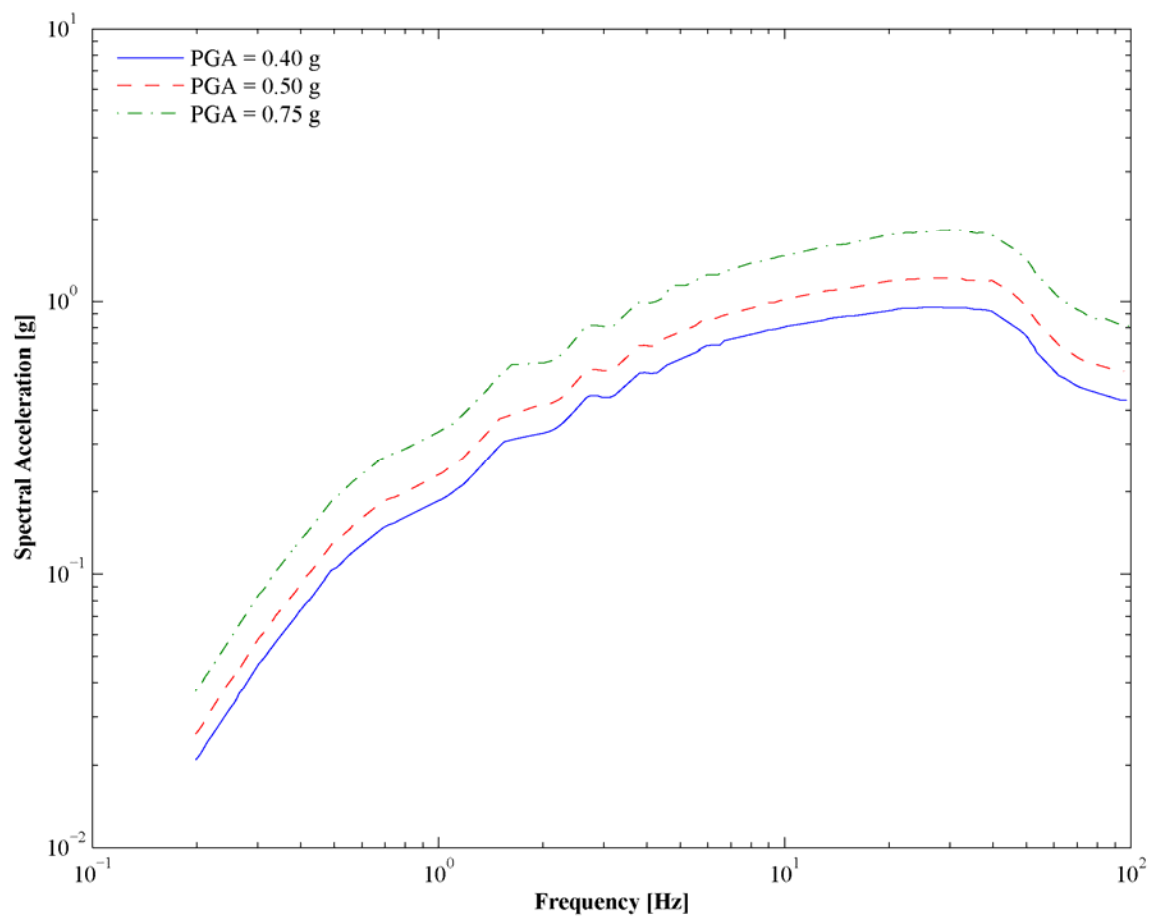
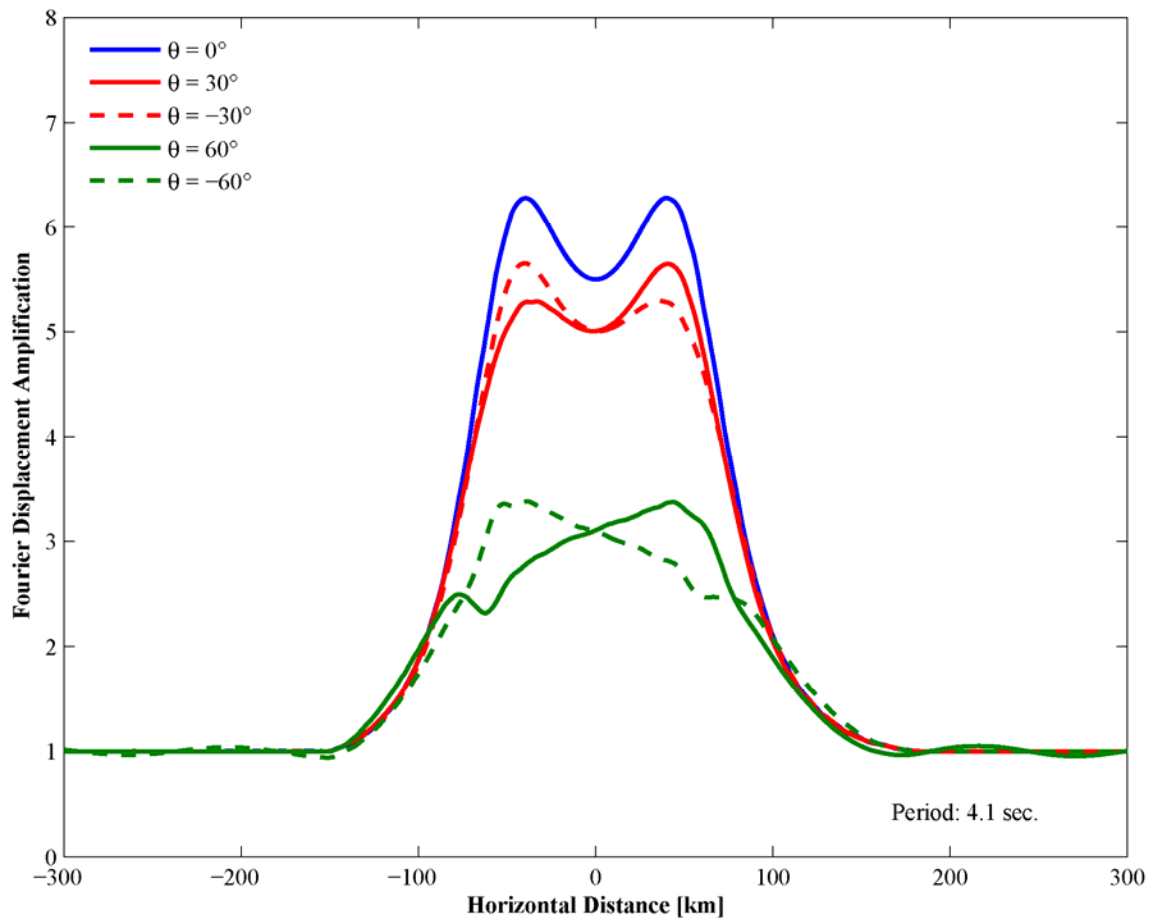


**Figure 5.18.** Response spectra of incident motions used in the analyses

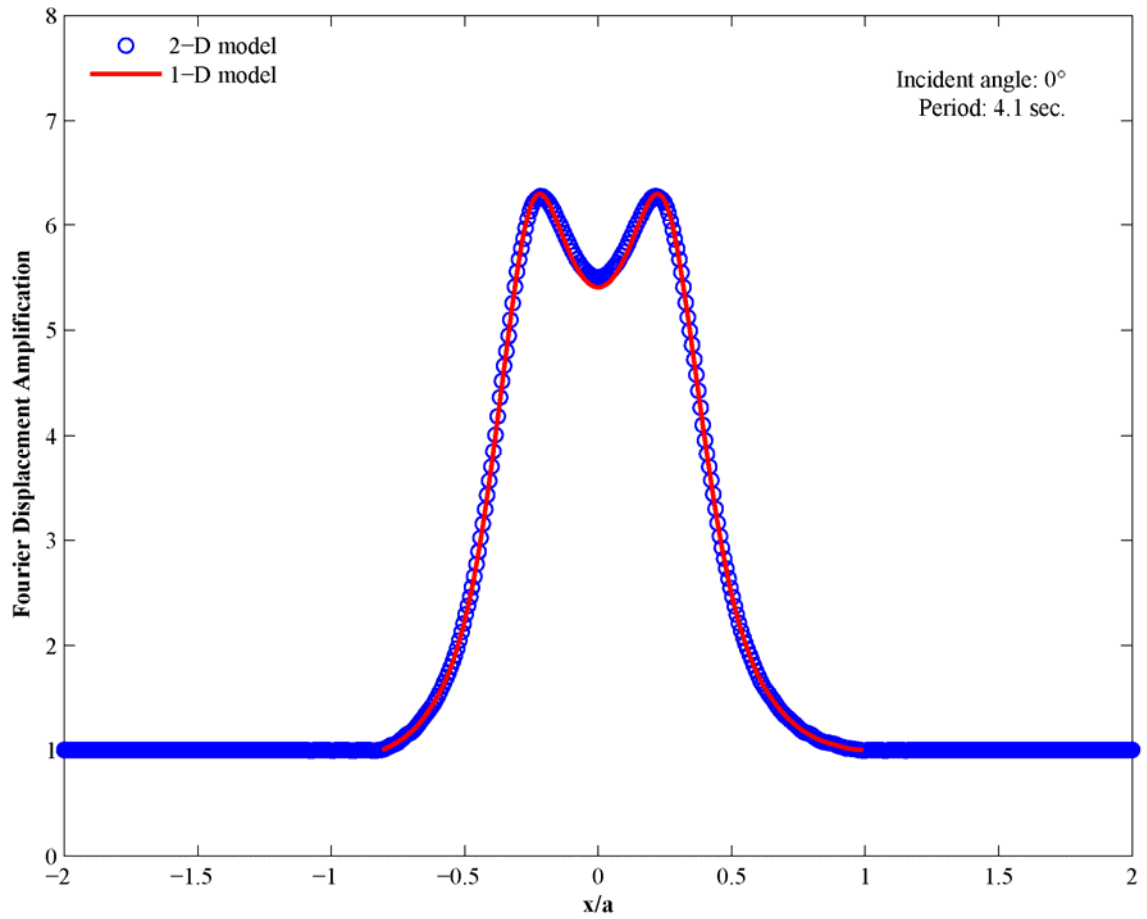
The analyses were performed for five angles of incidence including  $0^\circ$ ,  $30^\circ$ ,  $-30^\circ$ ,  $60^\circ$ , and  $-60^\circ$ . Negative angles were considered in the analyses to evaluate the symmetry of the model of the Embayment. Due to limited computational resources, the ground response analyses were performed for periods between 2 and 10 seconds. For shorter periods (i.e. high frequencies), the size of matrix **A** in Equation 5.20 is very large and difficult, if not impossible, to handle with the available computer resources. However, as confirmed below, basin effects were expected to occur in the long-period range. The minimum period used herein matches the minimum period implemented by Saikia et al. (2006) when evaluating the effects of the Mississippi Embayment on the amplification of ground motions. Saikia et al. (2006) also used this lower bound due to the limitation on computer resources.

Figure 5.19 compares the Fourier displacement amplification with respect to the free-field conditions for the five angles of incidence. Only small differences are observed between the response of the model to positive and negative angles, and therefore the model can be considered symmetric. Furthermore, in the context of probabilistic seismic hazard analysis, it is important to consider the average effects of all possible earthquakes of concern, which in this case come from the New Madrid seismic zone as indicated in Chapter 3. Therefore the results presented herein will be calculated as the average response of negative and positive incident angles.

Figure 5.20 through Figure 5.22 compare the 1-D and 2-D horizontal distribution of the Fourier displacement amplification with respect to the free field for the five angles of incidence and a period of 4.1 seconds. The input motion corresponds to the ground motion with PGA of 0.40 g. The 1-D response was calculated using the propagator matrices formulation provided by Ben-Menahem and Singh (1981). The Fourier amplification shown in Figure 5.21 and Figure 5.22 was calculated as the average of the response of negative and positive angles. It can be observed from the figures that there is no difference between the response of 1-D and 2-D models. This good agreement is due



**Figure 5.19.** Fourier displacement amplification at the surface of the Upper Mississippi Embayment



**Figure 5.20.** Comparison of 1-D and 2-D Fourier displacement amplifications vs. distance for the incident motion with PGA of 0.40g and incident angle of  $0^\circ$

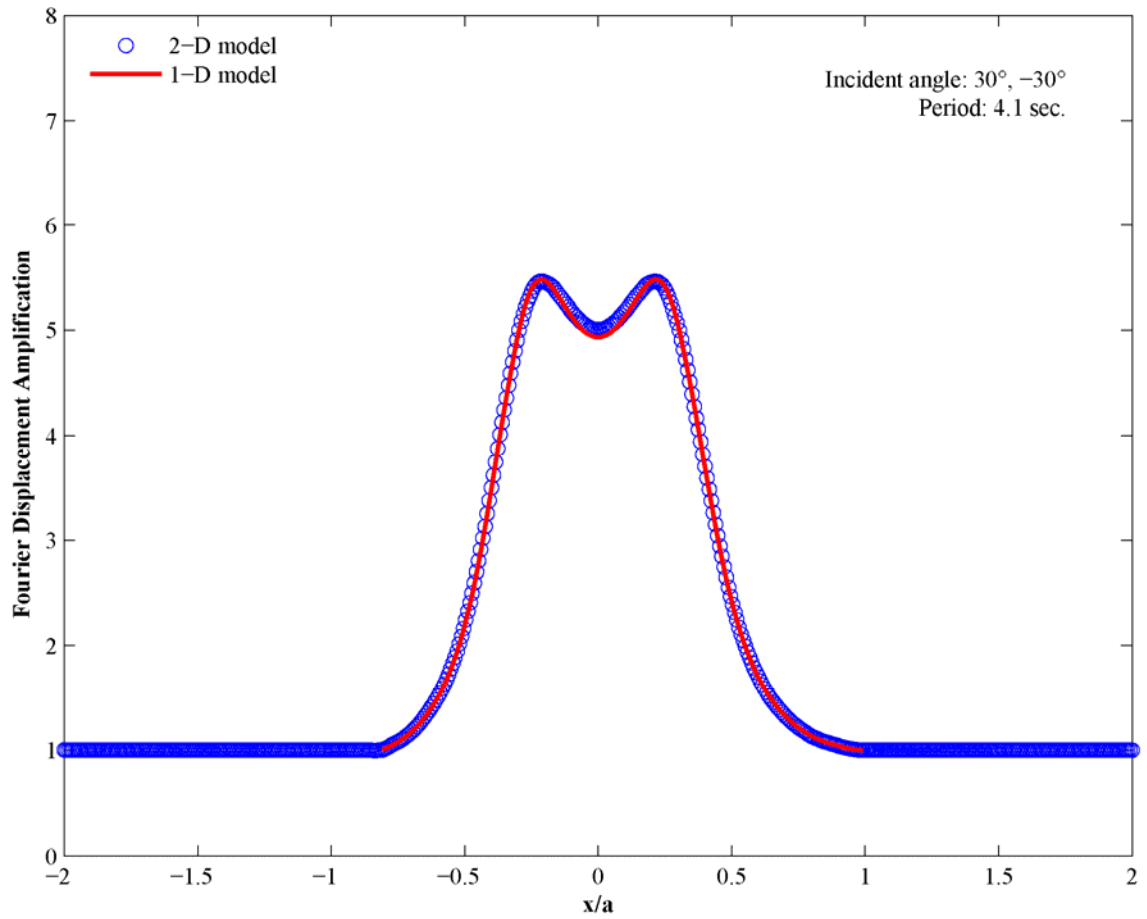


**Figure 5.21.** Comparison of 1-D and 2-D Fourier displacement amplifications vs. distance for the incident motion with PGA of 0.40g and incident angles of  $30^\circ$  and  $-30^\circ$

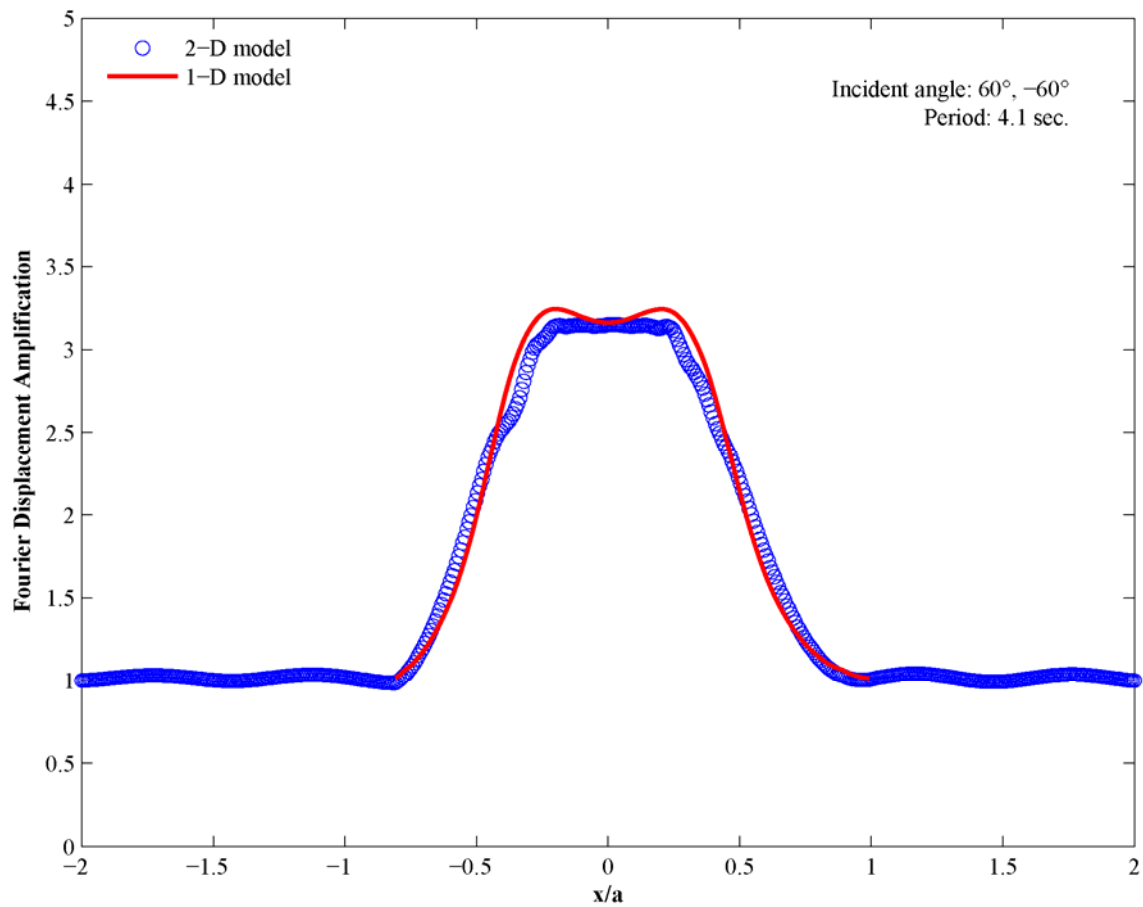


**Figure 5.22.** Comparison of 1-D and 2-D Fourier displacement amplifications vs. distance for the incident motion with PGA of 0.40g and incident angles of  $60^\circ$  and  $-60^\circ$

to the geometry of the Embayment as discussed later. Similar results were obtained for other spectral periods as shown in Figure 5.23. Figure 5.24 through Figure 5.26 compare the same Fourier displacement amplification for different locations at the surface of the Embayment. As shown in Figure 5.9 and Figure 5.11, 2-D effects are more evident at the center of the basin for vertical incidence. However, Figure 5.24 shows a good agreement between 1-D and 2-D Embayment models. For incident angles different than  $0^\circ$ , 2-D effects are more evident towards the edges of the basin as illustrated in Figure 5.10 and Figure 5.13. Figure 5.25 and Figure 5.26 show no significant difference between the Embayment response computed by 1-D and 2-D models.

Figure 5.27 to Figure 5.29 compare the 1-D and 2-D soil amplification for the seven Embayment depth categories used in Toro and Silva (2001). The response spectra were calculated from the Fourier spectra using the method proposed by Pfaffinger (1983). The 2-D amplification corresponds to the average of the response due to the five incident angles. For the central part of the Embayment (i.e. sediments depth from 30 to 1220 m) no difference is observed between the 1-D and 2-D models. However, for Embayment depths less than 30 m (i.e. the edges of the basin) and periods longer than 4 seconds, there is a significant difference between the 1-D and 2-D response. In these cases, the 2-D model predicts higher amplification and displays the characteristics of basin edge effects as defined by Kawase (1996; 2003), where constructive interference occurs between basin-induced surface waves and direct body waves propagating from the bottom of the basin. According to the Embayment model shown in Figure 5.17, basin edge effects are observed in areas up to 3 km from the west edge and 10 km from the east edge. These observations are consistent with the results of Saikia et al. (2006), where basin effects were observed only in a narrow area along the basin edge. Saikia et al. (2006) attributed these effects to the very strong velocity contrast between the rock and the upper sediments.

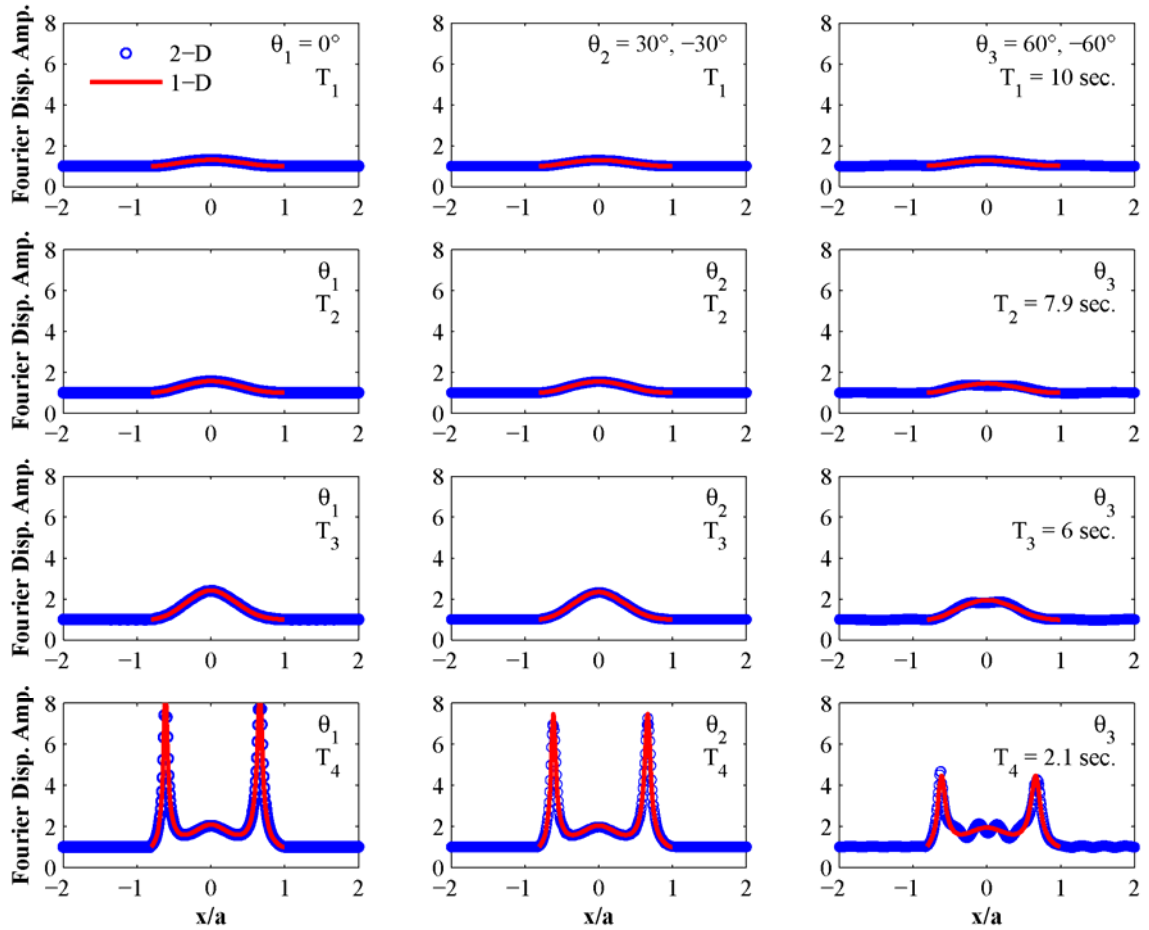


**Figure 5.23.** Comparison of 1-D and 2-D Fourier displacement amplifications vs. distance and spectral period for the incident motion with PGA of 0.40g

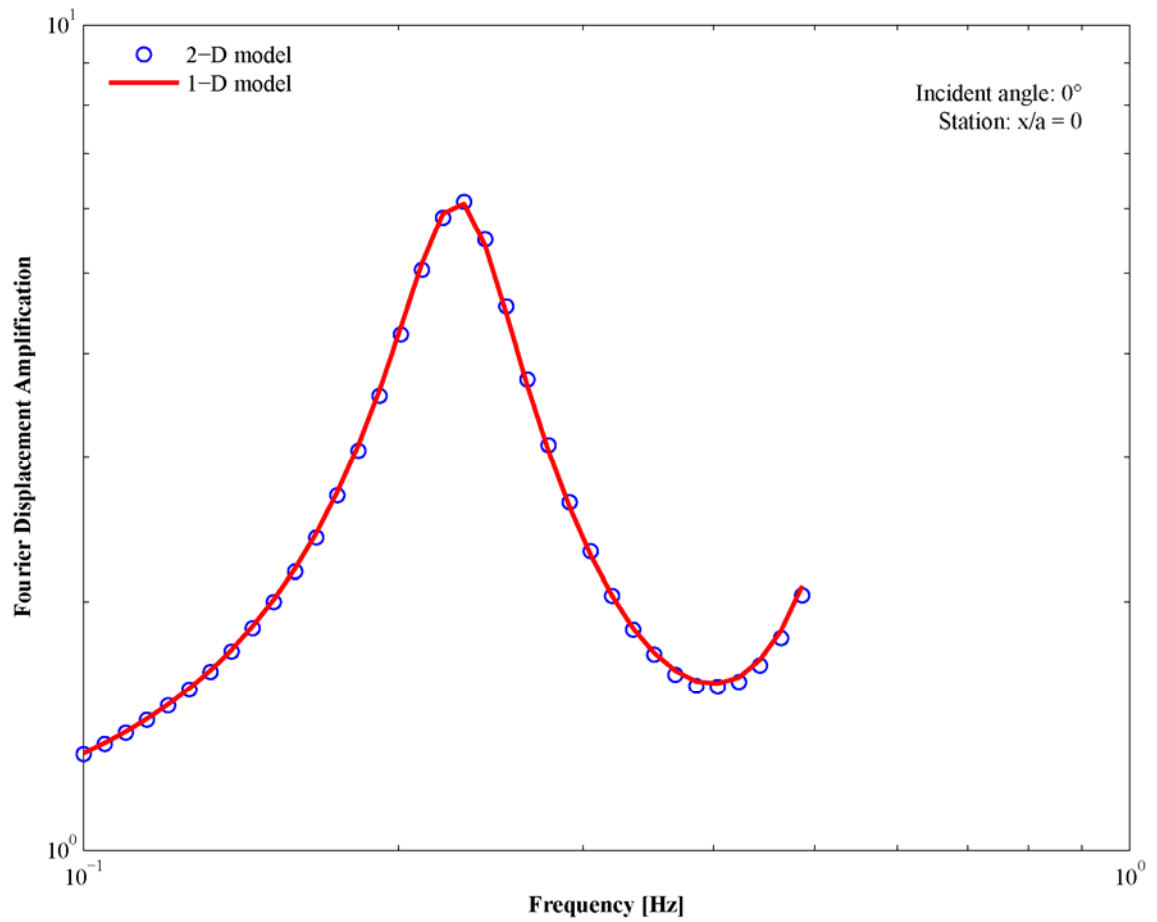


**Figure 5.24.** Comparison of 1-D and 2-D Fourier displacement amplifications vs. frequency for the incident motion with PGA of 0.40g and incident angle of  $0^\circ$

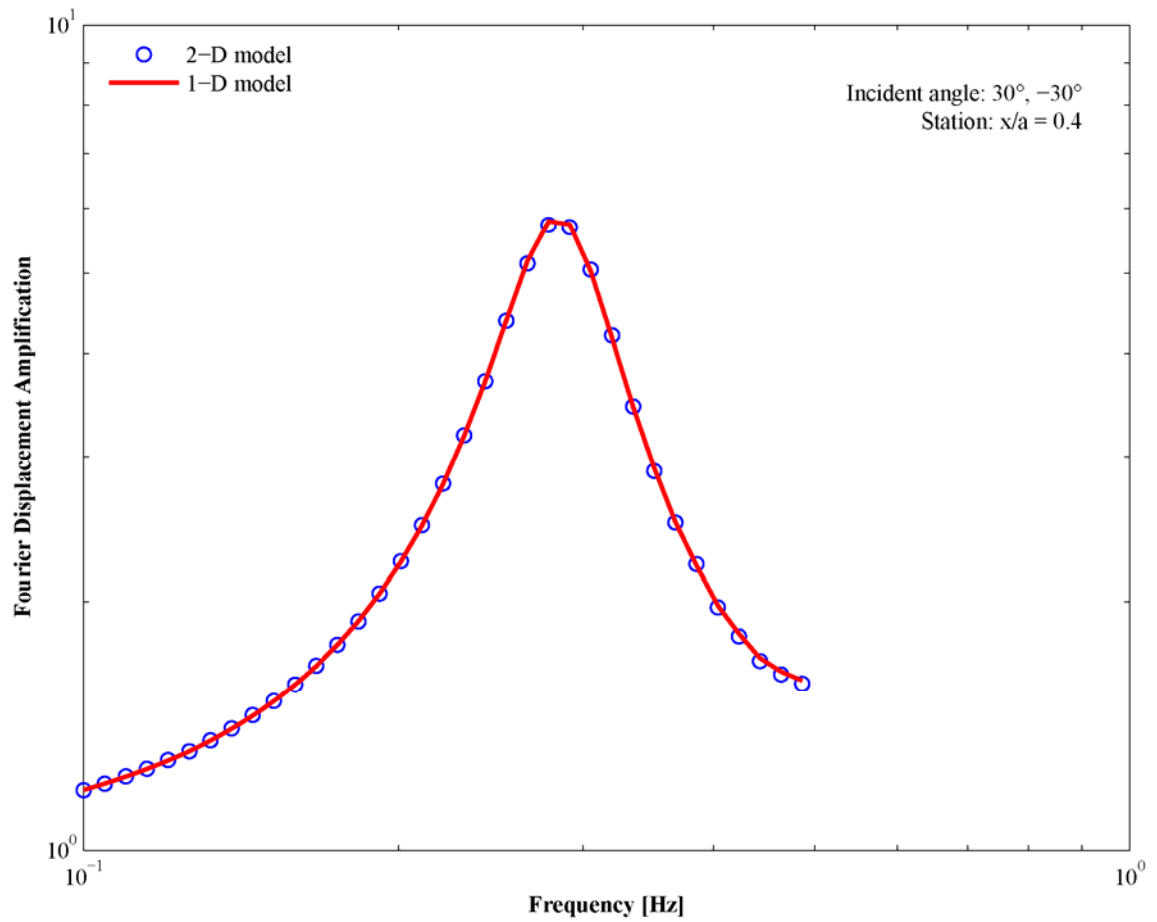


**Figure 5.25.** Comparison of 1-D and 2-D Fourier displacement amplifications vs. frequency for the incident motion with PGA of 0.40g and incident angles of  $30^\circ$  and  $-30^\circ$

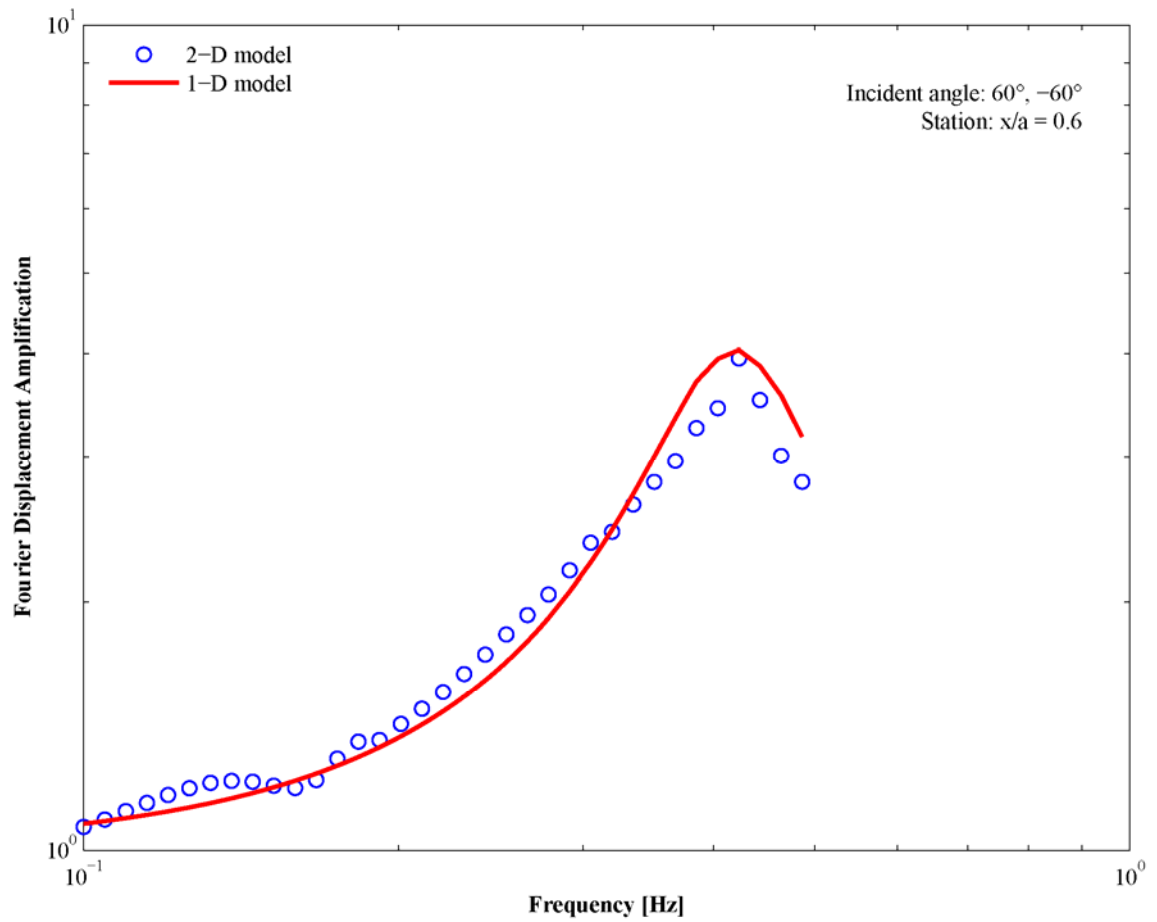


**Figure 5.26.** Comparison of 1-D and 2-D Fourier displacement amplifications vs. frequency for the incident motion with PGA of 0.40g and incident angles of  $60^\circ$  and  $-60^\circ$

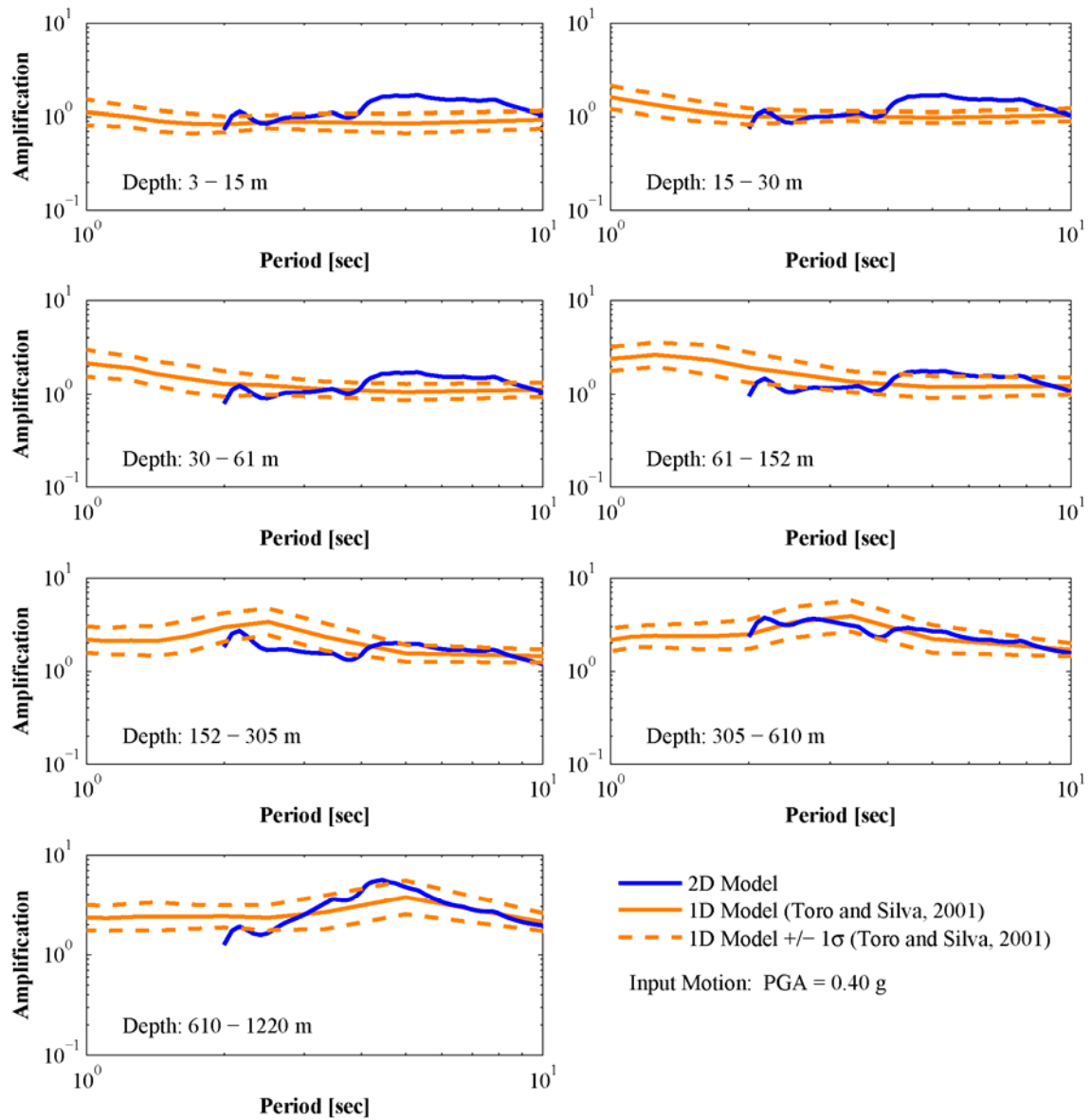


**Figure 5.27.** Comparison of 1D and 2D soil amplification for an incident motion with PGA of 0.40g

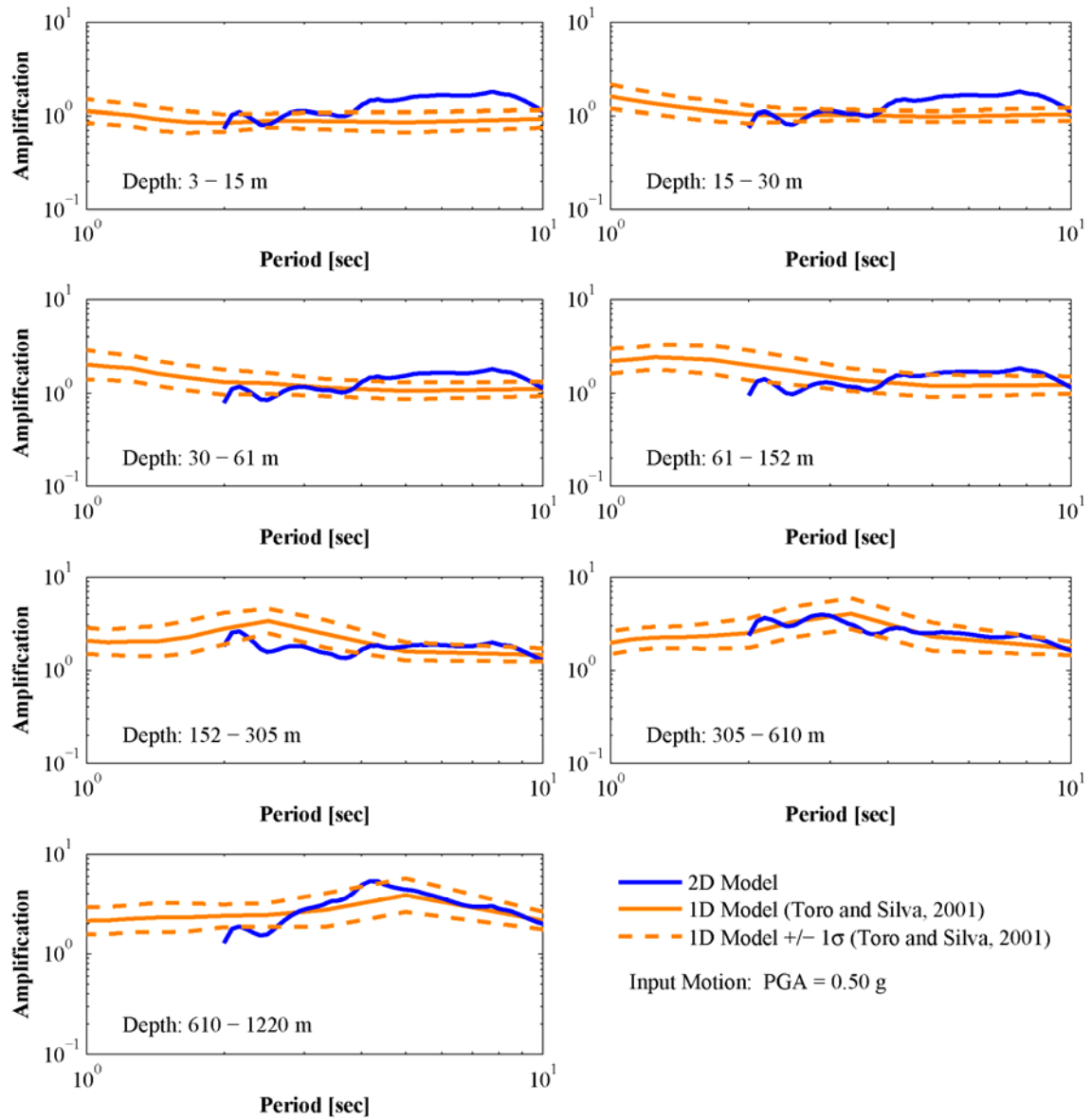


**Figure 5.28.** Comparison of 1D and 2D soil amplification for an incident motion with PGA of 0.50g

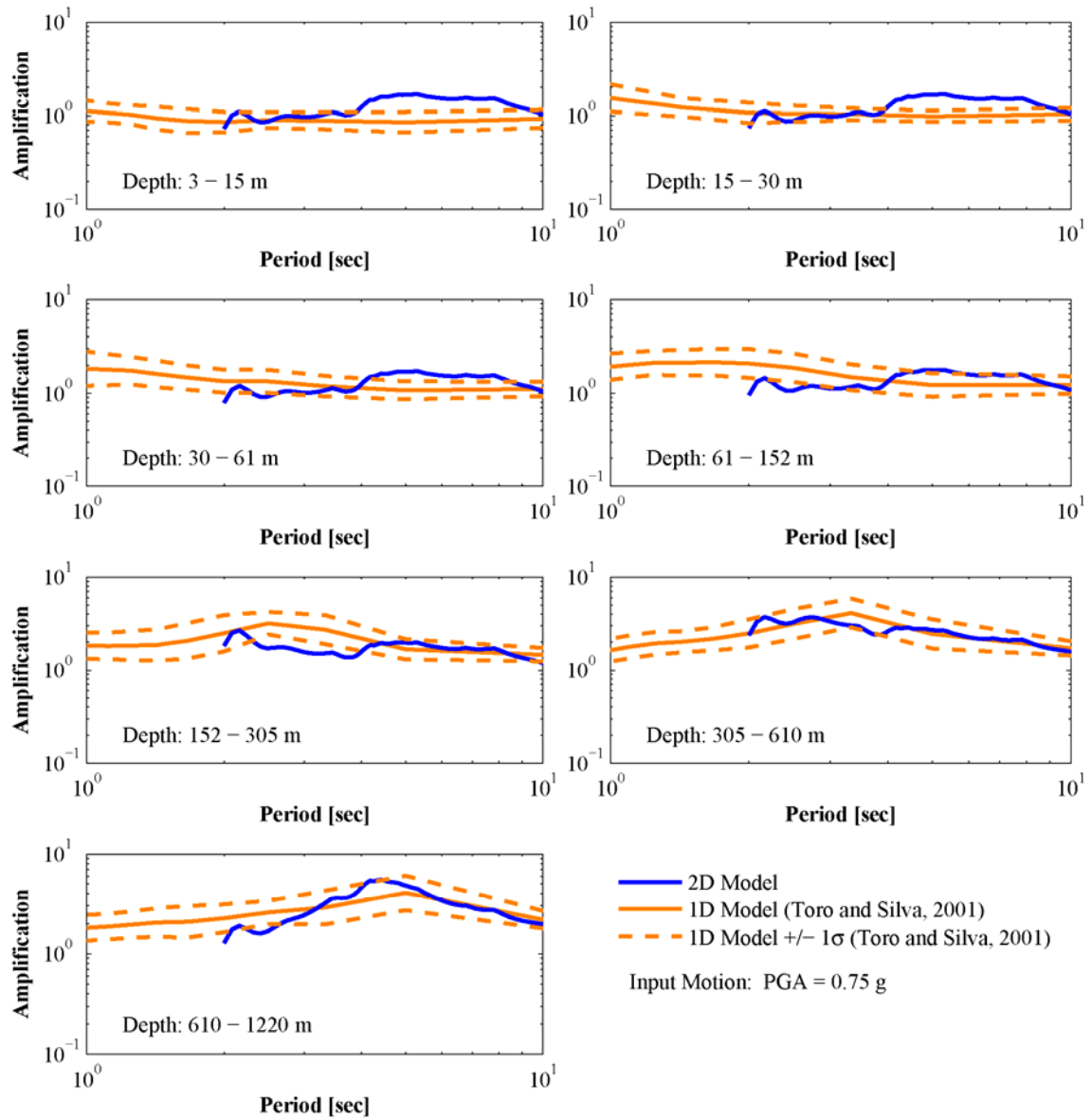


**Figure 5.29.** Comparison of 1D and 2D soil amplification for an incident motion with PGA of 0.75g

The good agreement between the seismic response of the 1-D and 2-D models, particularly in the central part of the basin, is due to the geometry of the Embayment. The longest spectral period considered in the analyses is 10 seconds, which corresponds to an incident wavelength of 35.2 km. This wavelength is approximately 10% of the total width of the model of the basin (~325 km) as shown in Figure 5.17. The longest wavelength is small compared to the dimension of the irregularity, and therefore the incident motion is not affected by the 2-D geometry of the basin. Longer wavelengths ( $T > 10$  sec.) comparable to the dimensions of the Embayment are needed to excite the 2-D response of the basin; however these wavelengths (or periods) are not important for engineering purposes. Input motions having shorter wavelengths with large values of angles of incidence might induce basin effects in the Embayment because the significant basin dimension decreases as the angle of incidence increases. However, as shown in Chapter 4, the seismic hazard in the Upper Mississippi Embayment is dominated by the New Madrid seismic zone, which is located in the central part of the Embayment. Therefore the probability of occurrence of a large earthquake generated outside this seismic source zone is low.

Previous studies have shown that 1-D site response analysis predicts reasonably accurate ground motion amplitudes in sedimentary basins with large width-to-depth ratios (i.e. shape ratio) (Yegian et al., 1994a, 1994b) as is the case in the Upper Mississippi Embayment with a shape ratio of approximately 300. Examples of basins with large shape ratios where 1-D models can be used to estimate site amplification are the Taipei basin with a shape ratio of 60 (Sokolov et al., 2000), the Turkey Flat test area near Parkfield, California with a shape ratio of 80 (Real et al., 2006; Stepp and Cramer, 1992), and Ashigara Valley test site in Japan with a shape ratio of 70 on the longitudinal axis (Kudo and Sawada, 1992; Shinozaki and Irikura, 1992). Kawase (2003) stated that for sedimentary basins with large shape ratios, body waves propagating vertically from the bottom of the structure arrive earlier at surface stations located in the central part of the

basin than surface waves generated at the edges, and therefore no 2-D effects are observed. Furthermore, high material damping can rapidly attenuate basin-induced surface waves (Bard and Riepl-Thomas, 2000). Studies at other basins have shown that the shape ratio is an important factor to consider when evaluating the 2-D response of these structures (Makra et al., 2005; 2002). It seems that for the central part of the Embayment, the 1-D model is sufficient to predict earthquake ground motions, confirming the conclusions of Saikia et al. (2006). These results are also consistent with Bodin and Horton (1999) and Bodin et al. (2001), who used microtremor observations to evaluate resonant periods of the Mississippi Embayment using the horizontal-to-vertical (H/V) spectral ratios. They found that the fundamental resonant periods correlate well with the depth of the Embayment, and that these periods can be estimated by assuming a 1-D wave propagation model.

The conclusions of this study are based on the amplitude of the ground motions. An analysis of the ground motions duration similar to the performed for the parabolic basin, will yield similar conclusions because the 1-D and 2-D Fourier amplitudes in the Embayment are the same. Furthermore, the numerical simulations of Saikia et al. (2006) were performed in the time domain and resulted in the same conclusions as this study.

Empirical studies of earthquakes recorded in Los Angeles basin concluded that basin depth is a good a predictor of basin effects (Field, 2000; Field et al., 2000; Hruby and Beresnev, 2003; Lee and Anderson, 2000; Mahdyar, 2002); however as discussed above, basin effects are related not only to basin depth, but also to the shape ratio. Furthermore, ground motion amplitudes based on basin depth alone result in higher amplification at sites located on the deepest part of the basin and cannot predict basin-edge effects as observed by Kawase (1996; 2003). This approach might be valid only for vertical incidence as illustrated in Figure 5.11. The empirical corrections proposed by Joyner (2000) are based on the distance from the edge where surface waves enter the

basin. This approach is more consistent with the displacement time histories shown in Figure 5.13 for incidence angles different than  $0^\circ$ .

An advantage of the method presented herein is that it can be easily incorporated into the stochastic method for ground motion simulation described in Chapter 3. The amplification function  $A(f)$  used to define the site effects term in Equation 3.1 can be computed using Equation 5.12, and the ground motions would be computed at locations horizontally distributed along the surface of the structure. However, the consideration of high frequencies in the analysis, particularly for large problems, like the Upper Mississippi Embayment, will be feasible only when significant computational resources are available. A disadvantage of the method is that it can only consider a flat surface and horizontal soil layers; however these assumptions are valid for many site response problems, or it can provide a first-order site response estimate for more complex geometries (Makra et al., 2002).

## **5.7. Conclusions**

The two-dimensional, non-linear seismic response of the Upper Mississippi Embayment has been evaluated by using a procedure that combines the indirect boundary element method and the discrete wavenumber representation of propagator matrices. Non-linear soil behavior was incorporated in the analysis by using an equivalent linear approach based on random vibration theory. This approach is more computationally efficient than domain methods since the discretization is performed only on the basin interface and the wave field in the sediments is estimated by propagator matrices, which permit a high resolution of the soil layers.

For the range of periods implemented in the analysis, no significant difference was observed between the soil amplification of the 1-D and 2-D models of the Upper Mississippi Embayment, except for sites located in a narrow region along the basin edge and periods longer than 4 seconds, where higher ground amplification was observed due

to basin-edge effects. Thus, basin effects are important for long-period structures located near the edges of the Embayment. If desired, the soil attenuation relationships developed in Chapter 3 can be corrected to account for higher amplification in the long period range ( $T \geq 4$  sec.) at shallow depths ( $\leq 30$  m); however most engineering applications in the Embayment will not be affected by basin effects.

The results obtained herein are consistent with the analyses performed by Saikia et al. (2006). In this study, only a 2-D model of Embayment was considered as opposed to Saikia et al. (2006) who implemented a 3-D model. However, this study incorporated a better characterization of the sediments by using a detailed shear-wave velocity profile and considered both edges of the basin. It is believed that both studies are complementary, and both conclude that basin effects in the Upper Mississippi Embayment are not important for earthquakes generated in the New Madrid seismic zone and sites located in the central part of the Embayment. This conclusion validates the use of a 1-D wave propagation approach in Chapters 3 and 4 when estimating earthquake ground motions in the region. A limitation of these studies is the lack of large-earthquake records to confirm the results obtained by numerical simulations.

An advantage of the method presented herein is that it can be easily incorporated into the stochastic method for ground motion simulation described in Chapter 2 to include 2-D effects. However, the consideration of high frequencies in the analysis, particularly for large problems like the Upper Mississippi Embayment, will be feasible only when significant computational resources are available. A disadvantage of the method is that it can only consider a flat surface and horizontal soil layers; however these assumptions are valid for many site response problems; in other cases it can provide a first-order site response estimate for more complex geometries.

## **CHAPTER 6**

### **SUMMARY, CONCLUSIONS, AND RECOMENDATIONS**

#### **6.1. Summary and Conclusions**

In this study, earthquake ground motions have been generated for the Upper Mississippi Embayment using a numerical wave propagation formulation. Source, path, and site effects have been considered simultaneously and the variability in the entire earthquake process has been incorporated. The effects of epistemic and aleatory uncertainties in the earthquake source, path, and site processes, the effects of non-linear soil behavior, and the effects of the geometry of the Embayment have been incorporated. The ground motions are intended to better characterize the seismic hazard in the Upper Mississippi Embayment by representing the amplitude and variability that might be observed in real earthquakes and to provide resources to evaluate the seismic risk in the region.

Chapter 3 describes the development of attenuation relationships for soil conditions in the Upper Mississippi Embayment. Typical geological units of the region, Embayment depth, and non-linear soil behavior were considered. Epistemic variability was accommodated with the use of three source models and three stress drop values. Aleatory variability was accommodated by the randomization of site, path, and site parameters. No other study of seismic hazard in the Upper Mississippi Embayment has incorporated epistemic and aleatory uncertainty in a manner as rigorous or complete as this study.

The consideration of epistemic variability in stress drop causes large difference in the mean ground motion amplitudes in the high-frequency range ( $f > 1$  Hz), illustrating the importance of this parameter when estimating high-frequency ground motions.

Epistemic variability in source model is an important factor to consider when estimating ground motion amplitudes of future earthquakes, particularly for areas with a low seismicity rate but capable of generating large earthquakes like in the CEUS. The soil attenuation relationships developed herein account for correlation among earthquake processes and therefore provide a direct approach for developing hazard-consistent soil motions that avoids difficulties involved in properly coupling probabilistic rock motions and site amplifications.

Chapter 4 documents the regional and site-specific seismic hazard analyses performed in the Upper Mississippi Embayment using the soil attenuation relationships developed in Chapter 3. Seismic hazard analyses were performed for seven selected cities in the Upper Mississippi Embayment. Regional analyses were also performed to develop probabilistic seismic hazard maps for the entire region. In general, probabilistic seismic hazard analyses conducted in this study are broadly comparable with probabilistic ground motions calculated in previous studies. However the UHS computed herein are believed to be more accurate since the variability in the entire earthquake process and site-specific conditions are included directly in the PSHA calculations by using soil attenuation relationships in the hazard integral.

Chapter 5 evaluates the two-dimensional effects of the geometry of the Upper Mississippi Embayment on earthquake ground motions in the region. The 2-D non-linear seismic response of the Upper Mississippi Embayment was evaluated by using a procedure that combines the indirect boundary element method and the discrete wavenumber representation of propagator matrices. Non-linear soil behavior was incorporated in the analysis by using an equivalent linear approach based on random vibration theory. This approach is more computationally efficient than domain methods since the discretization is performed only on the basin interface and the wave field in the sediments is estimated by propagator matrices that permit a high resolution of the soil layers.

For the range of periods implemented in the analysis, no significant difference was observed between the soil amplification of the 1-D and 2-D models, except for sites located in a narrow region along the basin edge and periods longer than 4 seconds, where higher ground amplification was observed due to basin edge effects. Thus, basin effects are important for long-period structures located near the edges of the Embayment. These observations validate the use of a 1-D wave propagation approach when estimating earthquake ground motions in most parts of the Embayment. A limitation of these studies is the lack of large-earthquake records to confirm the results obtained by numerical simulations.

The results of this study have been incorporated into MAEviz ([http://mae.ce.uiuc.edu/software\\_and\\_tools/maeviz.html](http://mae.ce.uiuc.edu/software_and_tools/maeviz.html)) to estimate surface ground motions in the Upper Mississippi Embayment. MAEviz is a seismic risk assessment software developed by the Mid-America Earthquake (MAE) Center and the National Center for Supercomputing Applications (NCSA).

## **6.2. Recommendations**

Recent site investigations in the southern part of the Upper Mississippi Embayment have determined shear modulus reduction and damping ratio curves that show a more linear behavior than the predicted by the EPRI (1993) curves (Silva, personal communication). The development of additional soil attenuations relationships using this new set of dynamic soil properties will help to better characterize their epistemic variability. As discussed in Chapter 3, the source model is an important factor to consider when estimating ground motions in the Embayment, and therefore the consideration of other source models (e.g., Boatwright and Choy, 1992; Haddon, 1996; Joyner, 1997) in the analyses will also improve the characterization of epistemic variability.

The selection of the method to conduct the seismic site response analysis in the development of the attenuation relationships may contribute to the uncertainty in soil ground motions estimation, and hence, the incorporation of other site response models such as a true non-linear analysis (e.g., Hashash and Park, 2001) and an equivalent linear analysis with frequency-dependent dynamic soil properties (e.g., Assimaki and Kausel, 2002; Kausel and Assimaki, 2002) will better characterize epistemic variability.

Few observed earthquakes of magnitudes and distances of engineering significance exist in the CEUS, particularly for the soil conditions of the Upper Mississippi Embayment, and an assessment of observed ground motion durations cannot be performed in the region at this moment. Therefore, the duration of the ground motion time histories developed herein might not represent the actual duration of large earthquakes observed at soil sites in the Embayment. Time domain scaling of ground motions is not recommended because the frequency content is modified and the process may generate unrealistic motions. Additional research is needed to evaluate the duration of ground motions in the Embayment and determine a methodology to incorporate it in the numerical simulations.

A limitation of the methodology described in Chapter 5 to evaluate basin effects is the homogenization of shear strains across each soil layer performed by the equivalent linear approach. Future work is required to evaluate the significance of this assumption on the results calculated by proposed method. The regions near the edges of the Embayment were greatly affected by basin-induced surface waves. A detailed analysis of these regions by other wave propagation methods (e.g., finite-difference and finite-element methods) will better characterize the seismic response of the edges of Upper Mississippi Embayment. Furthermore, the evaluation of basin effects using 2-D models of the Embayment at other latitudes will help to obtain a further insight of the effect of the geometry of the Embayment on earthquake ground motions in the region.

## **APPENDIX A**

### **MODEL REGRESSION COEFFICIENTS FOR THE SOIL ATTENUATION EQUATION**

This appendix includes an electronic supplement with the model regression coefficients for the soil attenuation relationships developed in Chapter 3. The regression coefficients are given in a portable document format (.pdf) file. Each set of coefficients is preceded by a header that indicates the combination of source model, stress drop case, soil profile, dynamic soil properties, and Embayment depth corresponding to that particular set. The format of the header is:

Regression Coefficients for Soil Attenuation Relationships by Fernandez (2007)

Upper Mississippi Embayment  
[Source model]  
[Stress drop case]  
[Soil profile]  
EPRI (1993) soil properties  
[Embayment depth]

The regression coefficients for the Atkinson and Boore (1995) source model are given only for the median stress drop value, as discussed in Chapters 3 and 4. The file containing the regression coefficients can be accessed [here](#).

## APPENDIX B

### SEISMIC HAZARD DEAGGREGATION

This appendix includes the seismic hazard deaggregation for the cities listed in Table 4.5 (except Memphis, TN, which is shown in Chapter 4) for peak ground acceleration (PGA) and 1-second spectral period and return period of 2475 years.

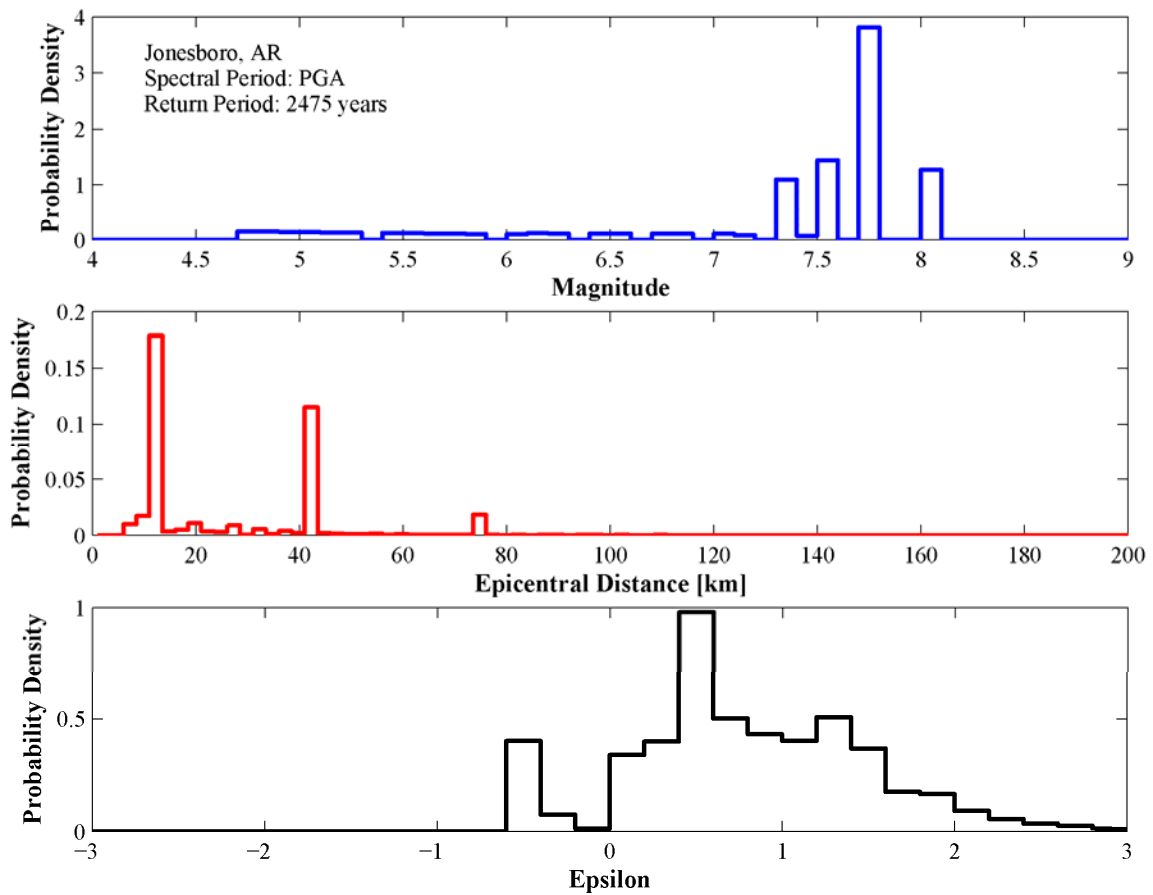


**Figure B.1** Hazard deaggregation for peak ground acceleration and return period of 2475 years in Jonesboro, AR

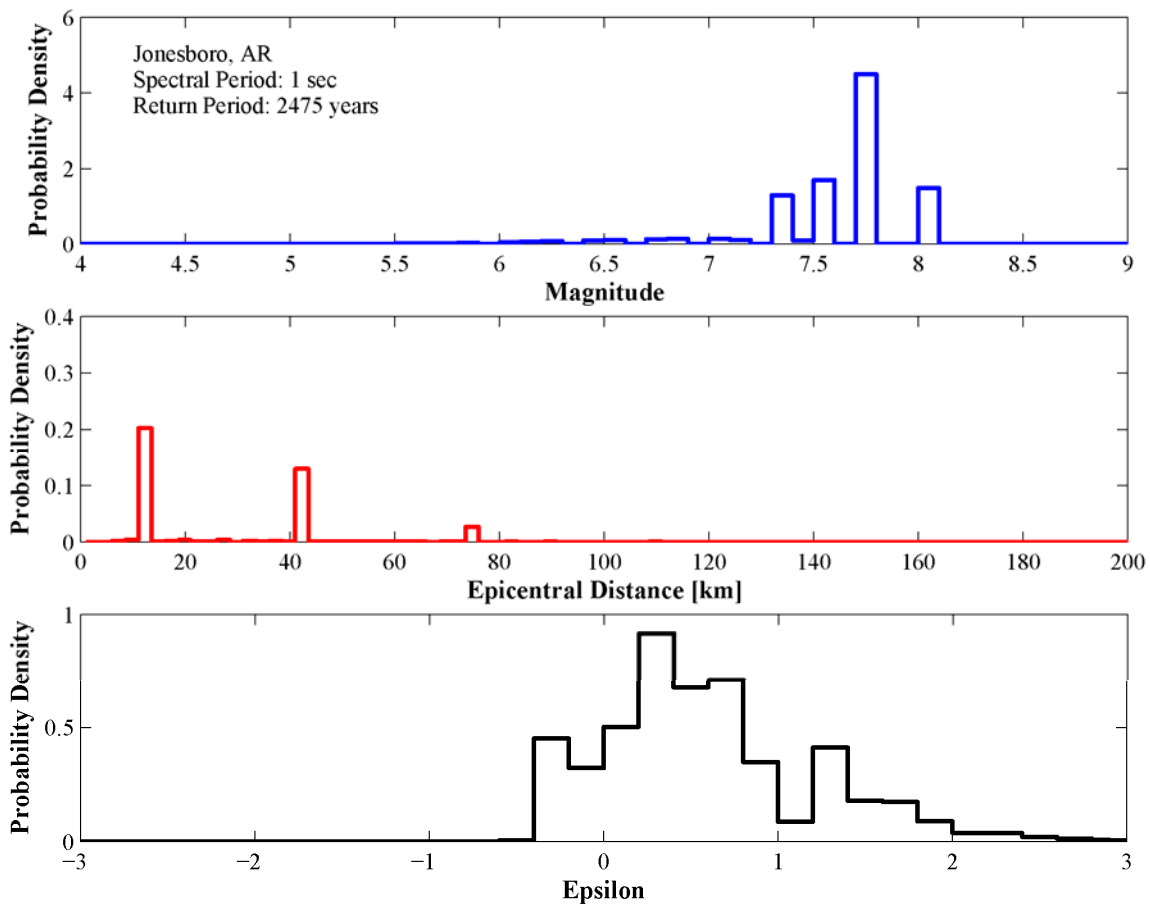


**Figure B.2.** Hazard deaggregation for 1-second spectral period and return period of 2475 years in Jonesboro, AR

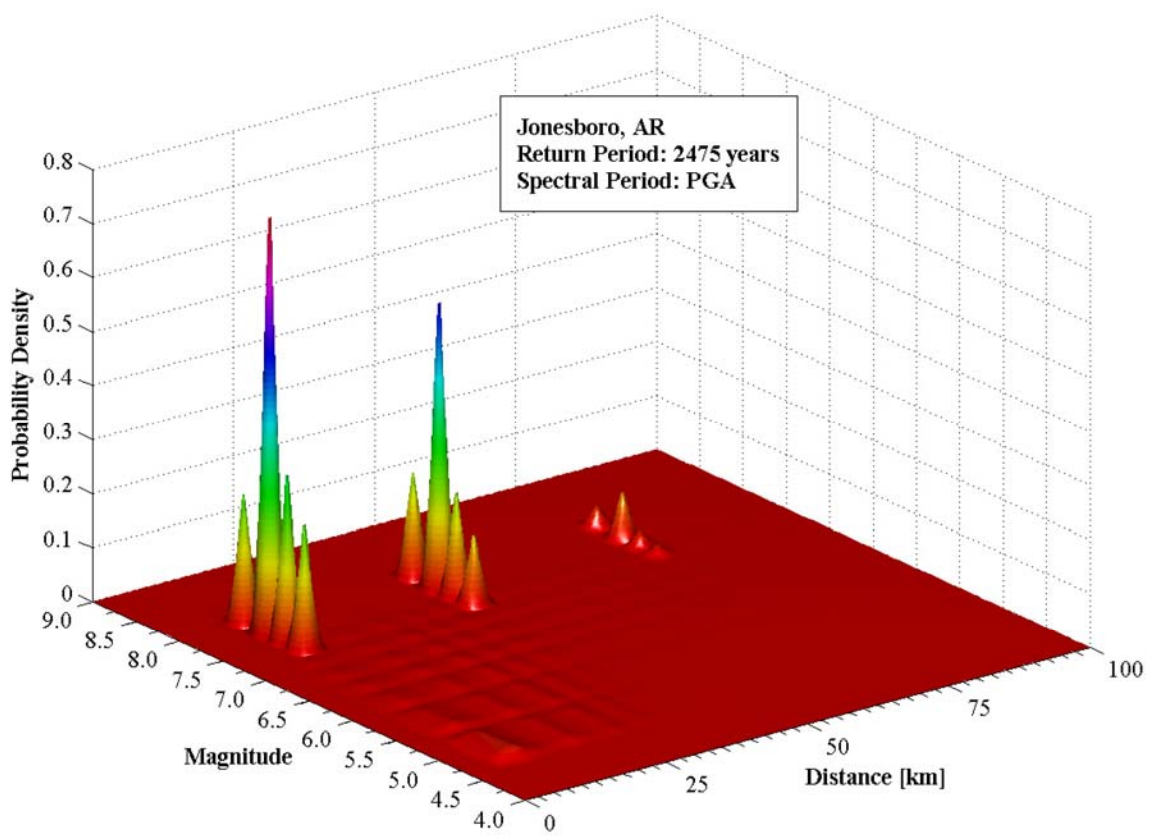


**Figure B.3.** Joint magnitude and distance hazard deaggregation for peak ground acceleration and return period of 2475 years in Jonesboro, AR

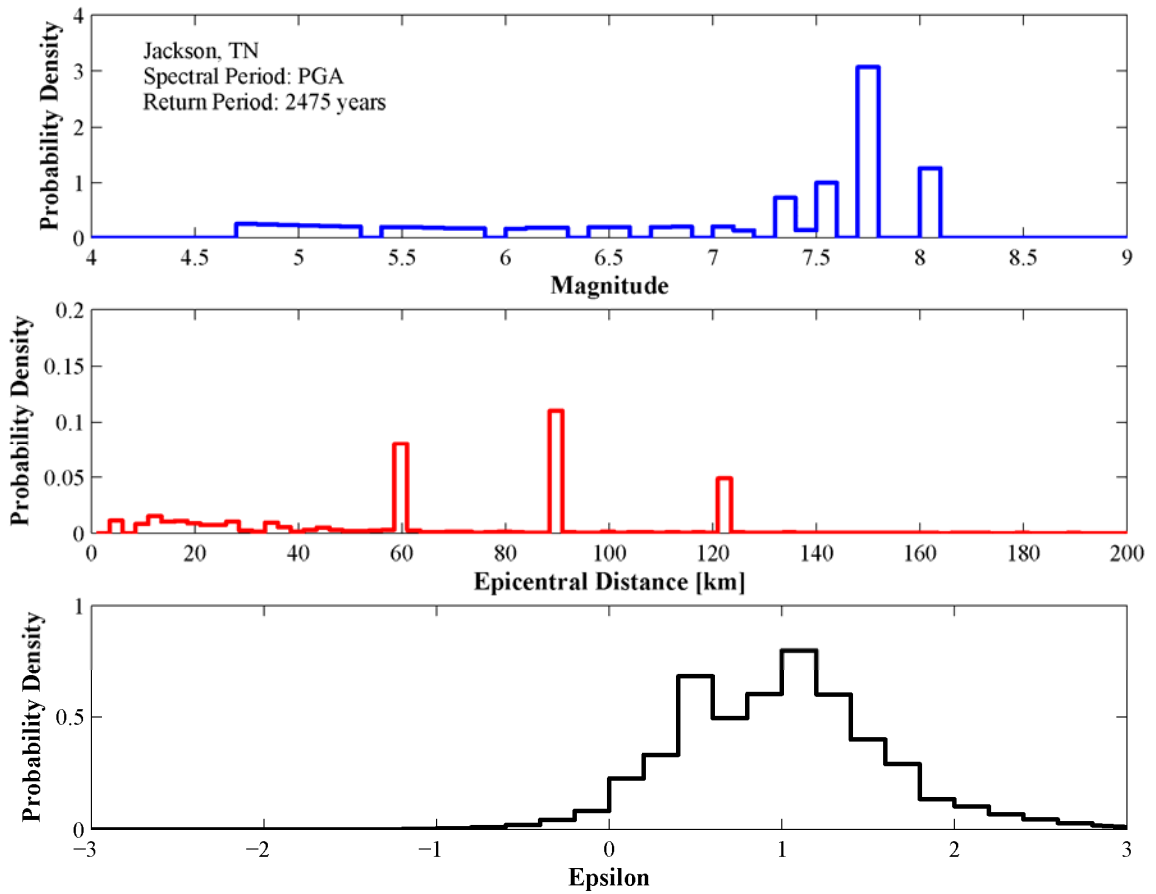


**Figure B.4.** Hazard deaggregation for peak ground acceleration and return period of 2475 years in Jackson, TN

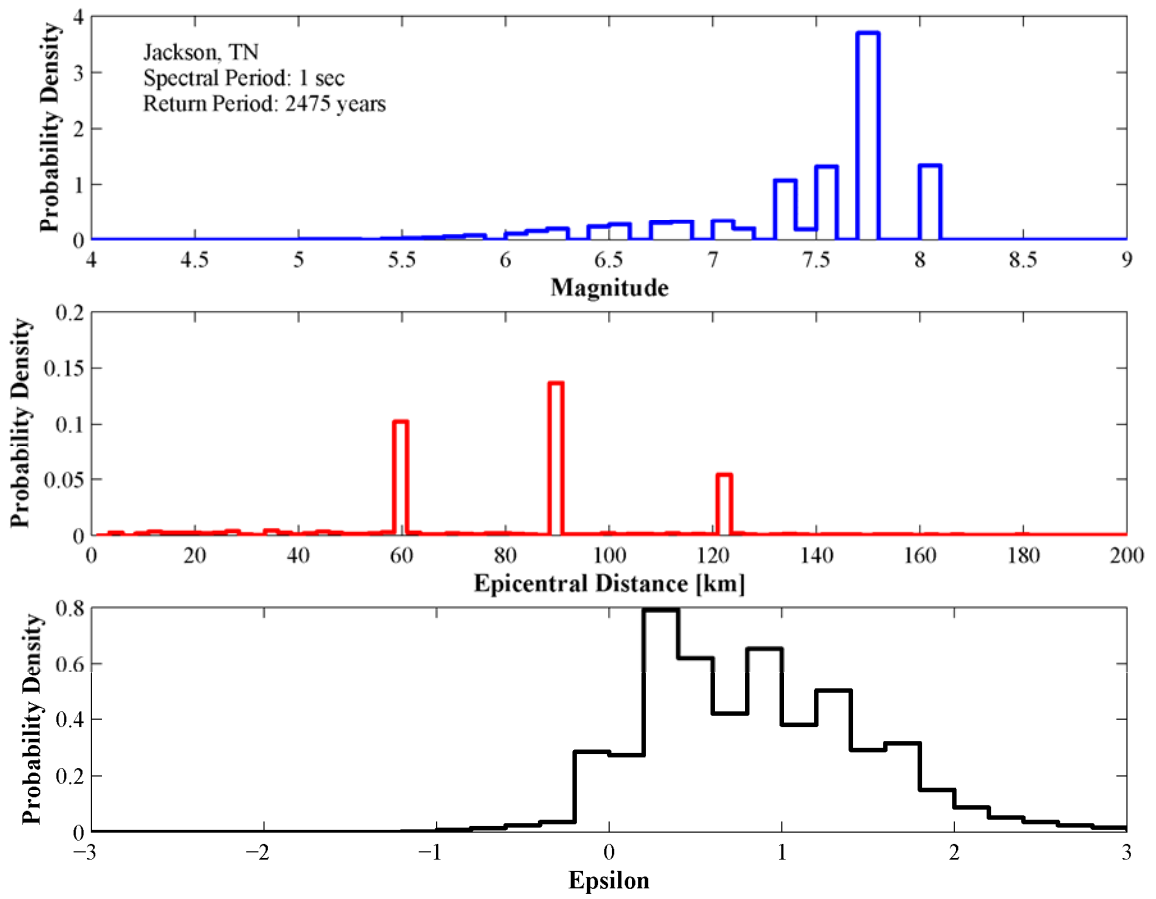


**Figure B.5.** Hazard deaggregation for 1-second spectral period and return period of 2475 years in Jackson, TN

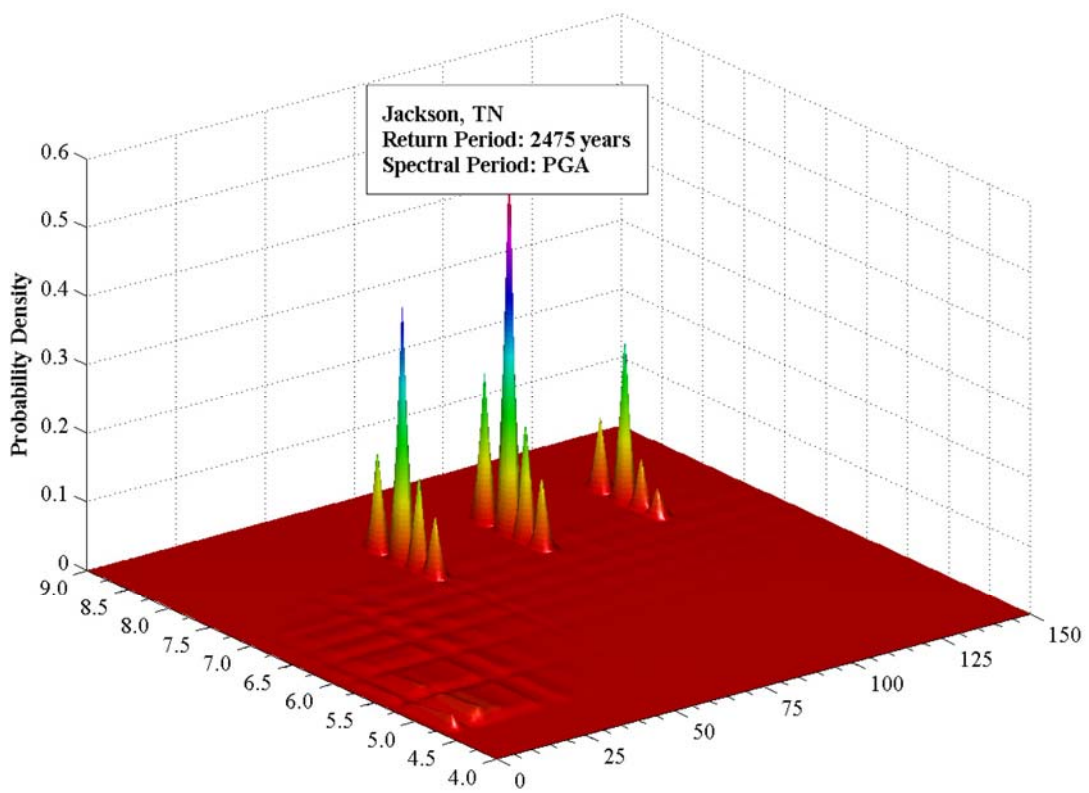


**Figure B.6.** Joint magnitude and distance hazard deaggregation for peak ground acceleration and return period of 2475 years in Jackson, TN

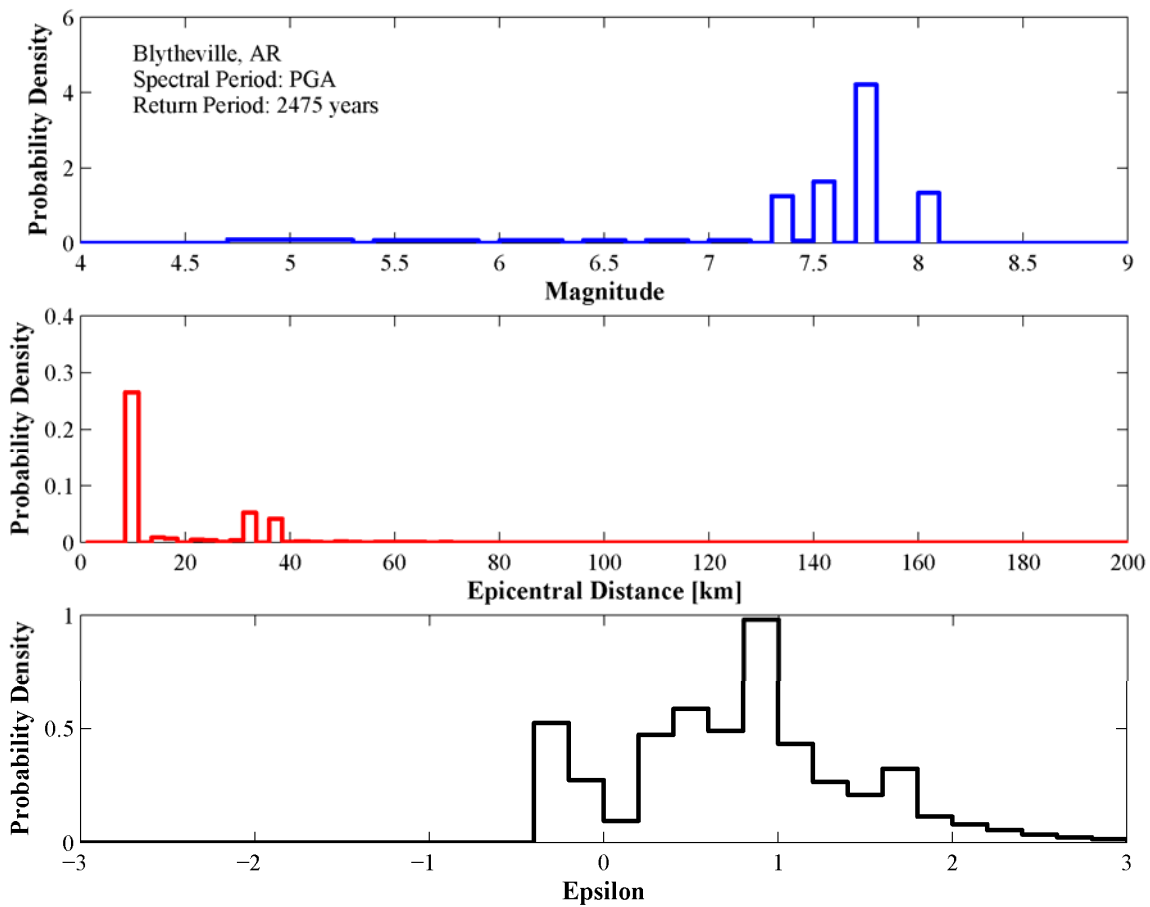


**Figure B.7.** Hazard deaggregation for peak ground acceleration and return period of 2475 years in Blytheville, AR

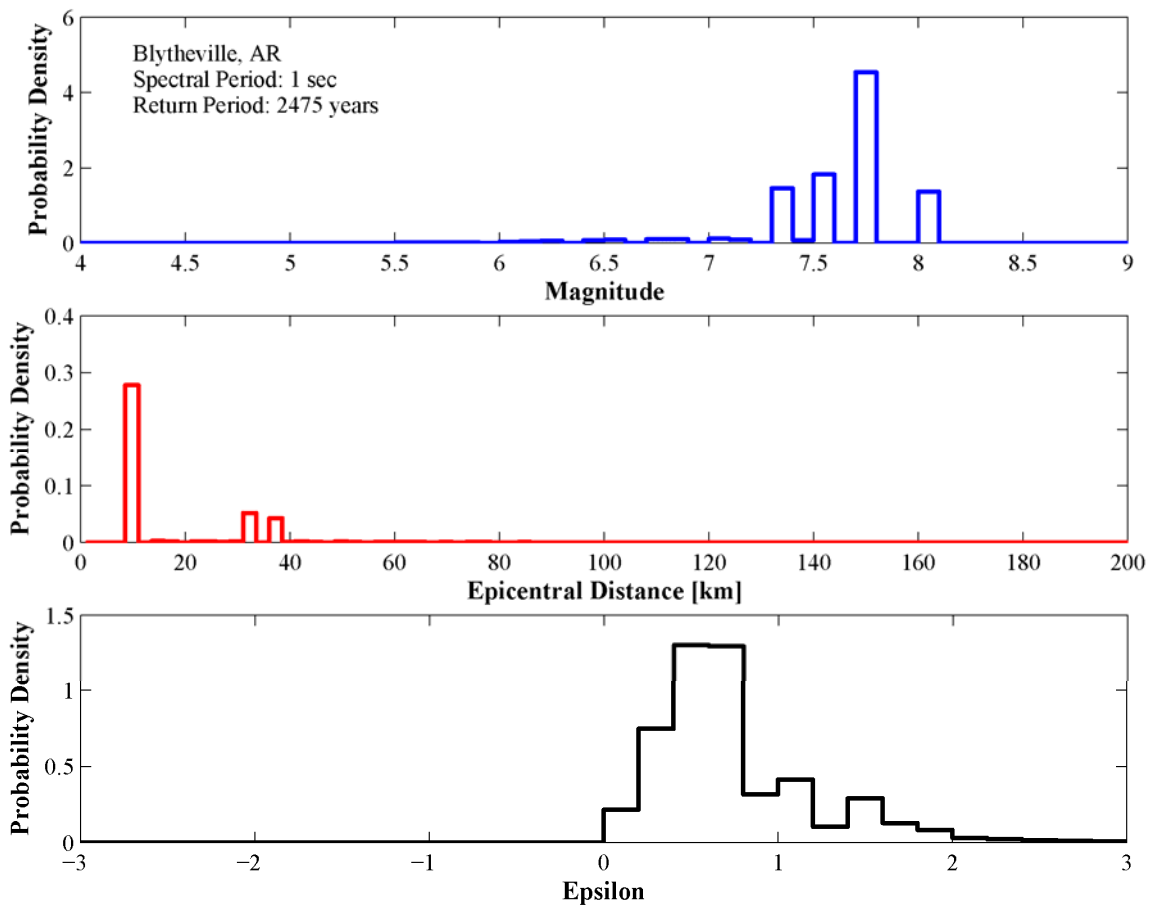


**Figure B.8.** Hazard deaggregation for 1-second spectral period and return period of 2475 years in Blytheville, AR

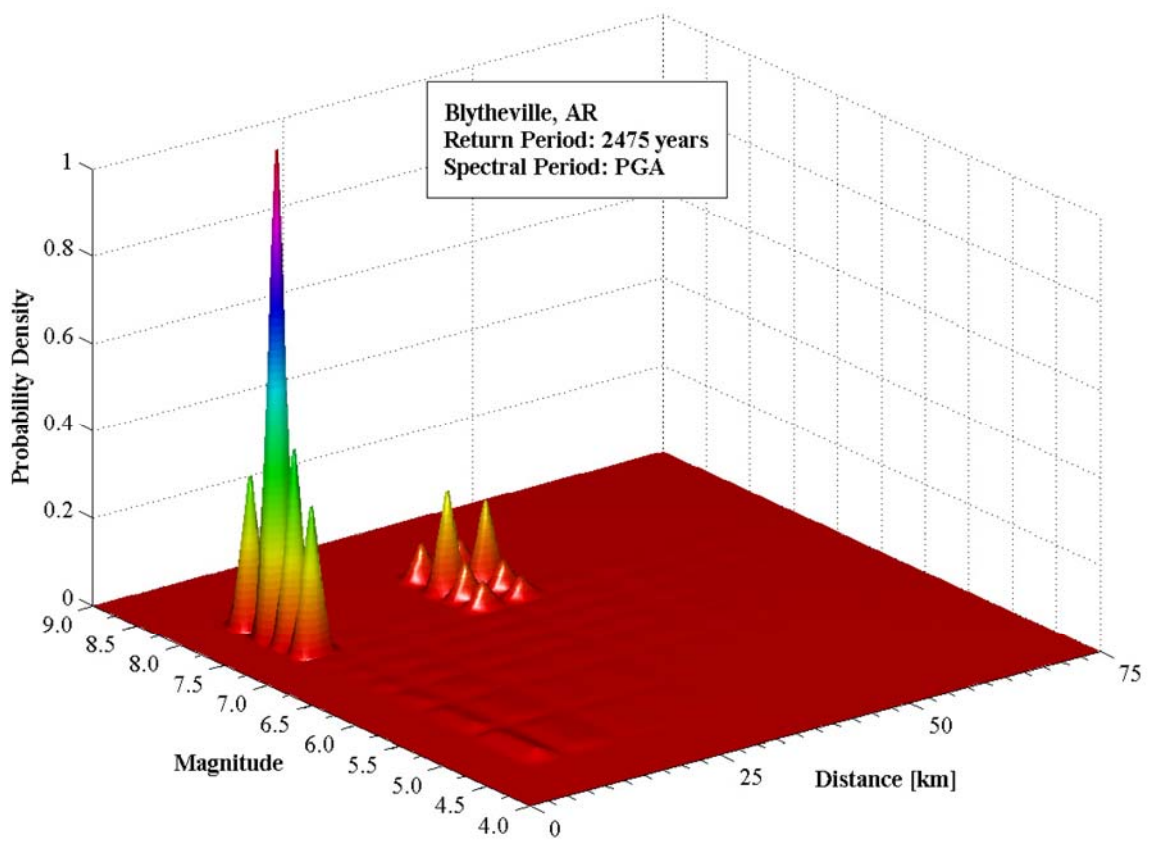


**Figure B.9.** Joint magnitude and distance hazard deaggregation for peak ground acceleration and return period of 2475 years in Blytheville, AR

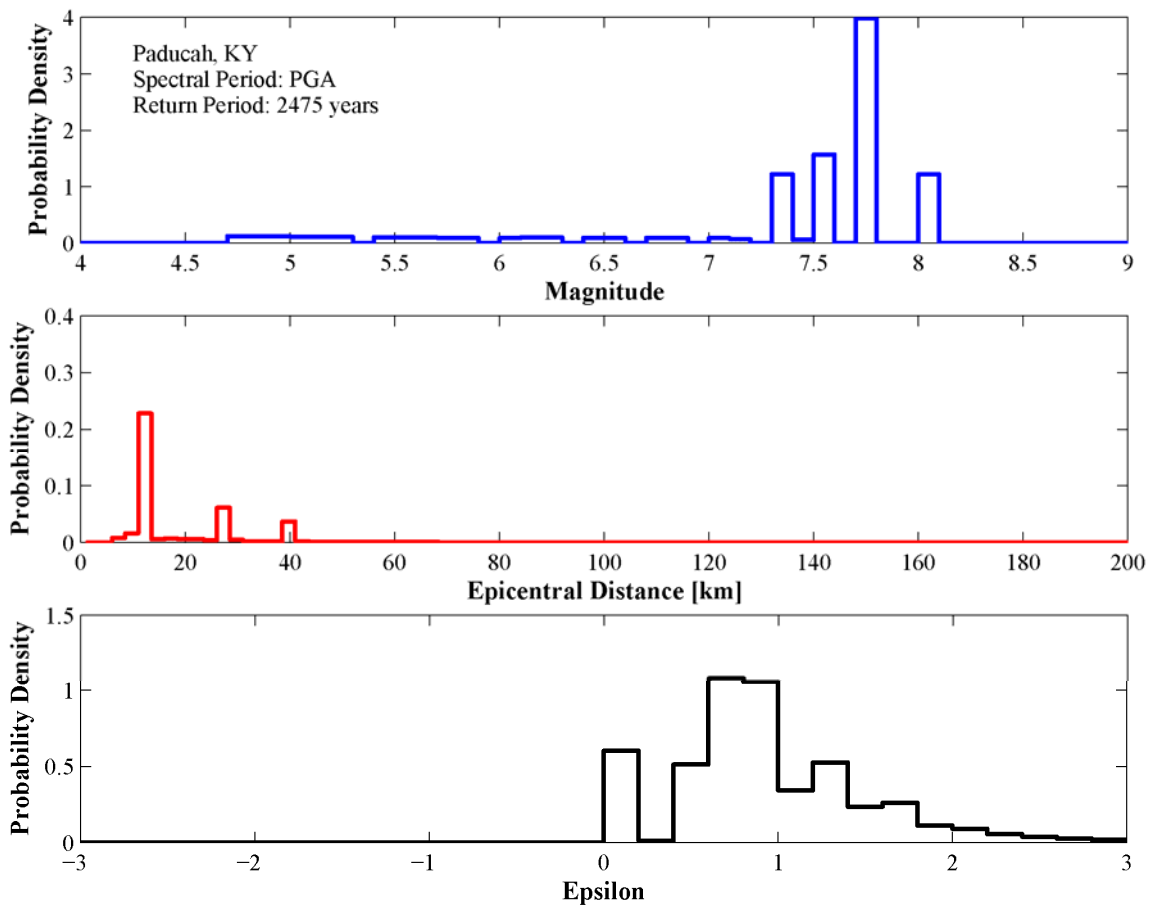


**Figure B.10.** Hazard deaggregation for peak ground acceleration and return period of 2475 years in Paducah, KY

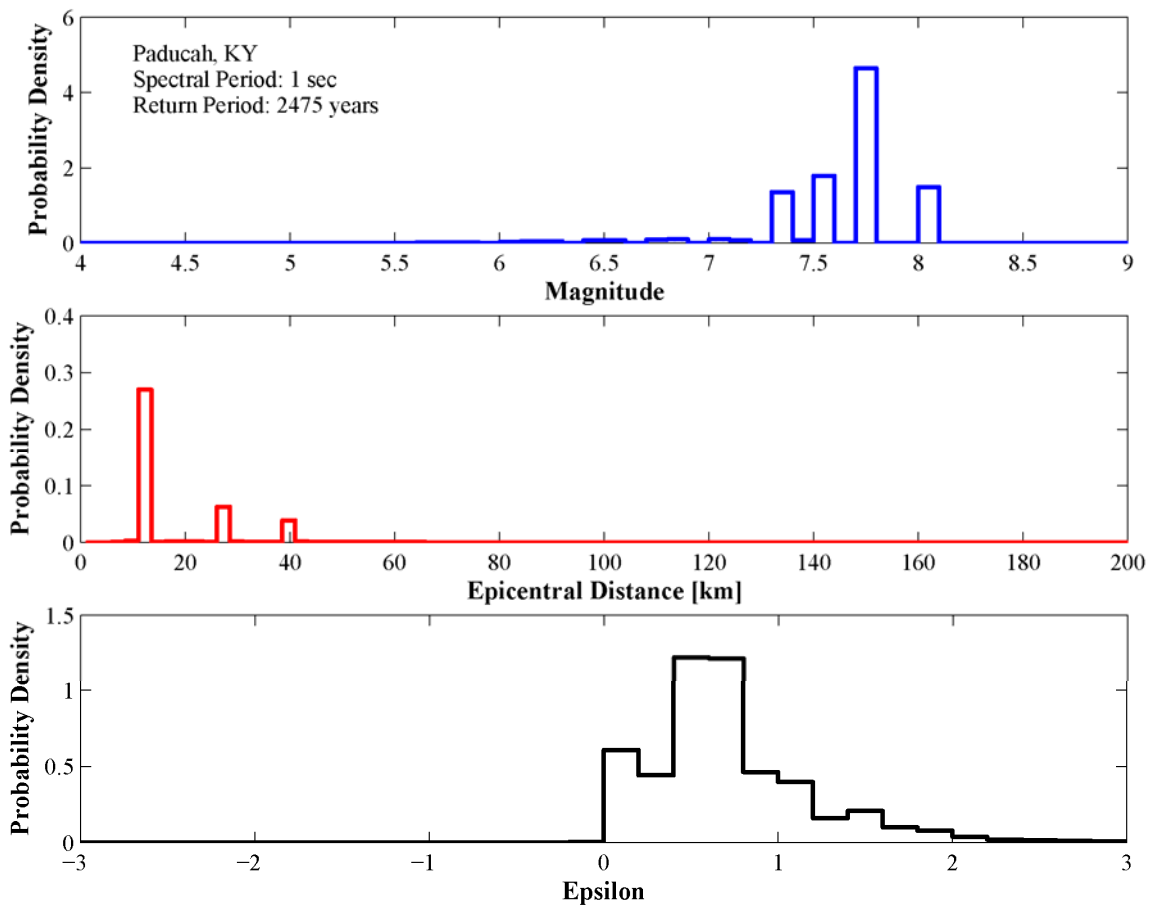


**Figure B.11.** Hazard deaggregation for 1-second spectral period and return period of 2475 years in Paducah, KY

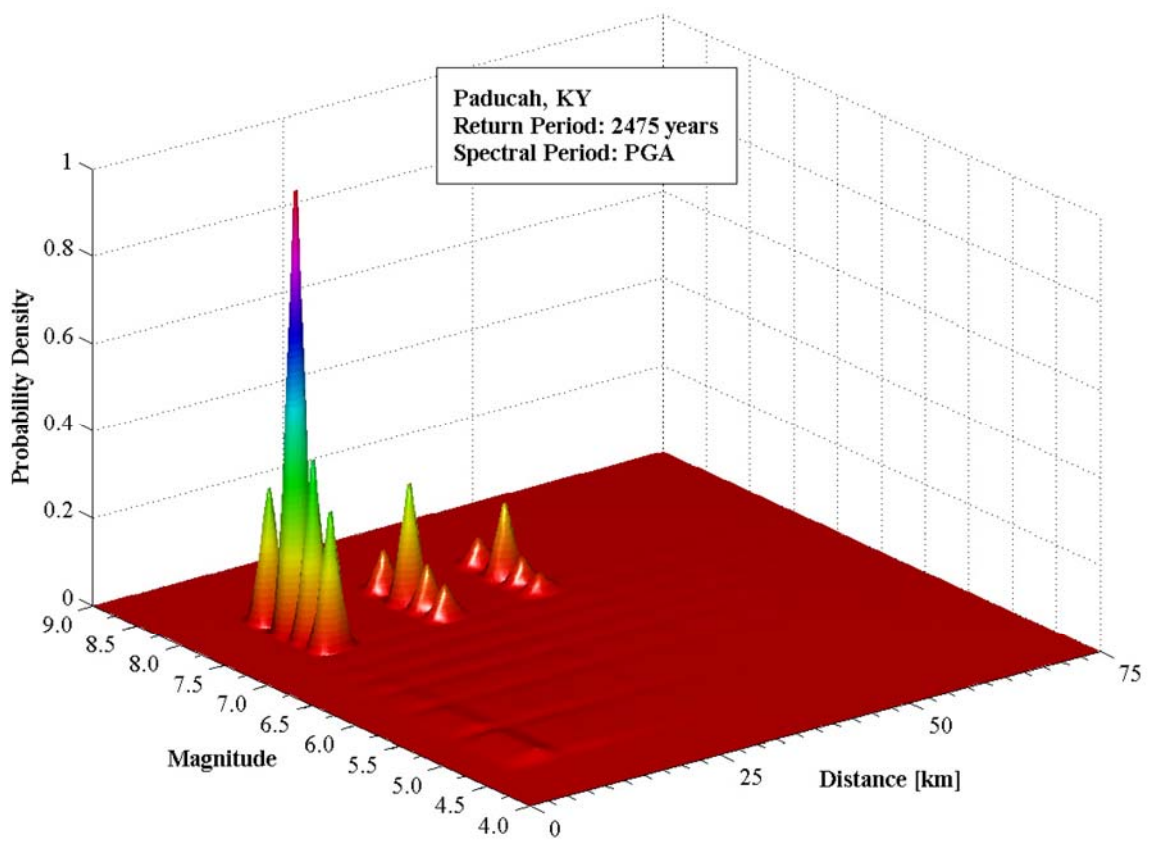


**Figure B.12.** Joint magnitude and distance hazard deaggregation for peak ground acceleration and return period of 2475 years in Paducah, KY

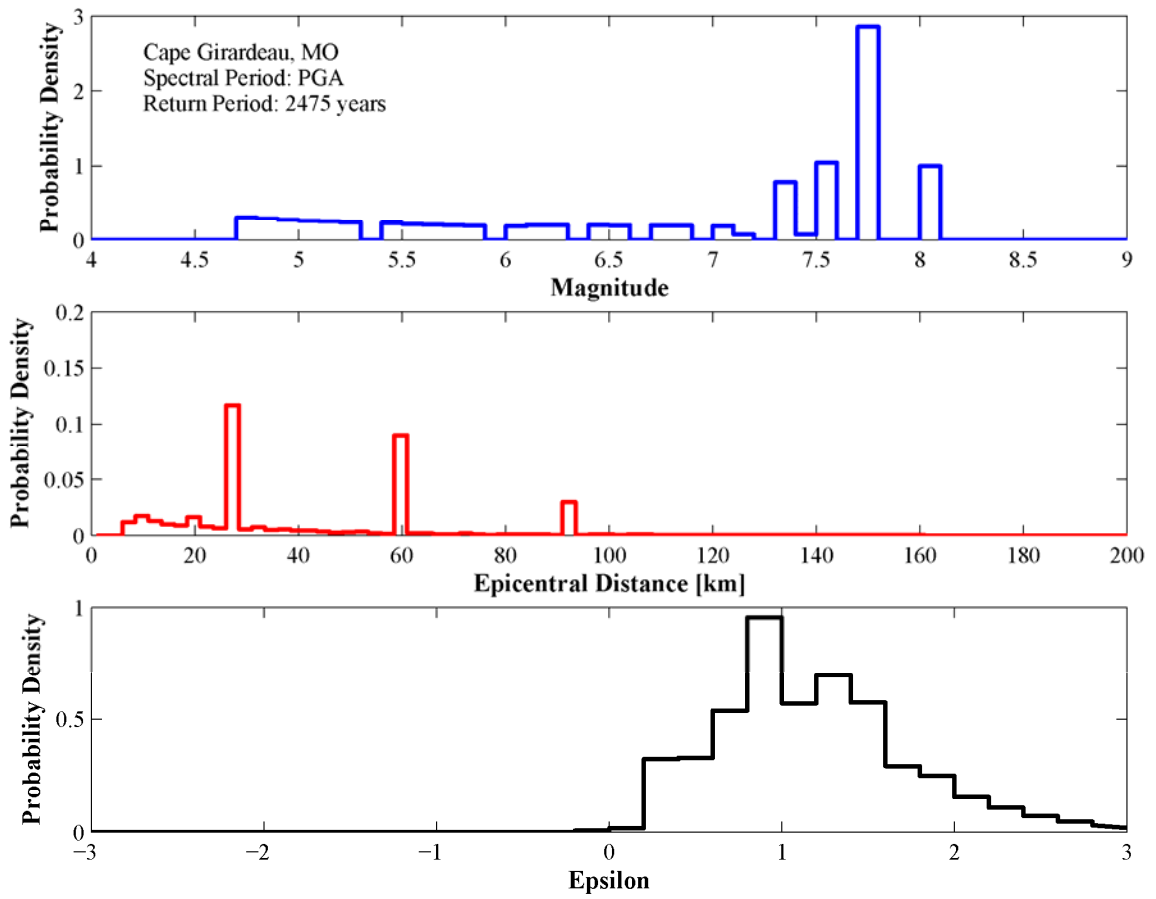


**Figure B.13.** Hazard deaggregation for peak ground acceleration and return period of 2475 years in Cape Girardeau, MO

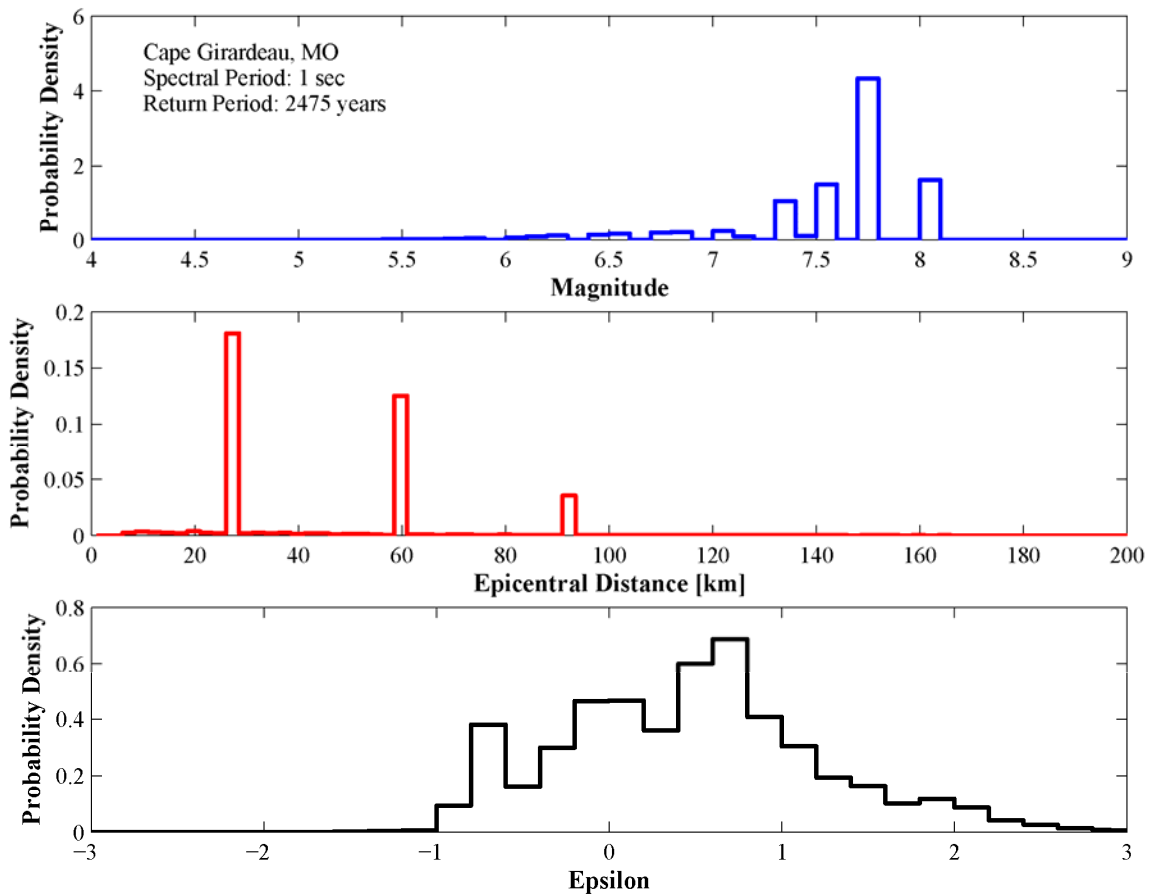


**Figure B.14.** Hazard deaggregation for 1-second spectral period and return period of 2475 years in Cape Girardeau, MO

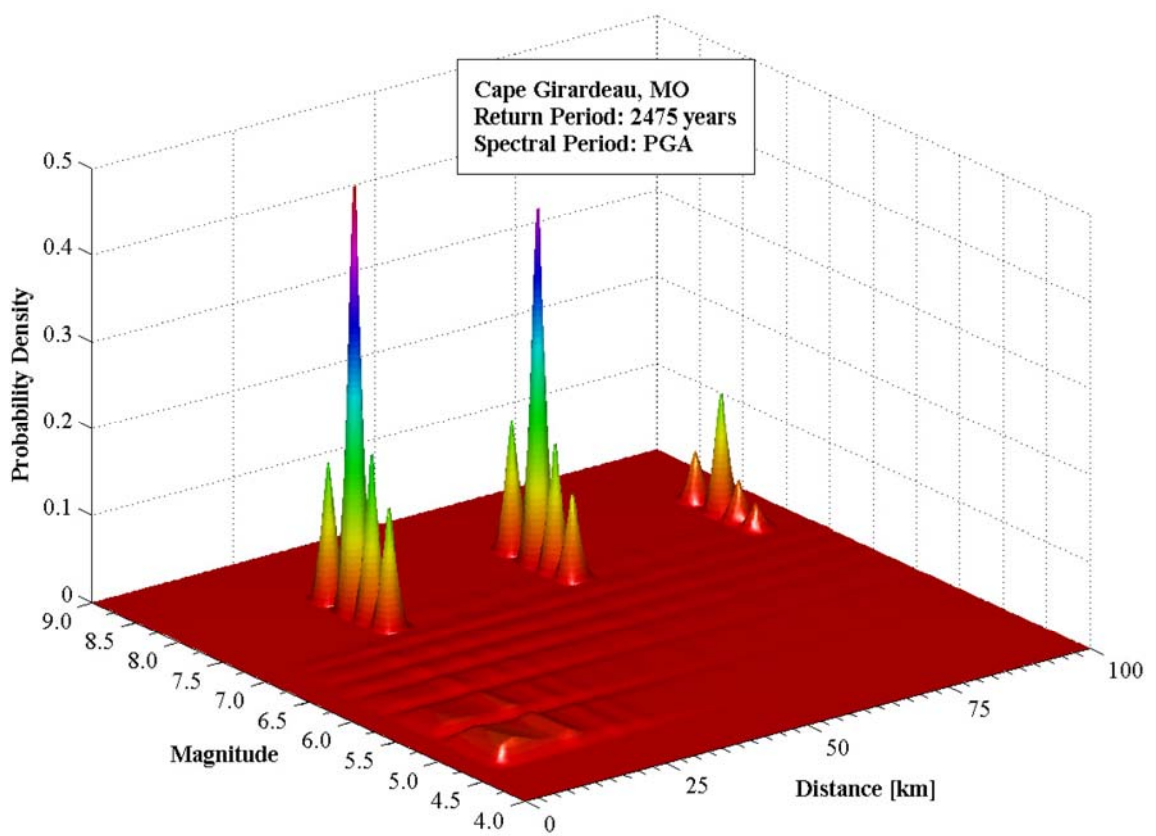


**Figure B.15.** Joint magnitude and distance hazard deaggregation for peak ground acceleration and return period of 2475 years in Cape Girardeau, MO

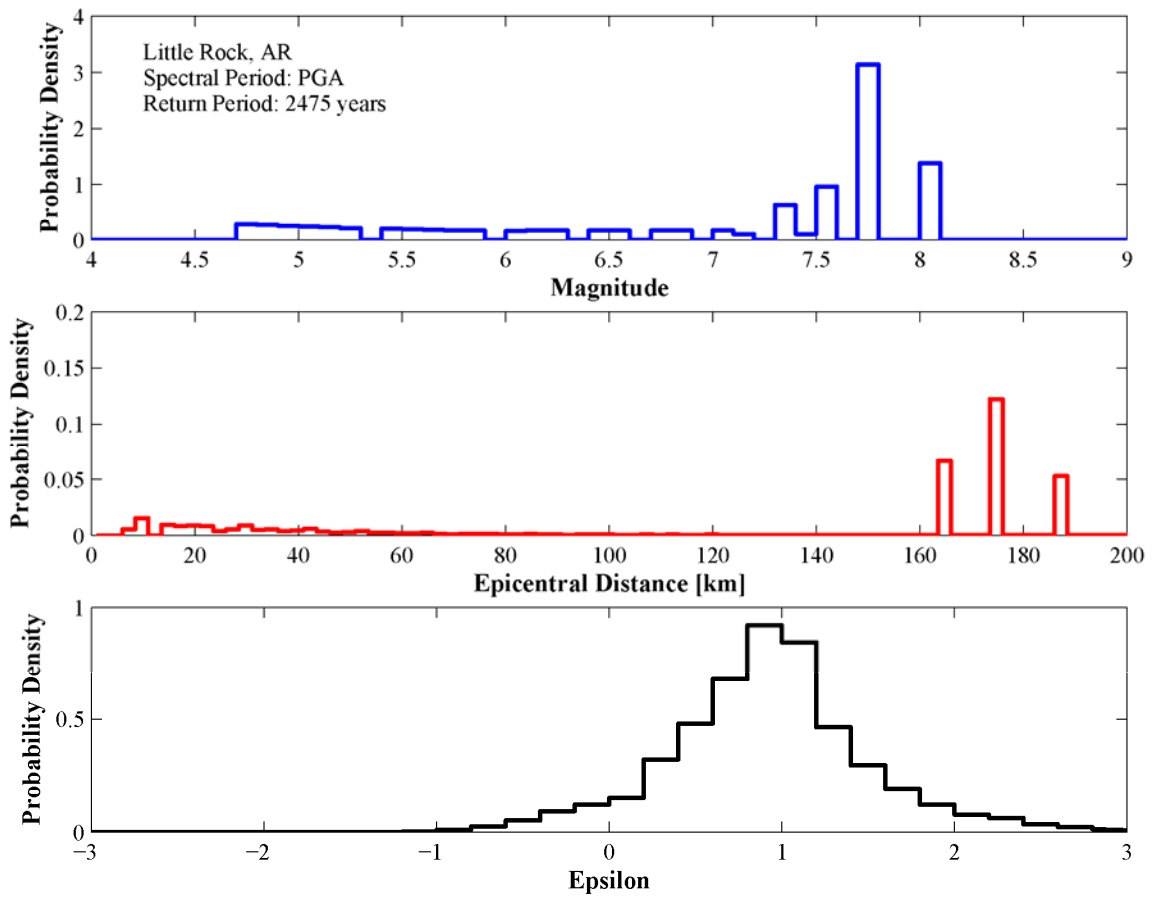


**Figure B.16.** Hazard deaggregation for peak ground acceleration and return period of 2475 years in Little Rock, AR

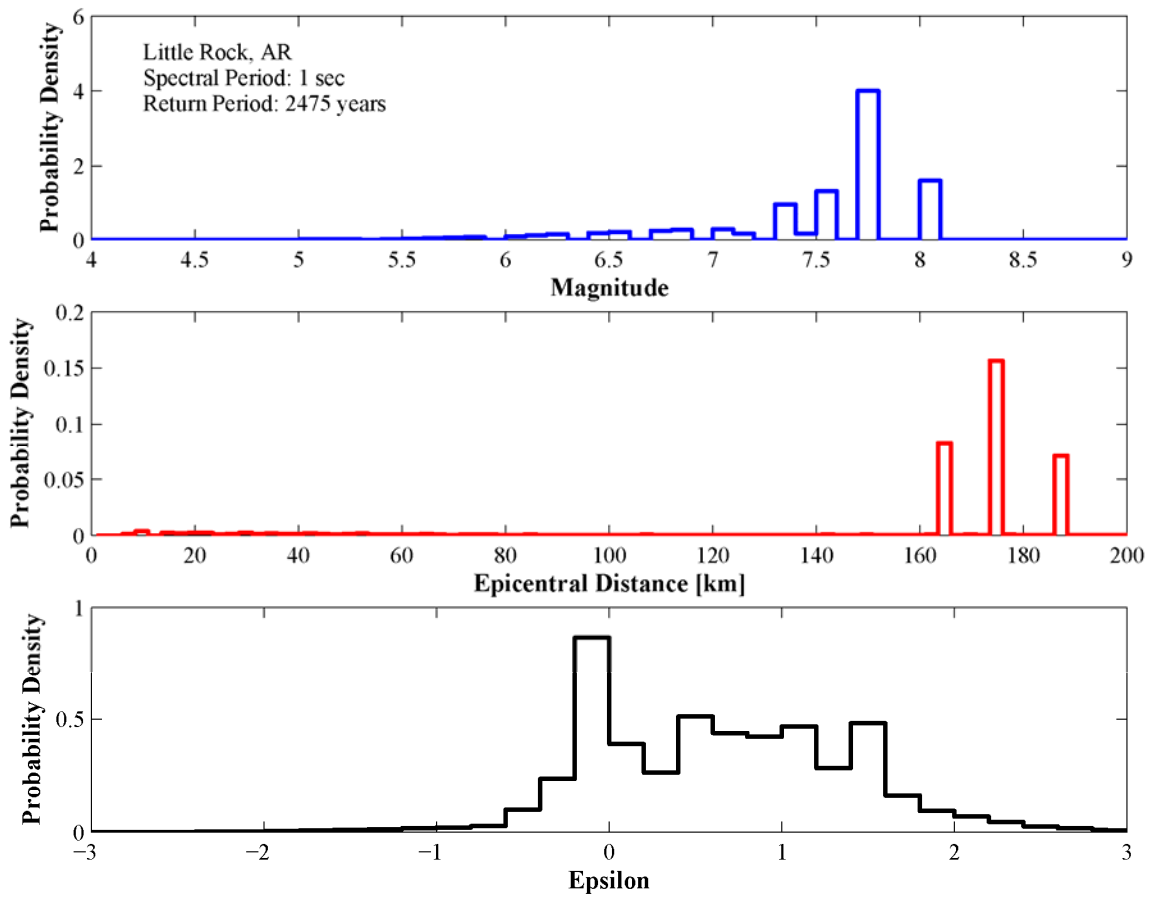


**Figure B.17.** Hazard deaggregation for 1-second spectral period and return period of 2475 years in Little Rock, AR

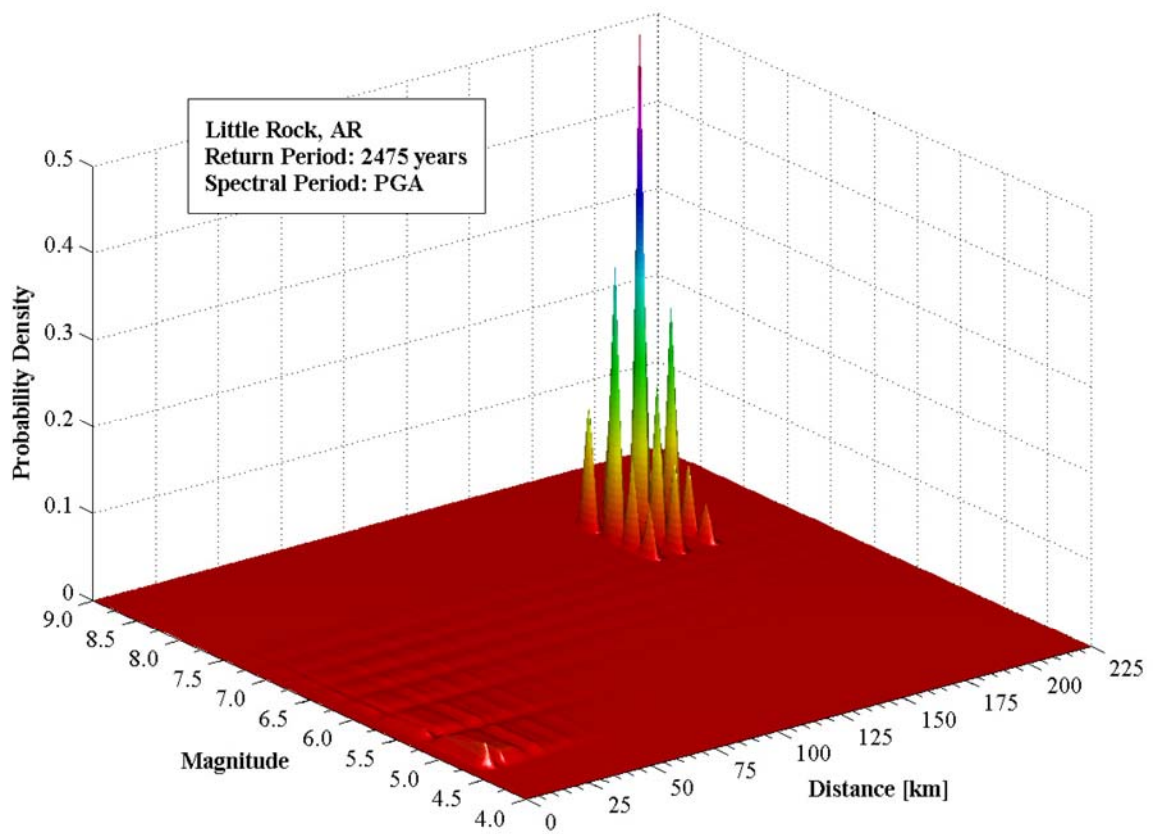


**Figure B.18.** Joint magnitude and distance hazard deaggregation for peak ground acceleration and return period of 2475 years in Little Rock, AR

## REFERENCES

- Abrahamson, N. A. (1992). "Non-Stationary Spectral Matching." *Seismological Research Letters*, 63(1), 30.
- Abrahamson, N. A., and Bommer, J. J. (2005). "Probability and Uncertainty in Seismic Hazard Analysis." *Earthquake Spectra*, 21(2), 603-607.
- Abrahamson, N. A., and Silva, W. J. (1997). "Empirical Response Spectral Attenuation Relations for Shallow Crustal Earthquakes." *Seismological Research Letters*, 68(1), 94-127.
- Abrahamson, N. A., Somerville, P. G., and Cornell, C. A. (1990). "Uncertainty in Numerical Strong Motion Predictions." *Proceedings of the Fourth U.S. National Conference on Earthquake Engineering*, Palm Springs, CA, USA, 407-416.
- Acevedo, A. B. (2003). "Seismological Criteria for Selecting and Scaling Real Accelerograms for Use in Engineering Analysis and Design," Masters Thesis, European School of Advanced Studies in Reduction of Seismic Risk, ROSE School, Pavia, Italy.
- Aki, K. (1967). "Scaling Law of Seismic Spectrum." *Journal of Geophysical Research*, 72(4), 1217-1231.
- Aki, K. (1988). "Local Site Effects on Strong Ground Motion." *Earthquake Engineering and Soil Dynamics II - Recent Advances in Ground-Motion Evaluation*, Park City, UT, USA, 103-155.
- Aki, K., and Larner, K. L. (1970). "Surface Motion of a Layered Medium having an Irregular Interface due to Incident Plane SH Waves." *Journal of Geophysical Research*, 75(5), 933-954.
- Aki, K., and Richards, P. G. (1980). *Quantitative Seismology. Theory and Methods.*, W.H. Freeman and Company, San Francisco, CA.
- Alvarez-Rubio, S., Sanchez-Sesma, F. J., Benito, J. J., and Alarcon, E. (2004). "The Direct Boundary Element Method: 2D Site Effects Assessment on Laterally

Varying Layered Media (Methodology)." *Soil Dynamics and Earthquake Engineering*, 24(2), 167-180.

Anderson, J. G. (2003). "Strong-Ground Motion Seismology." International Handbook of Earthquake and Engineering Seismology, Part B, W. H. Lee, H. Kanamori, P. C. Jennings, and C. Kisslinger, eds., Academic Press, 937-965.

Anderson, J. G., and Hough, S. E. (1984). "A Model for the Shape of the Fourier Amplitude Spectrum of Acceleration at High Frequencies." *Bulletin of the Seismological Society of America*, 74(5), 1969-1993.

Andrews, D. J. (1986). "Objective Determination of Source Parameters and Similarity of Earthquakes of Different Size." Earthquake Source Mechanics, Geophysical Monograph 37, S. Das, J. Boatwright, and C. H. Scholz, eds., American Geophysical Union, Washington, D.C, 259-268.

Arias, A. (1970). "A Measure of Earthquake Intensity." Seismic Design of Nuclear Reactors, R. J. Hansen, ed., MIT Press, 438-483.

Assimaki, D., and Kausel, E. (2002). "An Equivalent Linear Algorithm with Frequency- and Pressure-dependent Moduli and Damping for the Seismic Analysis of Deep Sites." *Soil Dynamics and Earthquake Engineering*, 22(9-12), 959-965.

Astroza, M., and Monge, J. (1991). "Regional Seismic Zonation in Central Chile." *Proceedings of the Fourth International Conference on Seismic Zonation*, Stanford, CA, 487-494.

Atkinson, G. M., and Beresnev, I. A. (1997). "Don't Call it Stress Drop." *Seismological Research Letters*, 68(1), 3-4.

Atkinson, G. M., and Beresnev, I. A. (2002). "Ground Motions at Memphis and St. Louis from M 7.5–8.0 Earthquakes in the New Madrid Seismic Zone." *Bulletin of the Seismological Society of America*, 92(3), 1015 - 1024.

Atkinson, G. M., and Boore, D. M. (1995). "Ground Motion Relations for Eastern North America." *Bulletin of the Seismological Society of America*, 85(1), 17 - 30.

- Atkinson, G. M., and Boore, D. M. (1998). "Evaluation of Models for Earthquake Source Spectra in Eastern North America." *Bulletin of the Seismological Society of America*, 88(4), 917-934.
- Atkinson, G. M., and Boore, D. M. (2001). "Preliminary Ground Motion Relations for Subduction Zone Earthquakes." *Seismological Research Letters*, 72, 282.
- Atkinson, G. M., and Boore, D. M. (2006). "Earthquake Ground-Motion Prediction Equations for Eastern North America." *Bulletin of the Seismological Society of America*, 96(6), 2181-2205.
- Atkinson, G. M., and Silva, W. (2000). "Stochastic Modeling of California Ground Motions." *Bulletin of the Seismological Society of America*, 90(2), 255-274.
- Baker, J., and Cornell, C. A. (2006a). "Correlation of Response Spectral Values for Multicomponent Ground Motions." *Bulletin of the Seismological Society of America*, 96(1), 215 - 227.
- Baker, J. W., and Cornell, C. A. (2006b). "Spectral Shape, Epsilon and Record Selection." *Earthquake Engineering and Structural Dynamics*, 35(9), 1077-1095.
- Bakir, B. S., Ozkan, M. Y., and Ciliz, S. (2002). "Effects of Basin Edge on the Distribution of Damage in 1995 Dinar, Turkey Earthquake." *Soil Dynamics and Earthquake Engineering*, 22(4), 335-345.
- Bao, H., Bielak, J., Ghattas, O., Kallivokas, L. F., O'Hallaron, D. R., Shewchuk, J. R., and Xu, J. (1998). "Large-Scale Simulation of Elastic Wave Propagation in Heterogeneous Media on Parallel Computers." *Computer Methods in Applied Mechanics and Engineering*, 152(1-2), 85-102.
- Bard, P.-Y., and Bouchon, M. (1980). "The Seismic Response of Sediment-Filled Valleys. Part 1. The Case of Incident SH Waves." *Bulletin of the Seismological Society of America*, 70(4), 1263-1286.
- Bard, P.-Y., and Bouchon, M. (1985). "The Two-Dimensional Resonance of Sediment-Filled Valleys." *Bulletin of the Seismological Society of America*, 75(2), 519-541.

- Bard, P.-Y., and Gariel, J.-C. (1986). "The Seismic Response of Two-Dimensional Sedimentary Deposits with Large Vertical Velocity Gradients." *Bulletin of the Seismological Society of America*, 76(2), 343-366.
- Bard, P.-Y., and Riepl-Thomas, J. (2000). "Wave Propagation in Complex Geological Structures and their Effects on Strong Ground Motion." *Wave Motion in Earthquake Engineering*, E. K. a. G. Manolis, ed., WIT Press, 37-98.
- Bard, P. Y. (1982). "Diffracted Waves and Displacement Field over Two Dimensional Elevated Topographies." *Geophysical Journal of the Royal Astronomical Society*, 71, 731-760.
- Bard, P. Y., Campillo, M., Chavez-Garcia, F. J., and Sanchez-Sesma, F. (1988). "Mexico Earthquake of September 19, 1985 - A Theoretical Investigation of Large- and Small-Scale Amplification Effects in the Mexico City Valley." *Earthquake Spectra*, 4(3), 609-633.
- Bard, P. Y., and Tucker, B. E. (1985). "Underground and Ridge Site Effects: A Comparison of Observation and Theory." *Bulletin of the Seismological Society of America*, 75(4), 905-922.
- Baturay, M. B., and Stewart, J. P. (2003). "Uncertainty and Bias in Ground-Motion Estimates from Ground Response Analyses." *Bulletin of the Seismological Society of America*, 93(5), 2025-2042.
- Bazzurro, P., and Cornell, C. A. (1999). "Disaggregation of Seismic Hazard." *Bulletin of the Seismological Society of America*, 89(2), 501-520.
- Bazzurro, P., and Cornell, C. A. (2004a). "Ground-Motion Amplification in Nonlinear Soil Sites with Uncertain Properties." *Bulletin of the Seismological Society of America*, 94(6), 2090-2109.
- Bazzurro, P., and Cornell, C. A. (2004b). "Nonlinear Soil-Site Effects in Probabilistic Seismic-Hazard Analysis." *Bulletin of the Seismological Society of America*, 94(6), 2110 - 2123.
- Bazzurro, P., and Cornell, C. A. (2006). "Reply to 'Comment on 'Nonlinear Soil-Site Effects in Probabilistic Seismic-Hazard Analysis' by Paolo Bazzurro and C. Allin Cornell' by Jonathan P. Stewart and Christine A. Goulet." *Bulletin of the Seismological Society of America*, 96(2), 748-749.

- Ben-Menahem, A., and Singh, S. J. (1981). *Seismic Waves and Sources*, Springer-Verlag, New York.
- Bielak, J., Ghattas, O., and Bao, H. (1998). "Ground Motion Modeling using 3D Finite Element Methods." *Proceedings of the Second International Symposium on the Effects of Surface Geology on Seismic Motion*, Yokohama, Japan, 121-133.
- Bielak, J., Xu, J., and Ghattas, O. (1999). "Earthquake Ground Motion and Structural Response in Alluvial Valleys." *Journal of Geotechnical and Geoenvironmental Engineering*, 125(5), 413-423.
- Boatwright, J., and Choy, G. L. (1992). "Acceleration Source Spectra Anticipated for Large Earthquakes in Northeastern North America." *Bulletin of the Seismological Society of America*, 82(2), 660-682.
- Boatwright, J., Fletcher, J. B., and Fumal, T. E. (1991). "A General Inversion Scheme for Source, Site, and Propagation Characteristics using Multiply Recorded Sets of Moderate-Sized Earthquakes." *Bulletin of the Seismological Society of America*, 81(5), 1754-1782.
- Bodin, P., and Horton, S. (1999). "Broadband Microtremor Observation of Basin Resonance in the Mississippi Embayment, Central US." *Geophysical Research Letters*, 26(7), 903-906.
- Bodin, P., Smith, K., Horton, S., and Hwang, H. (2001). "Microtremor Observations of Deep Sediment Resonance in Metropolitan Memphis, Tennessee." *Engineering Geology*, 62(1-3), 159-168.
- Bollinger, G. A., Chapman, M. C., and Sibol, M. S. (1993). "Comparison of Earthquake Damage Areas as a Function of Magnitude across the United States." *Bulletin of the Seismological Society of America*, 83(4), 1064-1080.
- Bommer, J. J. (2002). "Deterministic vs. Probabilistic Seismic Hazard Assessment: An Exaggerated and Obstructive Dichotomy." *Journal of Earthquake Engineering*, 6(Special Issue 1), 43-73.
- Bommer, J. J. (2003). "Uncertainty about the Uncertainty in Seismic Hazard Analysis." *Engineering Geology*, 70(1-2), 165-168.

- Bommer, J. J., Scott, S. G., and Sarma, S. K. (2000). "Hazard-Consistent Earthquake Scenarios." *Soil Dynamics and Earthquake Engineering*, 19(4), 219-231.
- Boore, D. M. (1983). "Stochastic Simulation of High-Frequency Ground Motions based on Seismological Models of the Radiated Spectra." *Bulletin of the Seismological Society of America*, 73(6), 1865-1894.
- Boore, D. M. (1999). "Basin Waves on a Seafloor Recording of the 1990 Upland, California, Earthquake: Implications for Ground Motions from a Larger Earthquake." *Bulletin of the Seismological Society of America*, 89(1), 317-324.
- Boore, D. M. (2003a). "Simulation of Ground Motion Using the Stochastic Method." *Pure and Applied Geophysics*, 160, 635 - 676.
- Boore, D. M. (2003b). "SMSIM - Fortran Programs for Simulating Ground Motions from Earthquakes: Version 2.0 - A Revision of OFR 96-80-A." U.S. Geological Survey.
- Boore, D. M. (2003c). "SMSIM – Fortran Programs for Simulating Ground Motions from Earthquakes: Version 2.0—A Revision of OFR 96-80-A." *A modified version of OFR 00-509*, U.S. Geological Survey.
- Boore, D. M. (2005). "On Pads and Filters: Processing Strong-Motion Data." *Bulletin of the Seismological Society of America*, 95(2), 745-750.
- Boore, D. M., and Atkinson, G. M. (1987). "Stochastic Prediction of Ground Motion and Spectral Response Parameters at Hard-Rock Sites in Eastern North America." *Bulletin of the Seismological Society of America*, 77(2), 440-467.
- Boore, D. M., and Atkinson, G. M. (2006). "Boore-Atkinson Provisional NGA Empirical Ground-Motion Model for the Average Horizontal Component of PGA, PGV and SA at Spectral Periods of 0.05, 0.1, 0.2, 0.3, 0.5, 1, 2, 3, 4, and 5 Seconds (Version 1.7)." *Report of Next Generation Attenuation (NGA) Models*, Pacific Earthquake Engineering Research Center.
- Boore, D. M., and Boatwright, J. (1984). "Average Body-Wave Radiation Coefficients." *Bulletin of the Seismological Society of America*, 74(5), 1615-1621.

- Boore, D. M., and Bommer, J. J. (2005). "Processing of Strong-Motion Accelerograms: Needs, Options and Consequences." *Soil Dynamics and Earthquake Engineering*, 25, 93-115.
- Boore, D. M., Harmsen, S. C., and Harding, S. T. (1981). "Wave Scattering from a Step Change in Surface Topography." *Bulletin of the Seismological Society of America*, 71(1), 117-125.
- Boore, D. M., Lerner, K. L., and Aki, K. (1971). "Comparison of Two Independent Methods for the Solution of Wave-Scattering Problems: Response of a Sedimentary Basin to Vertically Incident SH Waves." 76(2), 558-69.
- Borcherdt, R. D. (1970). "Effects of Local Geology on Ground Motion near San Francisco Bay." *Bulletin of the Seismological Society of America*, 60(1), 29-61.
- Borcherdt, R. D., Wentworth, C. M., Janssen, A., Fumal, T., and Gibbs, J. F. (1991). "Methodology for Predictive GIS Mapping of Special Study Zones for Strong Ground Motion Shaking in the San Francisco Bay Region." *Proceedings of the Fourth International Conference on Seismic Zonation*, Stanford, CA, 545-552.
- Bouchon, M. (2003). "A Review of the Discrete Wavenumber Method." *Pure and Applied Geophysics*, 160, 445-465.
- Bouchon, M., and Aki, K. (1977). "Discrete Wave-Number Representation of Seismic-Source Wave Fields." *Bulletin of the Seismological Society of America*, 67(2), 259-77.
- Brahana, J. V., Parks, W. S., and Gaydos, M. W. (1987). "Quality of Water from Freshwater Aquifers and Principal Well Fields in the Memphis Area, Tennessee." *Water-Resources Investigations Report 87-4052*, U.S. Geological Survey, Nashville, Tennessee.
- Bravo, M. A., Sanchez-Sesma, J., and Chavez-Garcia, F. J. (1988). "Ground Motion on Stratified Alluvial Deposits for Incident SH Waves." *Bulletin of the Seismological Society of America*, 78(2), 436-450.
- Brune, J. N. (1970). "Tectonic Stress and the Spectra of Seismic Shear Waves from Earthquakes." *Journal of Geophysical Research*, 75(26), 4997-5009.

- Brune, J. N. (1971). "Correction." *Journal of Geophysical Research*, 76, 5002.
- Campbell, K. W. (1997). "Empirical Near-Source Attenuation Relationships for Horizontal and Vertical Components of Peak Ground Acceleration, Peak Ground Velocity, and Pseudo-Absolute Acceleration Response Spectra." *Seismological Research Letters*, 68(1), 154-179.
- Campbell, K. W. (2003a). "Engineering Models of Strong Ground Motion." *Earthquake Engineering Handbook*, W.-F. Chen and C. Scawthorn, eds., CRC Press LLC, Boca Raton, Florida, USA.
- Campbell, K. W. (2003b). "Prediction of Strong Ground Motion Using the Hybrid Empirical Method and Its Use in the Development of Ground-Motion (Attenuation) Relations in Eastern North America." *Bulletin of the Seismological Society of America*, 93(3), 1012 - 1033.
- Campbell, K. W., and Bozorgnia, Y. (2006). "Campbell-Bozorgnia NGA Empirical Ground Motion Model for the Average Horizontal Component of PGA, PGV, PGD and SA at Selected Spectral Periods Ranging from 0.01–10.0 Seconds (Version 1.1)." *Report of Next Generation Attenuation (NGA) Models*, Pacific Earthquake Engineering Research Center.
- Carballo, J. E., and Cornell, C. A. (2000). "Probabilistic Seismic Demand Analysis: Spectrum Matching and Design." *Report No. RMS-41*, Reliability of Marine Structures Program, Stanford University.
- Cartwright, D. E., and Longuet-Higgins, M. S. (1956). "The Statistical Distribution of the Maxima of a Random Function." *Proceedings of the Royal Society of London. Series A, Mathematical and Physical Sciences*, 237(1209), 212-232.
- Catchings, R. D. (1999). "Regional  $V_p$ ,  $V_s$ ,  $V_p/V_s$ , and Poisson's Ratios across Earthquake Source Zones from Memphis, Tennessee, to St. Louis Missouri." *Bulletin of the Seismological Society of America*, 89(6), 1591 - 1605.
- Celebi, M. (1987). "Topographical and Geological Amplifications determined from Strong-Motion and Aftershock Records of the 3 March 1985 Chile Earthquake." *Bulletin of the Seismological Society of America*, 77(4), 1147-1167.
- Celebi, M. (1991). "Topographical and Geological Amplification. Case Studies and Engineering Implications." *Structural Safety*, 10(1-3), 199-217.

- Center for Earthquake Research and Information. (2007). "New Madrid Earthquake Catalog Search ([http://folkworm.ceri.memphis.edu/catalogs/html/cat\\_nm.html](http://folkworm.ceri.memphis.edu/catalogs/html/cat_nm.html))."
- Chapman, M. C. (1995). "Probabilistic Approach to Ground-Motion Selection for Engineering Design." *Bulletin of the Seismological Society of America*, 85(3), 937-942.
- Chavez-Garcia, F. J., and Bard, P.-Y. (1994). "Site Effects in Mexico City Eight Years after the September 1985 Michoacan Earthquakes." *Soil Dynamics and Earthquake Engineering*, 13(4), 229-247.
- Chavez-Garcia, F. J., Raptakis, D., Makra, K., and Pitilakis, K. (2000). "Site Effects at Euroseistest - II. Results from 2D Numerical Modeling and Comparison with Observations." *Soil Dynamics and Earthquake Engineering*, 19(1), 23-39.
- Ching, J.-Y., and Glaser, S. D. (2001). "1D Time-Domain Solution for Seismic Ground Motion Prediction." *Journal of Geotechnical and Geoenvironmental Engineering*, 127(1), 36-47.
- Chiou, B. S.-J., and Youngs, R. R. (2006). "Chiou and Youngs PEER-NGA Empirical Ground Motion Model for the Average Horizontal Component of Peak Acceleration and Pseudo-Spectral Acceleration for Spectral Periods of 0.01 to 10 Seconds." *Report of Next Generation Attenuation (NGA) Models. Interim Report for USGS Review*, Pacific Earthquake Engineering Research Center.
- Chiu, J. M., Johnston, A. C., and Yang, Y. T. (1992). "Imaging the Active Faults of the Central New Madrid Seismic Zone using PANDA Array Data." *Seismological Research Letters*, 63(3), 375-393.
- Cornell, C. A. (1968). "Engineering Seismic Risk Analysis." *Bulletin of the Seismological Society of America*, 58(5), 1583-1606.
- Cornell, C. A. (2005). "On Earthquake Record Selection for Nonlinear Dynamic Analysis." The Esteva Symposium, Mexico.
- Cornell, C. A., and Winterstein, S. R. (1988). "Temporal and Magnitude Dependence in Earthquake Recurrence Models." *Bulletin of the Seismological Society of America*, 78(4), 1522-1537.

- Cramer, C. H. (2001). "A Seismic Hazard Uncertainty Analysis for the New Madrid Seismic Zone." *Engineering Geology*, 62, 251 - 266.
- Cramer, C. H. (2003). "Site-Specific Seismic-Hazard Analysis that is Completely Probabilistic." *Bulletin of the Seismological Society of America*, 93(4), 1841-1846.
- Cramer, C. H. (2006a). "An Assessment of the Impact of the 2003 EPRI Ground-Motion Prediction Models on the USGS National Seismic-Hazard Maps." *Bulletin of the Seismological Society of America*, 96(3), 1159-1169.
- Cramer, C. H. (2006b). "Quantifying the Uncertainty in Site Amplification Modeling and Its Effects on Site-Specific Seismic-Hazard Estimation in the Upper Mississippi Embayment and Adjacent Areas." *Bulletin of the Seismological Society of America*, 96(6), 2008-2020.
- Cramer, C. H., Gomberg, J. S., Schweig, E. S., Waldron, B. A., and Tucker, K. (2004). "The Memphis, Shelby County, Tennessee, Seismic Hazard Maps." *U.S. Geological Survey Open File Report 04-1294*, U.S. Geological Survey, Memphis, TN.
- Darragh, B., Silva, W., and Gregor, N. (2006). "Validation and Comparison of One-Dimensional Ground Motion Methodologies." *Third International Symposium on the Effects of Surface Geology on Seismic Motion*, Grenoble, France.
- Davis, M. W. (1987). "Production of Conditional Simulations via the LU Triangular Decomposition of the Covariance Matrix." *Mathematical Geology*, 19(2), 91 - 98.
- Ding, G., and Dravinski, M. (1996). "Scattering of SH Waves in Multilayered Media with Irregular Interfaces." *Earthquake Engineering and Structural Dynamics*, 25(12), 1391-1404.
- Dobry, R., Borchardt, R. D., Crouse, C. B., Idriss, I. M., Joyner, W. B., Martin, G. R., Power, M. S., Rinne, E. E., and Seed, R. B. (2000). "New Site Coefficients and Site Classification System used in Recent Building Seismic Code Provisions." *Earthquake Spectra*, 16(1), 41-67.
- Dobry, R., Idriss, I. M., and Ng, E. (1978). "Duration Characteristics of Horizontal Components of Strong-Motion Earthquake Records." *Bulletin of the Seismological Society of America*, 68(5), 1487-1520.

- Douglas, J. (2003). "Earthquake Ground Motion Estimation Using Strong-Motion Records: A Review of Equations for the Estimation of Peak Ground Acceleration and Response Spectral Ordinates." *Earth-Science Reviews*, 61(1-2), 43-104.
- Dravinski, M. (2003). "Scattering of Elastic Waves by a General Anisotropic Basin. Part 2: a 3D Model." *Earthquake Engineering and Structural Dynamics*, 32, 653 - 670.
- Ebel, J. E., and Kafka, A. L. (1999). "A Monte Carlo Approach to Seismic Hazard Analysis." *Bulletin of the Seismological Society of America*, 89(4), 854-866.
- Electric Power Research Institute. (1993). "Guidelines for Determining Design Basis Ground Motions." *EPRI TR-102293*, Electric Power Research Institute, Palo Alto California.
- FEMA. (2001a). "NEHRP Recommended Provisions for Seismic Regulations for New Buildings and other Structures, 2000 Edition, Part 1: Provisions (FEMA 368)." Prepared by the Building Seismic Safety Council for the Federal Emergency Management Agency, Washington, D.C.
- FEMA. (2001b). "NEHRP Recommended Provisions for Seismic Regulations for New Buildings and other Structures, 2000 Edition, Part 2: Commentary (FEMA 369)." Prepared by the Building Seismic Safety Council for the Federal Emergency Management Agency, Washington, D.C.
- Field, E. H. (2000). "A Modified Ground Motion Attenuation Relationship for Southern California that Accounts for Detailed Site Classification and a Basin-Depth Effect." *Bulletin of the Seismological Society of America*, 90(6 PT B), 209-221.
- Field, E. H., Anderson, J. G., Henyey, T. L., Jackson, D. D., Joyner, W. B., Lee, Y., Magistrale, H., Minster, B., Olsen, K. B., Petersen, M. D., Steidl, J. H., Wald, L. A., and Wills, C. J. (2000). "Accounting for Site Effects in Probabilistic Seismic Hazard Analyses of Southern California: Overview of the SCEC Phase III Report." *Bulletin of the Seismological Society of America*, 90(6B), S1-S31.
- Field, E. H., and Jacob, K. H. (1993). "The Theoretical Response of Sedimentary Layers to Ambient Seismic Noise." *Geophysical Research Letters*, 20(24), 2925-2928.
- Field, E. H., and Jacob, K. H. (1995). "Comparison and Test of Various Site-Response Estimation Techniques, including Three that are not Reference-Site Dependent." *Bulletin of the Seismological Society of America*, 85(4), 1127-1143.

- Frankel, A. (1993). "Three-Dimensional Simulations of Ground Motions in the San Bernardino Valley, California, for Hypothetical Earthquakes on the San Andreas Fault." *Bulletin of the Seismological Society of America*, 83(4), 1020-1041.
- Frankel, A., Mueller, C., Barnhard, T., Perkins, D., Leyendecker, E. V., Dickman, N., Hanson, S., and Hopper, M. (1996). "National Seismic Hazard Maps: Documentation." *OFR 96-532*, U.S. Geological Survey.
- Frankel, A., Petersen, M., Mueller, C., Haller, K., Wheeler, R., Leyendecker, E. V., Wesson, R., Harmsen, S., Cramer, C., Perkins, D., and Rukstales, K. (2002). "Documentation for the 2002 Update of the National Seismic Hazard Maps." *U.S. Geological Survey OFR 02-420*.
- Frankel, A. D. (1995). "Mapping Seismic Hazard in the Central and Eastern United States." *Seismological Research Letters*, 66(4), 8-21.
- Fu, L.-Y., and Bouchon, M. (2004). "Discrete Wavenumber Solutions to Numerical Wave Propagation in Piecewise Heterogeneous Media. I. Theory of Two-Dimensional SH Case." *Geophysical Journal International*, 157(2), 481-98.
- Geli, L., Bard, P. Y., and Jullien, B. (1988). "The Effect of Topography on Earthquake Ground Motion: A Review and New Results." *Bulletin of the Seismological Society of America*, 78(1), 42-63.
- Giammarinaro, M. S., Tertulliani, A., Galli, G., and Leta, M. (2005). "Investigation of Surface Geology and Intensity Variability in the Palermo, Italy, Urban Area after the 6 September 2002 Earthquake." *Bulletin of the Seismological Society of America*, 95(6), 2318-2327.
- Gil-Zepeda, S. A., Montalvo-Arrieta, J. C., Vai, R., and Sanchez-Sesma, F. J. (2003). "A Hybrid Indirect Boundary Element - Discrete Wave Number Method Applied to Simulate the Seismic Response of Stratified Alluvial Valleys." *Soil Dynamics and Earthquake Engineering*, 23(1), 77-86.
- Goulet, C. A., and Stewart, J. P. (2007). "Probabilistic versus Deterministic Implementation of Nonlinear Site Factors in Seismic Hazard Analysis." *2007 Asian-Pacific Network of Centers for Earthquake Engineering Research (ANCER) Meeting*, Hong Kong, China.

- Goulet, C. A., Stewart, J. P., Bazzurro, P., and Field, E. H. (2007). "Integration of Site-Specific Ground Response Analysis Results into Probabilistic Seismic Hazard Analyses." *4th International Conference on Earthquake Geotechnical Engineering*, Thessaloniki, Greece, Paper No. 1486.
- Graves, R. W., Pitarka, A., and Somerville, P. G. (1998). "Ground-Motion Amplification in the Santa Monica Area: Effects of Shallow Basin-Edge Structure." *Bulletin of the Seismological Society of America*, 88(5), 1224-1242.
- Graves, R. W., and Wald, D. J. (2004). "Observed and Simulated Ground Motions in the San Bernardino Basin Region for the Hector Mine, California, Earthquake." *Bulletin of the Seismological Society of America*, 94(1), 131-146.
- Haddon, R. (1996). "Earthquake Source Spectra in Eastern North America." *Bulletin of the Seismological Society of America*, 86(5), 1300-1313.
- Hanks, T. C. (1975). "Strong Ground Motion of the San Fernando, California, Earthquake: Ground Displacements." *Bulletin of the Seismological Society of America*, 65(1), 193-225.
- Hanks, T. C., and McGuire, R. K. (1981). "The Character of High-Frequency Strong Ground Motion." *Bulletin of the Seismological Society of America*, 71(6), 2071-95.
- Hansen, C. (2001). "Regularization Tools. A Matlab Package for Analysis and Solution of Discrete Ill-Posed Problems. Version 3.1 for Matlab 6.0." Department of Mathematical Modelling, Technical University of Denmark, Lyngby, Denmark.
- Harik, I. E., Allen, D. L., Street, R. L., Guo, M., Graves, R. C., Harison, J., and Gawry, M. J. (1997). "Seismic Evaluation of Brent-Spence Bridge." *Journal of Structural Engineering*, 123(9), 1269-1275.
- Hartzell, S., Bonilla, L. F., and Williams, R. A. (2004). "Prediction of Nonlinear Soil Effects." *Bulletin of the Seismological Society of America*, 94(5), 1609-1629.
- Hashash, Y. M. A., and Park, D. (2001). "Non-linear One-dimensional Seismic Ground Motion Propagation in the Mississippi Embayment." *Engineering Geology*, 62(1-3), 185-206.

- Haskell, N. A. (1953). "The Dispersion of Surface Waves on Multilayered Media." *Bulletin of the Seismological Society of America*, 43, 17-34.
- Herrera, I. (1984). *Boundary Methods. An Algebraic Theory*, Pitman Advanced Publishing Program, Boston, Massachusetts.
- Herrmann, R. B. (1985). "An Extension of Random Vibration Theory Estimates of Strong Ground Motion to Large Distances." *Bulletin of the Seismological Society of America*, 75(5), 1447-1453.
- Hruby, C. E., and Beresnev, I. A. (2003). "Empirical Corrections for Basin Effects in Stochastic Ground-Motion Prediction, Based on the Los Angeles Basin Analysis." *Bulletin of the Seismological Society of America*, 93(4), 1679 - 1690.
- Hwang, H., and Huo, J.-R. (1997). "Attenuation Relations of Ground Motion for Rock and Soil Sites in Eastern United States." *Soil Dynamics and Earthquake Engineering*, 16(6), 363-372.
- Idriss, I. M., and Seed, H. B. (1968). "Seismic Response of Horizontal Soil Layers." *American Society of Civil Engineers Proceedings, Journal of the Soil Mechanics and Foundations Division*, 94(SM4), 1003-1031.
- Idriss, I. M., and Sun, J. I. (1992). "SHAKE 91. A Computer Program for Conducting Equivalent Linear Seismic Response Analyses of Horizontally Layered Soil Deposits." University of California, Davis.
- Iervolino, I., and Cornell, C. A. (2005). "Record Selection for Nonlinear Seismic Analysis of Structures." *Earthquake Spectra*, 21(3), 685 - 713.
- Johnston, A. C., and Schweig, E. S. (1996). "Enigma of the New Madrid Earthquakes of 1811-1812." *Annual Review of Earth and Planetary Sciences*, 24, 339-384.
- Joyner, W. (1997). "Ground Motion Estimates for the Northeastern U.S. or Southeastern Canada." in "Recommendations for Probabilistic Seismic Hazard Analysis: Guidance on Uncertainty and Use of Experts," prepared by R.J. Budnitz, G. Apostolakis, D.M. Boore, L.S. Cluff, K.J. Coppersmith, C.A. Cornell, and P.A. Morris, U.S. Nuclear Regulatory Commission, Report NUREG/CR-6372, Washington, DC.

- Joyner, W. B. (1984). "A Scaling Law for the Spectra of Large Earthquakes." *Bulletin of the Seismological Society of America*, 74(4), 1167-1188.
- Joyner, W. B. (2000). "Strong Motion from Surface Waves in Deep Sedimentary Basins." *Bulletin of the Seismological Society of America*, 90(6 PT B), 95-112.
- Joyner, W. B., Warrick, R. E., and Fumal, T. (1981). "The Effect of Quaternary Alluvium on Strong Motion in the Coyote Lake, California, Earthquake of 1979." *Bulletin of the Seismological Society of America*, 71(4), 1333-1349.
- Kanai, K. (1962). "On the Spectrum of Strong Earthquake Motions." *Bulletin of the Earthquake Research Institute*, 40(1), 71-90.
- Kanai, K., and Tanaka, T. (1961). "On Microtremors VIII." *Bulletin of the Earthquake Research Institute*, 39(1), 97-114.
- Kanai, K., Tanaka, T., and Yoshizawa, S. (1965). "On Microtremors IX." *Bulletin of the Earthquake Research Institute*, 43(3), 577-588.
- Kausel, E., and Assimaki, D. (2002). "Seismic Simulation of Inelastic Soils via Frequency-Dependent Moduli and Damping." *Journal of Engineering Mechanics*, 128(1), 34 - 47.
- Kausel, E., and Roesset, J. M. (1984). "Soil Amplification: Some Refinements." *Soil Dynamics and Earthquake Engineering*, 3(3), 116-123.
- Kawase, H. (1996). "The Cause of the Damage Belt in Kobe: "The Basin-Edge Effect", Constructive Interference of the Direct S-Wave with the Basin-Induced Diffracted/Rayleigh Waves." *Seismological Research Letters*, 67(5), 25-34.
- Kawase, H. (2003). "Site Effects on Strong Ground Motions." International Handbook of Earthquake and Engineering Seismology, Part B, W. H. Lee, H. Kanamori, P. C. Jennings, and C. Kisslinger, eds., Academic Press, 1013-1030.
- Kawase, H., and Aki, K. (1990). "Topography Effect at the Critical SV-Save Incidence: Possible Explanation of Damage Pattern by the Whittier Narrows, California, Earthquake of 1 October 1987." *Bulletin of the Seismological Society of America*, 80(1), 1-22.

- Keaton, J. R., Zeng, Y., and Anderson, J. G. (2000). "Procedure for Scaling Earthquake Records to Match Acceleration Response Spectra for Engineering Design." *Sixth International Conference on Seismic Zonation: Managing Earthquake Risk in the 21st Century*, EERI, Palm Springs, CA.
- Kempton, J. J., and Stewart, J. P. (2006). "Prediction Equations for Significant Duration of Earthquake Ground Motions Considering Site and Near-Source Effects." *Earthquake Spectra*, 22(4), 985-1013.
- Knapp, J. (2003). "Geology-Based Site Coefficients for the Upper Mississippi Embayment," Master Thesis, Georgia Institute of Technology, Atlanta, GA.
- Kramer, S. L. (1996). *Geotechnical Earthquake Engineering*, Prentice-Hall, Inc., Upper Saddle River, NJ.
- Krinitzsky, E. L. (1995). "Deterministic versus Probabilistic Seismic Hazard Analysis for Critical Structures." *Engineering Geology*, 40(1-2), 1-7.
- Krinitzsky, E. L. (1998). "Hazard in using Probabilistic Seismic Hazard Analysis for Critical Structures." Seattle, WA, USA, 164-165.
- Krinitzsky, E. L. (2002a). "Epistematic and Aleatory Uncertainty: A New Shtick for Probabilistic Seismic Hazard Analysis." *Engineering Geology*, 66(1-2), 157-159.
- Krinitzsky, E. L. (2002b). "How to Obtain Earthquake Ground Motions for Engineering Design." *Engineering Geology*, 65(1), 1-16.
- Krinitzsky, E. L. (2003). "How to Combine Deterministic and Probabilistic Methods for Assessing Earthquake Hazards." *Engineering Geology*, 70(1-2), 157-163.
- Kudo, K., and Sawada, Y. (1992). "Blind Prediction Experiments at Ashigara Valley, Japan." *Proceedings of the 10th World Conference on Earthquake Engineering*, Madrid, Spain, 6967-6971.
- Lachet, C., and Bard, P.-Y. (1994). "Numerical and Theoretical Investigations on the Possibilities and Limitations of the "Nakamura's" Technique." *Journal of Physics of the Earth*, 42, 377-397.

- Lachet, C., Hatzfeld, D., Bard, P.-Y., Theodulidis, N., Papaioannou, C., and Savvaidis, A. (1996). "Site Effects and Microzonation in the City of Thessaloniki (Greece) Comparison of Different Approaches." *Bulletin of the Seismological Society of America*, 86(6), 1692-1703.
- Lawrence, B. K., Rix, G. J., and Mayne, P. W. (2006). "Validation of Ground Motions in the Upper Mississippi Embayment." *Eighth U.S. National Conference on Earthquake Engineering 8NCEE*, San Francisco, CA.
- Lay, T., and Wallace, T. C. (1995). *Modern Global Seismology*, Academic Press, Inc., San Diego, California.
- Lee, Y., and Anderson, J. G. (2000). "Potential for Improving Ground-Motion Relations in Southern California by Incorporating Various Site Parameters." *Bulletin of the Seismological Society of America*, 90(6 PT B), 170-186.
- Lermo, J., and Chavez-Garcia, F. J. (1994). "Are Microtremors useful in Site Response Evaluation?" *Bulletin of the Seismological Society of America*, 84(5), 1350-1364.
- Leyendecker, E. V., Hunt, R. J., Frankel, A. D., and Rukstales, K. S. (2000). "Development of Maximum Considered Earthquake Ground Motion Maps." *Earthquake Spectra*, 16(1), 21-40.
- Lutes, L. D., and Sarkani, S. (1997). *Stochastic Analysis of Structural and Mechanical Vibrations*, Prentice Hall, Inc., Upper Saddle River, New Jersey.
- Luzon, F., Gil-Zepeda, S. A., Sanchez-Sesma, F. J., and Ortiz-Aleman, C. (2004). "Three-Dimensional Simulation of Ground Motion in the Zafarraya Basin (Southern Spain) up to 1.335 Hz under Incident Plane Waves." *Geophysical Journal International*, 156(3), 584-94.
- Mahdyiar, M. (2002). "Are NEHRP and Earthquake-Based Site Effects in Greater Los Angeles Compatible?" *Seismological Research Letters*, 73, 39-45.
- Makra, K., Chavez-Garcia, F. J., Raptakis, D., and Pitilakis, K. (2005). "Parametric Analysis of the Seismic Response of a 2D Sedimentary Valley: Implications for Code Implementations of Complex Site Effects." *Soil Dynamics and Earthquake Engineering*, 25(4), 303-315.

- Makra, K., Raptakis, D., Chavez-Garcia, F. J., and Pitilakis, K. (2002). "How Important is the Detailed Knowledge of a 2D Soil Structure for Site Response Evaluation?" 12th European Conference on Earthquake Engineering, London, UK.
- Manolis, G. D., and Beskos, D. E. (1988). *Boundary Element Methods in Elastodynamics*, Unwin Hyman Ltd., London, UK.
- McGuire, R. K. (1976). "FORTRAN Computer Program for Seismic Risk Analysis." *Open-File Report 76-67*, U.S. Geological Survey.
- McGuire, R. K. (1993). "Computations of Seismic Hazard." *Annali di Geofisica*, 36, 181-200.
- McGuire, R. K. (1995). "Probabilistic Seismic Hazard Analysis and Design Earthquakes: Closing the Loop." *Bulletin of the Seismological Society of America*, 85(5), 1275.
- McGuire, R. K. (2001). "Deterministic vs. Probabilistic Earthquake Hazards and Risks." *Soil Dynamics and Earthquake Engineering*, 21(5), 377-384.
- McGuire, R. K. (2004). *Seismic Hazard and Risk Analysis*, Earthquake Engineering Research Institute, Oakland, CA.
- McGuire, R. K., Cornell, C. A., and Toro, G. R. (2005). "The Case for Using Mean Seismic Hazard." *Earthquake Spectra*, 21(3), 879-886.
- McGuire, R. K., Silva, W. J., and Costantino, C. J. (2001). "Technical Basis for Revision of Regulatory Guidance on Design Ground Motions: Hazard- and Risk-Consistent Ground Motion Spectra Guidelines." *NUREG/CR-6728*, U.S. Nuclear Regulatory Commission, Washington, DC.
- Moczo, P., Labak, P., Kristek, J., and Hron, F. (1996). "Amplification and Differential Motion due to an Antiplane 2D Resonance in the Sediment Valleys Embedded in a Layer over the Half-Space." *Bulletin of the Seismological Society of America*, 86(5), 1434-1446.
- Moeen-Vaziri, N., and Trifunac, M. D. (1988). "Scattering and Diffraction of Plane SH-Waves by Two-Dimensional Inhomogeneities: Part I." *Soil Dynamics and Earthquake Engineering*, 7(4), 179-188.

- Mukherjee, S., and Gupta, V. (2002). "Wavelet-Based Generation of Spectrum-Compatible Time-Histories." *Soil Dynamics and Earthquake Engineering*, 22(9-12), 799-804.
- Musson, R. M. W. (1998). "On the Use of Monte Carlo Simulations for Seismic Hazard Assessment." 6th US. National Conference on Earthquake Engineering, Seattle, Washington.
- Musson, R. M. W. (1999). "Determination of Design Earthquakes in Seismic Hazard Analysis through Monte Carlo Simulation." *Journal of Earthquake Engineering*, 3(4), 463.
- Musson, R. M. W. (2000). "The use of Monte Carlo Simulations for Seismic Hazard Assessment in the UK." *Annali di Geofisica*, 43(1), 1-9.
- Musson, R. M. W. (2005). "Against Fractiles." *Earthquake Spectra*, 21(3), 887-891.
- Nakamura, Y. (1989). "Method for Dynamic Characteristics Estimation of Subsurface using Microtremor on the Ground Surface." *Quarterly Report of RTRI (Railway Technical Research Institute) (Japan)*, 30(1), 25-33.
- Narayan, J. P., and Singh, S. P. (2006). "Effects of Soil Layering on the Characteristics of Basin-Edge Induced Surface Waves and Differential Ground Motion." *Journal of Earthquake Engineering*, 10(4), 595-614.
- Nuttli, O. W. (1981). "Similarities and Differences between Western and Eastern United States Earthquakes, and Their Consequences for Earthquake Engineering." *Earthquakes and Earthquake Engineering: The Eastern United States*, Knoxville, Tennessee, 25-51.
- Papageorgiou, A. S., and Pei, D. (1998). "A Discrete Wavenumber Boundary Element Method for Study of the 3-D Response of 2-D Scatterers." *Earthquake Engineering and Structural Dynamics*, 27, 619 - 638.
- Park, D., and Hashash, Y. M. A. (2005). "Evaluation of Seismic Site Factors in the Mississippi Embayment. II. Probabilistic Seismic Hazard Analysis with Nonlinear Site Effects." *Soil Dynamics and Earthquake Engineering*, 25, 145 - 156.

- Paul, W. J. (2002). "Discussion on the Opinion Paper 'Epistematic and Aleatory Uncertainty: a New Shtick for Probabilistic Seismic Hazard Analysis' by Ellis L. Krinitzsky, *Engineering Geology* 66(1-2), 157-159." *Engineering Geology*, 66, 161.
- Pedersen, H., Le Brun, B., Hatzfeld, D., Campillo, M., and Bard, P. Y. (1994). "Ground-Motion Amplitude across Ridges." *Bulletin of the Seismological Society of America*, 84(6), 1786-1800.
- Pedersen, H. A., Campillo, M., and Sanchez-Sesma, F. J. (1995). "Azimuth Dependent Wave Amplification in Alluvial Valleys." *Soil Dynamics and Earthquake Engineering*, 14(4), 289.
- Pei, D., and Papageorgiou, A. S. (1996). "Locally Generated Surface Waves in Santa Clara Valley: Analysis of Observations and Numerical Simulation." *Earthquake Engineering and Structural Dynamics*, 25(1), 47-63.
- Pfaffinger, D. D. (1983). "Calculation of Power Spectra from Response Spectra." *Journal of Engineering Mechanics*, 109(1), 357-372.
- Pitilakis, K. (2004). "Site Effects." Recent Advances in Earthquake Geotechnical Engineering and Microzonation, A. Ansal, ed., Kluwer Academic Publishers, Dordrecht, The Netherlands, 139-197.
- Raptakis, D., Chavez-Garcia, F. J., Makra, K., and Pitilakis, K. (2000). "Site Effects at Euroseistest - I. Determination of the Valley Structure and Confrontation of Observations with 1D Analysis." *Soil Dynamics and Earthquake Engineering*, 19(1), 1-22.
- Rathje, E., Idriss, I. M., Somerville, P., Ansal, A., Bachhuber, J., Baturay, M., Erdik, M., Frost, D., Lettis, W., Sozer, B., Stewart, J., and Ugras, T. (2000). "Strong Ground Motions and Site Effects." *Earthquake Spectra*, 16(SUPPL A), 65-96.
- Real, C. R., Shakal, A. F., and Tucker, B. E. (2006). "Turkey Flat, U.S.A. Site Effects Test Area: Anatomy of a Blind Ground-Motion Prediction Test." Third International Symposium on the Effects of Surface Geology on Seismic Motion, Grenoble, France.
- Reiter, L. (1990). *Earthquake Hazard Analysis. Issues and Insights.*, Columbia University Press, New York.

- Restrepo, J. I., and Cowan, H. A. (2000). "'Eje Cafetero' Earthquake, Colombia of January 25 1999." *Bulletin of the New Zealand National Society for Earthquake Engineering*, 33(1), 1-29.
- Risk Engineering Inc. (2005). "EZ-FRISK Version 7.14, User's Manual." Risk Engineering Inc., Software for Earthquake Ground Motion Estimation.
- Roblee, C. J., Silva, W., Toro, G. R., and Abrahamson, N. A. (1996). "Variability in Site-Specific Seismic Ground-Motion Design Predictions." *Uncertainty in the Geologic Environment: from Theory to Practice, "Uncertainty '96", Geotechnical Special Publication No. 58*, Madison, WI, 1113-1133.
- Romero, S. M. (2001). "Ground Motion Amplification of Soils in the Upper Mississippi Embayment," Ph.D. Dissertation, Georgia Institute of Technology, Atlanta, GA.
- Saikia, C. K., Pitarka, A., and Ichinose, G. A. (2006). "Effects of Irregular Structure of the Mississippi Embayment on Ground-Motion Amplification." *Bulletin of the Seismological Society of America*, 96(4), 1448-1473.
- Sanchez-Sesma, F., Chavez-Perez, S., Suarez, M., Bravo, M. A., and Perez-Rocha, L. E. (1988). "Mexico Earthquake of September 19, 1985 - On the Seismic Response of the Valley of Mexico." *Earthquake Spectra*, 4(3), 569-589.
- Sanchez-Sesma, F. J. (1987). "Site Effects on Strong Ground Motion." *Soil Dynamics and Earthquake Engineering*, 6(2), 124-132.
- Sanchez-Sesma, F. J., and Esquivel, J. A. (1979). "Ground Motion on Alluvial Valleys under Incident Plane SH Waves." *Bulletin of the Seismological Society of America*, 69(4), 1107-1120.
- Sanchez-Sesma, F. J., Herrera, I., and Aviles, J. (1982). "A Boundary Method for Elastic Wave Diffraction: Application to Scattering of SH Waves by Surface Irregularities." *Bulletin of the Seismological Society of America*, 72(2), 473-490.
- Sanchez-Sesma, F. J., Ramos-Martinez, J., and Campillo, M. (1993). "An Indirect Boundary Element Method Applied to Simulate the Seismic Response of Alluvial Valleys for Incident P, S and Rayleigh Waves." *Earthquake Engineering and Structural Dynamics*, 22(4), 279-95.

- Sanchez-Sesma, F. J., Vai, R., Dretta, E., and Palencia, V. J. (2000). "Fundamentals of Elastic Wave Propagation for Site Amplification Studies: The Seismic Response of Alluvial Valleys." *Wave Motion in Earthquake Engineering*, E. K. a. G. Manolis, ed., WIT Press, 1-36.
- Santamarina, J. C., and Fratta, D. (1998). *Introduction to Discrete Signals and Inverse Problems in Civil Engineering*, ASCE Press, Reston, VA.
- Santamarina, J. C., Klein, K. A., and Fam, M. A. (2001). *Soils and Waves*, John Wiley & Sons Ltd., West Sussex, England.
- Satoh, T., Kawase, H., and Sato, T. (1995). "Evaluation of Local Site Effects and their Removal from Borehole Records Observed in the Sendai Region, Japan." *Bulletin of the Seismological Society of America*, 85(6), 1770-1789.
- Scawthorn, C. (2003). "Earthquakes: A Historical Perspective." *Earthquake Engineering Handbook*, W.-F. Chen and C. Scawthorn, eds., CRC Press LLC, Boca Raton, Florida, USA.
- Schnabel, P. B., Lysmer, J., and Seed, H. B. (1972). "SHAKE: A Computer Program for Earthquakes Response Analysis of Horizontally Layered Sites." *UCB/EERC-72/12*, Earthquake Engineering Research Center, University of California, Berkeley, California.
- Schwartz, D. P., and Coppersmith, K. J. (1984). "Fault Behaviour and Characteristic Earthquakes: Examples from the Wasatch and San Andreas Fault Zones." Snowbird, UT, USA, 5681-5698.
- Schweig, E. S., and Van-Arsdale, R. B. (1996). "Neotectonics of the Upper Mississippi Embayment." *Engineering Geology*, 45, 185 - 203.
- Scott, S. G., Bommer, J. J., and Sarma, S. K. (1998). "Definition of Hazard-Consistent Ground Motions through Multi-Parameter Seismic Hazard Assessment." *Seismic Design Practice into the Next Century. Research and Application*, Oxford, UK, 229-236.
- Seed, H. B., and Idriss, I. M. (1969). "Influence of Soil Conditions on Ground Motions during Earthquakes." *American Society of Civil Engineers, Journal of the Soil Mechanics and Foundations Division*, 95(SM1), 99-137.

- Seed, R. B., Dickenson, S. E., and Idriss, I. M. (1991). "Principal Geotechnical Aspects of the 1989 Loma Prieta Earthquake." *Soils and Foundations*, 31(1), 1-26.
- Seed, R. B., Dickenson, S. E., Riemer, M. F., Bray, J. D., Sitar, N., Mitchell, J. K., Idriss, I. M., Kayen, R. E., Kropp, A., L.F. Harder Jr., and Power, M. S. (1990). "Preliminary Report on the Principal Geotechnical Aspects of the October 17, 1989 Loma Prieta Earthquake." *Report No. UCB/EERC-90/05*, Earthquake Engineering Research Center, University of California at Berkeley.
- Seekins, L. C., Wennerberg, L., Margheriti, L., and Liu, H.-P. (1996). "Site Amplification at Five Locations in San Francisco, California: A Comparison of S Waves, Cudas, and Microtremors." *Bulletin of the Seismological Society of America*, 86(3), 627-635.
- Semblat, J. F., Duval, A. M., and Dangla, P. (2002). "Seismic Site Effects in a Deep Alluvial Basin: Numerical Analysis by the Boundary Element Method." *Computers and Geotechnics*, 29(7), 573-585.
- Semblat, J. F., Kham, M., Parara, E., Bard, P. Y., Pitilakis, K., Makra, K., and Raptakis, D. (2005). "Seismic Wave Amplification: Basin Geometry vs Soil Layering." *Soil Dynamics and Earthquake Engineering*, 25(7-10), 529-538.
- Shinozaki, Y., and Irikura, K. (1992). "Summary and Some Comments on results of Ashigara Valley Blind Prediction Test." *Proceedings of the 10th World Conference on Earthquake Engineering*, Madrid, Spain, 6973-6976.
- Shoji, Y., Tani, K., and Kamiyama, M. (2005). "A Study on the Duration and Amplitude Characteristics of Earthquake Ground Motions." *Soil Dynamics and Earthquake Engineering*, 25(7-10), 505-512.
- Shome, N., Cornell, C. A., Bazzurro, P., and Carballo, J. E. (1998). "Earthquakes, Records, and Nonlinear Responses." *Earthquake Spectra*, 14(3), 469 - 500.
- Silva, W. (1976). "Body Waves in a Layered Anelastic Solid." *Bulletin of the Seismological Society of America*, 66(5), 1539-1554.
- Silva, W. (1992). "Factors Controlling Strong Ground Motion and Their Associated Uncertainties." *Dynamic Analysis and Design Considerations for High-Level Nuclear Waste Repositories*, San Francisco, California, 132-161.

- Silva, W., Abrahamson, N. A., Toro, G. R., and Constantino, C. (1997). "Description and Validation of the Stochastic Ground Motion Model." *Report Prepared for the Engineering Research and Applications Division Department of Nuclear Energy, Pacific Engineering and Analysis, El Cerrito, CA.*
- Silva, W., and Costantino, C. (2002). "Development of Site-Specific Design Ground Motions in Western and Eastern North America." *Soil Dynamics and Earthquake Engineering*, 22, 755-764.
- Silva, W., Gregor, N., and Darragh, R. (2002). "Development of Regional Hard Rock Attenuation Relations for Central and Eastern North America." Pacific Engineering and Analysis, El Cerrito, CA.
- Silva, W., Gregor, N., and Darragh, R. (2003). "Development of Regional Hard Rock Attenuation Relations for Central and Eastern North America, Mid-Continent and Gulf Coast Areas." Pacific Engineering and Analysis, El Cerrito, CA.
- Silva, W., and Lee, K. (1987). "WES RASCALS Code for Synthesizing Earthquake Ground Motions." Pacific Engineering and Analysis, El Cerrito, CA.
- Silva, W. J., Lee, R., McGuire, R. K., and Cornell, C. A. (2000). "A Comparison of Methodologies to Achieve a Site-Specific PSHA (abstract)." *Seismological Research Letters*, 71, 247.
- Silva, W. J., Wong, I. G., and Darragh, R. B. (1991). "Engineering Characterization of Earthquakes Strong Ground Motions with Applications to the Pacific Northwest." *Open-File Report 91-441-H*, U.S. Geological Survey.
- Sokolov, V. Y., Loh, C.-H., and Wen, K.-L. (2000). "Empirical Study of Sediment-Filled Basin Response: The Case of Taipei City." *Earthquake Spectra*, 16(3), 681-707.
- Somerville, P., and Collins, N. (2003). "Ground Motion Time Histories for Use in Performance Based Seismic Engineering." *Report to the U.S. Geological Survey under award number 01HQGR0154*, URS Group, Inc.
- Somerville, P., and Saikia, C. (2001). "Ground Motion Attenuation Relations for the Central and Eastern United States." *Report to the U.S. Geological Survey under award number 99HQGR0098*, URS Group, Inc.

- Somerville, P., Smith, N., Punyamurthula, S., and Sun, J. (1997). "Development of Ground Motion Time Histories for Phase 2 of the FEMA/SAC Steel Project." *Report No. SAC/BD-97/04*, SAC Joint Venture, Sacramento, CA.
- Stepp, J. C., and Cramer, C. H. (1992). "A Brief Summary of the Results of the Turkey Flat Weak Motion Site Response Blind Prediction." *Proceedings of the 10th World Conference on Earthquake Engineering*, Madrid, Spain, 6963-6965.
- Stewart, J., Chiou, S.-J., Bray, J., Graves, R., Somerville, P., and Abrahamson, N. (2002). "Ground Motion Evaluation Procedures for Performance-Based Design." *Soil Dynamics and Earthquake Engineering*, 22(9-12), 765-772.
- Stewart, J. P., Goulet, C., Bazzurro, P., and Claassen, R. (2006). "Implementation of 1D Ground Response Analysis in Probabilistic Assessments of Ground Shaking Potential." *GeoCongress 2006, Geotechnical Engineering in the Information Technology Age*, Atlanta, GA.
- Stewart, J. P., and Goulet, C. A. (2006). "Comment on "Nonlinear Soil-Site Effects in Probabilistic Seismic-Hazard Analysis" by Paolo Bazzurro and C. Allin Cornell." *Bulletin of the Seismological Society of America*, 96(2), 745-747.
- Stover, C. W., and Coffman, J. L. (1993). "Seismicity of the United States, 1568-1989 (Revised)." U.S. Geological Survey Professional Paper 1527, United States Government Printing Office, Washington, 337.
- Street, R., Woolery, E. W., and Chiu, J.-M. (2004). "Shear-wave Velocities of the Post-Paleozoic Sediments across the Upper Mississippi Embayment." *Seismological Research Letters*, 75(3), 390 - 405.
- Su, F., Anderson, J. G., Der Ni, S., and Zeng, Y. (1998). "Effect of Site Amplification and Basin Response on Strong Motion in Las Vegas, Nevada." *Earthquake Spectra*, 14(2), 357-376.
- Takenaka, H., Furumura, T., and Fujiwara, H. (1998). "Recent Developments in Numerical Methods for Ground Motion Simulation." *Proceedings of the Second International Symposium on the Effects of Surface Geology on Seismic Motion*, Yokohama, Japan, 91-101.

- Thenhaus, P. C., and Campbell, K. W. (2003). "Seismic Hazard Analysis." *Earthquake Engineering Handbook*, W.-F. Chen and C. Scawthorn, eds., CRC Press LLC, Boca Raton, Florida, USA.
- Thomson, W. T. (1950). "Transmission of Elastic Waves Through a Stratified Solid Medium." *Journal of Applied Physics*, 21, 89-93.
- Toro, G. R. (1995). "Probabilistic Models of Site Velocity Profiles for Generic and Site-Specific Ground-Motion Amplification Studies." *Report prepared for Brookhaven National Laboratory, Under Contract 779574*, Risk Engineering, Inc., Boulder, CO.
- Toro, G. R., Abrahamson, N. A., and Schneider, J. F. (1997). "Model of Strong Ground Motions from Earthquakes in Central and Eastern North America: Best Estimates and Uncertainties." *Seismological Research Letters*, 68(1), 41-57.
- Toro, G. R., and McGuire, R. K. (1987). "Calculational Procedures for Seismic Hazard Analysis and its Uncertainty in the Eastern United States." *Developments in Geotechnical Engineering* 44. *Ground Motion and Engineering Seismology*, A. S. Cakmak, ed., Elsevier Science Publishing Company Inc., New York, NY, 195-206.
- Toro, G. R., and Silva, W. (2001). "Scenario Earthquakes for Saint Louis, MO, and Memphis, TN, and Seismic Hazard Maps for the Central United States Region Including the Effect of Site Conditions." *Technical Report, USGS Grant 1434-HQ-97-GR-02981*, Risk Engineering, Inc., Boulder, CO.
- Toshinawa, T., and Ohmachi, T. (1992). "Love-Wave Propagation in a Three-Dimensional Sedimentary Basin." *Bulletin of the Seismological Society of America*, 82(4), 1661-1677.
- Trifunac, M. D. (1971). "Surface Motion of a Semi-Cylindrical Alluvial Valley for Incident Plane SH Waves." *Bulletin of the Seismological Society of America*, 61(6), 1755-1770.
- Trifunac, M. D., and Brady, A. G. (1975). "A Study on the Duration of Strong Earthquake Ground Motion." *Bulletin of the Seismological Society of America*, 65(3), 581-626.

- Tsang, H.-H., and Chandler, A. M. (2006). "Site-Specific Probabilistic Seismic-Hazard Assessment: Direct Amplitude-Based Approach." *Bulletin of the Seismological Society of America*, 96(2), 392-403.
- Van Arsdale, R. B., and TenBrink, R. K. (2000). "Late Cretaceous and Cenozoic Geology of the New Madrid Seismic Zone." *Bulletin of the Seismological Society of America*, 90(2), 345-356.
- Vanmarcke, E. H. (1979). "State-of-the-art for Assessing Earthquakes Hazard in the United States: Representation of Earthquake Ground Motions - Scaled Accelerograms and Equivalent Response Spectra." *Miscellaneous Paper S-73-1, Report 14*, U.S. Army Corps of Engineers Waterways Experiment Station, Vicksburg, Mississippi.
- Vanmarcke, E. H., and Lai, S.-S. P. (1980). "Strong-Motion Duration and RMS Amplitude of Earthquake Records." *Bulletin of the Seismological Society of America*, 70(4), 1293-1307.
- Walsh, M. J. (2003). "Engineering and Design. Time-History Dynamics Analysis of Concrete Hydraulic Structures." *EM 1110-2-6051*, U.S. Army Corps of Engineers, Washington, DC.
- Watson-Lamprey, J., and Abrahamson, N. (2006a). "Selection of Ground Motion Time Series and Limits on Scaling." *Soil Dynamics and Earthquake Engineering*, 26(5), 477-482.
- Watson-Lamprey, J. A., and Abrahamson, N. A. (2006b). "Bias Caused by Use of Spectrum Compatible Motions." Proceedings of the 8th U.S. National Conference on Earthquake Engineering, San Francisco, California.
- Wells, D. L., and Coppersmith, K. J. (1994). "New Empirical Relationships among Magnitude, Rupture Length, Rupture Width, Rupture Area, and Surface Displacement." *Bulletin of the Seismological Society of America*, 84(4), 974-1002.
- Wen, Y. K., and Wu, C. L. (2001). "Uniform Hazard Ground Motions for Mid-America Cities." *Earthquake Spectra*, 17(2), 359-384.
- Wheeler, R. L., and Perkins, D. M. (2000). "Research, Methodology, and Applications of Probabilistic Seismic-Hazard Mapping of the Central and Eastern United States -

Minutes of a Workshop on June 13-14, 2000, at Saint Louis University " *Open-File Report 00-0390*, U.S. Geological Survey.

- Wollery, W., and Street, R. (2002). "3D Near-Surface Soil Response from H/V Ambient-Noise Ratios." *Soil Dynamics and Earthquake Engineering*, 22(9-12), 865-876.
- Wong, H. L., and Trifunac, M. D. (1974). "Surface Motion of a Semi-Elliptical Alluvial Valley for Incident Plane SH Waves." *Bulletin of the Seismological Society of America*, 64(5), 1389-1408.
- Yegian, M. K., Ghahraman, V. G., and Gazetas, G. (1994a). "Ground-Motion and Soil-Response Analyses for Leninakan, 1988 Armenia Earthquake." *Journal of Geotechnical Engineering*, 120(2), 330-348.
- Yegian, M. K., Ghahraman, V. G., and Gazetas, G. (1994b). "Seismological, Soil and Valley Effects in Kirovakan, 1988 Armenia Earthquake." *Journal of Geotechnical Engineering*, 120(2), 349-365.
- Youngs, R. R., and Coppersmith, K. J. (1985). "Implications of Fault Slip Rates and Earthquake Recurrence Models to Probabilistic Seismic Hazard Estimates." *Bulletin of the Seismological Society of America*, 75(4), 939-964.
- Zeng, Y., and Benites, R. (1998). "Seismic Response of Multi-Layered Basins with Velocity Gradients Upon Incidence of Plane Shear Waves." *Earthquake Engineering and Structural Dynamics*, 27(1), 15-28.
- Zheng, T., and Dravinski, M. (1998). "Amplification of SH Waves by an Orthotropic Basin." *Earthquake Engineering and Structural Dynamics*, 27(3), 243-257.

## **VITA**

José Alfredo Fernández León was born on October 24, 1975 in Guatemala City, Guatemala. He earned a B.S. degree in Civil Engineering and a Master of Science in Structural Engineering from Universidad del Valle de Guatemala in 1998 and 2002, respectively. He started his graduate studies at the Georgia Institute of Technology in the Fall of 2002. He received a Master of Science and a Ph.D. degree in Civil Engineering with emphasis in Geotechnical Engineering from this institution in 2004 and 2007, respectively. His main research topic during his doctoral studies was Geotechnical Earthquake Engineering, particularly in the development of earthquake ground motions in the Central and Eastern United States.